



UNIVERSITY OF  
PLYMOUTH



Peninsula Medical School Theses  
Faculty of Health Theses

2023

## Proteomic analysis of genetically stratified grade-I meningioma

Yeasmin Akther

*Let us know how access to this document benefits you*

### General rights

All content in PEARL is protected by copyright law. Author manuscripts are made available in accordance with publisher policies. Please cite only the published version using the details provided on the item record or document. In the absence of an open licence (e.g. Creative Commons), permissions for further reuse of content should be sought from the publisher or author.

### Take down policy

If you believe that this document breaches copyright please [contact the library](#) providing details, and we will remove access to the work immediately and investigate your claim.

Follow this and additional works at: <https://pearl.plymouth.ac.uk/pms-theses>

---

### Recommended Citation

Akther, Y. (2023) *Proteomic analysis of genetically stratified grade-I meningioma*. Thesis. University of Plymouth. Retrieved from <https://pearl.plymouth.ac.uk/pms-theses/40>

This Thesis is brought to you for free and open access by the Faculty of Health Theses at PEARL. It has been accepted for inclusion in Peninsula Medical School Theses by an authorized administrator of PEARL. For more information, please contact [openresearch@plymouth.ac.uk](mailto:openresearch@plymouth.ac.uk).



UNIVERSITY OF  
PLYMOUTH

PEARL

PHD

## Proteomic analysis of genetically stratified grade-I meningioma

Akther, Yeasmin

**Award date:**  
2023

*Awarding institution:*  
University of Plymouth

[Link to publication in PEARL](#)

All content in PEARL is protected by copyright law.

The author assigns certain rights to the University of Plymouth including the right to make the thesis accessible and discoverable via the British Library's Electronic Thesis Online Service (EThOS) and the University research repository (PEARL), and to undertake activities to migrate, preserve and maintain the medium, format and integrity of the deposited file for future discovery and use.

Copyright and Moral rights arising from original work in this thesis and (where relevant), any accompanying data, rests with the Author unless stated otherwise\*.

Re-use of the work is allowed under fair dealing exceptions outlined in the Copyright, Designs and Patents Act 1988 (amended), and the terms of the copyright licence assigned to the thesis by the Author.

In practice, and unless the copyright licence assigned by the author allows for more permissive use, this means,

That any content or accompanying data cannot be extensively quoted, reproduced or changed without the written permission of the author / rights holder

That the work in whole or part may not be sold commercially in any format or medium without the written permission of the author / rights holder

\* Any third-party copyright material in this thesis remains the property of the original owner. Such third-party copyright work included in the thesis will be clearly marked and attributed, and the original licence under which it was released will be specified. This material is not covered by the licence or terms assigned to the wider thesis and must be used in accordance with the original licence; or separate permission must be sought from the copyright holder.

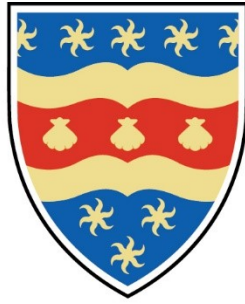


## **Copyright Statement**

This copy of the thesis has been supplied on the condition that anyone who consults it is understood to recognise that its copyright rests with its author and that no quotation from the thesis and no information derived from it may be published without the author's prior consent.







# UNIVERSITY OF PLYMOUTH

## **Proteomic analysis of genetically stratified grade-I meningioma**

By

**YEASMIN AKTHER**

A thesis submitted to the University of Plymouth

in partial fulfilment for the degree of

**DOCTOR OF PHILOSOPHY**

Peninsula Medical School

**September 2022**

## **Thesis supervisors**

### **Director of studies:**

Prof. Dr C. Oliver Hanemann MD, FRCP  
Chair in Clinical Neurobiology, Associate Head (Research) Peninsula Medical School  
Plymouth University Peninsula Schools of Medicine and Dentistry Plymouth, UK

### **2<sup>nd</sup> supervisor:**

Dr. Claudia Barros, PhD  
Associate Professor of Neuroscience  
Deputy Director of Doctoral College (Medical, Dental and Biomedical Schools)  
Faculty of Health, University of Plymouth

### **3<sup>rd</sup> supervisor:**

Dr. Claire L Adams BSc (Hons) PhD SRCS FIBMS  
Laboratory and Biobank Manager  
HTA person designate  
Faculty of Health, University of Plymouth

### **4<sup>th</sup> supervisor:**

Dr. Vikram Sharma, PhD  
Head Proteomics Core,  
School of Biomedical Sciences  
Plymouth University Peninsula Schools of Medicine and Dentistry

### **5<sup>th</sup> supervisor:**

Dr. Matthew Banton, PhD  
Research Fellow  
Faculty of Health, University of Plymouth, UK

## **Acknowledgements**

I want to start by expressing my gratitude to Prof. Oliver Hanemann, my director of studies, for providing me with the opportunity to work on my PhD project in your lab and for all of your supportive guidance throughout this process. I was very touched by your kindness and patience as you mentored me in becoming a research scientist and set goals for me to achieve. Besides science, I am also grateful to you for your kind support during my most difficult time.

I want to thank Dr Claire Adams for your unwavering guidance and encouragement during my PhD. You taught me to become a scientist by sharing your knowledge and skills in the field, which was a goal I never thought I'd be able to accomplish. You encouraged me to persevere when I got lost and taught me to have faith in my efforts. Without your dedication to genotyping the samples used in this project, along with your ongoing assistance in locating samples and ensuring that ethical standards were always upheld, this project would not have been possible.

I would like to thank Dr Vikram Sharma for your assistance with the mass spec sample processing and running the samples through the mass-spec machine. As my supervisor, you supported me through some difficult analyses, and your knowledge of proteomics and advice enabled me to succeed.

I would like to thank Dr Claudia Barros for your constructive feedback/comments throughout my PhD which help me to grow, especially in my scientific writing.

I also want to thank Dr Matthew Banton for your unwavering support, advice, and assistance with the analysis of my phosphopeptide data as well as for taking the time to address all of my bioinformatics-related inquiries.

Outside of my supervising team, I would want to express my gratitude to a number of researchers who provided technical support for my research studies. I want to express my profound gratitude to Dr. David Hilton and the other members of the Derriford neuropathology department for providing the vast majority of the rare samples used in this study. In particular, I am grateful to Dr. Hilton for helping to optimise the experiments, educating me on the fundamentals of neuropathology, and slides scoring.

Most significantly, a big thanks to Dr Emanuela Ercolano for your unconditional help and support in cell culturing and drug treatment experiments at the last moment of my lab work. You gave me most of the knowledge I have about cell cultures, and you were always there to provide a sympathetic ear or to gently remind me of reality. Also thanks to Dr. Leandro for his suggestions in my writing.

A huge thanks to the entire Hanemann group, past and present: Dr. Sara Ferluga, Dr.Sylwia, Dr. Jury, Dr. Sarah, Dr. Boh, Dr. Lucy, Dr. Foram, Bora, Dr. Jemma, Kevin, Ting and Laurien. You all helped me, gave me advice, and made my time in the lab more pleasurable. Outside of the Hanemann group, thanks to Julio, Lolita, Nsikan and Artjoms with whom I could discuss my bad days.

I consider myself exceedingly fortunate to have had my family's unwavering support during my PhD. Without the support of my parents, I genuinely would not have been able to complete my education. Even in their most difficult moment, they prioritised my study. I firmly believe, for their constant prayers I am here today.

Finally, a sincere thanks to my husband Raihan, It's probably difficult for me to put into words how thankful I am to have you in my life. You are always there to cheer me up and keep me going during my most difficult times. I dedicate this thesis to you.

## **Author's Declaration**

At no time during the registration for the degree of Doctor of Philosophy has the author been registered for any other University award without the prior agreement of the Doctoral College Quality Sub-Committee.

Work submitted for this research degree at the University of Plymouth has not formed part of any other degree either at the University of Plymouth or at another establishment.

This study was financed with the aid of a studentship from Brain Tumour Research.

## **Presentations at Conferences**

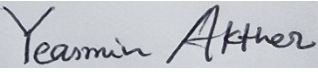
### **Virtual Oral presentation**

**Akther Y**, Adams CL, Sharma V, Barros CS, Banton M, Hilton DA, Hanemann CO. Proteomic analysis of genetically stratified low-grade meningiomas, BNOS, 9<sup>th</sup> July 2021

### **Virtual poster presentation**

**Akther Y**, Adams CL, Sharma V, Barros CS, Banton M, Hilton DA, Hanemann CO. Proteomic analysis of genetically stratified low-grade meningiomas, SNO, 15-16<sup>th</sup> July 2021

Word count of main body of thesis: 56341

Signed: 

Date: 09.09.2022

## Abbreviations

ABC	Ammonium bicarbonate
AE2	Anion exchange protein 2
AKT1	V-akt murine thymoma viral oncogene homolog 1
ANOVA	Analysis of variance
ANXA3	Annexin-A3
AURKB	Aurora kinase B
BCA	Bicinchoninic acid assay
BSA	Bovine serum albumin
CAFs	Cancer-associated fibroblasts
CAMK2A	Calcium/calmodulin-dependent protein kinase II alpha
CDH1	Cadherin 1
CHEK1	Checkpoint kinase 1
CHEK2	Checkpoint kinase 2
CLIC3	Chloride intracellular channel protein 3
CNS	Central nervous system
CRABP2	Cellular retinoic acid-binding protein 2
CSNK2A1	Casein kinase 2 alpha 1
DAB	Diaminobenzidine
DAVID	Database for Annotation, Visualization and Integrated Discovery
DEPs	Differentially expressed proteins
DMEM	Dulbecco's modified eagle medium
DMSO	Dimethyl sulfoxide
DTT	Dithiothreitol
ECL	Enhanced chemiluminescence
EDTA	Ethylene diamine tetra acetic acid antigen
EGFR	Epidermal growth factor receptor
EMT	Epithelial-mesenchymal transition
ERK7	Extracellular signal-regulated kinase 7
FAK	Focal adhesion kinase
FC	Fold changes
FDA	Food and drug administration
FDR	False discovery rate
FFPE	Formalin Fixed Paraffin Embedded
FRET	Fluorescence resonance energy transfer
GAPDH	Glyceraldehyde-3-phosphate dehydrogenase
GMDS	GDP- mannose 4, 6-dehydratase
GO	Gene ontology
GTR	Gross total resection
HIF-1 $\alpha$	Hypoxia-inducible factor-1 $\alpha$
HLA-DRA	Human Leukocyte Antigen – DR <i>Isotype</i>
HPLC	High performance liquid chromatography
IDH1	Isocitrate dehydrogenase-1
IgG	Immunoglobulin
IHC	Immunohistochemistry
IPA	Ingenuity pathway analysis
JNK	c-Jun N-terminal kinases

KASP	Kompetitive allele specific PCR
KEGG	Kyoto encyclopedia of genes and genomes
KLF4	Krupple like factor 4
LC MS/MS	Liquid chromatography tandem-mass spectrometry
LCK	Lymphocyte-specific protein-tyrosine kinase
LFQ	Label free quantification
MAPK	Mitogen-activated protein kinases
MLPA	Multiplex ligation-dependent probe amplification
MMP-2	Matrix metalloproteinase-2
MOI	Multiplicity of infection
NGS	Next generation sequencing
NMT	Normal meningeal tissue
OS	Overall survival
PBST	Phosphate-buffered saline and tween-20
PC	Pyruvate carboxylase
PCR	Polymerase chain reaction
PFS	Progression-free survival
pHi	Intracellular pH
PI3K	Phosphoinositide 3' kinase
PIK3CA	Phosphatidylinositol-4,5-biphosphate 3-kinase catalytic subunit alpha
POLR2A	Polymerase RNA II DNA directed polypeptide
PRKCA	Protein kinase C alpha
PTBE	Peritumoral brain oedema
PTGFRN	Prostaglandin F2 receptor negative regulator
RA	Retinoic acid
RhoGDI	Rho GDP-Dissociation Inhibitors
RIPA	Radioimmunoprecipitation assay
RPM	Revolutions per minute
RT	Room temperature
SEM	Standard error of the mean
shRNA	Short hairpin RNA
SLC29A1	Solute carrier family 29 member 1
SMO	Smoothened, frizzle family receptor
SNP	Single nucleotide polymorphisms
STAGE	Stop and go extraction
TBST	Tris-buffered saline and tween-20
TCA cycle	Tricarboxylic acid cycle
TFA	Trifluoroacetic acid
TGF- $\beta$	Transforming growth factor- $\beta$
THSD4	Thrombospondin type-1 domain-containing protein 4
TMTs	Tandem mass tags (TMTs)
TNF	Tumour necrosis factor
TRAF7	TNF receptor associated factor 7 (TRAF7)
VEGFR	Vascular endothelial growth factor receptor
VELI-3	Vertebrate lin-7 homolog 3



## Table of contents

<b>Abstract.....</b>	<b>1</b>
<b>1. Introduction.....</b>	<b>3</b>
1.1 Meningioma background.....	3
1.2 Incidence and risk factor of meningioma.....	4
1.3 Clinical presentation of meningioma .....	5
1.4 Histopathological classification of meningioma.....	6
1.5 Meningioma diagnosis .....	7
1.6 Cytogenetics .....	8
1.7 <i>NF2</i> mutation in meningioma .....	9
1.8 Non- <i>NF2</i> mutations in meningioma.....	11
1.9 Current therapies .....	16
1.9.1 Surgery.....	16
1.9.2 Radiotherapy.....	17
1.9.3 Systemic treatment for meningioma.....	17
1.9.4 Targeted molecular therapies.....	18
1.9.5 Immune therapy.....	20
1.10 Overview of omics research in meningioma.....	22
1.10.1 Genomics .....	23
1.10.2 Epigenomics .....	24
1.10.3 Transcriptomics .....	27
1.10.4 Proteomics .....	28
1.11 Biomarkers in neuro-oncology.....	33
1.12 Aim of this project.....	36
<b>2. Material and methods.....</b>	<b>39</b>
2.1 Tumour material and clinical data.....	39
2.2 Digestion of meningioma tumour and cell culture.....	41
2.3 DNA extraction and Next Generation Sequencing .....	42
2.4 KASP genotyping.....	42
2.5 Sanger sequencing.....	45
2.6 Tissue lysates preparations.....	47
2.7 Total protein preparation.....	47
2.8 Gel digestion .....	47
2.9 Peptide clean-up .....	48
2.10 Protein identification by liquid chromatography-tandem mass spectrometry .....	48

2.11 Enrichment of phosphoprotein .....	49
2.12 TMT Labelling and phospho-peptide enrichment.....	50
2.12.1 Nano-LC Mass Spectrometry .....	50
2.12.2 Data Analysis.....	51
2.13 Statistical and functional annotation analysis .....	52
2.14 Kinase identification .....	52
2.15 Western blotting .....	53
2.16 Simple wes assay.....	59
2.17 Immunohistochemistry.....	59
2.18 Functional validation of proteins <i>in-vitro</i> .....	61
2.18.1 Protein knockdown procedure .....	61
2.18.2 Drug treatment and ATP assay.....	61
<b>3. Results- Global proteomic analysis of mutational subtypes of meningioma grade-I ..65</b>	
3.1 Introduction .....	65
3.2 Confirmation of mutational background in meningioma specimens .....	66
3.2.1 <i>NF2<sup>-/-</sup></i> mutational status .....	66
3.2.2 <i>AKT1<sup>E17K</sup></i> and <i>TRAF7</i> mutational status .....	68
3.2.3 <i>KLF4<sup>K409Q</sup></i> and <i>TRAF7</i> mutational status .....	69
3.3 Global proteomic analysis of meningioma subtypes.....	70
3.3.1 Protein identification and quantification .....	70
3.3.2 Hierarchical clustering of meningioma mutational subtypes .....	72
3.3.3 Hierarchical clustering of differentially expressed proteins across meningioma sample groups .....	74
3.4 Meningiomas with <i>AKT1<sup>E17K</sup>/TRAF7</i> mutations.....	75
3.4.1 Meningioma with <i>AKT1<sup>E17K</sup>/TRAF7</i> mutational subtype-specific protein analysis	75
3.4.2 Distinct and overlapping proteins in meningioma with <i>AKT1<sup>E17K</sup>/TRAF7</i> mutational subtypes .....	77
3.4.3 Functional annotation enrichment analysis of <i>AKT1<sup>E17K</sup>/TRAF7</i> mutational meningioma subtypes .....	80
3.4.4 Functional annotation enrichment analysis of <i>AKT1<sup>E17K</sup>/TRAF7</i> -specific upregulated proteins .....	81
3.4.5 <i>AKT1<sup>E17K</sup>/TRAF7</i> mutant meningioma subtype-specific IPA pathway analysis .....	84
3.4.6 Validation of protein candidates for <i>AKT1<sup>E17K</sup>/TRAF7</i> mutational meningioma subtypes .....	86
3.5 Meningioma with <i>NF2<sup>-/-</sup></i> mutations.....	92
3.5.1 Meningioma with <i>NF2<sup>-/-</sup></i> mutational subtype-specific protein analysis .....	92

3.5.2 Distinct and overlapping proteins in meningioma with <i>NF2</i> <sup>-/-</sup> mutational subtypes .....	94
3.5.3 Functional annotation enrichment analysis of <i>NF2</i> <sup>-/-</sup> -specific proteins.....	97
3.5.4 <i>NF2</i> <sup>-/-</sup> mutant meningioma subtype-specific IPA pathway analysis:.....	99
3.5.5 Protein candidates of <i>NF2</i> <sup>-/-</sup> mutational meningioma subtypes for validation .....	102
3.6 Meningioma with <i>KLF4</i> <sup>K409Q</sup> mutational .....	107
3.6.1 Meningioma with <i>KLF4</i> <sup>K409Q</sup> mutational subtype-specific protein analysis .....	107
3.6.2 Distinct and overlapping proteins in meningioma with <i>KLF4</i> <sup>K409Q</sup> mutational subtypes .....	109
3.6.3 Functional annotation enrichment analysis of <i>KLF4</i> <sup>K409Q</sup> mutant meningioma specific proteins .....	113
3.6.4 <i>KLF4</i> <sup>K409Q</sup> mutant meningioma subtype-specific IPA pathway analysis .....	115
3.6.5 Protein candidates of <i>KLF4</i> <sup>K409Q</sup> / <i>TRAF7</i> mutant meningioma for validation .....	118
3.7 Meningioma grade-I.....	122
3.7.1 Meningioma grade-I protein analysis irrespective of genotype .....	122
3.7.2 Validation of meningioma grade I specific proteins via Simple WES or Western Blot .....	126
3.7.3 Immunohistochemistry of differentially regulated candidates for meningioma grade-I.....	128
3.8 Summary and conclusion of global proteomics data analysis.....	130
<b>4. Results- Phosphoproteomic and phosphopeptide analysis of mutational subtypes of meningioma grade-I.....</b>	<b>131</b>
4.1 Introduction .....	131
4.2 Phosphoproteomic analysis of meningioma subtypes.....	132
4.2.1 Phosphoproteins identification and quantification .....	132
4.2.2 Hierarchical clustering of meningioma mutational subtypes .....	133
4.3 Phosphopeptide analysis of meningioma subtypes .....	136
4.3.1 Detection of phosphorylated motifs .....	137
4.3.2 Quantitative changes in phosphorylation sites in meningioma mutational subtypes .....	138
4.4 Kinase prediction analysis.....	141
4.4.1 Predicted differential kinase activity in meningioma mutational subtypes.....	141
4.4.2 Validation of predicted kinases .....	144
4.4.3 Examination of PRKACA activity via immunohistochemistry .....	153
4.4.4 Functional validation of PRAKCA in benign meningioma subtypes.....	155
4.5 Conclusion.....	159

<b>5. Discussion.....</b>	<b>160</b>
5.1 Global proteomic data analysis .....	160
5.1.1 <i>AKT1</i> <sup>E17K</sup> / <i>TRAF7</i> mutant meningioma-specific upregulated protein candidates ..	161
5.1.2 <i>NF2</i> <sup>-/-</sup> mutant meningioma-specific upregulated protein candidates.....	171
5.1.3 <i>KLF4</i> <sup>K409Q</sup> / <i>TRAF7</i> mutated meningioma-specific upregulated protein candidates .....	176
5.1.4 Meningioma grade-I specific upregulated protein candidates.....	184
5.1.5 Functional annotation enrichment analysis of DEPs (differential expression of proteins) using DAVID .....	190
5.1.6 Pathway analysis of benign meningioma subtype via IPA.....	191
5.1.7 Global proteomic data analysis compared with previous proteomic studies of meningioma .....	197
5.2 Phospho-peptide proteomic data analysis .....	198
5.2.1 <i>AKT1</i> <sup>E17K</sup> / <i>TRAF7</i> specific kinase candidates.....	198
5.2.2 <i>NF2</i> <sup>-/-</sup> specific kinase candidates .....	202
5.2.3 <i>PRKCA</i> as a therapeutic target for benign mutational meningioma subtypes .....	206
5.3 Limitations of the study.....	207
5.4 Future directions.....	209
5.5 Conclusions .....	213
<b>References.....</b>	<b>215</b>
<b>Appendix.....</b>	<b>268</b>

<b>List of figures</b>	<b>Page no</b>
Figure 1: Schematic illustration of three meningeal layers	4
Figure 2: Structure and frequency of <i>NF2</i> mutations in meningioma.	10
Figure 3: Schematic representation of the mutational landscape of meningiomas.	12
Figure 4: Schematic of TRAF7 structure.	13
Figure 5: Point mutation of <i>AKT1</i> <sup>E17K</sup> in the PH (pleckstrin homology) domain.	14
Figure 6: Illustrating point mutation of <i>KLF4</i> <sup>K409Q</sup> in the zinc finger domain.	14
Figure 7: Illustrating overview of molecular signalling pathways and drug targets in meningioma.	20
Figure 8: Classification of meningioma based on DNA methylation	26
Figure 9: A summary of the biomarker categories situated along this clinical continuum.	34
Figure 10.1: Schematic representation of global proteome and phosphoproteome experimental strategy.	63
Figure 10.2: Schematic representation of phospho peptide proteome experimental strategy.	64
Figure 11: <i>NF2</i> <sup>-/-</sup> mutational status confirmation in meningioma tissue samples.	67
Figure 12: <i>AKT1</i> <sup>E17K</sup> and <i>TRAF7</i> mutational status confirmation in meningioma samples.	69
Figure 13: Distribution of identified proteins across all sample groups.	71
Figure 14: Meningioma samples clustering based on their proteomic profiles and comparative analysis of different mutational subtypes of meningioma and normal meninges.	73
Figure 15: Differential protein expression between sample groups.	76
Figure 16: <i>AKT1</i> <sup>E17K</sup> / <i>TRAF7</i> mutational subtype-specific proteins.	78
Figure 17: Functional annotation enrichment analysis of <i>AKT1</i> <sup>E17K</sup> / <i>TRAF7</i> -specific upregulated proteins.	82
Figure 18: KEGG pathways analysis via DAVID shows upregulated proteins in <i>AKT1</i> <sup>E17K</sup> / <i>TRAF7</i> mutant meningioma subtype are mostly found in metabolic pathways and oxidative phosphorylation terms.	83
Figure 19: A balloon plot showing IPA pathways analysis for three sets of differential expression data	85
Figure: 20 Illustrating <i>AKT1</i> <sup>E17K</sup> / <i>TRAF7</i> specific IPA canonical pathway analysis (oxidative phosphorylation pathway).	86
Figure 21: Validation of proteins identified as significantly upregulated in <i>AKT1</i> <sup>E17K</sup> / <i>TRAF7</i> vs. other mutational subtypes and NMT.	89
Figure 22: Immunohistochemistry analysis of <i>AKT1</i> <sup>E17K</sup> / <i>TRAF7</i> specific candidate proteins.	91
Figure 23: Differential protein expression between sample groups.	93
Figure 24: <i>NF2</i> <sup>-/-</sup> mutational subtype-specific proteins	95
Figure 25: Functional annotation of 54 proteins commonly significantly downregulated in meningioma <i>NF2</i> <sup>-/-</sup> mutational subtypes compared to NMT by the DAVID version 6.8.	99
Figure 26: A balloon plot showing IPA pathways analysis for three sets of differential expression data	101
Figure 27: Validation of proteins identified as significantly upregulated in <i>NF2</i> <sup>-/-</sup> vs. other mutational subtypes and NMT.	103
Figure 28: Immunohistochemistry analysis of <i>NF2</i> <sup>-/-</sup> specific candidate proteins.	105

Figure 29: Annexin-3 knock-down slightly affects the expression of cyclin-D1 in meningioma cell line Benmen-1	107
Figure 30: Differential protein expression between sample groups.	108
Figure 31: <i>KLF4<sup>K409Q</sup></i> mutational subtype-specific proteins.	110
Figure 32: Functional annotation of <i>KLF4<sup>K409Q</sup></i> mutant meningioma specific up-regulated proteins by the DAVID version 6.8.	113
Figure 33: Functional annotation of <i>KLF4<sup>K409Q</sup></i> mutant meningioma-specific down-regulated proteins by the DAVID version 6.8.	115
Figure 34: A balloon plot showing IPA pathways analysis for three sets of differential expression data	117
Figure 35: Validation of proteins identified as significantly upregulated in <i>KLF4<sup>K409Q</sup>/TRAF7</i> vs. other mutational subtypes and NMT.	120
Figure 36: Immunohistochemistry analysis of <i>KLF4<sup>K409Q</sup>/TRAF7</i> mutant meningioma-specific candidate proteins.	121
Figure 37: Meningioma grade I specific proteins regardless of mutations.	123
Figure 38: Validation of proteins identified as significantly upregulated in benign meningioma compared to NMT.	126
Figure 39: Immunohistochemistry analysis of meningioma grade I specific candidate proteins.	129
Figure 40: Distribution of identified phosphoproteins across all sample groups.	133
Figure 41: Meningioma samples clustering based on their phosphoproteomic profiles and comparative analysis of different mutational subtypes of meningioma and normal meninges.	134
Figure 42: Overview of the phosphopeptide data set.	137
Figure 43: Phosphosites-specific motif analysis by using motif-x method (MoMo).	138
Figure 44: Differential phosphosites expression between sample groups.	140
Figure 45: Differential kinases activity analysis between sample groups.	143
Figure 46: Validation of predicted kinases as significantly upregulated in <i>AKT1<sup>E17K</sup>/TRAF7</i> compared to <i>NF2<sup>-/-</sup></i> mutational subtype and NMT.	147
Figure 47: Validation of predicted kinases as significantly upregulated in <i>NF2<sup>-/-</sup></i> compared to <i>AKT1<sup>E17K</sup>/TRAF7</i> mutational subtype and NMT.	152
Figure 48: Immunohistochemistry analysis of PRKACA kinase in meningioma mutant subtypes compared to NMT.	154
Figure 49: Efficacy of PRKCA inhibitor (Go6976) in meningioma primary cell viability assay.	156
Figure 50: Go6976 was unable to inhibit PRKCA activity in benign meningioma subtypes by 72 hours.	158
Figure 51: AKT mediated cellular energy metabolism, cell growth and cell proliferation.	192
Figure 52: Illustrating RhoGDI pathway from IPA.	195

<b>List of tables</b>	<b>Page no</b>
Table 1: WHO classification (2021) of meningioma grading based on histological subtype and molecular markers.	7
Table 2.1: Clinical and histological details about the specimens are presented	41
Table 2.2: Endpoint genotyping primers	44
Table 3: Oligonucleotide details.	46
Table 4: Polyacrylamide gel recipes	54
Table 5: List of primary antibodies with their concentrations used in this study.	58
Table 6: <i>KLF4</i> <sup>K409Q</sup> and <i>TRAF7</i> mutational status confirmation in meningioma samples	70
Table 7: A partial list of significantly upregulated proteins common to <i>AKT1</i> <sup>E17K</sup> / <i>TRAF7</i> mutational subtype.	79
Table 8: A complete list of significantly downregulated proteins common to <i>AKT1</i> <sup>E17K</sup> / <i>TRAF7</i> mutational subtype.	80
Table 9: <i>AKT1</i> <sup>E17K</sup> / <i>TRAF7</i> mutant meningioma specific candidate's for validation.	87
Table 10: A Complete lists of significantly upregulated proteins unique to <i>NF2</i> <sup>-/-</sup> mutational subtype.	96
Table 11: A partial lists of significantly downregulated proteins unique to <i>NF2</i> <sup>-/-</sup> mutational subtype.	97
Table 12: <i>NF2</i> <sup>-/-</sup> mutant meningioma specific upregulated proteins for validation	102
Table 13: A partial lists of significantly upregulated proteins unique to <i>KLF4</i> <sup>K409Q</sup> mutated meningioma subtype.	111
Table 14: A partial lists of significantly downregulated proteins unique to <i>KLF4</i> <sup>K409Q</sup> mutated meningioma subtype.	112
Table 15: <i>KLF4</i> <sup>K409Q</sup> / <i>TRAF7</i> mutant meningioma specific upregulated proteins for validation	118
Table 16: A partial lists of significantly upregulated proteins unique to benign meningioma compared to NMT.	124
Table 17: A partial lists of significantly downregulated proteins unique to benign meningioma compared to NMT.	125
Table 18: Meningioma grade I specific upregulated proteins for validation	126

# **Proteomic analysis of genetically stratified grade-I meningioma**

## **Abstract**

**Introduction:** Meningioma is the most common primary intracranial tumour. Although often benign in nature, at least 20% have high rates of recurrence. Surgical resection and radiotherapy are the main therapeutic approach, yet tumour location can hamper complete resection and chemotherapies are ineffective. Therefore, more accurate prognostic biomarkers are needed to improve the clinical management of meningioma. The mutational profile of mutant meningioma is well defined, including in addition to most common NF2 loss, mutations of *TRAF7*, *KLF4*, and *AKT1*. The aim of this study is to identify novel biomarkers and therapeutic targets of genetically stratified meningioma by characterising the proteomic landscape.

**Materials and methods:** Frozen meningioma tissue samples were stratified according to mutational background: *AKT1<sup>E17K</sup>/TRAF7*, *KLF4<sup>K409Q</sup>/TRAF7* and *NF2<sup>-/-</sup>*. For global proteomics, proteins were fractionated by SDS-PAGE followed by in-gel tryptic digestion and sample preparation for LCMS analysis. Raw mass spectrometry data files were analysed using MaxQuant (1.6.2.10) and Perseus software (1.6.1.3). Quantitative phosphoproteomics was performed using TMT 10plex labelling approach followed by kinase prediction using KinswingR. GO enrichment analyses were performed using DAVID against all human proteins. Proteomics data were also further analysed for pathway analysis by the Ingenuity® Pathway Analysis (IPA®) software. Followed by mutational subtype specific potential protein and kinase candidates were validated via Western blot and immunohistochemistry techniques.

**Results:** In total, 4162 proteins were quantified across all meningioma mutational subtypes and normal meninges (n=31). Hierarchical clustering analysis showed distinct proteomic profiles of meningioma mutational subtypes and corresponding clusters of differentially expressed proteins. Comparative analysis showed only 10 proteins were commonly significantly upregulated ( $\log_2$  fold-change $\geq 1$ ;  $p < 0.05$ ) among all mutational subtypes vs. normal meninges which indicates mutational subtypes are very different from each other at



their protein expression level. Mutational subtype specific analysis identified 156 proteins to be commonly significantly upregulated ( $\log_2$  fold-change $\geq 1$ ;  $p < 0.05$ ) in *AKT1<sup>E17K</sup>/TRAF7*, 14 proteins in *KLF4<sup>K409Q</sup>/TRAF7*, and 7 proteins in *NF2<sup>-/-</sup>* mutant meningioma subtypes compared to normal meninges. IPA and gene ontology analysis showed that *AKT1<sup>E17K</sup>/TRAF7* mutant subtype-specific upregulated proteins were highly enriched in oxidative phosphorylation and metabolic pathways, while *KLF4<sup>K409Q</sup>/TRAF7* mutated meningioma-specific upregulated proteins were associated with extracellular matrix disassembly and focal adhesion GO terms. *AKT1<sup>E17K</sup>/TRAF7* mutated meningioma-specific top candidate protein expressions including CLIC3, CRABP2, GMDS, and Pyruvate carboxylase were validated via WB and Simple wes and an increased expression of *KLF4<sup>K409Q</sup>/TRAF7* specific protein Endoglin confirmed via both WB and IHC. *NF2<sup>-/-</sup>* mutated meningioma-specific one protein, Annexin-3 showed significant expression compared to other meningioma subtypes and NMT, and knocking down of this protein showed reduced Benmen-1 cell proliferation. Lastly, analysis of 6600 phosphosites (n=8) predicted regulatory kinases including PRKCA and EGFR, and the presence of an active form of PRKCA in benign meningioma was confirmed via both WB and IHC.

**Conclusion:** A proteomic approach is an effective tool to identify distinct protein expression in genetically distinct meningioma subgroups and has led to the identification of differentially expressed proteins and activated pathways in mutant subtypes. Further validation and functional verification of potential candidates will allow us to identify potential drug targets/biomarkers for benign meningiomas.

# 1. Introduction

Meningioma is the most common primary intracranial tumour of the central nervous system (CNS). Most meningiomas (80%) are low grade. However, some show high rates of recurrence, which causes mild to severe morbidity. Currently surgery, radiotherapy and stereotactic radiosurgery are the treatment options for meningioma and sometimes is not possible due to tumour location. Moreover, there is a lack of accurate prognostic or diagnostic markers for the diagnosis and management of meningiomas. With the advancement of sequencing technology, genomic studies have identified several meningioma driver mutations (Clark *et al.*, 2013; Clark *et al.*, 2016). These mutations and their molecular manifestations consequently affect the multiple signalling pathways which are potential therapeutic targets. The molecular mechanisms behind meningioma tumorigenesis are still not fully understood. Therefore, proteomics analysis of these mutations is highly relevant.

## 1.1 Meningioma background

Meningiomas are the most common primary intracranial tumour of the central nervous system (CNS) accounting for approximately 36.4% of all brain tumours (Ostrom *et al.*, 2014; Ostrom *et al.*, 2015; Ostrom *et al.*, 2021). The meninges consist of three protective tissue layers that cover the brain and spinal cord; the outermost thick layer called dura mater which is adjacent to the skull and vertebrae, the middle layer called arachnoid mater, a web-like structure filled with fluid that supports the brain and spinal cord, and the most inner thin layer referred to as pia mater which provides the lining for the brain and spinal cord (Wiemels *et al.*, 2010; Al-Rashed *et al.*, 2020) (Fig 1). Meningiomas are likely to originate from non-neuroepithelial arachnoid cap cells, which are a morphologically distinct and metabolically active subset of arachnoidal cells, involved in cerebrospinal fluid resorption (Marosi *et al.*, 2008). They are found in the apex of arachnoid villi, often within a dural sinus, and are accessible to venous blood flow (Marosi *et al.*, 2008) (Fig 1). Another study showed that meningioma tumours originate from prostaglandin D2 synthase (PGDS)-expressing arachnoid cells that emerge through the dura on arachnoid villi in genetically modified mice (Kalamarides *et al.*, 2011; Al-Rashed *et al.*, 2020). In summary, meningiomas are derived from the neoplastic transformation of the arachnoid barrier cells and less commonly from the dural border cells (Abbritti *et al.*, 2016). The majority of meningiomas are intracranial (90%) whilst a small minority occur in

the spine with the thoracic spine being the most common spinal site (Whittle *et al.*, 2004; Ostrom *et al.*, 2015).

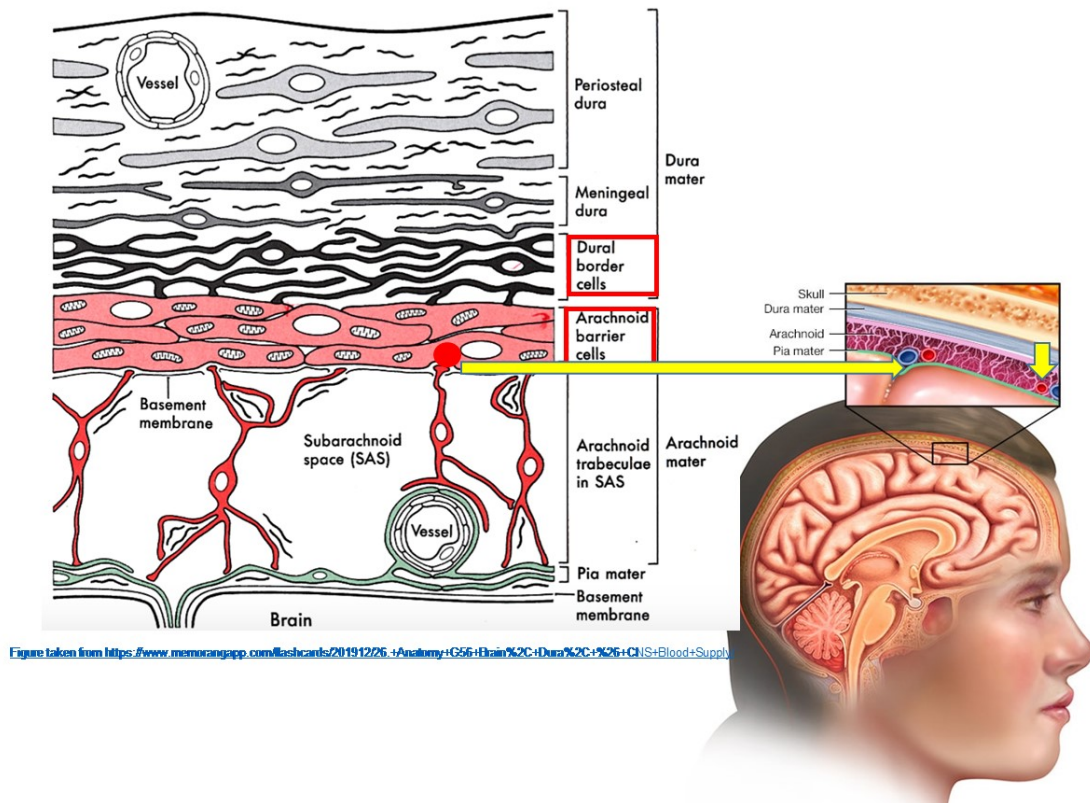


**Figure 1:** Schematic illustration of three meningeal layers (outer dura mater, middle arachnoid, and inner pia mater) and yellow arrows showing meningioma originates from arachnoid barrier cells. Image adapted from the sites (<https://www.memorangapp.com/flashcards/201912/26.+Anatomy+G56+Brain%2C+Dura%2C+%26+CNS+Blood+Supply/> and <https://middlesexhealth.org/learning-center/diseases-and-conditions/meningioma>)

## 1.2 Incidence and risk factor of meningioma

Meningioma is the most prevalent intracranial brain tumour, with an estimated incidence of 7.8 cases per 100,000 people each year (Baldi *et al.*, 2018; Ostrom *et al.*, 2021). Meningioma incidence rises with age, from 0.14 % 100,000 in children aged 0 to 19 years to 37.75 % 100,000 in people aged 75 to 84 years (Ostrom *et al.*, 2016). In addition, data show that African-Americans have a higher prevalence than Caucasians, with a 2.27:1 female predominance (Ostrom *et al.*, 2016) and, across all populations, the occurrence of meningioma is three and a half times more common in females compared to males (Tufan *et al.*, 2005; Klaeboe *et al.*, 2005). The increased prevalence of this tumour in women may be linked to the presence of progesterone receptors, which may play a role in meningioma pathogenesis (Claus

*et al.*, 2013). Another study reported the existence of oestrogen, progesterone, and androgen receptors in some meningiomas, with an additional link between breast cancer and meningiomas (Claus *et al.*, 2007). Meningiomas have been shown to fluctuate in size during the luteal phase of the menstrual cycle and during pregnancy, as well as the shrinkage of multiple tumours in a meningioma patient occurring when oestrogen agonist therapy is stopped (Claus *et al.*, 2007; Vadivelu *et al.*, 2010). However, the incidence of meningioma is not consistently associated with hormones (Wiemels *et al.*, 2010).

Established risk factors for meningioma include germline mutations in the *Neurofibromatosis 2 (NF2, merlin, neurofibromin 2)* gene and exposure to ionising radiation (Evans *et al.*, 2017; Schneider *et al.*, 2005; Flint-Richter *et al.*, 2011; Buerki *et al.*, 2018). Meningioma development is associated with a wide variety of familial disorders, with neurofibromatosis type 2 (NF2), an autosomal dominant condition, being the common hereditary cause (Evans *et al.*, 2017). Whilst ionizing radiation exposure at high levels has been shown to increase the chance of meningioma, at lower doses it may also increase the risk, but the exact types and doses are still debated (Wiemels *et al.*, 2010). There are other risk factors associated with meningiomas such as pre-existing diabetes mellitus and arterial hypertension (Sadetzki *et al.*, 2002; Perry *et al.*, 2001; Evans *et al.*, 2017; Schneider *et al.*, 2005; Flint-Richter *et al.*, 2011).

### **1.3 Clinical presentation of meningioma**

Meningioma tumours exhibit different clinical presentations depending on where they are located. Intracranial meningiomas are common whereas intraventricular meningiomas are rare in occurrence (Buerki *et al.*, 2018). Meningiomas are slow-growing, that present with a gradual development of symptoms. Meningiomas are often identified incidentally on imaging, with most patients asymptomatic (Buerki *et al.*, 2018). Symptoms occur when the tumour is large enough to cause a mass effect, and include: signs of raised intracranial pressure, focal neurological deficit, seizures, and death (Whittle *et al.*, 2004; Fathi and Roelcke, 2013). In addition to this, personality changes, anxiety, and a shift in state of consciousness are common in anterior (frontal) or parasagittal meningiomas, symptoms that can easily be mistaken as dementia or depression initially in the clinic (Buerki *et al.*, 2018).

## 1.4 Histopathological classification of meningioma

Meningiomas are classified according to the 2016 World Health Organisation (WHO) classification into three grades comprised of 15 different histopathological subtypes (Louis *et al.*, 2016). Approximately ~80% of meningioma is WHO grade I, encompassing nine histological subtypes, characterized by a benign nature with low mitotic activity (Riemenschneider *et al.*, 2006; Whittle *et al.*, 2004). Among these, meningothelial, fibroblastic and transitional are common; in contrast, metaplastic, and lymphoplasmacytic-rich subtypes are rare (Riemenschneider *et al.*, 2006).

Meningiomas classified as WHO grade II are more aggressive and invasive in nature, accounting for up to 15-20% of all meningiomas. There are three histological subtypes in this group (chordoid, clear cell, and atypical). Histopathologically grade II is characterized by 4-19 mitoses per 10 high power fields (HPF), increased cellularity, nuclear polymorphism, and tumour necrosis (Perry *et al.*, 1999; Riemenschneider, Perry and Reifenberger, 2006; Mawrin and Perry., 2010).

WHO grade III accounts for only 1-3% and consists of three subtypes: papillary, rhabdoid, and anaplastic. Malignant meningioma exhibits high mitotic activity, (more than 20 per 10 HPF) and is associated with an 80% risk of recurrence (Perry *et al.*, 1999; Riemenschneider, Perry and Reifenberger, 2006; Mawrin and Perry., 2010; Louis *et al.*, 2016). Higher-grade meningiomas demonstrate aggressive behaviour with grade III tumours exhibiting overtly malignant cytology (Louis *et al.*, 2016). Progression-free survival (PFS) and overall survival (OS) decrease as the grade increases, in that patients with a grade III meningioma have a poorer clinical outcome compared to grade I meningioma patients (Bi *et al.*, 2016). In addition to histopathological features, in 2021 WHO introduced molecular markers to define meningioma (Louis *et al.*, 2021; Goldbrunner *et al.*, 2021). WHO grade I does not include lymphoplasmacytic-rich subgroups in the new classification 2021 (Table 1). Furthermore, two histological subtypes (rhabdoid and papillary meningioma) previously linked to WHO grade III were not included in the new classification 2021 (Louis *et al.*, 2021; Goldbrunner *et al.*, 2021). These two subtypes are currently classified according to the same atypical and anaplastic criteria as other meningioma histological subtypes (Louis *et al.*, 2021; Goldbrunner *et al.*, 2021). WHO meningioma classification 2021 associated molecular markers are described in detail in sections 1.6, 1.7, 1.8 and 1.10.2.

	Common Mutations	CNVs	MC
WHO grade 1			
Meningothelial	<i>AKT1</i> (/ <i>TRAF7</i> ), <i>SMO</i>	None	ben-2
Fibroblastic	<i>NF2</i>	del 22q	ben-1
Transitional	<i>NF2</i>	del 22q	ben-1
Secretory	<i>KLF4</i> / <i>TRAF7</i> <sup>a</sup>	None	ben-2
Psammomatous	<i>NF2</i>	del 22q	ben-1
Metaplastic	<i>NF2</i>	gain 5	ben-3
Microcystic	<i>NF2</i>	gain 5	ben-3
Angiomatous	<i>NF2</i>	gain 5	ben-3
WHO grade 2			
Atypical	<i>NF2</i>	del 1p, del 22q	int-A/B
Chordoid	( <i>NF2</i> )	del 2p	int-A/B
Clear cell	<i>SMARCE1</i>	None	No specific
WHO grade 3			
Anaplastic	<i>NF2</i> , <i>TERT</i> promoter	del 1p, 10, 22q, homo del CDKN2A/B	Malignant
Formerly WHO grade 3			
Rhabdoid	<i>BAP1</i>	( <i>BAP1</i> locus)	No specific
Papillary	<i>PBRM1</i>	No specific	No specific

**Table 1. WHO classification (2021) of meningioma grading based on histological subtype and molecular markers.** The table is taken from Goldbrunner *et al.*, (2021). Abbreviations: ben, benign; CNVs, copy number variations; del, deletion; homo del, homozygous deletion; int, intermediate; MC, methylation class.22 (Goldbrunner *et al.*, 2021).

## 1.5 Meningioma diagnosis

MRI (Magnetic resonance imaging) is a common tool for meningioma diagnosis, alternatively computed tomography (CT) scans may be used in meningioma patients who are unable to undergo an MRI scan (Buerki *et al.*, 2018). In addition to MRI, there are other imaging techniques that are not yet routine medical practice, positron emission tomography (PET) using, for example, a 68-Ga-DOTATE-labeled somatostatin-receptor analogue (68-Ga-

DOTATE) can be used to monitor for recurrence in previously irradiated meningioma and to aid diagnosis when a surgical biopsy is not possible (Rachinger *et al.*, 2015; Afshar-Oromieh *et al.*, 2015). Despite the fact that these meningioma features are useful diagnostic aids, conventional MRI and other imaging techniques cannot predict meningioma pathology grade or growth potential. Further, conventional MRI can be ineffective at distinguishing early recurrence from treatment-related radiographic alterations like moderate dural thickening (Buerki *et al.*, 2018).

Currently, meningiomas are diagnosed based on both, radiological and histological features. Imaging may suggest the diagnosis of a meningioma, but does not indicate a grade; hence, the gold standard for diagnosis being histopathological analysis, using 2021 WHO diagnostic criteria (Louis *et al.*, 2021).

There are emerging molecular and genetic tools currently being developed to improve the stratification of meningiomas based on their predicted PFS and OS (Sahm *et al.*, 2017), but none are currently in wide clinical use yet. Therefore, the WHO histopathological criteria still remain the only diagnostic clinical tool, emphasising the pressing need for molecular markers to aid in meningioma diagnosis and stratification.

## 1.6 Cytogenetics

Meningioma has been linked to a variety of chromosomal changes, which have been shown to increase in correlation with tumour grade and aggressiveness (Lerner *et al.*, 2014; Al-Rashed *et al.*, 2020). The most common somatic copy number alteration (SCNA) in meningioma is chromosome 22 monosomy, which occurs in 56 % of cases and results in the deletion of the genomic locus containing *NF2* (22q12.2) (Ruttledge *et al.*, 1994; Brastianos *et al.*, 2013; Esaulova *et al.*, 2017). *NF2* mutations increase the risk of progression in benign meningiomas compared to those with a normal karyotype (Al-Rashed *et al.*, 2020). Furthermore, the prevalence of *NF2* abnormalities rises with tumour grade (Al-Rashed *et al.*, 2020). The second most common chromosomal aberration in meningioma is the loss of heterozygosity on chromosome 1p (Sulman *et al.*, 2004). Retinoblastoma protein-interacting zinc-finger gene 1 (RIZ1) is a tumour suppressor and methyltransferase protein identified on chromosome 1p, and it has been shown that reduced or loss of expression of RIZ1 is linked to meningioma development (Liu *et al.*, 2013). The deletion of the *CDKN2A/CDNK2B* (cyclin-dependent kinase inhibitor 2A/cyclin-dependent kinase 4 inhibitor B) gene on chromosome 9q is frequently associated with the development of atypical to anaplastic, and a recurrent

amplification of this locus is also seen in benign meningioma (Goutagny *et al.*, 2010; Everson *et al.*, 2018; Sievers *et al.*, 2020).

Loss of chromosomes 6q, 9p, 10q, 14, and 18q, along with gains in 17q and 20q, are also seen, although less frequently in higher grade meningioma (Bi *et al.*, 2017; Lee *et al.*, 2010; Goutagny *et al.*, 2010). A study has shown that changes in the chromosomal set of 1p, 1q, 7, 9, 10, 14, 18 and 22 were highly associated with an increased risk of recurrence. This study also demonstrated that tumours with a complex karyotype, or two or more defective chromosomes, were associated with considerably lower recurrence-free survival (RFS) than those with a single abnormal chromosome or a normal diploid karyotype (Domingues *et al.*, 2014). Angiomatous meningioma, a more aggressive form of meningioma, was shown to be associated with the existence of chromosome 5 polysomy, even when several other polysomies on chromosomes 20, 6, 12, and 13 were present (Abedalthagafi *et al.*, 2014). Higher grade meningiomas are extremely varied, as indicated by the detection of locus heterogeneity in different tumours from the same patient (Bi *et al.*, 2017).

### **1.7 *NF2* mutation in meningioma**

The most common genetic aetiology of meningioma is the absence of chromosome 22q and mutations at chromosome 22q12 causing inactivation of the *NF2* gene leading to loss of the tumour suppressor protein merlin (Trofatter *et al.*, 1993; Rouleau *et al.*, 1993). *NF2* mutations are reported in 40-60% of sporadic meningioma and are followed by loss of heterozygosity (LOH) (Riemenschneider *et al.*, 2006). Additionally, germline *NF2* mutations lead to the genetically inherited, autosomal dominant tumour predisposition syndrome, Neurofibromatosis type 2 (NF2), which can include the presence of multiple tumours, including bilateral vestibular schwannomas, meningioma, and ependymomas (Petrilli and Fernández-Valle, 2016; Evans *et al.*, 2017).

*NF2* splice site, nonsense, and missense mutations are observed, producing truncated and non-functional merlin (Fig-2) (Goutagny *et al.*, 2010). Nonsense or *NF2* deletion mutations are primarily associated with grade II, III meningioma, and a frameshift mutation in grade I (Perry *et al.*, 1999; Brastianos *et al.*, 2013; Goutagny *et al.*, 2010). *NF2* mutations are very common in convexities, the posterior skull base and spine meningiomas (Brastianos *et al.*, 2013; Clark *et al.*, 2016).

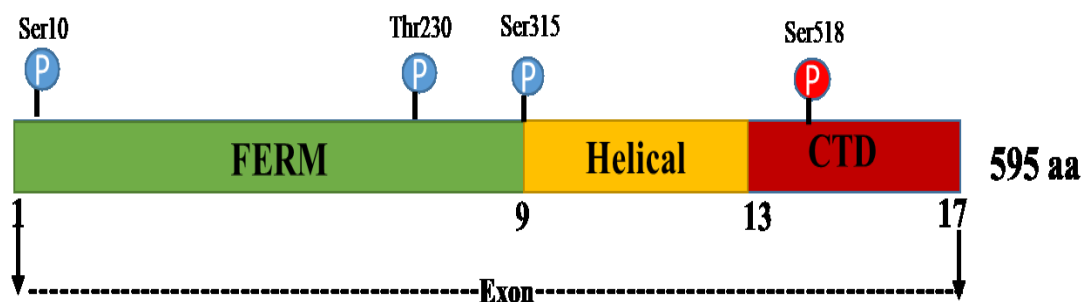


### Merlin structure and function:

The *NF2* gene encodes for merlin (moesin ezrin radixin like protein), which is a member of the 4.1 ezrin, radixin, and moesin (ERM) family exhibiting sequence homology with other family members. Merlin structure comprises an N-terminal FERM domain, a central helical domain and a C-terminal domain (CTD) (Fig-2) (Trofatter *et al.*, 1993). Phosphorylation at serine 518 of the CTD leads to the inhibition of merlin's tumour suppressor activity (Fig-2) (Sher *et al.*, 2012).

NF2 is a membrane-cytoskeleton scaffolding protein, forming a bridge between the plasma membrane and cytoskeleton, inhibiting contact-dependent cell proliferation by regulating several signalling pathways, including Hippo, PI3K/mTORC1/Akt, and receptor-dependent mitogenic signalling pathways, patched and Notch pathway (Curto *et al.*, 2007; Maitra *et al.*, 2006; Zhou and Hanemann, 2012; Petrilli and Fernández-Valle, 2016). Moreover, loss of the *NF2* gene results in the overexpression of Focal Adhesion Kinase (FAK) leading to increased cell migration and invasion (Shah *et al.*, 2014).

A



B

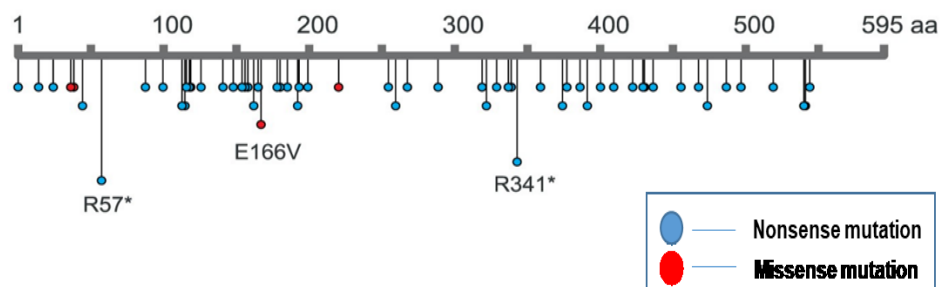


**Figure 2: Structure and frequency of *NF2* mutations in meningioma.** A) Domain organisation of *NF2* gene. Merlin is comprised of three domains: N-terminal FERM (the 4.1 ezrin, radixin, and moesin) domain (green) containing exon 1-9, central helical domain (yellow) containing exon 10-13, and C-terminal domain (red) containing 14-17 exon (Trofatter

*et al.*, 1993). Phosphorylation of serine 518 at CTD resulting the inhibition of Merlin's tumour suppressor activity (Sher *et al.*, 2012). B) Frequency of genetic alterations in the *NF2* gene where it showed nonsense (blue) and missense (red) mutations. Figure modified from Sato and Sekido, (2018).

## 1.8 Non-*NF2* mutations in meningioma

Mutations of the TERT promoter region, which encodes Telomere Reverses Transcriptase are observed in various cancers including glioma, bladder cancer, melanoma, and are found in 6% of meningioma (Vinagre *et al.*, 2013; Eckel-Passow *et al.*, 2015; Sahm *et al.*, 2015). Mutations in the TERT promoter region generate an extra transcriptional binding site, resulting in TERT overexpression and maintaining the tumour cell telomere length (Sahm *et al.*, 2015). TERT C228T and C250T variants are commonly found in grade I meningioma, showing high rates of recurrence and possible progression into higher-grade meningioma (Sahm *et al.*, 2015). Later TERT is also frequently found in high-grade meningioma (Mirian *et al.*, 2020). Around 80% of TERT mutations co-occur with an *NF2* mutation (Sahm *et al.*, 2015).

Rare somatic mutations in Subunit of Chromatin Remodelling Complex (*SMARCB1*) can coexist with *NF2* mutations, and *SMARCE1* mutations are specific to clear cell meningiomas (Yuzawa *et al.*, 2016). However, other driver gene mutations are associated with non-*NF2* meningiomas: Clark *et al.*, (2013) identified mutations of TNF receptor-associated factor 7(*TRAF7*), V-akt murine thymoma viral oncogene homolog 1 (*AKT1*), kruppel like factor 4 (*KLF4*) and smoothed, frizzle family receptor (*SMO*) in non-*NF2* meningioma by next-generation sequencing (summarised in Fig-3). *TRAF7*, *AKT1*, *KLF4*, *PIK3CA*, and *SMO* mutations are found in 28, 14, 12, 7 and 5% of meningiomas respectively (Bi *et al.*, 2016).

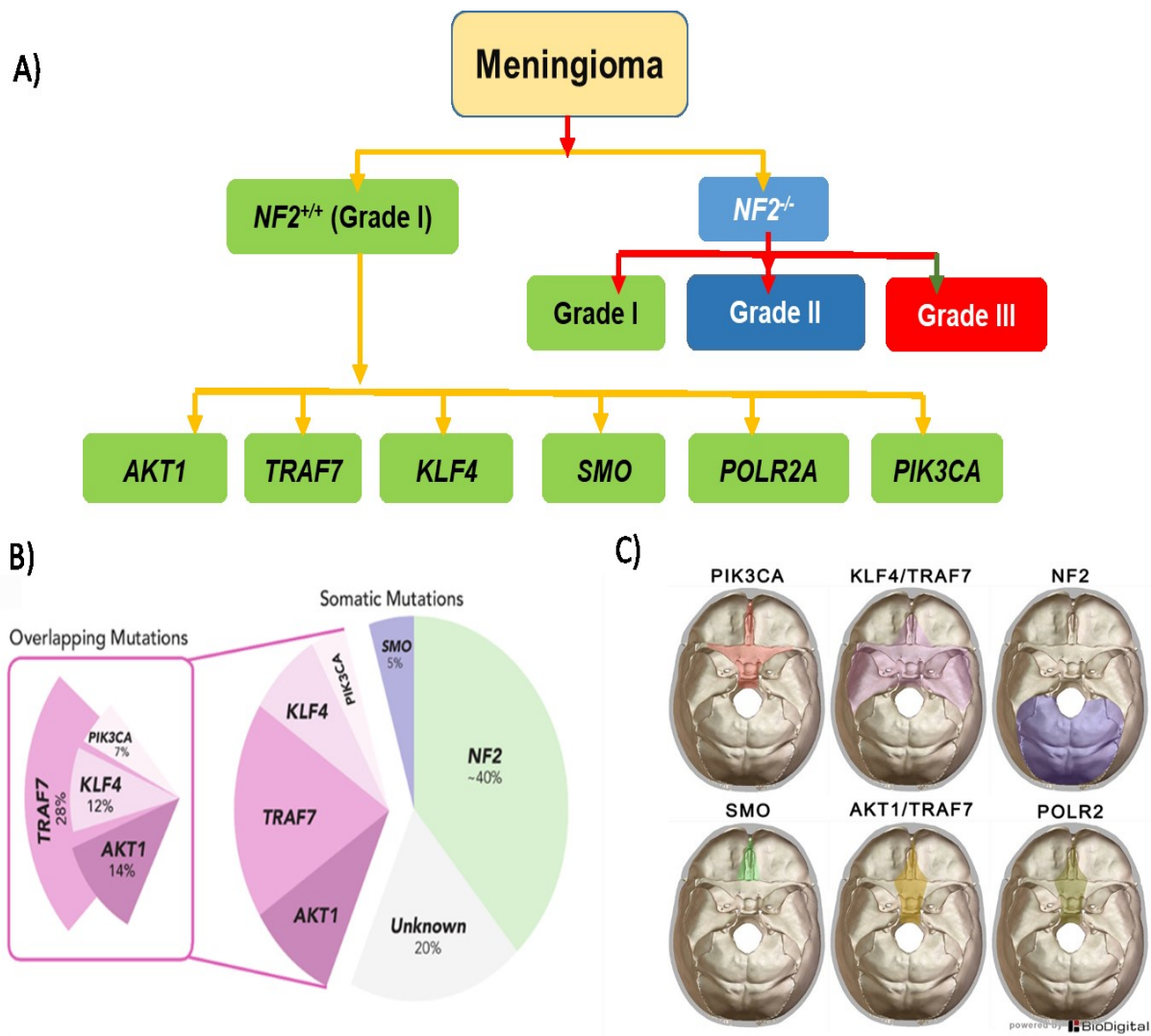


**Figure 3: Schematic representation of the mutational landscape of meningiomas. A)** *NF2* mutations are found in grade I, II and III meningiomas. Non-*NF2* mutations (*TRAF7*, *AKT1*, *KLF4*, *PIK3CA*, *SMO*, *POLR2A*) are mostly seen in the grade I meningioma. **B)** Percentage of occurrence of Non-*NF2* mutations and overlapping mutations. **C)** Occurrence of Non-*NF2* mutations are very specific to their location. Figure modified from (Bi *et al.*, 2016; Clark *et al.*, 2013; Clark *et al.*, 2016).

### *TRAF7* mutations:

*TRAF7* mutations are identified most commonly in grade I meningioma (Clark *et al.*, 2013). *TRAF7* is a member of the tumour necrosis factor associated receptor (TNF-R) superfamily, comprised of four domains; a ring finger domain, TRAF-zinc finger domain, coiled coil domain and WD40 repeats (Zotti *et al.*, 2012) (Fig-4). The *TRAF7* ring finger domain is involved in E3 ubiquitin ligase activity and targets C-FLIP (an anti-apoptotic protein) and initiates lysosomal degradation by inhibiting caspases activation in tumour cells (Tsuchiya *et al.*, 2015). In addition to this, *TRAF7* negatively regulates nuclear factor kappa B (NF- $\kappa$ B) activity by

promoting ubiquitination and lysosomal degradation of NEMO, an adaptor molecule very important for activating the NF- $\kappa$ B canonical pathway (Zotti *et al.*, 2011). *TRAF7* mutations are most frequent at WD40 repeats and at the coiled coil domain, regions through which TRAF7 maintains interactions with other proteins including mitogen activated protein kinase kinase kinase 3 (MEKK3), leading to the activation of Jun N-terminal Kinase (JNK) and p38 mitogen activated protein kinase (MAPK) pathways (Xu *et al.*, 2004) (Fig-4). Surprisingly, *TRAF7* mutations are exclusive of *NF2* mutations and usually co-exist with *AKT1*, *KLF4* or *PIK3CA* mutations (see below) (Clark *et al.*, 2013).

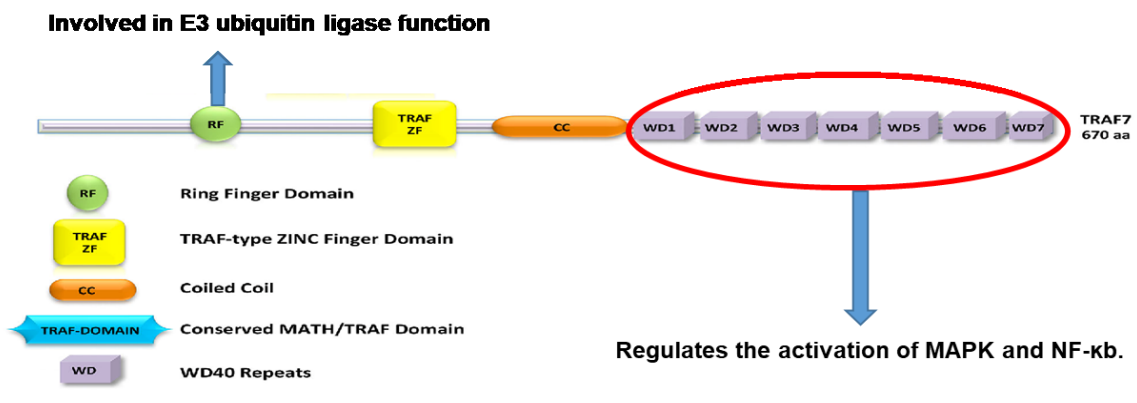


**Figure 4: Schematic of TRAF7 structure.** *TRAF7* mutations in the ring finger domain (green circle, involved in E3 ubiquitin ligase activity) and within the WD-40 repeat region (red circle) are the most frequent and affect TRAF7 interaction with proteins including MEKK3, subsequently activating JNK and p38 MAP kinase pathways. Figure modified from Zotti *et al.*, (2012).

#### *AKT1* mutations:

*AKT1* mutations are known to be oncogenic in breast, colorectal and lung cancer (Vivanco *et al.*, 2002; Chen *et al.*, 2020). *AKT1* mutations in the PH (pleckstrin homology) domain increase levels of AKT1 phosphorylation and its localisation to the plasma membrane (Fig-5), followed by activation of the phosphatidylinositol-3-kinase and protein kinase B (PI3K/AKT) signalling pathway, which inhibits apoptosis and increases cellular proliferation (Carpten *et al.*, 2007). *AKT1*<sup>E17K</sup> mutations are common in grade I meningioma but rare in grade II and III. *AKT1*<sup>E17K</sup> and *TRAF7* mutations have been found to co-occur in meningiothelial and transitional meningioma subtypes and are predominantly located in the anterior cranial base (Clark *et al.*, 2013; Clark *et al.*, 2016). AKT1 mutations are mutually exclusive of the *KLF4*<sup>K409Q</sup> mutation (see below) (Clark *et al.*, 2013).

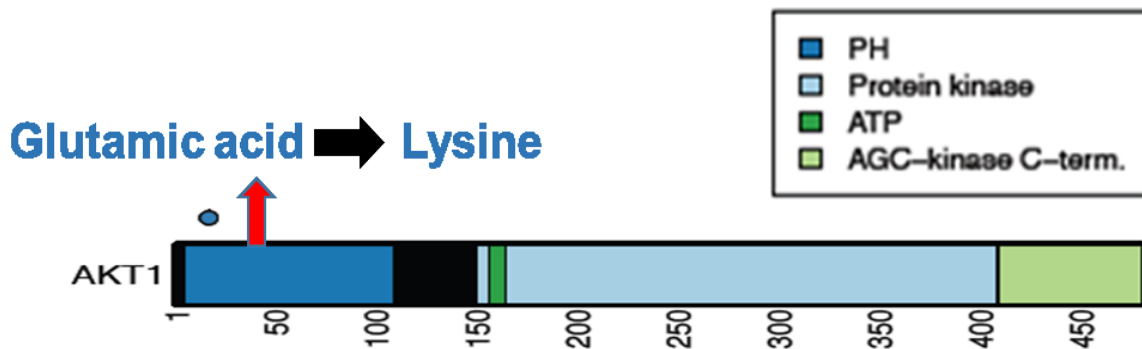


**Figure 5:** Point mutation of  $AKT1^{E17K}$  in the PH (pleckstrin homology) domain. Point mutations at nucleotide 49 results in a lysine substitution for glutamic acid at amino acid 17 ( $AKT1^{E17K}$ ) in the PH (Pleckstrin homology) domain (dark blue) of protein, disrupting the lipid binding pocket 9. Figure modified from Carpten *et al.*, (2007).

#### *KLF4* mutations:

*KLF4* is a transcription regulator, comprised of three Cys2-His2 zinc-finger motifs in the C-terminal region involved in DNA binding (Fig-6) (McConnell *et al.*, 2010). A recurrent  $KLF4^{K409Q}$  mutation in the first zinc finger domain results in changes in the DNA binding motifs and regulates reprogramming of somatic cells back into pluripotent stem cells, suggesting involvement of *KLF4* in stem cell maintenance (Schuetz *et al.*, 2011; Takahashi and Yamanaka, 2006). Furthermore, *KLF4* acts as a transcriptional repressor of mesenchymal genes thereby preventing epithelial mesenchymal transition and metastasis (Tiwari *et al.*, 2013).  $KLF4^{K409Q}$  and *TRAF7* mutations have been found to consistently co-occur in secretory meningiomas located in the medial or lateral skull base (Clark *et al.*, 2013; Yuzawa *et al.*, 2016).



**Figure 6:** Illustrating point mutation of  $KLF4^{K409Q}$  in the zinc finger domain. *KLF4* comprised of three Cys2-His2 zinc-finger motifs (red) in the C-terminal region involved in DNA binding (McConnell *et al.*, 2010). A recurrent mutational hotspot ( $KLF4$  p.Lys409Gln)

is identified in the first zinc finger domain (red arrow). Figure modified from Ghaleb and Yang, (2017).

#### *PIK3CA* mutations:

Phosphatidylinositol-4, 5-bisphosphate 3-kinase catalytic subunit alpha (*PIK3CA*) mutations co-occur with *TRAF7* mutations (Yuzawa *et al.*, 2016; Abedalthagafi *et al.*, 2016). *PIK3CA* is a known oncogene, mutations in *PIK3CA* result in the constitutive phosphorylation and activation of *AKT1* (Karakas *et al.*, 2006). *PIK3CA* mutations activate PI3K/AKT/mTOR signalling pathways in a similar way to *AKT1* mutants increasing cell proliferation and cell growth (Kang *et al.*, 2005; Apra *et al.*, 2018). *PIK3CA* mutations are mutually exclusive of *NF2*, *SMO* and *AKT1* but in some cases co-occur with *TRAF7* or *KLF4* mutations (Abedalthagafi *et al.*, 2016).

#### *SMO* mutations:

*SMO* mutations occur independently and are predominantly found in WHO grade I tumours (Clark *et al.*, 2013). *SMO* mutations dysregulate the activation of the Hedgehog (Hh) signalling pathway, which plays a role in both cell proliferation and differentiation, resulting in tumorigenesis (Briscoe and Thérond, 2013). There are two common variants of *SMO* mutations including L412F and W535L. The incidence of *SMO L412F* is high and commonly occurs in olfactory groove meningioma (Brastianos *et al.*, 2013; Clark *et al.*, 2013).

#### *POLR2A* mutations:

It is also reported that recurrent somatic *POLR2A* (polymerase RNA II DNA directed polypeptide) mutations occur in benign meningioma, causing dysfunctional transcription of protein coding genes including *WNT6* and *ZIC1/ZIC4* and tumours located in the tuberculum sellae (Clark *et al.*, 2016).

#### *BAP1* mutations:

Inactivating germline and somatic mutations in the tumour suppressor breast cancer (BRCA)–associated protein 1 (*BAP1*) gene were detected in high grade rhabdoid meningiomas (Abdel-Rahman *et al.*, 2011; Wadt *et al.*, 2012; Shankar *et al.*, 2017). Meningioma patients with germline *BAP1* mutations are prone to a variety of other tumours, including melanoma, mesothelioma, and other cancers. Focal deletion, nonsense mutations, frameshift mutations, and intrachromosomal fusion may cause inactivation of *BAP1* (Cheung and Testa, 2017;

Suppiah *et al.*, 2019). In addition to this, loss of chromosome 3p which encodes *BAP1* causes complete inactivation of *BAP1* tumour suppressor activity (Cheung and Testa, 2017). Interestingly, *BAP1* mutated mesothelioma tumour cells have been shown to be responsive to enhancer of zeste homolog 2 inhibitors, implying that pharmacologic inhibition of *BAP1*-mutant meningiomas is a possibility in the treatment of these tumours (Cheung and Testa, 2017).

## **1.9 Current therapies**

### **1.9.1 Surgery**

Surgical excision is the gold standard for meningioma treatment and, following gross total resection (GTR) between 38-80% of meningioma can be cured (Aghi *et al.*, 2009). Tumours can be surrounded by vital nerves and vasculature, which can hamper complete resection, as a result, these tumours tend to grow progressively or recur, thereby, creating therapeutic challenges in the clinical management of meningioma (Jenkinson *et al.*, 2016). WHO grade I meningiomas are benign in nature but may encroach on dural sinuses, skull, and intracranial regions (such as orbit, inaccessible soft tissue, and skin) making them more difficult to remove with surgery (Louis *et al.*, 2016).

The Simpson grade has long been used to determine the degree of resection, and both postoperative imaging and the neurosurgeon's evaluation are used to characterize the outcome (Simpson, 1957). Simpson grade V refers to a biopsy, grade IV to a subtotal resection, grade III to a macroscopic resection without dural excision or coagulation, grade II to a gross total resection with dural coagulation, and grade I to a complete resection that includes dural and surrounding bone resection (Simpson, 1957). While recurrence rates after complete resection are minimal in grade I meningiomas, they climb dramatically as the pathologic grade rises. Recurrence rates following gross total resection (GTR) after five years are reported to be 7–23% in grade I meningiomas, 50–55 % in grade II, and 72–78% in grade III (Rogers *et al.*, 2015; Ostrom *et al.*, 2016). On GTR (Simpson grade I to III), patients with tumours that originate on the convexity recovered more than parasagittal, parafalcine, or skull base meningioma patients. Hence, for WHO grade I skull base meningioma that have been entirely excised, routine surveillance imaging is recommended (Rogers *et al.*, 2015; Sun *et al.*, 2015). Adjuvant treatment is used for WHO grade I meningiomas that are incompletely removed (Simpson grade IV or V), as well as tumours of higher pathological grade (grade II or III) to help avoid or at least slowdown recurrence (Buerki *et al.*, 2018).

### **1.9.2 Radiotherapy**

Radiation therapy (RT) is not as effective as surgery. However, RT is frequently recommended for patients whose tumours are surgically inaccessible in order to control local tumour growth (Buerki *et al.*, 2018). In addition, radiotherapy can be recommended for recurring meningioma or meningioma with an aggressive histological characteristic. It can be used as monotherapy or as an adjuvant in conjunction with surgery (Apra *et al.*, 2018). Radiation therapy for meningioma includes fractionated external beam radiation therapy (EBRT), stereotactic radiosurgery (SRS), and rarely brachytherapy (Apra *et al.*, 2018). SRS and SFRT radiation therapy are known to be effective for local control of meningioma due to their site-specific delivery and limited damage to the surrounding tissue (Alexiou *et al.*, 2010).

Adjuvant radiotherapy has shown minimal benefit to overall patient survival in benign meningioma and its use is controversial due to the known link between radiation exposure and meningioma formation (Mawrin *et al.*, 2015). Furthermore, radiotherapy may cause further off-target effects including alopecia, seizures, oedema, radio-necrosis, impaired vision, and radiation-induced meningioma (Fathi and Roelcke, 2013; Yamanaka *et al.*, 2017).

### **1.9.3 Systemic treatment for meningioma**

There is no chemotherapy for meningioma that is proven to be successful (Gupta *et al.*, 2018). Traditional chemotherapeutics such as temozolomide, irinotecan, doxorubicin, and ifosfamide have not proven effective in meningioma (Chamberlain and Barnholtz-Sloan, 2011; Apra *et al.*, 2018).

In a retrospective case study, 60 patients with recurrent WHO grade 1 meningioma were treated with hydroxyurea and it has been demonstrated to be clinically well-tolerated but a majority of the patients experienced tumour growth after therapy (Chamberlain and Johnston, 2011; Kim *et al.*, 2017).

A recent phase II trial of trabectedin for recurrent WHO grade 2 or 3 meningiomas was conducted (Preusser *et al.*, 2022). When tetrahydroisoquinoline alkaloid trabectedin binds to the minor groove of DNA's double helix, it creates trabectedin-DNA adducts, which have pleiotropic anti-tumor, immunomodulatory, and antiangiogenic activities (Preusser *et al.*, 2012). In vitro preclinical studies of WHO grade 2 and 3 meningiomas revealed trabectedin's



clinical efficacy and safety (Preusser *et al.*, 2012). The trial was subsequently terminated due to the frequent adverse events and lack of efficacy among patients treated with trabectedin, despite the full patient enrollment of 90 individuals and favourable preclinical results supporting the use of trabectedin. Patients with non-benign meningiomas who received trabectedin had worse PFS and OS and it was more toxic than standard systemic therapy (Preusser *et al.*, 2022).

The impact of hormonal dysregulation on the development and progression of meningioma resulted in several hormone-targeting drugs being tested. The anti-estrogen drug tamoxifen, which is widely used, did not show a significant beneficial outcome (Goodwin *et al.*, 1993; Gupta *et al.*, 2018). Small trials of the anti-progesterone drug mifepristone have shown mixed results and demonstrated that stratifying patients based on progesterone receptor expression in the context of a trial could help to explain the efficacy of using this drug as a treatment in meningioma patients (Grunberg *et al.*, 1991; Grunberg *et al.*, 2006; Gupta *et al.*, 2018).

Although chemotherapeutics are ineffective for the majority of meningiomas although several FDA-approved drugs, for example Vismodegib, Vistusertib, Apelisisib and Trametinib etc. are currently in clinical trials (Mawrin *et al.*, 2015; Johnson *et al.*, 2008).

#### **1.9.4 Targeted molecular therapies**

Molecular therapeutic targets of meningioma have been explored, although to date, none have demonstrated significant therapeutic efficacy so far in controlled trials (Fig-7). Molecules such as, sunitinib, vatalanin, and bevacizumab were used to target endothelial growth factor receptor (EGFR) and platelet-derived growth factor receptor (PDGFR) in patients with recurrent grade II and III meningioma (Kaley *et al.*, 2014; Nunes *et al.*, 2013). Sunitinib showed favourable results in a prospective phase II trial and the use of bevacizumab showed prolonged progression-free survival in retrospective studies, although further validation is required (Andrae *et al.*, 2012). Nunes *et al.*, (2013) showed that bevacizumab has no effect on meningiomas with *NF2* mutation. Vismodegib and FAK inhibitor GSK2256098 are in phase II clinical trial (NCT02523014) for patients with progressive meningioma or those with *SMO* and *AKT1* mutations (<https://ClinicalTrials.gov/show/NCT02523014> (2015); Strickland *et al.*, 2017). A recent study demonstrated a favourable outcome for an AKT inhibitor (AZD5363) in a patient with multiple, recurring intracranial meningiomas who showed a sustained significant clinical and radiological response to the AZD5363 after one year of treatment (Weller *et al.*, 2017). However, our group treated *AKT1*<sup>E17K</sup> mutated grade I primary meningioma cells with

AZD5363 and showed a reduction in meningioma cell viability after AKT inhibition, albeit the results were inconsistent and the IC<sub>50</sub> values were high (Dunn *et al.*, 2019). These data suggest that inhibition of AKT with AZD5363 alone is not sufficient as a targeted therapy in meningioma (data not published). In addition AKT activation seem to be less in higher grade meningioma (Dunn *et al.*, 2019).

Another molecular targeted therapy the dual mammalian target of rapamycin complex 1 and 2 (mTORC/2) inhibitor Vistusertib (AZD2014) is currently in clinical trials for Neurofibromatosis type 2 patients with progressive or symptomatic meningioma (<https://ClinicalTrials.gov/show/NCT03071874> (2015); Beauchamp *et al.*, 2015).

The PI3K and AKT signaling pathways upstream of mTOR and have been identified as prevalent and possibly targetable mutations, as previously discussed. A forthcoming trial will look at the effects of Alpelisib (a PI3K inhibitor), in conjunction with Trametinib, a MEK inhibitor (NCT03631953). Blocking PI3K signaling alone without inhibiting mTOR, may not cause apoptosis. On the other hand, MEK inhibition in combination with PI3K inhibition caused cell death in meningioma primary cells. As a result, this combined therapy may be advantageous (Al-Rashed *et al.*, 2020).

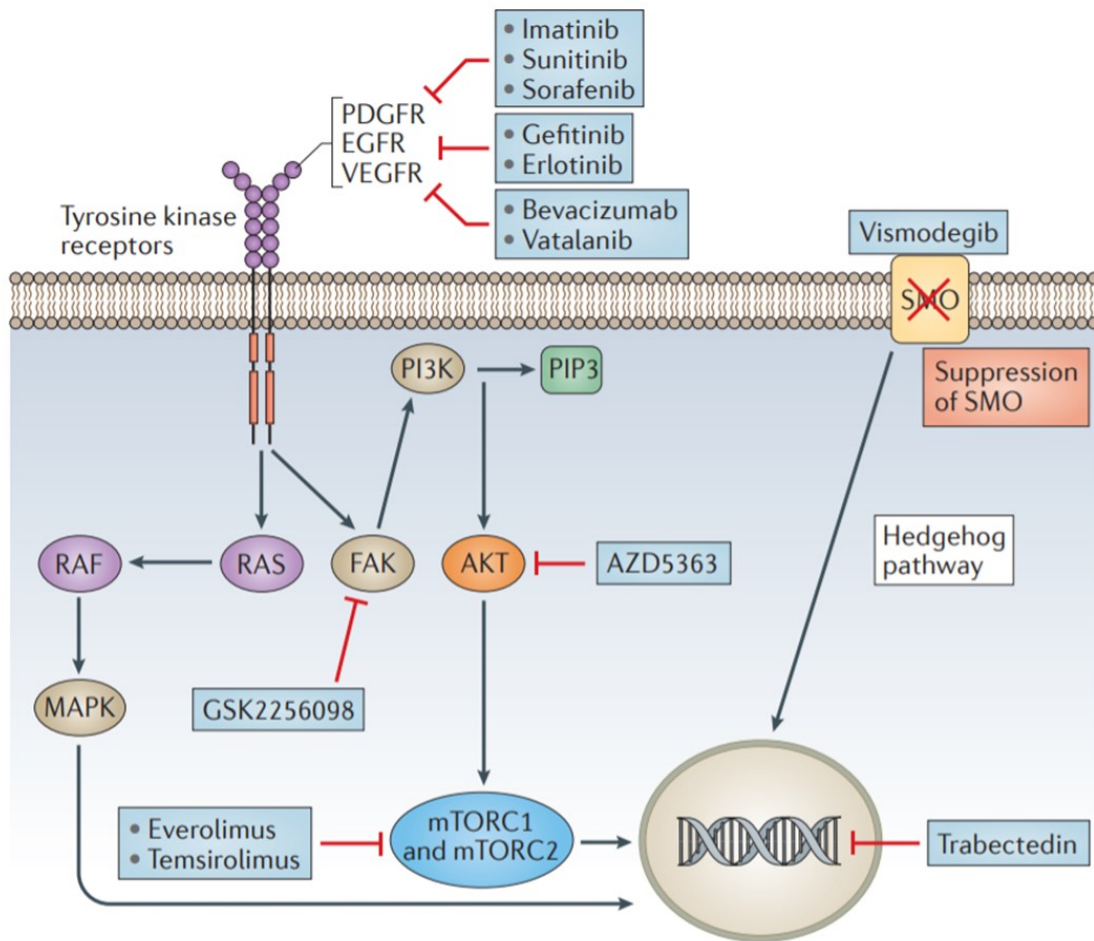


**Figure 7: Illustrating overview of molecular signalling pathways and drug targets in meningioma.** The MAPK (mitogen-activated protein kinase), the phosphoinositide 3kinase (PI3K)–AKT–mammalian target of rapamycin complex (mTORC) system, and the Hedgehog pathway are only a few of the cellular processes that have been linked to meningioma growth. The current medical therapy options for meningioma are summarised in this diagram, which target a number of molecular targets. Some of the available drugs are used because of their effects on molecular targets that could be used as biomarkers in the selection of patients. Figure taken from (Preusser *et al.*, 2018).

### 1.9.5 Immune therapy

Tumour-induced immunosuppression involves the overexpression of immunosuppressive molecules or their receptors, such as programmed death-ligand 1/programmed death-1 (PD-L1/PD-1), an immunological checkpoint that can prevent the activation of effector T cells, resulting in tumour immune escape (Chen *et al.*, 2019). Hence, previously, inhibiting immunological checkpoints has become a promising immunotherapy strategy for reversing immune suppression and restoring immune system function. PD-L1/PD-1 antagonists are the most common immune checkpoint blockers that have been approved by the FDA and are now in clinical development (Jiang *et al.*, 2019).

In meningioma, Du *et al.*, (2015) found significant overexpression of PD-L1 protein in anaplastic meningioma compared to benign meningioma. The positive correlation between PD-L1 expression and grade was confirmed by their investigation of PD-L1 mRNA expression. This research suggests that high-grade meningioma tumours have an immunosuppressive tumour microenvironment, and PD-L1 levels may contribute to the aggressive tumour behaviour. Wang *et al.*, (2018) showed that PD-L1 expression was linked with *NF1* and *NF2* gene mutations in various tumour types, such as meningioma, schwannoma, and neurofibroma, and confirmed PD-L1 expression in 40% of *NF2*-mutated meningiomas via immunohistochemistry. Another study showed higher PD-L1 immunoreactivity in *TRAF7*-mutated tumours compared to non-*TRAF7* mutated tumours in skull-based meningiomas (Hao *et al.*, 2019). These results support the hypothesis that somatic genetic changes in meningioma can affect checkpoint protein expression and should be taken into account in future immunotherapy patient stratification (Karimi *et al.*, 2021).

However, inhibitory PD-1 antibody-based treatments, are still being tested including, pembrolizumab (NCT03016091, NCT03279692), nivolumab alone (NCT02648997), a combination of ipilimumab (CTLA4 inhibitor NCT03604978) and avelumab (Karimi *et al.*, 2021). Dunn *et al.*, (2018) reported that nivolumab (anti-PD-1 antibody) had a considerable therapeutic efficacy in a recurrent, atypical meningioma patient from the early stages of phase II clinical trial (NCT 02648997). Avelumab (anti-PD-L1 antibody) was shown to produce antibody-dependent cellular cytotoxicity in meningioma and natural killer (NK) cell lines *in vitro* (Giles *et al.*, 2019). Anti-PD-L1 monoclonal antibodies have two potential negative effects on tumour growth; direct suppression of the PD-1/PD-L1 pathway and activation of natural killer cells (Dong *et al.*, 2019). However, previous research has revealed that a PD-1/PD-L1 antagonist has a poor therapeutic effect against solid tumours such as PDL1-positive metastatic melanoma, lung cancer, and colorectal cancer (Jiang *et al.*, 2019).

Collectively, these studies suggest that although several molecules have made it to clinical trial none have proven efficacious so far and there is still an urgent requirement to identify new molecular targets for pharmacological intervention or to act as biomarkers for meningioma progression.

## 1.10 Overview of omics research in meningioma

The word ‘omics’ originated from the Greek word ‘body’ and is used in molecular biology to designate a body of knowledge on a subset of biological molecular classes (Epstein and Lin, 2017). The study of genes (genomics), mRNA (transcriptomics), proteins (proteomics), lipids (lipidomics), and metabolites (metabolomics) in specific biological samples is referred to as ‘omics’ (Horgan and Kenny, 2011). Unbiased high-resolution and high-throughput technologies have given researchers an unprecedented picture of cancer omics to date (Vucic *et al.*, 2012). An omics study generates a large number of high-resolution datasets at several levels and scales in order to expose the complexity of cells and their surroundings. This type of research can lead to new frameworks for deciphering biological events or methods for testing ideas utilizing a variety of datasets (Heo *et al.*, 2021). The omics-based research has led to the discovery of biologically essential genes and pathways that are frequently dysregulated across a wide range of cancer types, improving our understanding of cancer as a disease and revealing clinically useful diagnostic, prognostic, and druggable targets (Vucic *et al.*, 2012). In addition to this, omics research will continue to aid in the development of more accurate risk factor classification, biomarker identification, detection of new therapeutic targets and development of effective treatment strategies to defeat drug resistance, and the introduction of advanced targeted immunotherapies for diagnosis and treatment of the cancer patients (Guang *et al.*, 2018).

Current breakthroughs in omics technologies (genomics, transcriptomics, epigenomics, and proteomics) have made it possible to screen a large number of biomarkers for meningiomas using tissue samples to determine their biological functions (Di Chen *et al.*, 2020). Combining multi-omics and clinical data to develop highly accurate prediction models for meningioma progression is a promising methodology for developing accurate prediction models, implying the possibility of early and accurate diagnosis, effective therapeutic strategies and a favourable prognosis for meningioma patients (Ramroach *et al.*, 2020; Liu *et al.*, 2020; Nassiri *et al.*, 2021; Maas *et al.*, 2021). The application of omics-based approaches in meningioma and their major significant findings will be reviewed in the following sections.

### 1.10.1 Genomics

With the advancement in sequencing technology, genomic studies played an essential role in the understanding of meningioma pathogenesis, providing further information on meningioma classification and diagnosis (Liu *et al.*, 2020). The genetic landscape of meningioma is well characterized and has already been discussed previously in section 1.7 and 1.8. Several more genomic studies will be reviewed that identified genomics signature of meningioma contributed to the meningioma pathogenesis, risk factor, and diagnosis.

A genomic signature *MLLT10* (encoding myeloid/lymphoid or mixed-lineage leukaemia translocated to 10) was detected to be a novel susceptibility locus for meningioma by Dobbins *et al.*, (2011), who conducted a genome-wide association study (GWAS) in 859 meningioma patients with a large number in the control group (n=704). Loss of heterozygosity for markers at chromosome 10p including *MLLT10* has been observed in approximately 30% of incidences (Mihaila *et al.*, 2003). *MLLT10* is a key promoter of Wnt-dependent transcription resulting in activation the of Wnt pathway (Mahmoudi *et al.*, 2010). The stimulation of the Wnt pathway has been linked to the development of anaplastic meningioma (Mawrin and Perry, 2010).

Hosking *et al.*, (2011) used high-density single-nucleotide polymorphism (SNP) arrays in 66 blood samples from radiation-induced meningioma patients and mapped variations in a number of genes, including *PIAS2* (*Protein Inhibitor Of Activated STAT 2*), *KATNAL2* (*Katanin Catalytic Subunit A1 Like 2*), *TCEB3CL* (*Transcription Elongation Factor B Polypeptide 3C-Like*), *TCEB3C* (*Transcription elongation factor B polypeptide 3C*), and *TCEB3B* (*Transcription elongation factor B polypeptide 3B*) to the 18q21.1 locus, which has been suggested as a risk factor for radiation-induced meningioma.

Another recent study identified a susceptible risk locus at 11p15.5 for meningioma via genome-wide association analysis and detected a number of genes localized to this region including *resistance to inhibitors of cholinesterase-8A* (*Ric-8A*) (Claus *et al.*, 2018). Ric8a plays an important role required in the development of the mammalian central nervous system, as it keeps the pial basement membrane intact and regulates cell division (Kask *et al.*, 2015). Ric8a knockout mice have been shown to have problems in meningeal layer development (Kask *et al.*, 2015). Hence, Claus *et al.*, (2018) suggested mutation in *Ric-8A* could be a risk factor for cranial neural crest-derived meningioma development although further investigations are required to confirm.

Aside from the probable relevance of genetic factors in meningioma, genomics has been used to diagnose and classify the disease (Liu *et al.*, 2020). Zhang *et al.*, (2014) performed whole-

exome sequencing in five malignant meningioma samples and identified mutational signature genes including *NF2* (*Neurofibromatosis type 2*), *MNI* (*a proto-oncogene and a transcription regulator*), *ARID1B* (*AT-Rich Interaction Domain 1B*), *SEMA4D* (*Semaphorin 4D*), and *MUC2* (*Mucin 2*) that have a role in the development of malignant meningioma. However, there are certain drawbacks to the study, such as the small number of samples and the fact that it only included the sequencing of malignant meningioma. Furthermore, AlSahlawi *et al.*, (2019) were the first to detect two novel missense mutations in *FGFR3* (fibroblast growth receptor-3): T932C and G1376C via NGS analysis in 71 meningioma samples. *FGFR3* mutations were found in benign meningioma and the study reported it as a marker for non-NF2 skull base meningioma with a good prognosis. Data from increased number of meningioma samples should be used to investigate this assertion further.

### 1.10.2 Epigenomics

Meningioma pathogenesis is influenced by epigenetic factors such as DNA methylation and histone modification (Drakos *et al.*, 2010). Methylation of DNA is an epigenetic process in which a methyl group is transferred to the C5 position of cytosine to generate 5-methylcytosine. A family of DNA methyltransferases (Dnmts) catalyzes DNA methylation and the majority of DNA methylation occurs at CpG sites (Bird, 1980; Moore *et al.*, 2013). Both hypomethylation and hypermethylation of DNA have been linked to meningioma progression (Gao *et al.*, 2013). *Tissue inhibitors of metalloproteinase 3* (*TIMP3*), *cyclin-dependent kinase inhibitor 2A* (*CDKN2A*), and *tumor protein 73* (*TP73*) are among the genes that have been found to be hypermethylated in at least 10% of meningioma tumours (Bello *et al.*, 2004). *TIMP3* hypermethylation suppresses its tumour suppressor activities by downregulating transcription (He *et al.*, 2013). *TIMP3* hypermethylation is common in grade III meningiomas and hypermethylation is correlated with reduced time of recurrence in meningioma (Bello *et al.*, 2004; Barski *et al.*, 2010). *TIMP3* is also present on chromosome 22q12, and nearly all cases of *TIMP3* hypermethylation had a 22q allelic deletion as well (Barski *et al.*, 2010). Another study found that aberrant *TP73* methylation is significant in higher grade meningioma but not in grade I implying that hypermethylation of *TP73* is a biomarker for high-grade meningioma (Nakane *et al.*, 2007). Furthermore, a study demonstrated that hypermethylation of *WNK2* is linked to loss of gene expression which is found to be higher in grade II and III meningioma. Loss of *WNK2*, a negative regulator of cell proliferation, is likely linked to more aggressive tumour growth (Bernhart *et al.*, 2014).

In 497 meningiomas and 309 extra-axial skull tumours, Sahm *et al.*, (2017) performed DNA methylation profiling to generate a genome-wide mapping of differentially methylated locations, this DNA methylation data can clearly differentiate all meningiomas from other skull base tumours across grades. In addition to this, DNA methylation profiling identified six clinically important methylation classes that were linked to common tumour locations, mutations, cytogenetic, and gene expression patterns (Sahm *et al.*, 2017). DNA methylation profiling identified two primary epigenetic patterns, groups A and B, which are further split into four and two methylation classes (MC) respectively (Fig-8). Three benign MCs, ben-1, ben-2, and ben-3, plus one intermediate MC, int-A, comprised methylation group A. Int-B and one malignant MC, introduced as mal, comprised methylation group B (Sahm *et al.*, 2017). Most of the *NF2* mutated meningioma samples were found to be in group A, while the majority of *TERT* mutations are found to be in group B. In addition to this, non-*NF2* such as *AKT1*, *KLF4*, and *SMO* mutations are referred to as the MC ben-2 class (Fig-8). Interestingly, these categories have higher accuracy than the WHO grade alone in predicting the length of progression-free survival (PFS) (Sahm *et al.*, 2017).

However, recent breakthroughs in meningioma epigenomics have mostly focused on DNA methylation, ignoring the importance of histone modification and chromosome arrangement (Liu *et al.*, 2020). Recently, it has been reported changes in the trimethylation of lysine 27 (K27) of histone H3 (H3K27me3), a histone modification. Loss of H3K27 trimethylation is closely connected to an increased risk of recurrence in meningioma (Katz *et al.*, 2018; Nassiri *et al.*, 2021).



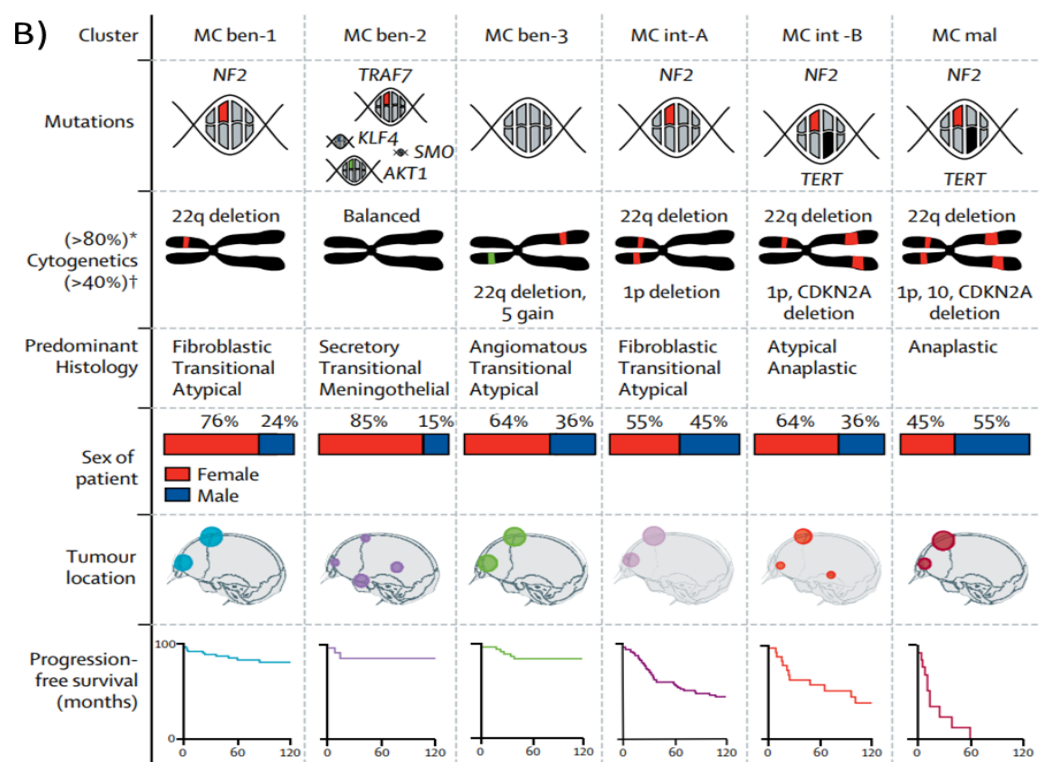
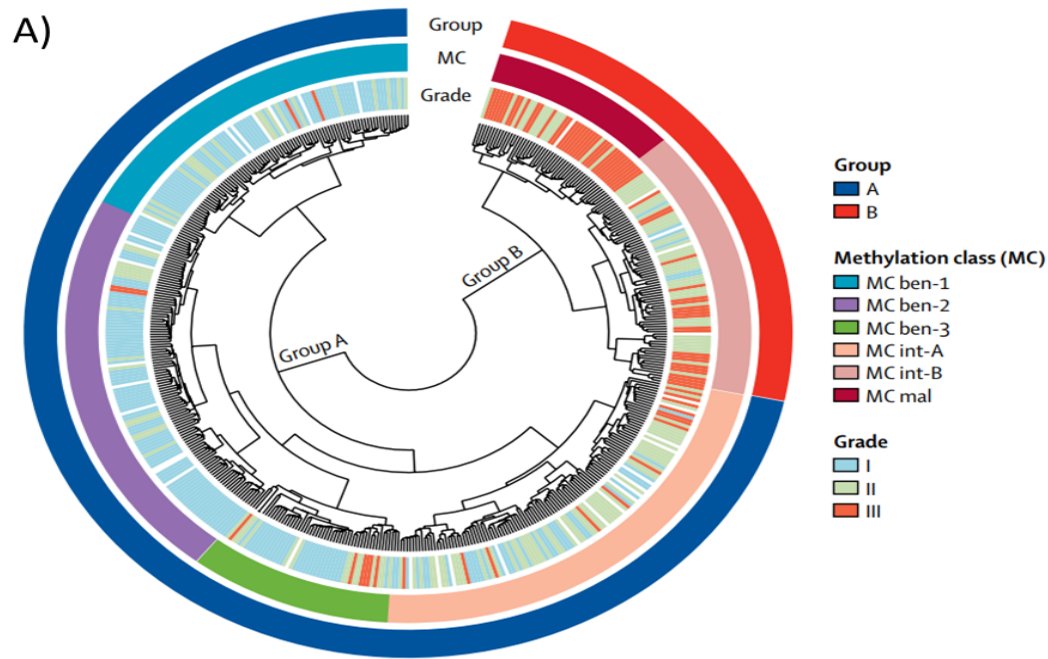


**Figure 8: Classification of meningioma based on DNA methylation** (Sahm *et al.*, 2017).  
 A) Unsupervised clustering of 497 meningioma samples based on DNA methylation profile.  
 B) Illustrating the six methylation classes identified, as well as their molecular and clinical properties (Sahm *et al.*, 2017).

### 1.10.3 Transcriptomics

Epigenetic changes, such as DNA methylation, have established subgroups of meningiomas with significant clinical implications. It stands to reason to see if these signatures can be translated in gene expression profiling (Suppiah *et al.*, 2019). Transcriptomic analysis can detect potential markers, which can be helpful in distinguishing benign meningiomas from those with a higher risk of progression or recurrence (Liu *et al.*, 2020).

Chen *et al.*, (2015) looked at 119 meningioma samples using two types of microarray expression profiling datasets, they discovered a 37-gene prognostic signature for meningioma patients that can be used to predict meningioma progression and survival. A study analysing microRNA (miRNA) profiles of 50 meningioma patients demonstrated that significant overexpression of miRNA-21 as the histopathological grade increased, but a significant decrease in miRNA-107 expression was observed with the increasing histopathological grade, indicative of poor prognosis (Katar *et al.*, 2017). The expression of miRNA-137 and miRNA-29b did not differ significantly by histopathologic grade (Katar *et al.*, 2017). However, there was no control group in this investigation, and only one grade III sample was considered.

Dalan *et al.*, (2017) used whole transcriptome microarray analysis on 14 meningioma tissue samples and one human meningeal cell line to show that MiR-29c-3p and *pentraxin-3* (*PTX3*, a tumour suppressor gene) are negatively correlated in tissues and meningioma cells, demonstrating that miR-29c-3p can control *PTX3* expression. The study also showed that inhibition of miR-29c resulted in an increase in *PTX3* expression and apoptosis in primary meningioma cells and decreased cell viability (Dalan *et al.*, 2017).

A member of our group Negroni *et al.*, (2020) studied microRNA levels in different grades of meningioma tissue samples and reported expression of the miR-497~195 cluster in meningioma decreases with the meningioma grade increases. Decrease expression of miR-497~195 cluster linked to Cyclin D1 overexpression. By regulating the expression of the miR-497~195 cluster, GATA binding protein 4, a transcription factor elevated in high grade meningioma which stimulates cell survival, resulting in increased Cyclin D1 expression (Negroni *et al.*, 2020). GATA-4 suppression was observed with the small-molecule inhibitor NSC140905 which reinstated miR-497~195 cluster expression, followed by lower cell viability and downregulation of Cyclin D1. This study suggested GATA-4 could be a new promising therapeutic target whereas miR-497 could be a non-invasive biomarker for high-grade meningioma (Negroni *et al.*, 2020).

Viaene *et al.*, (2019) used RNA-seq data to identify the transcriptome signature of grade I, II, and III meningiomas and discovered that *GREMLIN-2* (a bone morphogenetic proteins

pathway regulator) and short nucleolar RNAs (snoRNAs) such as *SNORA46* and *SNORA48* are significantly reduced as the meningioma WHO grade progresses. The study also showed that WHO grade I meningiomas that do not undergo progression are molecularly distinct from those that do; they have more RNA fusion transcripts and a considerably larger immune infiltration than grade II or III meningioma (Viaene *et al.*, 2019).

Schmidt *et al.*, (2016) conducted transcriptomic analysis of 62 meningiomas, including an exceptionally high proportion of WHO grade III tumours (n=28), as well as 14 grade II and 20 grade I tumours with a poor clinical outcome. The study found that a total of 332 differentially expressed transcriptome signature genes were common in clinically more aggressive meningioma subgroups independent of WHO grade, including recurrent or malignantly progressing grade I and II, and all grade III tumours when compared to non-recurrent grade-I meningioma. out of 332, only 10 genes were validated across the WHO grades, while *PTTGI* (*securin*) and *LEPR* (*leptin receptor*), revealed a strong correlation with recurrence irrespective of meningioma WHO grade progression, suggesting their potential use as biomarkers to predict the aggressive behaviour of meningiomas in the future.

However, most gene expression analyses have a small sample size and there is little overlap in the candidate genes found between studies (Katar *et al.*, 2017; Dalan *et al.*, 2017; Viaene *et al.*, 2019). Therefore, more research is needed to evaluate possible gene expression biomarkers (Suppiah *et al.*, 2019).

#### **1.10.4 Proteomics**

A gene's transcription level only gives an initial idea of its expression level into a protein (Abbott, 1999). It is now widely accepted that mRNA does not always translate into protein. The gene from which mRNA is transcribed, as well as the cell's current physiological state, dictate the amount of protein generated from a given amount of mRNA (Anderson and Seilhamer, 1997). Furthermore, a large amount of mRNA produced may undergo degradation or be translated incompetently, yielding a minimal amount of protein (Kowalski and Mager, 1998). Moreover, many proteins undergo post-translational changes including phosphorylation, glycosylation, acetylation, methylation, and ubiquitination, all of which have a significant impact on their functions. Some proteins, for example, do not become active until they are phosphorylated (Kia-Ki and Martinage, 1992). In addition to this, many transcripts produce several proteins as a result of alternative splicing or post-translational modifications

(Newman, 1998). Furthermore, many proteins are associated with other proteins or RNA molecules to create complexes and they only work when these other proteins or molecules are present (Diviani and Scott, 2001). Therefore, proteomic research is necessary to fully understand the effect of gene expression changes (Graves and Haystead, 2002).

The term proteome was introduced by Wilkins *et al.*, to describe the total set of proteins generated by tissue or an organism, as well as the alterations made to them, across time and under different (biological physiological, or pathological) conditions (Wilkins *et al.*, 1996). The study of proteins present in many types of biological materials referred to as proteomics can be used to discover their activities and structures, such as the identification of interaction sites or post-translational modifications. Whilst the majority of the analyses are carried out on cells and/or tissues, bodily fluid also appear to have great potential to identify biomarkers or therapeutic targets (Anderson *et al.*, 1998; Tyers and Mann, 2003; Apweiler *et al.*, 2009).

In 1975, the first investigations that meet the term "proteomic" research were done by developing two-dimensional (2D) gel electrophoresis (Graves and Haystead, 2002). For high-throughput and rapid protein expression analysis, protein microarrays or chips have been established. However, protein microarray is not sensitive enough to investigate the function of a complete genome (Sutandy *et al.*, 2013). Mass spectrometry (MS), X-ray crystallography, and nuclear magnetic resonance (NMR) spectroscopy are some of the additional methods used to analyse proteins (Zhang *et al.*, 2010).

Whilst for peptide and protein analysis, mass spectrometry (MS) has become an indispensable instrument because of its speed, accuracy, and adaptability (Zhang *et al.*, 2010). MS used to determine peptide amino acid sequences and characterise a range of post-translational changes like phosphorylation and glycosylation (Zhang *et al.*, 2010). Mass spectrometry can also estimate absolute and relative protein concentrations, as well as identify and quantify hundreds of proteins from complicated samples, making it a particularly useful tool for systems biology research (Pandey and Mann, 2000).

Global tissue proteome analysis enables a deeper understanding of the mechanisms underpinning tumorigenesis; helping identify potential biomarkers that can differentiate among meningioma subtypes (Sharma *et al.*, 2015). However, proteomic analysis is still limited in the meningioma field with only a handful of studies establishing differential proteomic profiles between meningioma grades (Suppiah *et al.*, 2019).

Okamoto *et al.*, (2006) were the first to identify proteome profiles and proteins that distinguish WHO grade I, II, and III meningioma. They investigated 24 human meningioma selective tissue microdissections to acquire a pure population of meningioma cells and then subjected them to two-dimensional gel electrophoresis (2D-GE) and LC-MS/MS mass spectrometry. This study reported nine proteins that were differentiated between WHO grades II and III where 15 proteins were identified as significantly differentially expressed between benign and atypical meningioma. In benign meningioma, six of the 15 differentiating proteins were shown to be overexpressed including calponin-1, an activator of 90-kDa heat shock protein ATPase homologue 1, serine-threonine kinase receptor-associated protein, placental ribonuclease inhibitor, vitamin D-binding protein, and apolipoprotein A-I. Overexpression of calponin-1 in benign meningioma was confirmed via both western blot and immunohistochemistry techniques and suggested reduced expression of calponin-1 to be indicative of progression of a low-grade to a higher-grade meningioma. However, the study did not consider a normal control and validated only one protein by IHC.

Cui *et al.*, (2014) performed protein profile screening on 10 samples of grade I meningioma tissue using the same technique (2D-GE and LC-MS/MS mass spectrometry), where adjacent arachnoid tissue was used as a control. Only six of the 43 significantly differentially expressed proteins between grade I meningioma and arachnoid tissue were confirmed by western blotting. According to their findings, the expression of galectin-3, vimentin, and endoplasmic reticulum chaperone protein was dramatically reduced, and significant overexpression of 40S ribosomal protein S12, glutathione S-transferase, and hypoxia up-regulated protein 1 was observed in benign meningioma compared to arachnoid control tissue. The study implied that these six proteins could play a role in meningioma progression. However, there were limitations such as the possible contamination of control tissue (which was taken adjacent to the tumour) with tumour cells and the small sample size. Later, the role of galectin-3 in meningioma was further studied by another group who found that overexpression of galectin-3 was related to brain invasion, recurrence and higher grade meningioma (Ahmed *et al.*, 2017). However, the involvement of galectin-3 in meningioma is still debated, and more research is needed to determine the specific mechanism of galectin-3 overexpression in meningioma (Liu *et al.*, 2020).

Wibom *et al.*, (2009) investigated the differences in protein expression patterns between bone-invasive and non-invasive meningioma using a protein spectrum and surface-enhanced laser desorption/ionization time-of-flight mass spectrometry (SELDI). By examining the protein

spectra in benign meningiomas, the researchers were able to discern between invasive and noninvasive growth behaviour in both fibrous and meningothelial grade I meningiomas. They found that early diagnosis of invasive grade I meningioma using protein spectra analysis is possible and that this information will be useful in determining follow-up tactics and whether to utilize early or late radiation therapy. However, no proteins specific to the invasive and non-invasive characteristics of meningioma were discovered in this investigation.

Saydum *et al.*, (2010) conducted proteomic analysis between grade I meningioma cell line (SF4433) and primary arachnoid cells as control via Gel-nanoLC-MS/MS. They identified 281 proteins significantly expressed and validation concentrated only on the upregulated minichromosome maintenance (MCM) family of proteins by qRT-PCR, suggesting that they could be used as biomarkers to diagnose benign meningiomas.

Two studies (Sharma *et al.*, 2014; Sharma *et al.*, 2015) conducted i-TRAQ based (Isobaric tags for relative and absolute quantification) proteomics to identify 2367 proteins that were differentially expressed across WHO grade I, II, and III meningiomas in meningioma patient's serum and tissue samples. The majority of the proteins were found to be shared among the groups, and silico functional analysis revealed that several of them were linked to a variety of signalling pathways, including Integrin, Wnt, RAS, EGFR, and FGFR. This study also used ELISA (enzyme-linked immunosorbent assay) to validate certain proteins, including vimentin, alpha-2 macroglobulin, apolipoprotein B and A-I, S-100A6, aldehyde dehydrogenase mitochondrial, AHNAK and antithrombin-III, all of which showed sequentially increases in serum levels as the grades increased (from grade I to III), implying that they might be used as prognostic indicators. However, the studies were limited by the use of only one grade III meningioma sample in their proteomic analysis.

Parada *et al.*, (2018) employed the unbiased iTRAQ LC-MS/MS and the biased Pamchip® peptide array techniques and reported phosphoproteomic and kinomic signature AKAP12-Ser-1587 protein (A-kinase anchor protein 12). They suggested that lower levels of AKAP12 were associated with high grade, invasive, and recurrent/progressive meningioma, establishing AKAP12 as a prognostic biomarker. The same group Parada *et al.*, (2020) revealed upregulation of RB1-S780 phosphosite in clinically aggressive WHO grade I meningioma (recurrent and progressive grade 1.5) compared to grade I and suggested the phosphorylation

of RB1-S780 in grade 1.5 meningiomas may play a role in the progression/recurrence phenotype that could be a viable predictive biomarker.

Our group Bassiri *et al.*, (2017) performed label-free quantitative mass spectrometry to analyse the proteome and phospho-proteome of genetically characterized *NF2* mutated human meningioma and schwannoma primary cells. This study identified 2000 proteins significantly differentially overexpressed in *NF2* mutated meningioma and schwannoma compared to control human meningeal and Schwann cells respectively. Among these, only one protein PDZ and LIM domain protein 2 (PDLIM2) was commonly significantly overexpressed in both *NF2* mutated meningioma and schwannoma compared to their respective controls, and significant overexpression of this protein was confirmed via WB. This study also found that knocking down *PDLIM2* with shRNA in both primary meningioma and schwannoma cells reduces cell growth. Furthermore, the phosphoproteomic analysis found PDLIM2 phosphoserine sites. However, due to a lack of phosphosite-specific commercial antibodies, phosphoserine-PDLIM2 could not be validated.

Another study from our group Dunn *et al.*, (2019) conducted a comprehensive analysis of proteins and phosphoproteins in meningioma tissue of all grades compared to healthy meninges. They identified a panel of potential therapeutic targets/biomarkers for all grades and validated the upregulation of NEK9, NEK9-T210, HK2, p-AKT1-S473, p-AKT2-S474, and SET, EGFR, and STAT2 proteins and phosphoproteins across all grades of meningioma compared to normal meninges. In addition to this, this study revealed that increased phosphorylation of AKT1-S473 was highly associated with grades I and II, while HK2 was a candidate for grade III. These findings have defined proteomic meningioma profiles that with the further investigation may hold therapeutic value.

Silva *et al.*, (2020) performed shotgun proteomics to compare the protein expression pattern between male and female patient's tissue samples of grade I meningioma. DDX42, BCAS2, DDX3, PRPF6, PRPF31 and S100-A4 proteins were considerably overexpressed in female meningioma patients compared to the male group in this study, and these proteins are highly enriched at RNA splicing and transport-related pathways. Male meningioma patient-specific proteins, on the other hand, were shown to be highly enriched in the extracellular matrix architecture, suggesting that they are linked to cancer aggressiveness and metastasis. Furthermore, the author points out that just because proteins are linked to one biological

condition does not mean they are entirely absent from another. Instead, their absence might be caused by the stochastic nature of data-dependent acquisition or by an abundance that is below the detection limits of the mass-spectrometry method (Silva *et al.*, 2020).

Our group recently carried out proteome analysis on WHO grade I and grade II primary meningioma cells (Sofela *et al.*, 2021). This study used meningioma cells, tissue and plasma samples to validate a biomarker for meningioma using Western blotting, immunohistochemistry, and real-time quantitative polymerase chain reaction (RT-qPCR), enzyme-linked immunosorbent assay (ELISA). Fibulin-2, a calcium-binding extracellular matrix glycoprotein, was the only protein whose expression results were consistent across all experimental settings. Fibulin-2 overexpression was shown to be significantly higher in grade II meningioma than in grade I meningioma in this investigation. Furthermore, a considerable increase in Fibulin-2 in the plasma implies that it is a biomarker for grade II meningioma. However, this study, solely compared grades and did not include any normal meninges as a control group.

### **1.11 Biomarkers in neuro-oncology**

In neuro-oncology, biomarkers are essential for both routine clinical care and the development of new treatments (Cagney *et al.*, 2018). The term "biomarker" refers to a variety of patient or disease assessments and when the terms are used imprecisely or without comprehending their definitions, confusion can result. In turn, this may delay their proper use, relevance, and adoption (Cagney *et al.*, 2018).

The Food and Drug Administration (FDA) and the National Institutes of Health (NIH) established the BEST (Biomarkers, Endpoints, and other Tools) glossary in 2016 to enable those organisations a common language to communicate in and to standardise and make plain terminology used in the development of medical products and translational science (Cagney *et al.*, 2018). According to FDA/NIH, a biomarker is "a particular characteristic that is determined as an indicator of normal biological processes, pathogenic processes, or responses to an exposure or intervention, including therapeutic interventions." A biomarker can be a molecular, histologic, radiographic, or physiological feature, but it is not an evaluation of how a person feels, behaves, or survives (FDA-NIH Biomarker Working Group, BEST (Biomarkers, Endpoints, and other Tools) Resource. Maryland, 2016; Cagney *et al.*, 2018). To summarize, biomarkers are characteristics that are evaluated at every stage within the clinical continuum,



from the pre-diagnosis of disease to the pre-treatment phase (which forms the basis for precision medicine), to the post-treatment phase (outcomes and endpoints) (Cagney *et al.*, 2018).

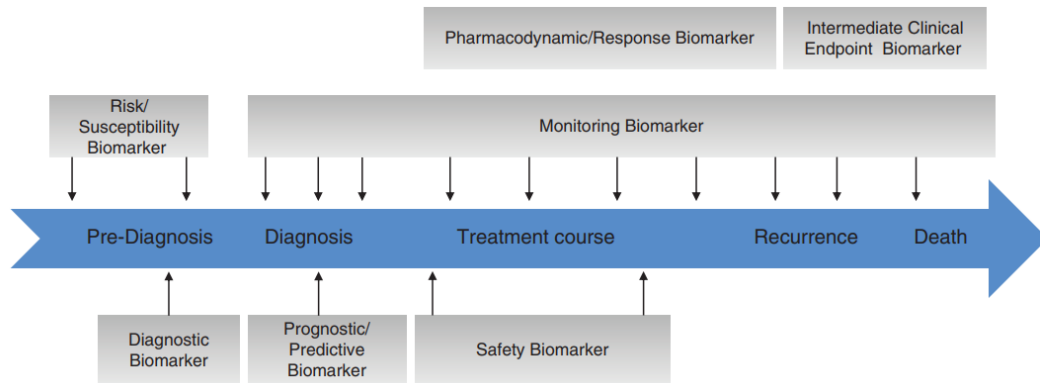


**Figure 9: A summary of the biomarker categories situated along this clinical continuum.** The figure is taken from Cagney *et al.*, 2018.

According to BEST (Biomarkers, Endpoints, and other Tools) Resource. Maryland, 2016, biomarkers are classified into seven categories based on their application: risk/susceptibility, diagnostic, monitoring, prognostic, predictive, pharmacodynamics/response, and safety biomarkers (Fig-9) (Cagney *et al.*, 2018).

**A susceptibility/risk biomarker** is a biomarker that predicts an individual's tendency to develop an illness or other medical condition over time even if they do not now show clinical symptoms of it (FDA-NIH Biomarker Working Group, BEST (Biomarkers, Endpoints, and other Tools) Resource. Maryland, 2016; Cagney *et al.*, 2018). For instance, a history of ionizing radiation (IR) exposure has been associated with both meningioma and glioma development suggesting that risk biomarkers are associated with the absorbed dosage of IR (Schwartzbaum *et al.*, 2006). Neurofibromatosis type 1 (NF1), NF2 gene alterations, RB1 or MYCN alterations (retinoblastoma), and tuberous sclerosis 1 (TSC1) and TSC2 mutations are inherited genetic disorders characterised by germline mutations of the p53 tumour suppressor gene that are associated with risk of development of meningioma and glioma (Ohgaki and Kleihues, 2005; Schwartzbaum *et al.*, 2006).

**A diagnostic biomarker** is used to detect people who have a disease or condition or to specify a subgroup of the disease (FDA-NIH Biomarker Working Group, BEST (Biomarkers, Endpoints, and other Tools) Resource. Maryland, 2016; Cagney *et al.*, 2018). Diagnostic biomarkers are routinely employed in neuropathology and are becoming increasingly important

for classifying brain tumours. In addition to histology, the 2021 World Health Organisation (WHO) classification included a number of molecular factors (Louis *et al.*, 2016; Louis *et al.*, 2021).

**A monitoring biomarker** that is serially evaluated to determine the state of a disease or medical condition, as well as to show if a patient has been exposed to (or experienced the effects of) a medication or an environmental factor (FDA-NIH Biomarker Working Group, BEST (Biomarkers, Endpoints, and other Tools) Resource. Maryland, 2016; Cagney *et al.*, 2018). Blood is the most convenient tissue source for monitoring biomarkers and is commonly used to evaluate disease status in malignancies such as prostate and ovarian cancer using serum biomarkers of prostate-specific antigen and cancer antigen 125, respectively. Blood-based monitoring biomarkers in neuro-oncology are mainly utilised to evaluate toxicity and safety for carrying out treatment. Blood-based monitoring biomarkers may be more challenging in the setting of neuro-oncology since the blood-brain barrier (BBB) prevents the reliable release of tumour-related biomarkers into the bloodstream (Cagney *et al.*, 2018). Meningiomas, it turns out, exist outside the BBB, therefore this restriction is less of a problem in this tumour type. However, the advantages may be significant and outweigh the disadvantages, supporting the study of blood-based biomarkers in neuro-oncology, such as exosomes, microRNAs, and circulating tumour cells (Shao *et al.*, 2012; Qiu *et al.*, 2013; Akers *et al.*, 2013). These biomarkers may also be helpful for response monitoring, as well as diagnostic, prognostic, and predictive purposes in addition to disease monitoring (Cagney *et al.*, 2018).

**A prognostic biomarker** can identify the risk of a clinical event, a disease recurrence, or the course of the disease in people with the target disease or condition (Cagney *et al.*, 2018). The association between these biomarkers and a specific outcome, such as overall survival (OS) or progression-free survival (PFS), is therefore frequently observed (Cagney *et al.*, 2018). IDH1/2 mutations, 1p/19q co-deletion status, and MGMT promoter methylation status are prognostic indicators in neuro-oncology (Weller *et al.*, 2010; Zhao *et al.*, 2014; Alexander and Mehta, 2011).

**Predictive biomarkers** are used to identify those who are more likely to suffer a favourable or adverse response to exposure to a medical product or an environmental agent (BEST (Biomarkers, Endpoints, and other Tools) Resource. Maryland. 2016; Cagney *et al.*, 2018).

**A pharmacodynamics/response biomarker** that demonstrates the occurrence of a biological response in a person after exposure to a drug or an environmental agent (BEST (Biomarkers,

Endpoints, and other Tools) Resource. Maryland. 2016; Cagney *et al.*, 2018). The most common type of blood-based pharmacodynamics biomarker used in neuro-oncology to date is the measurement of peripheral blood mononuclear cells using Western blot, for example, to assess the inhibition of targets like pAKT and pS6 after treatment with small molecules AKT inhibitors (Fouladi *et al.*, 2014).

**A safety biomarker** is used to detect the existence or level of toxicity related to a procedure or exposure (BEST (Biomarkers, Endpoints, and other Tools) Resource. Maryland. 2016; Cagney *et al.*, 2018). Weekly complete blood counts are the most often used safety biomarker in neuro-oncology to check for myelosuppression in patients receiving chemotherapy and radiotherapy for gliomas (Gerber *et al.*, 2007).

## 1.12 Aim of this project

Proteins carry out the majority of cell functions and are strongly linked to cell phenotype (Deracinois *et al.*, 2013). The relationship between mRNA levels and protein levels is not precise, therefore quantitative mRNA data alone is insufficient to predict protein expression levels or protein function (Gygi *et al.*, 1999).

Advances in DNA sequencing technologies have allowed for the base-pair resolution unravelling of cancer genomes, revealing cancer genomic alterations in the development of malignant tumours (Vogelstein *et al.*, 2013). However, it is becoming obvious that detection of gene mutations alone is insufficient in order to suggest biomarkers or therapeutic targets for personalized therapy due to the fact, that cellular function is executed at protein levels (Wu *et al.*, 2019). For example, when patients with *EGFR* mutations are treated with an EGFR inhibitor (Gefitinib), the patients did not respond and some patients with *BRAF V600E* mutations did not respond to treatment with BRAF inhibitor (Vemurafenib) (Goulart *et al.*, 2001; Paez *et al.*, 2004; Chapman *et al.*, 2011). Genomic and transcriptomic analysis may provide vital information about gene expression (Graves and Haystead, 2002), and the understanding the effect of genome alterations on protein function will advance the knowledge of meningioma biology.

The molecular landscape of meningioma has been relatively well characterized, therefore proteomic analysis of genetically-defined samples is highly relevant to understand pathogenesis, discover biomarkers and therapeutic targets of different genotypes.

The aim of this project is to identify novel biomarkers and/ or therapeutic targets in genetically stratified meningiomas to aid precision medicine for these patients. To achieve this, unbiased proteome analyses were performed on genetically defined meningioma subtypes such as *NF2*, *AKT1/TRAF7*, and *KLF4/TRAF7* mutations to identify novel molecular differences among the meningioma mutant subtypes, subsequently describe biomarker(s) for distinguishing meningioma mutant subtypes. Following that, bioinformatics and statistical analysis of proteomic data were used to generate a list of significantly differentially expressed proteins among the meningioma subtypes, from which I carried out validation experiments using meningioma tissue to confirm the expression observed in the proteomics analyses. Eventually, these experiments may help to identify a panel of proteins with the potential to serve as meningioma mutant subtype-specific biomarkers. In addition to this, phospho-peptide proteome analyses were performed to investigate abnormal protein phosphorylation and kinase signaling that are responsible for tumour development in different meningioma mutant subtypes.

## **Objectives:**

- **Screening for mutational hotspots:** To confirm mutational status by genotyping or genome sequencing, the screening for *NF2*, *TRAF7*, *AKT1*, *KLF4*, *PIK3CA*, *SMO*, *POLR2A*, *SMARCB1*, and *SMARCE1* mutational hotspots in meningioma tissue samples were undertaken for genetic stratification.
- **Proteomic Profiling:** Characterisation of proteomic signature of the meningioma mutational subtypes by performing unbiased global and as well as phospho-proteomic analysis followed by a comparison of the proteomic profiles of subtypes to establish the differential expression of proteins.
- **Functional annotation and pathway analysis:** Functional annotation and pathway analysis will be performed on differentially expressed proteins and phosphoproteins in order to gain a better understanding of the biology of each meningioma mutational group.
- **Expression validation:** Confirmatory experiments to validate potential targets/biomarkers using antibody-based techniques such as Western blot or immunohistochemistry. Examination of promising candidates using inhibitors such as FDA-approved or other commercially available drugs or lentiviral-mediated knockdown in

order to detect drug response or inhibition of a targeted potential candidate to observe the effect on meningioma cell growth *in vitro* before and after treatment.

## **2. Material and methods**

### **2.1 Tumour material and clinical data**

Meningioma samples under the ‘J’ series were received from the Brain Archive and Information Network (BRAIN UK) under ethical approval (REC No: 14/SC/0098; IRAS project ID: 143874, BRAIN UK Ref: 15/011; ‘Identifying and validating molecular targets in low-grade brain tumour’).

Meningioma (MN) were collected with patient consent during the surgical procedure and complied with national and local ethics approval (REC No: 14/SW/0119; IRAS project ID: 153351) (Plymouth Hospitals NHS Trust: R&D No: 14/P/056 and North Bristol NHS Trust: R&D No: 3458).

Two frozen normal meninges were obtained from Analytical Biological Services Inc. The grading was carried out based on the WHO 2021 grading system (Louis *et al.*, 2021) by a neuropathologist, and only meningioma grade I was included in this study.

Human meningioma cells (HMC) were purchased from Sciencell™ which is used as a control. The benign immortalised Ben-Men-1 cell line was acquired from the Leibniz Institute DSMZ -German Collection of Microorganisms and Cell Cultures (Cat# ACC-599, RRID: CVCL\_1959) (Puttmann *et al.*, 2005) and used in the functional validation procedure (knockdown experiment).

Clinical and histological details about the specimens are presented in supplementary data (S1) and also briefly presented below (Table- 2.1).

<b>Sample</b>	<b>WHO grade</b>	<b>Age</b>	<b>Gender</b>	<b>Histological subtypes</b>	<b>Location</b>
J5	I	50	F	Fibroblastic	Occipital
J6	I	37	F	Transitional	Parasagittal
J14	I	80	F	Fibroblastic	Frontal
MN005	I	59	F	Fibroblastic	Brain stem
MN017	I	51	F	Transitional	Frontal
MN164	I	-	F	Transitional	Left extra axial
MN274	I	68	F	Fibrous	Left parietal
MN160	I	48	F	Meningothelial	Anterior cranial fossa
MN257	I	34	F	Fibrous	Fibrous
MN325	I	-	F	Psammomatous	R- convexity
MN319	I	57	F	Mixed (fibrous+psammomatous)	R-posterior fossa
MN310	I	63	F	Psammomatous	R-temporal convexity
MN255	I	35	F	Meningothelial	Left sphenoid wing
MN149	I	63	F	Meningothelial	Right frontal extra axial
MN214	I	59	F	Meningothelial	Planum sphenoidale
MN197	I	62	F	Psammomatus	Sphenoid wing
MN109	I	48	F	Transitional	Frontal
MN330	I	-	F	Meningothelial	Left sphenoid wing
MN110	I	47	F	Transitional	Left lateral ventricle

MN306	I	-	F	Secretory	R-frontal
MN244	I	65	F	Not reported	Left frontal extra convexity
MN232	I	70	F	Secretory	R-sphenoid wing
MN331	I	75	F	A-Psammomatus	A- left olfactory groove
				B- Transitional	B- right tuberculum sella
MN348	I	-	F	-	-
MN315	I	-	F	Psammomatus	Left paraclinoid
MN125	I	41	F	Secretory	Left sphenoid wing
NFB23	I	-	-	Secretory	Cavernous sinus
NFB26	I	-	-	Secretory	Frontal
NFB28	I	-	-	Secretory	Skull base

**Table 2.1** Clinical and histological details of the tumour samples used in this proteomics study.

## 2.2 Digestion of meningioma tumour and cell culture

After the surgery, fresh meningioma specimens are directly sent to our lab in a sterile transferred media, Dulbecco's Modified Eagle Media (DMEM, Gibco, Life Technologies, Loughborough, UK), composed of 10% FBS (Sigma Aldrich, Gillingham, UK), 500 U/mL penicillin/streptomycin (Gibco, Life Technologies, Loughborough, UK), and 2.5 µg/mL amphotericin B (Sigma Aldrich, Gillingham, UK).

First, tumours are washed twice with sterile phosphate-buffered saline (PBS, Gibco, Life Technologies, Loughborough, UK) and then depending on the size of the tumour, tumours were dissected into a few pieces: DNA, tissue lysates (proteomics), RNA experiment and the rest of the tumour pieces process for primary cell generation. For primary cells, tumour pieces were made into a single cell suspension and incubated in a P100 sterile plate containing incubation medium (DMEM, Gibco, Life Technologies, Loughborough, UK), 10% FBS (Sigma Aldrich, Gillingham, UK), and 100 U/mL penicillin/streptomycin (Gibco, Life



Technologies, Loughborough, UK), and incubated at 37 °C in a humidified atmosphere (5% CO<sub>2</sub>) till digestion. In DMEM supplemented with 10% FBS, 100 U/mL penicillin/streptomycin (Gibco, Life Technologies, Loughborough, UK) and 20 U/mL Collagenase III (Worthington Biomedical Corp., Lakewood, NJ) overnight at 37 °C. After digestion, primary cells were pelleted at 1000 rpm for 5 minutes, removed supernatant, re-suspended the pellet in a complete media and seeded in tissue culture flasks. Meningioma primary cells (Grade-I) and Ben-Men-1 cell lines were routinely cultured in DMEM (Gibco, Life Technologies, Loughborough, UK) supplemented with 10% FBS (Sigma Aldrich, Gillingham, UK), 1% D-(+)- glucose (Sigma Aldrich, Gillingham, UK), 100 U/mL penicillin/streptomycin (Gibco, Life Technologies, Loughborough, UK) and 2 mM GlutaMAX™-I (Gibco, Life Technologies, Loughborough, UK) at 37 °C and 5% CO<sub>2</sub>.

Human meningeal cell lines were cultured in the commercially available HMC medium (Sciencell™, Buckingham, UK) at 37 °C and 5% CO<sub>2</sub>.

### **2.3 DNA extraction and Next Generation Sequencing**

DNA was extracted from each tumour sample by using Qiagen® DNeasy® Blood & Tissue Kit (Qiagen, Hilden, Germany; #69504) following the manufacturer's instructions. The quality and quantity of DNA were assessed by using a NanoDrop 2000 spectrophotometer (Thermo Scientific, US). Two micrograms of DNA were sent to the Manchester Centre for Genomic Medicine for detection of *NF2* mutations using NGS and Multiplex Ligation-dependent Probe Amplification (MLPA®) dosage test. NGS was used to identify single nucleotide polymorphisms (SNP) in *NF2* and MLPA® to identify whole exon deletions and duplications.

### **2.4 KASP genotyping**

Kompetitive allele-specific PCR is a fluorescence-based genotypic variant of polymerase chain reaction. It is based on allele-specific oligo extension and Fluorescence Resonance Energy Transfer for signal generation and is able to detect both SNP and insertion/deletion genotypes (He *et al.*, 2014; Adams *et al.*, 2020). KASP reactions were carried out in a final volume of 10 µl consisting of 2 µl of genomic DNA (20 ng/µl), 5 µl of 2x KASP mix [a mixture of FAM and HEX Fluorescence Resonance Energy Transfer (FRET) cassettes, ROX™ passive dye, an optimized buffer containing MgCl<sub>2</sub>, Taq polymerase and dNTPs], 0.14 µl primer mix (LGC, Queens Road, Middlesex, UK ) (Table-2.2) containing two allele-specific forward primers and a common reverse primer and 2.86 µl of sterile water. PCR amplification was performed in a

LightCycler® 480II (Roche) using the cycling conditions: 94°C for 15 min for hot-start Taq DNA polymerase activation, followed by a touchdown profile of 10 cycles at 94°C for 20 s and 61°C for 1 min with a 0.6°C reduction per cycle, followed by amplification at 26 cycles at 94°C for the 20s and 55°C for 1 min. Once the programme was finished extra five cycles were run at 57°C. Once the KASP reaction was finished end-point fluorescent images were visualised in a Cartesian plot, and the data were analyzed using KlusterCaller™ software ((LGC, Queens Road, Middlesex, UK).

Mutation	Primer allele FAM (x-axis)	Primer allele HEX (y-axis)	Common primer	Allele FAM	Allele HEX	WT genotype
<i>AKT1</i> E17K (SNP : rs121434592)	CACCCGCACGTCGTAGGGA	ACCCGCACGTCGTAGGGG	GTGGCCGCCAGGTC TTGATGTA	A	G	GG
<i>KLF4</i> K409Q	GTGCCTTGATGGGAACTCTT	GTGCCTTGAGATGGGAACTCTG	GATTACGGGGCTG CGGCAAAA	A	C	AA
<i>TRAF7</i> N520S	AGAAAGGAGCTCACAGGCCTCAA	GAAGGAGCTCACAGGCCTCA	GGTAGGAGCCGCTG TACAGGTA	A	G	AA
<i>SMO</i> L412F	GAAAGTAGCCTCCACGATGAG	GGAAGTAGCCTCCACGATGAA	GGGCTTCGTGCTGG CCCCAA	C	T	CC
<i>SMO</i> W535L (SNP : rs121918347)	GGCATGCCCATGAGCACCTG	GGCATGCCCATGAGCACCTT	TCCAGATGAGCAGC GTGGCCTT	G	T	GG
<i>POLR2A</i> Q403K	CCTCTTTCCTTCTAGACTTAAAGA ACTAGTGGCAGGGG	CCTCTTTCCTTCTAGACTTCAAGA ACTACTCCGCCAGGGG	Not supplied	A	C	CC
<i>PIK3CA</i> H1047R (SNP : rs121913279)	AAATGAATGATGCACATCATGGTG GCTGGAC	AAATGAATGATGCACGTCATGGTG GCTGGAC	Not supplied	A	G	AA
<i>PIK3CA</i> E345K (SNP : rs104886003)	CTCTCTGAAATCCTGAGCAGGAG AAAGATT	CTCTCTGAAATCACTAAGCAGGAG AAAGATT	Not supplied	G	A	GG
<i>POLR2A</i> L438_H439del	TTTCCACCCCAAGCCAGTGACCTT CACCTGCAGACCGGCTATAAG	TTTCCACCCCAAGCCAGTGACCTG AGACCGGCTATAAG	Not supplied	ACCTTC		ACCTCC
<i>SMARCB1</i> R374Q	GTGTTGGCAAGACGCCCTCATCT	GTGTTGGCAAGACGCCCTCATCC	CATTGCCCTCCCACTA CCTCTT	A	G	GG
<i>SMARCB1</i> R377H (SNP : rs387906812)	CGGGCCCGTGTGGCAAGAT	GGGGCCGTTTGGCAAGAC	CCACTCCTCTCCAGGA CGGAT	A	G	GG

**Table 2.2** Endpoint genotyping primers

## 2.5 Sanger sequencing

Primers (Table 3) were designed to cover areas of the WD40 region of TRAF7 DNA sequence (NC\_000016.10:2155752-2178129, Homo sapiens Chr 16, GRch38). Fragments were amplified in 50µl PCR reactions with 30ng template DNA, 10µM Primers and 2x LongAmp Taq master mix, using five minutes hot start at 94°C, 35 cycles of 94 °C 1 minute, 65°C 1 min, 72°C 4 min with five minutes 72°C final elongation, PCR products were run on a 1% Tris-Acetate EDTA (TAE) agarose gel and extracted using Qiaex II Gel extraction kit before quantification using the Nanodrop. 150ng of the template was sent to Eurofins, Surrey, UK for Sanger sequencing with 20µM of specifically designed sequencing primers.

### A) Primers used for PCR amplification

Name	Sequence (from 5' to 3')
AKT1 FOR EXON2	CTGGCCCTAAGAAACAGCTCC
AKT1 REV EXON2	TGCTTGCCAGCCCAGGACTT
TRAF7 R4 FOR	TTTCTGTTGGTGCTGATATTGCCTGGGGGCTGCTTCTCAG
TRAF7 R4 REV	ACTTGCCTGTCGCTCTATCTTCCAGAGCCTGTCCACCTATGC
KLF4 FOR EXON4	GGATGATGCTCACCCAC
KLF4 REV INTRON4	GGAGATCAAGGCGATAGACTGC

**B) Primers used for Sanger sequencing**

Name	Sequence (from 5' to 3')
AKT1 FOR SEQ	CACACCCAGTTCCTGCCTGG
AKT1 REV SEQ	CGCCACAGAGAAGTTGTTGA
TRAF7 WD1 FOR	ATCAACGCGCGGCTGAACAT
TRAF7 WD1 REV	GACTCACCCCTGGATGCAGA
TRAF7 WD4 FOR	AGCCCACAGTTGCAGCAAT
TRAF7 WD4 REV	CTGGCCTTGCACCCAGATG
TRAF7 WD5 FOR	ACCAACTGGCCCACGATTAC
TRAF7 WD5 REV	GACTTTGGTCTGGTCTGGCG
TRAF7 WD6 FOR	CAGTGTCTTTGACCTGCCT
TRAF7 WD6 REV	AGCAAGTCCAAACCTGCAG
KLF4 FOR SEQ	AGAGGAGCCCAAGCCAAAG
KLF4 REV SEQ	TGGGGCTGGAAGCTAACCTG

**C) PCR conditions**

	Initial denaturation	Amplification	Final elongation
<i>AKT1</i> and <i>KLF4</i>	98°C for 30 s	35 cycles : 98°C for 10 s 60°C for 30 s 72°C for 20 s	72°C for 2 min
<i>TRAF7</i>	95°C for 5 min	25 cycles : 98°C for 10 s 65°C for 15 s 68°C for 4-5 min	68°C for 5 min

**Table 3. Oligonucleotide details.** A) Primers used for PCR amplification. B) Primers used for Sanger sequencing. C) PCR conditions.

## 2.6 Tissue lysates preparations

Tumour samples were homogenised manually or using bullet blender (Bullet Blender® Next advance Storm Pro, 5E Pro, and Lite with Easy Touch Technology) in radio immunoprecipitation assay buffer (RIPA buffer) RIPA buffer (50 mM Tris/HCl P<sup>H</sup> 7.4, 1% SDS, 1% NP-40, 150 mM NaCl, 1 mM EDTA, 0.5% sodium deoxycholate) containing protease inhibitor (1:20) and phosphatase inhibitor cocktail (1:100) (Thermo Scientific™ RIPA Lysis and Extraction Buffer, UK). The volume of the lysis buffer added to the samples depends on the size of the tumour. Followed by tissue lysates were stored at -80 °C for at least 24 hours, then the samples were thawed on ice, vortex and centrifuged at maximum speed (16000 x g) for 15 minutes at 4°C. The supernatant was collected and protein concentration was measured. Protein concentration was determined using a colorimetric BCA protein assay (Thermo Fisher Scientific, Massachusetts, US; Cat: 23225) by measuring absorbance at 562 nm.

## 2.7 Total protein preparation

Total proteins (50 µg) were separated in 4-15% Mini-PROTEAN® TGX™ Precast Gels (Bio-Rad, Hercules, California, US). Gel was stained with Coomassie brilliant blue R-350 (GE Healthcare Life Sciences, Illinois, US) for 5 minutes or until sample lanes were visible. Followed by gel was kept in destaining solution (50% LC/MS grade water (Fisher Scientific; #W6212), 40% LC/MS grade methanol (Fisher Scientific; #A456-1) and 10% acetic acid) for overnight at room temperature. The gel was washed with LC/MS grade water and each lane was sliced into six fractions (each fraction = 1x1mm) and the whole process was performed in keratin-free conditions.

## 2.8 Gel digestion

For mass-spectrometry, separated proteins were in-gel digested according to the method described by Shevchenko *et al.*, (2006). The gel pieces were washed/dehydrated three times in 50 mM ammonium bicarbonate (ABC) pH 7.9/50 mM ABC + 50% acetonitrile (ACN). Subsequently, proteins were reduced with 10 mM dithiothreitol (Sigma-Aldrich®) for 20 minutes at 56 °C and alkylated with 50 mM iodoacetamide (Sigma-Aldrich®) for 20 min at room temperature (RT) in the dark. After two subsequent wash/dehydration cycles, the gel pieces were incubated overnight with 12.5 ng/µl trypsin (Promega, Wisconsin, US; #V5111) at 37 °C for digestion. Peptides were acidified by adding 2% trifluoroacetic acid (TFA) and incubated for 20 minutes on a shaker at 1400 rpm at RT and supernatant was collected in a

fresh Eppendorf® Protein LoBind 1.5 ml micro-centrifuge tubes. Followed by 200 µl of Buffer B (80% ACN, 0.5% acetic acid and 1% TFA) was added to extract the remaining peptides from the gel pieces. The volume was reduced to evaporate ACN in a vacuum centrifuge prior to peptide purification.

## **2.9 Peptide clean-up**

To purify peptides, the peptide clean-up stage tips protocol by Rappsilber *et al.*, (2003) was performed. Stage tips were made in-house by cutting polytetrafluoroethylene membrane (Empore™ Solid Phase Extraction Disks C18, 3M™; Fisher Scientific) into very small pieces. Followed by two small pieces were inserted into 200 µl pipettes tips which functioned as the column. C18 stage tips were placed into a micro-centrifuge tube and conditioned by adding 50 µl of LC/MS grade methanol and centrifuged at 1000 X g for min. Then 50 µl of buffer B was added to activate the C18 stage tip column and equilibrated adding 50 µl of buffer A (0.5% acetic acid and 1% TFA). Samples were loaded to the stage tip column and centrifuged at low speed at 1-2000 X g until the samples pass through the column completely. The tips were then washed twice using 50 µl of buffer A and then stage tips were placed into a fresh Eppendorf® Protein LoBind 1.5 ml micro-centrifuge tubes. Finally, samples were eluted from C18-StageTips by pipetting 50 µl of buffer B and concentrated using a SpeedVac at 30°C. Once dried out, samples were re-dissolve in 30 µl of Buffer A and stored at -20°C until run through Mass-spectrometry.

## **2.10 Protein identification by liquid chromatography-tandem mass spectrometry**

MS was carried out using an ultimate 3000 UPLC system (Thermo Fisher) connected to an Orbitrap Velos Pro mass spectrometer (Thermo Fisher). Proteins were identified with the Andromeda peptide database search engine integrated into the computational proteomics platform MaxQuant version (1.5.0.30). Andromeda parameters for protein identification were set at mass tolerance of 20 ppm and minimal peptide length was at 6 amino acids. Proteins were quantified with label-free quantification (LFQ) values representing normalised summed peptide intensities correlating with protein abundances, where the ‘match between run’ option was permitted between runs with a 0.7 minute elution time interval.

## 2.11 Enrichment of phosphoprotein

Commercially available Qiagen<sup>®</sup> PhosphoProtein Purification Kit (Qiagen, cat: 37101) was used to enrich phosphoprotein. This kit is composed of affinity chromatography which completely separates phosphorylated protein from non-phosphorylated protein. While tissue lysates run through the column, phosphorylated proteins are attached to the affinity column where non-phosphorylated proteins are washed away. The previous study has already described and suggested that 88% of elution of phosphoprotein is possible by this method (Bassiri *et al.*, 2017; Dunn *et al.*, 2019).

According to the manufacturer's instructions, the meningioma tumor pieces were homogenized by using pastel and mortar by adding 1ml of phosphoprotein lysis buffer, consisting of 0.25% CHAPS detergent, the DNase/RNase Benzonase<sup>®</sup> Nuclease, protease inhibitors (provided with the kit), phosphatase inhibitor cocktails B (Santa Cruz Biotechnology, Inc. cat: sc-45045) and C (Santa Cruz Biotechnology, Inc. cat: sc-45065) at the concentration of 1:1. The remaining phosphoprotein lysis buffer was added to the tissue lysates and incubated for 30 minutes at 4 °C and vortex briefly every 10 minutes. After incubation, centrifuge the tissue lysates at 10,000 x g and 4°C for 30 min. To equilibrate the phosphoprotein purification column, 4 ml of phosphoprotein lysis buffer containing 0.25% CHAPS was used. Then the supernatant was harvested and protein concentrations were determined by using the Pierce<sup>™</sup> BCA Protein Assay Kit (Thermo Fisher Scientific, Massachusetts, US; Cat: 23225). Depending on the size of the tumour, approximately the volume of 2.5 mg of total protein was taken and adjusted the protein concentrations to 0.1 mg/ml by diluting with 0.25% CHAPS containing phosphoprotein lysis buffer which will yield approximately 25 ml of lysates to the final volume. Then pipette half of the tissue lysates to the upper reservoir of phosphoprotein purification column and allowed to run through the column and enter into the gel bed. The same procedure was followed for the remaining half lysates. This step took about 50 minutes to an hour to complete and allowed enough time for phosphoproteins to bind to the affinity column. All these steps were performed at room temperature. Followed by 6 mL of 0.25% CHAPS containing phosphoprotein lysis buffer were pipetted to wash the column and allowed to flow through. Then 500 µl of 0.25% CHAPS containing phosphoprotein elution buffer was added to the column and eluted fraction was collected, and this step was repeated 5 times. The eluted phosphoproteins fractions were condensed to approximately 25 µL by using the Nanosep ultrafiltration column provided with the kit. Further, 6X loading buffer (375 mM Tris-HCl pH 6.8, 6% SDS, 50% glycerol, 9% β-mercaptoethanol, 0.03% bromophenol blue) was added to the phosphoproteins and stored at -



20 °C until separation by SDS-PAGE. The rest of the proteomics steps followed as total proteomics.

Be noted that, some tumours were small in size or fibrotic, could not make 2.5 mg of total protein. In that case, took the whole amount of lysates and adjusted the concentration of tissue lysates to 0.1 mg/ml accordingly.

## **2.12 TMT Labelling and phospho-peptide enrichment**

Aliquots of 100µg of each sample were digested with trypsin (2.5µg trypsin per 100µg protein; 37°C, overnight), labelled with Tandem Mass Tag (TMT) ten plex reagents according to the manufacturer's protocol (Thermo Fisher Scientific, Loughborough, LE11 5RG, UK) and the labelled samples were pooled.

The pooled sample was desalted using a SepPak cartridge according to the manufacturer's instructions (Waters, Milford, Massachusetts, USA). Eluate from the SepPak cartridge was evaporated to dryness and subjected to TiO<sub>2</sub>-based phosphopeptide enrichment according to the manufacturer's instructions (Pierce). The flow-through and washes from the TiO<sub>2</sub>-based enrichment were then subjected to FeNTA-based phosphopeptide enrichment according to the manufacturer's instructions (Pierce). The phospho-enriched samples were again evaporated to dryness and then re-suspended in 1% formic acid prior to analysis by nano-LC MSMS using an Orbitrap Fusion Lumos mass spectrometer (Thermo Scientific).

### **2.12.1 Nano-LC Mass Spectrometry**

The phospho-enriched peptides were further fractionated using an Ultimate 3000 nano-LC system in line with an Orbitrap Fusion Lumos mass spectrometer (Thermo Scientific). In brief, peptides in 1% (vol/vol) formic acid were injected onto an Acclaim PepMap C18 nano-trap column (Thermo Scientific). After washing with 0.5% (vol/vol) acetonitrile 0.1% (vol/vol) formic acid peptides were resolved on a 250 mm × 75 µm Acclaim PepMap C18 reverse phase analytical column (Thermo Scientific) over a 150 min organic gradient, using 7 gradient segments (1-6% solvent B over 1min., 6-15% B over 58min., 15-32%B over 58min., 32-40%B over 5min., 40-90%B over 1min., held at 90%B for 6min and then reduced to 1%B over 1min.) with a flow rate of 300 nl min<sup>-1</sup>. Solvent A was 0.1% formic acid and Solvent B was aqueous 80% acetonitrile in 0.1% formic acid. Peptides were ionized by nano-electrospray ionization at 2.0kV using a stainless-steel emitter with an internal diameter of 30 µm (Thermo Scientific) and a capillary temperature of 300°C.

All spectra were acquired using an Orbitrap Fusion Lumos mass spectrometer controlled by Xcalibur 3.0 software (Thermo Scientific) and operated in data-dependent acquisition mode using an SPS-MS3 workflow. FTMS1 spectra were collected at a resolution of 120 000, with an automatic gain control (AGC) target of 200 000 and a max injection time of 50ms. Precursors were filtered with an intensity threshold of 5000, according to charge state (to include charge states 2-7) and with monoisotopic peak determination set to Peptide. Previously interrogated precursors were excluded using a dynamic window (60s +/-10ppm). The MS2 precursors were isolated with a quadrupole isolation window of 0.7m/z. ITMS2 spectra were collected with an AGC target of 10 000, max injection time of 70ms and CID collision energy of 35%.

For FTMS3 analysis, the Orbitrap was operated at 50 000 resolution with an AGC target of 50 000 and a max injection time of 105ms. Precursors were fragmented by high energy collision dissociation (HCD) at a normalised collision energy of 60% to ensure maximal TMT reporter ion yield. Synchronous Precursor Selection (SPS) was enabled to include up to 5 MS2 fragment ions in the FTMS3 scan.

### **2.12.2 Data Analysis**

The raw data files were processed and quantified using Proteome Discoverer software v2.1 (Thermo Scientific) and searched against the UniProt Human database (downloaded October 2019: 150786 entries) using the SEQUEST algorithm. Peptide precursor mass tolerance was set at 10ppm, and MS/MS tolerance was set at 0.6Da. Search criteria included oxidation of methionine (+15.995Da), acetylation of the protein N-terminus (+42.011Da), Methionine loss plus acetylation of the protein N-terminus (-89.03Da) and phosphorylation of serine, threonine and tyrosine (+79.966) as variable modifications and carbamidomethylation of cysteine (+57.0214) and the addition of the TMT mass tag (+229.163) to peptide N-termini and lysine as fixed modifications. Searches were performed with full tryptic digestion and a maximum of 2 missed cleavages were allowed. The reverse database search option was enabled and all data was filtered to satisfy false discovery rate (FDR) of 5%.

TMT Labelling and phospho-peptide enrichment and data analysis procedure were performed by Dr Vikram Sharma.

## 2.13 Statistical and functional annotation analysis

LFQ values were  $\log_2$  transformed and imputed with normal distribution using the Perseus software suite 1.6.2.3. Statistical significance of protein changes in abundance were calculated by a two-tailed  $t$ -test, with p-values adjusted for multiple testing by a Benjamini-Hochberg FDR at 1%. Microsoft Excel was used to calculate log fold changes (FC) and a  $\log_2 \text{FC} \geq 1$  and  $\log_2 \text{FC} \leq -1$  with p-value  $< 0.05$  were used as selection criteria for further downstream analysis via Database for Annotation, Visualization and Integrated Discovery (DAVID) and Ingenuity Pathway Analysis (IPA). Differentially expressed proteins for hierarchical clustering were obtained by submitting relative expression profiles to Perseus and performing an ANOVA (p-value  $< 0.05$ ) on data imputation. Venn diagrams illustrating distribution of proteins/upregulated proteins among all meningioma subtypes using Venny 2.1 (<http://bioinfogp.cnb.csic.es/tools/venny/index.html>). GO enrichment analyses were performed using the Database for Annotation, Visualization and Integrated Discovery (DAVID) v6.8 (<https://david.ncifcrf.gov/>) against all human proteins. In addition to this, pathway analyses were performed on the selected significant proteins via Ingenuity® Pathway Analysis (IPA®) (QIAGEN Inc., <https://www.qiagenbioinformatics.com/products/ingenuity-pathway-analysis>).

## 2.14 Kinase identification

The identification of kinases from the phosphopeptide dataset was performed by Dr Matthew Banton using R (version 4.1) and the Bioconductor package KinSwingR (version 1.12.0) as previously described by Engholm-Keller *et al.*, (2019). The KinSwingR method takes the 15-mer peptides centralised on the phosphorylated residue, the fold change and p-value of each peptide, and a database of kinase-substrate peptides from PhosphoSitePlus (19<sup>th</sup> March 2020). It builds position weight matrix (PWM) models of the kinase substrates from the database and then statistically infers the phospho-peptide 15-mers to each PWM model to identify the most likely kinase that phosphorylates each phosphosite. KinSwingR then quantifies the activity of each kinase based on the direction of the fold change for each peptide and represents this activity in the KinSwingR “swing score”.

KinSwingR analysis for each comparison ( $NF2^{-/-}$  vs NMT,  $AKT1^{E17K}$  vs NMT and  $NF2^{-/-}$  vs  $AKT1^{E17K}$ ) was performed 100 times using randomly generated seeds in order to calculate an average swing score across 100 replicates and calculate the percentage of times a particular kinase was significant across the 100 analyses and the percentage of times a kinase is associated

with a particular phospho-peptide. The higher the percentage of occurrence the kinase was found to be significant ( $p \leq 0.05$ ) out of the 100 kinswingR analyses the more robust the kinase is in the kinswingR analysis and the better the candidate is for further validation.

The results columns of the KinSwingR output are:

- **kinase**: The kinase
- **pos**: Number of positively regulated kinase substrates
- **neg**: Number of negatively regulated kinase substrates
- **all**: Total number of regulated kinase substrates
- **pk**: Proportion of positively regulated kinase substrates
- **nk**: Proportion of negatively regulated kinase substrates
- **swing\_raw**: Raw - weighted score
- **n**: Number of substrate sequence in kinase PWM
- **swing**: Normalised (Z-score transformed) - weighted score
- **p\_greater**: probability of observing a swing score greater than
- **p\_less**: probability of observing a swing score less than

Values used to determine potential candidates for downstream analyses include: the kinase, the swing score (+ve = upregulated, -ve = downregulated) and the p-values.

## 2.15 Western blotting

The Western blotting procedure was followed in this study as previously described by Dunn *et al.*, (2019); Negroni *et al.*, (2020) and Sofela *et al.*, (2021).

### Sodium Dodecyl Sulphate- Polyacrylamide Gel Electrophoresis

Different percentage of polyacrylamide resolving gel (10 wells) was made in-house depending on the size of the molecular weight of protein interest (Table 4). I have also used readymade Criterion™ XT Precast gels (4-12% Bis-Tris Protein Gels (18 wells); Bio-Rad; cat no: 3450124) to accommodate a large number of samples. Tissue lysates were prepared (described previously in section 2.6) and an equal amount of 4X loading buffer (62.5 mM Tris-HCl pH 6.8, 10% glycerol, 1% SDS, 0.005% bromophenol blue) was added and then samples were heated at 95°C for 5 minutes prior to loading gel. The gel holder was placed in a running tank and 1L of 1x running buffer (14.3 gms of glycine and 3 gms of Tris mixed in 1L distilled water and then added 5ml of 20% SDS solution) was poured into the tank. For criterion gel, XT MOPS 20x readymade running buffer was used (BIO-RAD CAT: 1610788). Six microlitres of

pre-stained protein marker were loaded as a standard and 10µg of each tissue lysates were loaded in each well. The gels were run until the sample's dye had migrated to the bottom of the gel at a 120V constant current.

	<b>Percentage of resolving gel</b>			
<b>Reagents</b>	6%	8%	10%	15%
40% acrylamide	1.5 mL	2 mL	2.5 mL	3.75 mL
1.5 M Tris-HCl pH 8.8	2.5 mL	2.5 mL	2.5 mL	2.5 mL
10% SDS	100 µl	100 µl	100 µl	100 µl
10% ammonium persulfate (APS)	100 µl	100 µl	100 µl	100 µl
TEMED	10 µl	10 µl	10 µl	10 µl
Distilled H <sub>2</sub> O	5.79 mL	5.29 mL	4.79 mL	4.29 mL
	<b>4% of acrylamide stacking gel</b>			
Reagents	40% acrylamide			0.5 mL
	0.5 M Tris-HCl, 0.4% SDS pH 6.8			1.25 mL
	10% ammonium persulfate (APS)			50 µl
	TEMED			10 µl
	Distilled H <sub>2</sub> O			3.19 mL

**Table: 4** Polyacrylamide gel recipes

### **Electrophoretic protein transfer**

After SDS-PAGE electrophoresis, the gel was removed and placed on two filter papers ( for criterion gel Criterion <sup>TM</sup> blotter filter paper catalog: 1704085 Bio-rad used) which were pre-wetted with 1X transfer buffer (14.3 gms of glycine, 3 gms of Tris mixed, 800 mL of distilled water and 200 ml of methanol). A polyvinylidene difluoride membrane (Immuno-Blot® PVDF membrane, Bio-rad) was placed on top of the gel along with two filter papers. Followed by transferring the protein from gel to nitrocellulose membrane at a constant 250 mA for 90 -100 minutes at 4°C cold temperature. For overnight transfer, the current was set at a constant 175 mA.

### **Probing with primary antibodies**

After transfer nitrocellulose membrane were washed with PBS-T and blocked with 5% (w/v) non-fat skim milk in PBS-T for an hour. Then membranes were probed with species-specific primary antibodies at 4°C overnight (Table 5).

<b>Antibody</b>	<b>Manufacturer/ Catalogue number</b>	<b>Species</b>	<b>Applications &amp; dilution</b>
Merlin	Cell Signaling Technology - #6995	Rabbit	WB (1:1000)
p-Merlin- S518	Cell Signaling Technology - #9163	Rabbit	WB (1:500)
Chk-1	Cell Signaling Technology - # the 2360s	Mouse Monoclonal	WB (1:250)
p-CHK1 (S345)	Cell Signaling Technology - # 2341s	Rabbit	WB (1:250)
Chk-2	Cell Signaling Technology - # 2662s	Rabbit Polyclonal	WB (1:500)
p-Chk2 (T68)	Cell Signaling Technology - # 2661s	Rabbit Polyclonal	WB (1:500)
PKC - $\alpha$	Cell Signaling Technology - # 2056s (WB) Abcam-ab32376 (IHC)	Rabbit Polyclonal (WB) Rabbit Monoclonal (IHC)	WB (1:500) IHC (1:500) EDTA
p-PKC- $\alpha$ / beta II (t638/641) (rabbit) p-PKC- $\alpha$ (T638)	Cell Signaling Technology - # 9375S (WB) Abcam-ab32502 (IHC)	Rabbit Rabbit Monoclonal (IHC)	WB (1:500) IHC (1:3000) EDTA
p-PKC- $\alpha$ (S657)	Abcam- ab180848	Rabbit	WB (1:500) IHC (1:500) EDTA
p-PKC- $\alpha$ (T497)	Abcam- ab76016	Rabbit Monoclonal	WB (1:500) IHC (1:3000) EDTA
LCK	Cell Signaling Technology - # 2984s	Rabbit Monoclonal	WB (1:500)
p-LCK (Tyr394)	Thermo Fisher Scientific – PA537628	Rabbit Polyclonal	WB (1:500)
CSNK2A1	Cell Signaling Technology - # 2656s	Rabbit Monoclonal	WB (1:500)
p-CSNK2A1 (T360+S362)	Abcam- ab119410	Rabbit Polyclonal	WB (1:500)
AURKB	Abcam- ab2254	Rabbit Polyclonal	WB (1:500)
p-AURORA a/b/c (T288/238/398)	Cell Signaling Technology - # 2914s	Rabbit Monoclonal	WB (1:500)
p-CHK1 (S345)	Cell Signaling Technology - # 2341s	Rabbit Monoclonal	WB (1:250)
p-CAM2A (thr286) total CAM2A (DUET antibodies)	Cell Signaling Technology - # 81902	Rabbit Monoclonal	WB (1:500)
p-EGFR (Tyr1068) (D7A5)	Cell Signaling Technology - # 3777	Rabbit Monoclonal	WB (1:500)

<b>Antibody</b>	<b>Manufacturer</b>	<b>Type</b>	<b>Applications &amp; dilution</b>
p-EGFR (Tyr1173) (53A5)	Cell Signaling Technology - # 4407	Rabbit Monoclonal	WB (1:500)
EGFR (D38B1)	Cell Signaling Technology - # 4267	Rabbit Monoclonal	WB (1:500)
Cleaved Caspase-3 (Asp175)	Cell Signaling Technology - # 9664	Rabbit Monoclonal	WB (1:500)
Cyclin D1	Cell Signaling Technology - # 2922	Rabbit Polyclonal	WB (1:500)
Anion exchange protein 2 -SLC4A2	Sigma- SAB2701184 (WB), LOT NUMBER- GT40233 Sigma- HPA019339, LOT NUMBER- A104877 (IHC)	Rabbit  Rabbit Polyclonal IgG	WB (1:500)  IHC (1:3000)-Citrate
E-cadherin 1	Sigma- SAB4503751 LOT NUMBER- 310147	Rabbit	WB (1:500)  IHC (1:800)-Citrate
Endoglin	Sigma-HPA011862, LOT NUMBER- A81361	Rabbit Polyclonal IgG	WB (1:500)  IHC (1:600)-Citrate
Pyruvate carboxylase	Sigma- HPA043922, LOT NUMBER- 000002248	Rabbit Polyclonal IgG	WB (1:500)  IHC (1:70)-EDTA
GDP-mannose 4,6 dehydratase	Novus: NBP1-33424	Rabbit Polyclonal IgG	Simple Wes (1:50)  IHC (1:5000)-Citrate
Chloride intracellular channel protein 3	Sigma-HPA005963, LOT NUMBER: A115350	Rabbit Polyclonal IgG	Simple Wes (1:75)  IHC (1:100)-Citrate
Cellular retinoic acid-binding protein	Sigma- HPA004135, Lot number: B105867	Rabbit Polyclonal IgG	Simple Wes (1:50)  IHC (1:100)-Citrate
Annexin A3	Sigma- HPA013398, Lot number: a101914	Rabbit Polyclonal IgG	Simple Wes (1:250)  IHC (1:1500)-Citrate
Lin-7 homolog C	Abcam: ab127049	Rabbit Polyclonal	Simple Wes (1:10)  IHC (1:100)-Citrate
Prostaglandin F2 receptor negative regulator	Sigma- SAB2700379, Lot number: GT39735	Rabbit	WB (1:500)  IHC (1:800)-Citrate



Thrombospondin type-1 domain-containing protein 4	biorbyt.com, cat no-orb544020 (WB) Creative diagnostics: DPABH-20213 (IHC)	Rabbit Polyclonal Rabbit Polyclonal IgG	WB (1:500) IHC (1:400)-EDTA
Solute carrier family 29 member 1(SLC29A1) /ENT1	Novus-NBP3-02977	Rabbit Polyclonal IgG	WB (1:500) IHC (1:1500)-Citrate
<b>Antibody</b>	<b>Manufacturer</b>	<b>Type</b>	<b>Application &amp; dilution</b>
Vinculin	Sigma-Aldrich- V9131	Mouse Monoclonal HVIN-1	Simple Wes (1:500) WB (1:5000)
$\alpha$ -Tubulin	Bio-technne- NB100-690	Mouse Monoclonal DM1A	WB (1:5000)
GAPDH	Merck Millipore- MAB374	Mouse Monoclonal 6C5	WB (1:5000)

**Table: 5** List of primary antibodies with their concentrations used in this study. WB= Western Blot, IHC= Immunohistochemistry, SW= Simple Wes, EDTA= Ethylenediaminetetraacetic acid antigen retrieval method and citrate antigen retrieval method.

### Probing with secondary antibody, protein detection and quantification

Following incubation with primary antibody, membranes were washed with PBS-T three times for 10 mins. After washing, the corresponding horseradish-peroxidase-conjugated secondary antibody (1:5000) Rabbit (cat: 170-6516; Bio-Rad) or Mouse (cat: 172-1019; Bio-Rad) was added to the membrane for one hour at room temperature. Proteins were detected using ECL 1 or 2 (ThermoScientific) depending on signal strength. Followed by membranes were exposed to hyper film (GE Healthcare, Chalfont Saint Giles, UK) and developed in a Xenograph compact X4 X-ray film processor or via GENESYS. Films were scanned in greyscale at 600 dpi resolution using an HP Scanjet 2400. For Genesys development, images were saved at 300 dpi resolution. Band intensity was quantified using ImageJ software and normalised to loading control (gapdh, vinculin and  $\alpha$ -tubulin). For phosphoproteins, the band intensity of phosphoprotein was normalised to total protein/ loading control.

For phosphoprotein expression analysis, first membranes were immunoblotted with anti-phosphorylated antibodies and then stripped with stripping buffer solution (Thermo Fisher Scientific; cat: 46430) for 15 minutes. After stripping membranes were washed three times for 10 minutes, re-blocked with 5% skimmed milk-PBST solution, and re-probe with total primary antibodies overnight.

## 2.16 Simple wes assay

Simple Wes assay was previously described by Estoppey *et al.*, (2021) and Uchida *et al.*, (2021).

A Simple wes assay was performed on a Wes instrument (ProteinSimple, San Jose, CA) according to the manufacturer's instructions. Simple wes assay kit (SM-W004 SDS 12-230 kDa WES separation module kit) and 8x25 capillary cartridge obtained from Bio-technie. First, tissue lysates were further diluted with 0.1X SDS sample buffer (coming with the kit) to make a concentration of 0.5 mg/ml. Followed by a combined one part of pre-made 5X fluorescent Master Mix (10X SDS sample buffer and 400 mM DTT) with 4 parts of diluted samples. Tissue samples were denatured at 95 °C for 5 minutes before pipetting into a Simple wes plate. Five µl of Biotinylated ladder was also pipetted to detect protein molecular weight 12-230 kDa, 10 µl of Milk free antibody diluent added as blocking reagent, 10 µl of respective diluent primary antibodies (Table 5), 10 µl of HRP conjugated anti-rabbit (ProteinSimple cat: 043-426) or anti-mouse secondary antibodies (ProteinSimple cat: 042-205) and 15 µl of a mixture of (1:1) luminol (ProteinSimple cat: 043-311) and peroxide (ProteinSimple cat: 043-379 ) were added in the assay plate to generate chemiluminescence. The plate was centrifuged for 5 minutes at 2500 rpm (~100 X g) at room temperature. Further, chemiluminescence was captured by a charge-coupled device (CCD) camera. A Compass software (ProteinSimple, Santa Clara, CA) was used to analyse the digital image. Protein expression was estimated via correlating signal strength on digital images by representing a peak area. The values for the peak area of each sample were normalised to the corresponding peak area of loading control (Vinculin) from that run. Statistical significance was calculated using One-way ANOVA with Dunnett's multiple comparison tests or unpaired t-test in the GraphPad Prism software (version 9.1.2) as described in the figure legends. Values were displayed as standard error mean (SEM) and the number of biological replicates (n value) is indicated for each figure. Statistical significance is displayed on the figures with asterisks as follows: \*,  $p < 0.05$ ; \*\*,  $p < 0.01$ ; \*\*\*,  $p < 0.001$ ; \*\*\*\*,  $p < 0.0001$ ; ns was considered for not significant.

## 2.17 Immunohistochemistry

The four-micrometer thickness of Formalin Fixed Paraffin Embedded (FFPE) tissue section slides were received from the Department of Cellular Pathology at University Hospitals Plymouth and the Department of Cellular Pathology at Bristol Hospital. At first, slides sections were baked at 60 °C for an hour to get rid of all paraffin. Tissue sections were then de-waxed

by xylene (ThermoFisher Scientific, Loughborough, UK) and washed with 100% ethanol (VWR, Lutterworth, UK) to rehydrate. Followed by sections were washed by placing them under running tap water for 5 minutes. To stop endogenous peroxidase activity tissue sections were blocked with the solution containing 3% H<sub>2</sub>O<sub>2</sub> in MeOH for 30 minutes (Hilton *et al.*, 2016; Dunn *et al.*, 2019; Sofela *et al.*, 2021).

Antigen retrieval techniques were performed by using Tris/EDTA or citrate buffer solution (outlined in table-5) in a microwave for 30 minutes (Hilton *et al.*, 2016; Dunn *et al.*, 2019; Sofela *et al.*, 2021). After equilibration with TBS/Tween for 5 minutes, further, slides were blocked with normal horse serum and avidin-biotin ((Vector Laboratories Ltd; #SP-2001) blocking solution for 15 minutes to avoid non-specific binding. Sections were then incubated with respective primary antibodies overnight at 4 °C in a moist black box to avoid drying. The next day after a couple of washes tissue sections were incubated with biotinylated secondary antibody (Vectastain<sup>®</sup> Universal Elite ABC kit; #PK-6200; Vector Laboratories Ltd) for 30 mins and biotinylated HRP (Vectastain<sup>®</sup> Elite ABC Reagent; Vectastain<sup>®</sup> Universal Elite ABC kit) for 30 mins at room temperature for protein detection according to manufacturer's protocol as previously described by Hilton *et al.*, 2016; Dunn *et al.*, 2019; Sofela *et al.*, 2021. For negative control, tissue sections were incubated with 1xTBS-Tween overnight instead of adding primary antibodies and then followed the same procedure.

For protein visualisation, tissue sections were incubated with 3,3'-diaminobenzidine (DAB) solution (Sigma-Aldrich<sup>®</sup>; cat: D4293) for 5 minutes, rinsed with tap water for 5 minutes and then counterstaining of nuclei by Mayer's haematoxylin solution (Sigma-Aldrich<sup>®</sup>; #MHS1) for two minutes. Further, tissue sections were dehydrated with 100% ethanol and xylene twice for 5 minutes. Finally tissue section were mounted onto coverslip by using Pertex (Sigma Aldrich, Gillingham, UK).

Images were taken via Leica DMRB and semi-quantitative assessment of intensity of staining was performed blindly by consultant neuropathologist Dr David Hilton (Department of Cellular and Anatomical Pathology, University Hospitals Plymouth), and scored as follows: 0 = negative, 1 = when show weak immunoreactivity, 2 = when the staining signal was moderate and 3 = when showed strong staining signal (Dunn *et al.*, 2019; Sofela *et al.*, 2021). To observe clinical differences among the mutational meningioma subtypes, average of the tissue section slides scoring calculated for each group and graphically represented the comparison.

## 2.18 Functional validation of proteins *in-vitro*

### 2.18.1 Protein knockdown procedure

Lentiviral mediated shRNA knockdown procedure was previously described by Ammoun *et al.*, (2015) and Provenzano *et al.*, (2017).

Ben-men-1 (BM-1) cells were cultured until showed 70% of confluence in a 6-well plate. For Annexin-3 Knockdown, protamine sulphate 8 µg/ml (Sigma Aldrich, Gillingham, UK) and commercially available lentiviral shRNA particles containing three different construct (clone ID: V2LHS\_49622, Gene symbol- ANXA3, target sequence: CAACTACTATCCAATTAT, cat no: VGH5518-200188034; clone ID: V2LHS\_49695, Gene symbol- ANXA3, target sequence: CACCTTACTTCTTCTCATA, cat no: VGH5518-200190006; and clone ID: V3LHS\_331751, Gene symbol- ANXA3, target sequence: ACAGAGTTCAAGAAGCATT, cat no: VGH5518-200266161, Dharmacon Inc, USA ) were added to the media. Scramble used as a negative control obtained from Dharmacon, cat: RHS4348. Virus multiplicity of infection (MOI) was calculated by using the formula ( $MOI = \text{Virus titre (IU/ mL)} \times \text{Virus volume (mL)} / \text{Total cell number}$ ). Followed by BM-1 was infected with the media containing protamine sulphate and lentiviral shRNA particles for 72 hours. After infection, puromycin (2 µg/ml) selection was performed for 48 hours. Transfection efficiency in BM-1 was assessed by observing GFP expression under the Leica8 microscope. Lastly, cells were then lysed for protein extraction and WB was performed for Annexin-3 knockdown confirmation.

### 2.18.2 Drug treatment and ATP assay

Meningioma grade I primary cells, BM-1 and KT-21 cell lines were seeded in 96 well white plates (Greiner Bio-One; #655088) at 2500 cells per well and grow for 24 hours. Go6976 (A protein kinase C inhibitor) (TOCRIS, Bio-technique cat: 2253) was serially diluted in dimethyl sulfoxide (DMSO; Sigma-Aldrich®) to make the appropriate concentration (0.1 µM, 1 µM, 3 µM and 10 µM) in meningioma grade I medium at a final volume of 100 µl/well. Only DMSO 0.1% was used as a negative control (vehicle control). Cells were then treated with the drug for 72 hours or 7 days at 37 °C in humidified 5% CO<sub>2</sub>. Followed by cell viability was investigated using ‘CellTiter-Glo® Luminescent Cell Viability Assay’ (Promega; #G7570). According to the manufacturer’s instructions, 100 µl of CellTiter-Glo luminescent substrate was pipetted per well and incubated in the dark for 15 minutes. The luminescence signal was measured by an Omega plate reader (BMG Labtech, Aylesbury, UK). To observe the drug effect, cell viability was calculated as a percentage, and the value normalised at DMSO control in Graph pad prism.

To investigate drug effect at the protein level, meningioma primary cells were seeded in a 6 well plate at 70,000 cells per well. Then cells were treated with different concentrations (1  $\mu$ M, 3  $\mu$ M and 10  $\mu$ M) of the drug (Go6976) for 3 days. Followed by cells were lysed for protein extraction and immunoblotted for PKC- $\alpha$  expression to assess the degree of drug inhibition. DMSO was used as a negative control. PKC- $\alpha$  expression for different concentrations of drug-treated cells was normalised at untreated/DMSO and referred to as a value of '1' and for quantification, each treated drug concentration was divided by the average of the control value. Then one-way Anova was performed to determine significant inhibition by Go6976 drug.

Figures 10.1 and 10.2 below provide a schematic illustration of the experimental procedures used in this study.

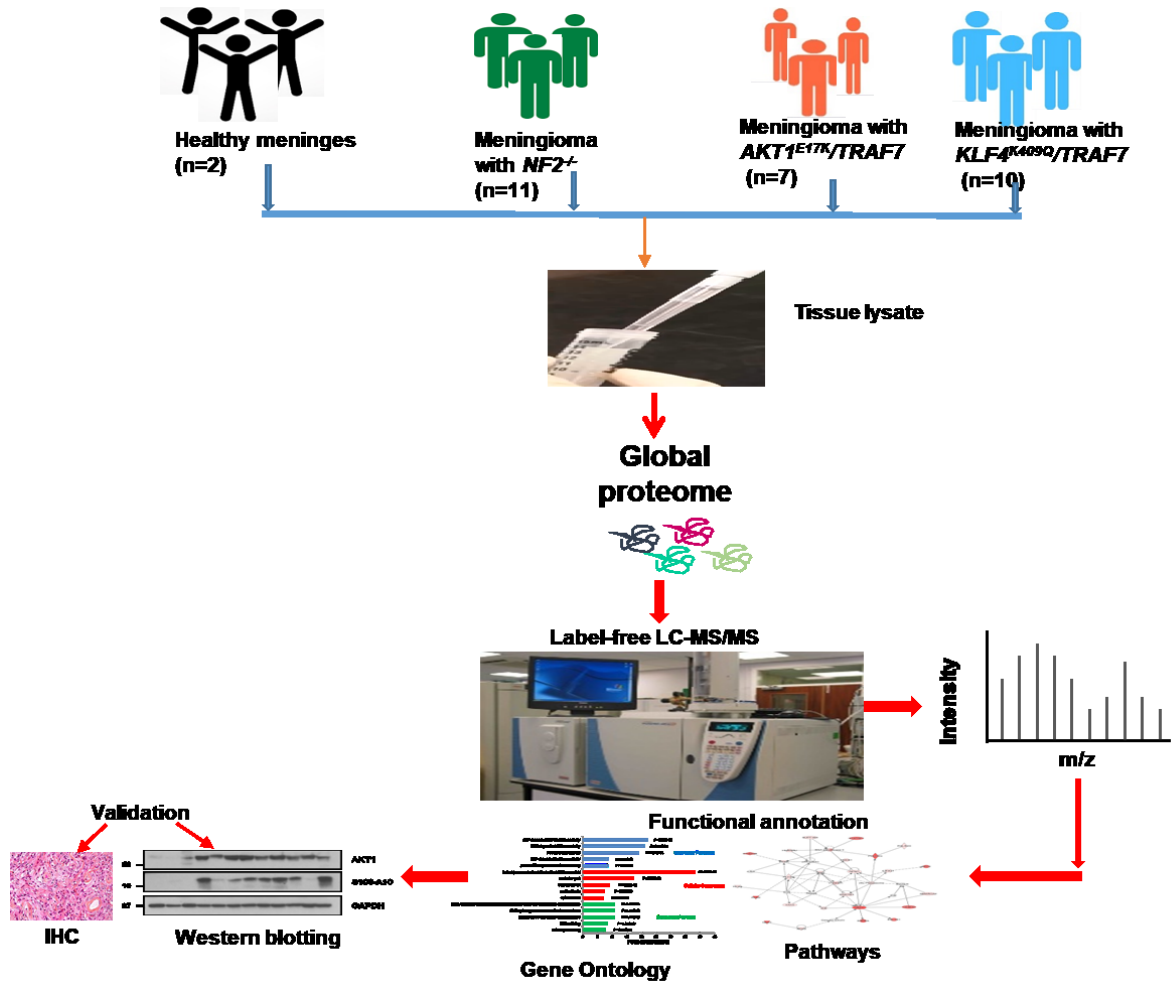


**Figure 10.1:** Schematic representation of global proteome and phosphoproteome experimental strategy. First mutational status in the frozen tissue samples is confirmed before homogenization of tumour tissue to extract proteins and process the samples for proteomics (peptide clean-up, phosphoprotein enrichment). Samples are then subjected to liquid chromatography-tandem mass spectrometry (LC-MS/MS). Followed by mass-spectrometry data analysis of differential expression between meningioma subtypes and healthy meninges. Functional annotation of differentially expressed proteins and phosphoproteins is carried out to identify associated biological processes as well as validation studies to confirm expression.

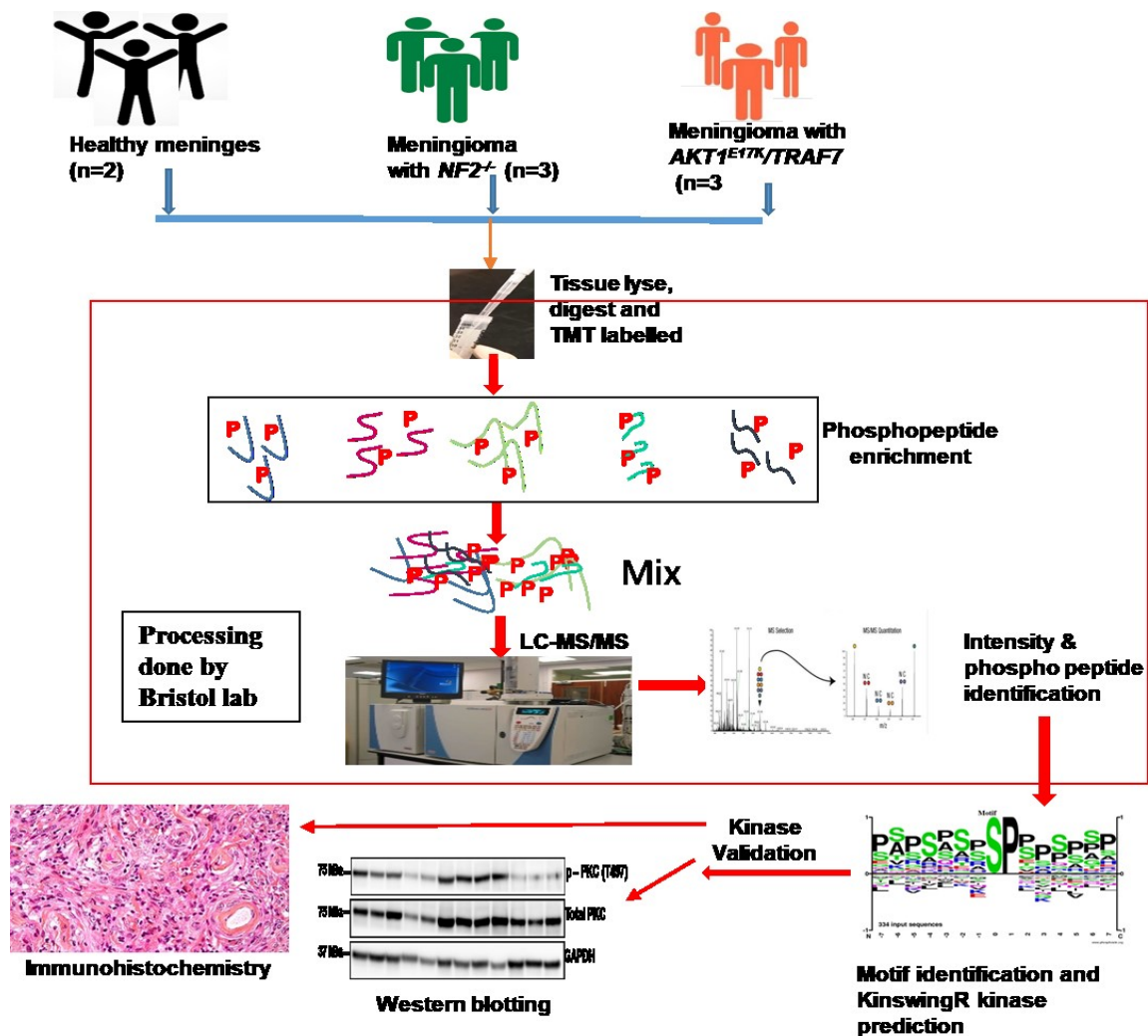


**Figure 10.2:** Schematic representation of phosphopeptide proteome experimental strategy. For phosphopeptide proteomics, tissue lysates were sent to Bristol laboratory for TMT labelled mass-spectrometry processing and analysis. Followed by mass-spectrometry data analysis of differential expression of phosphosites between meningioma subtypes and healthy meninges. From identified phosphosites motifs were identified using MOMO, followed by KinSwingR kinase analysis performed to predict kinases, as well as kinases validation via WB and IHC.

### 3. Results- Global proteomic analysis of mutational subtypes of meningioma grade-I

#### 3.1 Introduction

In order to discover new biomarkers, develop novel diagnostics, and track new therapeutic strategies, it is vital to be able to detect important differences between cellular states (both the molecular and cellular mechanisms) involved in biological processes. In recent years proteomics has become a crucial tool to investigate biological systems which allows for a direct comparison between different physiological conditions (Deracinois *et al.*, 2013).

In the last few years, mass spectrometry-based proteomics studies have suggested several potential biomarkers and therapeutic targets in meningiomas (Okamoto *et al.*, 2006; Cui *et al.*, 2014; Sharma *et al.*, 2014; Sharma *et al.*, 2015; Dunn *et al.*, 2019; Sofela *et al.*, 2021). However, these studies only compared between grades, without considering the genetic landscape of meningioma. Genetics plays a role in the development of tumours, and can be the cause of different protein expressions in patients (Kristensen *et al.*, 2019). A growing field of precision and personalized medicine (PPM) arose out of this inherent variability of tumours and is showing promise in the treatment of adult's brain tumours (Krzyszczyk *et al.*, 2018; Leibetseder *et al.*, 2022).

The molecular landscape of meningioma has been relatively well characterised (Clark *et al.*, 2013 and Clark *et al.*, 2016), therefore proteomic analysis of genetically defined samples may help us to identify biomarker or therapeutic targets to provide personalised medication in meningioma grade-I, since most biological functions are executed by proteins (Suppiah *et al.*, 2019). Understanding the effect of genome alterations on protein function will advance the knowledge of meningioma biology. In this study, I have only focused on meningioma grade-I tumours, and although they are benign, can show high rates of recurrence. Surgery is the main therapeutic approach, yet location can hamper complete resection and chemotherapies are ineffective. Moreover, accurate biomarkers for clinical management are lacking.

First, we stratified the fresh tumour samples based on their mutational status via Next Generation Sequencing (NGS) and KASP genotyping method and grouped them into three different mutational groups: *AKT1<sup>E17K</sup>/TRAF7*, *KLF4<sup>K409Q</sup>/TRAF7*, and *NF2<sup>-/-</sup>*. Then we performed a large-scale unbiased label-free mass spectrometry (MS) based proteomics approach in a total of 30 tissue samples (28 meningioma grade-I and two normal meninges).



Following MS data processing and analysis, we identified proteins and determined differential protein expression by comparing meningioma mutational subtypes and normal meninges. Additionally, mutational subtype specific proteins expressions have also been distinguished by overlapping the differential expression data sets. Furthermore, gene ontology (GO) enrichment and IPA pathway analysis was performed to determine dysregulated cellular pathways and biological processes among the meningioma mutational subtypes. To suggest potential biomarkers or therapeutic targets, I have started validation of proteomics data via different techniques such as Western blot (WB), Simple wes assay, immunohistochemistry (IHC), and functional validation (using shRNA knockdown). However, due to time limits and the lack of an ideal in-vitro model, extensive functional validation was not performed for all potential candidates, although further experiments will be conducted for the functional validation of potential protein candidates. In addition to this, due to the lack of samples only new possible targets were validated.

## **3.2 Confirmation of mutational background in meningioma specimens**

### **3.2.1 *NF2*<sup>-/-</sup> mutational status**

Upon receiving a meningioma tumour sample, the first step was to confirm its mutational status. Eleven meningiomas with *NF2*<sup>-/-</sup> mutation were included in this study. KASP genotyping method was not suitable due to the complicated nature of *NF2* mutations leading to *NF2* loss (Adams *et al.*, 2020). Five of these *NF2*<sup>-/-</sup> tumour samples were received from another group member (Dunn *et al.*, 2019) with confirmed mutations in the *NF2* gene by next-generation sequencing (NGS) and multiplex ligation-dependent probe amplification (MLPA) (Fig -11 A). Routine in-house screening of samples for *NF2* and phosphorylated (p*NF2*)-S518 by western blotting (WB) confirmed the remaining six samples to be *NF2*<sup>-/-</sup>. Western blot screening is shown in Figure-11 B; the red circles highlighted the six *NF2*<sup>-/-</sup> meningioma samples from this panel, which were included in the global proteomic analysis. However, the MN164 tumour sample showed a faint band for p-*NF2*-S518 (Fig-11 B), therefore it was sent for NGS to Bristol. For this instance, in this sample *NF2*<sup>-/-</sup> mutation was confirmed WB and NGS.

A

Sample	WHO grade	Mutational status
J5	I	<i>NF2</i> <sup>-/-</sup> (NGS/MLPA)
J6	I	<i>NF2</i> <sup>-/-</sup> (NGS/MLPA)
J14	I	<i>NF2</i> <sup>-/-</sup> (NGS/MLPA)
MN005	I	<i>NF2</i> <sup>-/-</sup> (NGS/MLPA)
MN017	I	<i>NF2</i> <sup>-/-</sup> (NGS/MLPA)
MN164	I	<i>NF2</i> <sup>-/-</sup> (WB & NGS/MLPA)
MN274	I	<i>NF2</i> <sup>-/-</sup> (WB)
MN257	I	<i>NF2</i> <sup>-/-</sup> (WB)
MN325	I	<i>NF2</i> <sup>-/-</sup> (WB)
MN319	I	<i>NF2</i> <sup>-/-</sup> (WB)
MN310	I	<i>NF2</i> <sup>-/-</sup> (WB)

B

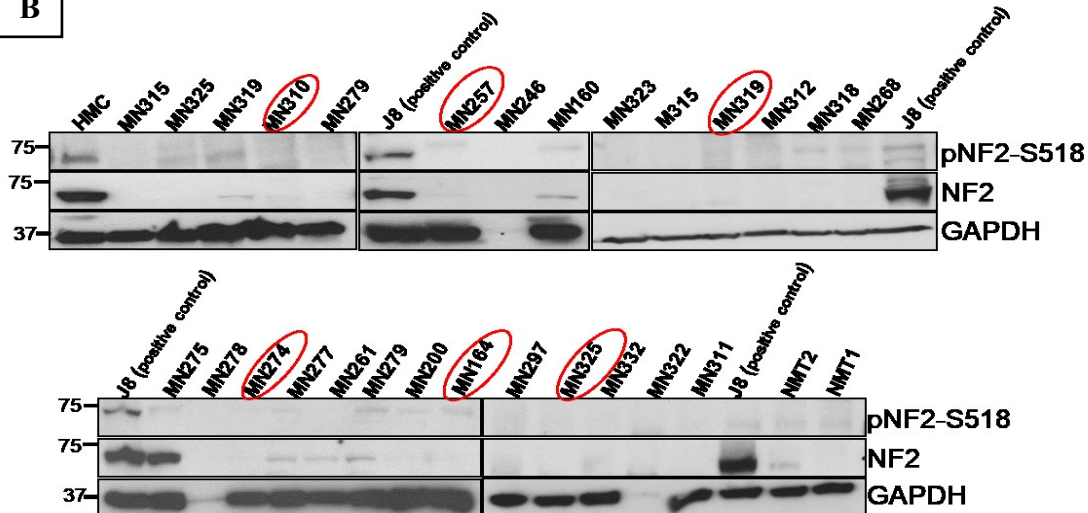


**Figure 11:** *NF2*<sup>-/-</sup> mutational status confirmation in meningioma tissue samples. A) Table shows meningioma specimens with confirmed *NF2*<sup>-/-</sup> mutational status and the method of confirmation (WB= western blotting). B) *NF2* mutational status confirmation by western blot, 25  $\mu$ g of each tissue lysate were blotted with *NF2* and p*NF2*-518 antibodies, J8 is a tissue positive control for *NF2* and GAPDH used as a loading control. Samples marked with red circles did not show any band for *NF2* or p*NF2*-518, therefore were included for MS analysis.

Our NGS/MPLA results showed that six meningioma grade-I including MN134 showed a deletion encompassing the whole of the *NF2* gene (supplementary data -S1).

### 3.2.2 *AKT1*<sup>E17K</sup> and *TRAF7* mutational status

In-house KASP genotyping was performed to screen the genes with mutational hotspots which are classed as non-NF2 meningioma (thus containing wild-type NF2 in their genome). The mutational hotspots screened include *AKT1*<sup>E17K</sup>, *KLF4*<sup>K409Q</sup>, *TRAF7*<sup>N520S</sup>, *SMO*<sup>L412F</sup>, *SMO*<sup>W535L</sup>, *SMARCB1*<sup>R374Q</sup>, *SMARCB1*<sup>R377H</sup> and *POLR2A*<sup>Q403K</sup> (Adams *et al.*, 2020). We were able to confirm seven meningioma tissue samples with *AKT1*<sup>E17K</sup> mutations. As previously mentioned, a majority of *AKT1*<sup>E17K</sup> mutated tumours mostly co-occur with *TRAF7* mutations, therefore, we also screened these seven samples for *TRAF7* mutations. Only one *AKT1*<sup>E17K</sup> mutant sample (MN214) showed a mutational hotspot for *TRAF7*<sup>N520S</sup> by KASP genotyping (Fig-12 A). The remaining six *AKT1*<sup>E17K</sup> mutant samples did not show *TRAF7*<sup>N520S</sup> hotspot mutation, suggesting these tumours harbour a *TRAF7* mutation in the other regions of the gene, including WD40 repeats. Therefore, *TRAF7* mutations in these samples were detected and confirmed by Sanger sequencing (Fig-12 B). Dr. Claire Adams confirmed all these mutational statuses in meningioma samples. Five of the seven meningiomas with *AKT1*<sup>E17K</sup> mutations analysed demonstrate mutations clustered within *TRAF7* WD40 domains, in line with previous data from Clark *et al.*, (2013) (Fig-12 B). Further, *TRAF7* mutation in the MN330 tumour sample has not yet been confirmed.

Sample	WHO grade	Mutational status	<i>AKT1</i> <sup>E17K</sup>	<i>TRAF7</i> <sup>N520S</sup>	<i>TRAF7</i> sequenced by Sanger
MN255	I	<i>AKT1</i> <sup>E17K</sup> / <i>TRAF7</i>	KASP	-	Yes
MN149	I	<i>AKT1</i> <sup>E17K</sup> / <i>TRAF7</i>	KASP	-	Yes
MN214	I	<i>AKT1</i> <sup>E17K</sup> / <i>TRAF7</i>	KASP	KASP	-
MN197	I	<i>AKT1</i> <sup>E17K</sup> / <i>TRAF7</i>	KASP	-	Yes
MN109	I	<i>AKT1</i> <sup>E17K</sup> / <i>TRAF7</i>	KASP	-	Yes
MN330	I	<i>AKT1</i> <sup>E17K</sup> / <i>TRAF7</i>	KASP	-	-
MN110	I	<i>AKT1</i> <sup>E17K</sup> / <i>TRAF7</i>	KASP	-	Yes

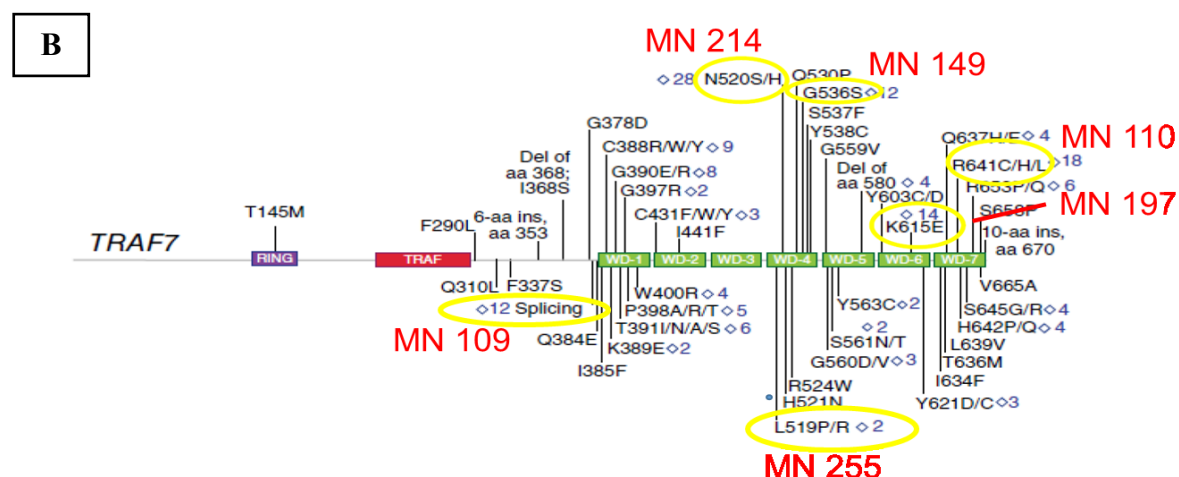


**Figure 12: *AKT1*<sup>E17K</sup> and *TRAF7* mutational status confirmation in meningioma samples.** A) Table shows meningioma specimens with confirmed *AKT1*<sup>E17K</sup>/*TRAF7* mutational status and the method of confirmation. B) Yellow circles depict the majority of *TRAF7* mutation occurring in the WD40 repeats region. Figure modified from Clark *et al.*, (2013).

### 3.2.3 *KLF4*<sup>K409Q</sup> and *TRAF7* mutational status

A total of ten meningioma samples with *KLF4*<sup>K409Q</sup> mutation were confirmed via in-house KASP genotyping (Table 6). Reuss *et al.*, (2013) reported that *KLF4*<sup>K409Q</sup> always co-occur with *TRAF7* in secretory meningioma. Six of the ten *KLF4*<sup>K409Q</sup> mutated meningiomas are secretory and in agreement with the previous study, we did not investigate *TRAF7* mutations by sequencing for these samples.

Sample	WHO grade	Mutational status	<i>KLF4</i> <sup>K409Q</sup>	<i>TRAF7</i> <sup>N520S</sup>	<i>TRAF7</i> sequenced by Sanger	Histological subtypes
MN306	I	<i>KLF4</i> <sup>K409Q</sup> / <i>TRAF7</i>	KASP	-	Not yet	Secretory
MN244	I	<i>KLF4</i> <sup>K409Q</sup> / <i>TRAF7</i>	KASP	-	Not yet	Not reported
MN232	I	<i>KLF4</i> <sup>K409Q</sup> / <i>TRAF7</i>	KASP	-	Not yet	Secretory
MN331	I	<i>KLF4</i> <sup>K409Q</sup> / <i>TRAF7</i>	KASP	-	Not yet	A-Psammomatus B- Transitional
MN348	I	<i>KLF4</i> <sup>K409Q</sup> / <i>TRAF7</i>	KASP	-	Not yet	-
MN315	I	<i>KLF4</i> <sup>K409Q</sup> / <i>TRAF7</i>	KASP	KASP	Not yet	Psammomatus
MN125	I	<i>KLF4</i> <sup>K409Q</sup> / <i>TRAF7</i>	KASP	-	Not yet	Secretory
NFB23	I	<i>KLF4</i> <sup>K409Q</sup> / <i>TRAF7</i>	KASP	-	Not yet	Secretory
NFB26	I	<i>KLF4</i> <sup>K409Q</sup> / <i>TRAF7</i>	KASP	-	Not yet	Secretory
NFB28	I	<i>KLF4</i> <sup>K409Q</sup> / <i>TRAF7</i>	KASP	-	Not yet	Secretory

**Table 6:** *KLF4*<sup>K409Q</sup> and *TRAF7* mutational status confirmation in meningioma samples.

A) Table shows meningioma specimens with confirmed *KLF4*<sup>K409Q</sup>/*TRAF7* mutational status and the method of confirmation.

Moreover, detailed genotyping information of all the meningioma samples included in this study can be found in supplementary data 1 (S1). Upon mutational status confirmation in meningioma tumour samples, they were then processed for proteomic analysis.

### 3.3 Global proteomic analysis of meningioma subtypes

#### 3.3.1 Protein identification and quantification

In total, 4162 proteins have been identified across 30 samples including 28 genetically defined meningiomas and two healthy normal meningeal tissues (NMT) as control with a 1% false discovery rate (FDR) by LC-MS based label-free proteomics according to (Dunn *et al.*, 2019; Sofela *et al.*, 2021). Among the 4162 proteins, 3868 were identified with at least two distinct ‘razor and unique’ peptides. Figure 13 depicts the distribution of the 4162 identified proteins among the sample groups of NMT, *NF2*<sup>-/-</sup>, *AKT1*<sup>E17K</sup>/*TRAF7* and *KLF4*<sup>K409Q</sup>/*TRAF7* mutant meningioma subtypes. 2909 proteins were identified within normal meninges (n=2) whilst, in meningioma tissue, 3490 proteins were identified across *AKT1*<sup>E17K</sup>/*TRAF7* mutant subtypes (n=7) and 3820 proteins identified in *NF2*<sup>-/-</sup> mutant subtypes (n=11) and 3179 proteins were identified in *KLF4*<sup>K409Q</sup>/*TRAF7* meningioma mutants (n=10).

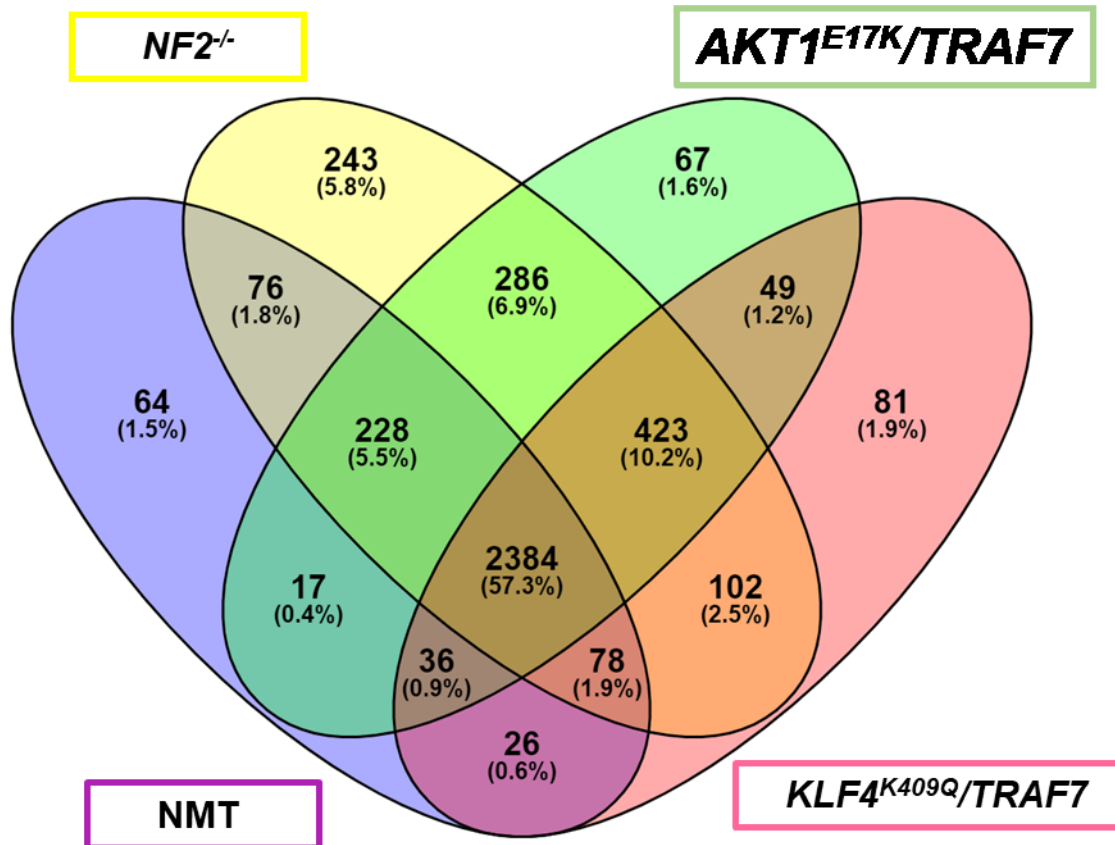


**Figure 13: Distribution of identified proteins across all sample groups.** Label-free quantitative (LFQ) proteomics by LC-MS/MS was used to identify 4162 proteins in *AKT1<sup>E17K</sup>/TRAF7* mutant meningioma ( $n=7$ ), *NF2<sup>-/-</sup>* mutant meningioma ( $n=11$ ), *KLF4<sup>K409Q</sup>/TRAF7* ( $n=10$ ), and normal meningeal tissue (NMT) ( $n=2$ ). Proteins were identified by at least two ‘razor and unique’ peptides with an FDR of 1%.

### 3.3.2 Hierarchical clustering of meningioma mutational subtypes

Unsupervised hierarchical clustering was performed via Perseus to identify tumour samples patterns based on protein expression profiles. As described previously, the data obtained from Max-Quant were  $\log_2$  transformed, imputed with normal distribution and normalised using Z scoring and median normalisation. This approach classified the panel of tumour samples into two overarching groups containing four clusters (Fig-14). All meningioma samples (n=7) with *AKT1*<sup>E17K</sup>/*TRAF7* mutation tended to cluster together and a similar pattern was observed for *KLF4*<sup>K409Q</sup>/*TRAF7* (n=10) group samples (Fig-14). In contrast, *NF2*<sup>-/-</sup> mutant samples grouped on either side of the *AKT1*<sup>E17K</sup>/*TRAF7* mutant samples and formed partial and mixed clusters (Fig-14). Additionally, hierarchical clustering showed the two normal meninges clustered together away from the meningioma subtypes (Fig-14).

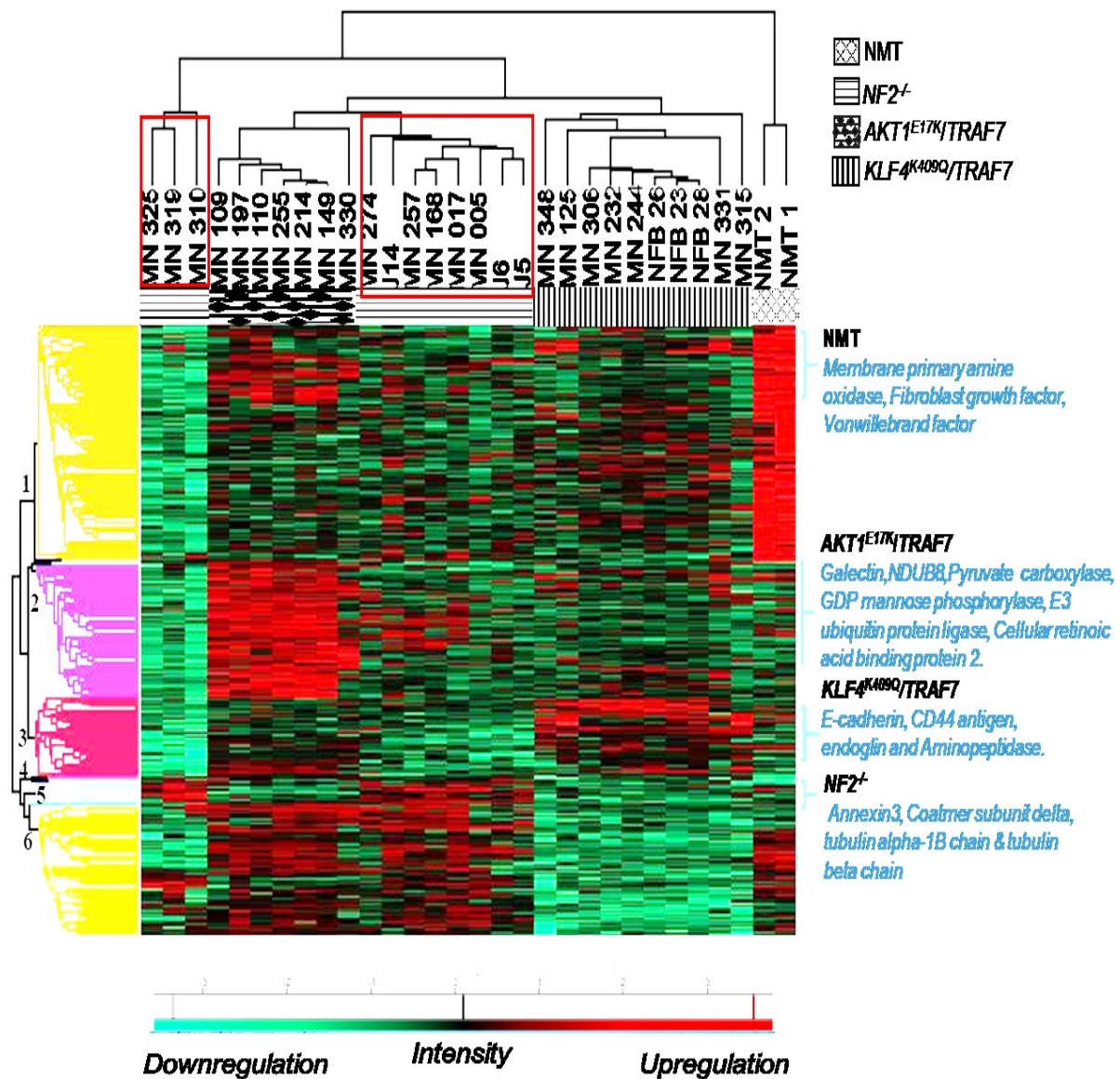


**Figure 14:** Meningioma samples clustering based on their proteomic profiles and comparative analysis of different mutational subtypes of meningioma and normal meninges. Hierarchical clustering was generated using  $\log_2$  LFQ values in Perseus version 1.6.2.3. The red boxes were demonstrating clustering of all  $NF2^{-/-}$  mutant samples on either side of samples with  $AKT1^{E17K}/TRAF7$  mutations and NMT clusters away from the tumour groups. Moreover, hierarchical clustering presented 663 proteins significantly differentially expressed across all groups based on relative expression values. Protein cluster numbers are shown on the left-hand side in different colours and numbered 1-6. Partial lists of proteins upregulated in each sample group are detailed in blue on the right-hand side. One-way ANOVA was carried out among four groups ( $AKT1^{E17K}/TRAF7$ ,  $KLF4^{K409Q}/TRAF7$ ,  $NF2^{-/-}$  and NMT), Benjamini-Hochberg adjusted  $p < 0.05$ . Clustering was created using Perseus 1.6.2.3 software.



### 3.3.3 Hierarchical clustering of differentially expressed proteins across meningioma sample groups

Analysis of variance (ANOVA) was performed to determine statistical significance identified 663 significantly differentially expressed proteins between meningioma subtypes and NMT (Benjamini-Hochberg adjusted  $p$ -value  $<0.05$ ). Hierarchical clustering of these 663 proteins showed six distinct clusters, the purple one of which (cluster 2, Fig-14) include 144 proteins that are specifically more highly expressed in meningioma with *AKT1<sup>E17K</sup>/TRAF7* mutations and a red cluster (cluster 3) showed a total of 84 proteins significantly upregulated in *KLF4<sup>K409Q</sup>/TRAF7* mutant meningioma. On the other hand, a small blue cluster (cluster 5) comprised of only 23 proteins, is highly expressed in *NF2<sup>-/-</sup>* mutant subtypes but demonstrate reduced expression in *AKT1<sup>E17K</sup>/TRAF7* and *KLF4<sup>K409Q</sup>/TRAF7* mutant subtypes and normal meninges (Fig-14). In contrast, a yellow cluster (cluster 6) showed overexpressed proteins were shared across the meningioma mutant groups (*NF2<sup>-/-</sup>* and *AKT1<sup>E17K</sup>/TRAF7*) and normal meninges (Fig-14) while those proteins were downregulated in *KLF4<sup>K409Q</sup>/TRAF7* mutant subtypes.

*AKT1<sup>E17K</sup>/TRAF7* mutant subtypes clusters (cluster 2) showed a significant increase in Pyruvate Carboxylase that may be associated with the TCA cycle and pyruvate metabolism; NADH dehydrogenase sub-complexes (NDUFB1, NDUFB3, NDUFA7 and NDUB8) and COX assembly mitochondrial protein homolog (CMC1), involved in regulating the electron-transport chain.

*KLF4<sup>K409Q</sup>/TRAF7* mutant subtypes associated cluster showed upregulation of Endoglin (a membrane glycoprotein) is a part of the TGF beta receptor complex; E-cadherin-1, a calcium ion binding protein plays a part in adherence junction; and Anion exchange protein 2 (AE2) involved in ion exchange and chloride transmembrane transporter activity (<https://www.proteinatlas.org/ENSG00000164889-SLC4A2>).

On the other hand, the *NF2<sup>-/-</sup>* mutant subtype cluster showed increases in ANAX3 (Annexin-3), a calcium ion binding protein; tubulin alpha 1 beta chain (Guanyl ribonucleotide binding protein), show GTPase activity and tubulin beta chain involved in hydrolase activity. Other proteins showing reduced expression in all meningioma subtypes were oxidoreductase enzyme AOC3 (membrane primary amine oxidase protein), VWF (Von Willebrand Factor) and FGF1 (Fibroblast Growth Factor 1).

### 3.4 Meningiomas with *AKT1<sup>E17K</sup>/TRAF7* mutations

#### 3.4.1 Meningioma with *AKT1<sup>E17K</sup>/TRAF7* mutational subtype-specific protein analysis

A two-sample *t*-test (volcano plot) was performed to identify differentially expressed protein candidates (DEPs) between the meningioma mutational subtypes and normal meninges (a similar analysis was carried out by Dunn *et al.*, (2019) (Fig-15). Proteins with  $\log_2 \text{FC} \geq 1$ ;  $p < 0.05$  were considered as significantly upregulated and proteins with  $\log_2 \text{FC} \leq -1$ ;  $p < 0.05$  as significantly downregulated. Comparative analysis between *AKT1<sup>E17K</sup>/TRAF7* meningioma subtypes and NMT identified 1100 significantly differentially expressed proteins; among them, 583 proteins were upregulated and 503 proteins were downregulated in *AKT1<sup>E17K</sup>/TRAF7* subtypes compared to NMT control (Fig-15 A). Proteins demonstrating the highest fold changes and thus most highly upregulated in *AKT1<sup>E17K</sup>/TRAF7* mutants compared to NMT include THSD4, S26A2 or sulphate transporter, pyruvate carboxylase, CLIC3 (chloride intracellular channel protein 3), GMDS (metabolic enzyme), PTGFRN (Prostaglandin F2 Receptor Negative Regulator), cell adhesion proteins, mitochondrial electron transporter (NDUB7, NDUB6 and COX1) and CRABP2 which is involved in transport retinoic acid to the nucleus glutathione metabolic process, may play a role in retinoid signalling pathway and an unfavourable prognostic marker in renal and endometrial cancer (The human protein atlas: <https://www.proteinatlas.org/>).

Differential analysis between the two mutational subtypes, *AKT1<sup>E17K</sup>/TRAF7* and *NF2<sup>-/-</sup>* showed a total of 835 significantly differentially expressed proteins. Among these 766 proteins were upregulated in the *AKT1<sup>E17K</sup>/TRAF7* mutational subtype while 46 proteins were downregulated compared to the *NF2<sup>-/-</sup>* meningiomas (Fig-15 B). Upregulated proteins observed in *AKT1<sup>E17K</sup>/TRAF7* mutant subtypes including Disks large homolog 3, sulphate transporter, Retinol-binding protein 1, CLIC3 and Synaptogyrin 1, a favourable prognostic marker in renal and pancreatic cancer (The human protein atlas: <https://www.proteinatlas.org/>). On the other hand, downregulated proteins in *AKT1<sup>E17K</sup>/TRAF7* mutant subtypes include myosin-10, Annexin-3, Heat shock protein 70 kDa, and Lim-2 cysteine rich domains protein 1.

In contrast, a comparison between *AKT1<sup>E17K</sup>/TRAF7* and *KLF4<sup>K409Q</sup>/TRAF7*, identified 1195 proteins to be significantly differentially expressed, among them only 1048 proteins upregulated in *AKT1<sup>E17K</sup>/TRAF7* mutant subtypes and 123 proteins that were significantly downregulated compared to the *KLF4<sup>K409Q</sup>/TRAF7* (Fig-15 C). Here, CRABP2 (Cellular retinoic acid binding protein 2) was identified as the most significantly differentially expressed protein

with the highest  $\log_2$  FC, suggesting this protein to be highly specific to the *AKT1<sup>E17K</sup>/TRAF7* mutational subtype. In addition to this, several potentially interesting proteins including Histamine N- Methyltransferase, Quinone oxidoreductase PIG3, CLIC3, and NDUA7 (NADH dehydrogenase [ubiquinone] 1 alpha sub complex subunit 7) showed a similar trend upon comparative analysis with  $\log_2$  FC $\geq$ 3 specific to the *AKT1<sup>E17K</sup>/TRAF7* mutational subtype. However, the fibrinogen beta chain, Histone H1.0 and CD44 antigen showed reduced expression in *AKT1<sup>E17K</sup>/TRAF7* mutational subtype compared to *KLF4<sup>K409Q</sup>/TRAF7* mutant meningioma (Fig-15 C).

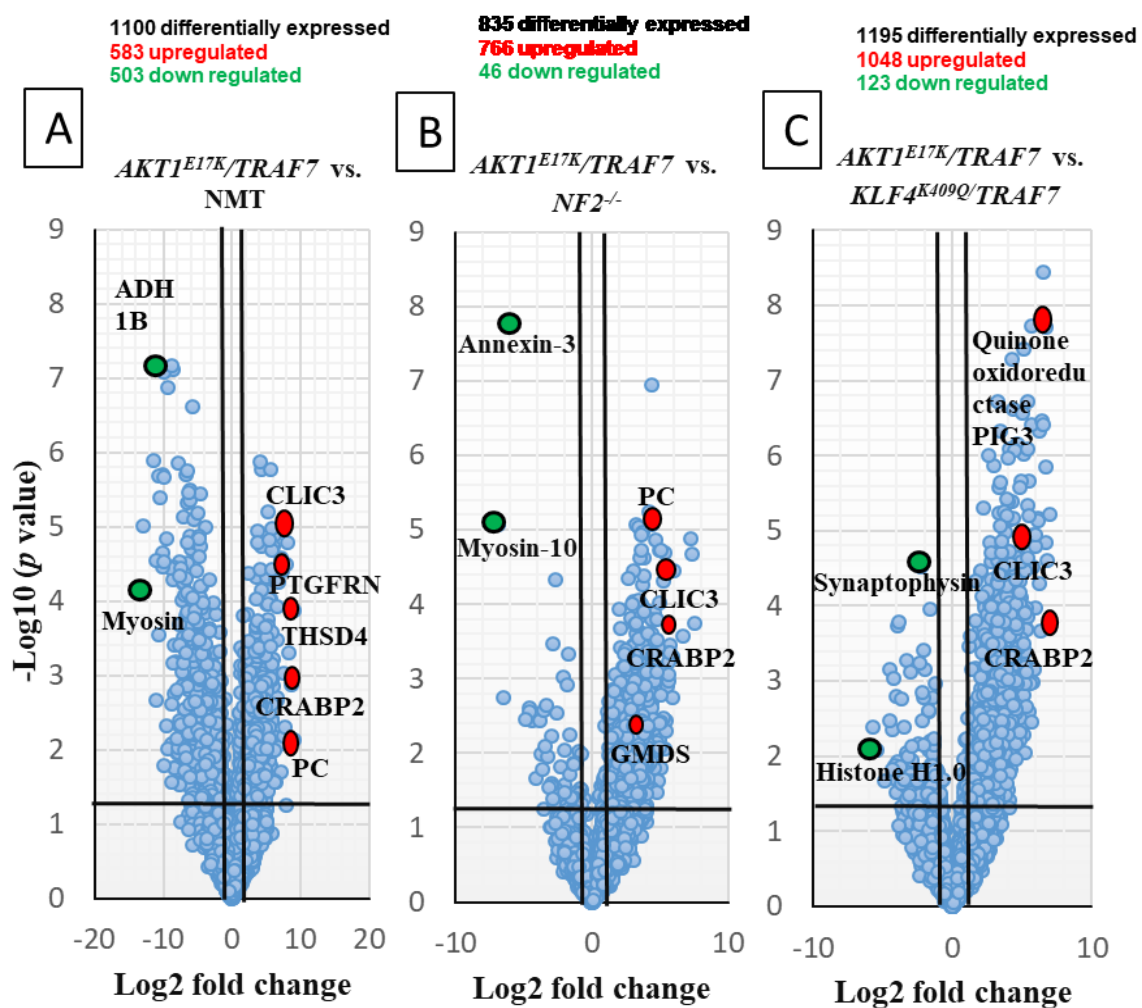


**Figure 15: Differential protein expression between sample groups.** Volcano plots of protein abundance between the mutational subtypes of meningioma and normal meningeal tissue (A, B, C). Depicted are  $\log_2$  fold changes vs.  $-\log_{10}$   $p$ -values (Student's  $t$ -test between replicate measurements). Black lines demarcate  $p$ -value < 0.05 and  $\log_2$  fold change of 1 and -1. Red dots: Upregulated proteins ( $\log_2$  FC $\geq$  1;  $p$ -value < 0.05). Green dots: Downregulated proteins ( $\log_2$  FC $\leq$  -1;  $p$ -value < 0.05). Highlighted proteins may be considered potential biomarker

candidates for further experimental validation. A) Comparative analysis between *AKT1<sup>E17K</sup>/TRAF7* meningioma subtypes vs. NMT. B) Differential analysis between two meningioma mutational subtypes *AKT1<sup>E17K</sup>/TRAF7* vs. *NF2<sup>-/-</sup>*. C) Comparative analysis between *AKT1<sup>E17K</sup>/TRAF7* and *KLF4<sup>K409Q</sup>/TRAF7*.

### 3.4.2 Distinct and overlapping proteins in meningioma with *AKT1<sup>E17K</sup>/TRAF7* mutational subtypes

Venn diagrams were used to determine distinct differential expression of proteins (upregulated and downregulated) in *AKT1<sup>E17K</sup>/TRAF7* meningioma subtypes as compared to *NF2<sup>-/-</sup>*, *KLF4<sup>K409Q</sup>/TRAF7* and NMT. Three data sets (*AKT1<sup>E17K</sup>/TRAF7* vs. NMT, *AKT1<sup>E17K</sup>/TRAF7* vs. *NF2<sup>-/-</sup>* and *AKT1<sup>E17K</sup>/TRAF7* vs. *KLF4<sup>K409Q</sup>/TRAF7*) were overlapped. Fold change criteria were set as follows: proteins demonstrating  $\log_2 FC \geq 1$ ;  $p < 0.05$  were considered as significantly upregulated and proteins with  $\log_2 FC \leq -1$ ;  $p < 0.05$  as significantly downregulated (Fig- 15). Overlapping data sets were visually represented in Venn diagrams (Fig-16).

From overlapping data sets, 162 proteins were revealed as commonly significantly upregulated in *AKT1<sup>E17K</sup>/TRAF7* mutant meningioma subtypes and only three proteins were commonly downregulated compared to the *NF2<sup>-/-</sup>* and *KLF4<sup>K409Q</sup>/TRAF7* meningioma subtypes and NMT (Fig-16 A and B). Partial list of commonly upregulated and a complete list downregulated proteins in *AKT1<sup>E17K</sup>/TRAF7* meningioma subtypes can be found in table -7 and 8 and the complete list of upregulated proteins can be found in appendix table- 1.

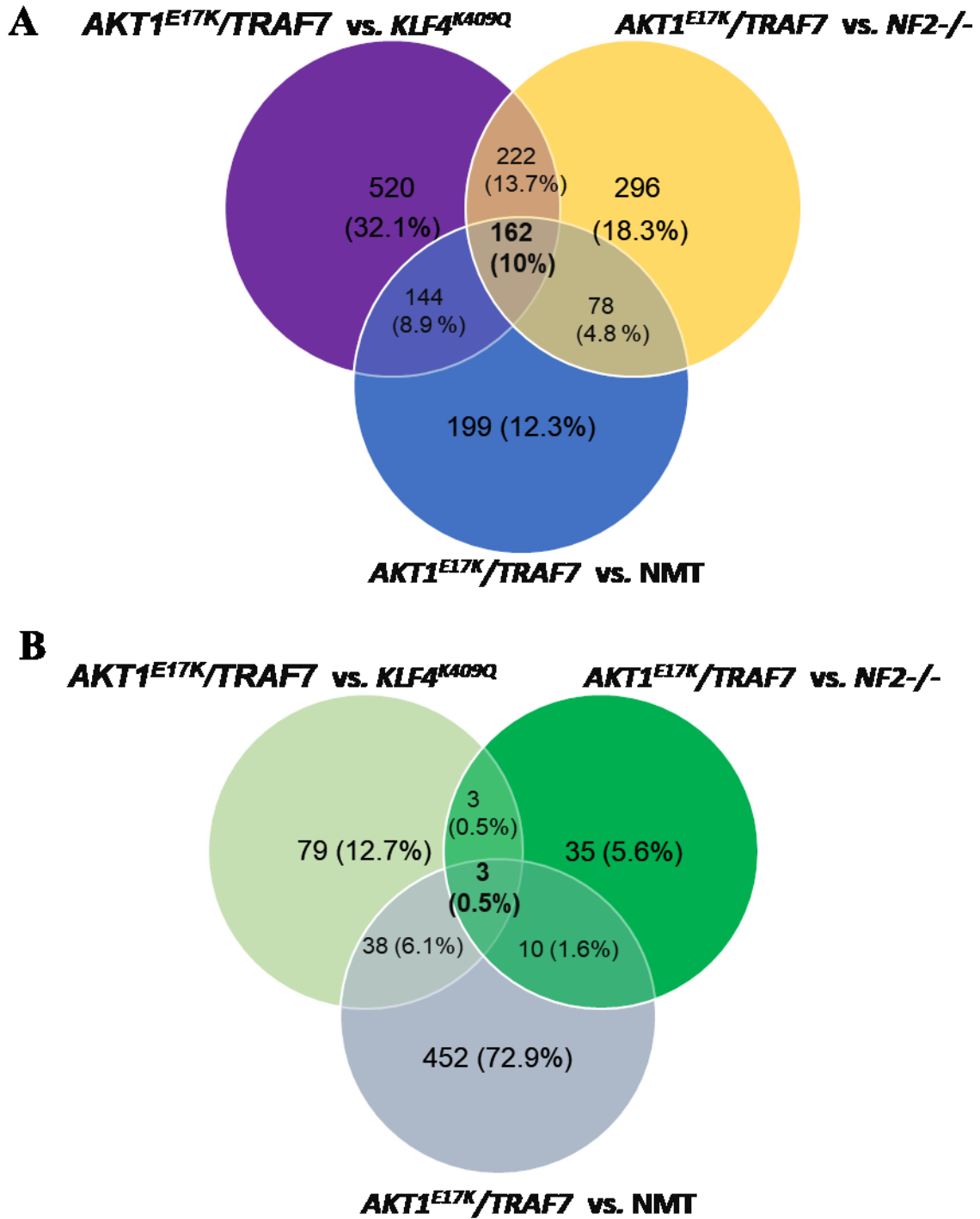


**Figure 16:** *AKT1<sup>E17K</sup>/TRAF7* mutational subtype-specific proteins. (A) Venn diagram illustrating the distinct and overlapping 162 upregulated proteins from differential expression analysis unique to the *AKT1<sup>E17K</sup>/TRAF7* mutational meningioma subtype. (B) Venn diagram illustrating the distinct and overlapping only three downregulated proteins from differential expression analysis unique to the *AKT1<sup>E17K</sup>/TRAF7* mutational meningioma subtype. Upregulated proteins ( $\log_2 \text{FC} \geq 1$ ;  $p\text{-value} < 0.05$ ). Downregulated proteins ( $\log_2 \text{FC} \leq -1$ ;  $p\text{-value} < 0.05$ ). Significance determined by Student's *t*-test.

Uniprot ID	Protein name	Log2 FC <i>AKT1<sup>E17K</sup>/TRAF7</i> vs. NMT	<i>P-value</i> <i>AKT1<sup>E17K</sup>/TRAF7</i> vs. NMT	Log2 FC <i>AKT1<sup>E17K</sup>/TRAF7</i> vs. <i>NF2<sup>-/-</sup></i>	<i>P-value</i> <i>AKT1<sup>E17K</sup>/TRAF7</i> vs. <i>NF2<sup>-/-</sup></i>	Log2 FC <i>AKT1<sup>E17K</sup>/TRAF7</i> vs. <i>KLF4<sup>K409Q</sup>/TRAF7</i>	<i>P-value</i> <i>AKT1AKT1<sup>E17K</sup>/TRAF7</i> vs. <i>KLF4<sup>K409Q</sup>/TRAF7</i>
A0A024R5C5	Pyruvate carboxylase (PC)	8.998	0.007346	4.969	0.006696	4.795	0.003284
O95833	Chloride intracellular channel protein 3 (CLIC3)	8.302	0.000489	5.460	0.003681	5.947	0.000105
A0A024RC61	Aminopeptidase	8.060	1.66E-05	4.202	0.000899	3.062	0.001302
Q96FL8	Multidrug and toxin extrusion protein 1	7.764	0.004934	4.410	0.002489	3.530	0.01284
P29373	Cellular retinoic acid-binding protein 2 (CRABP 2)	7.286	3.99E-05	4.803	0.007235	7.042	0.000192
Q53FA7	Quinone oxidoreductase PIG3	7.088	2.65E-05	2.212	0.004485	6.720	1.42E-06
O60547	GDP-mannose 4,6 dehydratase (GMDS)	6.109	4.15E-05	3.222	0.016223	2.901	0.008747
Q92542	Nicastrin	6.013	0.001413	3.139	0.013796	4.408	0.002519
Q6FGU2	DTYMK protein (Fragment)	5.960	1.81E-05	3.027	0.022986	2.937	0.000451
Q9BUH6	Protein PAXX	5.922	0.00116	3.220	0.020508	4.244	0.000599

**Table: 7** A partial list of significantly upregulated proteins common to *AKT1<sup>E17K</sup>/TRAF7* mutational subtype. Table showing a partial list of overlapping 162 upregulated proteins from differential expression analysis unique to the *AKT1<sup>E17K</sup>/TRAF7* mutational meningioma subtype detected via VENNY 2.1. Upregulated proteins ( $\log_2$  FC  $\geq$  1;  $p$ -value  $<$  0.05). Significance is determined by Student's  $t$ -test.

Uniprot ID	Protein name	Log2 FC <i>AKT1<sup>E17K</sup>/</i> <i>TRAF7</i> vs. NMT	<i>P</i> -value <i>AKT1<sup>E17K</sup>/</i> <i>TRAF7</i> vs. NMT	Log2 FC <i>AKT1<sup>E17K</sup>/</i> <i>TRAF7</i> vs. <i>NF2<sup>-/-</sup></i>	<i>P</i> -value <i>AKT1<sup>E17K</sup>/</i> <i>TRAF7</i> vs. <i>NF2<sup>-/-</sup></i>	Log2 FC <i>AKT1<sup>E17K</sup>/</i> <i>TRAF7</i> vs. <i>KLF4<sup>K409Q</sup></i> <i>/TRAF7</i>	<i>P</i> -value <i>AKT1AKT1<sup>E17K</sup>/</i> <i>TRAF7</i> vs. <i>KLF4<sup>K409Q</sup></i> <i>/TRAF7</i>
P12429	Annexin A3	-3.62737	0.016948	-6.09623	1.77E-08	-3.66919	0.001714
B7Z3I9	Delta-aminolevulinic acid dehydratase	-2.34556	0.004885	-1.35611	0.043625	-1.54507	0.025959
Q7Z7G0	Target of Nesh-SH3	-9.36123	1.32E-07	-4.51873	0.002774	-2.20294	0.026617

**Table: 8** A complete list of significantly downregulated proteins common to *AKT1<sup>E17K</sup>/TRAF7* mutational subtype. Table showing a complete list of overlapping three downregulated proteins from differential expression analysis unique to the *AKT1<sup>E17K</sup>/TRAF7* mutational meningioma subtype detected via VENNY 2.1. Downregulated proteins ( $\log_2 \text{FC} \leq -1$ ;  $p\text{-value} < 0.05$ ). Significance is determined by Student's *t*-test.

### 3.4.3 Functional annotation enrichment analysis of *AKT1<sup>E17K</sup>/TRAF7* mutational meningioma subtypes

To better understand the biology of each meningioma mutational and their differentially expressed proteins, the distribution of protein abundance within gene ontology (GO) categories (Biological Process', 'Molecular Function' and 'Cellular Component') was carried out. The functional annotation tool DAVID (Database for Annotation, Visualization and Integrated Discovery) was used to understand the potential biological significance of these proteins associated with diverse physiological pathways and their connection with meningioma pathophysiology. Following submission of a gene list, DAVID maps the genes of interest to related gene ontology terms and subsequently presents which of these terms are statistically enriched (Huang da *et al.*, 2009). Histograms illustrating significantly enriched GO terms in fold enrichment are shown in Figure-17 and 18. For this study, upregulated proteins specific to mutational meningioma subtypes were further investigated because their abundance may make them easier to target as a biomarker or in to discover molecular targets. However, in the future, downregulated proteins will also need to be investigated to further expand our knowledge of the molecular pathogenesis of meningiomas.

### 3.4.4 Functional annotation enrichment analysis of *AKT1<sup>E17K</sup>/TRAF7*-specific upregulated proteins

162 commonly upregulated proteins specific to *AKT1<sup>E17K</sup>/TRAF7* mutant meningiomas were subjected to GO enrichment analysis using DAVID. Cellular component analysis indicated significant numbers of the commonly upregulated proteins belonging to the extracellular exosome, while some were mitochondrial, cytoplasmic, and membranous proteins and only a few reside as mitochondrial inner proteins (Fig-17). Additionally, DAVID analysis revealed the association of *AKT1<sup>E17K</sup>/TRAF7* mutant meningioma signature proteins with different biological processes including negative regulation of proteasomal ubiquitin-dependent protein catabolic process (22.78 fold), endocytic recycling (15.6 fold), mitochondrial electron transport, NADH to ubiquinone (10.2 fold), chloride transport (9.3 fold), mitochondrial respiratory chain complex I assembly (7.9 fold) and positive regulation of cell growth (5.9 fold). Biological process analysis revealed that *AKT1<sup>E17K</sup>/TRAF7* mutant meningioma signature proteins, such as NDUFB7, NDUFB8, NADH dehydrogenase (ubiquinone) 1 alpha subcomplex 5 and NADH dehydrogenase (ubiquinone) 1 beta subcomplex 1 are highly enriched in both mitochondrial electron transport, NADH to ubiquinone and mitochondrial respiratory chain complex I assembly processes results suggesting that targeting these proteins could be a potential biomarker for *AKT1<sup>E17K</sup>/TRAF7* mutant meningioma. In addition to this, GO analysis showed that *AKT1<sup>E17K</sup>/TRAF7* mutant specific CLIC3 protein was highly enriched in two biological processes; chloride transport and chloride transmembrane transport. These results suggest that targeting CLIC3 could be a potential biomarker for *AKT1<sup>E17K</sup>/TRAF7* mutant meningioma (Fig-17).

Molecular function analysis indicated *AKT1<sup>E17K</sup>/TRAF7* mutant meningioma specific proteins are significantly enriched in voltage-gated ion channel activity (12.08 fold), NADH dehydrogenase ubiquinone (10.73 fold), metallopeptidase activity (6 .36 fold), cadherin binding involved in cell-cell adhesion (3.99 fold), GTPase activity (3.30 fold) and protein binding (1.28) fold). However, the highest number of proteins showed involvement in protein binding including pyruvate carboxylase, CLIC3, and cellular retinoic acid-binding protein 2, while 9 proteins were associated with cadherin binding involved in cell-cell adhesion (Fig-17).



Collectively, these results indicate that most *AKT1<sup>E17K</sup>/TRAF7* mutant meningioma subtype signature proteins are involved in protein folding, mitochondrial electron transport, chloride transmembrane transport, and voltage-gated ion channel activity.

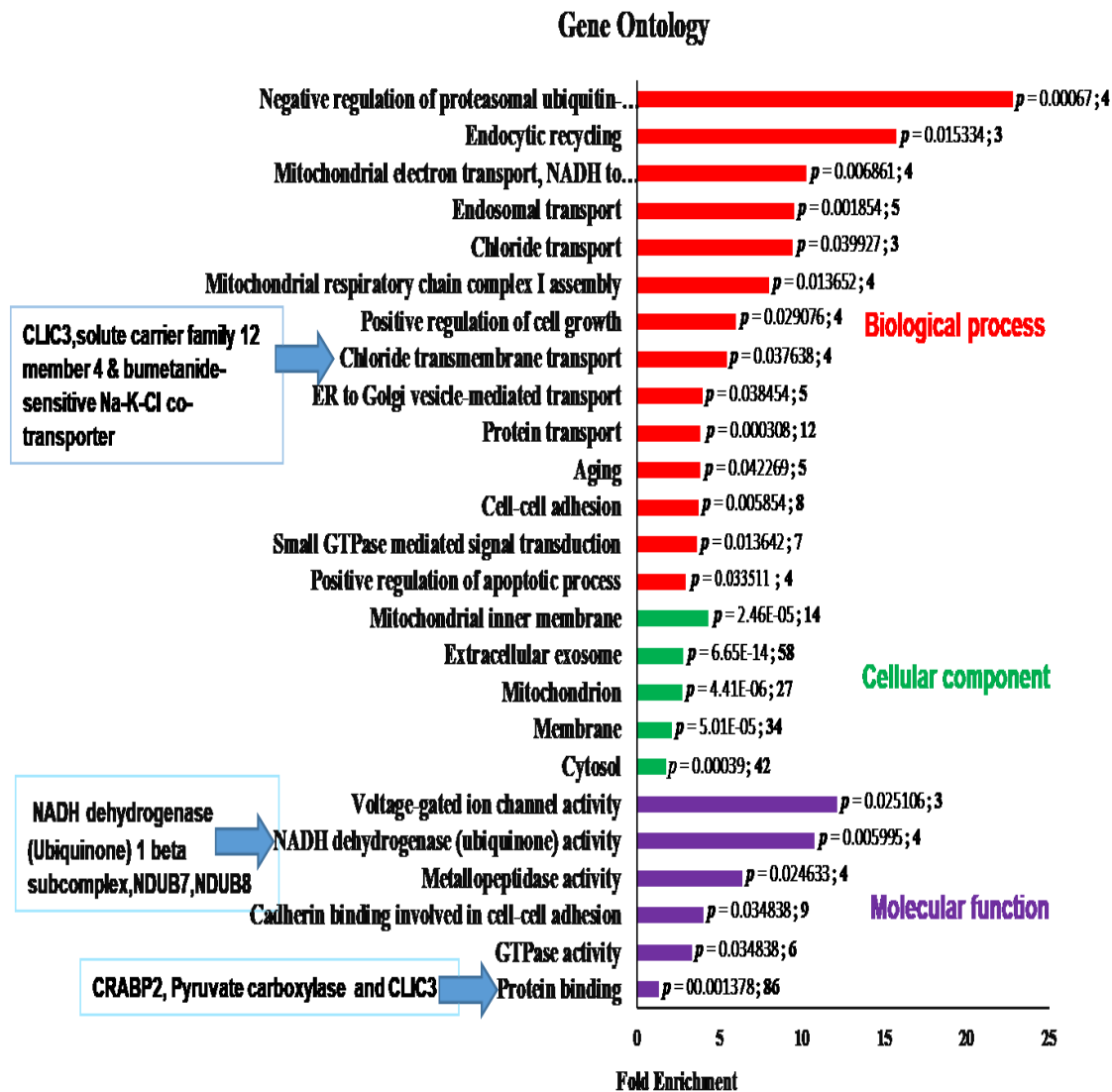


**Figure 17: Functional annotation enrichment analysis of *AKT1<sup>E17K</sup>/TRAF7*-specific upregulated proteins.** Gene Ontology (GO) enrichment analysis of 162 significantly upregulated *AKT1<sup>E17K</sup>/TRAF7*-specific proteins. GO analysis was performed using DAVID v6.8. Fold enrichment relative to the *H. sapiens* proteome is displayed on the x-axis. Terms containing at least three proteins with  $p < 0.05$  value and number of proteins are shown. Gene ontologies representing molecular function are presented in purple, cellular components in green and biological process in red.

Functional pathway analysis by DAVID, identified only five pathways under KEGG (Kyoto encyclopaedia of genes and genomes) including oxidative phosphorylation, metabolic pathway, Huntington's disease pathway, Parkinson's disease and endocytosis (Fig-18), with the highest number of proteins (24) occurring in the metabolic pathway comprised of pyruvate

carboxylase, amino-peptidase, GMDS, NDUFB1 and NDUFB8 proteins. Further analysis of the metabolic pathway may enable us to identify potential therapeutic targets in *AKT1<sup>E17K</sup>/TRAF7* mutant meningioma subtype. Additionally, KEGG pathway enrichment analysis also revealed that *AKT1<sup>E17K</sup>/TRAF7* mutant meningioma subtype-specific proteins (COX6B1, NDUFA5, NDUFB7, NDUFB1, NDUFB8 and ATPK) were highly enriched within the oxidative phosphorylation pathway which would be interesting for future research in this field.

KEGG Pathway analysis by DAVID suggests that most *AKT1<sup>E17K</sup>/TRAF7* mutant meningioma subtype signature proteins (24 proteins) such as pyruvate carboxylase, GMDS, COX6B1 are involved in metabolic pathways.

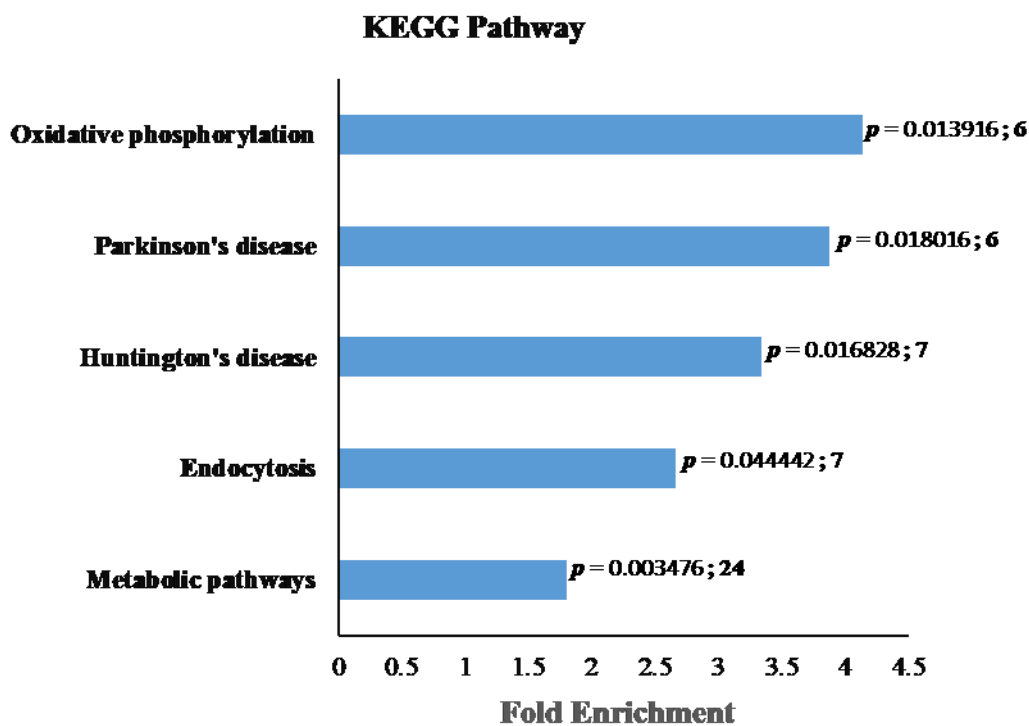


**Figure 18:** KEGG pathways analysis via DAVID shows upregulated proteins in *AKT1<sup>E17K</sup>/TRAF7* mutant meningioma subtype are mostly found in metabolic pathways and oxidative phosphorylation terms. GO analysis was performed using DAVID v6.8. Fold enrichment relative to the *H. sapiens* proteome is displayed on the x-axis. Terms containing at least three proteins with  $p < 0.05$  value and number of proteins are shown.

Unfortunately, due to the low number of unique proteins commonly significantly down-regulated in *AKT1<sup>E17K</sup>/TRAF7* mutant meningioma, it was not possible to carry out GO analysis for downregulated proteins by DAVID.

### 3.4.5 *AKT1<sup>E17K</sup>/TRAF7* mutant meningioma subtype-specific IPA pathway analysis

To increase confidence in our pathway analysis, ingenuity pathway analysis (IPA) was performed in three differential expression data set (*AKT1<sup>E17K</sup>/TRAF7* vs. NMT, *AKT1<sup>E17K</sup>/TRAF7* vs. *NF2<sup>-/-</sup>* and *AKT1<sup>E17K</sup>/TRAF7* vs. *KLF4<sup>K409Q</sup>/TRAF7*) and balloon plots generated (Fig 19). In total, 373 enriched canonical pathways were detected using IPA from differential expression data set with the complete list of IPA canonical pathways will be found in the supplementary data (S2). Among these, only 82 enriched canonical pathways were detected at thresholds  $-\log_{10}(P\text{-value}) > 3$ , Upregulated pathways ( $Z\text{-score} \geq 3$ ) marked by reddish to the yellowish scale (red arrow); Downregulated pathways ( $Z\text{-score} \leq -3$ ) marked by purple to blackish dot in the balloon plot (Fig-19). From the IPA analysis balloon plot, ‘Oxidative phosphorylation pathway’ showed the highest ranked among the signalling pathways with  $-\log_{10}(P\text{-value})$  ranges from  $>6.5$  to 15.05 and  $Z\text{-score}$  ranges from  $\geq 4.1$  to 5.19. In addition to this, the oxidative phosphorylation pathway is the only pathway that is always activated or upregulated in *AKT1<sup>E17K</sup>/TRAF7* mutant meningioma subtype whether compared with *NF2<sup>-/-</sup>*, *KLF4<sup>K409Q</sup>/TRAF7*, or NMT (Fig-19). Proteins such as COX6B1, ATPK (ATP synthase subunit f), NDUFA5, NDUFB7, NDUFB1 and NDUFB8 are overexpressed in the oxidative phosphorylation pathway. These results suggest that the oxidative phosphorylation pathway is a key pathway for meningiomas in the *AKT1<sup>E17K</sup>/TRAF7* mutant group.



**Figure 19:** A balloon plot showing IPA pathways analysis for three sets of differential expression data ( $AKT1^{E17K}/TRAF7$  vs.  $NF2^{-/-}$ ,  $AKT1^{E17K}/TRAF7$  vs.  $KLF4^{K409Q}/TRAF7$  and  $AKT1^{E17K}/TRAF7$  vs. NMT) together. Criteria were set to create balloon plot follows: pathways demonstrating  $-\log_{10}(P\text{-value}) > 3$ , Upregulated pathways ( $Z\text{-score} \geq 3$ ) marked by reddish to the yellowish dot; Downregulated pathways ( $Z\text{-score} \leq -3$ ) marked by purple to the blackish dot. The bigger the dot indicates the most significant pathways. IPA pathway analysis shows oxidative phosphorylation pathway is the most significantly upregulated in  $AKT1^{E17K}/TRAF7$  mutant meningioma subtype.

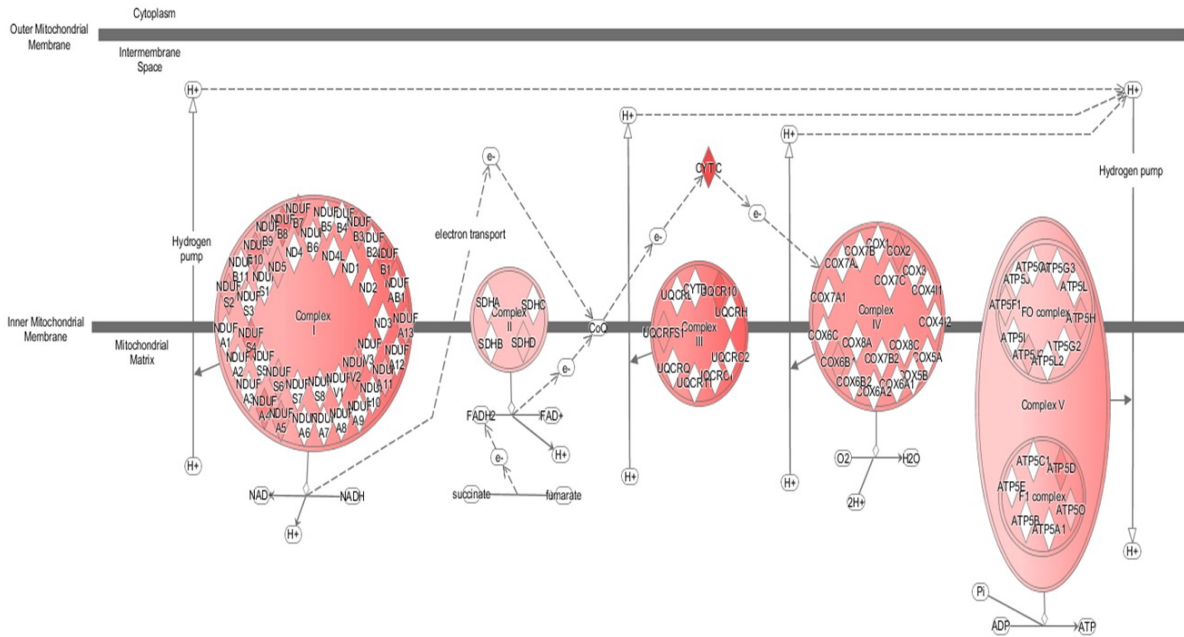


**Figure: 20** Illustrating *AKT1<sup>E17K</sup>/TRAF7* specific IPA canonical pathway analysis (oxidative phosphorylation pathway).

In both sets of pathway analysis (KEGG and IPA) it was observed that the oxidative phosphorylation pathway was highly enriched. Therefore, these results suggesting targeting and validation of this pathway for *AKT1<sup>E17K</sup>/TRAF7* mutant meningioma subtype would have the potential to suggest biomarkers or identify therapeutic targets. Unfortunately, due to samples limitations, this was out of the scope of this project and is a possibility for future work in this area.

### 3.4.6 Validation of protein candidates for *AKT1<sup>E17K</sup>/TRAF7* mutational meningioma subtypes

Following these mass-spectrometry data analyses, I have identified and quantified numerous proteins in mutant meningioma subtypes with the challenging task to determine which proteins should be chosen for further validation using alternative approaches. For selection, I considered different criteria including intensity or LFQ value, significant protein expression, fold change, number of peptides, and biological significance of the protein. Proteins with more than one peptide were our priority as candidates of choice however, proteins identified with only one peptide should not necessarily be discarded because they might be associated with essential biological pathways. Additionally, the proteins with subcellular location, involvement in targeted diseases and disorders from functional annotation analysis were also considered. After considering all these categories, I came up with several potential candidates for further validation in tissue (see Table 9).

Protein name	Fold change increase compared to <i>KLF4</i> <sup>K409Q</sup>	Fold change increase compared to <i>NF2</i> <sup>-/-</sup> mutant subtype	Fold change increase compared to normal (NMT)	Represented in functional annotation analysis
Pyruvate carboxylase	4.795141166	4.969	8.998654502	Metabolic pathways
Chloride intracellular channel protein 3	5.947419425	5.460	8.302536079	Chloride transmembrane transport
Cellular retinoic acid-binding protein 2	7.04222686	4.803	7.286500522	Protein binding
GDP-mannose 4,6 dehydratase	2.901418822	3.222457	6.109984	Metabolic pathways

**Table 9:** *AKT1*<sup>E17K</sup>/*TRAF7* mutant meningioma specific candidate's for validation with their fold change from differential expression analysis and functional annotation analysis.

For *AKT1*<sup>E17K</sup>/*TRAF7* mutant meningioma subtype, CRABP2 (cellular retinoic acid binding protein 2) and CLIC3 (chloride intracellular channel protein 3) always showed significant over-expression with the highest fold change and enriched in protein binding. Another two proteins, GMDS (GDP- mannose 4, 6 dehydratase) and PC (pyruvate carboxylase) were also significantly upregulated in *AKT1*<sup>E17K</sup>/*TRAF7* mutant meningioma and functional annotation analysis showed they were highly enriched in metabolic processes. In addition, significant proteins such as PC, CLIC3, and CRABP2 were identified with more than 50% sequence coverage using mass spectrometry (supplementary data- S3).

### 3.4.6.1 Validation of differential expression of proteins via Simple WES or Western Blot

Only a small number of samples and small amount of tissue lysates were left after mass-spectrometry sample analysis. Taking into consideration, to begin with, I wanted to prioritise the validation of potential target proteins as best as possible. I, therefore, started with the Simple Wes technique where only a few micrograms (0.5- 3 µg) of samples are required. Whilst still generating highly sensitive, reproducible and quantitative data that requires less time to detect compared to Western blot (Beekman *et al.*, 2018). However, the Simple wes assay limits the detection because the system is not fully developed to detect all commercially available antibodies yet. After initial validation of the antibody combinations, if the signal detection was good, I progressed with the Simple wes assay. Unfortunately, for the candidate proteins which were not able to be detected via Simple wes, the Western blot technique was used to validate those proteins in tissue lysates.

For the Simple wes assay, Vinculin was used as a loading control, as α-tubulin antibody did not show a signal in the Simple wes assay, and in some cases, the molecular weight of target protein and GAPDH (commonly used as a loading control) were very close. In addition to this, GAPDH gives noisy peaks and highly saturated bands which interfere with quantification.

From Simplex assay quantification, it was observed that CLIC3, CRABP2, and GMDS showed significant overexpression in *AKT1<sup>E17K</sup>/TRAF7* mutated meningioma compared to *NF2<sup>-/-</sup>*, *KLF4<sup>K409Q</sup>/TRAF7*, and NMT (Fig- 21 A, B and C). These observations agreed with Mass-spectrometry data analysis (Table 7). On the other hand, only one candidate protein pyruvate carboxylase was validated by Western blot and quantitative analysis showed significant overexpression in *AKT1<sup>E17K</sup>/TRAF7* compared to *NF2<sup>-/-</sup>* mutant meningioma. Whereas upregulated expression of pyruvate carboxylase was not significant but showed a trend towards a higher expression in *AKT1<sup>E17K</sup>/TRAF7* mutant meningioma compared to *KLF4<sup>K409Q</sup>/TRAF7* mutant meningioma and NMT (Fig- 21 D).

Unfortunately, we could not expand our validation to an independent cohort because of the rarity of this mutational meningioma tumour sample.

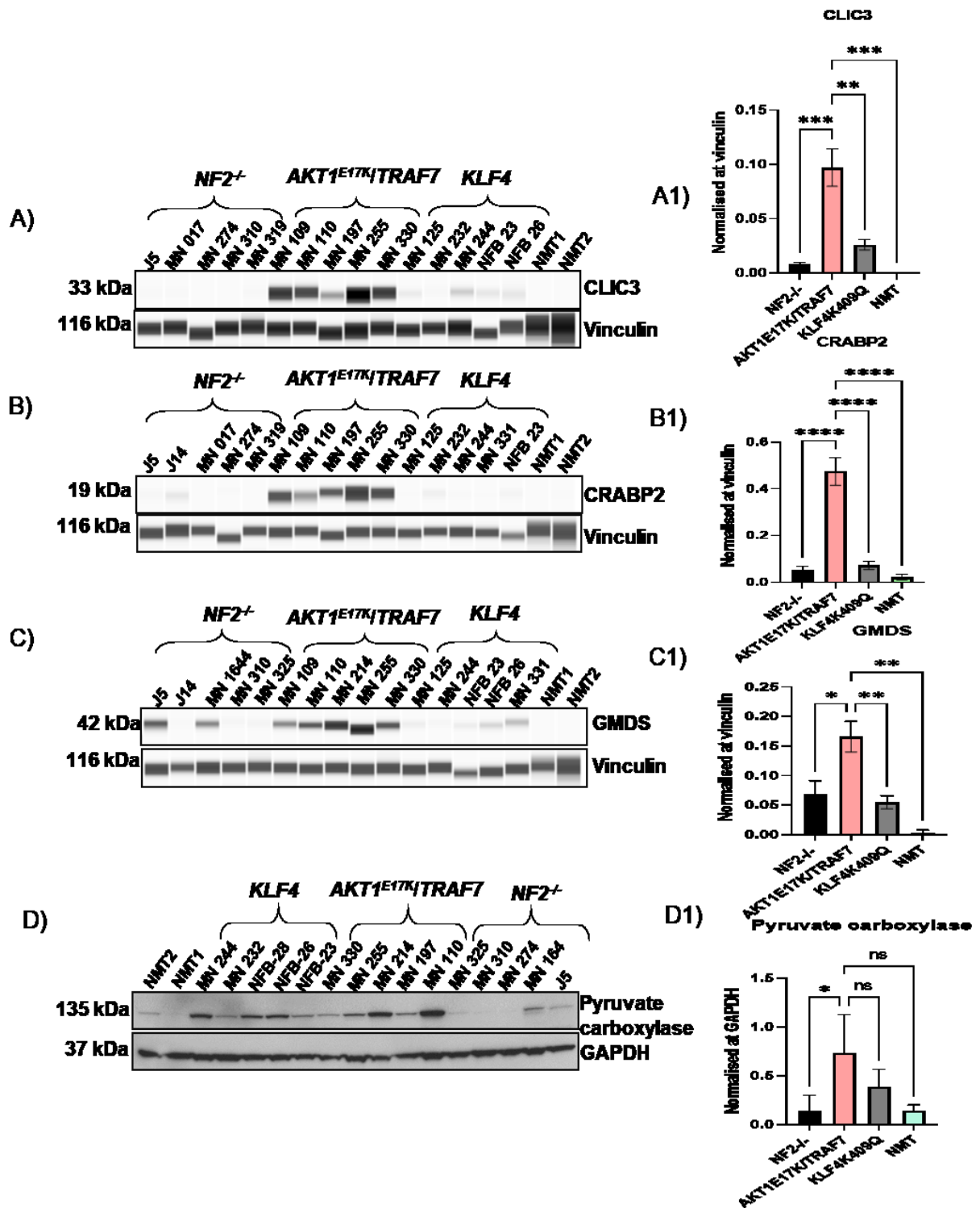


**Figure 21:** Validation of proteins identified as significantly upregulated in *AKT1*<sup>E17K</sup>/*TRAF7* vs. other mutational subtypes and NMT. (A, B, C and D) Western blot analysis of upregulated proteins in *AKT1*<sup>E17K</sup>/*TRAF7*, GAPDH and vinculin as loading control. NMT ( $n=2$ ); *NF2*<sup>-/-</sup> ( $n=5$ ), *AKT1*<sup>E17K</sup>/*TRAF7* ( $n=5$ ) and *KLF4*<sup>K409Q</sup> ( $n=5$ ). (A1, B1, C1 and D1) Histogram showing quantification of proteins (CLIC3, CRABP2, GMDS and Pyruvate Carboxylase) respectively. Data represented as  $\pm$ SEM and statistical significance One-way ANOVA is shown by: ns= not significant;  $p > 0.05$ ; \*  $p \leq 0.05$ ; \*\*  $p \leq 0.01$ ; \*\*\*  $p \leq 0.001$ ; \*\*\*\*  $p \leq 0.0001$ .



### 3.4.6.2 Immunohistochemistry of differentially regulated protein candidates for *AKT1<sup>E17K</sup>/TRAF7* mutant meningioma

I also carried out immunohistochemistry (IHC) to detect the biomarker candidates. Though the IHC technique is a semi-quantitative approach, it is routinely used in the clinical setting, unlike Western blot. Besides protein identification via the IHC technique, localisation can also be detected which strengthens the validation results and provides a more in-depth picture of the involvement of these proteins. The two normal meninges used as a control tissue throughout previous experiments (MS and WB) were not used for the immunohistochemistry approach. I have expanded the validation as an independent cohort by adding four different cases of normal meninges tissue section to validate the candidates. As with Western blot analysis, it was not possible to expand the validation to an independent cohort via IHC because the rarity of the mutated meningioma samples. Altogether I have used five tissue section slides per meningioma mutant group (*AKT1<sup>E17K</sup>/TRAF7*, *NF2<sup>-/-</sup>* and *KLF4<sup>K409Q</sup>/TRAF7*) and four different cases of NMT sections to verify our target proteins expression.

From immunohistochemistry average scoring analysis, it has been observed that *NF2<sup>-/-</sup>* mutant meningioma group and NMT showed weak immunostaining for pyruvate carboxylase which was mostly detected in the cytoplasm. These results showed a similar trend to Western blot analysis (Fig- 21 D; Fig- 22 A and Ba). On the other hand, *AKT1<sup>E17K</sup>/TRAF7* and *KLF4<sup>K409Q</sup>/TRAF7* mutant meningioma group both showed moderate staining for pyruvate carboxylase where only one sample from *AKT1<sup>E17K</sup>/TRAF7* meningioma group showing a weak immunoreaction (Fig- 22 Ba).

CRABP2 and GMDS showed a similar pattern in IHC staining, where the highest average score was observed in *KLF4<sup>K409Q</sup>/TRAF7* mutant meningioma and did not produce any clear differences among the meningioma mutational subtypes and NMT (Fig- 22 Bc and Bd). In addition, in IHC staining, both proteins were predominantly found in the cytoplasm (Fig-22 A). The staining results for CRABP2 and GMDS were not reflective of Western Blot and Mass-spectrometry analysis (Fig-21 B and C).

CLIC3 showed strong immunostaining across all meningioma mutant subtypes compared to NMT which showed a weak signal and was predominantly detected as focal nuclear and cytoplasmic (Fig-22 A). These results revealed distinct differences between *AKT1<sup>E17K</sup>/TRAF7* and NMT (Fig- 22 Bb).

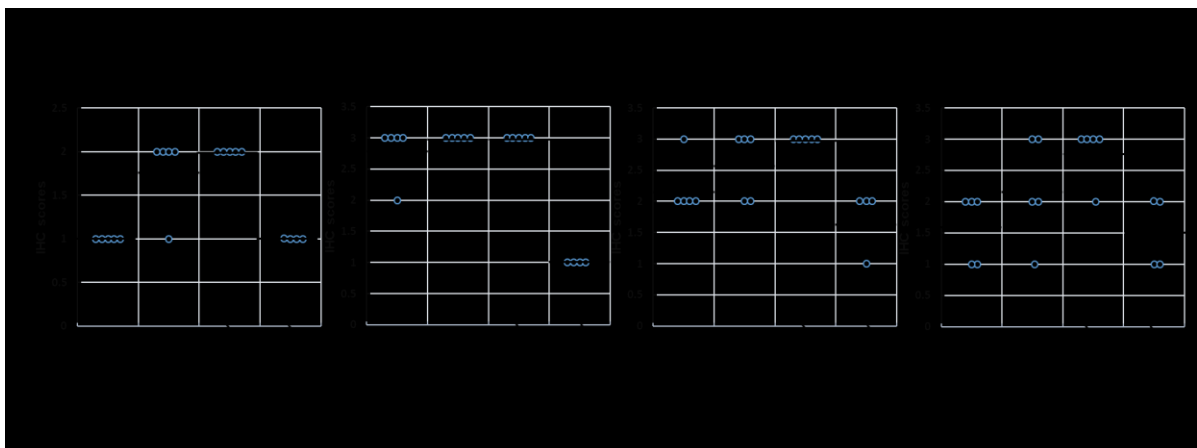
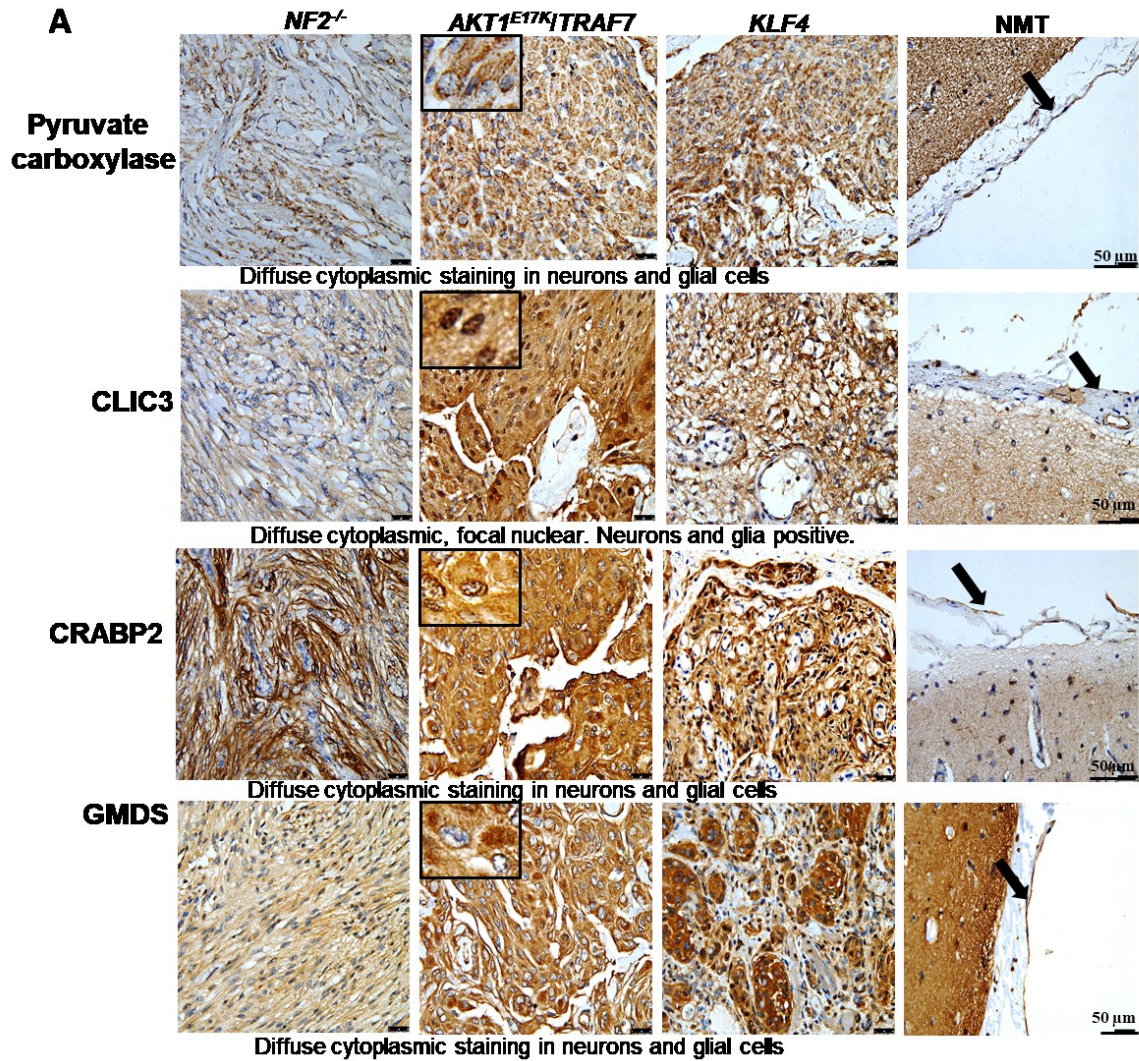


**Figure 22: Immunohistochemistry analysis of *AKT1<sup>E17K</sup>/TRAF7* specific candidate proteins.** A) Immunostaining images of pyruvate carboxylase, CLIC3, CRABP2 and GMDS in meningioma mutational subtypes and NMT at 40x magnification. B) Corresponding IHC scoring of pyruvate carboxylase, CLIC3, CRABP2 and GMDS (a, b, c, and d) respectively represent as mean calculated based on staining score shown in the black bold line for each group. Scoring criteria 0 = absent, 1= Weak, 2 = moderate and 3 = strong.

Unfortunately, I was unable to further examine the target proteins for functional validation due to the lack of a suitable meningioma model with *AKT1<sup>E17k</sup>* mutation. However, these results providing a foundation for the development of a new project providing possible directions for this validation by developing a new meningioma cell line holding this *AKT1<sup>E17k</sup>* point mutation.

### 3.5 Meningioma with *NF2<sup>-/-</sup>* mutations

#### 3.5.1 Meningioma with *NF2<sup>-/-</sup>* mutational subtype-specific protein analysis

A two-sample *t*-test (volcano plot) was performed to detect differentially expressed proteins in *NF2<sup>-/-</sup>* mutant meningioma versus other mutational meningioma subtypes and NMT. A total of 560 proteins were differentially expressed in comparison between *NF2<sup>-/-</sup>* and NMT, where only 68 proteins significantly upregulated ( $\text{Log}_2 \text{FC} \geq 1$ ;  $p < 0.05$ ) in *NF2<sup>-/-</sup>* mutant meningioma and 491 proteins downregulated ( $\text{Log}_2 \text{FC} \leq -1$ ;  $p < 0.05$ ) compared to NMT. Upregulated proteins with the highest fold change included; THSD4 (thrombospondin type 1 domain containing 4 may be involved in hydrolase activity), HLA-DRA (Human Leukocyte Antigen – DR isotype is a favourable prognostic marker in colorectal cancer) (<https://www.proteinatlas.org/ENSG00000204287-HLA-DRA>), Serpin peptidase inhibitor, Catenin delta-1 (a favourable prognostic marker in renal cancer, may involve in regulating cell adhesion) (<https://www.proteinatlas.org/ENSG00000198561-CTNND1>) and Solute carrier family 29 members 1 (a transmembrane glycoprotein involved in regulating the intake of nucleosides from the neighbouring cellular medium (<https://www.proteinatlas.org/ENSG00000197119-SLC25A29>)) (Fig-23 A).

Differential expression analysis between *NF2<sup>-/-</sup>* and *AKT1<sup>E17K</sup>/TRAF7* already explained in (Fig-15 B) and again created the image to show upregulated proteins in *NF2<sup>-/-</sup>* compared to *AKT1<sup>E17K</sup>/TRAF7* mutant meningioma (Fig-23 B). Annexin 3 (Calcium and phospholipid-binding protein may act as a phospholipase A2 inhibitor and also a favourable prognostic marker in renal cancer) (<https://www.proteinatlas.org/ENSG00000138772-ANXA3>), myosin 10 (a prognostic marker in renal and urethral cancer) (<https://www.proteinatlas.org/ENSG00000133026-MYH10>), target of Nesh-sh3, LIM and cysteine-rich domain and solute carrier family 29 and member 1 protein showed increased expression proteins in *NF2<sup>-/-</sup>* compared to *AKT1<sup>E17K</sup>/TRAF7* mutant meningioma.

On the other hand, differential analysis between *NF2<sup>-/-</sup>* and *KLF4<sup>K409Q</sup>* mutant meningioma by *t*-test volcano plot revealed that the expression of a total of 731 proteins were significantly different, among them 273 proteins were upregulated and 431 were downregulated in *NF2<sup>-/-</sup>*

mutant meningioma compared to the *KLF4<sup>K409Q</sup>* mutant meningioma group. In this case, upregulated proteins in *NF2<sup>-/-</sup>* mutant meningioma with the highest fold change comprised: fatty acid-binding protein 5, heat shock 70 kDa protein 12A (HS12A), four and half Lim Domains 1 variant, histamine N-methyl transferase, and myosin 10 (Fig-23 C).

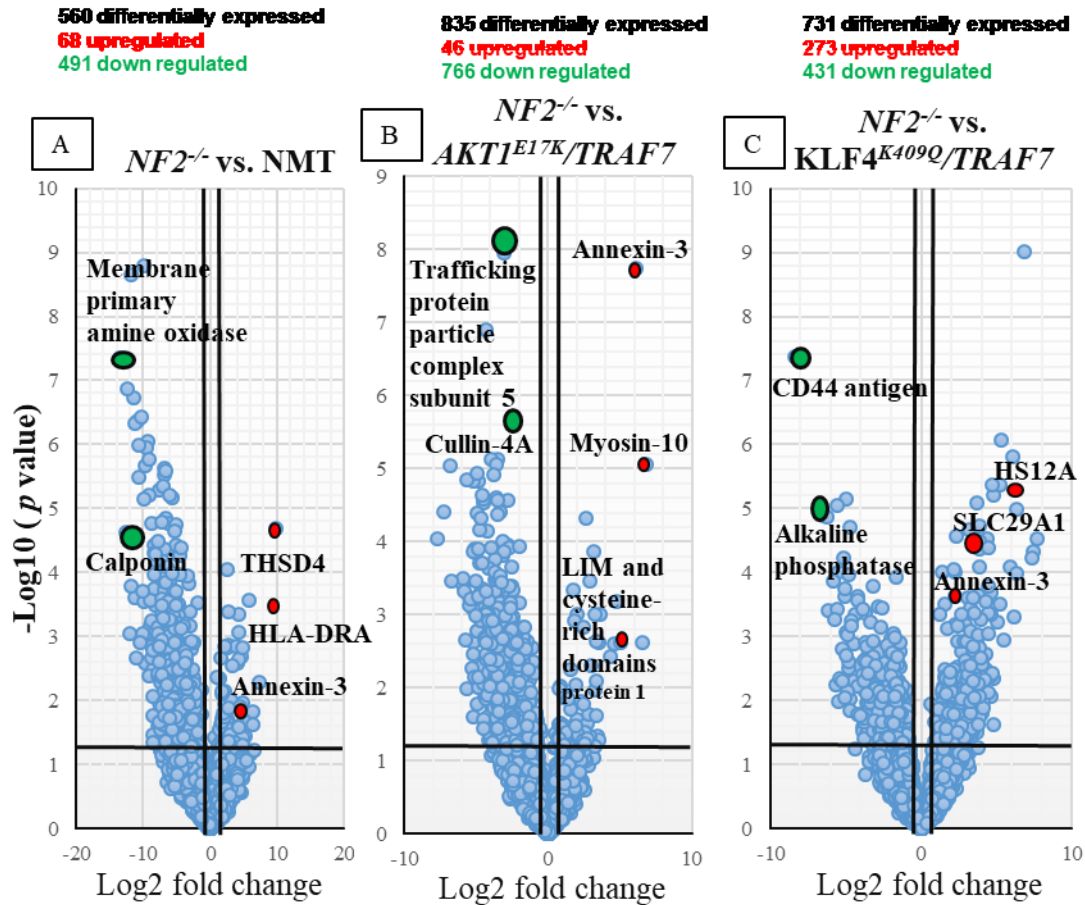


**Figure 23: Differential protein expression between sample groups.** Volcano plots of protein abundance between the mutational subtypes of meningioma and normal meningeal tissue (A, B and C). Depicted are  $\log_2$  fold changes vs.  $-\log_{10} p$ -values (Student's *t*-test between replicate measurements). Black lines demarcate  $p$ -value < 0.05 and  $\log_2$  fold change of 1 and -1. Red dots: Upregulated proteins ( $\log_2$  FC  $\geq$  1;  $p$ -value < 0.05). Green dots: Downregulated proteins ( $\log_2$  FC  $\leq$  -1;  $p$ -value < 0.05). Highlighted proteins may be considered potential biomarker candidates for future experimental validation.

### 3.5.2 Distinct and overlapping proteins in meningioma with *NF2*<sup>-/-</sup> mutational subtypes

Venn diagrams were used to determine distinct differential expression of proteins (upregulated and downregulated) in *NF2*<sup>-/-</sup> meningioma subtypes as compared to *AKT1*<sup>E17K</sup>/*TRAF7*, *KLF4*<sup>K409Q</sup>/*TRAF7*, and NMT. Three data sets (*NF2*<sup>-/-</sup> vs. NMT, *NF2*<sup>-/-</sup> vs. *AKT1*<sup>E17K</sup>/*TRAF7* and *NF2*<sup>-/-</sup> vs. *KLF4*<sup>K409Q</sup>/*TRAF7*) were overlapped. Fold change criteria were set as follows: proteins demonstrating  $\log_2 \text{FC} \geq 1$ ;  $p < 0.05$  were considered as significantly upregulated (Fig- 24 A) and proteins with  $\log_2 \text{FC} \leq -1$ ;  $p < 0.05$  as significantly downregulated (Fig- 24 B). Overlapping data sets were visually represented in Venn diagrams (Fig-24).

From overlapping data sets, only 7 proteins showed commonly significant overexpression while 54 proteins were commonly significantly downregulated in *NF2*<sup>-/-</sup> meningioma subtypes compared to the *AKT1*<sup>E17K</sup>/*TRAF7*, *KLF4*<sup>K409Q</sup>/*TRAF7* meningioma subtypes, and NMT (Fig-24 A and B). A complete list of commonly upregulated and a partial list downregulated proteins in *NF2*<sup>-/-</sup> meningioma subtypes can be found in table -10 and 11. Complete list of commonly significantly downregulated proteins in *NF2*<sup>-/-</sup> meningioma subtypes can be found in appendix table-2.

From the analysis of the overlapping data set, it was observed that the number of commonly significantly overexpressed proteins (162) were high in *AKT1*<sup>E17K</sup>/*TRAF7* meningioma subtypes compared to the number of commonly downregulated proteins (only 3) which is very low (Fig-16 A and B). On the other hand, an opposite trend was revealed in *NF2*<sup>-/-</sup> mutational meningioma subtypes while a higher number of commonly significantly down-regulated proteins (54) were identified compared to the number of overexpressed proteins (Fig-24 A and B).



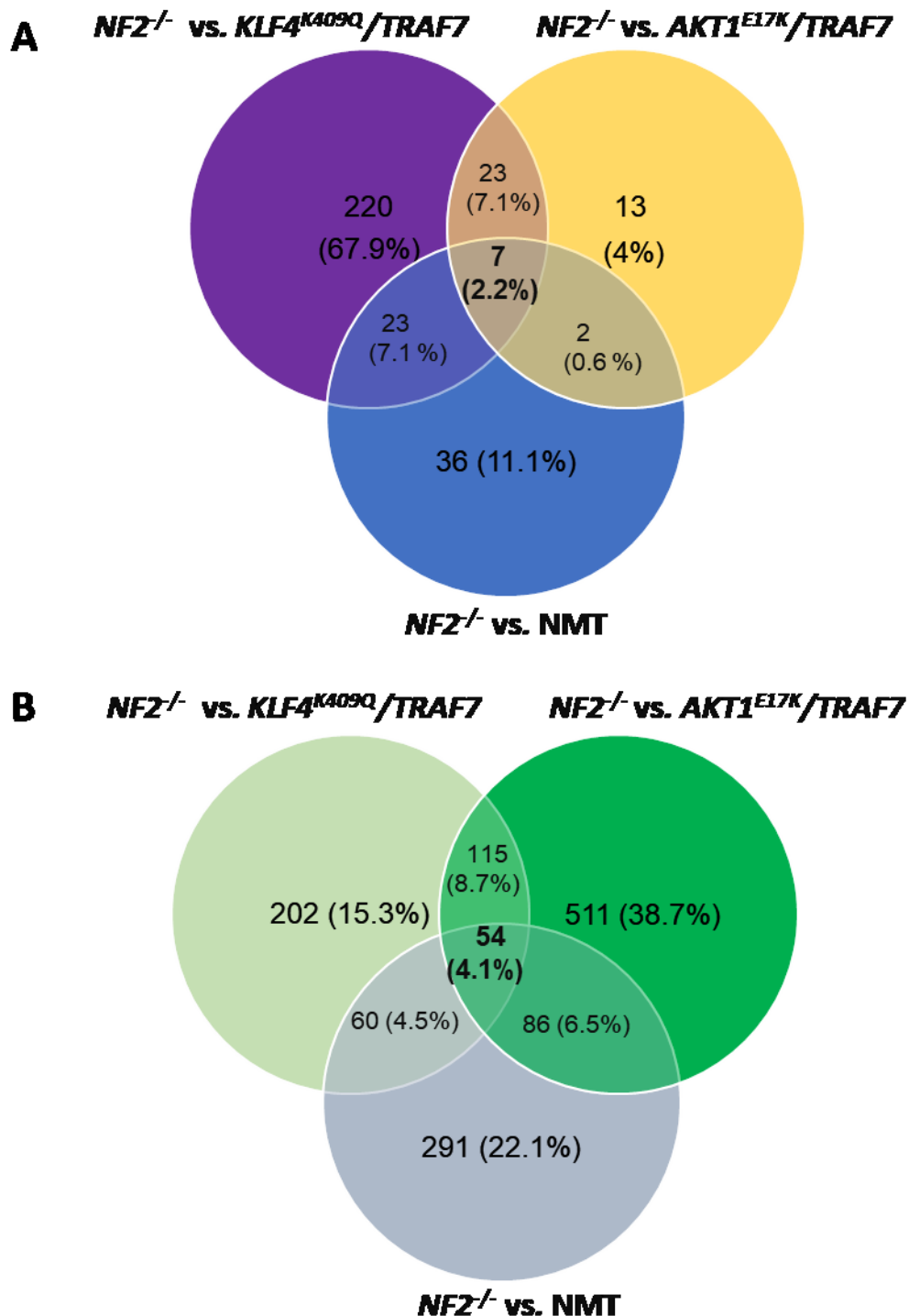


**Figure 24: *NF2*<sup>-/-</sup> mutational subtype-specific proteins.** (A) Venn diagram illustrating the distinct and overlapping only 7 upregulated proteins from differential expression analysis unique to the *NF2*<sup>-/-</sup> mutational meningioma subtype. (B) Venn diagram illustrating the distinct and overlapping only 54 downregulated proteins from differential expression analysis unique to the *NF2*<sup>-/-</sup> mutational meningioma subtype. Upregulated proteins ( $\log_2 \text{FC} \geq 1$ ;  $p\text{-value} < 0.05$ ). Downregulated proteins ( $\log_2 \text{FC} \leq -1$ ;  $p\text{-value} < 0.05$ ). Significance determined by Student's *t*-test.

Uniprot ID	Protein Name	Log2 FC <i>NF2<sup>-/-</sup></i> vs. <i>AKT1<sup>E17K</sup>/TRAF7</i>	P-value <i>NF2<sup>-/-</sup></i> vs. <i>AKT1<sup>E17K</sup>/TRAF7</i>	Log2 FC <i>NF2<sup>-/-</sup></i> vs. <i>KLF4<sup>K409Q</sup>/TRAF7</i>	P-value <i>NF2<sup>-/-</sup></i> vs. <i>KLF4<sup>K409Q</sup>/TRAF7</i>	Log2 FC <i>NF2<sup>-/-</sup></i> vs. NMT	P-value <i>NF2<sup>-/-</sup></i> vs. NMT
P12429	Annexin A3	6.096226184	1.76827E-08	2.427033407	0.004996556	2.468851263	0.020809851
A0A220K8H0	Solute carrier family 29 member 1 (Augustine blood group)	3.589353338	0.000996222	3.280741605	0.000829894	4.837815198	0.010709557
Q9BQS8	FYVE and coiled-coil domain-containing protein 1	3.22618648	0.010456117	3.451730537	0.001413961	4.822268486	0.038245444
P06737	Glycogen phosphorylase, liver form	2.870296949	0.000345626	3.849839817	1.83424E-05	2.762715947	0.038015733
V9HWJ7	Epididymis secretory protein Li 37	1.714252249	0.000460482	1.531175908	0.000308577	1.529196652	0.023974948
Q8IZ29	Tubulin beta chain	1.364134504	0.014118856	1.673272011	0.004595065	2.568250916	0.019391934
P68363	Tubulin alpha-1B chain	1.121571801	0.013715348	2.00540416	0.003672012	1.949174187	0.024525429

**Table: 10** A Complete lists of significantly upregulated proteins unique to *NF2<sup>-/-</sup>* mutational subtype. Table showing a complete list of overlapping seven upregulated proteins from differential expression analysis unique to the *NF2<sup>-/-</sup>* mutational meningioma subtype detected via VENNY 2.1. Upregulated proteins ( $\log_2 \text{FC} \geq 1$ ;  $p\text{-value} < 0.05$ ). Significance is determined by Student's *t*-test.

Uniprot ID	Protein Name	Log2 FC <i>NF2<sup>-/-</sup></i> vs. <i>AKT1<sup>E17K</sup>/T</i> <i>RAF7</i>	P-value <i>NF2<sup>-/-</sup></i> vs. <i>AKT1<sup>E17K</sup>/T</i> <i>RAF7</i>	Log2 FC <i>NF2<sup>-/-</sup></i> vs. <i>KLF4<sup>K409Q</sup>/</i> <i>TRAF7</i>	P-value <i>NF2<sup>-/-</sup></i> vs. <i>KLF4<sup>K409Q</sup>/</i> <i>TRAF7</i>	Log 2 FC <i>NF2<sup>-/-</sup></i> vs. NMT	P-value <i>NF2<sup>-/-</sup></i> vs. NMT
E9PN66	Tumor protein p53-inducible protein 11 (Fragment)	-2.77858	0.026205	-2.74788	0.00407	-6.40615	0.002673
Q53EW7	Branched-chain-amino-acid aminotransferase (Fragment)	-4.86843	1.49E-05	-4.37141	0.000442	-7.63052	0.000211
O43405	Cochlin	-1.01525	0.024436	-1.11593	0.045237	-5.03383	3.75E-05
Q53HG3	Peroxisomal D3,D2-enoyl-CoA isomerase isoform 1 variant (Fragment)	-2.97296	0.002052	-2.13039	0.04309	-4.62381	0.00769
O75891	Cytosolic 10-formyltetrahydrofolate dehydrogenase	-3.8657	0.002568	-3.07241	0.010052	-8.5665	0.001306

**Table: 11** A partial lists of significantly downregulated proteins unique to *NF2<sup>-/-</sup>* mutational subtype. Table showing a partial list of overlapping downregulated proteins from differential expression analysis unique to the *NF2<sup>-/-</sup>* mutational meningioma subtype detected via VENNY 2.1. Downregulated proteins ( $\log_2 \text{FC} \leq -1$ ;  $p\text{-value} < 0.05$ ). Significance is determined by Student's *t*-test.

### 3.5.3 Functional annotation enrichment analysis of *NF2<sup>-/-</sup>*-specific proteins

Unfortunately, due to the very low number of unique proteins commonly significantly upregulated in *NF2<sup>-/-</sup>* mutant meningioma, it was not possible to detect statistically significant enriched Gene Ontology terms for upregulated proteins by DAVID. However, 54 commonly significantly down-regulated proteins specific to *NF2<sup>-/-</sup>* mutant meningioma subtype were subjected to GO enrichment analysis using DAVID. In the GO biological process analysis, the down-regulated *NF2<sup>-/-</sup>* mutant meningioma subtype signature proteins were mainly enriched in the glucose metabolism process, cell-matrix adhesion, regulation of cell shape, extracellular matrix organization, and cell adhesion. Downregulated proteins including pyruvate dehydrogenase (acetyl transferring) kinase isozyme 3, glucose 1, 6 bi-phosphate synthases, and apolipoprotein D were highly enriched in glucose metabolism biological processes. The highest



number of downregulated proteins were enriched in cell adhesion GO terms which consist of tenascin X, sorbin and SH3 domain-containing protein 2, integrin alpha 7, and CD44 antigen (Fig- 25) in the *NF2<sup>-/-</sup>* mutant meningioma subtype. However, an opposite trend was observed where *AKT1<sup>E17K</sup>/TRAF7* mutant meningioma specific signature up-regulated proteins were highly enriched in cell-cell adhesion GO terms (Fig-17).

In the molecular function group, downregulated proteins were mainly enriched in a structural constituent of muscle (27.18 fold), Extracellular matrix structural constituent (22.90 fold), and collagen binding (19 fold) (Fig-25). Proteins associated with collagen binding included CD44 antigen, cochlin, and collagen alpha 1 (x-iv) chain.

The cellular component analysis showed *NF2<sup>-/-</sup>* mutant meningioma-specific down-regulated genes were significantly enriched in the mitochondrial matrix, extracellular exosome, and mitochondrion, the opposite results of functional annotation analysis of *AKT1<sup>E17K</sup>/TRAF7* mutant meningioma specific upregulated proteins (Fig- 17).

Collectively, these results indicate that most *NF2<sup>-/-</sup>* mutant meningioma subtype specific downregulated proteins are significantly enriched in collagen binding, cell-matrix adhesion, cell adhesion, and glucose metabolism processes.

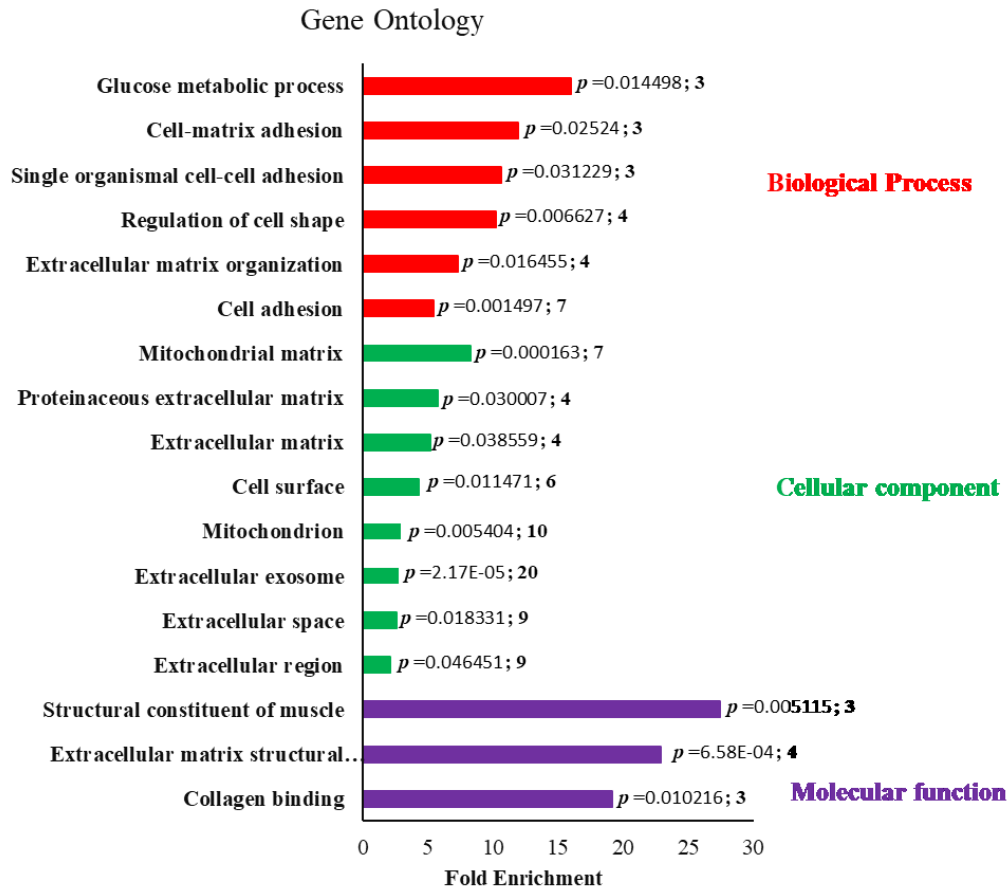


**Figure 25:** Functional annotation of 54 proteins commonly significantly downregulated in meningioma  $NF2^{-/-}$  mutational subtypes compared to NMT by the DAVID version 6.8. Fold enrichment relative to the *H. sapiens* proteome is displayed at the *x*-axis. Terms containing at least three proteins with significant  $p < 0.05$  are shown. Gene Ontologies representing molecular function are presented in purple, cellular component in green and biological process in red.

### 3.5.4 $NF2^{-/-}$ mutant meningioma subtype-specific IPA pathway analysis:

Similar ingenuity pathway analysis (IPA) was performed in three differential expression data set ( $NF2^{-/-}$  vs. NMT,  $NF2^{-/-}$  vs.  $AKT1^{E17K}/TRAF7$  and  $NF2^{-/-}$  vs.  $KLF4^{K409Q}/TRAF7$ ) and balloon plot generated (Fig-26). A total of 255 enriched canonical pathways were detected using IPA from the differential expression data set and the complete list of IPA canonical pathways can be found in supplementary data (S4). Among these, only 39 enriched canonical pathways were detected at thresholds  $-\log_{10}(P\text{-value}) > 3$ , Upregulated pathways (Z-score  $\geq 3$ ) marked by reddish to the yellowish dot; Downregulated pathways (Z-score  $\leq -3$ ) marked by purple to blackish dot in the balloon plot (Fig-26). From the IPA analysis balloon plot, ‘Sirtuin signalling pathway’ showed the highest rank in  $NF2^{-/-}$  mutant meningioma among the signalling pathways when compared to  $AKT1^{E17K}/TRAF7$  mutant group with  $-\log_{10}(P\text{-value}) > 14.012$  and Z-score  $\geq 2.646$ . Sirtuin signalling pathway was also significantly upregulated in  $NF2^{-/-}$  mutant

meningioma compared to NMT with  $-\log_{10}(P\text{-value}) > 3.230$  and  $Z\text{-score} \geq 0.302$ . In contrast, there were no significant differences between *NF2<sup>-/-</sup>* and *KLF4<sup>K409Q</sup>/TRAF7* mutant meningioma groups for sirtuin signalling pathway activation or upregulation ( $-\log_{10}(P\text{-value}) > 2.305$  and  $Z\text{-score} \geq 0$ ) (Fig- 26). Other than this, I was unable to find any pathways which showed consistent upregulation or downregulation in *NF2<sup>-/-</sup>* mutant meningioma compared to other groups (Fig- 26). These results suggest targeting sirtuin signalling pathways could be interesting for a better understanding of the *NF2<sup>-/-</sup>* mutant meningioma subtype. However, this was not possible currently due to sample limitations.



**Figure 26:** A balloon plot showing IPA pathways analysis for three sets of differential expression data ( $NF2^{-/-}$  vs. NMT,  $NF2^{-/-}$  vs.  $AKT1^{E17K}/TRAF7$  and  $NF2^{-/-}$  vs.  $KLF4^{K409Q}/TRAF7$ ) together. Criteria were set to create balloon plot follows: pathways demonstrating  $-\log_{10}(P\text{-value}) > 3$ , Upregulated pathways ( $Z\text{-score} \geq 3$ ) marked by reddish to the yellowish dot; Downregulated pathways ( $Z\text{-score} \leq -3$ ) marked by purple to the blackish dot. The bigger the dot indicates the most significant pathways. IPA pathway analysis shows the Sirtuin signaling pathway is the most significantly upregulated in  $NF2^{-/-}$  mutant meningioma when compared to  $AKT1^{E17K}/TRAF7$  mutant meningioma subtype.

### 3.5.5 Protein candidates of *NF2*<sup>-/-</sup> mutational meningioma subtypes for validation

I began to validate upregulated proteins first, as there were only seven upregulated proteins specific for *NF2*<sup>-/-</sup> mutant meningioma compared to other groups (Fig-24 A). For validation, priority is given to those proteins with the highest fold change and based on their significant expression from mass-spectrometry analysis, only the top two highly upregulated proteins, annexin-3 and solute carrier family 29 member 1, were chosen for further validation due to the limitation of sample amount (Table 12).

Uniprot ID	Protein Name	Log2 FC <i>NF2</i> <sup>-/-</sup> vs. <i>AKT1</i> <sup>E17K</sup> / <i>TRAF7</i>	P-value <i>NF2</i> <sup>-/-</sup> vs. <i>AKT1</i> <sup>E17K</sup> / <i>TRAF7</i>	Log2 FC <i>NF2</i> <sup>-/-</sup> vs. <i>KLF4</i> <sup>K409Q</sup> / <i>TRAF7</i>	P-value <i>NF2</i> <sup>-/-</sup> vs. <i>KLF4</i> <sup>K409Q</sup> / <i>TRAF7</i>	Log2 FC <i>NF2</i> <sup>-/-</sup> vs. NMT	P-value <i>NF2</i> <sup>-/-</sup> vs. NMT
P12429	Annexin A3	6.096226184	1.76827E-08	2.427033407	0.004996556	2.468851263	0.020809851
A0A220K8H0	Solute carrier family 29 member 1 (Augustine blood group)	3.589353338	0.000996222	3.280741605	0.000829894	4.837815198	0.010709557

**Table: 12** *NF2*<sup>-/-</sup> mutant meningioma specific upregulated proteins for validation with their significant *P*-value and Log2 fold change from differential expression analysis of mass-spectrometry data.

#### 3.5.5.1 Validation of differential expression of protein via Simple wes or Western blot

Simple wes analysis demonstrated significant over-expression of annexin-3 in *NF2*<sup>-/-</sup> mutant meningioma compared to *AKT1*<sup>E17K</sup>/*TRAF7*, *KLF4*<sup>K409Q</sup>/*TRAF7*, and NMT which is in line agreement with mass-spectrometry data analysis (Fig- 27 A and A1).

On the other hand, Western blot analysis showed solute carrier family 29 member 1 (Augustine blood group) protein significantly upregulated in both *AKT1*<sup>E17K</sup>/*TRAF7* and *KLF4*<sup>K409Q</sup>/*TRAF7* mutant meningioma compared to *NF2*<sup>-/-</sup> mutated group which is the opposite of what was found with mass-spectrometry analysis. Furthermore, NMT showed an increased tendency of solute carrier family 29 member 1 protein expression compared to *NF2*<sup>-/-</sup> mutant meningioma which again is not reflective of mass-spectrometry analysis (Fig- 27 B and B1).

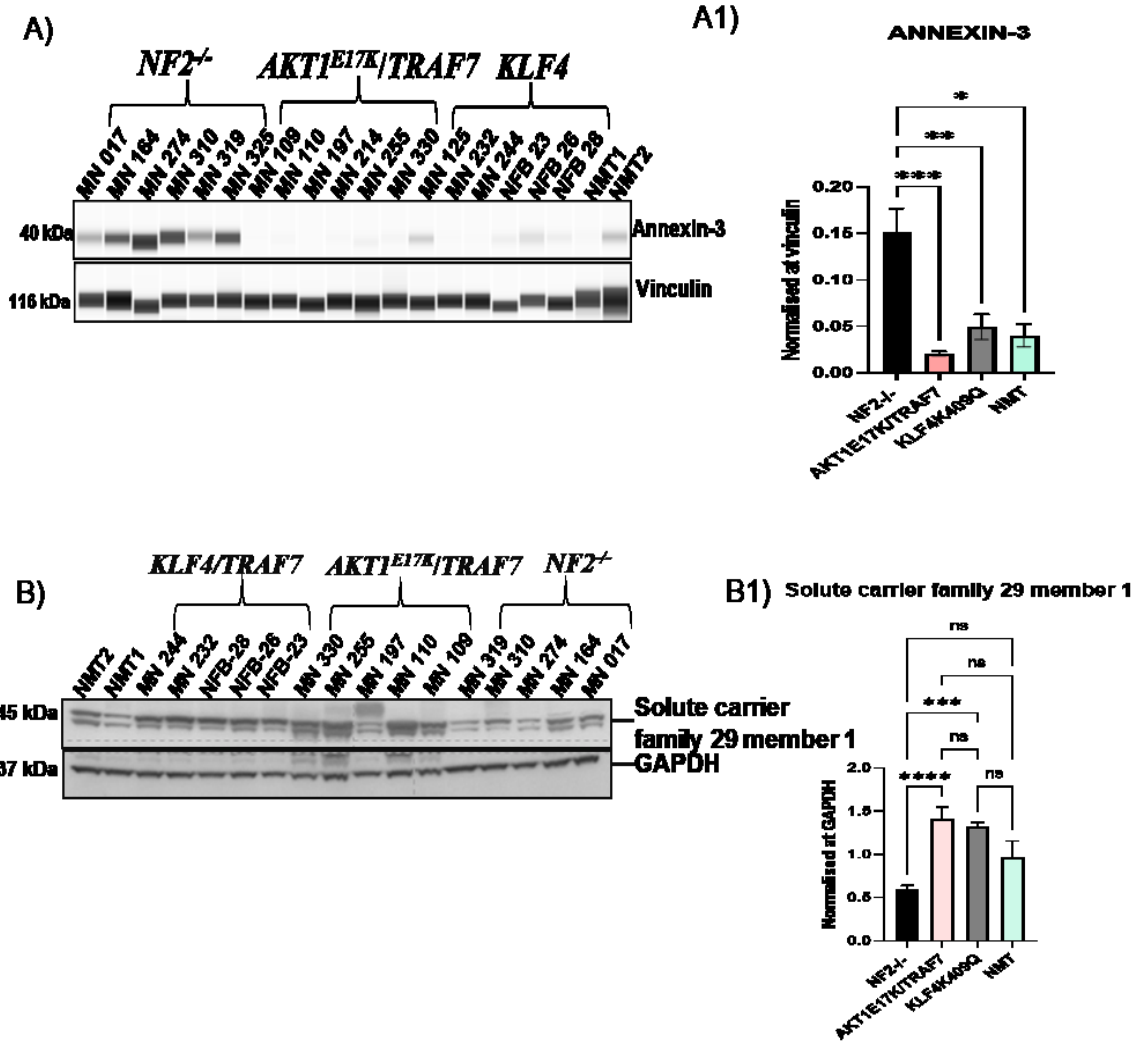


**Figure 27:** Validation of proteins identified as significantly upregulated in *NF2*<sup>-/-</sup> vs. other mutational subtypes and NMT. (A and B) Western blot analysis of upregulated proteins in *NF2*<sup>-/-</sup>, GAPDH and vinculin as a loading control. NMT ( $n=2$ ); *NF2*<sup>-/-</sup> ( $n=6$ ), *AKT1*<sup>E17K</sup>/*TRAF7* ( $n=6$ ) and *KLF4*<sup>K409Q</sup> ( $n=6$ ). (A1 and B1) Histogram showing quantification of proteins annexin-3 and solute carrier family 29 members 1 respectively. Data represented as  $\pm$ SEM and statistical significance One-way ANOVA is shown by: ns= not significant;  $p > 0.05$ ; \*  $p \leq 0.05$ ; \*\*  $p \leq 0.01$ ; \*\*\*  $p \leq 0.001$ ; \*\*\*\*  $p \leq 0.0001$ .

### 3.5.5.2 Immunohistochemistry of differentially regulated protein candidates for *NF2*<sup>-/-</sup> mutant meningioma

From IHC average scoring analysis, it was observed that *NF2*<sup>-/-</sup> mutant meningioma group showed the highest-scoring compared to other meningioma mutational subtypes and NMT for annexin-3, with this protein being mostly detected in the cytoplasm. Out of five *NF2*<sup>-/-</sup> mutant meningioma samples, three showed strong immunostaining whereas two of them only showed mild staining (Fig-28 A and Ba). On the other hand, almost all tissue sections of

*AKT1*<sup>E17K</sup>/*TRAF7* mutant meningioma and NMT both showed weak staining for annexin-3 expression (Fig-28 A and Ba). These results showed a similar trend as Simple was analysis (Fig-27 A and A1).

Solute carrier family 29 members 1 protein demonstrated the highest average score in IHC staining in *KLF4*<sup>K409Q</sup>/*TRAF7* mutant meningioma with strong immunoreaction. However, there was no significant differences in expression among the meningioma mutational subtypes and NMT (Fig-28 A and Bb) with solute carrier family 29 member 1 being predominantly detected as focal nuclear and cytoplasmic staining (Fig-28 A). The staining results for solute carrier family 29 members 1 protein were not reflective of Western blot and mass-spectrometry analysis. Therefore, I chose to proceed with this candidate for functional validation. On the other hand, annexin-3 overexpression in *NF2*<sup>-/-</sup> mutant meningioma was consistent in both WB and IHC. Therefore, further functional validation of annexin-3 was carried out.

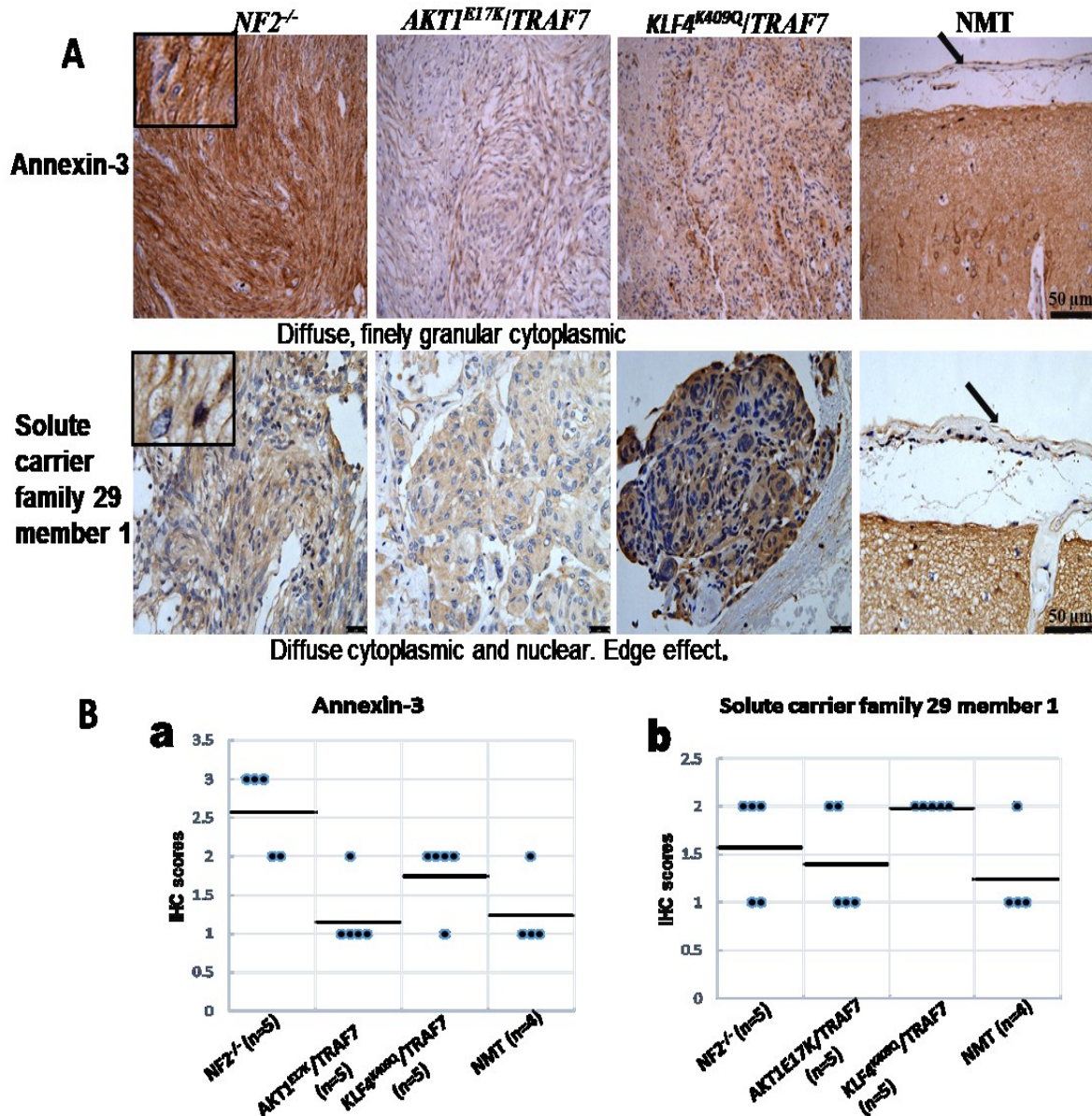


**Figure 28: Immunohistochemistry analysis of *NF2<sup>-/-</sup>* specific candidate proteins. A)** Immunostaining images of annexin-3 and solute carrier family 29 member 1 at 40x magnification. **Ba)** Corresponding IHC scoring of annexin-3 represent as mean shown in the black bold line for each group. **Bb)** Corresponding IHC scoring of solute carrier family 29 member 1 represent as mean calculated based on staining score shown in the black bold line for each group. Scoring criteria 0 = absent, 1= Weak, 2 = moderate and 3 = strong.

### 3.5.5.3 Functional study of Annexin-3

The grade-I; *NF2<sup>-/-</sup>* mutated meningioma cell line Benmen-1 was used to carry out functional validation of annexin-3 using shRNA knockdown. I was able to conclude annexin-3 expression in Benmen-1 cells using Western blotting. However, as expected, the KT21 cell line (grade-III; *NF2<sup>-/-</sup>* cell line) showed strong expression and IOMLEE (grade-III; *NF2<sup>+/+</sup>* cell line) showed low expression supporting my hypothesis and previous results (Fig- 29 a). Ready-made



GFP lentivirus particles with three distinct knockdown sequences were ordered from Dharmacon Inc, USA to deplete the expression of annexin-3 in Benmen-1 to observe the impact on cell proliferation.

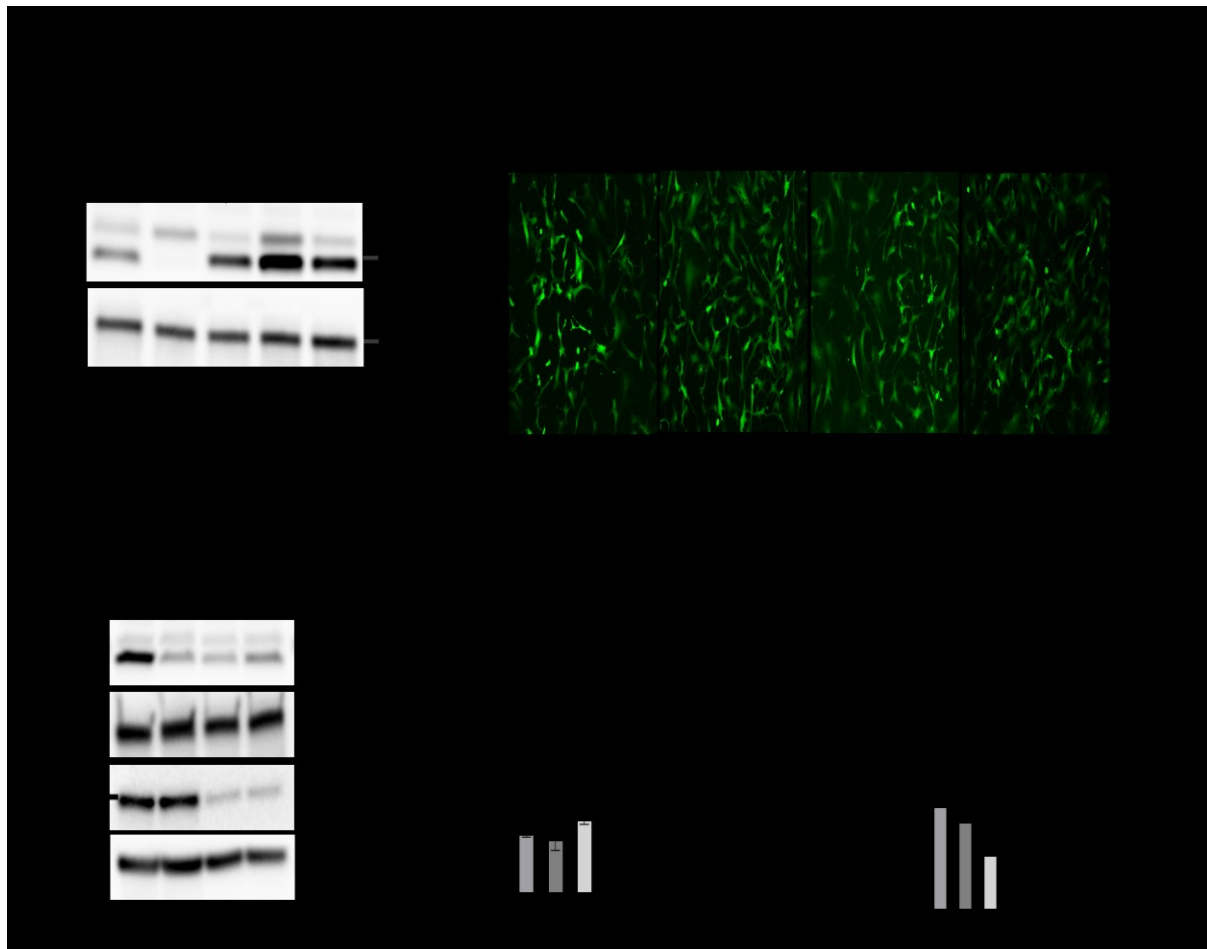


**Figure 29: Annexin-3 knock-down slightly affects the expression of cyclin-D1 in meningioma cell line Benmen-1.** a) Benmen-1 cell line expresses Annexin-3. b) Benmen-1 were infected with scramble shRNA (SCR-negative control) and Annexin-3 shRNA (constructs 622, 695 and 751) for 72 hrs or until all cells were GFP-positive. c) Immunoblot showing the expression of Annexin-3 and Cyclin-D1. Vinculin was used as a loading control. d) Western blot assay analysis of Annexin-3 levels in three constructs transfected with ANXA3-shRNA in Benmen-1 cells. Data were normalized to SCR. ANOVA with multiple comparison tests was performed using GraphPad Prism software. e) Bar chart showing knock-down of Annexin-3 shRNA (constructs 622, 695 and 751) in meningioma cell line Benmen-1 (n=3), resulted in slightly decreases in cyclin-D1 (cell proliferation marker) levels. Western blot assay analysis was performed using anti-cyclin D1, Statistical analysis was calculated by ANOVA with multiple comparison test using GraphPad Prism analysis software. Cyclin-D1, technical repeat n=3, ns=not significant, P= >0.2791.

To gain a better understanding of the biological functions of annexin-3 in meningioma, Benmen-1 cells were transfected with commercially (Dharmacon Inc, USA) available 622-shAnnexin3, 695- shAnnexin3, 751- shAnnexin3, and scramble (scr) shRNA used as control,

after which cells were selected using puromycin (2µg/ml). After knocking down, annexin-3 protein levels were significantly decreased compared to scramble (Fig-29 c). The role of annexin3 on Benmen-1 cell proliferation was investigated using the proliferation marker cyclin D1. Western blot analysis showed cyclin D1 tended to be suppressed in the Benmen-1 after annexin-3 knockdown but not to a significant degree (Fig-29 c and e).

Overall, these results suggest that the knockdown of annexin-3 suppresses meningioma cell proliferation although additional experiments are needed to confirm this.

### 3.6 Meningioma with *KLF4*<sup>K409Q</sup> mutational

#### 3.6.1 Meningioma with *KLF4*<sup>K409Q</sup> mutational subtype-specific protein analysis

A two-sample *t*-test (volcano plot) was performed again to detect differentially expressed proteins in *KLF4*<sup>K409Q</sup> mutant meningioma compared to other mutational subtypes and NMT. A total of 793 proteins were differentially expressed in comparison between *KLF4*<sup>K409Q</sup> and NMT, 128 proteins were significantly upregulated (Log2 FC≥1; *p*< 0.05) in *KLF4*<sup>K409Q</sup> mutant meningioma and 664 proteins were downregulated (Log2 FC≤-1; *p*< 0.05) compared to NMT. Upregulated proteins with the highest fold change including THSD4, Elongation factor Tu (TUFM) involve in promoting GTP dependent binding of aminoacyl-tRNA to the ribosomal site for protein synthesis and also regulates autophagy and innate immunity (<https://www.proteinatlas.org/ENSG00000178952-TUFM>), calcium-binding protein P22, HLA-DRA, prostaglandin F2 receptor negative regulator, anion exchange protein 2 may play a role in maintaining intracellular pH & secretion of biliary bicarbonate, also regulates chloride uptake and a prognostic marker for Liver and renal cancer (<https://www.proteinatlas.org/ENSG00000164889-SLC4A2>), and MHC class I antigen ( a cancer-related gene, may play a role in adaptive immunity, innate immunity and host-virus interaction, in addition to this it is a favourable prognostic marker for ovarian and endometrial cancer (<https://www.proteinatlas.org/ENSG00000206503-HLA-A>) (Fig-30 A).

Differential expression analysis between *KLF4*<sup>K409Q</sup>/*TRAF7* and *AKT1*<sup>E17K</sup>/*TRAF7* already explained in Fig- 15 C, has been included again for easy visualization in *KLF4*<sup>K409Q</sup> compared to *AKT1*<sup>E17K</sup>/*TRAF7* mutant meningioma (Fig-30 C). The top significantly overexpressed proteins include histone H1.0, aldehyde dehydrogenase is a favourable prognostic marker for head and neck cancer (<https://www.proteinatlas.org/ENSG00000108602-ALDH3A1>), actively takes part in alcohol originated acetaldehyde detoxification and helps to metabolize corticosteroids, neurotransmitters and lipid peroxidation (Hsu *et al.*, 1992), CD44, anion

exchange protein 2, and ribosomal protein S6 kinase (RBP6) (Yamashita *et al.*, (2013) demonstrated that RBP6 take part in regulating cell growth and proliferation via translocating specific mRNA classes.

On the other hand, differential analysis between *KLF4<sup>K409Q</sup>/TRAF7* and *NF2<sup>-/-</sup>* revealed that upregulated proteins in *KLF4<sup>K409Q</sup>* mutant meningioma include CD44, anion exchange protein 2, alkaline phosphatase, E-cadherin 1, and endoglin, a glycoprotein of vascular endothelium that takes part in regulating angiogenesis and TGF $\beta$  signaling pathways (Castonguay *et al.*, 2011; Bellón *et al.*, 1993; Alt *et al.*, 2012) compared to *NF2<sup>-/-</sup>* mutant meningioma subtypes (Fig-30 B).

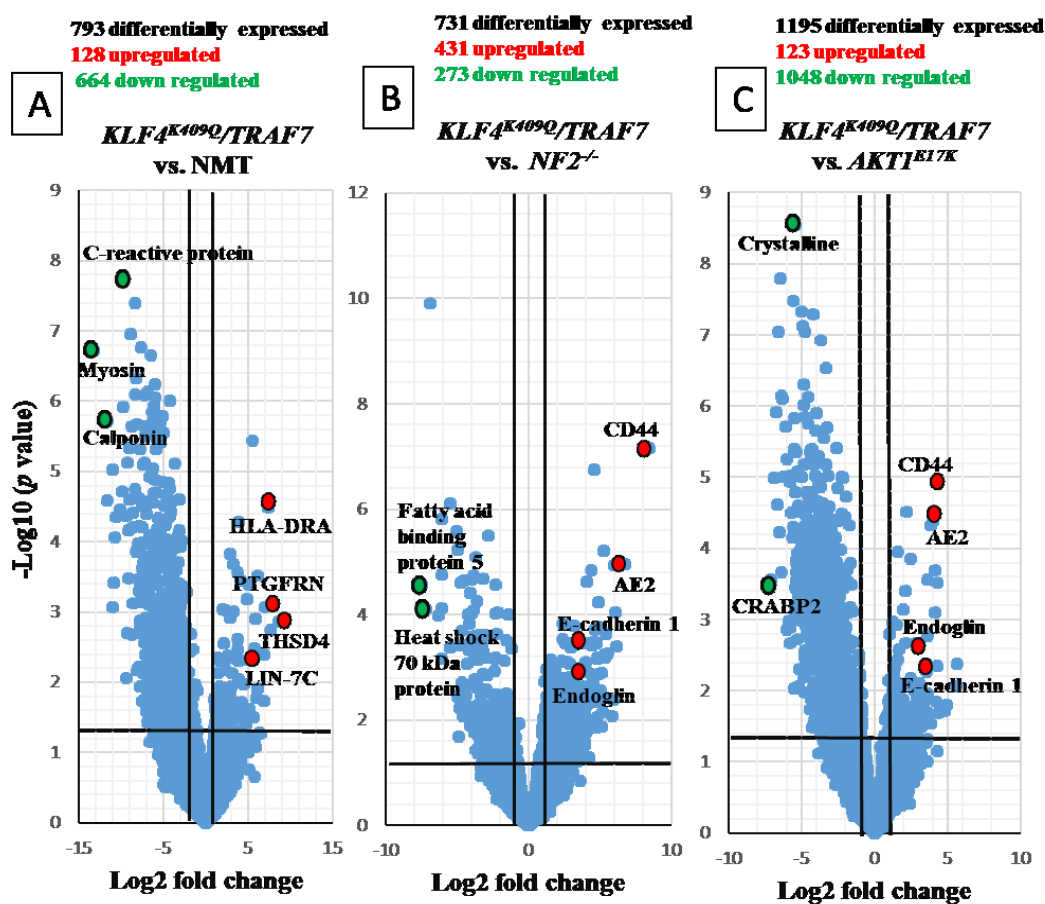


**Figure 30: Differential protein expression between sample groups.** Volcano plots of protein abundance between the mutational subtypes of meningioma and normal meningeal tissue (A, B and C). Depicted are  $\log_2$  fold changes vs.  $-\log_{10}$   $p$ -values (Student's  $t$ -test between replicate measurements). Black lines demarcate  $p$ -value < 0.05 and  $\log_2$  fold change of 1 and -1. Red dots: Upregulated proteins ( $\log_2$  FC  $\geq$  1;  $p$ -value < 0.05). Green dots: Downregulated proteins ( $\log_2$  FC  $\leq$  -1;  $p$ -value < 0.05). Highlighted proteins may be considered potential biomarker candidates for future experimental validation.

### 3.6.2 Distinct and overlapping proteins in meningioma with *KLF4*<sup>K409Q</sup> mutational subtypes

Venn diagrams were again used to determine distinct differential expression of proteins (upregulated and downregulated) in *KLF4*<sup>K409Q</sup> meningioma subtypes as compared to *AKT1*<sup>E17K</sup>/*TRAF7*, *NF2*<sup>-/-</sup>, and NMT. Three data sets (*KLF4*<sup>K409Q</sup> vs. NMT, *KLF4*<sup>K409Q</sup> vs. *AKT1*<sup>E17K</sup>/*TRAF7*, and *KLF4*<sup>K409Q</sup> vs. *NF2*<sup>-/-</sup>) were overlapped. Fold change criteria were set as follows: Proteins demonstrating  $\log_2 \text{FC} \geq 1$ ;  $p < 0.05$  were considered as significantly upregulated (Fig- 31 A) and proteins with  $\log_2 \text{FC} \leq -1$ ;  $p < 0.05$  as significantly downregulated (Fig- 31 B). Overlapping data sets were visually represented in Venn diagrams (Fig-31).

From overlapping data sets, only 14 proteins showed commonly significant expression in *KLF4*<sup>K409Q</sup> mutant subtype and 66 proteins were commonly significantly downregulated compared to the *AKT1*<sup>E17K</sup>/*TRAF7*, *NF2*<sup>-/-</sup> meningioma subtypes, and NMT (Fig-31 A and B). Partial lists of commonly upregulated and downregulated proteins in *KLF4*<sup>K409Q</sup> meningioma subtypes can be found in table -13 and 14 and complete lists can be found in appendix table-3 and 4.

Overall, *KLF4*<sup>K409Q</sup> mutant subtypes specific overlapping data set analysis showed a similar trend as *NF2*<sup>-/-</sup> mutational meningioma subtypes, where a lower number of significantly upregulated proteins were identified as distinct for this group compared to the number of down-regulated proteins (Fig-31 A and B).

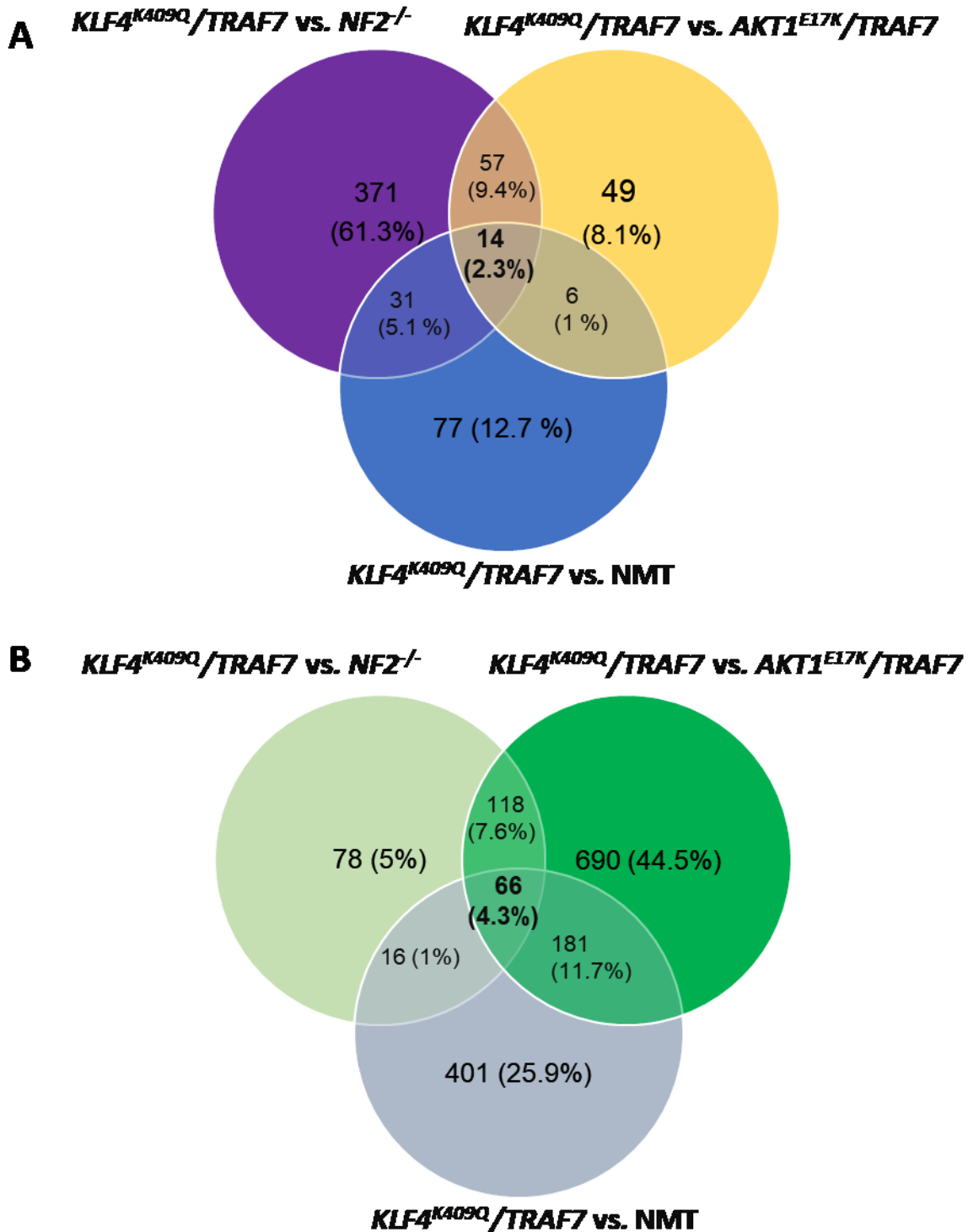


**Figure 31:** *KLF4<sup>K409Q</sup>* mutational subtype-specific proteins. (A) Venn diagram illustrating the distinct and overlapping only 14 upregulated proteins from differential expression analysis unique to the *KLF4<sup>K409Q</sup>* mutational meningioma subtype. (B) Venn diagram illustrating the distinct and overlapping only 66 downregulated proteins from differential expression analysis unique to the *KLF4<sup>K409Q</sup>* mutational meningioma subtype. Upregulated proteins ( $\log_2 \text{FC} \geq 1$ ;  $p\text{-value} < 0.05$ ). Downregulated proteins ( $\log_2 \text{FC} \leq -1$ ;  $p\text{-value} < 0.05$ ). Significance determined by Student's *t*-test.

Uniprot ID	Protein name	Log2 FC <i>KLF4</i> <sup>K409Q</sup> / <i>TRAF7</i> vs. <i>AKT1</i> <sup>E17K</sup> / <i>TRAF7</i>	P-value <i>KLF4</i> <sup>K409Q</sup> / <i>TRAF7</i> vs. <i>AKT1</i> <sup>E17K</sup> / <i>TRAF7</i>	Log2 FC <i>KLF4</i> <sup>K409Q</sup> / <i>TRAF7</i> vs. <i>NF2</i> <sup>-/-</sup>	P-value <i>KLF4</i> <sup>K409Q</sup> / <i>TRAF7</i> vs. <i>NF2</i> <sup>-/-</sup>	Log2 FC <i>KLF4</i> <sup>K409Q</sup> / <i>TRAF7</i> NMT	P-value <i>KLF4</i> <sup>K409Q</sup> / <i>TRAF7</i> NMT
P04920	Anion exchange protein 2	4.311079	0.004411	6.715718	1.1E-05	6.890585	0.018494
D3XNU5	E-cadherin 1	3.073486	0.010845	3.939768	0.006387	5.714101	0.003263
H0YD13	CD44 antigen	4.311307	0.000305	8.425873	7.01E-08	3.314977	0.00021
Q5T9B9	Endoglin (Osler-Rendu-Weber syndrome 1)	2.079189	0.000397	2.201567	0.002244	2.841178	0.001218
B2R8K9	Aminopeptidase	4.137402	0.000781	5.232938	6.12E-06	6.093094	0.000304
E9PQW1	Caspase recruitment domain-containing protein 16 (Fragment)	1.431636	0.009845	1.684484	0.000861	1.793876	0.047454
A0A0S2Z548	Sulfatase modifying factor 2 isoform 3	1.603546	0.01292	2.497712	0.035562	1.88763	0.012925
Q8NF91	Nesprin-1	2.71291	0.028219	2.575034	0.033208	3.246015	0.034617

**Table: 13** A partial lists of significantly upregulated proteins unique to *KLF4*<sup>K409Q</sup> mutated meningioma subtype. Table showing a partial list of overlapping 14 upregulated proteins from differential expression analysis unique to the *KLF4*<sup>K409Q</sup> mutational meningioma subtype detected via VENNY 2.1. Upregulated proteins ( $\log_2$  FC  $\geq$  1;  $p$ -value  $<$  0.05). Significance is determined by Student's  $t$ -test.

Uniprot ID	Protein name	Log2 FC <i>KLF4</i> <sup>K409Q</sup> / <i>TRAF7</i> vs. <i>AKT1</i> <sup>E17K</sup> / <i>TRAF7</i>	P-value <i>KLF4</i> <sup>K409Q</sup> / <i>TRAF7</i> vs. <i>AKT1</i> <sup>E17K</sup> / <i>TRAF7</i>	Log2 FC <i>KLF4</i> <sup>K409Q</sup> / <i>TRAF7</i> vs. <i>NF2</i> <sup>-/-</sup>	P-value <i>KLF4</i> <sup>K409Q</sup> / <i>TRAF7</i> vs. <i>NF2</i> <sup>-/-</sup>	Log2 FC <i>KLF4</i> <sup>K409Q</sup> / <i>TRAF7</i> NMT	P-value <i>KLF4</i> <sup>K409Q</sup> / <i>TRAF7</i> NMT
Q6ZN40	Tropomyosin 1 (Alpha), isoform	-6.3347	0.000219	-6.2827	0.000103	-10.9713	0.000865
Q53FI7	Four and a half LIM domains 1 variant (Fragment)	-6.873	1.02E-05	-7.22534	7.91E-05	-10.1997	3.54E-05
A0A024RBB5	Cysteine and glycine-rich protein 2, isoform	-2.4665	0.005647	-3.19157	0.00132	-9.88956	1.95E-08
P13591	Neural cell adhesion molecule 1	-5.1497	0.000117	-3.92071	0.011197	-9.11525	6.84E-05
V9HWC9	Superoxide dismutase [Cu-Zn]	-3.8219	0.001119	-4.688	0.00195	-9.07859	0.000337
P01861	Immunoglobulin heavy constant gamma 4	-3.1529	0.009836	-3.21098	0.024828	-8.75455	2.31E-06
A0A0S2Z3X8	Rab GDP dissociation inhibitor (Fragment)	-3.5417	0.000973	-5.52259	7.92E-07	-8.27719	0.000141

**Table: 14 A partial lists of significantly downregulated proteins unique to *KLF4*<sup>K409Q</sup> mutated meningioma subtype.** Table showing a partial list of overlapping downregulated proteins from differential expression analysis unique to the *KLF4*<sup>K409Q</sup> mutational meningioma subtype detected via VENNY 2.1. Downregulated proteins ( $\log_2 \text{FC} \leq -1$ ;  $p\text{-value} < 0.05$ ). Significance is determined by Student's *t*-test.

### 3.6.3 Functional annotation enrichment analysis of *KLF4<sup>K409Q</sup>* mutant meningioma specific proteins

GO analysis of *KLF4<sup>K409Q</sup>* specific upregulated proteins were highly enriched in the extracellular matrix disassembly biological processes with proteins making up this GO category including CD44 antigen, E-cadherin-1, and endoglin (Fig-32).

The cellular component analysis showed that *KLF4<sup>K409Q</sup>* mutant meningioma-specific upregulated proteins were highly enriched in the nuclear membrane, focal adhesion, mitochondrial inner membrane, and cell surface. However, the highest number of proteins were found in the focal adhesion terms including anion exchange protein 2, calcium-binding protein 22, CD44 antigen, E-cadherin-1 and endoglin (Fig-32). Due to the low number of upregulated proteins input into DAVID, no significant enrichment was observed in molecular function GO terms. For the same reasons, it was not possible to carry out KEGG pathway analysis for upregulated proteins via DAVID.

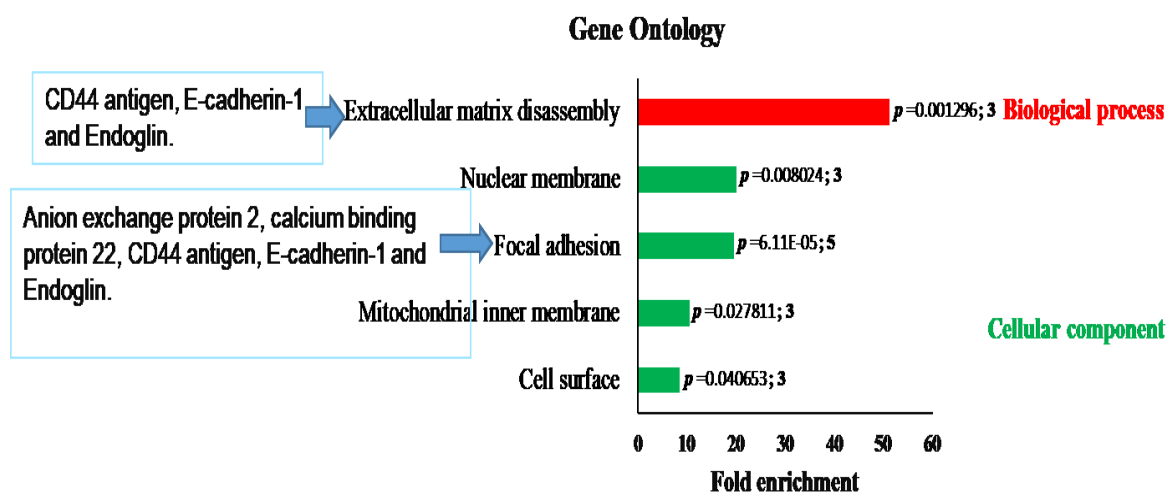


**Figure 32:** Functional annotation of *KLF4<sup>K409Q</sup>* mutant meningioma specific up-regulated proteins by the DAVID version 6.8. Fold enrichment relative to the *H. sapiens* proteome is displayed at the x-axis. Terms containing at least three proteins with  $p < 0.05$  are shown. Gene Ontologies representing Cellular Component in green and Biological Process in red.

In contrast, functional annotation analysis of *KLF4<sup>K409Q</sup>* specific downregulated proteins were highly enriched in the regulation of endocytosis, regulation of the cellular amino acid metabolic process, antigen processing and presentation of exogenous peptide antigen via MHC class I, TAP-dependent, NIK/NF-kappaB signalling, Negative regulation of ubiquitin-protein ligase activity involved in mitotic cell cycle, positive regulation of ubiquitin-protein ligase activity involved in the regulation of mitotic cell cycle transition and Wnt signalling pathway biological



GO terms (Fig-33). Within molecular function GO terms, downregulated proteins were significantly enriched in cytoskeletal protein binding, actin filament binding, actin binding, protein homodimerization activity and protein binding (Fig-33). The highest number of *KLF4<sup>K409Q</sup>* specific downregulated proteins were highly enriched in protein binding GO terms which is the complete opposite result of *AKT1<sup>E17K</sup>/TRAF7* mutant meningioma subtypes specific upregulated proteins functional annotation analysis at molecular function GO terms (Fig-17).

Overall, *KLF4<sup>K409Q</sup>* -specific upregulated proteins are enriched in extracellular matrix disassembly and focal adhesion GO terms, and downregulated are enriched in regulation of endocytosis and cytoskeletal protein binding GO term (Fig- 32 and 33).

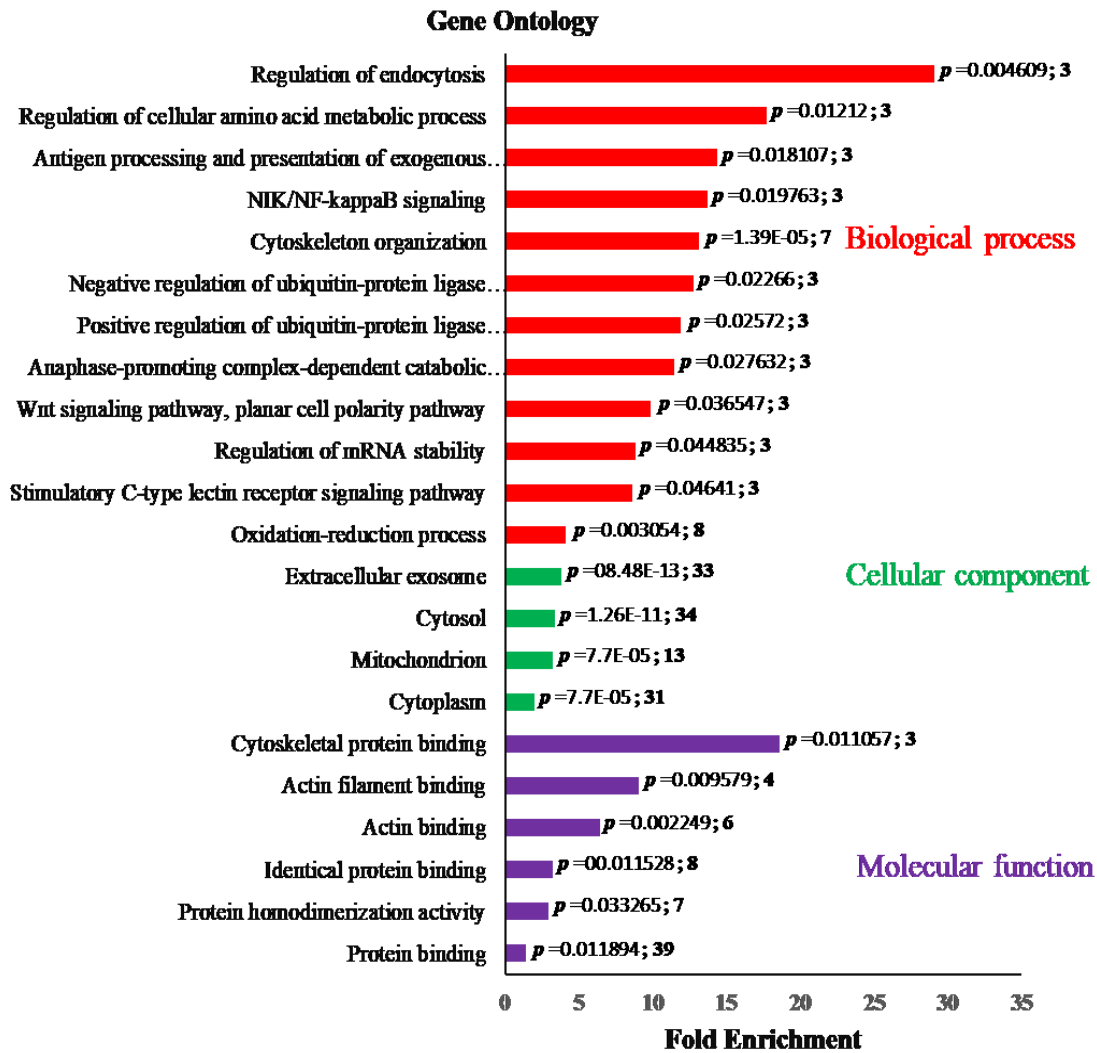


**Figure 33:** Functional annotation of *KLF4<sup>K409Q</sup>* mutant meningioma-specific down-regulated proteins by the DAVID version 6.8. Fold enrichment relative to the *H. sapiens* proteome is displayed at the x-axis. Terms containing at least three proteins with  $p < 0.05$  are shown. Gene Ontologies representing Cellular Component in green and Biological Process in red and Molecular function in purple.

### 3.6.4 *KLF4<sup>K409Q</sup>* mutant meningioma subtype-specific IPA pathway analysis

Similar IPA was performed for three differential expression data sets (*KLF4<sup>K409Q</sup>/TRAF7* vs. NMT, *KLF4<sup>K409Q</sup>/TRAF7* vs. *AKT1<sup>E17K</sup>/TRAF7* and *KLF4<sup>K409Q</sup>/TRAF7* vs. *NF2<sup>-/-</sup>*) and a balloon plot generated (Fig-34). A total of 375 enriched canonical pathways were detected using IPA from the differential expression data sets, and the complete list of IPA canonical pathways can be found in the supplementary data- S5. Among these, only 100 enriched canonical pathways were detected at thresholds  $-\log_{10}(P\text{-value}) > 3$ , upregulated pathways ( $Z\text{-score} \geq 3$ ) marked by reddish to the yellowish dot; downregulated pathways ( $Z\text{-score} \leq -3$ ) marked by purple to

blackish dot in the balloon plot (Fig- 34). Like *NF2<sup>-/-</sup>* mutant meningioma, IPA analysis balloon plot showed significant upregulation of sirtuin signalling pathway in *KLF4<sup>K409Q</sup>* mutant meningioma among the signalling pathways when compared to *AKT1<sup>E17K</sup>/TRAF7* mutant group with  $-\log_{10} p\text{-value} > 10.64$  and  $Z\text{-score} \geq 2.92$ . However, unlike *NF2<sup>-/-</sup>* mutant meningioma, sirtuin signalling pathway was significantly downregulated in *KLF4<sup>K409Q</sup>* mutant meningioma compared to NMT with  $-\log_{10} p\text{-value} > 3.81$  and  $Z\text{-score} \geq -0.471$ . As mentioned previously, there were no significant differences between *NF2<sup>-/-</sup>* and *KLF4<sup>K409Q</sup>/TRAF7* mutant meningioma groups for sirtuin signalling pathway activation ( $-\log_{10} p\text{-value} > 2.305$  and  $Z\text{-score} \geq 0$ ) (Fig-34). These results show clear differences between *KLF4<sup>K409Q</sup>* and *AKT1<sup>E17K</sup>/TRAF7* mutant meningioma group.

In addition to this, RhoGDI signalling pathway which showed significant upregulation in *KLF4<sup>K409Q</sup>* mutant meningioma compared to *AKT1<sup>E17K</sup>/TRAF7* mutant group ( $-\log_{10} p\text{-value} > 6.28$  and  $Z\text{-score} \geq 3.27$ ) and NMT ( $-\log_{10} p\text{-value} > 4.21$  and  $Z\text{-score} \geq 1.604$ ) groups respectively. On the other hand, this pathway was significantly down-regulated in *KLF4<sup>K409Q</sup>* mutant meningioma compared to *NF2<sup>-/-</sup>* mutant group ( $-\log_{10} p\text{-value} > 3.81$  and  $Z\text{-score} \geq -1.291$ ) (Fig-34).

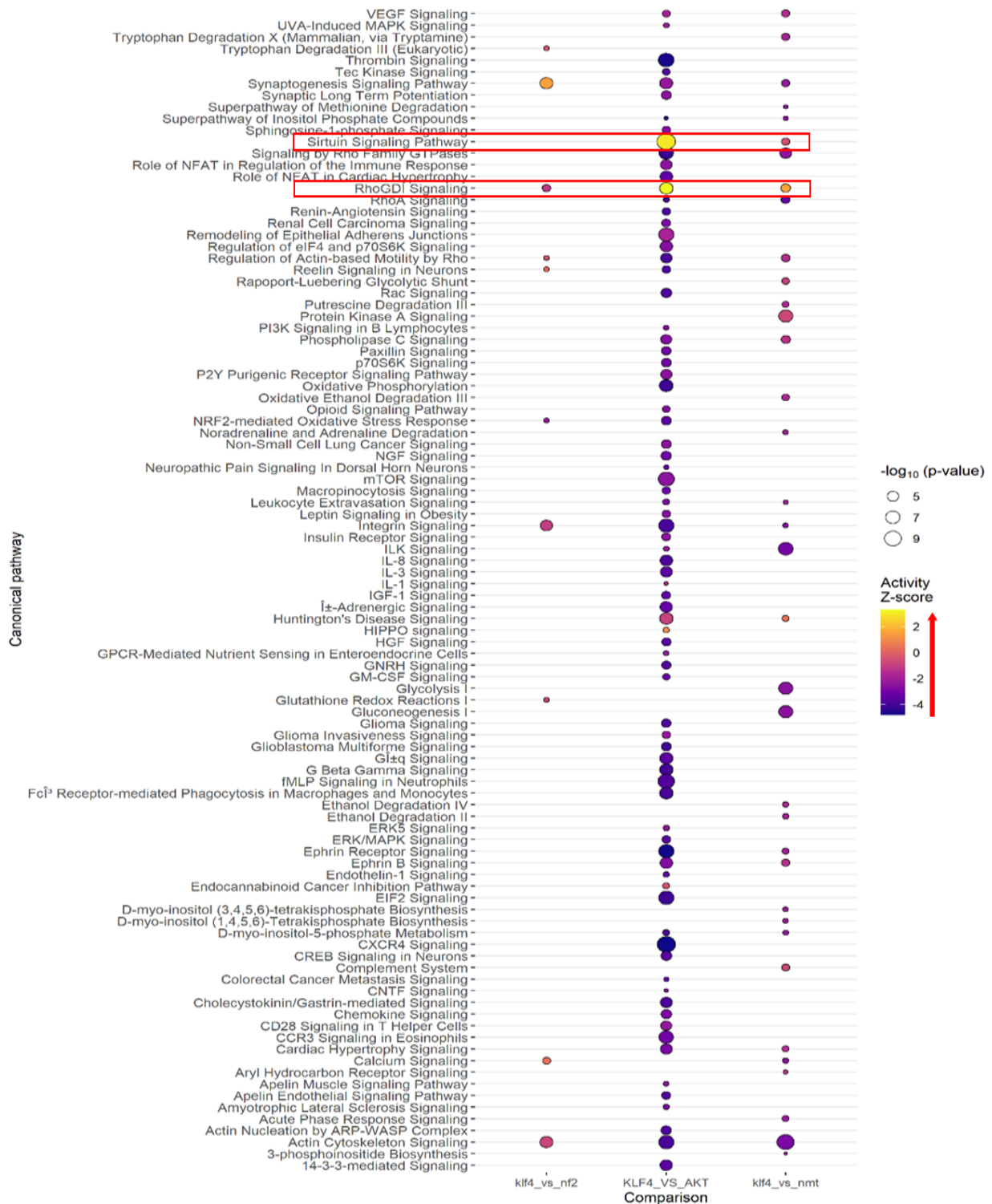


**Figure 34:** A balloon plot showing IPA pathways analysis for three sets of differential expression data ( $KLF4^{K409Q}/TRAF7$  vs. NMT,  $KLF4^{K409Q}/TRAF7$  vs.  $AKT1^{E17K}/TRAF7$ , and  $KLF4^{K409Q}/TRAF7$  vs.  $NF2^{-/-}$ ) together. Criteria were set to create balloon plot follows: pathways demonstrating  $-\log_{10}(P\text{-value}) > 3$ , Upregulated pathways (Z-score  $\geq 3$ ) marked by reddish to the yellowish dot; Downregulated pathways (Z-score  $\leq -3$ ) marked by purple to the blackish dot. The bigger the dot indicates the most significant pathways. IPA pathway analysis shows the sirtuin and RhoGDI signaling pathways were the most significantly upregulated in  $KLF4^{K409Q}/TRAF7$  mutant meningioma when compared to  $AKT1^{E17K}/TRAF7$  mutant meningioma subtype in the bold red box.

### 3.6.5 Protein candidates of *KLF4<sup>K409Q</sup>/TRAF7* mutant meningioma for validation

Only 14 upregulated proteins were very specific for *KLF4<sup>K409Q</sup>/TRAF7* mutant meningioma compared to other groups (Fig- 31 A). For validation, priority is given to those proteins with the highest fold change and based on their significant expression from mass-spectrometry analysis, and only three proteins were chosen for further validation due to the limitation of sample amount (Table 15).

Protein name	Fold change increase compared to <i>AKT1E17K/TRAF7</i>	Fold change increase compared to <i>NF2<sup>-/-</sup></i> mutant subtype	Fold change increase compared to normal (NMT)	Represented in functional annotation analysis
E-cadherin 1	3.073486	3.939768	5.714101	<b>Extracellular matrix disassembly and focal adhesion</b>
CD44 antigen	4.311307	8.425873	3.314977	<b>Extracellular matrix disassembly and focal adhesion</b>
Endoglin (Osler-Rendu-Weber syndrome 1)	2.079189	2.201567	2.841178	<b>Extracellular matrix disassembly and focal adhesion</b>
Anion exchange protein 2	4.311079	6.715718	6.890585	<b>Focal adhesion</b>

**Table 15:** *KLF4<sup>K409Q</sup>/TRAF7* mutant meningioma specific upregulated proteins for validation with fold change from differential expression analysis of Mass-spectrometry data and corresponding GO terms.

#### 3.6.5.1 Validation of differential expression of protein via Western blot

Western blot analysis showed an increased expression of endoglin in *KLF4<sup>K409Q</sup>/TRAF7* mutant meningioma compared to other mutational meningioma subtypes and NMT (Fig-35 A and A1) but not to a significant degree as mass-spectrometry analysis showed. In mass-spectrometry data, endoglin was identified at 67 kDa but in Western blot, I have observed a double band with one isoform at 67 kDa and another isoform at 70 kDa (<https://www.uniprot.org/uniprot/Q5T9B9>). For statistical analysis, I have calculated the intensity value for both bands. Out of five *KLF4<sup>K409Q</sup>/TRAF7* mutant meningioma tissue lysates, only three samples showed strong bands at 70 kDa where all samples showed very thin bands at 67 kDa (Fig-35 A).

E-cadherin 1 has numerous cleavage sites which in turn produces multiple bands at Western blot analysis, bands expected from 80-120 kDa. In mass spectrometry data set proteins were detected at 97 kDa and in Western blot analysis, E-cadherin 1 expression was detected at around 100 kDa and 80kDa. Kuefer *et al.*, (2003) observed E-cadherin 1 fragment at 80 kDa band in metastatic prostate cancer at serum protein level. They have suggested 80 kDa fragment is actively correlated with metastatic tumour progression (Kuefer *et al.*, 2003). Likewise, in the

Western blot, almost all *KLF4<sup>K409Q</sup>/TRAF7* mutant meningioma showed 80kDa fragments for E-cadherin 1 while other tumour samples and normal meninges did not show the band at this molecular weight (Fig-35 A). For confirmation an additional antibody is required. Overall WB analysis of E-cadherin 1 showed the highest expression in *AKT1<sup>E17K</sup>/TRAF7* (Fig-35 A and A2) which is not in agreement with mass-spectrometry results. In contrast E-cadherin 1 overexpression trend is observed in *KLF4<sup>K409Q</sup>/TRAF7* mutant meningioma compared to *NF2<sup>-/-</sup>* mutant meningioma and NMT but not significantly so.

Whilst mass-spectrometry data analysis identified anion exchange protein 2 as the most significant with the highest fold change expression for *KLF4<sup>K409Q</sup>/TRAF7* mutant meningioma (Fig-35 B and B2), only a very faint band was observed for anion exchange protein 2 at 135 kDa in WB with no clear differences in expression among the meningioma mutational subtypes and NMT.

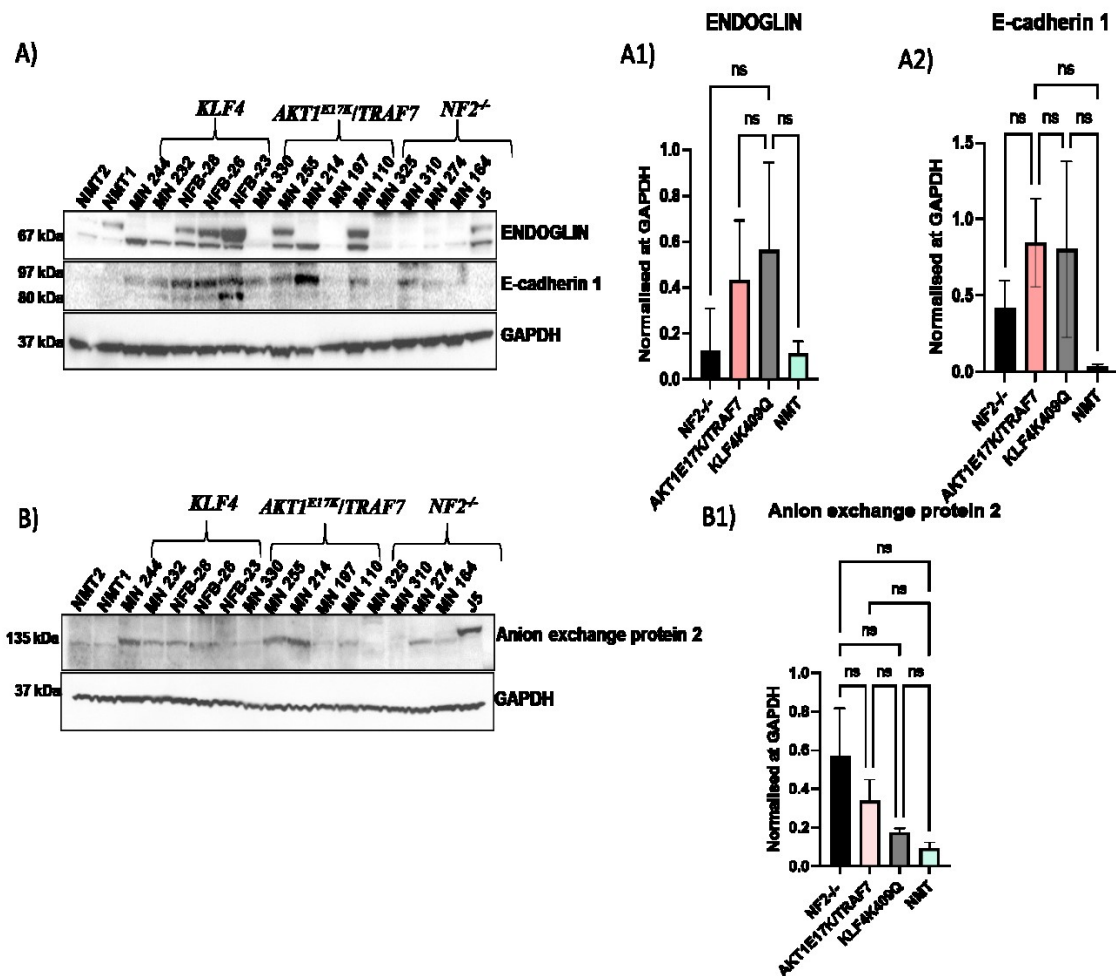


**Figure 35:** Validation of proteins identified as significantly upregulated in *KLF4*<sup>K409Q</sup>/*TRAF7* vs. other mutational subtypes and NMT. (A and B) Western blot analysis of upregulated proteins endoglin, E-cadherin 1 and anion exchange protein 2 in *KLF4*<sup>K409Q</sup>/*TRAF7*, GAPDH as a loading control. NMT ( $n=2$ ); *NF2*<sup>-/-</sup> ( $n=5$ ), *AKT1*<sup>E17K</sup>/*TRAF7* ( $n=5$ ) and *KLF4*<sup>K409Q</sup> ( $n=5$ ). (A1, A2 and B1) Histogram showing quantification of proteins Endoglin, E-cadherin 1 and Anion exchange protein 2 respectively. Data represented as  $\pm$ SEM and statistical significance One-way ANOVA is shown by: ns= not significant;  $p>0.05$ ; \*  $p\leq 0.05$ ; \*\*  $p\leq 0.01$ ; \*\*\*  $p\leq 0.001$ ; \*\*\*\*  $p\leq 0.0001$ .

### 3.6.5.2 Immunohistochemistry of differentially regulated protein candidates for *KLF4*<sup>K409Q</sup>/*TRAF7* mutant meningioma

From IHC average scoring analysis, it was observed that *KLF4*<sup>K409Q</sup>/*TRAF7* mutant meningioma group showed the highest scoring compared to other meningioma mutational subtypes and NMT for both endoglin and E-cadherin 1, with these proteins mostly detected in the cytoplasm (Fig-36 a, a1, b and b1). Immunostaining results of endoglin reflected the mass-spectrometry data and WB analysis.



On other hand, strong immunostaining was observed for anion exchange protein 2 in all meningioma subtypes compared to NMT with no clear differences among meningioma mutant subtype groups (Fig-36 c and c1). The staining results for anion exchange protein 2 were not reflective of Western blot and mass-spectrometry analysis. To be noted for IHC validation a different manufacturer of anion exchange protein 2 antibody used.

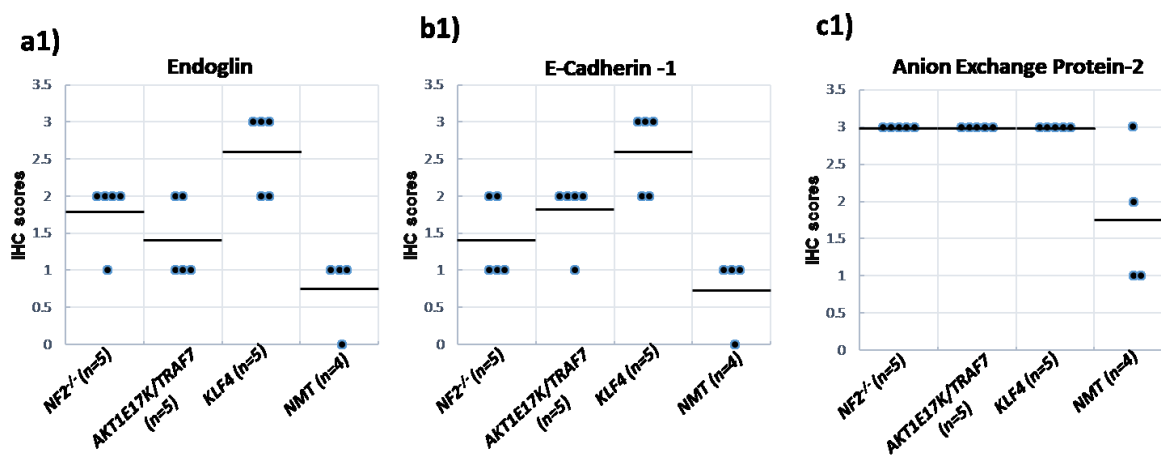
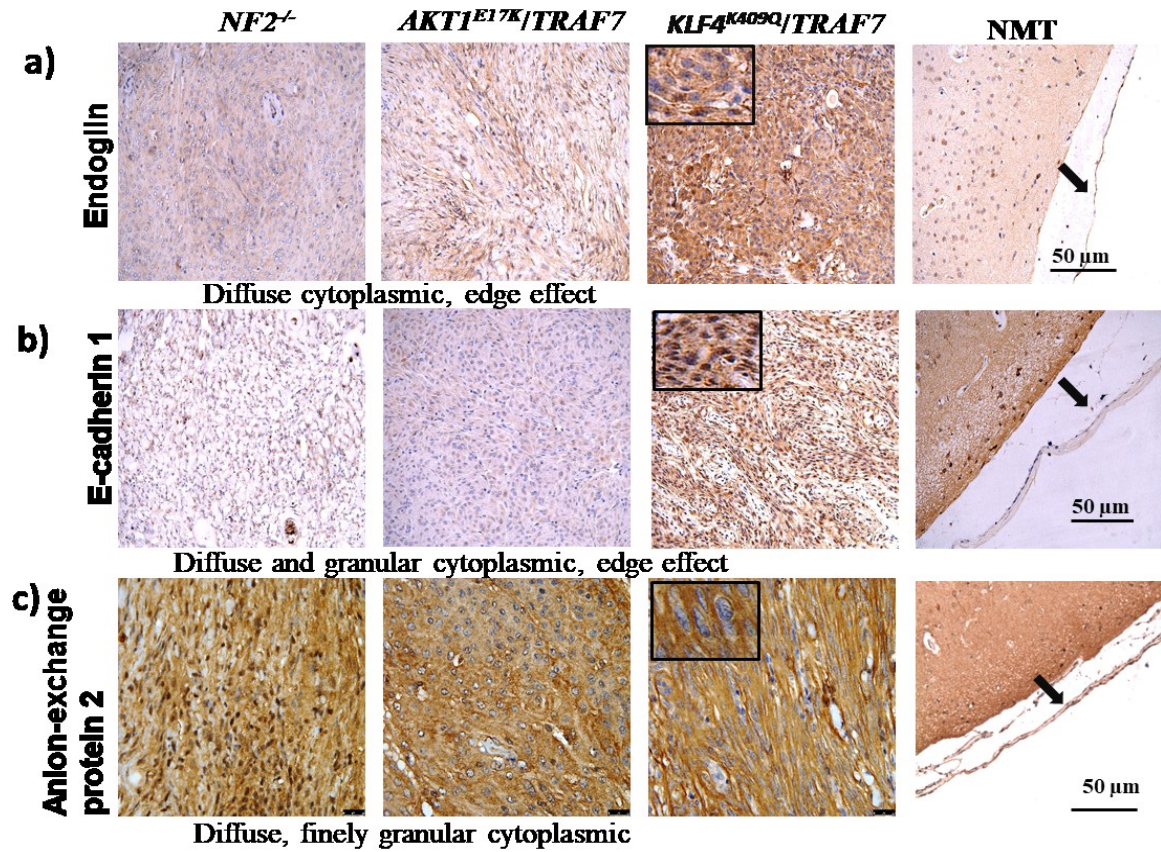


**Figure 36:** Immunohistochemistry analysis of *KLF4*<sup>K409Q</sup>/*TRAF7* mutant meningioma-specific candidate proteins. a, b and c) Immunostaining images of Endoglin, E-cadherin 1 and Anion exchange protein 2 at 40x magnification. a1, b1 and c1) Corresponding IHC scoring



of Endoglin, E-cadherin 1 and Anion exchange protein 2 respectively represent as mean calculated based on staining score shown in the black bold line for each group. Scoring criteria 0 = absent, 1= Weak, 2 = moderate and 3 = strong.

### **3.7 Meningioma grade-I**

#### **3.7.1 Meningioma grade-I protein analysis irrespective of genotype**

Finally, I wanted to see which proteins had increased expression across all meningioma tumours, regardless of their mutational status, in comparison to NMT. Subsequently, distinct proteins in meningioma were identified by overlapping three sets of data (*AKT1<sup>E17K</sup>/TRAF7* vs. NMT, *NF2<sup>-/-</sup>* vs. NMT and *KLF4<sup>K409Q</sup>* vs. NMT) using venn diagrams (Fig-37). Fold change criteria were the same as the previous set as follows: Proteins demonstrating  $\log_2 \text{FC} \geq 1$ ;  $p < 0.05$  were considered as significantly upregulated (Fig- 37 A) and proteins with  $\log_2 \text{FC} \leq -1$ ;  $p < 0.05$  as significantly downregulated (Fig- 37 B).

Only 10 proteins consistently showed increased expression amongst all benign meningioma, while 253 proteins were consistently downregulated compared to NMT (Fig-38 A and B). These results imply that the proteomic landscape of mutational subtypes is highly variable. Tables -16 and 17 contain partial lists of commonly upregulated and downregulated proteins in benign meningioma and the complete list can be found in appendix tables 5 and 6 respectively.

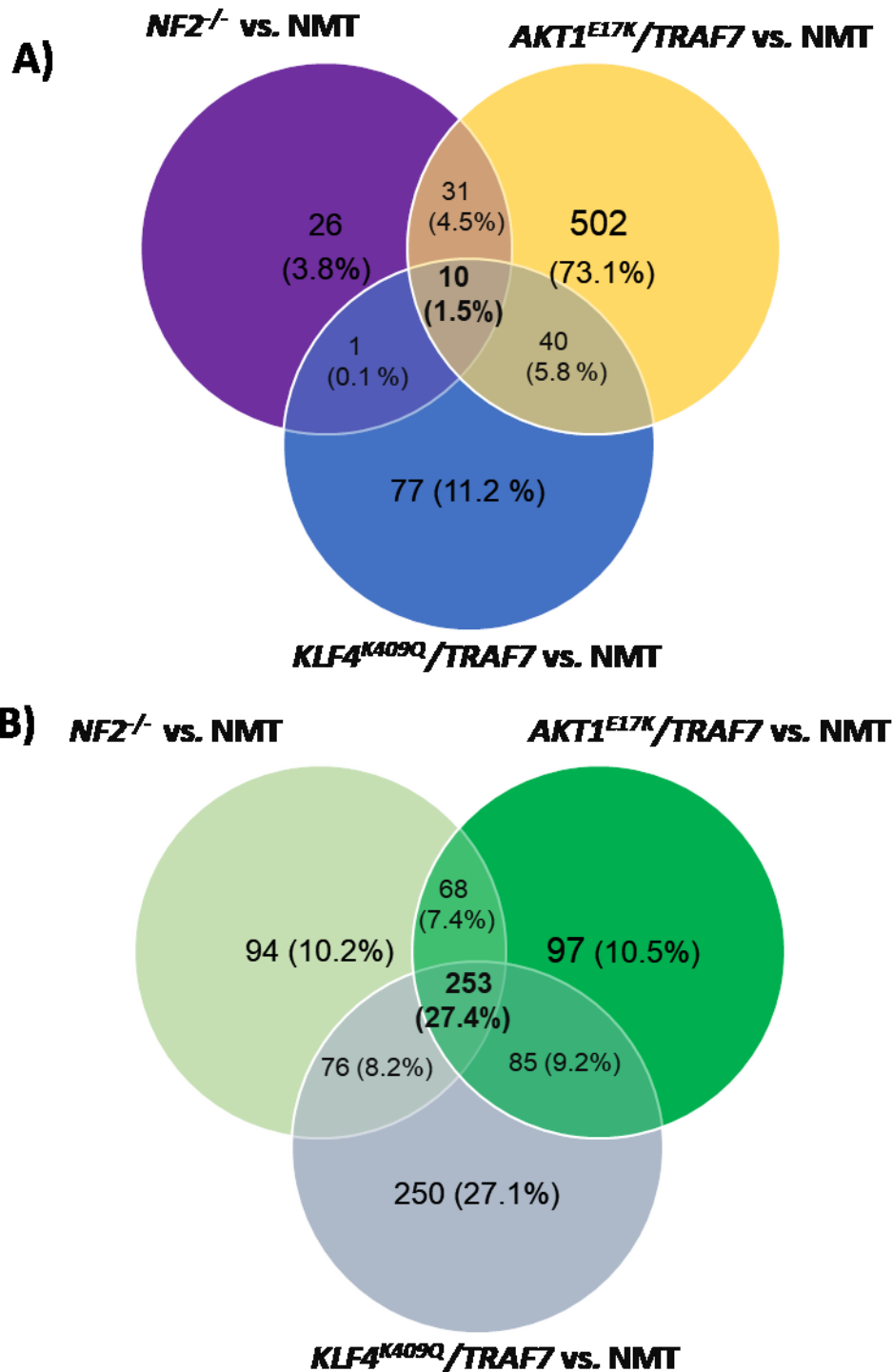


**Figure 37: Meningioma grade I specific proteins regardless of mutations.** (A) Venn diagram illustrating the distinct and overlapping only 10 upregulated proteins from differential expression analysis unique to the benign meningioma in comparison to NMT. (B) Venn diagram illustrating the distinct and overlapping only 253 downregulated proteins from differential expression analysis unique to the meningioma. Upregulated proteins ( $\log_2 \text{FC} \geq 1$ ;  $p\text{-value} < 0.05$ ). Downregulated proteins ( $\log_2 \text{FC} \leq -1$ ;  $p\text{-value} < 0.05$ ). Significance determined by Student's *t*-test.

Uniprot ID	Protein name	Log2 FC <i>AKT1</i> <sup>E17K</sup> / <i>T</i> <i>RAF7</i> vs. NMT	P-value <i>AKT1</i> <sup>E17K</sup> / <i>T</i> <i>RAF7</i> vs. NMT	Log2 FC <i>KLF4</i> <sup>K409Q</sup> / <i>T</i> <i>RAF7</i> vs. NMT	P-value <i>KLF4</i> <sup>K409Q</sup> / <i>T</i> <i>RAF7</i> vs. NMT	Log2 FC <i>NF2</i> <sup>-/-</sup> vs. NMT	P value <i>NF2</i> <sup>-/-</sup> vs. NMT
Q6ZMP0	Thrombospondin type-1 domain-containing protein 4	9.0513	0.000134	8.681101	0.001383	9.76963	2.07E-05
Q9P2B2	Prostaglandin F2 receptor negative regulator	7.872114	3.21E-05	7.022715	0.000844	4.313749	0.026003
B0UXD8	HUMAN HLA-DRA	5.720575	0.000101	7.636087	0.000784	7.309523	0.005213
Q07812	Apoptosis regulator BAX	5.101104	4.7E-05	4.852595	0.000659	4.31843	0.002286
Q53FX5	Lin-7 homolog C variant	6.618656	0.000119	4.809913	0.040019	4.555417	0.078835

**Table: 16** A partial lists of significantly upregulated proteins unique to benign meningioma compared to NMT. Table showing a partial list of overlapping upregulated proteins from differential expression analysis unique to the mutational meningioma subtype detected via VENNY 2.1. Upregulated proteins ( $\log_2 \text{FC} \geq 1$ ;  $p\text{-value} < 0.05$ ). Significance is determined by Student's *t*-test.

Uniprot ID	Protein name	Log2 FC <i>AKT1</i> <sup>E17K</sup> / <i>T</i> <i>RAF7</i> vs. NMT	P-value <i>AKT1</i> <sup>E17K</sup> / <i>T</i> <i>RAF7</i> vs. NMT	Log2 FC <i>KLF4</i> <sup>K409Q</sup> / <i>T</i> <i>RAF7</i> vs. NMT	P-value <i>KLF4</i> <sup>K409Q</sup> / <i>T</i> <i>RAF7</i> vs. NMT	Log2 FC <i>NF2</i> <sup>-/-</sup> vs. NMT	P value <i>NF2</i> <sup>-/-</sup> vs. NMT
A0A024QZJ4	Myosin, heavy polypeptide 11, smooth muscle, isoform	-13.2699	7.79E-05	-13.3154	1.88E-07	-8.67893	0.002138
Q16853	Membrane primary amine oxidase	-12.9434	9.61E-06	-11.6156	2.62E-05	-13.5585	4.57E-08
D6RGG3	Collagen alpha-1(XII) chain OS	-11.4378	1.28E-06	-9.4238	0.008816	-11.7305	0.000163
K7EMP8	Glial fibrillary acidic protein OS	-11.0712	0.002148	-10.7083	8.64E-05	-11.2581	4.74E-07
V9HWA5	Calponin OS	-10.9918	2.91E-05	-11.6264	1.93E-06	-12.6444	2.33E-05
P23141	Liver carboxylase 1 OS	-10.633	0.000288	-10.9765	9.43E-06	-12.4123	1.37E-07
A0A0U4BW16	Non-muscle myosin heavy chain 9 OS	-10.6194	2.09E-06	-9.22858	7.34E-06	-10.7338	1.05E-06
O94875	Sorbin and SH3 domain-containing protein 2 OS	-10.5649	4.02E-06	-9.36423	4.22E-05	-10.7652	4.27E-07

**Table: 17** A partial lists of significantly downregulated proteins unique to benign meningioma compared to NMT. Table showing a partial list of overlapping downregulated proteins from differential expression analysis unique to the mutational meningioma subtype detected via VENNY 2.1. Downregulated proteins ( $\log_2 \text{FC} \leq -1$ ;  $p\text{-value} < 0.05$ ). Significance is determined by Student's *t*-test.

### 3.7.2 Validation of meningioma grade I specific proteins via Simple WES or Western Blot

Due to sample limitation, only three proteins were chosen for further validation; Lin-7 homolog C variant (LIN-7C), thrombospondin type-1 domain-containing 4 (THSD4), and prostaglandin F2 receptor negative regulator (PTGFRN). Priority is given to those proteins with the highest fold change, and based on their significant expression from mass-spectrometry analysis (Table 16).

Uniprot ID	Protein name	Log2 FC AKT1 <sup>E17K</sup> /TRAF 7 vs. NMT	P-value AKT1 <sup>E17K</sup> /TRAF 7 vs. NMT	Log2 FC KLF4 <sup>K409Q</sup> /TRAF 7 vs. NMT	P-value KLF4 <sup>K409Q</sup> /TRAF 7 vs. NMT	Log2 FC NF2 <sup>-/-</sup> vs. NMT	P value NF2 <sup>-/-</sup> vs. NMT
Q6ZMP0	Thrombospondin type-1 domain-containing protein 4	9.0513	0.000134	8.681101	0.001383	9.76963	2.07E-05
Q9P2B2	Prostaglandin F2 receptor negative regulator	7.872114	3.21E-05	7.022715	0.000844	4.313749	0.026003
Q53FX5	Lin-7 homolog C variant	6.618656	0.000119	4.809913	0.040019	4.555417	0.078835

**Table 18:** Meningioma grade I specific upregulated proteins for validation with fold change and *p*-value from differential expression analysis of Mass-spectrometry data.

LIN-7C expression was commonly significantly higher in *NF2*<sup>-/-</sup> mutant meningioma compared to NMT initially. Later one tumour sample from *NF2*<sup>-/-</sup> mutant meningioma group turned out to be *NF2*<sup>+/+</sup> from next-generation sequence results. Subsequently, the sample had to be excluded from the mass-spectrometry analysis which then rendered the cohort to show that LIN-7C was not significantly differentially expressed between *NF2*<sup>-/-</sup> mutant meningioma compared to NMT. Due to the high fold change of LIN-7C expression in *NF2*<sup>-/-</sup> mutant meningioma it was still considered for further validation (Table 18). In the Simple wes analysis, LIN-7C showed significant overexpression in both *NF2*<sup>-/-</sup> and *AKT1*<sup>E17K</sup>/*TRAF7* mutant meningioma compared to NMT which is in line agreement with the mass-spectrometry analysis. Conversely, in comparison to NMT higher expression of LIN-7C was seen in *KLF4*<sup>K409Q</sup> mutant meningioma, however, it was not significant in comparison to NMT (Fig-38 B and B1).

The mass-spectrometry analysis detected PTGFRN at 97 kDa molecular weight, however, in WB analysis, a double band was observed around 100 kDa. This double band is likely due to glycosylation as André *et al.*, (2007) observed 17 glycosylated isoforms in their 2-D PAGE and lectin blot analyses for PTGFRN expression. Therefore, I quantified the intensity for both bands and observed PTGFRN significantly overexpressed in both *KLF4*<sup>K409Q</sup> and *AKT1*<sup>E17K</sup>/*TRAF7* mutant meningioma compared to NMT which reflects our mass-

spectrometry results. However, the WB image showed that PTGFRN expressions were variable among the different tumour samples. PTGFRN is expressed as a single band in all *NF2*<sup>-/-</sup> mutant meningioma samples, whereas almost all merlin positive samples (*KLF4*<sup>K409Q</sup> and *AKT1*<sup>E17K</sup>/*TRAF7* mutant meningioma) showed a double band for PTGFRN (Fig-38 A and A2). Further experiments are needed to confirm and unpick this distinct variation.

THSD4 protein was detected at 112 kDa via mass-spectrometry but in WB analysis two isoforms were observed; one isoform around 112 kDa and another isoform at 80 kDa. Almost all tumour samples showed a strong band for 80 kDa THSD4 (a faint band was observed in one sample of NMT), whilst 112 kDa THSD4 expression was absent in NMT. WB statistical analysis demonstrated that THSD4 is significantly overexpressed in *NF2*<sup>-/-</sup> mutant meningioma samples compared to NMT (Fig-38 A and A1). However, THSD4 expression showed an increased tendency in both *KLF4*<sup>K409Q</sup> and *AKT1*<sup>E17K</sup>/*TRAF7* mutant meningioma compared to NMT. These results support mass-spectrometry findings.

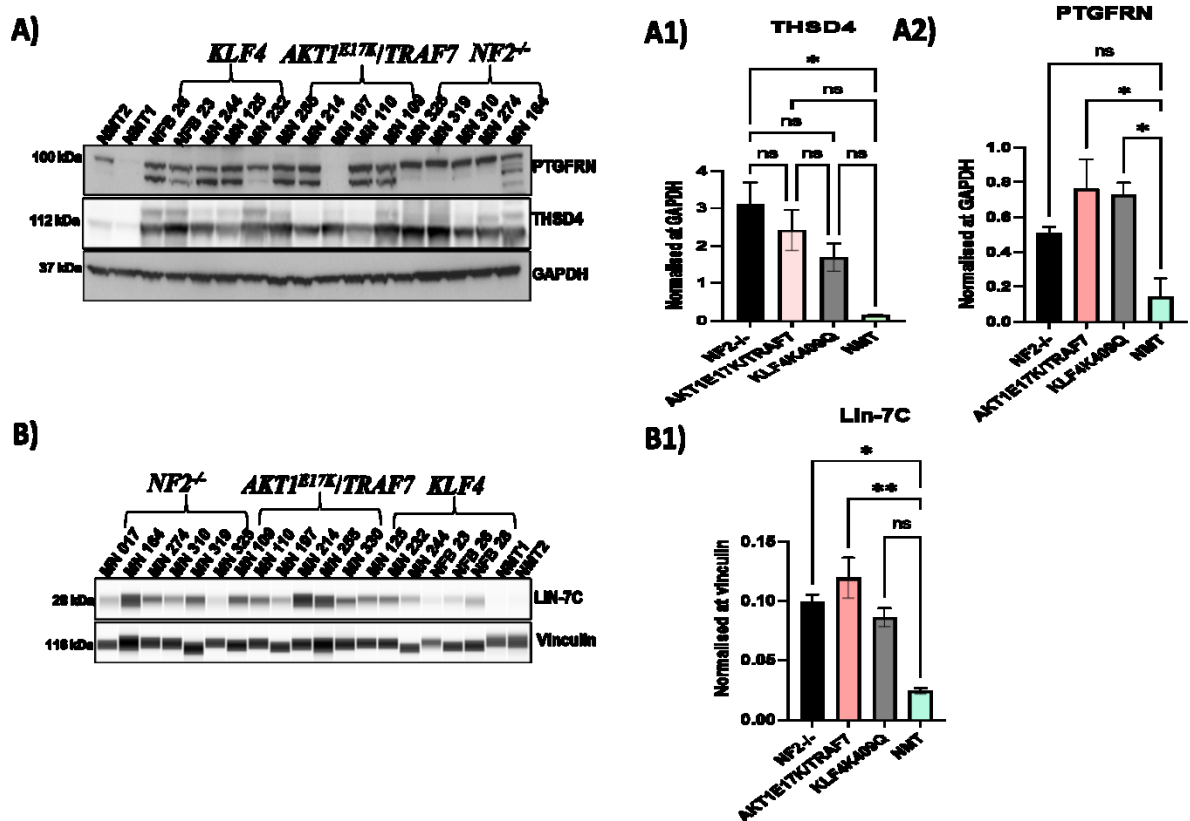


**Figure 38:** Validation of proteins identified as significantly upregulated in benign meningioma compared to NMT. (A) Western blot images of upregulated proteins (PTGFRN and THSD4) in meningioma, GAPDH as a loading control. NMT (*n*=2), *NF2*<sup>-/-</sup> (*n*=5), *AKT1*<sup>E17K</sup>/*TRAF7* (*n*=5) and *KLF4*<sup>K409Q</sup> (*n*=5). A1 and A2) Histogram showing quantification of corresponding proteins (THSD4 and PTGFRN) respectively. (B) Simple wes image of

upregulated protein LIN7C expression in meningioma, Vinculin as a loading control. NMT ( $n=2$ ),  $NF2^{-/-}$  ( $n=5$ ),  $AKT1^{E17K}/TRAF7$  ( $n=5$ ) and  $KLF4^{K409Q}$  ( $n=5$ ). B2) Data represented as  $\pm$ SEM and statistical significance One-way ANOVA is shown by: ns= not significant;  $p>0.05$ ; \*  $p\leq 0.05$ ; \*\*  $p\leq 0.01$ ; \*\*\*  $p\leq 0.001$ ; \*\*\*\*  $p\leq 0.0001$ .

### 3.7.3 Immunohistochemistry of differentially regulated candidates for meningioma grade-I

LIN7C immunostaining was strong in almost all tumour tissue sections, compared to normal meninges sections, which showed moderate staining (Fig-39 a and a1). These findings, again back up mass spectrometry and WB findings.

In terms of PTGFRN expression in IHC, there was a noticeable difference between  $KLF4^{K409Q}$  mutant meningioma and NMT, with  $KLF4^{K409Q}$  mutant meningioma scoring strongly and NMT scoring only weakly (Fig-39 b and b1). On other hand, no differences in staining were observed between the other mutational subtypes ( $AKT1^{E17K}/TRAF7$  and  $NF2^{-/-}$  mutational meningioma subtypes) and NMT.

The  $NF2^{-/-}$  mutant meningioma group had the highest average scoring compared to other meningioma mutational subtypes and NMT for THSD4 where it was predominantly found in the cytoplasm (Fig-39 c and c1). The results of THSD4 immunostaining were consistent with our mass-spectrometry and WB analysis. These data imply that THSD4 could be a promising candidate for further investigation, such as functional validation in benign meningiomas compared to normal meninges.

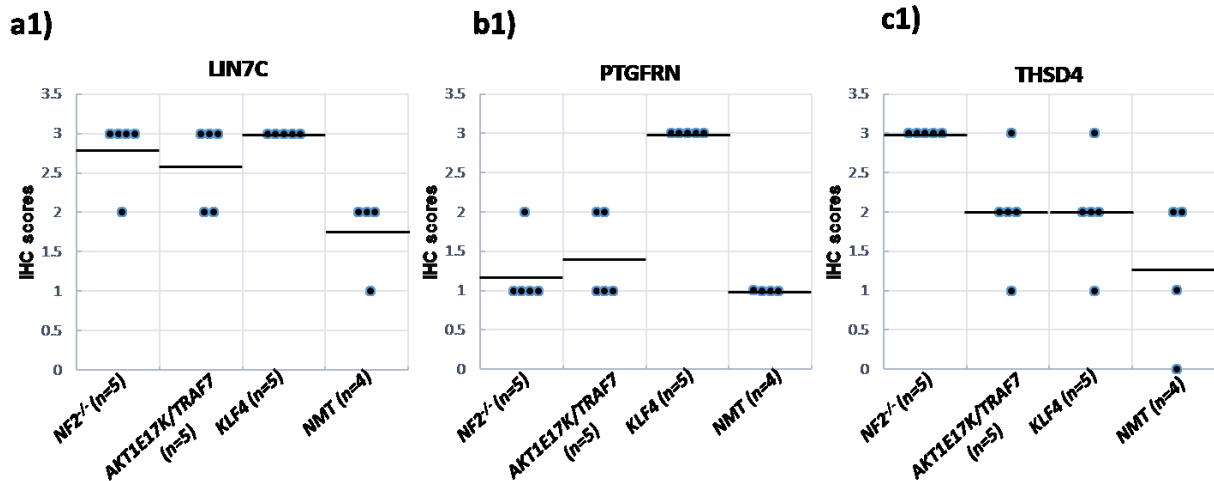
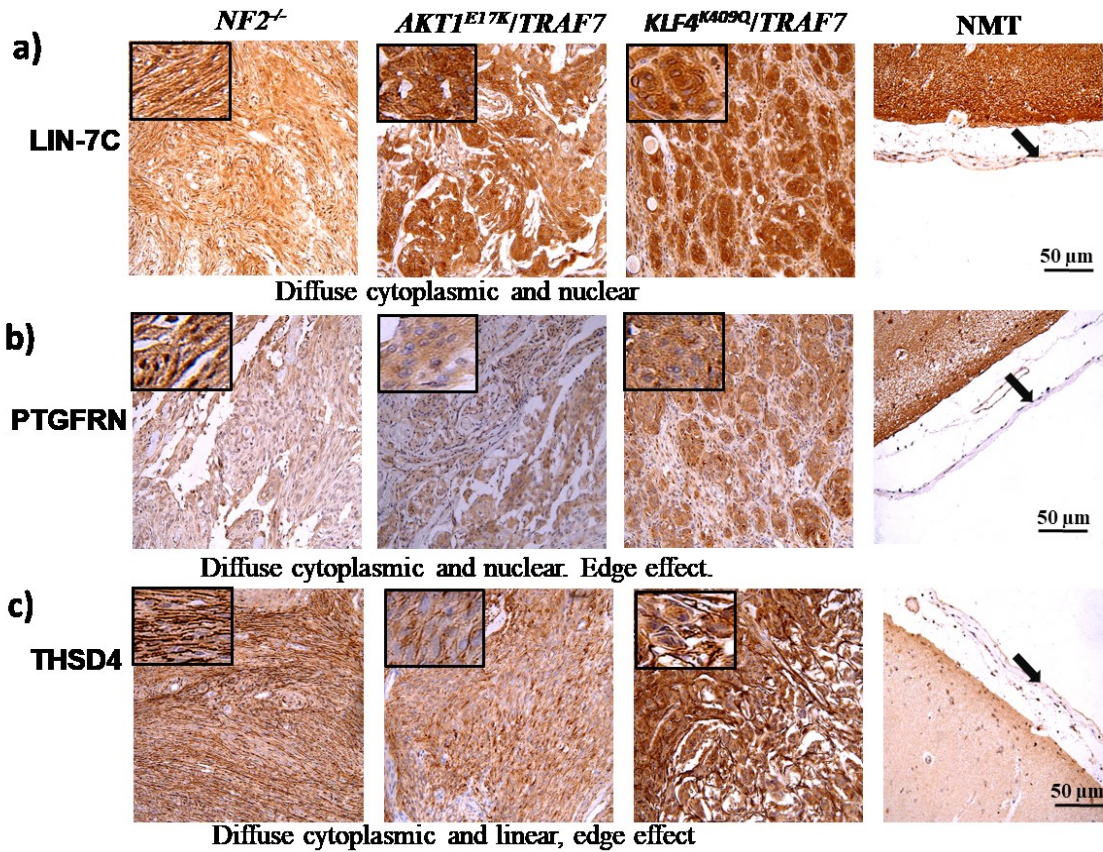


**Figure 39:** Immunohistochemistry analysis of meningioma grade I specific candidate proteins. a, b and c) Immunostaining images of LIN7C, PTGFRN, and THSD4 at 40x magnification. a1, b1 and c1) Corresponding IHC scoring of LIN7C, PTGFRN, and THSD4 respectively represent as mean calculated based on staining score shown in the black bold line for each group. Scoring criteria 0 = absent, 1= Weak, 2 = moderate and 3 = strong.



### 3.8 Summary and conclusion of global proteomics data analysis

This study is the first proteomic analysis of *AKT1<sup>E17K</sup>/TRAF7* and *KLF4<sup>K409Q</sup>* mutational subtypes in meningioma to date and has identified a total of 3490 and 3179 proteins respectively in these subtypes. Hierarchical clustering showed mutational subtypes grouped together based on their global proteomic profiles except for *NF2<sup>-/-</sup>* meningioma mutational subtype.

*AKT1<sup>E17K</sup>/TRAF7*, *KLF4<sup>K409Q</sup>* and *NF2<sup>-/-</sup>* differential expression analysis revealed upregulated proteins specific to these groups. Pyruvate carboxylase, GMDS, CLIC3 and CRABP2 are highly specific for *AKT1<sup>E17K</sup>/TRAF7* meningioma mutational subtype and confirmed via WB and Simple wes. Endoglin is highly expressed in *KLF4<sup>K409Q</sup>* meningioma mutational subtype also validated via WB and IHC. Annexin-3 expression was significantly high for *NF2<sup>-/-</sup>* meningioma mutational subtype compared to other mutational meningioma subtypes and NMT which is validated via both Simple wes and IHC. Knocking down of this protein reduced Benmen-1 cell proliferation.

*AKT1<sup>E17K</sup>/TRAF7* mutant meningioma show 162 upregulated proteins enriched in the following cellular function: mitochondrial electron transport, chloride transmembrane transport, NADH dehydrogenase activity, and oxidative phosphorylation pathway. Conversely, the *KLF4<sup>K409Q</sup>* meningiomas subtype specific 14 upregulated proteins which were highly enriched in extracellular matrix disassembly and focal adhesion GO terms.

Across all meningioma subtypes, THSD4, LIN7C, and PTGFRN showed significant expression compared to NMT and these are validated via WB/Simple wes and IHC.

Further validation and functional verification (with drug inhibition or knockdown approaches) of potential candidates will allow us to identify potential drug targets/biomarkers for these benign meningiomas.

## **4. Results- Phosphoproteomic and phosphopeptide analysis of mutational subtypes of meningioma grade-I**

### **4.1 Introduction**

Phosphorylation is an important post-translational alteration involved in regulating several biological events such as cellular protein activity, subcellular localisation, degradation, cell division, cell growth, cell differentiation, and cellular communication. It is the most important key to regulating cell signalling (Hunter, 2000; Pawson and Scott, 2005). Protein phosphorylation on serine, threonine, and tyrosine residues are most common (Hunter, 2009). Thus, it may be required to determine which amino acid residues are phosphorylated in order to fully comprehend phosphorylation and its effect. Identifying phosphorylation sites may indicate which protein kinase regulates a protein, aiding in the understanding of the signal transduction pathways' biological function and relevance (Yates III, 1998; Aebersold and Mann, 2003; Zhou *et al.*, 2009). Furthermore, phosphorylation induces protein activation or inactivation, leading to changes in function which are linked to the various diseases (Narumi *et al.*, 2012). As a result, phosphoproteomics analysis can help identify critical biomarkers for assessing disease etiology and detect therapeutic targets (Narumi *et al.*, 2012). Validation of large-scale phosphoproteome analysis greatly increases the value of discovering biomarkers (Narumi *et al.*, 2012; Lopez *et al.*, 2013).

The use of mass spectrometry (MS) based technologies for phosphoprotein and phosphosite identification has become common place in recent years to detect disease markers. Phosphoproteomics investigations using mass spectrometry have identified a small number of possible biomarkers and therapeutic targets in meningioma in recent years (Dunn *et al.*, 2019; Prada *et al.*, 2018; Prada *et al.*, 2020).

This study consisted of a large-scale unbiased label-free mass-spectrometry-based phosphoproteomics approach in a total of 14 tissue samples (12 meningioma grade I of different mutational subtypes and two normal meninges). Following subsequent MS data processing and analysis, phosphoproteins and differential protein expression were determined by comparing meningioma mutational subtypes and normal meninges.

In addition to this, mass-spectrometry incorporated with isobaric tandem mass tags (TMTs) was also performed to identify large-scale site-specific phosphorylated peptides in a total of

eight tissue samples (six meningioma grade I mutational subtypes and two normal meninges). Following that differential phosphosites expression analysis was performed among the mutational subtypes. To provide biological insight, the phosphopeptide data set was analysed using KinSwingR package in order to predict the differential kinases activity in the meningioma samples which could lead to the identification of novel drug targets for meningioma. Subsequently, significantly upregulated kinases have been predicted by comparing different meningioma mutational subtypes groups and normal meninges.

Finally, to suggest potential biomarkers or therapeutic targets, validation of several upregulated kinases via different techniques such as WB, IHC, and functional assay (drug treatment) was performed.

## **4.2 Phosphoproteomic analysis of meningioma subtypes**

### **4.2.1 Phosphoproteins identification and quantification**

In total, 3193 phosphoproteins have been identified across 14 tissue samples including 12 meningiomas and two healthy normal meningeal tissues (NMT) as control with a 1% false discovery rate (FDR) by LC-MS based label-free phosphoproteomics and similar analysis also done by Bassiri *et al.*, (2017); Dunn *et al.*, (2019). Among the 3193 phosphoproteins, 2781 were identified with at least two distinct ‘razor and unique’ peptides. Figure 41 depicts the distribution of the 3193 identified phosphoproteins among the sample groups of NMT, *NF2<sup>-/-</sup>*, *AKT1<sup>E17K</sup>/TRAF7*, and *KLF4<sup>K409Q</sup>/TRAF7 mutant* meningioma subtypes. 1516 phosphoproteins were identified within normal meninges (n=2) whilst, in meningioma tissue, 1860 phosphoproteins were identified across *AKT1<sup>E17K</sup>/TRAF7* mutant subtypes (n=3), 2520 phosphoproteins identified in *NF2<sup>-/-</sup>* mutant subtypes (n=6) and 2008 phosphoproteins were identified in *KLF4<sup>K409Q</sup> /TRAF7* meningioma mutants (n=3) (Fig-40).

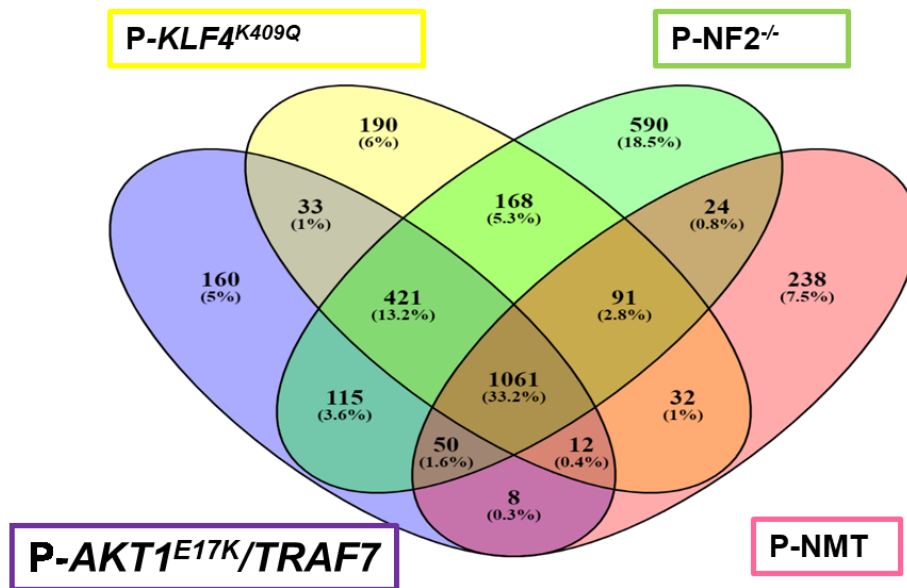


**Figure 40: Distribution of identified phosphoproteins across all sample groups.** Label-free quantitative (LFQ) phosphoproteomics by LC-MS/MS was used to identify 3193 phosphoproteins in *AKT1<sup>E17K</sup>/TRAF7* mutant meningioma ( $n=3$ ), *NF2<sup>-/-</sup>* mutant meningioma ( $n=6$ ), *KLF4<sup>K409Q</sup>/TRAF7* ( $n=3$ ), and normal meningeal tissue (NMT,  $n=2$ ). Phosphoproteins were identified by at least two ‘razor and unique’ peptides with an FDR of 1%.

#### 4.2.2 Hierarchical clustering of meningioma mutational subtypes

Similar to global proteomics, unsupervised hierarchical clustering was performed to identify tumour samples similarities based on phosphoprotein expression profiles. As described previously, the data obtained from Max-Quant were  $\log_2$  transformed, imputed with normal distribution, and normalised using Z scoring and median normalisation. This approach classified the panel of tumour samples into two overarching groups containing four clusters (Fig-41). All meningioma samples with *AKT1<sup>E17K</sup>/TRAF7* mutation ( $n=3$ ) tended to cluster together and a similar pattern was observed for *KLF4<sup>K409Q</sup>/TRAF7* ( $n=3$ ) group samples (Fig-41). In contrast, *NF2<sup>-/-</sup>* mutant samples grouped on either side of the *AKT1<sup>E17K</sup>/TRAF7* mutant samples, forming partial and mixed clusters (Fig-41). These results suggest variability among the meningioma *NF2* mutant subtypes detected by phosphoproteomics. Additionally, hierarchical clustering showed the two normal meninges clustered together away from the meningioma subtypes (Fig-41). Hierarchical clustering of meningioma mutational tumour samples based on phosphoprotein expression profile showed an identical pattern to that on the global proteomics data set (Fig-14).

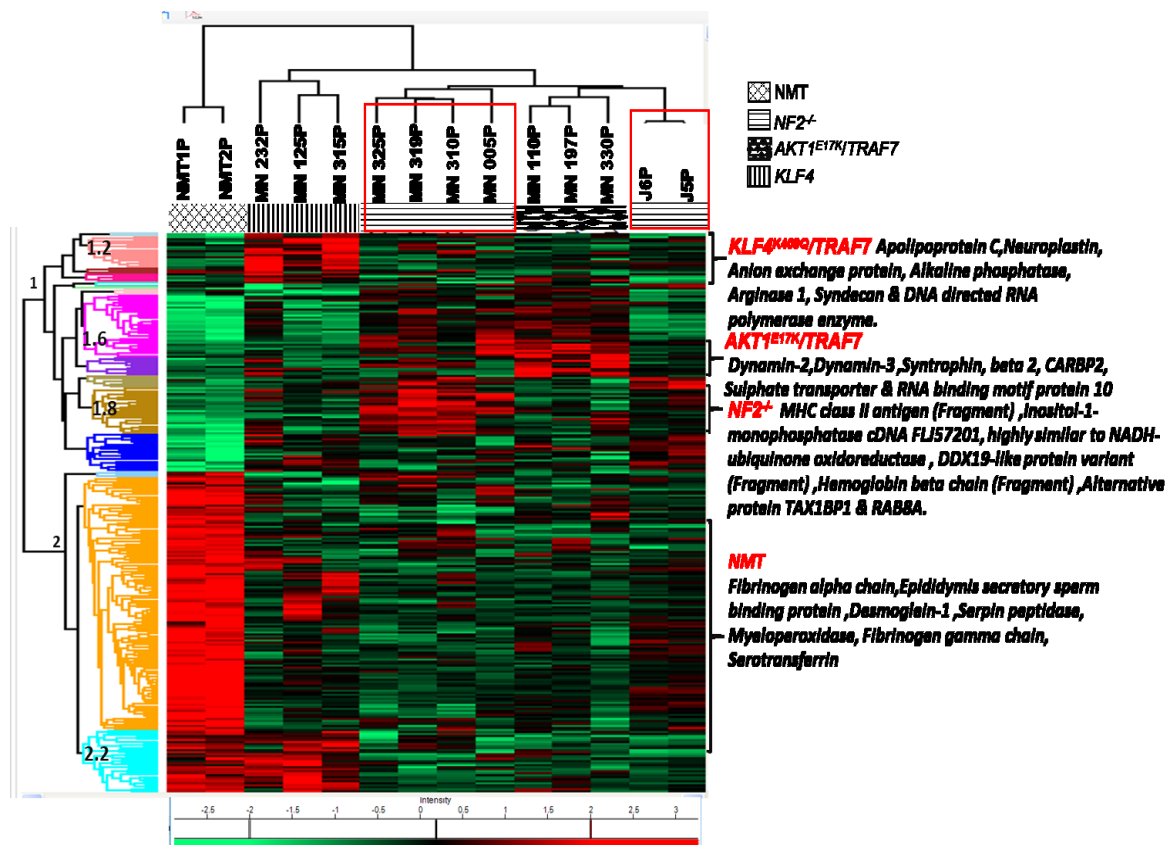


**Figure 41: Meningioma samples clustering based on their phosphoproteomic profiles and comparative analysis of different mutational subtypes of meningioma and normal meninges.** Hierarchical clustering was generated using  $\log_2$  LFQ values in Perseus version 1.6.2.3. The red boxes demonstrate clustering of all  $NF2^{-/-}$  mutant samples on either side of samples with  $AKT1^{E17K}/TRAF7$  mutations and NMT clusters away from the tumour groups. Moreover, hierarchical clustering presented 270 phosphoproteins significantly differentially expressed across all groups based on relative expression values. Protein cluster numbers are shown on the left-hand side in different colours and numbered 1 and 2. Partial lists of the most significant phosphoproteins upregulated in each sample group are detailed in blue on the right-hand side. One-way ANOVA was carried out among four groups ( $AKT1^{E17K}/TRAF7$ ,  $KLF4^{K409Q}/TRAF7$ ,  $NF2^{-/-}$  and NMT) with  $p < 0.05$ . Clustering was created using Z scoring and median normalisation via Perseus 1.6.2.3 software.

Analysis of variance (ANOVA) was performed in order to determine statistical significance identified 270 significantly differentially expressed phosphoproteins between meningioma subtypes and NMT ( $p$ -value  $< 0.05$ ). Hierarchical clustering of these 270 phosphoproteins showed two distinct clusters, one of which (Fig-41; clusters 1) diverges into several small clusters including phosphoproteins that are specifically more highly expressed in meningioma with  $AKT1^{E17K}/TRAF7$ ,  $KLF4^{K409Q}/TRAF7$ , and  $NF2^{-/-}$  mutations compared to NMT. Conversely, the big cluster-2 was fractionated into three which consists of a total of 154 phosphoproteins that showed overexpression in NMT compared to meningioma mutational

subtypes. However, the cluster highlighted in turquoise colour (cluster 2.2) showed overexpressed phosphoproteins were shared between normal meninges and *KLF4<sup>K409Q</sup>/TRAF7* mutant subtypes (Fig-41).

The cluster in pink (cluster 1.2) comprised a total of 17 phosphoproteins specific to *KLF4<sup>K409Q</sup>/TRAF7* mutant subtypes including apolipoprotein C, arginase-1, anion exchange protein, alkaline phosphatase, DNA-directed RNA polymerase I subunit RPA1, syndecan, periplakin, and neuroplastin (Fig-41).

*AKT1<sup>E17K</sup>/TRAF7* mutant subtypes from cluster-1.6 (pink & purple) consist of 37 phosphoproteins and showed a significant increase in dynamin-2, dynamin-3, syntrophin, beta 2, CARBP2, sulphate transporter & RNA binding motif protein 10, insulin-like growth factor binding protein 5, insulin-like growth factor binding protein 1 and integrin Beta 1 (Fig-41).

The *NF2<sup>-/-</sup>* mutant subtype specific cluster in brown (cluster-1.8) showed increases in MHC class II antigen, inositol-1-monophosphatase cDNA FLJ57201, highly similar to NADH-ubiquinone oxidoreductase, DDX19-like protein variant, hemoglobin beta chain, alternative protein TAX1BP1 and RAB8A, member RAS oncogene family and glutathione S-transferase phosphoprotein (Fig-41).

Tumour samples with similar genetic backgrounds tended to cluster together based on their differentially expressed phosphoproteins.

Unfortunately, after all these analyses it was not possible to proceed further with this phosphoprotein data because I was not confident with this phosphoproteins data. During sample processing, some fibrotic types of tumour samples after the phosphoprotein enrichment procedure did not yield an equal amount of phosphoproteins. Thus, the sample amount for each tissue lysates was not equal. The standard amount was 2.5 mg protein per sample for phosphoprotein analysis. From some tumours, this amount was achieved after the phosphoprotein enrichment procedure but some did not yield this amount particularly, *KLF4<sup>K409Q</sup>/TRAF7* and *AKT1<sup>E17K</sup>/TRAF7* mutated meningioma which gave approximately 300 µg and 500 µg respectively. It was initially thought that data would be normalised to the lowest concentrations of samples in MAXQUANT, however, upon receiving the data, there were a lot of ‘0’'s indicating phosphoproteins were not identified by mass-spectrometry due to the low amount of samples in that run. Therefore, mass-spectrometry incorporated with isobaric tandem mass tags (TMTs) was performed using 120 µg of meningioma tissue samples in order

to identify large-scale site-specific phosphorylated peptides and their corresponding phosphoproteins.

### 4.3 Phosphopeptide analysis of meningioma subtypes

The phosphorylation status in the meningioma mutational subtypes was studied to measure the post-translational modification of proteins in these samples. The investigation of the phosphorylation status of the serine (S), threonine (T), and tyrosine (Y) residues of the proteins was performed using TiO<sub>2</sub>-based enrichment techniques on eight tissue samples. In total, 6584 phosphorylated sites of each phosphopeptide and their corresponding total of 2388 phosphoproteins have been identified across eight tissue samples including six meningiomas (*AKT1<sup>E17K</sup>/TRAF7* mutant subtypes n=3 and *NF2<sup>-/-</sup>* mutant subtypes n=3) with two healthy normal meningeal tissues (NMT) used as a control with a 5% false discovery rate (FDR) by LC-MS/MS-based TMTs phosphopeptideomics. *KLF4<sup>K409Q</sup>/TRAF7* mutated tumour samples were not included in this experiment due to the lack of tissue lysates. The pie chart (Fig-42) depicts the distribution of the mapped phosphorylation sites of which serine (pS) is 80.69%, threonine (pT) is 5.3%, and tyrosine (pY) is 1.1% (Fig-42). Similar patterns in the percentage of phosphorylation sites were also reported by previous studies (Al-Momani *et al.*, 2018; Dunn *et al.*, 2019). In addition to this, 12.80% ambiguously phosphorylated sites were also identified. This is thought to occur when numerous S, T, and Y candidate residues are present in one phosphopeptide, therefore making it difficult to determine the particular site of phosphorylation (Villén *et al.*, 2007) (Fig-42).

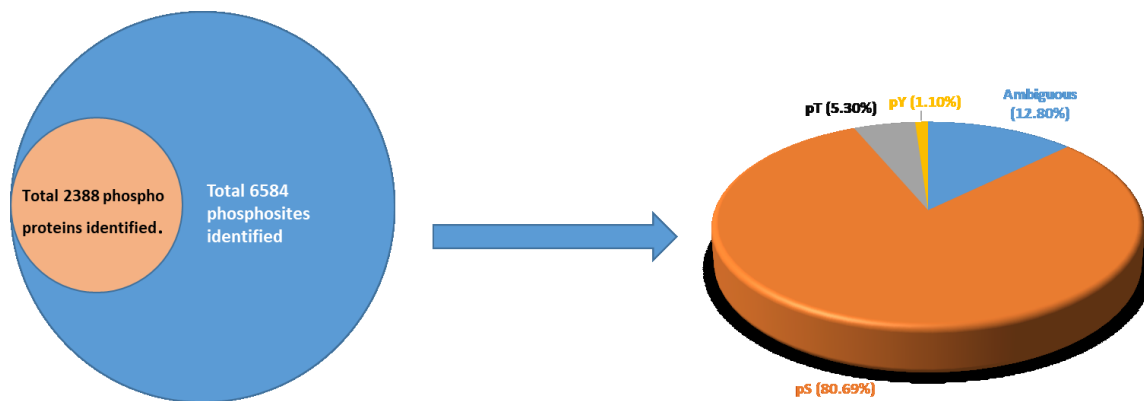


**Figure 42: Overview of the phosphopeptide data set.** Tandem mass tagging (TMTs) phosphopeptide-omics by LC-MS/MS was used to identify 2388 phosphoproteins and 6684 phosphopeptide in *AKT1<sup>E17K</sup>/TRAF7* mutant meningioma ( $n=3$ ), *NF2<sup>-/-</sup>* mutant meningioma ( $n=3$ ) and normal meningeal tissue (NMT) ( $n=2$ ). Phosphopeptides were identified with an FDR of 5%. Pie chart illustrating the distribution of amino acid phosphorylation for serine, threonine, and tyrosine among the mutational meningioma subtypes (*NF2<sup>-/-</sup>* and *AKT1<sup>E17K</sup>/TRAF7*) and NMT.

#### 4.3.1 Detection of phosphorylated motifs

A motif is a short area of a protein's three-dimensional structure or amino acid sequence that is conserved in multiple proteins. They are recognised areas of protein structure that are characterized (or not) by a specific chemical or biological activity (Xiong, 2006). As some motifs are frequently linked to certain kinases, motif analysis was performed to understand the biological input of these identified phosphosites (Peri *et al.*, 2004). First, 15-mer peptides were produced, centered on the identified phosphorylated site, and these were then used to detect 'phosphorylation motifs' in the phosphopeptide data composed of 4620 phosphosites, using the motif-x algorithm within MoMo (MEME suite). A total of 116 motifs were identified among the sample groups *NF2<sup>-/-</sup>*, *AKT1<sup>E17K</sup>/TRAF7* and NMT, of which 105 motifs were significantly mapped at serine (pS) residue, 11 motifs were across threonine (pT) while only one was at a tyrosine (pY) residue by at least two occurrences with  $p < 0.001$ . A binary decision tree was used to further classify motifs/phosphosites based on their chemical characteristics (Villén *et al.*, 2007). Proline-directed (33 %) and acidic (24 %) sites were the most common, followed by basic (13 %), others (4 %), and ambiguous (26 %) (Fig-43), a very similar pattern to which has been reported by previous studies (Villén *et al.*, 2007; Dunn *et al.*, 2019). After motif identification, the corresponding potential kinases could then be predicted that phosphorylated the identified motifs using PhosphoMotif finder from the Human Protein Reference Database. Within the phosphopeptide data set calmodulin-dependent protein kinase II substrate (CAM



family), protein kinase C (PRKC) and AKT kinases were detected against basophilic motifs such as LxRxxs, RRxs and RxRxxs respectively, similar findings observed by Villén *et al.*, (2007) in mouse liver tissue phosphorylation analysis. In contrast, some acidic motifs such as sxDxExE, sxxEE, sDxE, and sDxD recognised casein kinase II, while proline-directed motifs (PxsP and PxtP) were identified in MAPK2 and Ras-related family kinases (GSK-3, ERK1, ERK2 and CDK5). Motif analysis at serine and threonine residue and their corresponding kinases can be found in supplementary data 6 (S6).

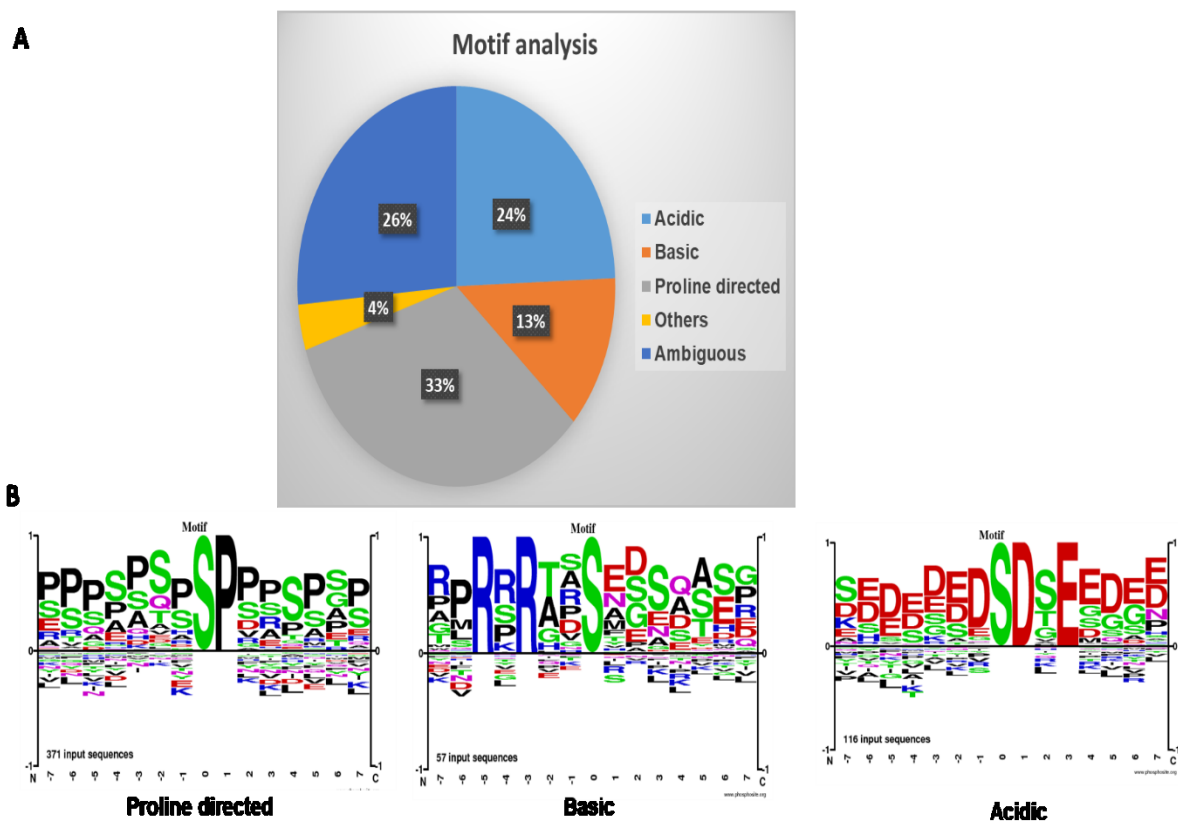


**Figure 43: Phosphosites-specific motif analysis by using motif-x method (MoMo).** A) Pie chart illustrating the distribution of motifs identified based on their chemical properties. B) Examples of sequence logos, phosphorylated serine is in center and Proline is at +1 then classified as proline-directed, Two or more lysine(K)/arginine (R) at -6 to -1, classified as a basic and aspartate(D)/glutamic acid (E) at +1/+2 OR +3 then classified as an acidic motif.

#### 4.3.2 Quantitative changes in phosphorylation sites in meningioma mutational subtypes

A two-sample *t*-test (volcano plot) was performed to identify differentially expressed phosphosites (DEPs) between the meningioma mutational subtypes and normal meninges (Fig 45). Phosphosites with  $\log_2 FC \geq 1$ ;  $p < 0.05$  were considered as significantly upregulated and phosphosites with  $\log_2 FC \leq -1$ ;  $p < 0.05$  as significantly downregulated. Comparative analysis

between *AKT1<sup>E17K</sup>/TRAF7* meningioma subtypes and NMT identified 2917 significantly differentially expressed phosphosites; among them, 2805 phosphosites were upregulated and 99 phosphosites were downregulated in *AKT1<sup>E17K</sup>/TRAF7* subtypes compared to NMT control (Fig-44 A). Phosphosites demonstrating the highest fold changes and thus most highly upregulated in *AKT1<sup>E17K</sup>/TRAF7* mutants compared to NMT include vacuolar protein sorting-associated protein 13D T-1144 (VPS13D T-1144), vimentin (S-10), vigilin (S-944), golgi integral membrane protein 4 S-364 (GOLIM4 S-364), chloride intracellular protein 3 (S-49) (CLIC3 S-49) and sulfate transporter S-36 (S26A2 S-36).

In contrast, a comparison between *NF2<sup>-/-</sup>* mutated meningioma and NMT, identified 2215 phosphosites to be significantly differentially phosphorylated, among them only 2064 phosphosites were upregulated in *NF2<sup>-/-</sup>* mutant subtypes, and 128 phosphosites were significantly downregulated compared to the control (Fig-44 B). Upregulated phosphosites were observed in *NF2<sup>-/-</sup>* mutant subtypes including coatamer subunit alpha (COPA) S-173, PDZ and LIM domain protein 4 (PDLIM4) S-120, neuroblast differentiation-associated protein AHNAK (AHNAK) S-511 and ATP dependent RNA helicase DDX55 (S-594), MHC class-1 antigen (Y-26) and proline-rich AKT1 substrate (S-212).

Differential analysis between the two mutational subtypes, *AKT1<sup>E17K</sup>/TRAF7* and *NF2<sup>-/-</sup>* showed a total of 265 significantly differentially phosphorylated sites. Among these 163 phosphosites were upregulated in the *AKT1<sup>E17K</sup>/TRAF7* mutational subtype while 75 phosphosites were downregulated compared to the *NF2<sup>-/-</sup>* meningiomas (Fig-44 C). Here, golgi integral membrane protein 4 (S-364) was identified as the most significantly differentially phosphorylated phosphosites with the highest log<sub>2</sub> FC, suggesting this phosphosite to be highly specific to the *AKT1<sup>E17K</sup>/TRAF7* mutational subtype. In addition to this, several potentially interesting phosphosites including RNA binding motif protein X-linked-like-1 S-208 (RBMXL1 S-208), sulfate transporter S-12 (S26A2 S-12), golgi apparatus protein 1 S-714 (GLG1 S-714) and chloride intracellular protein 3 S-49 (CLIC3 S-49) showed a similar trend upon comparative analysis with log<sub>2</sub> FC ≥ 2.5 specific to the *AKT1<sup>E17K</sup>/TRAF7* mutational subtype.

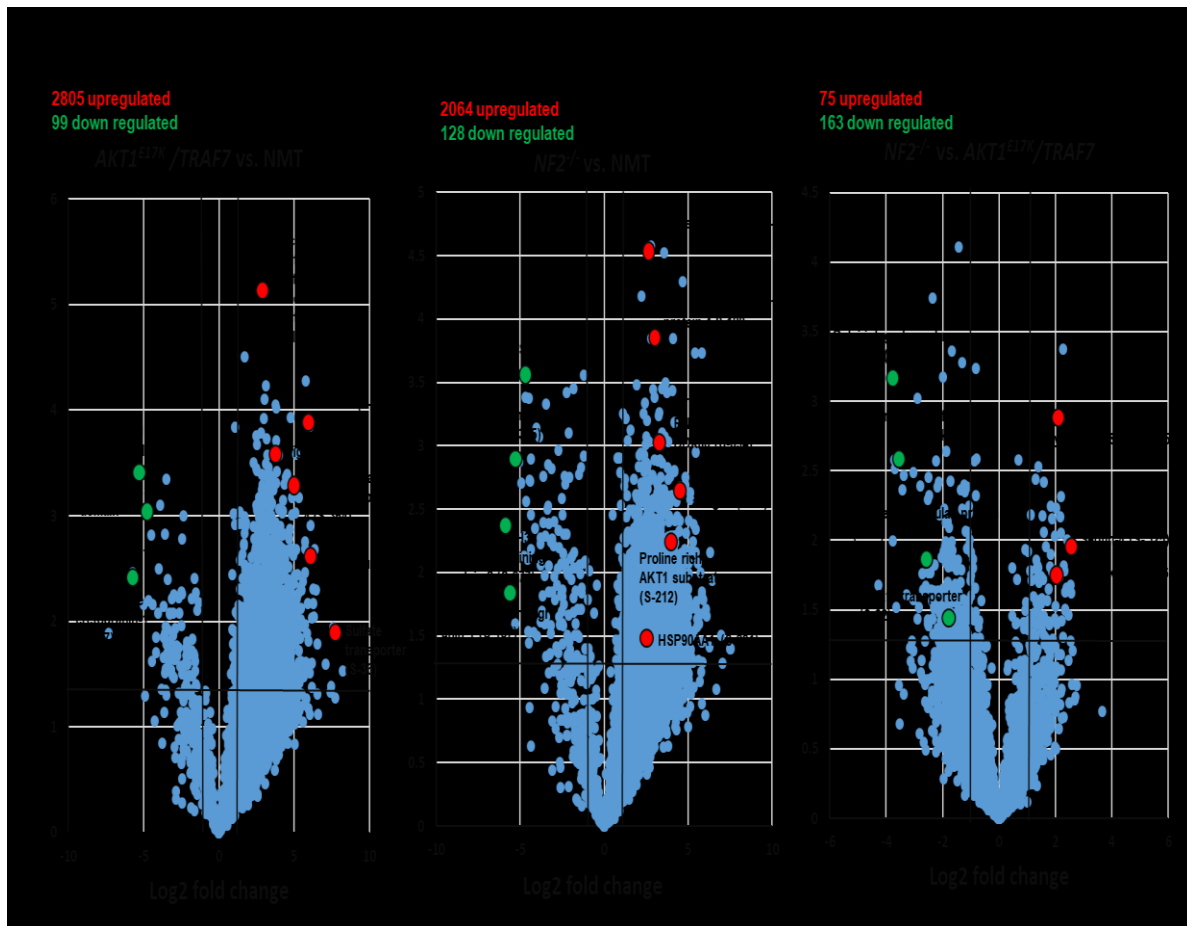


**Figure 44: Differential phosphosites expression between sample groups.** Volcano plots of phosphosites abundance between the mutational subtypes of meningioma and normal meningeal tissue (A, B, C). Depicted are  $\log_2$  fold changes vs.  $-\log_{10} p$ -values (Student's  $t$ -test between replicate measurements). Black lines demarcate  $p$ -value < 0.05 and  $\log_2$  fold change of 1 and -1. Red dots: Upregulated phosphosites ( $\log_2$  FC  $\geq$  1;  $p$ -value < 0.05). Green dots: Downregulated phosphosites ( $\log_2$  FC  $\leq$  -1;  $p$ -value < 0.05). Highlighted phosphosites may be considered potential biomarker candidates for future experimental validation. A) Comparative analysis between  $AKT1^{E17K}/TRAF7$  meningioma subtypes vs. NMT. B) Differential analysis between  $NF2^{-/-}$  vs. NMT C) Comparative analysis between two meningioma mutational subtypes  $AKT1^{E17K}/TRAF7$  vs.  $NF2^{-/-}$ .

## 4.4 Kinase prediction analysis

We identified 6584 phosphosites in total and subsequently performed kinase prediction analysis to be able to infer extensive information on the protein kinase activity (Wirbel *et al.*, 2018).

Despite the fact that just 518 kinases have been identified among about 30,000 human proteins, kinase-mediated phosphorylation affects more than 30% of human proteins, and almost half of the kinases (244) are closely correlated to malignancies and other illnesses (Manning *et al.*, 2002; Chen *et al.*, 2011). Since kinase dysregulation is linked to a variety of disease progression and a variety of novel kinase inhibitors have been approved or are being developed for various cancer types as well as targeted antibodies to inhibit kinase activity (Zhang *et al.*, 2009; Gonzalez de Castro *et al.*, 2013). For the study of diseases and the development of new therapeutics, a thorough understanding of the kinase signalling mechanism is required (Wirbel *et al.*, 2018).

### 4.4.1 Predicted differential kinase activity in meningioma mutational subtypes

Motif analysis and prediction of kinase activity were performed using the KinSwingR package (Engholm-Keller *et al.*, 2019). KinSwingR is able to predict the kinases that phosphorylate each phosphosite and then quantify the activity of each kinase by giving it a swing score derived from *p*-value and log<sub>2</sub>FC of each predicted target phosphosite. KinSwingR analysis of the phosphopeptide data set was used to compare the meningioma subtypes to each other and to the controls (*AKT1<sup>E17K</sup>/TRAF7* vs. NMT, *NF2<sup>-/-</sup>* vs. NMT, and *NF2<sup>-/-</sup>* vs. *AKT1<sup>E17K</sup>/TRAF7*), significant kinases with swing score  $\geq 1$ ;  $p < 0.05$  were considered as significantly upregulated and kinases with swing score  $\leq -1$ ;  $p < 0.05$  as significantly downregulated (Fig-45).

From the phosphosites comparative analysis between *AKT1<sup>E17K</sup>/TRAF7* mutant meningioma and normal meninges, a total of 11 kinases were predicted as significantly differentially activated, among them seven kinases were upregulated and four kinases were downregulated in *AKT1<sup>E17K</sup>/TRAF7* subtypes compared to NMT (Fig-45 A). The upregulated kinases in *AKT1<sup>E17K</sup>/TRAF7* mutants compared to NMT included PRKCA (protein kinase C alpha), CAM2A (calcium/calmodulin Dependent Protein Kinase II Alpha), CHEK1 (checkpoint kinase 1), CHEK2 (checkpoint kinase 2), PRKG1 (protein kinase CGMP-dependent 1), AKT2

(AKT Serine/Threonine kinase 2) and PRKAA2 (protein kinase AMP-activated catalytic subunit alpha 2). In contrast, downregulated kinases are JAK3 (Janus kinase 3), ERBB2 (ErbB2 receptor tyrosine kinase 2), MARK1 (microtubule affinity regulating kinase 1), and PKM (pyruvate kinase muscle isozyme). Among these predicted kinases, PRKCA is the most significantly activated kinases with the highest swing score (swing score= 3.7) in *AKT1<sup>E17K</sup>/TRAF7* mutational subtype compared to NMT.

On the other hand, a comparison of *NF2<sup>-/-</sup>* mutant meningioma and NMT prediction found five kinases significantly differently activated including two kinases that were upregulated and three downregulated (Fig-45 B). The two upregulated kinases are AURKB (aurora kinase B) with a swing score of 2.5 and LCK (lymphocyte-specific protein-tyrosine kinase) with a swing score of 2.3.

A total of 17 significantly differently active kinases were predicted by KinSwingR between the two meningioma mutational subtypes, *AKT1<sup>E17K</sup>/TRAF7* and *NF2<sup>-/-</sup>*. In comparison to *AKT1<sup>E17K</sup>/TRAF7* mutated meningiomas, 10 kinases were upregulated in the *NF2<sup>-/-</sup>* mutational subtype, while seven were downregulated (Fig-45 C). The most significantly differentially activated kinase with the highest swing score (swing score = 3.25) was CSNK2A1 (casein kinase 2 alpha 1), suggesting that this kinase is particularly unique to the *NF2<sup>-/-</sup>* mutated meningioma subtype. In addition to this, several potential kinases including EGFR (epidermal growth factor receptor), FYN (FYN protein tyrosine kinase), EEF2K (eukaryotic elongation factor-2 kinase), and PKM (pyruvate kinase muscle isozyme) were also activated with swing scores more than 1.5 in *NF2<sup>-/-</sup>* mutated meningioma subtype compared to *AKT1<sup>E17K</sup>/TRAF7* mutated meningiomas. In contrast, PRKCD (protein kinase C delta) was significantly activated with the highest swing score (swing score= 2.69) in *AKT1<sup>E17K</sup>/TRAF7* mutated meningiomas compared to *NF2<sup>-/-</sup>* mutated meningioma subtype indicating PKCD would be a potential therapeutic target and/or biomarker for this group.

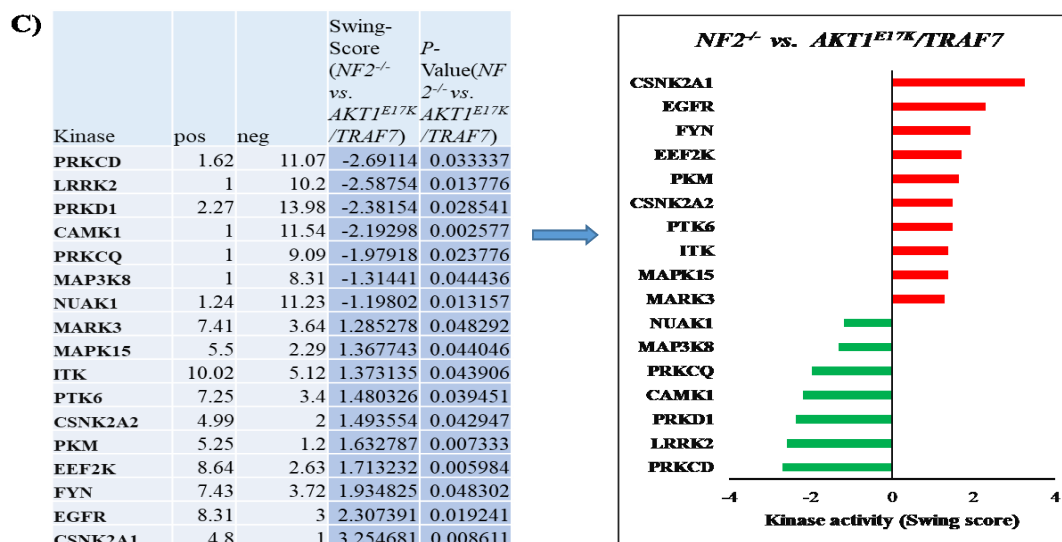
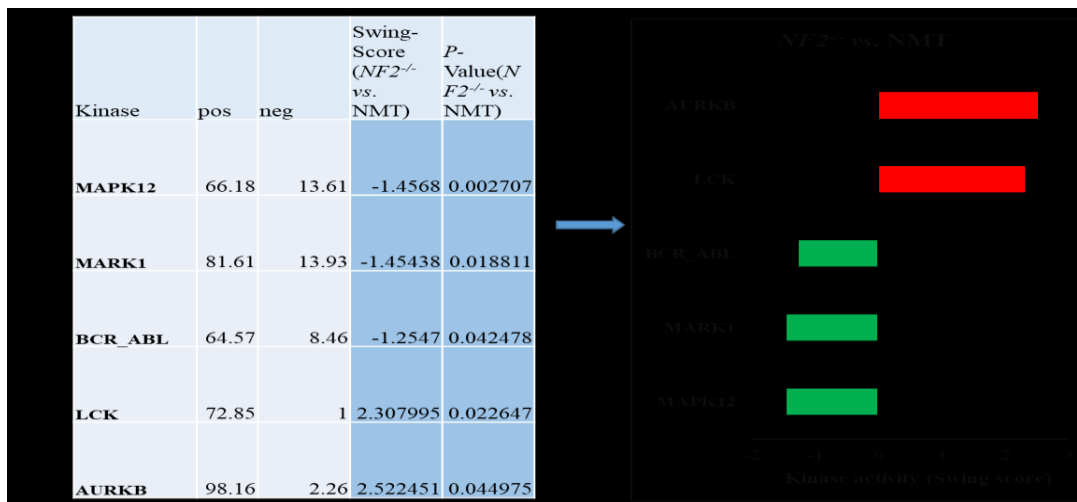
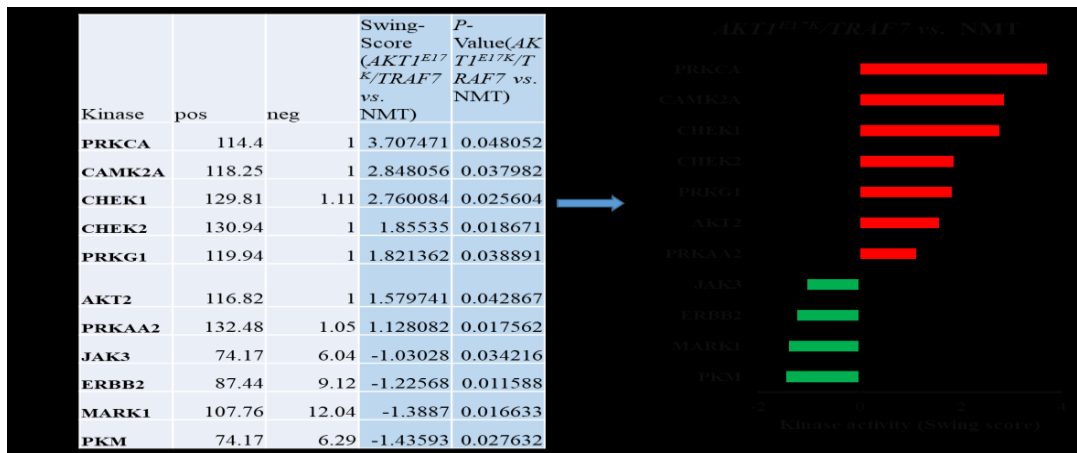


**Figure 45: Differential kinases activity analysis between sample groups.** The table showed the list of predicted significant kinases with swing score and *p*-value and a bar chart illustrating the up and downregulated predicted kinase activity between the mutational subtypes of meningioma and normal meningeal tissue (A, B and C). Red bar: Upregulated kinases (swing score  $\geq 1$ ; *p*-value  $< 0.05$ ). Green bar: Downregulated kinases (swing score  $\leq -1$ ; *p*-value  $< 0.05$ ). A) Comparative analysis between *AKT1<sup>E17K</sup>/TRAF7* meningioma subtypes vs. NMT. B)

Differential analysis between *NF2<sup>-/-</sup>* vs. NMT. C) Comparative analysis between two meningioma mutational subtypes *NF2<sup>-/-</sup>* vs. *AKT1<sup>E17K</sup>/TRAF7*.

#### 4.4.2 Validation of predicted kinases

In order to validate the KinSwingR kinase activity predictions, the activity of several differentially active kinases was assessed by WB for the active phosphorylated forms of these kinases. Anti-phospho kinase antibodies for measuring the activities of the kinases were identified using literature searches and the most cited phosphosites from PhosphoSitePlus<sup>®</sup> database. Due to the lack of sample amount, the priority was given to the kinases which showed a significant KinSwingR swing score  $\geq 1.5$ .

##### 4.4.2.1 Validation of *AKT1<sup>E17K</sup>/TRAF7* specific kinase candidates via WB

**CAMK2A** is a member of the calcium/calmodulin-dependent protein kinase II family largely expressed in the brain, particularly in the postsynaptic region (Liu *et al.*, 2012; Hell *et al.*, 2014). CAMK2 phosphorylation at Thr286 for the isoform CAMK2A isoforms has been proven as an activation site for CAMK2A signalling (Colbran *et al.*, 1989; Hudmon and Schulman, 2002). Here, CAMK2A kinase has been predicted to increase activation in *AKT1<sup>E17K</sup>/TRAF7* mutated meningioma compared to NMT with a high swing score of more than 2.5 (Fig-46 A). Besides literature search, PhosphoSitePlus<sup>®</sup> also showed the most cited phosphorylated active site is Thr286 for CAMK2A kinase activation, therefore I have conducted validation of this phosphosite via WB. However, p-CAMK2A-Thr286 in WB quantitative analysis showed increased activity in NMT compared to *AKT1<sup>E17K</sup>/TRAF7* and *NF2<sup>-/-</sup>* mutated meningioma which is the opposite of KinSwingR kinase prediction analysis (Fig-46 A).

**CHEK1** (Checkpoint kinase 1) is a Serine/Threonine protein kinase that regulates the progression from G2 to the M phase during DNA damage (Waworth *et al.*, 1993). CHEK1 controls a variety of cellular processes, such as DNA damage repair, gene transcription, embryo development, and somatic cell survival (Liu *et al.*, 2000; Takai *et al.*, 2000; Sørensen *et al.*, 2005; Shimada *et al.*, 2008). CHEK1 does not undergo phosphorylation at Ser-317 and 345 without being triggered by DNA damage when cells are prepared to enter mitosis. Some important intermediary proteins including RPA, ATR, and CtIP are required to regulate this DNA damage event, which is a prerequisite for CHEK1 phosphorylation (Xu *et al.*, 2010), and interestingly, PKB/AKT are involved in regulating this process (Xu *et al.*, 2010). In this phosphopeptide data set CHEK1 kinases have been predicted against a total of 488 phosphosites and 156 phosphoproteins and KinSwingR analysis showed upregulation of this

kinase in *AKT1<sup>E17K</sup>/TRAF7* subtypes compared to NMT (Fig-45 A). The phosphorylation site for CHEK1 we chose from phosphosite plus (<https://www.phosphosite.org/proteinAction.action?id=586&showAllSites=true>) showed most cited phosphosite is S-345. Due to the sample limitation, CHEK1-S-317 was not validated. However, by WB analysis, the activity of CHEK1-S345 and total CHEK1 was not detectable at 56kDa (Fig-46 B) unlike as reported by King *et al.*, (2004), even after trialling two different antibodies. Therefore, further validation was not carried out on this kinase.

**CHEK2** (Checkpoint Kinase 2) is a Ser/Thr protein kinase 2 triggered in response to DNA double-strand breakage (Ahn *et al.*, 2004; Bartek and Lukas, 2003; Pommier *et al.*, 2005; Harper and Elledge, 2007; Zoppoli *et al.*, 2012). Ataxia-telangiectasia mutant kinase (ATM), or other phosphatidyl-inositol-3 kinase family kinases ataxia telangiectasia-related kinase (ATR), and DNA-dependent protein kinase (DNAPK) phosphorylates CHEK2 at Thr68 (Matsuoka *et al.*, 2000; Ahn *et al.*, 2000; Bartek and Lukas, 2003; Li and Stern, 2005). As a result of phosphorylation, CHEK2 undergoes homodimerization and autophosphorylation (Ahn and Prives, 2002; Ahn and Prives, 2004; Zoppoli *et al.*, 2012). Followed by active CHEK2 kinase phosphorylates CDC25A, CDC25C, p53, E2F1, and other substrate proteins that are associated with cell cycle arrest, apoptosis, DNA damage response, and mitotic spindle assembly (Powers *et al.*, 2004; Matsuoka *et al.*, 1998; Hirao *et al.*, 2000; Falck *et al.*, 2001; Stevens *et al.*, 2003; Pommier *et al.*, 2005; Zoppoli *et al.*, 2012).

However, in this study CHEK2 has been significantly predicated as an upregulated kinase in *AKT1<sup>E17K</sup>/TRAF7* mutated meningioma compared to NMT, and this kinase was predicted against 430 phosphosites and 135 phosphoproteins with swing score 1.8 (Fig-45 A). According to the phosphosite plus and literature, Thr68 is identified as an active site for CHEK2 kinase signaling. Therefore, CHEK2-Thr68 phosphorylated sites were taken for validation in meningioma tissue samples. In WB, expression of CHEK2-T68 was observed at 56 kDa in only two samples of *NF2<sup>-/-</sup>* mutated meningioma, while there was no signal in *AKT1<sup>E17K</sup>/TRAF7* mutated meningioma samples and NMT, thus expression analysis could not reach a significant level (Fig-46 C). This result is not reflective of our KinswingR kinase prediction. One possible reason could be tumour variability because the two samples (MN017 and MN257) of *NF2<sup>-/-</sup>* mutated meningioma showed the expression of CHEK2-Thr68 at WB were not included in the phosphopeptide proteomics experiments (samples number for phosphopeptide proteomics is MN325, MN310, and MN164). On the other hand, interestingly, overexpression of total CHEK2 was observed in *AKT1<sup>E17K</sup>/TRAF7* mutated meningioma samples compared to the



*NF2*<sup>-/-</sup> mutated meningioma and NMT (Fig-46 C and C2). Due to the time limitations, no further validation experiments were conducted.

**PRKCA** (Protein kinase C alpha) is a Ser/Thr protein kinase that regulates numerous cellular activities including cell growth, differentiation, and apoptosis as a result of various stimuli (Michie and Nakagawa, 2005). There are three phosphorylation sites that have been detected in PRKCA including the activation loop (Thr-497), turn motif (Thr-638), and hydrophobic C terminal motif (Ser-657) in the catalytic domain of PRKCA (Parekh *et al.*, 2000; Newton, 2001).

PRKCA kinase has been significantly predicted with the highest swing score (swing score=3.70) in *AKT1*<sup>E17K</sup>/*TRAF7* mutant meningioma compared to normal meninges (Fig-45 A). PRKCA kinase has been detected against a total of 470 phosphopeptides and 123 phosphoproteins which provided high confidence for validation of this candidate in *AKT1*<sup>E17K</sup>/*TRAF7* mutant meningioma compared to NMT. To proceed with this candidate, all three phosphorylation sites (Thr-497), (Thr-638), and (Ser-657) of PRKCA have been analysed via WB (Fig-46 D). Interestingly, PRKCA-Ser-657 showed statistically significant overexpression in *NF2*<sup>-/-</sup> mutant meningioma compared to *AKT1*<sup>E17K</sup>/*TRAF7* mutated meningioma and NMT (Fig-46 D and D1). However, examining the results for the 5 samples, only one sample of *NF2*<sup>-/-</sup> mutant meningioma showed a very intense band for PRKCA-Ser-657 and the other two samples showed a very faint band at 75 kDa. Almost all samples of *AKT1*<sup>E17K</sup>/*TRAF7* mutated meningioma expressed this PRKCA-Ser-657 kinase strongly and in NMT it was very faint or absent (Fig-46 D).

On the other hand, PRKCA-Thr-638 was significantly activated in *AKT1*<sup>E17K</sup>/*TRAF7* compared to *NF2*<sup>-/-</sup> mutated meningioma and NMT (Fig-46 D and D1). This result is in agreement with KinswingR kinase prediction analysis. In contrast, there was no increased expression of PRKCA-Thr-638 in *NF2*<sup>-/-</sup> mutant meningioma compared to NMT (Fig-46 D and D1). While increased expression of PRKCA-Thr-497 was observed in both meningioma subtypes but was not significant compared to NMT (Fig-46 D and D1).

These results suggest that phosphorylation of PRKCA-Ser-657 was prominent in some *NF2*<sup>-/-</sup> mutated meningioma, while PRKCA-Thr-638 is found more predominantly activated in *AKT1*<sup>E17K</sup>/*TRAF7* mutant meningioma. Overall the data suggest that PRKCA kinase is a potential target candidate for benign meningioma albeit further experiments are required to establish it.

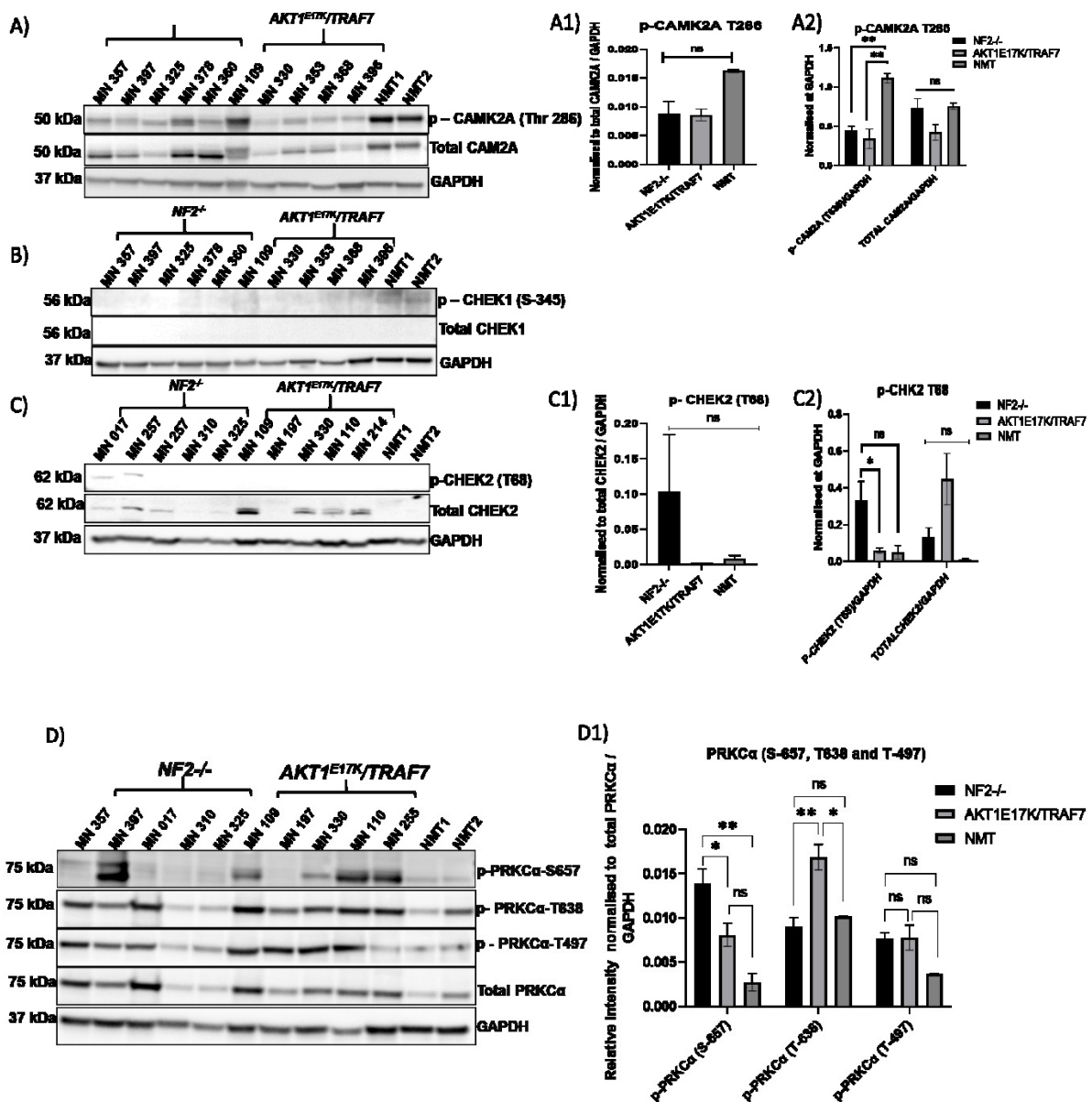


**Figure 46:** Validation of predicted kinases as significantly upregulated in *AKT1*<sup>E17K</sup>/*TRAF7* compared to *NF2*<sup>-/-</sup> mutational subtype and NMT. (A, B, C and D) Western blot analysis of upregulated kinases (p-CAM2A-Thr286, Total CAM2A, p-CHEK1-S345, Total CHEK1, p-CHEK2-Thr68, Total CHEK2, PRKCA-Ser-657, PRKCA-Thr-638, PRKCA-Thr-497, and Total PRKCA respectively) in *AKT1*<sup>E17K</sup>/*TRAF7* mutated meningioma. GAPDH as a loading control. NMT ( $n=2$ ); *NF2*<sup>-/-</sup> ( $n=5$ ) and *AKT1*<sup>E17K</sup>/*TRAF7* ( $n=5$ ). (A1, C1 and D1) Histogram showing quantification of kinases (p-CAM2A-Thr286, p-CHEK2-Thr68, PRKCA-Ser-657, PRKCA-Thr-638, and PRKCA-Thr-497 respectively). Data represented as  $\pm$ SEM and statistical significance One-way ANOVA is shown by: ns= not significant;  $p > 0.05$ ; \*  $p \leq 0.05$ ; \*\*  $p \leq 0.01$ ; \*\*\*  $p \leq 0.001$ ; \*\*\*\*  $p \leq 0.0001$ .

#### 4.4.2.2 Validation of *NF2<sup>-/-</sup>* specific kinase candidates via WB.

**EGFR** (Epidermal Growth Factor Receptor ) is a receptor tyrosine kinase and a member of the ErbB family that regulates cellular motility, proliferation, and differentiation by binding to a series of ligands such as EGF, TGF- $\alpha$  (Transforming Growth Factor-alpha), heparin-binding EGF (Olayioye *et al.*, 2000; Yamaoka *et al.*, 2011). There are six autophosphorylation sites for EGFR including Y-992, Y-1045, Y-1068, Y-1086, Y-1148, and Y-1173. Upon phosphorylation, these sites act as binding regions for intracellular signalling proteins and permit communication of external stimulus and internal signal transduction pathways (Shoelson, 1997).

In this experiment EGFR kinase has been predicted as the significant kinase with the second-highest swing score (swing score=2.30) in *NF2<sup>-/-</sup>* mutated meningioma compared to *AKT1<sup>E17K</sup>/TRAF7* meningioma mutant (Fig-45 C).

As mentioned EGFR has six autophosphorylation sites and due to the sample limitation, I have proceeded with only two sites EGFR Y-1173 and Y-1068 for validation via WB because these two sites are most cited in phosphosite plus (<https://www.phosphosite.org/proteinAction.action?id=592&showAllSites=true>). Interestingly, p-EGFR-Y1173 showed over-activated in *NF2<sup>-/-</sup>* mutated meningioma compared to *AKT1<sup>E17K</sup>/TRAF7* mutant meningioma and NMT but this did not reach a statistical significance level due to tumour variability (Fig-47 A and A1). Out of five samples with *NF2<sup>-/-</sup>* mutation, three (MN 164, MN 310, and MN257) showed a strong band for p-EGFR-1173, and these samples were processed for phosphopeptide proteomics. In contrast, out of three samples with *AKT1<sup>E17K</sup>/TRAF7* meningioma mutant included in the phosphopeptide proteomics experiment, only one sample showed strong expression for p-EGFR-1173 and expression was absent in NMT (Fig-47 A and A1). These results are in agreement with KinSwingR kinase prediction analysis.

On the other hand, p-EGFR-1068 showed strong expression in *AKT1<sup>E17K</sup>/TRAF7* meningioma mutant compared to *NF2<sup>-/-</sup>* mutated meningioma and NMT (Fig-47 A and A1). These results suggest EGFR kinase activity is present in both meningioma subtypes where the expression of this kinase is totally absent in normal meninges.

**LCK** is a lymphocyte-specific protein tyrosine kinase that regulates T-cell growth and homeostasis and is mostly active in T-cells. It is also expressed in natural killer cells (NK) and in the brain (Palacios and Weiss, 2004; Van Laethem *et al.*, 2013; Vahedi *et al.*, 2015). LCK is a plasma membrane-related protein that triggers intracellular signaling from the membrane T-cell receptor (TCR) (Yasuda *et al.*, 2000; Chueh and Yu, 2012). LCK has three domains; one SH3 at the amino terminus, one SH2 at the carboxy terminus, and the kinase domain at the carboxy terminus which is responsible for its activity (Palacios and Weiss, 2004; Singh *et al.*, 2018). There are two phosphorylation sites (Tyr394 and Tyr505) in the kinase domain responsible for LCK activity where phosphorylation of Tyr394 generates an open/active LCK conformation. In contrast, the phosphorylation of Tyr505 at the C-terminus kinase domain triggers an inactive form of LCK (Courtney and Weiss, 2018). In this study, LCK kinase has been predicted as most significantly upregulated in *NF2*<sup>-/-</sup> mutated meningioma compared to NMT with a high swing score (swing score=2.30) (Fig-45 B). A total of 98 phosphosites and 78 phosphoproteins significantly predicted LCK kinase in *NF2*<sup>-/-</sup> mutated meningioma. LCK kinase activity has not yet been reported in meningioma. For LCK validation I have proceeded with only the Tyr394 site which is responsible for kinase activation and due to the limited tissue lysates there was insufficient sample left to validate the LCK-Tyr505 site in meningioma tissue as well. In WB analysis p-LCK-Tyr394 showed increased activation in *NF2*<sup>-/-</sup> mutated meningioma compared to *AKT1*<sup>E17K</sup>/*TRAF7* meningioma and NMT (Fig-47 B and B1) in agreement with KinswingR kinase prediction analysis. However, total LCK did not show a clear band in all samples which makes the analysis difficult to interpret. Two different antibodies were used in order to get a clear signal for Total LCK, with one of which there was no signal. However, looking at the blot all samples with *NF2*<sup>-/-</sup> mutated meningioma showed a band for p-LCK- Tyr394 whereas one sample from NMT showed a strong band for this phospho-kinase. These results suggest active LCK kinases present in the *NF2*<sup>-/-</sup> mutated meningioma but a good antibody is required for total LCK in order to measure appropriate kinase activity among the samples.

**AURKB** (Aurora kinase B) is a serine/threonine-protein kinase and a member of the Aurora kinase family (Nigg, 2001). AURKB plays a role in cell cycle regulation by phosphorylating histone H3 at Ser-10 which is required for chromosomal separation following cell replication (Crosio *et al.*, 2002).

In this experiment, AURKB kinase has been predicted as upregulated in *NF2*<sup>-/-</sup> mutated meningioma compared to NMT with the highest swing score (swing score=2.50) (Fig-45 B).

Previous studies reported that the catalytic T-loop in the C-terminal kinase domain is responsible for AURKB activation when it is autophosphorylated at Thr232 (Cheetham *et al.*, 2002; Willems *et al.*, 2018). Therefore, I have proceeded to examine AURKB phosphorylated at the Thr232 site via WB. In WB analysis, p-AURKB-Thr232 showed increased activation in normal meninges (Fig-47 C and C1) compared to both meningioma mutational subtypes which is the opposite of KinswingR kinase prediction analysis. In WB blot there are double bands at 40-45 kDa, an upper band for p-AURKA-Thr288 and a lower one for p-AURKB-Thr232. The bands were too close to easily disseminate, therefore their intensity had to be calculated together. There were no available commercial antibodies other than this to proceed with for validation.

**CSNK2A1** (Casein kinase II) is a highly conserved Ser/Thr protein kinase and it has been reported that CSNKII targets more than 300 substrates which phosphorylates and is involved in a variety of cellular functions such as cell cycle progression, DNA synthesis and repair, growth and differentiation, gene regulation, cell signaling, tumorigenesis, and cell death (Meggio and Pinna, 2003; St-Denis *et al.*, 2009; Guerra and Issinger, 1999; Loizou *et al.*, 2004; Götz and Montenarh, 2017; Ghavidel and Schultz, 2001; Seldin *et al.*, 2005; Ahmad *et al.*, 2008; Lek *et al.*, 2016; Jiang *et al.*, 2019).

CSNK2A1 has been predicted as the most significant kinase with the highest swing score (swing score=3.25) in *NF2*<sup>-/-</sup> mutated meningioma compared to *AKT1*<sup>E17K</sup>/*TRAF7* meningioma mutant (Fig-45 C). CSNK2A1 prediction was made against a total of 463 phosphosites and 194 phosphoproteins via KinswingR. In addition to this, this kinase was detected 109 times in motif analysis in the whole phosphopeptide data set (data can be found in supplementary data-S7) suggesting CSNK2A1 is highly abundant in meningioma and a potential candidate for validation in *NF2*<sup>-/-</sup> mutated meningioma. However, there is not much literature mentioning the active site for CSNK2A1. Bosc *et al.*, (1995) reported that Thr-344, Thr-360, Ser-362, and Ser-370 are the active sites for CSNK2A1 and these sites undergo phosphorylation during cell mitosis by cyclin-dependent kinase 1 (CDK1). In this study for WB validation, there was only one commercial antibody (CSNK2A1-Thr360+Ser-362) available, therefore I have proceeded with that. It has been observed that p-CSNK2A1-Thr360+Ser-362 showed increased activation at 45 kDa in NMT compared to meningiomas in WB analysis (Fig-47 D and D1), which

contradicts KinswingR kinase prediction (Fig-45 C). One possible reason could be that the identified phosphorylation sites in the phosphopeptide data set could not map the sites Thr360 and Ser-362 for CSNK2A1, therefore the results showed the opposite of kinase prediction.

I have further analysed the total expression of CSNK2A1 in WB. Looking at the blot it has been observed that total CSNK2A1 showed significant overexpression at 45 kDa in both meningioma subtypes (*NF2*<sup>-/-</sup> and *AKT1*<sup>E17K</sup>/*TRAF7* meningioma) compared to NMT (Fig-47 D and D2, when total CSNK2A1 alone was normalised to GAPDH) and even expression was higher in *NF2*<sup>-/-</sup> mutated meningioma compared to *AKT1*<sup>E17K</sup>/*TRAF7* meningioma mutant. These results suggesting *NF2*<sup>-/-</sup> mutated meningioma tumour could be regulated by total CSNK2A1 but further experiments are required to confirm this.

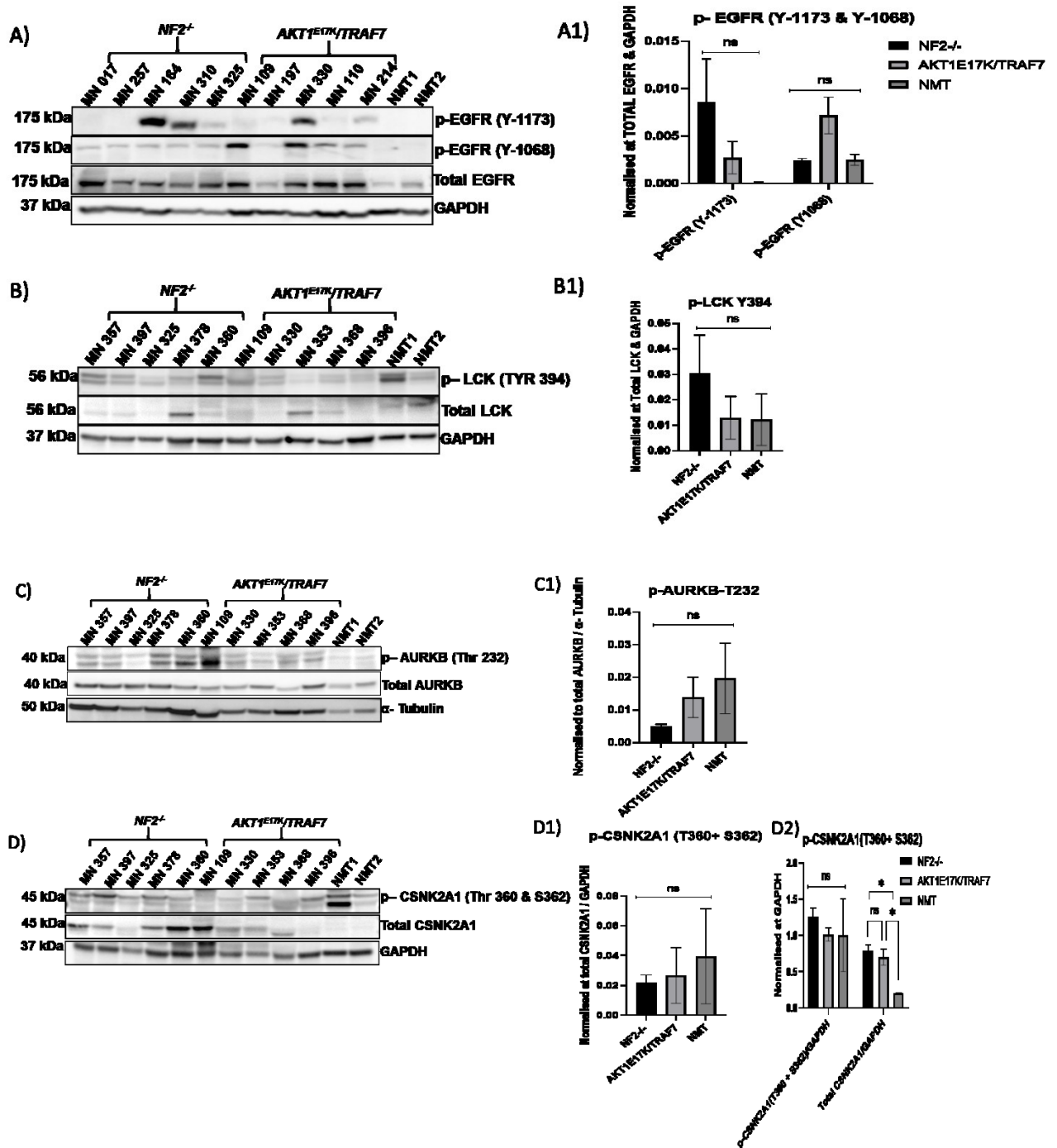


**Figure 47:** Validation of predicted kinases as significantly upregulated in *NF2*<sup>-/-</sup> compared to *AKT1*<sup>E17K</sup>/*TRAF7* mutational subtype and NMT. (A, B, C and D) Western blot analysis of upregulated kinases (p-EGFR-Y1173, p-EGFR-Y1048, Total EGFR, p-LCK-Y394, Total LCK, p-AURKB-Thr232, Total AURKB, p-CSNK2A1-Thr360+Ser-362, and Total CSNK2A1 respectively) in *NF2*<sup>-/-</sup> mutated meningioma. GAPDH as a loading control. NMT (*n*=2), *NF2*<sup>-/-</sup> (*n*=5) and *AKT1*<sup>E17K</sup>/*TRAF7* (*n*=5). (A1, B1, C1 and D1) Histogram showing quantification of kinases (p-EGFR-Y1173, p-EGFR-Y1048, p-LCK-Y394, p-AURKB-Thr232, and p-CSNK2A1-Thr360+Ser-362 respectively). Data represented as  $\pm$ SEM and statistical significance One-way ANOVA is shown by: ns= not significant;  $p > 0.05$ ; \*  $p \leq 0.05$ ; \*\*  $p \leq 0.01$ ; \*\*\*  $p \leq 0.001$ ; \*\*\*\*  $p \leq 0.0001$ .

#### 4.4.3 Examination of PRKACA activity via immunohistochemistry

Due to limited access to tissue section slides, I could not verify the expression of other potential kinases such as EGFR via immunohistochemistry (IHC) experiments. Only PRKCA was taken for IHC validation because PRKCA showed significantly increased activity in meningioma subtypes in comparison to NMT in WB analysis. Similar to global proteomics experiments, five tissue section slides per meningioma mutant group (*AKT1<sup>E17K</sup>/TRAF7* and *NF2<sup>-/-</sup>*) and four different cases of normal meningeal tissue sections were used to verify target kinases expression and their localization. It has been reported that cytoplasmic PRKCA expression indicates an inactive form of this kinase and its membranous expression is indicative of an active form of PRKCA (Newton, 2018; Hsu *et al.*, 2018).

From IHC analysis, all samples from both meningioma subtypes (*AKT1<sup>E17K</sup>/TRAF7* and *NF2<sup>-/-</sup>*) showed moderate immunostaining for p-PRKCA-S657, while p-PRKCA-S657 immunostaining was weak in two NMT samples out of four cases. In terms of localisation, p-PRKCA-S657 showed both membranous and cytoplasmic staining across all tumour samples, while only two samples from *NF2<sup>-/-</sup>* mutated and two samples from *AKT1<sup>E17K</sup>/TRAF7* mutated meningioma showed focal nuclear and membranous expression, with the remaining samples showing expression in the cytoplasm. Overall analysis suggests an increased expression of p-PRKCA-S657 in meningioma subtypes compared to NMT which is consistent with Western blot analysis and KinSwingR kinase prediction (Fig- 48 A and A1).

IHC staining of p-PRKCA-T638, p-PRKCA-T497, and total PRKCA did not show any detectable differences between meningioma subtypes and normal meninges (Fig-48 B1, C1, and D1). Immunostaining of p-PRKCA-T497 showed moderate membranous staining across all tumour samples which suggests p-PRKCA-T497 was active in all meningioma subtypes and the expression result is consistent with the WB results (Fig-46 D). In contrast, immunostaining of p-PRKCA-T638 showed moderate membranous expression in four samples of *NF2<sup>-/-</sup>* mutated meningioma and in two samples with *AKT1<sup>E17K</sup>/TRAF7* mutated meningioma which is the opposite of WB results (Fig-46 D). It could be because the same antibody was not used for both experiments and the results potentially indicate variability in antibody binding type especially targeting a specific site on the protein. There were no commercial antibodies available for p-PRKCA-T638 which can be used in both techniques, resulting in the same expression pattern not being observed in both WB and IHC. Overall, these results confirmed the presence of active forms of PRKCA present in benign meningioma via IHC.



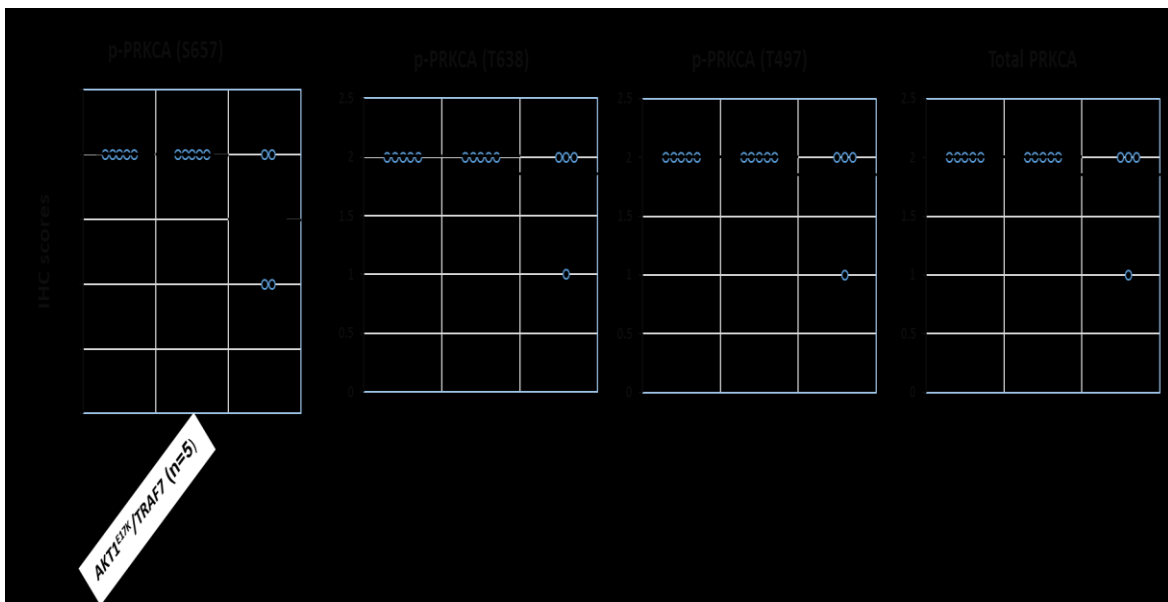
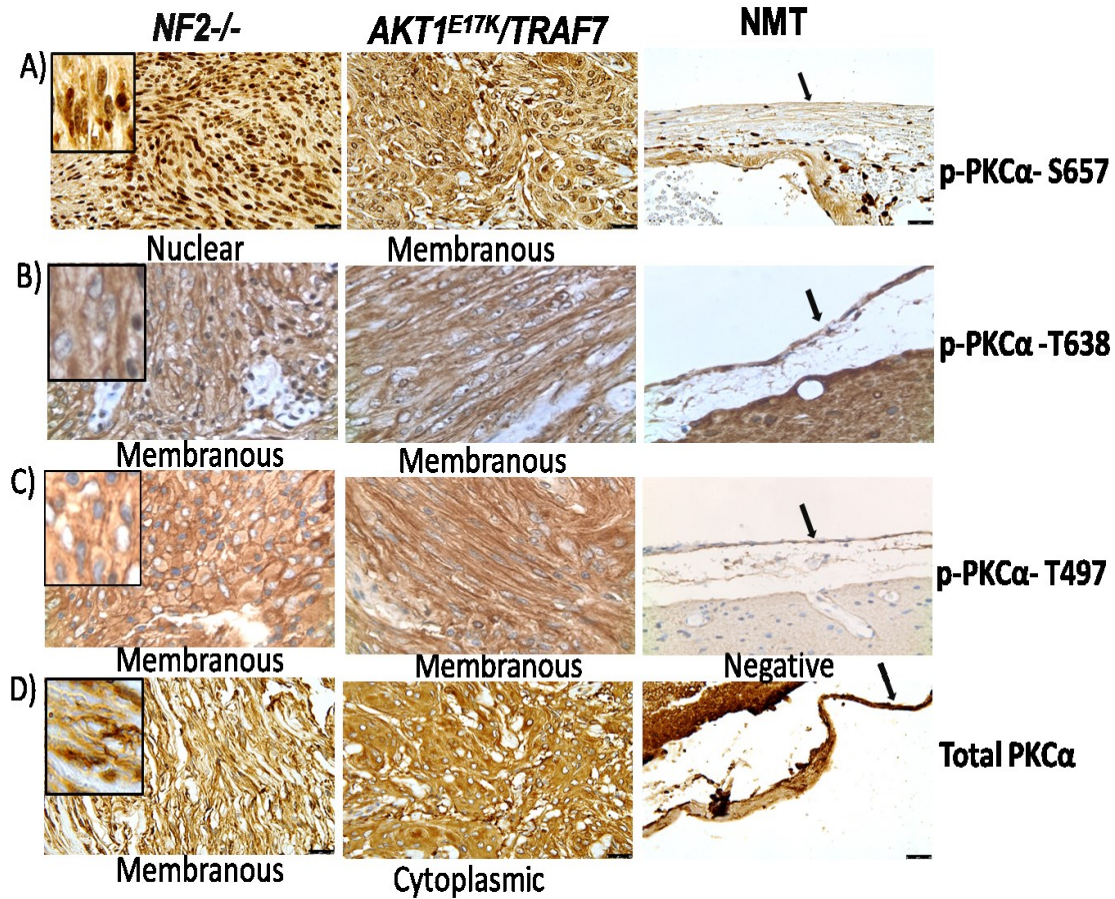


**Figure 48:** Immunohistochemistry analysis of PRKACA kinase in meningioma mutant subtypes compared to NMT. A, B, C and D) Immunostaining images of p-PRKCA-S657, p-PRKCA-T638, p-PRKCA-T497, and Total p-PRKCA respectively in meningioma mutational subtypes and NMT at 40x magnification. A1, B1, C1, and D1) Corresponding IHC scoring of p-PRKCA-S657, p-PRKCA-T638, p-PRKCA-T497, and Total p-PRKCA respectively represent as mean calculated based on staining score shown in the black bold line for each group. Scoring criteria 0 = absent, 1= Weak, 2 = moderate and 3 = strong.

#### 4.4.4 Functional validation of PRAKCA in benign meningioma subtypes.

Upon confirmation of increased activity of PRKCA kinase in meningioma using WB and IHC, functional validation of PRKCA was then used to identify it as a therapeutic target candidate for benign mutational meningioma subtypes. A classical PRKCA kinase inhibitor Go6976 (Koivunen *et al.*, 2006) was used to suppress the activity of PRKCA and establish it as a drug target for mutational meningioma subtypes. This inhibitor has previously been demonstrated to be effective in reducing PRKCA phosphorylation of breast cancer cells and inhibition of invasion has also been demonstrated in urinary bladder cancer cells (Tan *et al.*, 2006; Aaltonen *et al.*, 2007).

To investigate the efficacy of Go6976, a cell viability assay was performed using cultured meningioma primary cells. Three different meningioma primary cell cultures with *NF2*<sup>-/-</sup> mutations (MN 414, MN 360, and MN397) and three meningioma primary cell cultures with *AKT1*<sup>E17K</sup>/*TRAF7* mutations (MN 110, MN 255, and MN 330) were treated with different concentrations (0.1 µM, 1 µM, 3 µM and 10 µM) of Go6976 for both 72 hours and seven days. After 72 hours of treatment, it was observed that Go6946 affects the viability of all *NF2*<sup>-/-</sup> mutated primary meningioma cells with the lowest IC<sub>50</sub> of 7.95 µM in MN 360 sample. Go6946 affected the viability of one (MN 110) out of three meningiomas with *AKT1*<sup>E17K</sup>/*TRAF7* mutation, with an IC<sub>50</sub> of 16.10 µM. An IC<sub>50</sub> dose could not be reached in the other two tumour samples (Fig-49 A and B). To be noted respective primary meningioma cells only with DMSO were used as a control for each experiment.

After seven days of Go6976 treatment, all primary meningioma samples from both meningioma subtypes showed a concentration-dependent decrease in cell viability compared to DMSO control. Following seven days of treatment, IC<sub>50</sub> values of Go6976 ranged from 3.75 µM to 26.78 µM in *NF2*<sup>-/-</sup> mutated primary meningiomas cells, whereas all *AKT1*<sup>E17K</sup>/*TRAF7* mutated primary cells showed a reduction in viability with having the lowest IC<sub>50</sub> value of 9.63 µM in MN 110 sample (Fig-49 A1 and B1). According to the results of the cells viability assay, benign meningioma primary cells needed to be treated with Go6976 for more than seven days in order to observe stronger inhibitory effects on cell viability, and some of the meningioma primary cells require treatment with a higher concentration of Go6976.

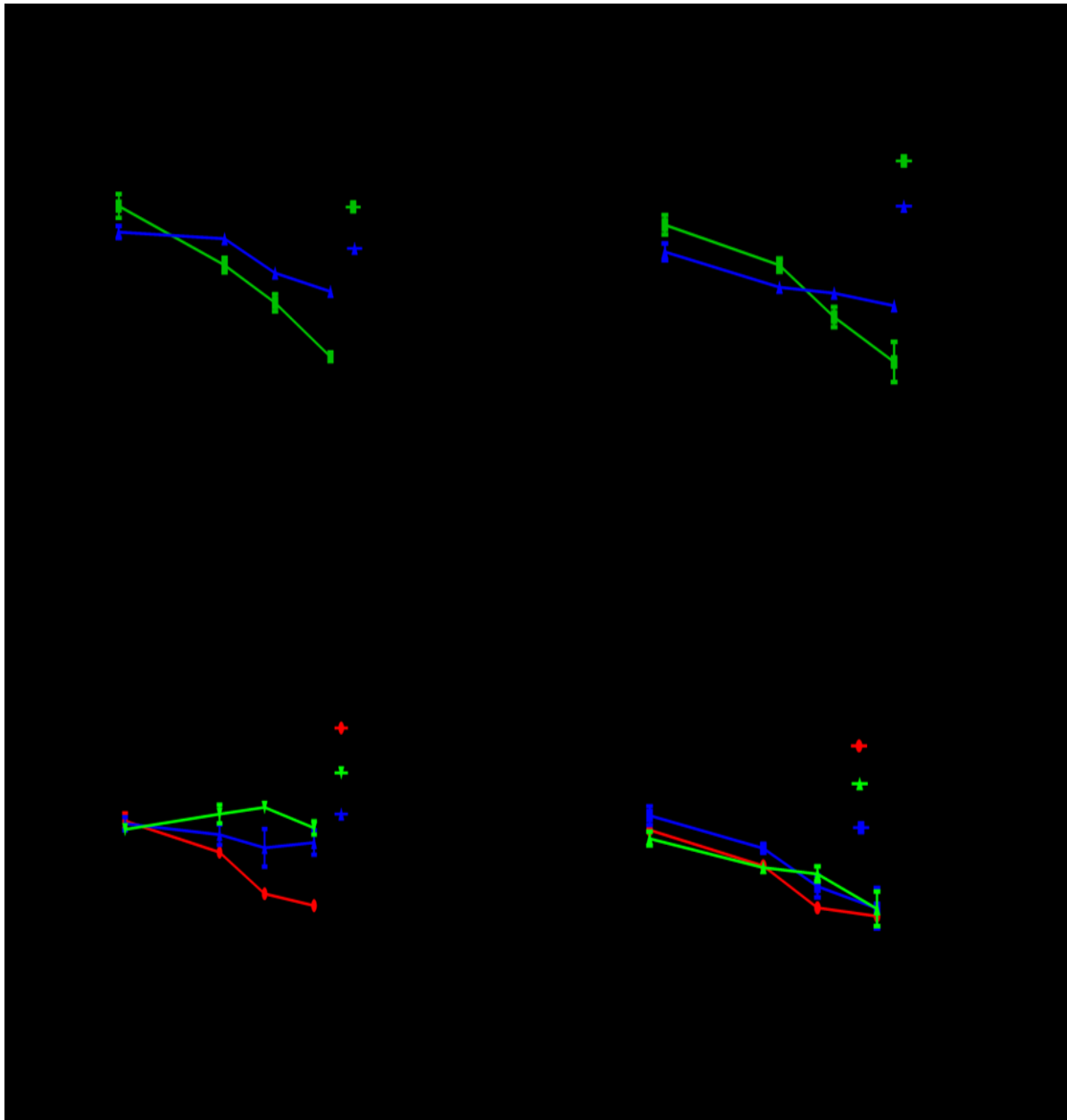


**Figure 49: Efficacy of PRKCA inhibitor (Go6976) in meningioma primary cell viability assay.** A) Illustrating Go6976 decreased viability of *NF2*<sup>-/-</sup> mutated primary cells after 72 hours of treatment. A1) Illustrating Go6976 decreased viability of *NF2*<sup>-/-</sup> mutated primary cells after 7 days of treatment. B) A) Illustrating Go6976 decreased viability of *AKT1*<sup>E17K</sup>/*TRAF7* mutated primary cells after 72 hours of treatment. B1) Illustrating Go6976 decreased viability of *AKT1*<sup>E17K</sup>/*TRAF7* mutated primary cells after 7 days of treatment. Corresponding IC<sub>50</sub> values were noted and to observe drug effect, cell viability was calculated as a percentage, and the value normalized against DMSO control in Graph pad prism.

To investigate the drug effect on meningioma cell proliferation, meningioma primary cells were treated with different concentrations (1  $\mu$ M, 3  $\mu$ M and 10  $\mu$ M) of Go6976 for 72 hours. Cells were then lysed for protein extraction and immunoblotted for all phospho-PRKCA site activity to assess the degree of drug inhibition. After treatment with Go6976, there was a dose-dependent increase in the activity of p-PRKCA-S657 in meningioma with *NF2*<sup>-/-</sup> mutant primary cells compared to control DMSO (dimethyl sulphoxide), but no discernible changes in the activity of the other two phospho-sites (p- PRKCA-T638 and p- PRKCA-T497) (Fig-50 A and A1).

However, in *AKT1*<sup>E17K</sup>/*TRAF7* mutated primary meningioma cells, a dose-dependent increase in activity of p-PRKCA-T497 was detected, while a very minor decrease in the activity of p-PRKC-S657 was observed compared to control DMSO (Fig-50 B and B1). There was no influence on the proliferation of primary meningioma cells in both cases as measured by Cyclin D1 expression (Fig-50 A and B). However, a dose-dependent overexpression of Caspase-3 (apoptosis marker) was observed in both meningioma mutational subtypes compared to control DMSO (Fig-50 B and B1) but was not significant, which could be due to the small number of technical repeats. Induction of apoptosis by Go6976 was also observed in previous studies (Aaltonen *et al.*, 2007). Cell viability assay and WB produced inconsistent results suggesting the Go6976 drug is not an ideal choice to inhibit PRKCA in benign meningioma primary cells.

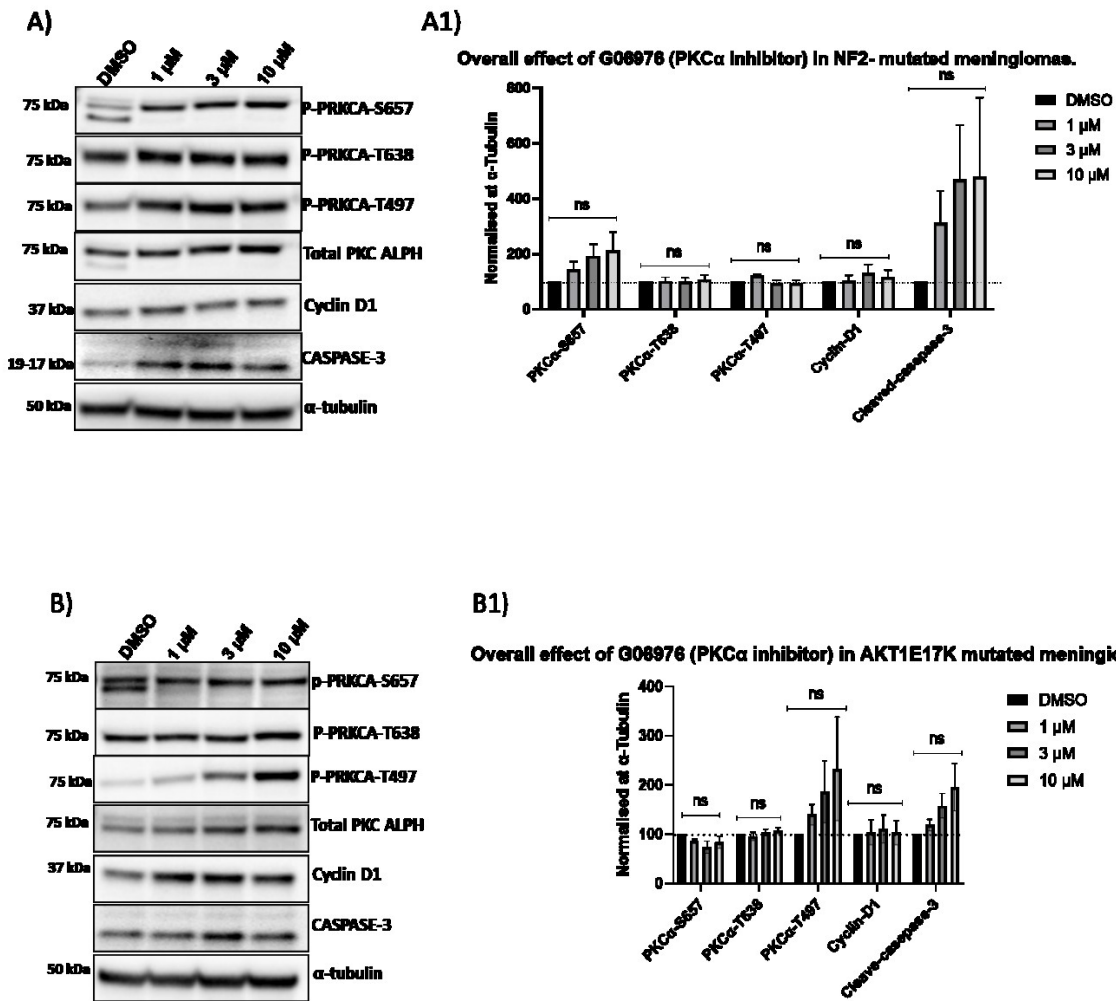


**Figure 50:** Go6976 was unable to inhibit PRKCA activity in benign meningioma subtypes by 72 hours. A and A1) Western blot analysis of p-PRKCA-S657, p-PRKCA-T638, p-PRKCA-T497, Total PRKCA, CyclinD1, and Caspase-3 expression after 72 hours of treatment of Go6976 in *NF2*<sup>-/-</sup> mutated meningioma primary cells (n=3) and DMSO as a control,  $\alpha$ -tubulin as a loading control. B and B1) Western blot analysis of p-PRKCA-S657, p-PRKCA-T638, p-PRKCA-T497, Total PRKCA, CyclinD1, and Caspase-3 expression after 72 hours of treatment of Go6976 in *AKT1*<sup>E17K</sup>/*TRAF7* mutated meningioma primary cells (n=3) and DMSO as a control,  $\alpha$ -tubulin as a loading control. Data represented as  $\pm$ SEM and statistical significance One-way ANOVA is shown by: ns= not significant;  $p > 0.05$ ; \*  $p \leq 0.05$ ; \*\*  $p \leq 0.01$ ; \*\*\*  $p \leq 0.001$ ; \*\*\*\*  $p \leq 0.0001$ .

## 4.5 Conclusion

This is the first TMT labelled phosphopeptide analysis of *NF2<sup>-/-</sup>* and *AKT1<sup>E17K</sup>/TRAF7* mutational meningioma subtypes to date. We have identified a total of 6584 phosphosites and 2388 phosphoproteins across 6 meningiomas (*AKT1<sup>E17K</sup>/TRAF7* mutant subtypes n=3 and *NF2<sup>-/-</sup>* mutant subtypes n=3) and two healthy normal meningeal tissues (NMT) as control with a 5% false discovery rate (FDR).

To understand the biological input of these identified phosphosites, motif analysis was performed and a total of 4620 phosphorylated motifs have been identified among the sample groups *NF2<sup>-/-</sup>*, *AKT1<sup>E17K</sup>/TRAF7*, and NMT, of which 105 motifs were significantly mapped at serine (pS) residue, 11 motifs were across threonine (pT) while only one at tyrosine (pY) residue by at least two occurrences with  $p < 0.001$ .

Differential expression analysis of *AKT1<sup>E17K</sup>/TRAF7*, *NF2<sup>-/-</sup>* and NMT predicted a total of 33 potential kinases in meningioma subtypes via KinswingR. PRKCA was predicted as a significant kinase in *AKT1<sup>E17K</sup>/TRAF7* mutant meningioma group compared to NMT. Validation of PRKCA was confirmed via WB where a significant increase in activity of PRKCA in both meningioma subtypes (*AKT1<sup>E17K</sup>/TRAF7* and *NF2<sup>-/-</sup>*) was observed, which turned out to be a candidate for a meningioma subtype-specific kinase. Active forms of PRKCA were also confirmed via IHC. Unfortunately, validation of PRKCA as a therapeutic target using drug inhibition was unsuccessful. Before rejecting PRKCA as a promising therapeutic target based on the initial results presented here, more research should be conducted to inhibit PRKCA such as using another drug (PRKCA inhibitor) or knocking down *PRKCA* using shRNA to see whether a reduction in meningioma cell proliferation is observed.

## 5. Discussion

In this chapter, the findings of the global proteomics data analysis will be discussed first (section-5.1), the experimental validation of meningioma subtypes specific upregulated twelve protein candidates that have been detected from differential protein expression analysis will be discussed along with their biological role in meningioma tumorigenesis. The functional annotation analysis of meningioma subtypes with different driver mutation-specific upregulated proteins and their associated pathways will also be discussed.

In the second part (section-5.2), kinase prediction using phosphopeptide proteomics will be discussed including the experimental validation of kinase activity in various meningioma subtypes with different driver mutations.

### 5.1 Global proteomic data analysis

The aim of the present study is to refine our understanding of meningioma biology via analysis of an integrated proteo-genomic landscape and to discover biomarker candidates and therapeutic targets for the clinical management of benign meningioma patients. To my knowledge, this is the first deep, quantitative proteomic study of the benign meningioma subtypes with different mutations. It characterises how proteomics can enhance our understanding of mutant subtype-specific driver's mechanisms. First, we confirmed the mutational status in benign meningioma before undertaking proteomic analysis (Section-3.2). The investigation of a large proteomic data set facilitated the extraction of potential biologically meaningful differences between the mutant meningioma subtypes. In this study, tissue samples from the three mutant meningioma subtypes, *AKT1<sup>E17K</sup>/TRAF7* (n=7), *NF2<sup>-/-</sup>* (n=11) and *KLF4<sup>K409Q</sup>/TRAF7* (n=10) were compared (Fig-14). However, as it is often challenging to obtain suitable control samples for meningioma, we were able to include only two healthy meningeal tissue samples for our experiment.

We investigated proteome differences within and between mutational subtypes based on global protein expression levels. Unsupervised hierarchical clustering showed tumour similarity at the proteome level. All meningioma samples (n=7) with *AKT1<sup>E17K</sup>/TRAF7* mutation tended to cluster together and a similar pattern observed for *KLF4<sup>K409Q</sup> /TRAF7* (n=10) group samples (Fig-14). In contrast, *NF2<sup>-/-</sup>* mutant samples (n=11) grouped on either side of the *AKT1<sup>E17K</sup>/TRAF7* mutant samples and formed partial and mixed clusters (Fig-14). These results

suggest variability among the meningioma *NF2* mutant subtypes detected by proteomics, which could be due to individual differences in the microenvironment or heterogeneity amongst the *NF2*<sup>-/-</sup> mutated tumours themselves. To summarise, these results suggested that meningioma samples with similar genetic backgrounds tend to group together based on their proteomic profile (Fig-14), while non-tumour tissue samples (healthy meninges n=2) clustered away from benign meningioma mutational subtypes.

From the global proteomic differential expression analysis, unsupervised hierarchical clustering revealed a big cluster-2 containing 144 proteins over-expressed in *AKT1*<sup>E17K</sup>/*TRAF7* mutant meningioma compared to the *KLF4*<sup>K409Q</sup>/*TRAF7* and *NF2*<sup>-/-</sup> meningioma subtypes and NMT. On the other hand, the smallest cluster-5 containing 23 proteins showed overexpression in *NF2*<sup>-/-</sup> mutant meningioma subtypes compared to the *AKT1*<sup>E17K</sup>/*TRAF7*, *KLF4*<sup>K409Q</sup>/*TRAF7* mutant meningioma and NMT (Fig-14). These proteins including CRABP2, CLIC3, PC, ANXA3 and endoglin could be interesting candidates for further confirmation/validation experiments.

### 5.1.1 *AKT1*<sup>E17K</sup>/*TRAF7* mutant meningioma-specific upregulated protein candidates

Using comparative differential expression analysis (Fig- 15 and Fig- 16 A) 162 proteins were detected that are commonly and significantly upregulated in *AKT1*<sup>E17K</sup>/*TRAF7* mutant meningioma compared to the *KLF4*<sup>K409Q</sup>/*TRAF7*, *NF2*<sup>-/-</sup> mutant meningioma subtypes and NMT including pyruvate carboxylase, GMDS, CLIC3, CRABP2, COX6B1, NDUFA5, NDUFB7, NDUFB1, NDUFB8 and ATPK, none of which have been reported previously in the context of benign meningioma (partial list in table 7 and a complete list at appendix table-1). Subsequently, below is a more detailed discussion of these candidates. Four upregulated proteins (pyruvate carboxylase, GMDS, CLIC3, CRABP2) from this group were further validated by Western blotting and/or Simple wes assay and immunohistochemistry.

**Pyruvate carboxylase (PC):** In this current study, the Western blot analysis confirmed the significant overexpression of PC in *AKT1*<sup>E17K</sup>/*TRAF7* compared to *NF2*<sup>-/-</sup> mutant meningioma. Whereas increased expression of PC in *AKT1*<sup>E17K</sup>/*TRAF7* mutant meningioma was observed compared to *KLF4*<sup>K409Q</sup>/*TRAF7* mutant meningioma and NMT, it did not reach a significant level (Fig- 21 D and D1), this could potentially be explained by the limited sample number. In mass-spectrometry analysis, PC has been identified as most significantly upregulated in



*AKT1<sup>E17K</sup>/TRAF7* compared to NMT with the highest fold change (Log2 FC= 8.998) (Table 7). Average scoring for PC immunostaining showed the highest in *KLF4<sup>K409Q</sup>/TRAF7* mutant meningioma with moderate staining compared to the other groups, where only one sample from the *AKT1<sup>E17K</sup>/TRAF7* meningioma group showed a weak immunoreaction, and the other four samples showed moderate staining (Fig- 22 Ba). This IHC result is in contrast to the proteomics data and WB analysis, however, IHC is a non-quantitative method.

PC is a metabolic enzyme, which catalyzes the carboxylation of pyruvate to oxaloacetate (OAA), this reaction is important in replenishing tricarboxylic acid cycle (TCA cycle) cycle intermediates, and has been linked to metabolic reprogramming and tumour growth (Kiesel *et al.*, 2021). Glycolysis, glutaminolysis, and macromolecule syntheses such as nucleic acids, amino acids and lipids, are the key metabolic processes deregulated during tumour development. These metabolic shifts are regulated by increased activation of cancer-related signalling pathways such as PI3K/Akt/mTOR, cMyc, and hypoxia-inducible factor-1 $\alpha$  (HIF-1 $\alpha$ ) (DeBerardinis *et al.*, 2008; Kiesel *et al.*, 2021). In adverse conditions, such as nutrient-deficient environments, cancer cells can maintain increased demands for both macromolecule synthesis for daughter cell formation and energy production. As a result, the ability to use a variety of energy substrates, such as glucose, glutamine, and fatty acids, is crucial for tumour growth, with evidence suggesting that cancer cells change their metabolic pathways as they proceed through tumour development stages (DeBerardinis *et al.*, 2008; Kiesel *et al.*, 2021). The capability of cancer cells to utilize available nutrient resources to promote survival and growth in an adverse environment is known as metabolic plasticity (McGuirk *et al.*, 2020). The tricarboxylic acid cycle (TCA cycle) produces energy and metabolic intermediates as a result of nutrient metabolism, which is required for cell development (Owen *et al.*, 2002; McGuirk *et al.*, 2020). Metabolic reprogramming is referred to as the Warburg effect in tumour cells in which, tumour cells prefer glucose metabolism via aerobic glycolysis for proliferation regardless of the presence of oxygen (Warburg *et al.*, 1927). Cells with Warburg-effect metabolism have an abundant supply of carbon backbones for the molecules they need to proliferate (DeBerardinis and Chandel, 2020). One of the most important carbon entry points into the TCA cycle in cells is the conversion of pyruvate to either oxaloacetate (OAA) via pyruvate carboxylase reaction or acetyl coenzyme A (acetyl-CoA) by pyruvate dehydrogenase (DeBerardinis and Cheng, 2010; Kiesel *et al.*, 2021). Another route is glutamine anaplerosis, which leads to the formation of the TCA cycle intermediate ketoglutarate ( $\alpha$ KG) (DeBerardinis and Cheng, 2010; Kiesel *et al.*, 2021). The capability of fatty acid synthesis and its utilization

is also essential for metabolic plasticity during tumour progression, as well as the OAA produced by the PC reaction may also help to protect against oxidative damage which is predominantly caused by enhanced metabolism (Pavlova and Thompson, 2016). Accordingly, PC may play a role in metabolic plasticity by regulating glucose metabolism, fatty acid synthesis, and defending against oxidative stress (Kiesel *et al.*, 2021). This current study also showed that PC is highly enriched in metabolic pathways via gene ontology KEGG pathway analysis (Fig-18). This result suggests overactive AKT1 may aid to increase pyruvate carboxylase metabolic activity by increasing the expression of PC in *AKT1<sup>E17K</sup>/TRAF7* mutated meningioma tumorigenesis (DeBerardinis *et al.*, 2008).

Overexpression of PC was reported in several cancer including lung cancer, gall bladder cancer, breast cancer, papillary thyroid cancer, and glioma (Shackelford *et al.*, 2013; Ma *et al.*, 2016; Phannasil *et al.*, 2015; Strickaert *et al.*, 2019; Izquierdo-Garcia *et al.*, 2014). Phannasil *et al.*, (2015) observed that overexpression of PC in breast cancer tissues is strongly associated with tumour size, volume, and advanced stages, but not with hormone receptor expression. Another study showed that overexpression of PC at the mRNA level was linked to poor prognosis in patients with metastatic breast cancer (Shinde *et al.*, 2018). In addition to this, knockdown of PC in the highly invasive breast cancer cell line MDA-MB-231 showed decreased production of serine, glycine, aspartate, nucleotides, and de novo fatty acid synthesis from glucose, resulting in a reduction of cell growth and motility (Phannasil *et al.*, 2017). Overexpression of PC at mRNA and protein levels was also observed in solid malignant lung tissue. In addition to this, <sup>13</sup>C isotopomer-based metabolomic study demonstrates that pyruvate carboxylation flux is higher in malignant lung tissue than in non-cancerous lung tissue, implying that anaplerosis via pyruvate carboxylation is required to meet the high anabolic demand of lung tumours during primary carcinogenesis (Sellers *et al.*, 2015). Further, overexpression of PC at protein level demonstrated in isocitrate dehydrogenase1 (IDH1) mutated low-grade glioma cells line and suggested as a promising therapeutic target for IDH1 mutated glioma (Izquierdo-Garcia *et al.*, 2014). Furthermore, Pichumani *et al.*, (2019) used NMR-based [U-<sup>13</sup>C] glucose isotopic tracing methods to investigate the metabolic fate of glucose in atypical meningioma primary cells and discovered that the presence of significant pyruvate carboxylase activity resulted in active anaplerosis in these patient-derived atypical meningioma cells. To my knowledge, we are the first to report PC expression in benign meningioma.

According to these results, it can be concluded that further investigation should be made into this candidate and published literature, including glioma, suggests that PC as a potential therapeutic target in solid tumours.

**GDP- mannose 4, 6-dehydratase (GMDS):** In this current study, GMDS was identified as significantly commonly upregulated in *AKT1<sup>E17K</sup>/TRAF7* compared to *NF2<sup>-/-</sup>*, *KLF4<sup>K409Q</sup>/TRAF7* mutant meningioma, and NMT via MS, and Simple wes analysis showed the consistent result as MS (Table 7, Fig- 21 C and C1). In IHC analysis, increased expression of GMDS was revealed in *AKT1<sup>E17K</sup>/TRAF7* compared to *NF2<sup>-/-</sup>* mutant meningioma and NMT which showed consistency with MS and Simple wes analysis (Fig- 22 A and Bd). However, no clear differences were observed in IHC staining for GMDS expression between *AKT1<sup>E17K</sup>/TRAF7* and *KLF4<sup>K409Q</sup>/TRAF7* mutant meningioma which does not reflect MS and Simple wes analysis (Fig- 22 Bd). As previously mentioned, IHC is not a quantitative technique. In addition, it may be due to factors associated with the IHC staining techniques which produce different results than WB, one possible reason could be I have received half of my tissue section slides from University *Hospitals Bristol* NHS Foundation, and sections were baked where the remaining slides from University *Hospitals Plymouth* NHS Foundation were non-baked which may produce variation in antigen retrieval processing.

GMDS is an intracellular enzyme and is reported as a prognostic marker in endometrial and renal cancer (cancer genome atlas database). GMDS is a mannose dehydrogenase enzyme that catalyses the production of GDP-fucose from GDP-mannose. The GMDS is the main contributor to fucosylation, one of the most common glycosylation changes associated with tumour development (Christiansen *et al.*, 2014). Fucosylated glycans are known to regulate cell-cell adhesion, and thus GMDS may play a role in the regulation of cell migration and cancer development (Noda *et al.*, 2003). Aberrant fucosylation has been reported in several cancer including colorectal cancer, hepatocellular carcinoma, and papillary carcinoma of the thyroid (Muinelo-Romay *et al.*, 2008; Noda *et al.*, 2003; Li *et al.*, 2001; Ito *et al.*, 2003). Overexpression of GMDS at mRNA and protein levels has been confirmed in human lung adenocarcinoma as compared to adjacent normal tissue (Wei *et al.*, 2018). In addition to this, the same study also reported that GMDS knockdown impairs cell proliferation and survival in human lung adenocarcinoma. Furthermore, GMDS knockdown also decreased tumour growth in the xenograft tumour mouse model (Wei *et al.*, 2018).

Overexpression of GMDS has not yet been reported in meningioma. In this current study, KEGG pathway analysis showed GMDS involve in metabolic pathways suggesting metabolic alterations are responsible for *AKT1<sup>E17K</sup>/TRAF7* mutant meningioma (Fig-18). In summary, validation results and GO analysis showed that GMDS is a potential target for further investigation in meningioma whose expression clearly differentiates between *NF2<sup>-/-</sup>* and *NF2<sup>+/+</sup>* mutant meningioma and also NMT. Therefore, the functional role or metabolic intervention of GMDS should be studied in benign meningioma, which we aim to do in future studies.

**Chloride intracellular channel protein 3 (CLIC3):** Significant overexpression of CLIC3 in *AKT1<sup>E17K</sup>/TRAF7* compared to *NF2<sup>-/-</sup>*, *KLF4<sup>K409Q</sup>/TRAF7* mutant meningioma and NMT was confirmed via Simple wes which reflected MS analysis (Table 7, Fig-21 A and A1). IHC analysis of CLIC3 expression did not produce any clear differences among the meningioma mutational subtypes which did not support MS and Simple wes results (Fig- 22 Bb). Although clear differences were observed between *AKT1<sup>E17K</sup>/TRAF7* mutant meningioma and NMT (Fig- 22 Bb). However, focal nuclear and cytoplasmic staining of CLIC3 in meningioma is supported by previous immuno-histochemical images from the Human protein atlas database (<https://www.proteinatlas.org/ENSG00000169583-CLIC3/pathology>) (Fig- 22 A).

CLIC3 is a member of the chloride intracellular channel (CLIC) family involved in regulating essential physiological functions such as cell membrane potential stabilization, transepithelial transport, intracellular pH maintenance, and cell volume regulation (Bretag, 1987; Steinmeyer *et al.*, 1991; Welsh, 1990; Strange, 1991; Worrell *et al.*, 1989). In addition to this, it has been shown that CLIC3 binds to ERK7 (Extracellular signal-regulated kinase 7), a protein that inhibits DNA synthesis and translocates into the nucleus, implying that CLIC3 is involved in cell growth regulation (Qian *et al.*, 1999). The same study also showed significant cytoplasmic expression of CLIC3 than ERK7, suggesting that it may act independently of ERK7. CLIC3 has been found to be expressed in the placenta, lung, and heart, with moderate expression in skeletal muscle, kidney, pancreas, and brain (Money *et al.*, 2007; Qian *et al.*, 1999; Wang *et al.*, 2015).

Secretomes from cancer and stromal cells create a tumour microenvironment that promotes tumour cell invasion and angiogenesis (Hernandez-Fernaud *et al.*, 2017). The secretomes of normal and cancer-associated fibroblasts (CAFs) were analysed using a mass spectrometry approach, and it was shown that CLIC3 is an abundant component of the CAF secretome

(Hernandez-Fernaud *et al.*, 2017). The study confirmed the significant overexpression of CLIC3 in breast cancer-associated fibroblasts compared to normal mammary fibroblasts via WB. In vivo and in 3D cell culture models also demonstrated that secreted CLIC3 stimulates invasive behaviour of endothelial cells to drive angiogenesis and increases the invasiveness of breast cancer cells, and this needs active transglutaminase-2 (TGM2) (Hernandez-Fernaud *et al.*, 2017). CLIC3 functions as a glutathione-dependent oxidoreductase that reduces TGM2 at cysteine 22 and alters TGM2 binding to its regulatory cofactors  $\alpha_5\beta_1$  integrin, where cysteine 22 is required for activating TGM2-dependent extracellular pro-invasive CLIC3 activities. The resulting TGM2 activation stiffens the ECM and promotes integrin-dependent invasive behaviours (Hernandez-Fernaud *et al.*, 2017).

Increased expression of CLIC3 was also linked to high-grade pancreatic ductal adenocarcinomas, locally invasive tumours, and lymph node involvement, implying that it plays a role in invasion and lymph node metastasis (Dozynkiewicz *et al.*, 2012). In pancreatic tumours with elevated CLIC3 expression, survival was reduced, and a poor prognosis was observed when both Rab25 (Ras-related protein Rab-25) and CLIC3 expression were increased. In multivariate cox proportional-hazard regression analysis for those tumours, a high level of CLIC3 was found to be an independent predictor of poor prognosis (Dozynkiewicz *et al.*, 2012). When Rab25 acts as a tumour suppressor, Rab25 binds  $\alpha_5\beta_1$  integrin and directs active integrin to the lysosome and degrades integrin signalling. On the other hand, in tumours where Rab25 promotes CLIC3 overexpression,  $\alpha_5\beta_1$  integrin that travels through the lysosome is not destroyed; instead, lysosomally transported active integrins are channelled to the plasma membrane via CLIC3. Thus, preventing degradation and allowing continuous integrin signalling for tumour development (Dozynkiewicz *et al.*, 2012). Though the role of CLIC3 has a published role in the malignant tumour, this study is the first to report CLIC3 overexpression in *AKT1<sup>E17K</sup>/TRAF7* mutant meningioma which is a grade I benign meningioma. As previous studies have shown that *AKT1<sup>E17K</sup>* mutated meningiomas are highly recurrent and show poor prognosis (Yesilöz *et al.*, 2017; John *et al.*, 2022). The role of CLIC3 overexpression should be investigated further in the development of recurrent *AKT1<sup>E17K</sup>/TRAF7* mutated meningioma.

A genome-wide RNAi screen revealed that the CLIC3 gene expressing ErbB2 positive breast carcinoma cell line SKBR-3 showed resistance to small-molecule tyrosine kinase inhibitor neratinib (HKI-272) (Seyhan *et al.*, 2012). Another study found that in the presence of fibronectin, CLT1, an anti-angiogenic peptide, increased apoptosis in CLT1 sensitive tumour cell lines via a process involving up-regulation of tumour cell integrin  $\alpha_5\beta_1$  and CLIC3. CLIC3

knockdown decreased CLT1-mediated cell death, and CLIC3 co-localization with CLT1 in tumour cells showed a connection between CLIC3 and CLT1 internalisation (Knowles *et al.*, 2013). Wang *et al.*, (2015) showed that CLIC3 gene expression was much higher in mucoepidermoid carcinoma (MEC) of the salivary gland than in normal tissue. The study also showed hypomethylation of CLIC3 in MEC samples compared to normal samples, which was then linked to increased gene expression and increased protein expression in the same MEC tumour samples. However, this study was conducted on a small number of MEC tumour samples and suggested further experiments should be carried out to confirm these findings. Liu *et al.*, (2019) reported overexpression of the CLIC3 gene associated with poor prognosis in lung cancer patients.

Further, Glioma cell invasion is reportedly regulated by several ion channels, including potassium and chloride channels that maintain cell volume, whereas glioma cells use Cl<sup>-</sup> as an osmotically active anion (Sontheimer, 2008). The invasiveness of human glioma cells has been demonstrated to be regulated by CLIC3 (Sontheimer, 2008; Lui *et al.*, 2010). In glioma cells, CLIC3 was shown to be overexpressed on the cytoplasmic membrane and intracellular vesicles confirmed via immunofluorescence staining (Habela *et al.*, 2008; Sontheimer, 2008). CLIC3 knockdown reduces chloride accumulation in glioma cells, resulting in a decrease in the swelling induced by chloride currents and an ultimate reduction in cell invasion (Sontheimer, 2008, Olsen *et al.*, 2003). Furthermore, another study found that chlorotoxin (a chloride channel inhibitor) suppressed high CLIC3 expression and slowed cell migration in the U87 glioma cell line by binding to matrix metalloproteinase-2 (MMP-2) and blocking CLIC3 chloride currents (Qin *et al.*, 2014). As in the current study, functional annotation analysis also showed that CLIC3 was highly enriched in chloride transmembrane transport and voltage-gated ion channel activity (Fig-17). One study has shown that *AKT1<sup>E17K</sup>* mutated xenograft mice developed larger meningioma tumours than AKT1 wt mice (John *et al.*, 2022). Like in glioma, there could be a link between *AKT1<sup>E17K</sup>* mutated tumour size and CLIC3 expression. A further experiment should be employed in order to observe an increased accumulation of chloride in *AKT1<sup>E17K</sup>* mutated meningioma cells to unravel the role of CLIC3 in meningioma tumour size. To summarise, CLIC3 involve in tumorigenesis and overall functional annotation and validation results suggest the functional relevance of CLIC3 in *AKT1<sup>E17K</sup>/TRAF7* mutant meningioma warrants further study, which we intend to conduct in the future.

**Cellular retinoic acid-binding protein 2 (CRABP2):** To date, this study is the first to report overexpression of CRABP2 protein in benign meningioma. A previous microarray gene-expression data analysis reported that upregulation of CRABP2 in meningiomas grade I compared to schwannomas (Torres-Martin *et al.*, 2014). However, the study did not verify CRABP2 expression at the mRNA and protein levels. In this current study, MS data differential expression analysis showed CRABP2 as commonly significantly upregulated in *AKT1<sup>E17K</sup>/TRAF7* mutated meningioma compared to *NF2<sup>-/-</sup>*, *KLF4<sup>K409Q</sup>/TRAF7* mutated meningioma and NMT (Fig- 15 and Table 7) and consistent significant overexpression of CRABP2 observed in *AKT1<sup>E17K</sup>/TRAF7* mutated meningioma compared to other groups confirmed via Simplex assay (Fig- 21 B and B1). The IHC staining results for CRABP2 were not consistent with WB and MS analysis (Fig- 22 Bc, Fig-21 B and B1). It could be due to the heterogeneity of fixed tissue used in IHC staining may produce a different result than WB which I have mentioned earlier for another candidate protein, GMDS.

CRABP2 is a member of the intracellular lipid-binding protein family that binds retinoid and fatty acids like retinoic acid (RA) (Vaezeslami *et al.*, 2006). CRABP2 expression is described in skin, uterus, ovary, choroid plexus, testis, and hematopoietic cells, and their increased expression is regulated by all-trans retinoic acid (ATRA) (Zheng *et al.*, 1996; Wardlaw *et al.*, 1997; Yamamoto *et al.*, 1998; Kreutz *et al.*, 1998; Fischer-Huchzermeyer *et al.*, 2017). ATRA is a vitamin A metabolite that binds to CRABP2 and activates nuclear RA receptors and peroxisome proliferator-activated receptors  $\beta/\delta$  (PPAR $\beta/\delta$ ) (Chambon, 1996; Michalik and Wahli, 2007; Schroeder *et al.*, 2008). This leads to transcriptional activation of ATRA-targeted pathways which controls the ligand-dependent transcription factors that are involved in regulating several biological processes including embryonic development, tissue remodelling, neural plasticity, lipid metabolism, and glucose homeostasis (Michalik and Wahli, 2007; Desvergne *et al.*, 2006). CRABP2 also plays a role in tissue differentiation and proliferation as a transcriptional co-activator, as well as controls axonal regeneration, neurite initiation, and neurite branching in mice by activating RA signalling (Eller *et al.*, 1995; Dieplinger *et al.*, 2007).

The role of CRABP2 in tumorigenesis is complicated. While RAR activation causes cell cycle arrest, apoptosis, and differentiation, which inhibits tumour growth (Budhu and Noy, 2002; Soprano *et al.*, 2004; Donato and Noy, 2005; Donato *et al.*, 2007; Noy, 2010). PPAR $\beta/\delta$  activation causes increased proliferation and survival, which can promote tumour formation (Schug *et al.*, 2007; Di-Poi *et al.*, 2002; Di-Poi *et al.*, 2003; Wang *et al.*, 2006). Overexpression

of CRABP2 with RA inhibits tumour growth resulting in RAR signalling activation (Schug *et al.*, 2007; Schug *et al.*, 2008; Manor *et al.*, 2003). In contrast, in the presence of another component, fatty acid-binding protein 5 (FABP5), CRABP2 mediates proliferative activity through retinoic acid-induced peroxisome proliferator-activated receptor  $\beta/\delta$  activation, rather than activating RAR signalling (Schug *et al.*, 2007). Following PPAR $\beta$  activation, ILK and PDK1 are upregulated, while PTEN is downregulated, resulting in AKT1 activation in a PI3K-dependent manner (Di-Poï *et al.*, 2002). In response to this activation, the activity of several of its targets, including Bad, FKHR, and NF- $\kappa$ B, are altered, resulting in apoptosis suppression and changes in cell adhesion/migration (Di-Poï *et al.*, 2002). The above literature suggests there is a link between overexpression of CRABP2 and AKT1 kinase activity. Therefore, RAR and PPAR $\beta$  signalling should be investigated in meningioma with *AKT1<sup>E17K</sup>/TRAF7* mutation. Supporting this one study has demonstrated that overexpression of CRABP2 increases AKT1 phosphorylation resulting in suppression of apoptosis in human osteoblast cells (Zhang *et al.*, 2021). In meningioma samples, it has been confirmed that *AKT1<sup>E17K</sup>* mutation increases the phosphorylation at AKT1-S473 and AKT1-T308 (John *et al.*, 2022). We could also investigate the association between CRABP2 expression and AKT1 kinase activity (AKT1-P-S473 and AKT1-P-T308) at the protein level by knockdown of CRABP2.

A proteomic study showed that increased expression of CRABP2 indicates poor prognosis in estrogen receptor-negative breast cancers and strong staining of CRABP2 is also confirmed in stage III invasive ductal carcinoma (IDC) compared to healthy tissue via IHC (Geiger *et al.*, 2012). This study also showed that significant overexpression of CRABP2 at the mRNA level was linked to reduced overall survival in breast cancer patients (Geiger *et al.*, 2012). Another proteomic study found that CRABP2 protein expression was highly specific to serous histologic subtypes of ovarian cancer when compared to clear cell, endometrioid, and mucinous ovarian cancer. Significant overexpression of CRAB2 was confirmed via WB, and strong CRABP2 staining was also confirmed for this group compared to other groups, implying that it could be used as a biomarker for these serous subtypes (Toyama *et al.*, 2012). Overexpression of CRABP2 was also found to be associated with tumour grade and ovarian cancer stage in this investigation (Toyama *et al.*, 2012). Further, another proteomic analysis revealed significant CRABP2 overexpression in retinoblastoma tissues compared to normal retinal tissues, as well as consistent results in quantitative RT-PCR analysis of CRABP2 mRNA level and strong immunostaining of CRABP2 via IHC, suggesting that CRABP2 could be used as a biomarker for prognostic monitoring and therapeutic use for retinoblastoma (Mallikarjuna *et al.*, 2010).



High CRABP2 levels were shown to be linked to lymph node metastases, poor overall survival, and higher recurrence in clinical samples (Wu *et al.*, 2019). Knocking down of CRABP2 in C10F4 lung cancer cells showed reduced migration, invasion, anoikis resistance, and in vivo metastasis (Wu *et al.*, 2019). This study also demonstrated the role of CRABP2 in lung cancer metastasis in which CRABP2 co-immunoprecipitated with HuR, and CRABP2 overexpression accelerated HuR levels, promoting integrin/FAK/ERK signalling (Wu *et al.*, 2019). The enhancing effect of CRABP2 in migration, invasion, and anoikis resistance was reversed when HuR or integrin 1/FAK/ERK signalling was inhibited (Wu *et al.*, 2019). In addition to this, in several studies overexpression of CRABP2 was also observed in non-small cell lung cancer (NSCLC) tumour tissues compared to normal lung tissue (Han *et al.*, 2014; Codreanu *et al.*, 2017; Zhang *et al.*, 2015). Kim *et al.*, (2018) showed that CRABP2 protein levels were significantly higher in plasma samples from NSCLC patients compared to plasma samples from healthy control group without malignancy and pulmonary diseases and were indicated as a diagnostic marker for patients with NSCLC.

In pancreatic ductal adenocarcinoma tissues, CRABP2 has also been reported to be strongly, significantly, and more frequently expressed in high-grade precursor malignant lesions compared to low-grade lesions (Xiao *et al.*, 2014). Finally, Fischer-Huchzermeyer *et al.*, (2017) demonstrated that strong cytoplasmic expression of CRABP2 in malignant peripheral nerve sheath tumours (MPNSTs) compared to normal schwann cells and knocking down of CRABP2 in MPNST cell lines (S462, T265, NSF1) reduces viability and proliferation while inducing apoptosis, cytotoxicity, and interferon signalling. These findings imply that overexpression of CRABP2 promotes the survival of MPNST cells in vitro, independent of retinoic acid, and targeting CRABP2 overexpression for the therapy of human MPNSTs could be potential (Fischer-Huchzermeyer *et al.*, 2017).

On the other hand, CRABP2 is epigenetically downregulated in several cancers, including prostate cancer, human head and neck cancer, and astrocytic gliomas (Okuducu *et al.*, 2005; Calmon *et al.*, 2009; Campos *et al.*, 2012). In addition to this, significant down-regulation of CRABP2 at mRNA level was observed in oesophageal tumour samples compared to normal oesophageal tissue and their functional experiments showed that overexpression of CRABP2 significantly inhibited cell proliferation in EC109 cells stably transfected with CRABP2 compared to EC109 cells transfected with vector (Yang *et al.*, 2016).

Though IHC for CRABP2 expression did not reveal any distinct patterns among the meningioma mutational subtypes. The average IHC score for CRABP2 expression was high in meningioma mutational subtype's tissue sections in comparison to NMT tissue sections (Fig- 22 Bc). In addition to this, strong staining was observed for CRABP2 expression in *AKT1<sup>E17K</sup>/TRAF7* and *KLF4<sup>K409Q</sup>/TRAF7* mutated meningioma compared to *NF2<sup>-/-</sup>* mutated meningioma samples where most of the tissue sections were strongly stained (Fig- 22 Bc). However, IHC staining demonstrated that CRABP2 proteins were predominantly found in the cytoplasm (Fig-22 A), which is in line with previous findings (Fischer-Huchzermeyer *et al.*, 2017; Liu *et al.*, 2016). Though the staining results were not reflective of Simple wes and Mass-spectrometry analysis, *AKT1<sup>E17K</sup>/TRAF7* mutant meningioma-specific CRABP2 protein should not be dismissed. Significant overexpression of CRABP2 from WB results and predominant cytoplasmic expression of CRABP2 from IHC suggest further investigation should be made on how CRABP2 protein involve in *AKT1<sup>E17K</sup>/TRAF7* mutated meningioma tumorigenesis and could be a potential target for therapeutic use for *AKT1<sup>E17K</sup>/TRAF7* mutated meningioma group.

### 5.1.2 *NF2<sup>-/-</sup>* mutant meningioma-specific upregulated protein candidates

Seven commonly and significantly upregulated proteins were identified for *NF2<sup>-/-</sup>* meningioma subtypes compared to other mutant meningioma and NMT (Fig-24 A). These include Annexin A3, Solute carrier family 29 member 1, FYVE and coiled-coil domain-containing protein 1, Glycogen phosphorylase, Tubulin beta chain, and Tubulin alpha-1B chain (Table 10), only two proteins with the highest fold change were taken for further validation and all the confirmation results will be discussed below.

Comparing *AKT1<sup>E17K</sup>/TRAF7* and *NF2<sup>-/-</sup>* mutational meningioma subtypes it is important to note that the number of commonly significantly overexpressed proteins (162) were high in *AKT1<sup>E17K</sup>/TRAF7* meningioma subtypes compared to the number of commonly downregulated proteins (only 3) which is very low (Fig-16 A and B). On the other hand, an opposite trend was revealed in *NF2<sup>-/-</sup>* mutational meningioma subtypes while a higher number of commonly significantly down-regulated proteins (54) were identified compared to the number of overexpressed proteins (Fig-24 A and B).

**Annexin-A3 (ANXA3):** In meningioma expression of ANXA3 has not yet been reported. This study is the first to detect ANXA3 as a commonly significantly overexpressed in *NF2<sup>-/-</sup>* mutant meningioma compared to *AKT1<sup>E17K</sup>/TRAF7*, *KLF4<sup>K409Q</sup>/TRAF7*, and NMT in mass-spectrometry data analysis (Table 10) and ANXA3 overexpression confirmed via Simplex assay and IHC which is in line agreement with mass-spectrometry data analysis (Fig- 27 A and A1, Fig-28 A and Ba).

ANXA3 is a member of the annexin family proteins and is also referred to as lipocortin III and placental anticoagulant protein III (Gerke and Moss, 2002; Moss and Morgan, 2004). There are two ANXA3 isoforms with molecular weights of 33 and 36 kDa that has been identified, the 36 kDa ANXA3 isoform is mostly found in monocytes, whereas the 33 kDa ANXA3 isoform is more common in neutrophils (Le Cabec and Maridonneau-Parini, 1994). ANXA3 consists of four conserved structural domains in which the N-terminus domain containing two tryptophan residues are crucial for protein stability and interaction with intracellular calcium ions and negatively charged phospholipids, allowing ANXA3 to regulate a wide range of biological processes (Hofmann *et al.*, 2000; Sopkova *et al.*, 2002; Yang *et al.*, 2021). Annexin3 is a calmodulin-dependent phospholipid-binding protein that is involved in regulating a wide range of molecular and cellular processes, including calcium ion current regulation, membrane trafficking, cellular adhesion, cell signalling, the maintenance of cytoskeleton and extracellular matrix integrity, development and differentiation, inflammation, blood coagulation, and so on (Swairjo and Seaton, 1994; Gerke and Moss, 2002; Mussunoor and Murray, 2008). It has been reported that the dysregulation of ANXA3 protein expression has been linked to tumour growth and progression. However, the evidence to date on its expression in various malignancies is contradictory (Yang *et al.*, 2021). Overexpression of ANXA3 has been observed in several cancer types such as breast, colorectal, bladder, ovarian, gastric, pancreatic, and hepatocellular and nasopharyngeal carcinoma (Du *et al.*, 2018; Kim *et al.*, 2018; Li *et al.*, 2018; Zhou *et al.*, 2018; Xu *et al.*, 2019; Tsai *et al.*, 2018; Jiang *et al.*, 2019; Wang and Li, 2016; Wan *et al.*, 2020; Tong *et al.*, 2018; Ruan *et al.*, 2010; Yang *et al.*, 2021). On the other hand, downregulation of ANXA3 was reported in renal cancer, prostate cancer, and papillary thyroid cancer (Bianchi *et al.*, 2010; Peraldo-Neia *et al.*, 2011; Jung *et al.*, 2010; Yang *et al.*, 2021).

Wang and Li, (2016) observed overexpression of ANXA3 in gastric cancer tumour tissue compared to neighbouring normal tissue at both mRNA and protein levels. This study also looked at 183 paraffin-embedded GC tissue section slides, and their univariate and multivariate analysis found that strong ANXA3 expression was significantly correlated with tumour size,

depth of tumour infiltration (T stage), TNM stage (the tumour, node and metastasis) and metastasis, implying that ANXA3 could be a potential prognostic marker for GC patients. Moreover, they also revealed knockdown of ANXA3 significantly reduced GC cell proliferation and colony formation, these findings suggesting ANXA3 is involved in GC carcinogenesis (Wang and Li, 2016). Likewise, knockdown of ANXA3 expression in primary hepatocellular carcinoma cells significantly decreased cell proliferation and tumorigenesis (Pan *et al.*, 2015). Similar to these, in this current study, functional analysis using knockdown of ANXA3 in the benmen-1 reduced cell proliferation but not to a significant degree (Fig- 29 e). This could be due to the fact that benmen-1 being an immortalized cell line and maybe knocking down the ANXA3 in primary merlin negative cells would give us more significant results. The functional role of ANXA3 in meningioma should be followed up by additional experiments. To sum up, knockdown of ANXA3 decreased *NF2*<sup>-/-</sup> mutated Benmen-1 cell proliferation and the result was supported by previous cancer studies (Wang and Li, 2016; Pan *et al.*, 2015).

Proteomic study of bladder cancer tissue revealed overexpression of ANXA3 relative to neighbouring normal tissue, and further higher levels of ANXA3 were verified through WB and ELISA in urine samples from BC patients, implying that ANXA3 is a diagnostic marker for BC (Tsai *et al.*, 2018). Likewise, another proteomic investigation found higher expression of ANXA3 in colon cancer tissue compared to normal mucosal tissue, with WB and IHC confirming significant ANXA3 overexpression. In IHC, ANXA3 displayed medium to mild staining in colon cancer tissue sections, while ANXA3 expression was missing or hardly detectable in normal mucosal tissue, and it was mostly found in the cytoplasm (Yang *et al.*, 2018). Similar to this, IHC experiments of the current study, ANXA3 showed strong to moderate staining in *NF2*<sup>-/-</sup> mutant meningioma samples where *AKT1*<sup>E17K</sup>/*TRAF7* and *KLF4*<sup>K409Q</sup>/*TRAF7* mutant meningioma and NMT showed moderate to weak staining for annexin-3 expression (Fig-28 A and Ba). ANXA3 expression is predominantly observed in the cytoplasm and a similar pattern of observation is reported in other cancer studies (Liu *et al.*, 2009; Yang *et al.*, 2018).

ANXA3 has been demonstrated to activate the Notch and MAPK/ERK/JNK signalling pathways in hepatocellular carcinoma, leading to increased cell proliferation and stem-cell-like properties (Pan *et al.*, 2015; Tong *et al.*, 2015). In vitro findings from colorectal cancer showed that phosphorylation of ERK and JNK was greatly reduced if ANXA3 was depleted using small interfering RNA (siRNA) (Xu *et al.*, 2019). Supporting these findings, a further investigation

of chemoresistant non-small cell lung cancer (NSCLC) cells found that a high amount of ANXA3 released by cancer-associated fibroblasts (CAFs) in the tumour microenvironment stimulated JNK/survivin signalling, allowing cancer cells to escape cisplatin-induced apoptosis (Wang *et al.*, 2019). As in this study, NF2 loss in meningioma may lead to ANXA3 upregulation, which could contribute to MAPK/ERK/JNK pathway activation, resulting in cell cycle progression which should be investigated further in *NF2*<sup>-/-</sup> mutated meningioma subtypes (Shaw *et al.*, 2001; Curto *et al.*, 2007; Maitra *et al.*, 2006; Zhou and Hanemann, 2012; Petrilli and Fernández-Valle, 2016).

Some studies also reported that ANXA3 may also involve in inducing cancer cell migration (Yang *et al.*, 2021). An increased level of epithelial-mesenchymal transition (EMT) was observed in ANXA3 overexpressing gastric cancer (GC) cells and GC tumour samples, as evident by western blot results showing increased expressions of mesenchymal markers vimentin and  $\beta$ -catenin, decreased expression of epithelial marker E-cadherin, and increased expressions of EMT-related transcription factors fibronectin, Slug, and Snail (Wang and Li, 2016). A similar observation was also confirmed in Hepatocellular Carcinoma cells (Pan *et al.*, 2015).

Further, some studies suggested that ANXA3 may also be involved in tumour angiogenesis (Yang *et al.*, 2021). The expressions of ANXA3 and HIF1 $\alpha$  were found to be positively correlated, suggesting that ANXA3 is involved in the pro-angiogenic activity (Pan *et al.*, 2015). Wan *et al.*, (2020) also observed silencing of ANXA3 in pancreatic cancer cells caused a reduction in the expression of vascular endothelial growth factor receptor 3 (VEGFR3), a protein that has been linked to lymphatic vascularization in pancreatic cancer. The hypoxia-inducible factor-1 (HIF1 $\alpha$ )/VEGF pathway is the well-known response of cancer cells to promote angiogenesis (Xu *et al.*, 2018; Zhang *et al.*, 2018; Yang *et al.*, 2021). Bianchi *et al.*, (2010) reported that ANXA3 has a role in renal cell carcinoma metastasis by promoting angiogenesis via elevated VEGF levels induced by HIF1 $\alpha$ . Furthermore, overexpression of ANXA3 in hepatocellular carcinoma has been shown to suppress apoptosis induced by PKC $\delta$ /p38 (Tong *et al.*, 2018).

Our findings, combined with those of other cancer findings, strongly suggest that overexpression of ANXA3 could be a possible therapeutic target for *NF2*<sup>-/-</sup> mutated meningioma.

**Solute carrier family 29 member 1** (SLC29A1) also known as human equilibrative nucleoside transporter 1 (hENT1) and a member of the SLC29 (Solute carrier family 29) gene family (Park, 2012; Young *et al.*, 2013). SLC29A1 acts as an intracellular transporter for purine and pyrimidine nucleosides, as well as certain nucleobases (Park, 2012; Young *et al.*, 2013). In this current study, SLC29A1 was identified as commonly significantly upregulated in *NF2*<sup>-/-</sup> mutated meningioma compared to *AKT1*<sup>E17K</sup>/*TRAF7* and *KLF4*<sup>K409Q</sup>/*TRAF7* mutant meningioma and NMT (Table 10). However, the result was not consistent with WB and IHC findings (Fig- 27 B and B1; Fig-28 A and Bb). In WB analysis, *NF2*<sup>-/-</sup> mutated meningioma showed the lowest expression for SLC29A1 compared to other meningioma subtypes and lower expression compared to NMT which is not reflective of mass-spectrometry analysis (Fig- 27 B and B1). No clear differences were observed among the meningioma mutational subtypes and NMT in the IHC analysis (Fig-28 A and Bb).

A recent immunohistochemistry study showed significant overexpression of SLC29A1 in high-grade meningioma compared to low-grade meningioma and also reported increased levels of SLC29A1 expression were linked to a shorter progression-free survival (PFS) (Yamamoto *et al.*, 2021). This study also established the role of SLC29A1 in the meningioma cell proliferation and survival, revealing that SLC29A1 expression is essential to prevent DNA damage and maintain meningioma cell growth in vitro and in vivo (Yamamoto *et al.*, 2021). However, another study has shown that overexpression of SLC29A1 was linked to a high Ki-67 labelling index in a cholangiocarcinoma cell line and knockdown of SLC29A1 expression resulting in G1/S arrest (Tavolari *et al.*, 2019). Yamamoto *et al.*, (2021) also investigated gemcitabine sensitivity in meningioma cell lines and revealed that the growth inhibitory effects of gemcitabine treatment were higher in high-grade meningioma cell lines (IOMM-Lee) than in low-grade meningioma cell lines (M-20-U and M-10-S) and normal human fibroblasts cells (IMR90) and suggesting SLC29A1 as a prognostic marker for high-grade meningioma. However, NF2 gene is intact in IOMM-Lee cell line. This current WB findings suggest expression of SLC29A1 is abundant not only in benign meningioma but also in normal meninges which contradicts previous studies, though the Yamamoto *et al.*, (2021) study used normal fibroblast tissue as a control and compared it to WHO meningioma grades, while the current study only looked in grade I benign meningioma.

With all the evidence pointing that there are inconsistencies between the analysis of the MS data and the findings of the validation of SLC29A1 expression in *NF2*<sup>-/-</sup> mutant meningioma;

hence, further investigation will not be conducted for this candidate. However, future studies could show additional functions that have not been described to date.

### 5.1.3 *KLF4*<sup>K409Q</sup>/*TRAF7* mutated meningioma-specific upregulated protein candidates

Only 14 upregulated proteins were very specific for *KLF4*<sup>K409Q</sup>/*TRAF7* mutant meningioma compared to other groups (Fig- 31 A). The proteins include endoglin, E-cadherin 1, CD44, anion exchange protein 2 member 1, etc. (Table 13). Due to the shortage of tissue lysates for this mutational subtype, only three proteins were chosen for further validation which will be discussed below.

CD44 is an interesting candidate for *KLF4*<sup>K409Q</sup>/*TRAF7* mutant meningioma and has already been reported in meningioma. Unfortunately, due to the shortage of meningioma tissue samples, CD44 expression was not validated via WB. Yan *et al.*, (2016) revealed that *KLF4* and CD44 proteins are involved in regulating cancer stemness and metastasis, reporting that knockdown of *KLF4* generates significant upregulation of CD44 in mouse cancer cell lines and tumour tissue. Previously a significant correlation between CD44 expression and grading has been reported. Mostafa *et al.*, (2017) showed that CD44 expression was higher in grade-II and grade-III (81.8%) compared to grade-I (18.2%), suggesting that increased expression of CD44 is a marker for aggressive meningioma. Lewy-Trenda *et al.*, (2004) have also observed similar findings, strong immunostaining for CD44 expression in atypical meningioma and moderate expression in benign meningioma. However, this current study did not look at total *KLF4* protein expression between mutational subtypes and NMT, and only focused on specific *KLF4* mutation at the 409 coding region. No western blot analysis for CD44 has yet been reported for meningioma in the literature.

**Endoglin** was identified as commonly significantly overexpressed in *KLF4*<sup>K409Q</sup>/*TRAF7* mutant meningioma compared to *AKT1*<sup>E17K</sup>/*TRAF7*, *NF2*<sup>-/-</sup> mutant meningioma, and NMT in mass-spectrometry data analysis (Table 13). One study has shown that endoglin-positive kidney tumour primary cells (Caki-2) and metastatic renal carcinoma cells (ACHN), both showed high expression of human mesenchymal stem cell (MSC) markers CD44 compared to a healthy kidney epithelial cell line (ASE-5063) (Khan *et al.*, 2016). Similarly, current proteomic data analysis showed endoglin and CD44 proteins both commonly significantly expressed in *KLF4*<sup>K409Q</sup>/*TRAF7* mutant meningioma compared to other mutational meningioma subtypes and normal meninges (Table 13; Fig- 31). Western blot analysis showed an increased expression of endoglin in *KLF4*<sup>K409Q</sup>/*TRAF7* mutant meningioma compared to

other mutational meningioma subtypes and NMT (Fig-35 A and A1) but not to a significant degree as mass-spectrometry analysis showed. It could be due to the small number of normal meningeal tissue. Future analysis by adding more tumour samples may exhibit significant expression in meningioma compared to NMT. Furthermore, in mass-spectrometry, endoglin was identified at 67 kDa but in Western blot, a double band between 60 and 75 kDa was observed (<https://www.uniprot.org/uniprot/Q5T9B9>) (Fig-35 A and A1). A previous study reported that the ultimate molecular weight of endoglin might vary between 90 and 95 kDa for two isoforms, depending on its glycosylation state in different tissues (Gougos and Letarte, 1990). Burghardt *et al.*, (2021) showed endoglin expression in glioma cell lysates as a double band of around 100 kDa, and endoglin expression was not confirmed in tissue lysates. These findings suggest that due to the glycosylation nature of endoglin, its size may differ from cell to cell. In agreement with WB, IHC analysis of *KLF4<sup>K409Q</sup>/TRAF7* mutant meningioma showed strong to moderate staining for endoglin expression whereas other mutant meningioma groups showed moderate to weak and NMT showed weak or absent expression (Fig-36 a and a1). Similar findings were observed in other cancer studies including glioblastoma and gastric cancer (Burghardt *et al.*, 2021; Nikiteas *et al.*, 2007). Like the current study, strong cytoplasmic expression of endoglin was also observed in other cancer studies such as glioblastoma, breast, papillary thyroid, melanoma, and osteosarcoma (Fig-36 a) (Nikiteas *et al.*, 2007; Postiglione *et al.*, 2005). IHC findings suggest strong cytoplasmic expression of endoglin could be used as a diagnostic marker for *KLF4<sup>K409Q</sup>/TRAF7* mutant meningioma.

Endoglin is a transmembrane glycoprotein, also referred to as CD105, mostly found in endothelial cells and acts as a co-receptor for transforming growth factor-  $\beta$  (TGF- $\beta$ ) (Siegel and Massague, 2003; Waite and Eng, 2003; Perez-Gomez *et al.*, 2005). The family of transforming growth factor-  $\beta$  (TGF- $\beta$ ) consists of TGF- $\beta$  isoforms, activins, inhibins, and bone morphogenetic proteins (BMPs) which are involved in regulating important cellular functions including cell growth, differentiation, migration, adhesion, angiogenesis, and the immune response (Siegel and Massague, 2003; Waite and Eng, 2003; Perez-Gomez *et al.*, 2005). In the presence of signalling receptors TGF $\beta$ RII, endoglin interacts with TGF- $\beta$ 1, TGF- $\beta$ 3, activin-A, and BMP-7; endoglin also interacts with BMP-2 in the presence of TGF $\beta$ RI; it can bind directly to BMP-9 or -10 (Cheifetz *et al.*, 1992; Barbara *et al.*, 1999; David *et al.*, 2007; Castonguay *et al.*, 2011; González Muñoz *et al.*, 2021). In a heterodimeric receptor complex, TGF $\beta$ RI and TGF $\beta$ RII receptors are then activated by endoglin, leading to phosphorylation of cytoplasmic domain of endoglin containing serine (Ser) 631 and 635 residues in the case of



TGF $\beta$ RII, while TGF $\beta$ RI phosphorylates ENG at threonine (Thr) residues (Koleva *et al.*, 2006; Guerrero-Esteo *et al.*, 2002; Lastres *et al.*, 1994). In addition to this, the endoglin ligand-receptor interaction accelerates the phosphorylation activity of TGF $\beta$ RI, which transmits the signals to phosphorylate downstream proteins receptor-regulated SMAD (R-SMADs) (Koleva *et al.*, 2006; Guerrero-Esteo *et al.*, 2002). To understand the role of endoglin in meningioma development, it will be interesting to further examine endoglin-mediated TGF $\beta$  signalling pathways in *KLF4*<sup>K409Q</sup>/*TRAF7* mutated meningioma.

Endoglin has two isoforms with different cytoplasmic domains; the large isoform, L- endoglin, contains 47-aminoacid residue of the cytoplasmic domain, but the smaller isoform, S-endoglin, only has a 14-aminoacid of cytoplasmic tail (Gougos and Letarte, 1990; Bellon *et al.*, 1993; Perez-Gomez *et al.*, 2005). Although both endoglin isoforms can bind ligands, their phosphorylation levels and ability to regulate TGF- $\beta$  -dependent responses differ (Bellon *et al.*, 1993; Lastres *et al.*, 1994; Lastres *et al.*, 1996). For example, S-endoglin is shown to activate the ALK5/SMAD2/PAI-1 (activin receptor-like kinase 5/ SMAD2/plasminogen activator inhibitor type 1) pathways, which increased TGF- $\beta$ 1-induced collagen-I and connective tissue growth factor expression resulting in reduction of endothelial and myoblast cell proliferation (Velasco *et al.*, 2008). In contrast, L-endoglin decreased TGF- $\beta$ 1-induced collagen-I and connective tissue growth factor expression by activating ALK1/SMAD1/ID-1 (activin receptor-like kinase 5/ SMAD2/ inhibitor of DNA binding 1) pathways, resulting in increasing TGF- $\beta$ 1-induced endothelial and myoblasts cell proliferation (Velasco *et al.*, 2008). Moreover, endoglin is involved in regulating angiogenesis in endothelial cells (EC) by activating the SMAD1/5/8 pathway (Tian *et al.*, 2012).

Endoglin plays a role in tumour cell development and progression (Rosen *et al.*, 2014; González Muñoz *et al.*, 2021). In addition to endoglin expression in tumour vasculature, overexpression of endoglin has been reported in several cancers tissue, such as melanoma, renal cell carcinoma (RCC), leukemias, some subtypes of sarcomas, and breast, ovarian, endometrial, and prostate cancer (González Muñoz *et al.*, 2021; Pardali *et al.*, 2011; Hu *et al.*, 2017; Kauer *et al.*, 2019; Oplawski *et al.*, 2018, Hara, 2012; Oxmann *et al.*, 2008; Madhav *et al.*, 2018; Zhang *et al.*, 2019). Endoglin primarily affects cancer cell malignancy via TGF $\beta$ /BMP signalling, but it also drives tumorigenesis through non-SMAD pathways including mitogen-activated protein kinases (MAPK)/ERK, p38, and c-Jun N-terminal kinases (JNK) and phosphoinositide 3' kinase (PI3K)/Akt (Pérez-Gómez *et al.*, 2010; González Muñoz *et al.*, 2021). Pardali *et al.*, (2011) showed overexpression of endoglin increases BMP

signalling or activating the FAK (focal adhesion kinase) and PI3K pathways resulting in tumour plasticity in both Ewing sarcoma and melanoma, and knockdown of endoglin inhibits tumour cell plasticity and decreases invasiveness and progression of sarcoma and melanoma cells in vitro. Likewise, in this current study, gene ontology analysis showed that endoglin is involved in extracellular matrix disassembly and focal adhesion GO term (Fig-32). For cellular stability, focal adhesion provides a signal transduction system through which cells can interact with the extracellular matrix. This is fundamental for numerous cellular processes including mitosis, motility, and cellular polarity. Dysfunction in the proteins associated with focal adhesion has been associated with diseases including cancer (Charras and Sahai, 2014; Alberts *et al.*, 2013). This result indicates overexpression of endoglin may be involved in regulating cellular motility or migration and in order to confirm this focal adhesion kinase activity should be investigated in *KLF4<sup>K409Q</sup>/TRAF7* mutated meningioma.

Fujiwara *et al.*, (2013) found that pancreatic cancer tissue had higher levels of endoglin compared to normal surrounding tissue. This study also showed that E-cadherin mRNA (epithelial marker) expression was reduced whereas vimentin mRNA (mesenchymal marker) was overexpressed in endoglin-positive pancreatic cancer cells, implying that endoglin-positive pancreatic cancer cells undergo epithelial-mesenchymal transition (Fujiwara *et al.*, 2013). In agreement with this, another study demonstrated that endoglin-expressing kidney cancer primary cells have a higher ability to form spheres in vitro than non-cancerous cells, and a similar observation in endoglin-expressing tumours in xenograft mice model (Hu *et al.*, 2017). In vitro, shRNA-mediated knockdown of endoglin diminished stemness markers and sphere-formation abilities (Hu *et al.*, 2017). Where cancer stem cells (CSCs) require endoglin to preserve their stem cell properties and NANOG, C-MYC, KLF4, and CDA are possible mediators of endoglin that increase self-renewal and chemoresistance (Hu *et al.*, 2017). Interestingly, a previous study of meningioma, demonstrated that *KLF4<sup>K409Q</sup>* mutation may enhance the KLF4 protein stability by increasing the expression of KLF4 as confirmed via WB (Von Spreckelsen *et al.*, 2020). In agreement with this, the current proteomic analysis showed expression of endoglin positively correlated with *KLF4<sup>K409Q</sup>/TRAF7* mutated meningioma, it could be postulated that KLF4 expression maintains stem cell properties via endoglin. As mentioned previously total KLF4 protein expression was not confirmed between mutational meningioma subtypes which should be investigated further. Downregulation of endoglin significantly reduced tumorigenicity and gemcitabine resistance suggesting endoglin is a

promising therapeutic target for renal cell carcinoma (Hu *et al.*, 2017). In ovarian cancer patients, overexpression of endoglin is linked to drug resistance, poor differentiation, advanced disease stage, and a high rate of recurrence (Ziebarth *et al.*, 2013; Bai *et al.*, 2019). Inhibition of endoglin with small interfering RNA (siRNA) in ovarian cancer cells results in a less aggressive phenotype, as well as the activation of apoptosis and increased carboplatin sensitivity in vivo models (Ziebarth *et al.*, 2013; Bai *et al.*, 2019). Moreover, Immunohistochemistry analysis of acute myeloid leukaemia tissue sections showed high levels of endoglin have been linked to poor overall survival (OS) and progression-free survival (PFS) (Kauer *et al.*, 2019).

Furthermore, endoglin expression is increased in actively proliferating endothelial cells of tumour-associated vasculature in numerous cancers, suggesting endoglin can be used as a tumour angiogenesis marker (González Muñoz *et al.*, 2021). Endoglin plays a role in regulating angiogenesis in a variety of cancers including pediatric adrenocortical tumors, pediatric rhabdomyosarcoma, astrocytomas, hepatocellular (HCC) and oral squamous cell carcinomas, breast, lung, prostate, colorectal (CRC), ovarian, gastric, endometrial, esophageal, and head and neck and renal cancers (Nassiri *et al.*, 2011; Dos Santos Dias *et al.*, 2015; Di Paolo *et al.*, 2018; González Muñoz *et al.*, 2021). It has been reported that endoglin overexpression increases VEGF secretion in glioma cells via Smad2/3 and Smad1/5/8-dependent signalling (Seystahl *et al.* 2015). Increased expression of endoglin was confirmed via IHC staining of glioblastoma tissue sections, and a high density of endoglin-expressing microvessels has been linked to a poor prognosis for glioblastoma patients (Yao *et al.*, 2005; Burghardt *et al.*, 2021). A previous study confirmed that *KLF4*<sup>K409Q</sup> mutation is involved in regulating tumour angiogenesis via activation of VEGF signalling which is responsible for peritumoral brain edema (PTBE) in *KLF4*<sup>K409Q</sup> mutated meningioma (Von Spreckelsen *et al.*, 2020). These results show a relationship between endoglin and KLF4 that has to be further investigated because both proteins play significant roles in tumour angiogenesis via VEGF production.

To summarise, all the findings imply that endoglin could be a potential diagnostic and therapeutic target for *KLF4*<sup>K409Q</sup>/*TRAF7* mutant meningioma.

**E-cadherin (Cadherin 1):** To date, this is the first study reporting increased E-cadherin expression in *KLF4*<sup>K409Q</sup>/*TRAF7* mutant meningioma or secretory meningioma compared to *AKT1*<sup>E17K</sup>/*TRAF7*, *NF2*<sup>-/-</sup> mutant meningioma, and NMT in mass-spectrometry data analysis (Table 13). Though in WB analysis, 4 samples from *AKT1*<sup>E17K</sup>/*TRAF7* mutant meningioma

showed expression of E-cadherin at 97 kDa and did not display any band at 80 kDa (Fig-35 A). In contrast, almost all samples from *KLF4<sup>K409Q</sup>/TRAF7* mutant meningioma group expressed E-cadherin at both molecular weights which is consistent with mass-spectrometry data analysis (Table 13; Fig-35 A and A2). IHC staining for E-cadherin expression supported MS data analysis where *KLF4<sup>K409Q</sup>/TRAF7* mutant meningioma showed strong to moderate E-cadherin expression, *AKT1<sup>E17K</sup>/TRAF7* and *NF2<sup>-/-</sup>* mutant meningioma both showed moderate to weak staining while NMT showed weak or absent expression (Fig-36 b and b1). Similar to this IHC finding in benign meningioma, Burandt *et al.*, (2021) showed overexpression of E-cadherin in 24 different tumour types compared to normal cells including testicular germ cell tumours, sarcoma and renal cell carcinomas (RCC). The author showed that upregulation of E-cadherin in papillary and clear cell RCCs originated from E-cadherin negative proximal tubule (Burandt *et al.*, 2021). Burandt *et al.*, (2021) also showed several normal tissues were negative for E-cadherin in immunostaining including the cerebellum and cerebrum. Interestingly, in the WB (Fig-35 A) it was observed that NMT did not show a band for E-cadherin suggesting normal meninges express E-cadherin low or not at all. Four different cases of NMT in IHC showed weak or absent staining for E-cadherin expression also confirming WB findings. However, more normal meningeal samples should be investigated to confirm these observations. It is still unclear which cellular functions are involved in the upregulation of E-cadherin and drive tumorigenesis (Burandt *et al.*, 2021). Some studies showed overexpression of E-cadherin inhibits anoikis, promotes the development of multicellular spheroids, and hence facilitates anchorage-independent cell proliferation (Kang *et al.*, 2007; Kantak *et al.*, 1998; Burandt *et al.*, 2021).

E-cadherin is a membrane glycoprotein that plays a key function in calcium-dependent cellular adhesion and polarity maintenance. E-cadherin is mostly expressed in epithelial cells (Powell *et al.*, 1984; Van Roy and Berx, 2008; Niessen *et al.*, 2011; Burandt *et al.*, 2021). E-cadherin consists of 5 domains; the extracellular domain regulates the calcium-dependent homophilic interaction to maintain epithelial cell-cell contact (Kemler, 1993; Saha *et al.*, 2008). While the E-cadherin intracellular C-terminal domain binds  $\alpha$ -catenin and  $\beta$ -catenins, as well as p120, and forms complexes followed by interaction with the actin cytoskeleton to keep normal epithelial tissue differentiation and polarity (Kemler, 1993; Saha *et al.*, 2008). Reduced or loss of E-cadherin expression suggests a loss of E-cadherin-mediated cell-cell contact, resulting in increased cell motility, which has been associated with tumour progression, invasive growth, and metastasis (Mendonsa *et al.*, 2018; Burandt *et al.*, 2021). Numerous immunohistochemistry

studies investigated the role of E-cadherin expression in tumour progression. Decreased or loss of E-cadherin expression has been linked to a high grade and advanced stage and shows poor prognosis in oesophageal, lung, squamous head and neck tumours, pancreatic, and cervical malignancies (Guilford, 1999; Pećina-Šlaus, 2003). Like previous studies, reduce E-cadherin expression was associated with a higher grade, triple-negative receptor status, and poor prognosis in invasive breast carcinoma of no particular type, triple-negative receptor status in lobular carcinoma of the breast, and lymph node metastasis in colorectal cancer (Burandt *et al.*, 2021).

Moreover, mutations in the E-cadherin (*CDH1*) cause inactivation of E-cadherin function has been found to be common in infiltrating lobular breast carcinomas and diffuse gastric carcinoma, endometrium, ovary, and thyroid (Huiping *et al.*, 1999; Berx *et al.*, 1998; Machado *et al.*, 1999; Pećina-Šlaus, 2003). Most of these mutations occur in tandem with the loss of heterozygosity of the wild-type allele (Pećina-Šlaus, 2003). Loss of heterozygosity of *CDH1* (E-cadherin 1) gene was linked to E-cadherin down-regulation also reported in high-grade meningiomas (Pećina-Šlaus *et al.*, 2010). These findings suggest overexpression of E-cadherin is indicative of low-grade benign meningioma which is in agreement with proteomic data analysis.

Zhou *et al.*, (2010) reported the role of E-cadherin and  $\beta$ -catenin expression in meningioma. E-cadherin and  $\beta$ -catenin expression levels were conversely linked to the WHO meningioma grade, with 92.69 %, 33.33 %, and 0% of grades I, II, and III respectively. Atypical and malignant meningioma had much lower levels of E-cadherin and  $\beta$ -catenin expression. E-cadherin and  $\beta$ -catenin expression levels were also found to be inversely related to meningioma invasion status, tumour size, and meningioma recurrence probabilities (Zhou *et al.*, 2010). A similar observation in meningioma was also confirmed by another group where the investigation showed E-cadherin expression was lower in anaplastic meningiomas, and the intensity of E-cadherin staining was reduced in neoplastic cells in atypical and anaplastic meningiomas that did not express Slug or Twist (Nagaishi *et al.*, 2012). Slug and Twist, both proteins are found to have a role in mesoderm formation. Slug and Twist interact with the E-cadherin promoter and inhibits the transcription of E-cadherin (Vesuna *et al.*, 2008; Larue *et al.*, 2005; Nagaishi *et al.*, 2012). Slug and Twist, which are required for epithelial to mesenchymal transition (EMT) are expressed by neural crest cells during embryonic development (Taylor and LaBonne, 2007; Thiery *et al.*, 2009; Nagaishi *et al.*, 2012).

Finally, two previous studies showed E-cadherin expression is positively correlated with KLF4 expression in breast and colorectal cancer (Yori *et al.*, 2010; Tang *et al.*, 2014). Yori *et al.*, (2010) showed that E-cadherin is a direct transcriptional target for KLF4, and this transcriptional regulation is required to maintain the epithelial phenotype in mammary epithelial cells. The study also shows that forcing KLF4 expression in the highly metastatic MDA-MB231 breast cancer cell line restores E-cadherin expression, resulting in decreased migration and invasion (Yori *et al.*, 2010). These observations support our findings, even though we did not confirm KLF4 protein expression in benign meningioma subtypes. As mentioned previously, *KLF4<sup>K409Q</sup>* mutation in meningioma may enhance the KLF4 protein activity by increasing the expression of KLF4 as confirmed via WB (Von Spreckelsen *et al.*, 2020) suggesting a positive link between KLF4 and E-cadherin expression in *KLF4<sup>K409Q</sup>/TRAF7* mutant meningioma.

**Anion exchange protein 2 (AE2)** is a plasma membrane protein, also known as SLC4A2, which acts as a sodium-independent chloride/bicarbonate transporter and involve in regulating intracellular pH and maintaining acid-base balance across the cell plasma membrane (Kopito *et al.*, 1989; Kopito, 1990; Holappa *et al.*, 2001). Intracellular pH (pHi) is vital for the regulation of important cellular activities and functions (Feske *et al.*, 2012; Celay *et al.*, 2018).

To date, the current study is the first to report AE2 in benign meningioma and an increased expression of AE2 was observed in meningioma mutational subtypes with the highest expression in *NF2<sup>-/-</sup>* mutational meningioma subtypes compared to NMT in WB (Fig-35 B and B2), which was not significant and also does not reflect mass spectrometry data analysis where AE2 was identified as the most significantly commonly upregulated in *KLF4<sup>K409Q</sup>/TRAF7* mutant meningioma (Table 13). However, anti-AE2 did not produce a clear signal and for confirmation, an additional new antibody should be tested. A strong cytoplasmic expression was observed for anion exchange protein 2 in all meningioma subtypes compared to NMT with no clear differences among meningioma mutant subtype groups (Fig-36 c and c1) suggesting it could be a potential marker for meningioma subtypes regardless of mutational status. The staining results for anion exchange protein 2 were not reflective of Western blot and mass-spectrometry analysis (Fig-35 B and B2; Fig-36 c and c1). To be noted for IHC validation a different manufacturer of anion exchange protein 2 antibody was used.

A gene expression data analysis in brain cells reported that KLF4 may play a role in regulating osmoadaptation-related AE genes (Maallem *et al.*, 2008). Osmoadaptation is a cellular process

where in the first stage cell shrinkage activates Na<sup>+</sup>, K<sup>+</sup>, 2 Cl<sup>-</sup> transporters (NKCC), Na<sup>+</sup> /H<sup>+</sup> exchangers (NHE), and Cl<sup>-</sup>/ HCO<sub>3</sub><sup>-</sup> anion exchangers (AE), allowing intracellular storage of inorganic ions (Na<sup>+</sup>, K<sup>+</sup>, and Cl<sup>-</sup> and subsequent osmosis-driven water input to restore cell volume (Hoffmann and Dunham, 1995; O'Neill, 1999; Maallem *et al.*, 2008). However, this study did not show any further confirmation of the mechanism of how KLF4 regulates AE genes in brain cells.

To summarise validation results, AE2 is not an ideal candidate for *KLF4*<sup>K409Q</sup>/*TRAF7* mutant meningioma as suggested by MS data analysis. Though AE2 overexpression was observed in mutational meningioma subtypes compared to NMT suggesting AE2 can be used as a therapeutic target for benign meningioma irrespective of mutational.

#### **5.1.4 Meningioma grade-I specific upregulated protein candidates**

Only 10 proteins are commonly upregulated amongst all benign meningioma compared to NMT (Fig-37 A; Table 16). These results imply that the proteomic landscape of mutational subtypes is highly variable (Fig-37 A; Table 16). Upregulated proteins include thrombospondin type-1 domain-containing protein 4, prostaglandin F2 receptor negative regulator, HLA-DRA, apoptosis regulator BAX, and Lin-7C (Table 16). Only three protein expressions were validated in benign meningioma regardless of mutational status compared to NMT which will be discussed below along with other two proteins (HLA-DRA and apoptosis regulator BAX) already been reported in meningioma.

From the overlapping data from these investigations, HLA-DRA (*Human Leukocyte Antigen – DR Isotype*) showed increased expression across all meningioma compared to NMT (Fig-37 A; Table 16), which is already been reported in meningioma by Ohara *et al.*, (1992). They have revealed that HLA-DRA expression was higher in fibrous and transitional histological subtypes compared to meningotheliomatous. In 1993, Kavanagh *et al.*, first reported the correlation between HLA-DRA expression and patient survival in large bowel carcinoma where high HLA-DRA expression was associated with a favourable prognosis. Several studies in a variety of malignancies such as colorectal, gastric, and breast cancer since then have revealed the same trend with tumours that were overexpressed HLA-DR having a better clinical outcome (Andrea *et al.*, 1998; Silva *et al.*, 2013; Chiba *et al.*, 1988). On the other hand, Fan *et al.*, (2017) demonstrated that glioma patients with high HLA-DRA scores showed increased *HLA-DRA* mRNA expression, had a poor clinical prognosis, and their results were supported by a prior study Esteban *et al.*, (1990) which looked at HLA-DRA protein levels in

glioma patients. However, in meningioma, no such correlation has yet been reported but Batchu *et al.*, 2021 observed in their transcriptomic analysis that HLA-DRA expression was higher in WHO grades I and II compared to grade III. This current study reporting higher expression of HLA-DRA in grade-I meningioma irrespective of mutational subtypes though we did not compare our data with grade II and grade III (Table 16).

Another protein, apoptosis regulator BAX showed consistent overexpression with high fold change in benign meningioma mass-spectrometry analysis compared to NMT. Lee *et al.*, (2015) reported that tumour with BAX overexpression showed a longer time to recurrence than those with lower expression in meningioma, suggesting a marker for slow-growing benign meningioma which supported the current mass-spectrometry analysis of benign meningioma (Table 16).

**PTGFRN** was detected as a candidate for benign meningioma subtypes and a significant overexpression was observed in  $AKT1^{E17K}/TRAF7$  and  $KLF4^{K409Q}/TRAF7$  mutant meningioma and an increased expression in  $NF2^{-/-}$  mutated meningioma compared to NMT via WB which in line with mass spectrometry data analysis (Table 16; Fig-38 A and A2). In addition to this, PTGFRN expressions at molecular weight level were variable among the different tumour samples (Fig-38 A and A2) which we can further investigate to confirm PTGFRN glycosylation by performing de-glycosylation assays (Provenzano *et al.*, 2017). However, in IHC, there was a noticeable difference between  $KLF4^{K409Q}$  mutant meningioma and NMT which is in agreement with MS data and WB results (Table 16; Fig-38 A and A2; Fig-39 b and b1). No differences in staining were observed between the other mutational subtypes ( $AKT1^{E17K}/TRAF7$  and  $NF2^{-/-}$  mutational meningioma subtypes) and NMT which could be due to the variation in tissue section slides (previously mentioned for GMDS) (Fig-39 b and b1) or non-specific expression by other cell types such as macrophages, epithelial or glial cells (Sofela *et al.*, 2021).

PTGFRN is a transmembrane protein with Ig domain, also known as CD9P-1, and is a member of the tetraspanin-enriched microdomains (TEMs) (Sala-Valdés *et al.*, 2006; Aguila *et al.*, 2019). TEMs consist of tetraspanins, growth factors, integrins, complement regulating proteins, signalling enzymes, and proteoglycans (Sala-Valdés *et al.*, 2006; Yáñez-Mó *et al.*, 2009; André *et al.*, 2009; Aguila *et al.*, 2019). PTGFRN functions as a scaffolding protein, interacting with other proteins to modulate downstream signalling pathways involved in a variety of cellular activities such as cell adhesion, migration, differentiation, proliferation, and



malignancy (Maecker *et al.*, 1997; Sala-Valdés *et al.*, 2006). In addition to this, Orlicky *et al.*, (1998) showed that PTGFRN is involved in lipid synthesis and accumulation in preadipose cells.

It has been reported that PTGFRN directly initiates cell motility or migration in HEK-293 cells by interacting with other tetraspanins CD9 or CD81, and PTGFRN expression is conversely correlated with CD9 and CD81 expression (Chambrion and Le Naour, 2010). A shotgun proteomics analysis showed PTGRN overexpression in xenograft tumour-derived metastatic MDA-MB-435 cells compared to non-metastatic cells, which was verified at the mRNA and protein levels and suggested that PTGFRN could be used as a marker for tumour metastasis (Karhemo *et al.*, 2012). Another study showed overexpression of PTGFRN in metastatic human lung tumours compared to non-metastatic lung tumours and surrounding normal tissue and demonstrated that PTGFRN overexpression significantly correlated with metastatic status of the lung cancer (Guilmain *et al.*, 2011). MicroRNA and immunohistochemistry analysis confirmed that overexpression of PTGFRN was significantly linked to tumour stage and histological grade and high PTGFRN expression was also linked to a worse overall survival rate in several cancer including hepatocellular carcinoma, renal carcinoma, and glioblastoma multiforme (Huang *et al.*, 2020; Tan *et al.*, 2021; Aguila *et al.*, 2019).

PTGFRN has also been involved in blocking prostaglandin F2 $\alpha$  binding to its receptor by reducing receptor numbers instead of receptor affinity (Orlicky, 1996; Pridham *et al.*, 2017). Higher levels of prostaglandin F2 $\alpha$  resulted in enhanced prostaglandin F2 $\alpha$  receptor-mediated signalling in prostate cancer, which has stimulated tumour cell proliferation and radiation resistance (Wang *et al.*, 2008; Sun *et al.*, 2016). While PTGFRN has been demonstrated to decrease the number of F2 $\alpha$  receptor receptors, lowering PTGFRN results in increased prostaglandin F2 $\alpha$  receptors, permitting for prostaglandin F2 $\alpha$  binding and signalling (Wang *et al.*, 2008; Sun *et al.*, 2016). However, Aguila *et al.*, (2019) showed a reduction of PTGFRN has no effect on prostaglandin F2 $\alpha$  receptor protein levels suggesting that PTGFRN does not modulate prostaglandin signalling in glioblastoma cells by reducing the amount of prostaglandin F2 $\alpha$  receptors. This study also showed that overexpression of PTGFRN has a role in promoting GBM tumour formation and development via PI3K/AKT signalling, and knockdown of PTGFRN resulted in a significant decrease in PI3K p110 $\beta$  and phosphorylated AKT expression followed by an ultimate reduction in GBM0821 and GBM0913 cell proliferation (Aguila *et al.*, 2019). Furthermore, inhibition of PTGFRN reduces nuclear PI3K p110 $\beta$ , resulting in reduced DNA damage detection and repair suggesting PTGFRN as a

potential therapeutic target for GBM (Aguila *et al.*, 2019). Accordingly, the highest PTGFRN expression was observed in *AKT1<sup>E17K</sup>/TRAF7* mutated meningioma confirmed via WB. This suggests that PTGFRN overexpression may contribute to the development of meningioma tumours via p-AKT signalling, similar to prior GBM investigations (Aguila *et al.*, 2019).

PTGFRN expression in meningioma tumorigenesis is not reported yet. Due to inconsistency in IHC results, we should not dismiss this candidate, more benign meningioma mutational tumour samples should be investigated for PTGFRN expression as other cancer studies showed PTGFRN as a marker for metastasis and a potential therapeutic target.

**Thrombospondin, type I, domain containing 4 (THSD4)** is cell surface glycoprotein, a member of the ADAMTS (A disintegrin and metalloproteinase with thrombospondin motifs) superfamily, and known as ADAMTSL6 (Stenina *et al.*, 2007; Iruela-Arispe *et al.*, 1993; O'shea *et al.*, 1998). The current study observed a significant overexpression of THSD4 in *NF2<sup>-/-</sup>* mutated benign meningioma samples, an increased tendency in both *KLF4<sup>K409Q</sup>* and *AKT1<sup>E17K</sup>/TRAF7* mutant meningioma compared to NMT compared to NMT in WB analysis and IHC staining (Fig-38 A and A1; Fig-39 c and c1). These findings were in agreement with mass-spectrometry data analysis (Table 16) and suggested THSD4 as a candidate for benign meningioma regardless of mutations.

THSD4 is mostly found in the extracellular matrix and plays a role in the production of elastic fibres and microfibrils (fibrillin-1) by regulating ECM-associated TGF- $\beta$  signal transduction pathways (Tsutsui *et al.*, 2010; Hubmacher and Apte, 2015). Mutations in THSD4 cause impairment in fibrillin-1 matrix assembly formation and haploinsufficiency and THSD4 knockout mice showed progressive dilation of the thoracic aorta suggesting THSD4 involve in the pathogenesis of thoracic aortic aneurysm and dissection (TAAD) (Elbitar *et al.*, 2021).

Aberrant expression of THSD4 was reported in several cancer types including oesophageal carcinoma, glioma, hepatocellular carcinoma, prostate cancer, breast cancer, lung, and colorectal cancer (Su *et al.*, 2016; Ma *et al.*, 2015; Theret *et al.*, 2021; Cohen *et al.*, 2014; Wu *et al.*, 2020; Zhang *et al.*, 2021; Liu *et al.*, 2021). THSD4 function is critical in cancer, however, a clear mechanism is not known yet (Su *et al.*, 2016; Cohen *et al.*, 2014; Zhang *et al.*, 2021). Overexpression of THSD4 is reported in the MCF7 breast cancer cell line and its expression is directly mediated by tumour suppressor protein GATA3 (Cohen *et al.*, 2014). In human mammary epithelial cells (HMEC) overexpression of GATA3 led to downregulation of THSD4 indicating that expression of THSD4 inversely correlated to GATA3 expression. These

findings suggesting the GATA3-mediated transition of normal cells into breast cancer may be accompanied by THSD4 deregulation (Cohen *et al.*, 2014). Overexpression of THSD4 was observed in hepatocellular carcinoma tissue compared to normal adjacent tissue and knockdown of THSD4 suppresses hepatocellular cancer cell progression (Honda *et al.*, 2017; Theret *et al.*, 2021). Another study reported single nucleotide polymorphisms of the *THSD4* gene may involve in hepatocellular cancer progression (Kim *et al.*, 2008).

In contrast, hypermethylation of THSD4 was reported in glioblastoma multiforme and hypermethylation of THSD4 was correlated with poor survival of glioblastoma patients (Ma *et al.*, 2015). A tissue microarray analysis showed downregulation of THSD4 in oesophageal cancer tissue compared to adjacent normal tissue and did not show the role of the downregulated expression of THSD4 in oesophageal cancer tumorigenesis, which suggested further investigation of this candidate (Su *et al.*, 2016). Down-regulation of THSD4 expression at mRNA level was also reported in prostate cancer tissue compared to normal adjacent tissue and their functional annotation analysis suggested THSD4 may involve in prostate cancer by regulating BMP5-BAMBI mediated TGF-beta signalling pathway (Wu *et al.*, 2020). Reduced expression of THSD4 at mRNA level was also reported in colorectal cancer tissue compared to the normal intestinal mucosa (Liu *et al.*, 2021). This study demonstrated downregulation of THSD4 transcriptionally activates ZNF37A (Zinc finger protein 37A) expression resulting in promoting TGF- $\beta$  signalling and activating cancer-associated fibroblasts (CAFs) in metastatic CRC (Liu *et al.*, 2021). Zhang *et al.*, (2021) demonstrated small cell lung cancer (NSCLC) patients with low expression of THSD4 had significantly longer progression-free survival (PFS) than those with high expression.

One study has reported, tumours that overexpress thrombospondin-1 grow slower, have less angiogenesis, and have fewer metastases (Isenberg *et al.*, 2005). Accordingly, the current study also observed overexpression of THSD4 in benign meningioma compared to NMT confirmed via WB and IHC both, these data imply that THSD4 could be a promising candidate for benign meningiomas.

**Lin-7C** is a PDZ domain-containing cell surface protein also referred to as vertebrate lin-7 homolog 3 (VELI-3) or mammalian lin-seven protein 3 (MALS-3), an integral part of the mature cadherin-based cellular junction involved in regulating protein-protein interactions by binding with COOH-terminal tails of other cellular junctional proteins (Perego *et al.*, 2002;

Onda *et al.*, 2007). Perego *et al.*, (2002) demonstrated that the PDZ domain-containing Lin-7C binds directly with a specific target sequence of  $\beta$ -catenin and creates a cadherin- $\beta$ -catenin complex, resulting in maintaining cadherin-regulated cell adhesion. This study also reported the binding of Lin-7C with  $\beta$ -catenin-containing cell-cell contacts is a slow process and the accumulation of Lin-7C was used to indicate the level of cadherin-mediated adhesion maturation (Perego *et al.*, 2002). While an invasive glioma T98G cell line showed a lack of Lin-7C accumulation in their cellular junction indicating an immature junction of migration and invasiveness of the glioma cell lines (Perego *et al.*, 2002). A proteomic analysis identified Lin-7C as significantly downregulated in oral squamous cell carcinoma (OSCC) tissue compared to normal oral tissues which were confirmed at mRNA and protein levels (Onda *et al.*, 2007). The study also demonstrated hypermethylation of Lin-7C strongly correlated with the development of OSCC lymph node metastasis (Onda *et al.*, 2007). Forced overexpression of Lin-7C in the OSCC cell line had no effect on cell proliferation but significantly reduced motility and invasiveness by increasing the expression of  $\beta$ -catenin (Onda *et al.*, 2007). Whereas  $\beta$ -catenin is involved in regulating cell adhesion by stimulating the Wnt signalling pathway, the expression of Lin-7C is positively correlated with the expression of  $\beta$ -catenin (Polakis, 2000; Bánkfalvi *et al.*, 2002; Onda *et al.*, 2007). Furthermore, an *in vivo* experiment revealed that blocking of Lin-7C in OSCC causes induction of tumour cell invasion but had no effect on the development of the primary tumour (Onda *et al.*, 2007). These findings suggest Lin-7C is a marker for OSCC metastasis and its early identification and targeting can stop OSCC metastasis (Onda *et al.*, 2007). Another study has shown that mirtazapine (a drug that inhibits metastasis) treated metastatic human squamous cell carcinomas (hSCCs) cell line and human melanoma-derived cell line showed reduced cellular migration or invasion by restoring the activity of Lin-7C/  $\beta$ -catenin pathway without affecting the cell proliferation (Uzawa *et al.*, 2014).

In this current proteomic study, Lin-7C was identified as commonly upregulated in benign meningioma subtypes regardless of mutational status compared to NMT (Table 16). Overexpression of Lin-7C in *NF2*<sup>-/-</sup>, *AKT1*<sup>E17K</sup>/*TRAF7*, and *KLF4*<sup>K409Q</sup>/*TRAF7* mutant meningioma compared to NMT confirmed via Simple wes and IHC (Fig-38 B and B1; Fig-39 a and a1), which is in line agreement with the mass-spectrometry analysis. These findings suggest overexpression of Lin-7C can be used as a marker for benign meningioma and further investigations by comparing its expression with high-grade meningioma should confirm this.

### 5.1.5 Functional annotation enrichment analysis of DEPs (differential expression of proteins) using DAVID

Functional annotation enrichment analysis of DEPs (differential expression of proteins) revealed subtle differences among three meningioma subtypes. At the cellular component level, GO showed that *AKT1<sup>E17K</sup>/TRAF7* mutant meningioma-specific proteins (COX6B1, NDUFA5, NDUFB7, NDUFB1, NDUFB8 and ATPK) were highly enriched in the mitochondrion and mitochondrial inner membrane and extracellular exosome (Fig-17). In contrast, an opposite trend was observed where *NF2<sup>-/-</sup>* meningioma subtype-specific downregulated proteins were enriched within mitochondrion and extracellular exosome (Fig-25).

In terms of *KLF4<sup>K409Q</sup>/TRAF7* mutant meningioma-specific upregulated proteins were highly enriched in focal adhesion cellular component GO term (Fig-32). Anion exchange protein 2, calcium-binding protein 22, CD44 antigen, E-cadherin-1, and endoglin proteins are related to focal adhesion. (Fig-32). Focal adhesions are protein complexes comprising integrin that create a bridge between intracellular actin filaments and the extracellular matrix or substrate (Abercrombie and Dunn, 1975). There are several identified physiological processes including initiation, clustering, growth, maturation, and disassembly that can be used to characterise the creation and function of focal adhesions (Lloyd, 1980). Focal adhesions act as anchors that prevent membrane tension and facilitate projection at the leading edge and allow cell migration and spreading (Morgan *et al.*, 2007). A time-lapse video from a study that described the progression of meningioma cells through the formation of focal adhesions revealed that the *TRAF7* mutation in the HMC enhanced changes in the actin cytoskeleton by causing contraction, retraction, and protrusions at the leading and rear edges with an increased number of focal adhesions (Najm *et al.*, 2021). These findings strongly imply that *KLF4<sup>K409Q</sup>/TRAF7* mutations may involve in meningioma tumorigenesis by affecting the actin cytoskeleton.

Moreover, GO term biological process analysis also distinguished the meningioma mutant subtypes, where it showed *AKT1<sup>E17K</sup>/TRAF7* mutant meningioma subtype-specific proteins were mainly associated with mitochondrial electron transport, chloride transmembrane transport (discussed for CLIC3) (Fig-17), whereas *KLF4<sup>K409Q</sup>* meningiomas subtype-specific upregulated proteins were highly enriched in extracellular matrix disassembly function (discussed for endoglin) (Fig-32).

At the molecular function level, GO showed that *AKT1<sup>E17K</sup>/TRAF7* mutant meningioma-specific upregulated proteins were associated with voltage-gated ion channel activity via CLIC3 already discussed, NADH dehydrogenase ubiquinone, cadherin binding involved in

cell-cell adhesion terms (Fig-17). In contrast, we were unable to detect any protein enrichment at the molecular function GO term for *KLF4*<sup>K409Q</sup>/*TRAF7* and *NF2*<sup>-/-</sup> mutated meningioma group due to the very small number of unique upregulated proteins were identified in these groups.

### 5.1.6 Pathway analysis of benign meningioma subtype via IPA

Of the 162, *AKT1*<sup>E17K</sup>/*TRAF7* mutant-specific upregulated proteins under pathway analysis by KEGG, 24 proteins were involved in metabolic pathways and six proteins were linked to oxidative phosphorylation (Fig-18). In addition to this, IPA pathway analysis showed oxidative phosphorylation pathway commonly significantly upregulated in *AKT1*<sup>E17K</sup>/*TRAF7* mutant meningioma compared to other meningioma mutant groups and normal meninges (Fig-19).

These metabolic alterations are supported by previous studies (Robay and Hay, 2009) where it has been reported that constitutive AKT activation increased cellular ATP production by increasing both glycolytic and oxidative metabolism. Additionally, AKT accelerated oxidative phosphorylation by increasing metabolic incorporation of glycolysis and oxidative phosphorylation via mitochondrial hexokinase (Robay and Hay, 2009). AKT increased glucose uptake by increasing the expression of glucose transporters (GLUT1, GLUT2, and GLT4) and increasing their translocation to the plasma membrane (Robay and Hay, 2009). Hyperactive AKT activates mTORC1, which stimulates HIF1 (hypoxia-inducible factor 1) accumulation in normoxic conditions and increases the abundance of GLUT1, hexokinase, and lactate dehydrogenase (Gottlob *et al.*, 2001), subsequently, increasing glucose transport and metabolism. Additionally, AKT increases cellular ATP levels to maintain the AMP-activated protein kinase that is required for full mTORC1 activation. MTOR is an important downstream regulator of AKT, and is responsible for AKT-mediated cell growth, proliferation and susceptibility to oncogenic transformation (Robay and Hay, 2009) (Fig-51). Our proteome profile suggests, for the first time, the molecular evidence for this metabolic pathway, which is specific to the *AKT1*<sup>E17K</sup>/*TRAF7* mutant meningioma subtype.

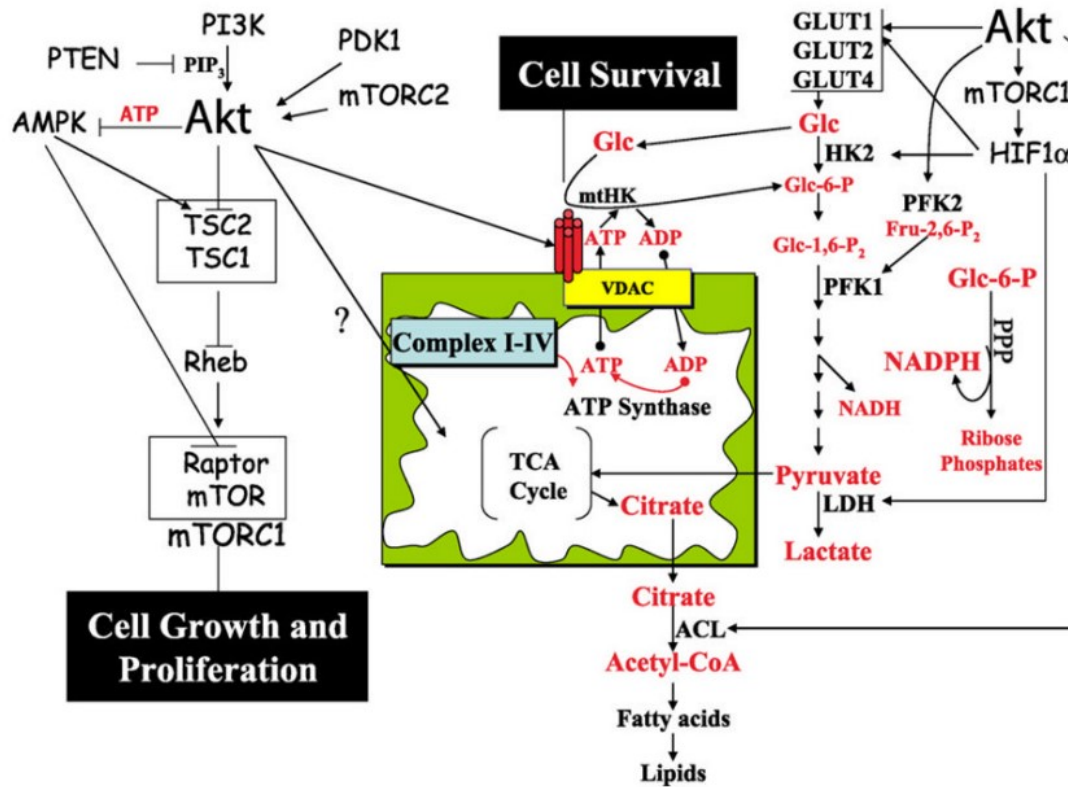


**Figure 51: AKT mediated cellular energy metabolism, cell growth and cell proliferation.** AKT regulates TCA cycle flux and increases cellular ATP levels to maintain low AMPK activity which is the requirement for activation of mTORC1, a downstream regulator of AKT which stimulates AKT-mediated cell growth and proliferation. The figure is taken from (Robay and Hay, 2009).

Oxidative phosphorylation pathway-associated proteins (COX6B1, NDUFA5, NDUFB7, NDUFB1, NDUFB8 and ATPK) were upregulated in *AKT1<sup>E17K</sup>/TRAF7* mutant meningioma (Fig-20). In the normal cell, the presence of oxygen significantly inhibits glycolysis (Pasteur, 1861). According to Otto Warburg, cancer cells, even those with adequate oxygenation, consume a lot of glucose and generate a lot of lactates, resulting in glycolysis being hyperactive (Warburg *et al.*, 1927). Oxidative phosphorylation (OXPHOS) is assumed to be consistently downregulated in cancer, as evidenced by the observation that cancer cells exhibit higher glycolysis compared to healthy cells (Ashton *et al.*, 2018). In contrast, there are several cancer studies including leukaemias, lymphomas, pancreatic ductal adenocarcinomas, subtype melanoma, and endometrial carcinoma reported upregulation of OXPHOS with active glycolysis (Weinberg *et al.*, 2015; Rodriguez-Enriquez *et al.*, 2007; Ashton *et al.*, 2018), which is also supporting our KEGG and IPA pathway analysis of *AKT1<sup>E17K</sup>/TRAF7* mutated meningioma (Fig-18 and Fig-19). Another proteomic study from our group reported the

upregulation of oxidative phosphorylation in high-grade meningioma via GO analysis (Dunn *et al.*, 2020). Ashton *et al.*, (2018) described the mechanism of how cancer cell exhibits upregulation of OXPHOS even with active anaerobic glycolysis. A possible mechanism would be oxidative metabolic processes that produce ATP by transporting electrons via a series of mitochondrial inner transmembrane protein complexes, called electron transport chain (ETC) where, NADH, FADH<sub>2</sub>, and succinate serves as electron donor, when electrons pass through the ETC protein complex protons are pushed out of the mitochondrial matrix into the intermembrane space, resulting in ATP synthesis. This suggests that while OXPHOS is active, there is a strong proton gradient across the membrane, where oxygen serves as a final electron acceptor (Ashton *et al.*, 2018). Therefore, OXPHOS inhibitors (non-clinically used metformin, atovaquone, and arsenic trioxide) may be employed to treat hypoxic tumours by targeting upregulated OXPHOS proteins (Ashton *et al.*, 2018).

To summarise, MS data analysis and literature from other cancer studies suggest targeting and validating the oxidative phosphorylation pathway for the *AKT1<sup>E17K</sup>/TRAF7* mutant meningioma subtype may reveal biomarkers or therapeutic targets for this meningioma subtypes..

IPA pathway analysis showed upregulation of RhoGDI signalling pathway in *KLF4<sup>K409Q</sup>* mutant meningioma compared to *AKT1<sup>E17K</sup>/TRAF7* mutant and NMT and down-regulation compared to *NF2<sup>-/-</sup>* mutant group (Fig-34).

Rho GDP-Dissociation Inhibitors pathway-associated proteins (RhoGDI1, RhoGDI2) are involved in inhibiting Rho small GTPase family proteins activity (Harding *et al.*, 2010). Small Rho GTPases family is comprised of large Ras-related proteins including RhoA, Rac1, and CDC42 (Lelias *et al.*, 1993; Harding *et al.*, 2010). Small Rho GTPase family proteins are involved in stimulating downstream signal transducers including P-21 Activated Kinase 1 (PAK1), PKC $\alpha$ , etc which are involved in regulating several cellular processes such as cell division, phenotype, migration, vesicular trafficking, and gene expression (Lu *et al.*, 2009; Oxford and Theodorescu, 2003; Karlsson *et al.*, 2009; Vega *et al.*, 2008; Harding *et al.*, 2010). RhoGDI controls the location and activity of small Rho GTPase family proteins and maintains cellular physiological processes. Small Rho GTPase proteins downstream signalling are activated when signal transducers switch from an inactive (GDP bound state) to an active (GTP bound state) (Harding *et al.*, 2010). GTPase activator proteins (GAPs) and guanine nucleotide exchange factors (GEFs) regulate the conversion of GDP to GTP and when GAPs and GEFs



interact with GTP, active Rho proteins bind to several downstream effector molecules (Vega *et al.*, 2008; Harding *et al.*, 2010). RhoGDIs are thought to inhibit Rho proteins in several different ways. RhoGDIs suppress the function of the GTPase by inhibiting the catalytic activity of Rho, as well as the release of GDP from the hydrolysed Rho protein. In addition to this, Rho GDIs act as shuttle where RhoGDIs directly bind prenylated Rho proteins, and shift them from the membrane to the cytoplasm, resulting in inhibiting the interactions of RhoGEFs and RhoGAPs with Rho GTPase proteins and the binding of other Rho activity regulators (Johnson *et al.*, 2009; Lin *et al.*, 2003; Harding *et al.*, 2010). Theodorescu *et al.*, (2004) showed downregulation of RhoGDIs enhanced bladder cancer cell metastasis and overexpression of RhoGDI did not affect bladder cancer cell (T24T) growth in a bladder organotypic invasion assay but reduced cell motility and invasion. Schunke *et al.*, (2007) showed upregulation of RhoGDI reduced MDA-MB-231 breast cancer cell migration. Regarding the current study upregulation of RhoGDI was observed in grade-I *KLF4<sup>K409Q</sup>/TRAF7* mutant meningiomas which are not aggressive.

Najm *et al.*, (2021) demonstrated that TRAF7 mutation in human meningeal cells (HMCs) promoted changes in the actin filaments and anchorage-independent meningioma development by activating CDC42 and RAS/ MAPK signalling. Following the incorporation of KLF4 mutation into HMCs, the authors demonstrated opposite results where small Rho GTPase proteins were suppressed by overexpression of semaphorin, a negative regulator of small GTPases (Najm *et al.*, 2021). Likewise, our IPA pathway analysis showed upregulation of the RhoGDI signalling pathway in *KLF4<sup>K409Q</sup>/TRAF7* mutant meningioma compared to *AKT1<sup>E17K</sup>/TRAF7* and NMT, where downregulation of small Rho GTPase proteins were observed including PAK1, MRAS, RHOA, RHOB, RHOC, RAC1, PRKCa and etc. (Fig-52, supplementary data- S5). On the other hand, only two proteins E-cadherin and CD44 showed upregulation in this pathway. Previous studies reported that Rho small GTPases like Rac1 involve in regulating cell adherence by interacting with the E-cadherin (Lozano *et al.*, 2008; Pujuguet *et al.*, 2003). Liu *et al.*, (2009) demonstrated that the expression of E-cadherin inversely correlated with the expression of RhoA, CDC42, and Rac1 in lung cancer tissue which supports our IPA analysis. However, the role of CD44 in the RhoGDI pathway is not clear. On the other hand, the RhoGDI pathway was downregulated in *KLF4<sup>K409Q</sup>/TRAF7* compared to *NF2<sup>-/-</sup>* mutant meningioma group where only associated upregulated proteins were Rho/Rac guanine nucleotide exchange factor 2 (ARHGEF2) (Fig-52, supplementary data- S5). As mentioned earlier, ARHGEF2 activates Rho GTPases by switching GDP into GTP (Harding *et al.*, 2010). Incontrast, it has been shown in schwannoma cells that NF2 loss leads to

activation of small GTPases RAC1 and CDC42 (Kaempchen *et al.*, 2003). However, we did not identify the expression of small GTPases RAC1 and CDC42 proteins in  $KLF4^{K409Q}/TRAF7$  compared to  $NF2^{-/-}$  mutant meningioma and NMT. To summarise it will be interesting to validate this pathway for  $KLF4^{K409Q}/TRAF7$  group.

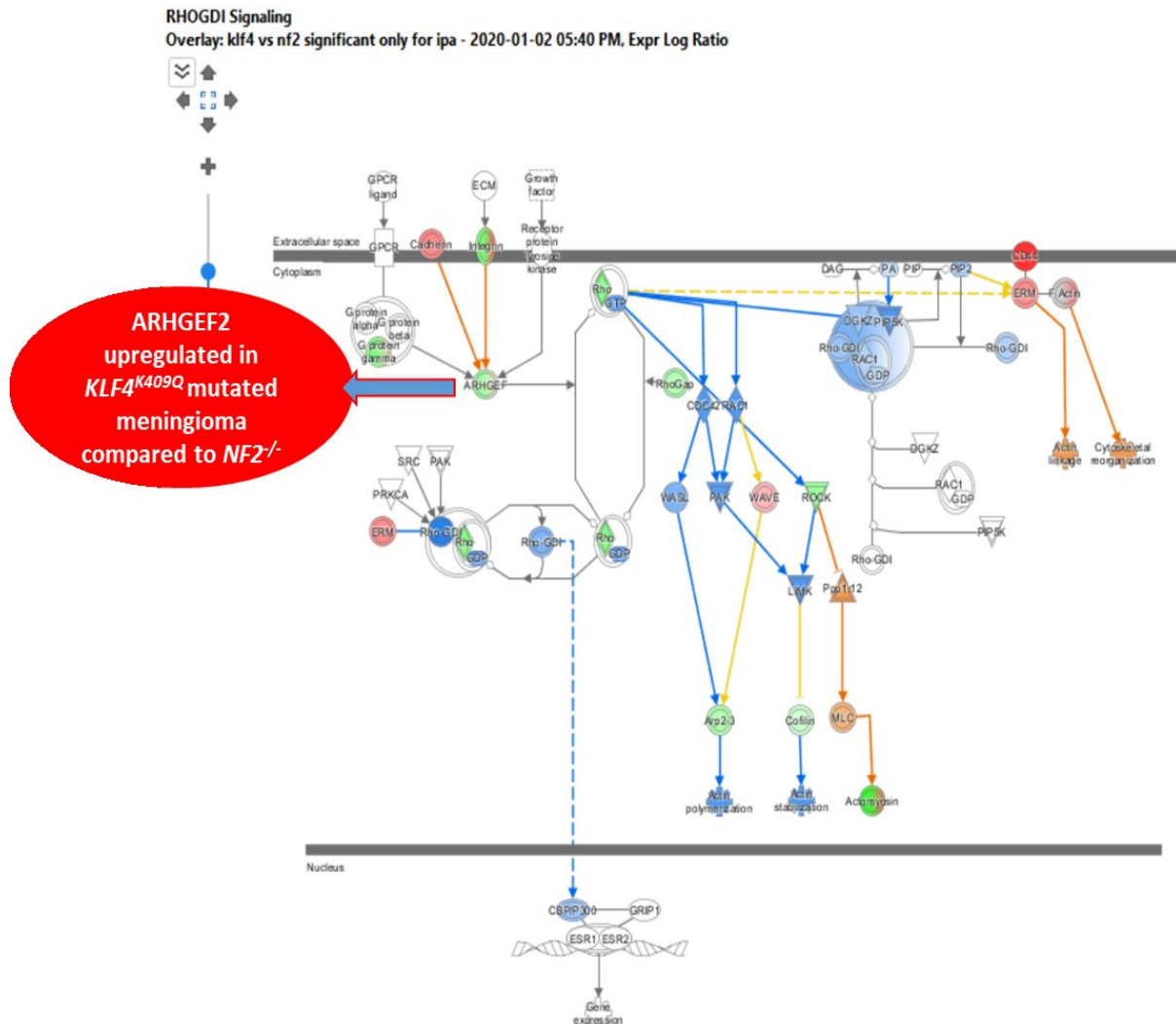


**Figure 52: Illustrating RhoGDI pathway from IPA.** This figure shows ARHGEF2 upregulated in  $KLF4^{K409Q}/TRAF7$  compared to  $NF2^{-/-}$  mutant meningioma group, resulting in down regulation of RhoGDI signalling as ARHGEF2 is an activator of Rho small GTPase family proteins.

On the other hand, in IPA analysis balloon plot, ‘Sirtuin signalling pathway’ showed the highest ranked in  $NF2^{-/-}$  mutant meningioma among the signalling pathways when compared to  $AKT1^{E17K}/TRAF7$  mutant group, also significantly upregulated in  $NF2^{-/-}$  mutant meningioma compared to NMT. There were no significant differences between  $NF2^{-/-}$  and  $KLF4^{K409Q}/TRAF7$  mutant meningioma groups (Fig- 26).

Sirtuins are NAD<sup>+</sup>-dependent histone deacetylases that control vital metabolic pathways and play a key role in a variety of biological processes, including cell survival, cell metabolism, senescence, proliferation, and apoptosis (Carafa *et al.*, 2016). So far, the Sirtuin family comprised of a total of seven members SIRT1 to SIRT7 and their activities and modulators are different (Carafa *et al.*, 2016), but in the current proteomic study only SIRT2 and SIRT3 both identified as significantly down regulated in *NF2*<sup>-/-</sup> and *KLF4*<sup>K409Q</sup>/*TRAF7* mutant meningioma respectively compared to *AKT1*<sup>E17K</sup>/*TRAF7* mutant meningioma in mass-spectrometry data analysis (supplementary data-S4).

SIRT2 contributes to apoptosis by regulating the p53 pathway. SIRT2 is also involved in cell cycle progression by mediating cell cycle checkpoints for G2/M transition (Serrano *et al.*, 2013; Inoue *et al.*, 2007). In addition to this, SIRT2 has revealed that it plays a role in metabolic processes such as adipogenesis (Jing *et al.*, 2007). SIRT2 targeting molecules including histone deacetylases (H4K16ac, H3K56 and H3K18), p300, FOXO1, FOXO3 $\alpha$ , tubulin and decreased expression of SIRT2 was observed in breast, liver, prostate cancer and glioblastoma (Aventaggiato *et al.*, 2021). In contrast, SIRT3 involve in cancer cell progression by deacetylating and activating several mitochondrial proteins, and preventing the production of reactive oxygen species (ROS) in the mitochondria which affect cell growth, survival and differentiation (Jing *et al.*, 2007; Finley *et al.*, 2011). In addition to this, SIRT3 inhibits glycolysis metabolism once pyruvate dehydrogenase is activated and deacetylated, where SIRT3 acts as a tumour suppressor (Jing *et al.*, 2007; Finley *et al.*, 2011). SIRT3 targets PGC-1 $\alpha$ , GDH, IDH2, SOD2, and ACECS2 and decrease expression of SIRT3 observed in breast, gastric, ovarian, lung cancer and medullblastoma (Aventaggiato *et al.*, 2021).

In comparison between *NF2*<sup>-/-</sup> versus *AKT1*<sup>E17K</sup>/*TRAF7* meningioma, a total of 36 proteins were associated with the Sirtuin pathway, where only three proteins including H1.5 linker histone, cluster member, tubulin alpha 1b and lactate dehydrogenase B showed upregulation in *NF2*<sup>-/-</sup> compared to *AKT1*<sup>E17K</sup>/*TRAF7* and rest of the proteins were downregulated (supplementary data- S4). On the other hand, no significant expression of SIRT2 and SIRT3 was observed when *NF2*<sup>-/-</sup> compared to NMT, only consistency was observed in tubulin alpha 1b expression (supplementary data- S4). Both analysis is suggesting the presence of upregulation of tubulin alpha 1b as part of upregulation of the Sirtuin pathway in *NF2*<sup>-/-</sup> mutated meningioma. It has been reported that SIRT2 is involve in  $\alpha$ -tubulin deacetylation which is vital for the regulation of cell division and differentiation (North *et al.*, 2003; Li *et al.*, 2007). However, inconsistency

of protein expression in two comparisons made it difficult to conclude how the Sirtuin pathway is upregulated in *NF2*<sup>-/-</sup> mutated meningioma.

### **5.1.7 Global proteomic data analysis compared with previous proteomic studies of meningioma**

There are few studies using proteomic-based analysis of benign meningiomas, the majority of which compared meningiomas of different grades. Okamoto *et al.*, (2006) identified 24 proteins differentially expressed between grades and, for grade I meningiomas, identified upregulated proteins including calponin-1, activator of 90-kDa Heat shock protein, Serine threonine kinase receptor associated protein and Apolipoprotein A-1. Of this list, Calponin-1 was significantly expressed in our data set with very low expression in meningioma subtypes, with the rest of the proteins not differentially expressed compared to the NMT. Saydam *et al.*, (2010) focused only on Minichromosome maintenance family (MCM2, MCM3, MCM4, MCM6, MEM7) proteins, validated by qRT-PCR, which were suggested as novel diagnostic marker for meningioma. However, in our proteomic data set, we observed no significant changes in the expression of these proteins in meningioma mutant subtypes. Cui *et al.*, (2013) reported differential expression of Galectin-3, Vimentin, Endoplasmic reticulum chaperone protein, Annexin A2, GSTP and 14-3-3 protein in benign meningioma and validated in tissue by WB. However, only Galectin-3 protein was significantly upregulated in *AKT1*<sup>E17K</sup>/*TRAF7* mutant meningioma subtype in our dataset. Bassiri *et al.*, (2017) suggested PDZ and LIM domain protein 2 (PDLIM2) as a novel therapeutic target for *NF2* deficient meningioma by comparing merlin deficient benign meningioma primary cells and foetal human meningeal cell line control (HMC). However, in our tissue dataset, the differential expression between *NF2*<sup>-/-</sup> mutational meningioma vs. NMT showed no significant changes in expression of PDLIM2. This may reflect differences between primary cells and the microenvironment of tissue samples.

Dunn *et al.*, (2018) compared meningiomas of different grades (grade I, II and III) and showed over-expression of Epithelial Growth Factor Receptor (EGFR), Cytoskeleton associated protein 4 (CKAP4), Signal Transducer and Activation of Transcription 1 (STAT1) and Hexo Kinase-2 (HK-2) across all grades compared to NMT and reported over-expression of HK-2 protein is very specific for higher grades (grade II and III) meningiomas. However, we observed no significant changes in the expression of these proteins in meningioma mutant subtypes compared to NMT.

## 5.2 Phospho-peptide proteomic data analysis

To date, this is the first study performed mass-spectrometry incorporated with isobaric tandem mass tags (TMTs) and identified a total of 6584 phosphorylated sites of each phosphopeptide and their corresponding total of 2388 phosphoproteins across eight tissue samples including six meningiomas (*AKT1<sup>E17K</sup>/TRAF7* mutant subtypes n=3 and *NF2<sup>-/-</sup>* mutant subtypes n=3) with two healthy normal meningeal tissues (NMT) in order to investigate post-translational regulatory function in meningioma tumorigenesis (Fig-42).

Followed by the phosphopeptide data was used to predict kinase activity in the meningioma tumour samples as this would give insight into which signaling pathways have been active in meningioma in comparison to normal tissues. Identifying kinase activity would also help to detect therapeutic targets for meningioma subtypes. We performed motif analysis and used the KinswingR package to predict kinase activity. KinswingR uses a probabilistic approach to predict the likely kinases that phosphorylate an identified phosphorylated site using known protein kinase substrate motifs. KinswingR is able to quantify the activity of each kinase by giving it a swing score based on the p-value and Log2FC of each phosphosite from a paired comparison (Engholm-Keller *et al.*, 2019). Indicating KinswingR predicts kinases by considering each identified phosphosites which is unbiased. While other kinase predictor such as kinase enrichment analysis 2 (KEA2) analysis predicts kinases based on overrepresented substrate/sequences present in the phosphopeptide data (Wiredja *et al.*, 2017). KinswingR package predicted a total of 33 upregulated kinase from three sets of comparison (*AKT1<sup>E17K</sup>/TRAF7* vs. NMT, *NF2<sup>-/-</sup>* vs. NMT and *NF2<sup>-/-</sup>* vs. *AKT1<sup>E17K</sup>/TRAF7*) (Fig-45). Due to the lack of tissue lysates availability, out of 33 kinases, only eight predicted upregulated kinases were taken for validation via WB and the findings will be discussed in the following sections (section 5.2.1 and 5.2.2)

### 5.2.1 *AKT1<sup>E17K</sup>/TRAF7* specific kinase candidates

To date, this study is the first to predict that CAMK2A is significantly upregulated in *AKT1<sup>E17K</sup>/TRAF7* mutated meningioma compared to *NF2<sup>-/-</sup>* mutated meningioma and NMT via KinSwingR analysis (Fig-45 A). CAMK2 has two distinct domains including calcium and calmodulin domains that are required for CAMK2 kinase activation (Brzozowski *et al.*, 2019). When calcium concentration increases inside the cell and at least four calcium molecules are bound to calmodulin, calmodulin is able to bind CAMK2, followed by stimulation of

phosphorylation at Thr286 for the CAMK2A isoform or at Thr287 for the  $\beta$ ,  $\gamma$ , and  $\delta$  (Fong *et al.*, 1989; Brzozowski *et al.*, 2019). Subsequently, this phosphorylation promotes and maintains CaMK2 activation (Meyer *et al.*, 1992; Skelding and Rostas., 2009; Coultrap *et al.*, 2010). Phosphorylation of CAMK2A at T286 induces breast cancer cell growth, migration, and invasion by stimulating downstream targets such as FAK, STAT5, and AKT (Chi *et al.*, 2016). In addition to this, Zhang *et al.*, (2018) reported CAMK2A as an important prognostic biomarker for Glioblastoma and showed that GBM patients with increased CAMK2 mRNA expression may have a poor prognosis. Further increased phosphorylation of CAMK2A at Thr286 was reported in gastric cancer tissues with metastasis and in high-grade metastatic gastric cancer cell lines (Liu *et al.*, 2014). This study also showed that the increased expression of CAMK2A resulted in a significant increase in NF- $\kappa$ B and Akt-mediated matrix metalloproteinase-9 (MMP-9) production. Thus suggesting CAMK2A-driven migration and invasiveness in gastric cancer cells may be dependent on MMP9 synthesis mediated by NF- $\kappa$ B and Akt (Liu *et al.*, 2014).

As Thr286 is an active site for CAMK2A, this site was considered for validation via WB. However, WB quantitative analysis showed increased activity of p-CAMK2A-Thr286 in NMT which is not in line with KinSwingR kinase prediction analysis (Fig-46 A). There was a clear discrepancy between results obtained from KinSwing and WB analysis of CAMK2A. WB results show CAMK2A is activated in all tumour samples and even in normal meninges samples. One explanation for this is that other kinases might also be phosphorylating the identified phosphosites other than CAMK2A. For example, KinSwingR identified several potential kinases that phosphorylate the substrate Caveolae-associated protein 3 including: BRSK1 (49%) CAMK2A (100%) CAMK4 (100%) Chk1 (99%) Chk2 (86%) CK1E (70%) MKK4 (3%) PKN1 (100%) AMPKA1 (34%) AMPKA2 (100%) PRKD2 (100%) and LKB1 (100%) (Supplementary data- S8). This means there could be shared substrates/proteins phosphorylated by multiple kinases. Future experiments are needed to validate all the kinases which share similar substrates. It is unrealistic to validate all kinases with similar substrates for CAM2A establishment in meningioma with limited tissue lysates.

**CHEK1** is another kinase candidate that showed significant upregulation in *AKT1<sup>E17K</sup>/TRAF7* mutated meningioma compared to NMT via KinSwingR analysis (Fig-45 A). Likewise, Puc *et al.*, (2005) demonstrated that PTEN loss and subsequent AKT activation degrade CHEK1 through phosphorylation, ubiquitination, and reduced nuclear localization, promoting genomic instability in tumour cells. Overexpression of CHEK1 has been reported in several cancer,

including breast, colon, liver, gastric and nasopharyngeal carcinoma (Hong *et al.*, 2012; Cho *et al.*, 2005; Madoz-Gurpide *et al.*, 2007; Verlinden *et al.*, 2007; Yao *et al.*, 2010; Sriuranpong *et al.*, 2004; Zhang *et al.*, 2014). It was also observed that overexpression of CHEK1 is positively correlated with tumour grade and recurrence (Hong *et al.*, 2012; Yao *et al.*, 2010; Lundgren *et al.*, 2008). It has also been reported that CHEK1 may possibly have a role in therapeutic resistance. Cancer cells, such as cancer stem cells from brain glioblastoma, prostate, and lung NSCLC, became resistant to chemotherapy and radiotherapy, including HDAC inhibitors, due to increased activation of CHEK1 (Bao *et al.*, 2006; Lee *et al.*, 2011; Bartucci *et al.*, 2012; Wang *et al.*, 2012; Zhang *et al.*, 2014). In addition to this, high expression of Ser-345-phosphorylated CHEK1 protein was linked to increased radio-resistance reported in the metastatic brain (Seol *et al.*, 2011; Zhang *et al.*, 2014). In this current study as predicted by KinSwingR kinase analysis, neither the expression of CHEK1-S345 nor total CHEK1 were found at 56kDa via WB analysis despite using two distinct antibodies, none of them were able to produce a signal for CHEK1 kinase (Fig-46 B) unlike as reported by King *et al.*, (2004). Looking at the WB, the CHEK1 signal is weak, this could be an antibody issue or a lack of CHEK1 expression across samples. Due to the very weak band, it was hard to draw conclusions from this. In addition to this, lack of tissue lysates, further validation was not attempted for this kinase activity in meningioma.

A comparison between *AKT1<sup>E17K</sup>/TRAF7* mutated meningioma and NMT also showed another checkpoint kinase (CHEK2) upregulation in *AKT1<sup>E17K</sup>/TRAF7* mutated meningioma via KinSwingR analysis (Fig-45 A). Overexpression of CHEK2-T68 has been detected in a variety of malignancies including breast cancer and pancreatic cancer (Bahassi *et al.*, 2007; Gorgoulis *et al.*, 2005; Zoppoli *et al.*, 2012). Yang *et al.*, 2012 reported numerous alternative variants of the CHEK2 gene without kinase domain in meningioma with NF2 mutation. This study showed that an alternative splicing and deletion of the CHEK2 cause chromosomal instability in the NF2 gene. Thus, alternative splicing of CHEK2 and NF2 genes, as well as frequent co-deletion, leads to genomic instability and progresses to aggressive meningiomas (Yang *et al.*, 2012). However, in this study, KinSwingR kinase analysis is predicated as an upregulated kinase in benign *AKT1<sup>E17K</sup>/TRAF7* mutated meningioma. However WB analysis contradicts KinSwingR kinase prediction, CHEK2-T68 activity was observed in two samples of meningioma with *NF2<sup>-/-</sup>* mutation, while there was no signal in samples with *AKT1<sup>E17K</sup>/TRAF7* mutation and NMT, (Fig-46 C and C1). As mentioned in the result section one possible reason could be tumour variability because the two samples (MN017 and MN257) of *NF2<sup>-/-</sup>* mutated meningioma

showed the expression of CHEK2-Thr68 at WB were not included in the phosphopeptide proteomics experiments (samples number for phosphopeptide proteomics is MN325, MN310, and MN164). These results suggest tumour variability affected KinswingR kinase prediction as mentioned previously for CHEK1, only a very few numbers of samples were considered for this analysis.

In contrast, interestingly, an increased expression of total CHEK2 was observed in *AKT1<sup>E17K</sup>/TRAF7* mutated meningioma samples compared to the *NF2<sup>-/-</sup>* mutated meningioma and NMT when the relative intensity of total CHEK2 was normalised at GAPDH only (Fig-46 C and C2) though due to the small number of samples could not reach significance. In addition to this, expression of total CHEK2 was not seen in all tumour samples as expected (Fig-46 C). However, due to time limitations, it was not possible to test more samples for this kinase activity confirmation via WB, as well as *AKT1<sup>E17K</sup>/TRAF7* mutated samples were very rare to acquire.

Final kinase candidate KinswingR kinase analysis predicted PRKCA in *AKT1<sup>E17K</sup>/TRAF7* mutant meningioma compared to normal meninges (Fig-45 A). PRKCA activity is controlled by and functionally interacts with a number of proto-oncogenes in order to carry out these biological functions such as cell proliferation, differentiation, and growth. Therefore it's not unexpected that dysregulation of PRKCA is linked to a variety of malignancies (Michie and Nakagawa, 2005). Upregulation of PRKCA in human MCF-7 breast cancer cells and malignant U87 glioma cells has been demonstrated to increase their proliferation potential (Mandil *et al.*, 2001; Ways *et al.*, 1995). The increase in proliferative ability found in cells overexpressing PRKCA is likely because activated PRKCA has been demonstrated to target downstream proteins directly, such as phosphorylates Raf-1 kinase, causing the extracellular signal-regulated kinase-mitogen-activated protein kinase (ERK-MAPK) cascade to be activated, and increasing cellular proliferation in a variety of cell types (Kolch *et al.*, 1993; Schönwasser *et al.*, 1998). In addition to this, PRKCA has been linked to cell cycle progression. Interestingly, catalytically active PRKCA triggers cell cycle development by increasing cyclin D1 production via activating the AP-1 region of the cyclin D1 promoters (Soh and Weinstein, 2003). In glioma cells, activation of PRKCA increases cell cycle progression (Besson and Yong, 2000). Parekh *et al.*, (2000) and Newton, (2001) reported three phosphorylation sites for PRKCA including the activation loop (Thr-497), which acts as a trans-phosphorylation site that gives a binding site for cofactors to be activated (Cazaubon *et al.*, 1994), turn motif (Thr-638) involved in PRKCA catalytic activity (Bornancin and Parker, 1996), and C terminal (Ser-657)



in the catalytic domain is crucial for PRKCA membrane stabilization and maturation (Gysin and Imber, 1996; Bornancin and Parker, 1997).

To date, this study is the first to report PRKCA activity in meningioma. However, WB validation analysis showed increased activity of PRKCA in meningioma regardless of mutation compared to NMT (Fig-46 D and D1). Where the significant activity of PRKCA-Ser-657 was observed in *NF2*<sup>-/-</sup> mutant meningioma compared to *AKT1*<sup>E17K</sup>/*TRAF7* mutated meningioma and NMT (Fig-46 D and D1) which is not in agreement with KinswingR kinase prediction. However, only one of the five samples of *NF2*<sup>-/-</sup> mutant meningioma that was analysed on the blot displayed a very large and intense band for PRKCA-Ser-657, whereas the other two samples displayed a very faint band at 75 kDa. While this PRKCA-Ser-657 kinase was substantially expressed in almost all samples of *AKT1*<sup>E17K</sup>/*TRAF7* mutant meningioma, it was either completely absent or very mild in NMT (Fig-46 D and D1). Due to the lack of tissue lysates, it was not possible to repeat WB analysis for PRKCA-Ser-657 activity confirmation. It would be worthwhile to do so in the future to determine whether PRKCA-Ser-657 is a candidate for *AKT1*<sup>E17K</sup>/*TRAF7* mutant meningioma by analysing the PRKCA-Ser-657 activity in an independent cohort.

In contrast, PRKCA-Thr-638 was confirmed by WB, and quantitative analysis revealed significant expression in *AKT1*<sup>E17K</sup>/*TRAF7* compared to *NF2*<sup>-/-</sup> mutated meningioma and NMT, which is consistent with the KinswingR kinase prediction (Fig-46 D and D1). Although both meningioma subtypes showed elevated expression of PRKCA-Thr-497, it was not significantly higher than NMT (Fig-46 D and D1).

WB quantitative analysis suggests PRKCA-Ser-657 phosphorylation is more prevalent in *NF2*<sup>-/-</sup> mutated meningioma while PRKCA-Thr-638 is more active in *AKT1*<sup>E17K</sup>/*TRAF7* mutant meningiomas. These findings collectively imply that PRKCA kinase is a viable target candidate for benign meningioma. In addition to this, the presence of an active form of PRKCA is also confirmed via IHC across all meningioma subtypes which is in line with WB analysis (Fig-48 and Fig-46 D and D1). However, additional research is required to confirm this.

### **5.2.2 *NF2*<sup>-/-</sup> specific kinase candidates**

The current study predicted significant upregulation of EGFR in *NF2*<sup>-/-</sup> mutated meningioma compared to *AKT1*<sup>E17K</sup>/*TRAF7* meningioma mutant (Fig-45 C). EGFR forms homodimers and heterodimers with other ErbB receptors in response to ligand (EGF and TGF- $\alpha$ ) interaction, resulting in stimulation of the receptor's protein tyrosine kinase activity and resulting in trans-

autophosphorylation of certain tyrosine residues within the cytoplasmic domain (Böni-Schnetzler and Pilch, 1987; Downward *et al.*, 1984; Margolis *et al.*, 1989). As mentioned previously in the results section EGFR consists of six autophosphorylation sites including Y-992, Y-1045, Y-1068, Y-1086, Y-1148, and Y-1173. Upon phosphorylation, these sites act as binding regions for intracellular signalling proteins and permit communication of external stimulus and certain internal signal transduction pathways (Shoelson, 1997). For example, EGFR phosphorylation at Y-1068 generates a docking site for Grb2, resulting in the stimulation of the MAPK/ERK signalling cascade, as well as a binding site for Gab1, causing activation of AKT by binding to the p85 subunit of phosphatidylinositol 3-kinase (PI 3-kinase) (Batzler *et al.*, 1994; Rojas and Lin, 1996; Rodrigues *et al.*, 2000). EGFR phosphorylation at Y-1173 promotes MAPK/ERK signaling activity by generating a binding site for the Shc adaptor protein (Sakaguchi *et al.*, 1998).

Several previous studies have already reported overexpression of EGFR in meningioma (Andersson *et al.*, 2004; Wickremesekera *et al.*, 2010; Caltabiano *et al.*, 2013; Baxter *et al.*, 2014). In addition to this, activation and overexpression of EGFR was also reported in merlin negative vestibular schwannomas (VS), as well as overexpression of the downstream signalling protein ERK1/2 (Ammoun *et al.*, 2010).

An increased expression of p-EGFR-Y1173 was observed in *NF2*<sup>-/-</sup> mutated meningioma compared to *AKT1*<sup>E17K</sup>/*TRAF7* mutant meningioma and NMT which is in line with KinswingR prediction but this finding was not statistically significant due to tumour variability, and a small number of samples included in this experiment (Fig-47 A and A1). However, statistical significance can be achieved by adding more samples. On the other hand, only one sample showed strong expression for p-EGFR-1173 in *AKT1*<sup>E17K</sup>/*TRAF7* mutated meningioma, while expression was absent in NMT (Fig-47 A and A1) and these WB results reflect KinswingR kinase prediction analysis.

In contrast, *AKT1*<sup>E17K</sup>/*TRAF7* mutant meningioma was shown to have higher levels of p-EGFR-1068 expression compared to *NF2*<sup>-/-</sup> mutated meningioma and NMT (Fig-47 A and A1). These results may suggest that EGFR-Y-1173 promotes *NF2*<sup>-/-</sup> mutated meningioma by binding Shc adaptor protein which results in activation of MAPK/ERK signalling (Sakaguchi *et al.*, 1998). In contrast, EGFR phosphorylation at Y-1068 stimulates Gab1, followed by activation of AKT and MAPK/ERK signalling cascade resulting in *AKT1*<sup>E17K</sup>/*TRAF7* mutated meningioma

tumorigenesis (Batzer *et al.*, 1994; Rojas and Lin, 1996; Rodrigues *et al.*, 2000). To confirm this hypothesis further experiments could be performed.

In general, these results suggest EGFR kinase activity is present in both meningioma subtypes irrespective of mutations where the expression of this kinase is totally absent in normal meninges which is in agreement with the previous study (Andersson *et al.*, 2004) and this experiment confirmed overexpression of EGFR kinase in meningioma compared to normal tissue via WB. Due to the lack of available tissue section accessibility, it was not possible to perform an IHC experiment to examine EGFR kinase activity in meningioma mutant subtypes. However, future research could examine these active EGFR phosphosites (EGFR-Y-1173 and p-EGFR-1068) by using a different tumour sample cohort and conducting additional experiments to look for EGFR activity in meningioma tumour that could serve as a viable therapeutic target for meningioma mutational subtypes.

Another kinase LCK has been predicted with a high KinswingR score and is most significantly upregulated in *NF2*<sup>-/-</sup> mutated meningioma compared to NMT (Fig-45 B). LCK overexpression and abnormal activity have been studied in leukaemia (Majolini *et al.*, 1999) and also seen in solid tumours including glioblastoma, breast, colorectal, and prostate cancers (Kim *et al.*, 2010; Elsberger *et al.*, 2010; Veillette *et al.*, 19987; Robinson *et al.*, 1996). LCK has been demonstrated to increase tumour growth and angiogenesis in breast cancer (Elsberger *et al.*, 2010) and has also been linked to radiation-induced proliferation and resistance in glioma patients (Kim *et al.*, 2010). LCK phosphorylates a variety of proteins, including ZAP70, ITK, protein kinase C, and PI3K, to govern cell functions like cell cycle control, cell adhesion, cell motility, cell proliferation, and cell differentiation (Weiss, 1993; Singh *et al.*, 2018).

This is the first study reporting LCK kinase activity in benign meningioma via KinswingR kinase prediction. In WB validation analysis p-LCK-Tyr394 activation was higher in *NF2*<sup>-/-</sup> mutant meningioma than in *AKT1*<sup>E17K</sup>/*TRAF7* mutant meningioma and NMT (Fig-47 B and B1) which reflects KinswingR kinase prediction. However, these observations produced ambiguous results because total LCK expression was not observed in all tissue samples (Fig-47 B). These findings imply that LCK kinase candidates for *NF2*<sup>-/-</sup> mutated meningioma should not be dismissed, however, accurate LCK phospho-kinase activity measurements between samples need a reliable total LCK antibody.

**AURKB** overexpression in malignancies has been demonstrated to cause aneuploidy and genomic instability, which results in tumour progression, migration, and dissemination (Marumoto *et al.*, 2005). AURKB overexpression or amplification has been seen in a variety of human malignancies, including breast cancer, ovarian cancer, gastric/gastrointestinal cancer, and neuroblastoma, and has been linked to a poor prognosis (Cirak *et al.*, 2015; Davidson *et al.*, 2014; Honma *et al.*, 2014; Ramani *et al.*, 2015). Schmidt *et al.*, (2016) reported AURKB expression in meningioma via transcriptomic analysis. In qPCR analysis, the authors observed significant overexpression of AURKB in recurrent malignant WHO grade I meningioma compared to non-recurrent meningioma and suggested it as a prognostic biomarker for meningioma. The current study predicted that AURKB kinase has been upregulated in *NF2*<sup>-/-</sup> mutated meningioma compared to NMT (Fig-45 B).

However, WB analysis showed the opposite of KinSwingR kinase prediction analysis, where overexpression of p-AURKB-Thr232 was observed in normal meninges (Fig-47 C and C1) compared to both meningioma mutational subtypes. The reason for the opposite result could be similar to the previously explained for CAMK2A which implies there are other kinases differentially activated or shared substrates/proteins phosphorylated by multiple kinases in *NF2*<sup>-/-</sup> mutated meningioma samples (Supplementary data- S9, where phosphosites are marked in red which showed 100% AURKB sequence similarity with other kinases). With these opposite findings, we did not do any further analysis on this kinase candidate.

**CSNK2A1** expression and kinase activity are higher in malignant tumour cells than in normal corresponding cells, and it has been proposed that CSNK2A1 is involved in tumorigenesis in breast, lung, kidney, and colorectal cancers (Bae *et al.*, 2016; Wang *et al.*, 2010; Xie *et al.*, 2018; Rabjerg, 2016; Slattery *et al.*, 2018; Zhang *et al.*, 2019). CSNK2A1-induced tumorigenesis occurs by regulating Wnt signaling, Hedgehog signaling, JAK/STAT, NF-κB, and PTEN/PI3K/Akt-PKB (Dominguez *et al.*, 2005; Dominguez *et al.*, 2009; Jia *et al.*, 2010; Zheng *et al.*, 2011; Di Maira *et al.*, 2005). CSNK2A1 stimulates Wnt signaling by activating and increasing the expression of the transcriptional co-factor β-catenin (Dominguez *et al.*, 2005). In addition to this, CSNK2A1 has been identified as a possible anticancer target and there are cell-permeable CK2 inhibitors advancing to preclinical and clinical studies including CX-4945 and CIGB-300 (Chua *et al.*, 2017).

In meningioma CSNK2A1 expression has not yet been reported. CSNK2A1 has been predicted as significantly upregulated in *NF2*<sup>-/-</sup> mutated meningioma compared to *AKT1*<sup>E17K</sup>/*TRAF7*

mutated meningioma via KinswingR analysis (Fig-45 C). However, WB validation analysis showed the opposite of the KinswingR analysis, where p-CSNK2A1-Thr360+Ser-362 showed increased expression in NMT compared to meningioma subtypes (Fig-47 D and D1). In contrast, significant overexpression of total CSNK2A1 was observed in both meningioma subtypes (*NF2*<sup>-/-</sup> and *AKT1*<sup>E17K</sup>/*TRAF7* meningioma) compared to NMT, while the highest expression was observed in *NF2*<sup>-/-</sup> mutated meningioma (Fig-47 D and D2). These findings imply that total CSNK2A1 could be involve in regulating meningioma tumour growth, although additional research is needed to substantiate this claim.

Overall KinswingR kinase prediction and WB results showed discrepancies for the majority of the kinases validated in meningioma mutational subtypes, and potential reasons why this might be the case has been described above. In addition to this, there are several factors including heterogeneity inherent to the tumour samples and the need for validation of these results in samples from independent cohorts as the phosphorylation status results could be affected by multiple freeze-thaw cycles while processing the samples. Another possible explanation is variability within control samples such as NMT as we have observed huge variations within samples obtained from the same or different vendors. Besides this, since there were only two samples used as a control, statistical significance was difficult to achieve with these two samples. After all these limitations, only the activity of the PRKCA kinase was found to be statistically significantly different in benign meningioma via WB and IHC which is in agreement with KinswingR kinase prediction analysis. Further experiments should be carried out on PRKCA kinase to establish if it could be used as a biomarker or therapeutic target for benign meningioma.

### **5.2.3 PRKCA as a therapeutic target for benign mutational meningioma subtypes**

Following confirmation of the presence of active PRKCA kinase in meningioma mutational subtypes, a preliminary functional validation of PRKCA was performed to identify it as a potential therapeutic target candidate for benign mutational meningioma subtypes. PRKCA inhibitor Go6976 was used to treat *NF2*<sup>-/-</sup> and *AKT1*<sup>E17K</sup>/*TRAF7* mutated primary cells in order to inhibit the activate PRKCA. From the cell viability assay, Go6976 decreased cell viability after seven days of treatment in all meningioma mutant subtypes. However, some of the meningioma primary cells required a higher concentration of Go6976 (more than 10 µM which is considerably higher) to reach IC50 (Fig-49). In addition to this meningioma primary cells

are required to treat with Go6976 for more than 7 days in order to observe strong effects on cell viability. These findings imply a limited therapeutic potential for PRKCA inhibition by Go6976.

From WB analysis, it was also observed that treatment with Go6976 was unable to inhibit the expression of active phospho-sites (p-PRKCA-S657, p-PRKCA-T638, and p-PRKCA-T497) of PRKCA in both meningioma subtypes (Fig-50 A and B). In addition to this, the Go6976 treatment had no effect on CyclinD1 expression (Fig-50 A and B). Unlike this study, Merzoug-Larabi *et al.*, (2017) demonstrated that 1 $\mu$ M Go6976 significantly suppresses CyclinD1 expression in patient-derived melanoma metastatic M4T2 cells after 48 h of treatment. In this study, it is clear that Go6976 did not suppress PRKCA activity it could be due to the fact that Go6976 suppresses the PRKCA activity by inhibiting the binding of phorbol ester to PRKCA (Martiny-Baron *et al.*, 1993; Cohen *et al.*, 2006; Merzoug-Larabi *et al.*, 2017). PRKCA consists of two domains including regulatory and catalytic/kinase domains and PRKCA can be activated by both domains (Silinsky and Searl, 2003). Regulatory domains act as receptors or binding sites for tumour-promoting phorbol ester, a plant-derived compound involved in mimicking diacylglycerol (DAG) (Zhang *et al.*, 1995). Upon binding of the phorbol ester to the PRKCA regulatory domain, it facilitates translocation of PRKCA to the membrane and activates downstream signalling (Silinsky and Searl, 2003). This mechanism clearly indicates that Go6976 is unable to inhibit active PRKCA phosphosites consisting of catalytic /kinase domain which reflects current WB results. Although there are currently no commercially available PRKCA phosphosite-specific inhibitors, knocking down *PRKCA* using a shRNA could be employed to test if this reduces meningioma cell proliferation.

### **5.3 Limitations of the study**

Mass-spectrometry-based proteomic analysis is currently a widely used method in neurooncology in order to discover diagnostic markers or therapeutic targets by identifying proteins that are differently expressed between the various groups. However, despite its widespread use in biomarker identification research, there are still a number of constraints to be overcome. It is still difficult to generate high-quality proteomic data from tissue lysates in order to obtain the full coverage of protein identification because a large number of high-quality biological tissue samples are required in order to obtain enough protein for the generation of precise proteomic data analysis (Alaiya *et al.*, 2005). In addition, mass spectrometry still has difficulty detecting a significant portion of low-abundance proteins

(Alaiya *et al.*, 2005). In addition to this, there is a significant chance of sample loss throughout each step of the washing and elution stage of sample processing prior to mass spectrometry (Feist and Hummon, 2015). Therefore, many proteomic studies use huge amounts of protein starting material mostly in the mg range in order to effectively enrich peptides or phosphopeptides that are at considerably lower abundance in a sample and discover as many peptides or phosphopeptides as feasible (Solari *et al.*, 2015). This current study performed proteomic analysis on rare mutational meningioma subtypes, tumours we received vary in their size, and most of the tumours did not yield mg of protein concentration, especially after the phosphoprotein enrichment procedure. Therefore, we could not proceed with phosphoproteomic data analysis. For global proteomic analysis, we used 50 µg and for phosphopeptide/kinase analysis we used 120 microgram which is considerably low for proteomic analysis. In contrast to the present study, Nassiri *et al.*, (2021) employed 1 to 2 mg of frozen meningioma tissue samples for proteome analysis, while a prior study found 36,000 phosphorylation sites in 10 mg of mouse brain tissue (Huttlin *et al.*, 2010). Additionally, Solari *et al.*, (2015) reviewed a number of studies using at least 1 mg of a tissue sample to detect 10,000 phosphosites.

Furthermore, the process of sample preparation before LC-MS analysis might significantly affect the outcomes (Solari *et al.*, 2015). Mertins *et al.*, (2014) recently studied the proteome and phosphoproteome of human ovarian tumour and breast cancer tissue and revealed that while the proteome does not change after the tissue is cut off from its blood supply for 60 minutes, up to 24 percent of the phosphoproteome had fast phosphorylation alterations, especially in pathways associated with cancer. In this current study, tissue samples were carefully handled in order to minimise technical variation in sample processing. Despite the fact that our normal meningeal tissues were very old, the continuous freezing and thawing of those NMT tissues may have affected the phosphopeptide identification dataset, which was reflected in our kinase validation as most of the kinase validation WB results were inconsistent with the KinswingR kinase prediction analysis.

Identified protein candidate validation via different techniques has advantages and limitations. Although the antibody-based WB approach is reproducible, sensitive, and quantitative. In contrast, it has a low potential for clinical practice since it is time-consuming and technically difficult (Ghosh *et al.*, 2014) and requires at least 10 µg of samples to run. After proteomic sample preparation, there was a relatively low amount of samples remaining for validation through WB. To address this, a Simple wes assay was added for validation, using only 1-3 µg

samples and requiring little time. However, this assay is not sufficiently developed to generate signal intensity against all antibodies.

Immunohistochemistry is reproducible and routinely used for the clinical diagnosis of central nervous system tumour (Louis *et al.*, 2016). IHC has several drawbacks, including the inability to quantify results, and the potential for experimental bias (during specimen fixation, antigen retrieval, detection, etc. (De Matos *et al.*, 2010). As I have observed inconsistencies between WB and IHC results for protein candidates including CLIC3, CRABP2, GMDS, and PTGFRN.

Furthermore, we could not validate protein candidates in an independent cohort, as mentioned previously mutational subtypes *AKT1<sup>E17K</sup>/TRAF7* and *KLF4<sup>K409Q</sup>/TRAF7* mutant meningioma are very rare about 14 and 12% respectively (Bi *et al.*, 2016). It took several years to acquire seven *AKT1<sup>E17K</sup>/TRAF7* mutated meningioma tumour for this study. In addition to this, we did not overlap global proteomic and phosphopeptide datasets due to the fact that two different protein identification techniques (label-free and TMT-labelled LC-MS) were performed, small samples size and the number of tumour samples was not equal in each data set, and the lack of *KLF4<sup>K409Q</sup>/TRAF7* mutant meningioma samples which was excluded from the phosphopeptide experiment.

## 5.4 Future directions

**Some future experiments are warranted to further confirm the findings presented in this thesis:**

Following mass-spectrometry data analyses, I have identified a panel of upregulated proteins, which can differentiate different meningioma mutant subtypes considered as biomarkers or therapeutic targets for each group which were then validated using WB and IHC. The data from the mass spectrometry analysis, Western blotting, and immunohistochemistry, meningioma (protein) biomarker/therapeutic studies sometimes produced inconsistent results for example: SLC29A1 and Anion exchange protein 2 (showed a discrepancy between MS detection and validation experiments) data among the different meningioma subtypes. This could be because of the various experimental sensitivities, but it could also be because of the recently described principle of intra-tumour heterogeneity (Magill *et al.*, 2020; Nigim *et al.*, 2018). One of our group members (Ting Zhang) now investigating the tumour microenvironment in various genotypes of meningioma to identify the markers related to the interaction between tumour cells and immune cells. She is using the Opal staining method from Akoya to detect immune markers on tissue, including CD68, CD163, CD3, TMEM119, and P2RY12, the last two are



microglia markers. In this experiment, she included the same tissue samples of *AKT1<sup>E17K</sup>/TRAF7* and *KLF4<sup>K409Q</sup>/TRAF7* mutant meningioma subtypes that were used for this proteomics study and she hypothesized that targeting these immune markers would aid in the treatment of various genotypes of meningioma.

To increase the confidence in the validation results, the next vital steps include the curation and analysis of independent *NF2<sup>-/-</sup>*, *AKT1<sup>E17K</sup>/TRAF7*, and *KLF4<sup>K409Q</sup>/TRAF7* mutant meningioma subtypes cohorts, further WB and IHC validation should then be carried out on these independent cohorts of tumour tissue. I recognise that whilst WB is an effective and established technique for quantifying protein expression differences among the different meningioma mutant subtypes, it is not practical for routine clinical use and is susceptible to irreproducible results due to variations in lab protocols (Ghosh *et al.*, 2014). Therefore, other techniques such as qPCR and ELISA (dependent on access to commercially available/validated antibodies) and mass spectrometry-based multiple reaction monitoring (MRM) quantifications should be employed further, to strengthen the validity of the results, and to describe biomarkers suitable for clinical translation where limited amounts of samples are concerned. Our research group, Abdelrahman *et al.*, (2022) evaluated the correlation between serum circulating miRNA and the methylation status in meningioma. They performed qPCR for miRNA quantification and showed that combined two miRNAs (miR-497 and miR-219) in the blood of meningioma patients are predictive of grade. For this project, potential protein candidate validation via qPCR combined with methylation profiling can be performed on a subset of tumour tissue samples to classify or predict meningioma mutant subtypes.

Another study from our group, Sofela *et al.*, (2021) used meningioma cells, tissue and plasma samples to validate a biomarker for meningioma using Western blotting, immunohistochemistry, and real-time quantitative polymerase chain reaction (RT-qPCR), enzyme-linked immunosorbent assay (ELISA). Fibulin-2, a calcium-binding extracellular matrix glycoprotein, was the only protein whose expression results were consistent across all experimental settings. Fibulin-2 overexpression was shown to be significantly higher in grade II meningioma than in grade I meningioma in this investigation and found a significant correlation between high plasma fibulin-2 levels and more aggressive methylation classes, irrespective of meningioma grade. Similar to this study, different clinical specimens and validation techniques should be applied to establish a sensitive biomarker from identified potential protein candidates for these meningioma mutant subtypes group. Enzyme-linked immunosorbent assays (ELISAs), which are very inexpensive and can handle large numbers of

samples fast using clinically approved tools and protocols, are frequently used in validation methods. The multiplexing powers of ELISA can be relatively restricted, and antibodies must be produced against each protein or peptide target of interest (Van Gool *et al.*, 2020). Additionally, assays may cross-react with molecules with similar protein or peptide structures, giving false-positive or higher values, depending on the molecule's structure (Van Gool *et al.*, 2020). Targeted MS-based techniques should be employed as an alternative because they make it easier to validate as highly multiplexed assays and are antibody independent (Parker and Borchers, 2014). These targeted mass spectrometric approaches have been developed using orbitrap or triple quadrupole mass spectrometers, and the output is given as protein concentrations which can be assessed with clinical samples with precision and accuracy (Parker and Borchers, 2014). In addition to this, a future proteomic analysis must focus on increasing the sample sizes to statistically validate these differences among the meningioma mutant subtypes as reliable biomarkers.

However, differential protein expression analysis revealed clearly upregulated proteins specific to these meningioma *AKT1<sup>E17K</sup>/TRAF7*, *KLF4<sup>K409Q</sup>* and *NF2<sup>-/-</sup>* mutant subtypes. Such as Pyruvate carboxylase, GMDS, CLIC3 and CRABP2 are highly specific for *AKT1<sup>E17K</sup>/TRAF7* meningioma mutational subtype, Endoglin is highly expressed in *KLF4<sup>K409Q</sup>* meningioma mutational subtype and. Annexin-3 expression was significantly high for *NF2<sup>-/-</sup>* meningioma mutational subtype compared to other mutational meningioma subtypes and NMT. The prognostic role will need to be investigated further as we currently do not have enough evidence to suggest a correlation between these candidate protein expressions and patient outcome (overall survival and recurrence-free survival). To achieve this, first, we need to establish a positive link between *AKT1<sup>E17K</sup>/TRAF7*, *KLF4<sup>K409Q</sup>* and *NF2<sup>-/-</sup>* mutations and their specific candidate protein expression in the meningioma cell lines (*in-vitro*). Further evidence that Annexin-3 overexpression was observed in *NF2<sup>-/-</sup>* mutated meningioma cell lines suggests there is a positive correlation between *NF2<sup>-/-</sup>* mutation and Annexin-3 overexpression. Where the Benmen-1 cell line (grade-I; *NF2<sup>-/-</sup>* cell line) and the KT21 cell line (grade-III; *NF2<sup>-/-</sup>* cell line) showed strong expression compared to IOMLEE (grade-III; *NF2<sup>+/+</sup>* cell line) supporting my hypothesis and previous results (Fig- 29 a). However, this has to be confirmed in *NF2<sup>-/-</sup>* mutated patient-derived tumour cells. A similar experiment should apply to other meningiomas mutant subtypes-specific protein candidates. Due to the lack of a suitable meningioma cell line model with *AKT1<sup>E17k</sup>* and *KLF4<sup>K409Q</sup>* mutation, these results provide a foundation for the development of a new project providing possible directions for this validation by developing a

new meningioma cell lines holding these *AKT1*<sup>E17k</sup> and *KLF4*<sup>K409Q</sup> point mutations using CRISPER-Cas9 (clustered regularly interspaced short palindromic repeats and CRISPR-associated protein 9). Secondly, we need to further investigate the functional relevance of these significant meningioma subtypes specific upregulated candidate proteins by performing a lentiviral-mediated RNA knockdown, using short hairpin RNA (shRNA) sequences. It was evident that annexin-3 knockdown reduced Benmen-1 cell proliferation which suggests a novel therapeutic option for *NF2*<sup>-/-</sup> mutated meningioma subtypes (Fig: 29 c and e). However, these experiments must be repeated in primary cells to draw conclusions. Similar lentiviral-mediated knockdown experiments can be applied to other potential candidate proteins for functional validation to observe the effect on meningioma cell growth. In addition to this, our biobank and associated clinical dataset is less than ten years old, we did not have long enough observation period to carry out statistical analysis on patient outcomes. Further, one should carry out univariate and multivariate statistical analysis linking the level of the biomarker in a particular genomic group to age, gender, tumour recurrence, and death to compare the patient outcomes between the different mutant subtypes.

KEGG and IPA pathway analysis of *AKT1*<sup>E17K</sup>/*TRAF7* mutated meningioma showed upregulation of oxidative phosphorylation (Fig-18 and Fig-19). Oxidative phosphorylation pathway-associated proteins (COX6B1, NDUFA5, NDUFB7, NDUFB1, NDUFB8 and ATPK) (Fig-20) will need to be validated via WB, IHC or targeted MS-based techniques to establish this pathway for *AKT1*<sup>E17K</sup>/*TRAF7* mutated meningioma subtypes. In both sets of pathway analysis (KEGG and IPA), it was observed that the oxidative phosphorylation pathway was highly enriched. These findings pointing to the targeting and validation of this pathway for the *AKT1*<sup>E17K</sup>/*TRAF7* mutant meningioma subtype may therefore point to novel biomarkers or therapeutic targets. OXPHOS inhibitors (non-clinically used metformin, atovaquone, and arsenic trioxide) may be employed to treat hypoxic tumours by targeting upregulated OXPHOS proteins (Ashton *et al.*, 2018). Additionally, the Agilent Seahorse XF ATP Real-Time rate assay can be employed (which measures the metabolic activity or oxidative phosphorylation) in *AKT1*<sup>E17K</sup>/*TRAF7* mutated meningioma cells to investigate metabolic rewiring to support rapid tumour growth, understand which nutrients fuel *AKT1*<sup>E17K</sup>/*TRAF7* mutated meningioma, and learn how metabolism affects the tumour microenvironment. Further, investigation of the methylation profile of the mutated meningioma subtypes tumour samples (n=28) used in this study would allow us to establish

whether samples clustering in a specific class share the same molecular characteristics regarding the Oxidative phosphorylation pathway-associated proteins (COX6B1, NDUFA5, NDUFB7, NDUFB1, NDUFB8 and ATPK) expression (Sahm *et al.*, 2017).

In future studies, the initial analysis of downregulated proteins detected in meningioma mutant subtypes in this study will be expanded upon.

## 5.5 Conclusions

Proteomic technologies have advanced significantly, enabling detailed investigation of protein expression patterns in several clinical samples. However, the categorization of meningioma using proteomics is still in its early stage. Consequently, there are limited numbers of data on protein biomarkers or therapeutic targets that are specifically associated with characterizing meningioma grades only. The genetic landscape of benign meningioma is well characterised, however, it is still unclear how these genetic changes affect the proteomic landscape as more than 20% of benign meningioma exhibit clinically aggressive behaviour (Nassiri *et al.*, 2021). This study aims to characterise the proteomic landscape of these benign meningioma subtypes. To date, this study performed the first comprehensive analysis of proteins in meningioma tissue harbouring *AKT1<sup>E17K</sup>/TRAF7*, *KLF4<sup>K409Q</sup>/TRAF7*, and *NF2<sup>-/-</sup>* mutant meningioma samples (n=28). Proteomic analysis of hierarchical clustering showed how mutational subtypes cluster based on their overall proteomic profiles, and at the same time, proteome analysis revealed information on the heterogeneity of *NF2<sup>-/-</sup>* mutant meningioma tumours.

This proteomic study successfully identified a panel of proteomic signatures that differentiated between benign meningioma mutational subtypes, including *AKT1<sup>E17K</sup>/TRAF7* mutant meningioma-specific upregulated proteins including GMDS, CLIC3, and CRABP2, and their significant expression was confirmed via Simple wes; *KLF4<sup>K409Q</sup>/TRAF7* mutant subtype-specific upregulated protein endoglin, and differential expression of this protein was confirmed by WB and IHC; *NF2<sup>-/-</sup>* mutant meningioma specific upregulated protein Annexin-3 and significant expression of this protein confirmed via both WB and IHC. Additionally, functional assay investigation revealed that overexpression of Annexin-3 may contribute to the proliferation of *NF2<sup>-/-</sup>* mutant meningioma cells.

Functional annotation analysis of proteins (eg: GMDS and PC) upregulated in *AKT1<sup>E17K</sup>/TRAF7* subtype indicated key alterations in metabolism processes. While upregulation of endoglin and E-cadherin point toward changes in focal adhesion and extracellular matrix disassembly processes across *KLF4<sup>K409Q</sup>/TRAF7* mutant subtypes. These proteomic alterations could provide us with a panel of proteins forming distinctive signatures providing us with developing biomarkers/therapeutic targets for mutational meningioma subtype and require further validation.

Although mutational landscape and DNA methylation are promising in meningioma diagnosis. Based on DNA methylation and mRNA abundance analyses, an integrative molecular investigation designated meningiomas with the mutations *AKT1<sup>E17K</sup>/TRAF7* and *KLF4<sup>K409Q</sup>/TRAF7* into MG2 (Meningioma2), and their gene expression pathway analysis showed enrichment for vascular angiogenesis (Nassiri *et al.*, 2021). According to recent proteomic research, *AKT1<sup>E17K</sup>/TRAF7* mutant meningioma-specific PC, CLIC3, and *KLF4<sup>K409Q</sup>/TRAF7* subtype-specific endoglin may all play a role in vascular angiogenesis (Kiesel *et al.*, 2021; Hernandez-Fernaud *et al.*, 2017; González Muñoz *et al.*, 2021), however, future research is needed to verify this. This current proteome investigation also serves as a foundation for future confirmation of the involvement of upregulated proteins that are specific to meningiomas with the *AKT1<sup>E17K</sup>/TRAF7* mutation in the oxidative phosphorylation pathway. Furthermore, phosphopeptide analysis confirmed the presence of an active form of PRKCA in benign meningiomas. However, additional validation in a different cohort and knockdown of PRKCA for functional validation would provide additional evidence that PRKCA might be a promising therapeutic target for the clinical management of benign meningioma.

Finally, improvements in the proteomic investigation, such as the acquisition of sufficient quantities of optimally collected tumour tissue samples, as well as developments in MS proteomics to decrease sample input and increase sensitivity for low abundance proteins and modified peptides, are necessary for the larger-scale exploration of discovery proteomics in the clinical setting.

## References

- Aaltonen, V., Koivunen, J., Laato, M. and Peltonen, J., 2007. PKC inhibitor Go6976 induces mitosis and enhances doxorubicin-paclitaxel cytotoxicity in urinary bladder carcinoma cells. *Cancer letters*, 253(1), pp.97-107.
- Abbott, A., 1999. A post-genomic challenge: learning to read patterns of protein synthesis. *Nature*, 402(6763), pp.715-716.
- Abbritti, R.V., Polito, F., Cucinotta, M., Giudice, C.L., Caffo, M., Tomasello, C., Germano, A. and Aguenouz, M., 2016. Meningiomas and proteomics: focus on new potential biomarkers and molecular pathways. *Cancer Genomics-Proteomics*, 13(5), pp.369-379.
- Abdelrahman, A., Negroni, C., Sahm, F., Adams, C.L., Urbanic-Purkart, T., Khalil, M., Vergura, R., Morelli, C. and Hanemann, C.O., 2022. miR-497 and 219 in blood aid meningioma classification. *Journal of Neuro-Oncology*, 160(1), pp.137-147.
- Abdel-Rahman, M.H., Pilarski, R., Cebulla, C.M., Massengill, J.B., Christopher, B.N., Boru, G., Hovland, P. and Davidorf, F.H., 2011. Germline BAP1 mutation predisposes to uveal melanoma, lung adenocarcinoma, meningioma, and other cancers. *Journal of medical genetics*, 48(12), pp.856-859.
- Abedalthagafi, M., Bi, W.L., Aizer, A.A., Merrill, P.H., Brewster, R., Agarwalla, P.K., Listewnik, M.L., Dias-Santagata, D., Thorner, A.R., Van Hummelen, P. and Brastianos, P.K., 2016. Oncogenic PI3K mutations are as common as AKT1 and SMO mutations in meningioma. *Neuro-oncology*, 18(5), pp.649-655.
- Abedalthagafi, M.S., Merrill, P.H., Bi, W.L., Jones, R.T., Listewnik, M.L., Ramkissoon, S.H., Thorner, A.R., Dunn, I.F., Beroukhi, R., Alexander, B.M. and Brastianos, P.K., 2014. Angiomatous meningiomas have a distinct genetic profile with multiple chromosomal polysomies including polysomy of chromosome 5. *Oncotarget*, 5(21), p.10596.
- Abercrombie, M. and Dunn, G.A., 1975. Adhesions of fibroblasts to substratum during contact inhibition observed by interference reflection microscopy. *Experimental cell research*, 92(1), pp.57-62.
- Adams, C.L., Ercolano, E., Ferluga, S., Sofela, A., Dave, F., Negroni, C., Kurian, K.M., Hilton, D.A. and Hanemann, C.O., 2020. A rapid robust method for subgrouping non-NF2 meningiomas according to genotype and detection of lower levels of M2 macrophages in AKT1 E17K mutated tumours. *International journal of molecular sciences*, 21(4), p.1273.
- Aebersold, R. and Mann, M., 2003. Mass spectrometry-based proteomics. *Nature*, 422(6928), pp.198-207.
- Aebersold, R. and Mann, M., 2003. Mass spectrometry-based proteomics. *Nature*, 422(6928), pp.198-207.
- Afshar-Oromieh, A., Wolf, M.B., Kratochwil, C., Giesel, F.L., Combs, S.E., Dimitrakopoulou-Strauss, A., Gnirs, R., Roethke, M.C., Schlemmer, H.P. and Haberkorn, U., 2015. Comparison of 68Ga-DOTATOC-PET/CT and PET/MRI hybrid systems in patients with cranial meningioma: initial results. *Neuro-oncology*, 17(2), pp.312-319.

- Aghi, M.K., Carter, B.S., Cosgrove, G.R., Ojemann, R.G., Amin-Hanjani, S., Martuza, R.L., Curry Jr, W.T. and Barker, F.G., 2009. Long-term recurrence rates of atypical meningiomas after gross total resection with or without postoperative adjuvant radiation. *Neurosurgery*, 64(1), pp.56-60.
- Aguila, B., Morris, A.B., Spina, R., Bar, E., Schraner, J., Vinkler, R., Sohn, J.W. and Welford, S.M., 2019. The Ig superfamily protein PTGFRN coordinates survival signaling in glioblastoma multiforme. *Cancer letters*, 462, pp.33-42.
- Ahmad, K.A., Wang, G., Unger, G., Slaton, J. and Ahmed, K., 2008. Protein kinase CK2-a key suppressor of apoptosis. *Advances in enzyme regulation*, 48, p.179.
- Ahmed, R.A., Shebl, A.M. and Habashy, H.O., 2017. Expression levels of  $\beta$ -catenin and galectin-3 in meningioma and their effect on brain invasion and recurrence: a tissue microarray study. *Cancer biology & medicine*, 14(3), p.319.
- Ahn, J. and Prives, C., 2002. Checkpoint kinase 2 (Chk2) monomers or dimers phosphorylate Cdc25C after DNA damage regardless of threonine 68 phosphorylation. *Journal of Biological Chemistry*, 277(50), pp.48418-48426.
- Ahn, J., Urist, M. and Prives, C., 2004. The Chk2 protein kinase. *DNA repair*, 3(8-9), pp.1039-1047.
- Ahn, J.Y., Schwarz, J.K., Piwnica-Worms, H. and Canman, C.E., 2000. Threonine 68 phosphorylation by ataxia telangiectasia mutated is required for efficient activation of Chk2 in response to ionizing radiation. *Cancer research*, 60(21), pp.5934-5936.
- Akers, J.C., Ramakrishnan, V., Kim, R., Skog, J., Nakano, I., Pingle, S., Kalinina, J., Hua, W., Kesari, S., Mao, Y. and Breakefield, X.O., 2013. MiR-21 in the extracellular vesicles (EVs) of cerebrospinal fluid (CSF): a platform for glioblastoma biomarker development. *PLoS one*, 8(10), p.e78115.
- Alaiya, A., Al-Mohanna, M. and Linder, S., 2005. Clinical cancer proteomics: promises and pitfalls. *Journal of proteome research*, 4(4), pp.1213-1222.
- Alarcón, S., Toro, M.D.L.Á., Villarreal, C., Melo, R., Fernández, R., Ayuso Sacido, A., Uribe, D., San Martín, R. and Quezada, C., 2020. Decreased equilibrative nucleoside transporter 1 (ENT1) activity contributes to the high extracellular adenosine levels in mesenchymal glioblastoma stem-like cells. *Cells*, 9(8), p.1914.
- Alberts, B., Bray, D., Hopkin, K., Johnson, A.D., Lewis, J., Raff, M., Roberts, K. and Walter, P., 2013. *Essential cell biology*. Garland Science.
- Alexander, B.M. and Mehta, M.P., 2011. Role of isocitrate dehydrogenase in glioma. *Expert review of neurotherapeutics*, 11(10), pp.1399-1409.
- Alexiou, G.A., et al., 2010. *Management of meningiomas*. *Clin Neurol Neurosurgery*, 112(3), pp. 177-82.
- Al-Momani, S., Qi, D., Ren, Z. and Jones, A.R., 2018. Comparative qualitative phosphoproteomics analysis identifies shared phosphorylation motifs and associated biological processes in evolutionary divergent plants. *Journal of proteomics*, 181, pp.152-159.
- Alper, S.L., Darman, R.B., Chernova, M.N. and Dahl, N.K., 2002. The AE gene family of Cl/HCO<sub>3</sub>-exchangers. *Journal of nephrology*, 15, pp.S41-53.

- Al-Rashed, M., Foshay, K. and Abedalthagafi, M., 2020. Recent advances in meningioma immunogenetics. *Frontiers in Oncology*, 9, p.1472.
- AlSahlawi, A., Aljelaify, R., Magrashi, A., AlSaeed, M., Almutairi, A., Alqubaishi, F., Alturkistani, A., AlObaid, A., Abouelhoda, M., AlMubarak, L. and AlTassan, N., 2019. New insights into the genomic landscape of meningiomas identified FGFR3 in a subset of patients with favorable prognoses. *Oncotarget*, 10(53), p.5549.
- Alt, A., Miguel-Romero, L., Donderis, J., Aristorena, M., Blanco, F.J., Round, A., Rubio, V., Bernabeu, C. and Marina, A., 2012. Structural and functional insights into endoglin ligand recognition and binding. *PloS one*, 7(2), p.e29948.
- Ammoun, S., Cunliffe, C.H., Allen, J.C., Chiriboga, L., Giacotti, F.G., Zagzag, D., Hanemann, C.O. and Karajannis, M.A., 2010. ErbB/HER receptor activation and preclinical efficacy of lapatinib in vestibular schwannoma. *Neuro-oncology*, 12(8), pp.834-843.
- Ammoun, S., Schmid, M.C., Zhou, L., Hilton, D.A., Barczyk, M. and Hanemann, C.O., 2015. The p53/mouse double minute 2 homolog complex deregulation in merlin-deficient tumours. *Molecular oncology*, 9(1), pp.236-248.
- Anderson, L. and Seilhamer, J., 1997. A comparison of selected mRNA and protein abundances in human liver. *Electrophoresis*, 18(3-4), pp.533-537.
- Anderson, N.L. and Anderson, N.G., 1998. Proteome and proteomics: new technologies, new concepts, and new words. *Electrophoresis*, 19(11), pp.1853-1861.
- Andersson, U., Guo, D., Malmer, B., Bergenheim, A.T., Brännström, T., Hedman, H. and Henriksson, R., 2004. Epidermal growth factor receptor family (EGFR, ErbB2–4) in gliomas and meningiomas. *Acta neuropathologica*, 108(2), pp.135-142.
- Andrae, N., Kirches, E., Hartig, R., Haase, D., Keilhoff, G., Kalinski, T. and Mawrin, C., 2012. Sunitinib targets PDGF-receptor and Flt3 and reduces survival and migration of human meningioma cells. *European Journal of Cancer*, 48(12), pp.1831-1841.
- André, M., Chambrion, C., Charrin, S., Soave, S., Chaker, J., Boucheix, C., Rubinstein, E. and Le Naour, F., 2009. In situ chemical cross-linking on living cells reveals CD9P-1 cis-oligomer at cell surface. *Journal of proteomics*, 73(1), pp.93-102.
- André, M., Morelle, W., Planchon, S., Milhiet, P.E., Rubinstein, E., Mollicone, R., Chamot-Rooke, J. and Le Naour, F., 2007. Glycosylation status of the membrane protein CD9P-1. *Proteomics*, 7(21), pp.3880-3895.
- Andrea Cavani, C.A. and Girolomoni, G., 1998. Interferon- $\gamma$ -stimulated human keratinocytes express the genes necessary for the production of peptide-loaded MHC class II molecules. *Journal of investigative dermatology*, 110(2), pp.138-142.
- Apra, C., Peyre, M. and Kalamarides, M., 2018. Current treatment options for meningioma. *Expert review of neurotherapeutics*, 18(3), pp.241-249.
- Apweiler, R., Aslanidis, C., Deufel, T., Gerstner, A., Hansen, J., Hochstrasser, D., Kellner, R., Kubicek, M., Lottspeich, F., Maser, E. and Mewes, H.W., 2009. Approaching clinical proteomics: current state and future fields of application in fluid proteomics. *Clinical chemistry and laboratory medicine*, 47(6), pp.724-744.



- Ashton, T.M., McKenna, W.G., Kunz-Schughart, L.A. and Higgins, G.S., 2018. Oxidative phosphorylation as an emerging target in cancer therapy. *Clinical Cancer Research*, 24(11), pp.2482-2490.
- Aventaggiato, M., Vernucci, E., Barreca, F., Russo, M.A. and Tafani, M., 2021. Sirtuins' control of autophagy and mitophagy in cancer. *Pharmacology & Therapeutics*, 221, p.107748.
- Bae, J.S., Park, S.H., Jamiyandorj, U., Kim, K.M., Noh, S.J., Kim, J.R., Park, H.J., Kwon, K.S., Jung, S.H., Park, H.S. and Park, B.H., 2016. CK2 $\alpha$ /CSNK2A1 phosphorylates SIRT6 and is involved in the progression of breast carcinoma and predicts shorter survival of diagnosed patients. *The American Journal of Pathology*, 186(12), pp.3297-3315.
- Bahassi, E.M., Penner, C.G., Robbins, S.B., Tichy, E., Feliciano, E., Yin, M., Liang, L., Deng, L., Tischfield, J.A. and Stambrook, P.J., 2007. The breast cancer susceptibility allele CHEK2\*1100delC promotes genomic instability in a knock-in mouse model. *Mutation Research/Fundamental and Molecular Mechanisms of Mutagenesis*, 616(1-2), pp.201-209.
- Bai, S., Zhu, W., Coffman, L., Vlad, A., Schwartz, L.E., Elishaev, E., Drapkin, R. and Buckanovich, R.J., 2019. CD105 is expressed in ovarian cancer precursor lesions and is required for metastasis to the ovary. *Cancers*, 11(11), p.1710.
- Baldi, I., Engelhardt, J., Bonnet, C., Bauchet, L., Berteaud, E., Grüber, A. and Loiseau, H., 2018. Epidemiology of meningiomas. *Neurochirurgie*, 64(1), pp.5-14.
- Bánkfalvi, A., Kraßbort, M., Buchwalow, I.B., Vég, A., Felszeghy, E. and Piffkó, J., 2002. Gains and losses of adhesion molecules (CD44, E-cadherin, and  $\beta$ -catenin) during oral carcinogenesis and tumour progression. *The Journal of Pathology: A Journal of the Pathological Society of Great Britain and Ireland*, 198(3), pp.343-351.
- Bao, S., Wu, Q., McLendon, R.E., Hao, Y., Shi, Q., Hjelmeland, A.B., Dewhirst, M.W., Bigner, D.D. and Rich, J.N., 2006. Glioma stem cells promote radioresistance by preferential activation of the DNA damage response. *Nature*, 444(7120), pp.756-760.
- Barbara, N.P., Wrana, J.L. and Letarte, M., 1999. Endoglin is an accessory protein that interacts with the signaling receptor complex of multiple members of the transforming growth factor- $\beta$  superfamily. *Journal of Biological Chemistry*, 274(2), pp.584-594.
- Barski, D., Wolter, M., Reifenberger, G. and Riemenschneider, M.J., 2010. Hypermethylation and transcriptional downregulation of the TIMP3 gene is associated with allelic loss on 22q12.3 and malignancy in meningiomas. *Brain pathology*, 20(3), pp.623-631.
- Bartek, J. and Lukas, J., 2003. Chk1 and Chk2 kinases in checkpoint control and cancer. *Cancer cell*, 3(5), pp.421-429.
- Bartek, J., Falck, J. and Lukas, J., 2001. CHK2 kinase—a busy messenger. *Nature reviews Molecular cell biology*, 2(12), pp.877-886.
- Bartucci, M., Svensson, S., Romania, P., Dattilo, R., Patrizii, M., Signore, M., Navarra, S., Lotti, F., Biffoni, M., Pillozzi, E. and Duranti, E., 2012. Therapeutic targeting of Chk1 in NSCLC stem cells during chemotherapy. *Cell Death & Differentiation*, 19(5), pp.768-778.
- Bassiri, K., Ferluga, S., Sharma, V., Syed, N., Adams, C.L., Lasonder, E. and Hanemann, C.O., 2017. Global proteome and phospho-proteome analysis of merlin-deficient meningioma and schwannoma identifies PDLIM2 as a novel therapeutic target. *EBioMedicine*, 16, pp.76-86.

- Batchu, S., Henry, O.S. and Yu, S., 2021. Transcriptomic deconvolution reveals unique tumor microenvironmental interactions across intracranial meningioma WHO grades. *Gene Reports*, 25, p.101388.
- Batzer, A.G., Rotin, D., Urena, J.M., Skolnik, E.Y. and Schlessinger, J., 1994. Hierarchy of binding sites for Grb2 and Shc on the epidermal growth factor receptor. *Molecular and cellular biology*, 14(8), pp.5192-5201.
- Batzer, A.G., Rotin, D., Urena, J.M., Skolnik, E.Y. and Schlessinger, J., 1994. Hierarchy of binding sites for Grb2 and Shc on the epidermal growth factor receptor. *Molecular and cellular biology*, 14(8), pp.5192-5201.
- Baxter, D.S., Orrego, A., Rosenfeld, J.V. and Mathiesen, T., 2014. An audit of immunohistochemical marker patterns in meningioma. *Journal of Clinical Neuroscience*, 21(3), pp.421-426.
- Beauchamp, R.L., James, M.F., DeSouza, P.A., Wagh, V., Zhao, W.N., Jordan, J.T., Stemmer-Rachamimov, A., Plotkin, S.R., Gusella, J.F., Haggarty, S.J. and Ramesh, V., 2015. A high-throughput kinome screen reveals serum/glucocorticoid-regulated kinase 1 as a therapeutic target for NF2-deficient meningiomas. *Oncotarget*, 6(19), p.16981.
- Beekman, C., Janson, A.A., Baghat, A., van Deutekom, J.C. and Datson, N.A., 2018. Use of capillary Western immunoassay (Wes) for quantification of dystrophin levels in skeletal muscle of healthy controls and individuals with Becker and Duchenne muscular dystrophy. *PloS one*, 13(4), p.e0195850.
- Bello, M.J., Amiñoso, C., Lopez-Marin, I., Arjona, D., Gonzalez-Gomez, P., Alonso, M.E., Lomas, J., de Campos, J.M., Kusak, M.E., Vaquero, J. and Isla, A., 2004. DNA methylation of multiple promoter-associated CpG islands in meningiomas: relationship with the allelic status at 1p and 22q. *Acta neuropathologica*, 108(5), pp.413-421.
- Bellón, T., Corbi, A., Lastres, P., Calés, C., Cebrián, M., Vera, S., Cheifetz, S., Massague, J., Letarte, M. and Bernabéu, C., 1993. Identification and expression of two forms of the human transforming growth factor- $\beta$ -binding protein endoglin with distinct cytoplasmic regions. *European journal of immunology*, 23(9), pp.2340-2345.
- Bernhart, E., Damm, S., Heffeter, P., Wintersperger, A., Asslaber, M., Frank, S., Hammer, A., Strohmaier, H., DeVaney, T., Mrfka, M. and Eder, H., 2014. Silencing of protein kinase D2 induces glioma cell senescence via p53-dependent and-independent pathways. *Neuro-oncology*, 16(7), pp.933-945.
- Berx, G., Becker, K.F., Höfler, H. and Van Roy, F., 1998. Mutations of the human E-cadherin (CDH1) gene. *Human mutation*, 12(4), pp.226-237.
- Besson, A. and Yong, V.W., 2000. Involvement of p21Waf1/Cip1 in protein kinase C alpha-induced cell cycle progression. *Molecular and cellular biology*, 20(13), pp.4580-4590.
- Bi, W.L., Greenwald, N.F., Abedalthagafi, M., Wala, J., Gibson, W.J., Agarwalla, P.K., Horowitz, P., Schumacher, S.E., Esaulova, E., Mei, Y. and Chevalier, A., 2017. Genomic landscape of high-grade meningiomas. *NPJ genomic medicine*, 2(1), pp.1-14.
- Bi, W.L., Zhang, M., Wu, W.W., Mei, Y. and Dunn, I.F., 2016. Meningioma genomics: diagnostic, prognostic, and therapeutic applications. *Frontiers in surgery*, 3, p.40.

- Bianchi, C., Bombelli, S., Raimondo, F., Torsello, B., Angeloni, V., Ferrero, S., Di Stefano, V., Chinello, C., Cifola, I., Invernizzi, L. and Brambilla, P., 2010. Primary cell cultures from human renal cortex and renal-cell carcinoma evidence a differential expression of two spliced isoforms of Annexin A3. *The American journal of pathology*, 176(4), pp.1660-1670.
- Bird, A.P., 1980. DNA methylation and the frequency of CpG in animal DNA. *Nucleic acids research*, 8(7), pp.1499-1504.
- Bodenbach, L., Fauss, J., Robitzki, A., Krehan, A., Lorenz, P., Lozeman, F.J. and Pyerin, W., 1994. Recombinant human casein kinase II: A study with the complete set of subunits ( $\alpha$ ,  $\alpha'$  and  $\beta$ ), site-directed autophosphorylation mutants and a bicistronically expressed holoenzyme. *European journal of biochemistry*, 220(1), pp.263-273.
- Böni-Schnetzler, M. and Pilch, P.F., 1987. Mechanism of epidermal growth factor receptor autophosphorylation and high-affinity binding. *Proceedings of the National Academy of Sciences*, 84(22), pp.7832-7836.
- Bornancin, F. and Parker, P.J., 1996. Phosphorylation of threonine 638 critically controls the dephosphorylation and inactivation of protein kinase Ca. *Current Biology*, 6(9), pp.1114-1123.
- Bornancin, F. and Parker, P.J., 1997. Phosphorylation of protein kinase C- $\alpha$  on serine 657 controls the accumulation of active enzyme and contributes to its phosphatase-resistant state. *Journal of Biological Chemistry*, 272(6), pp.3544-3549.
- Bosc, D.G., Slominski, E., Sichler, C. and Litchfield, D.W., 1995. Phosphorylation of Casein Kinase II by p34cdc2: Identification of phosphorylation sites using phosphorylation site mutants *in vitro*. *Journal of Biological Chemistry*, 270(43), pp.25872-25878.
- Brastianos, P.K., Horowitz, P.M., Santagata, S., Jones, R.T., McKenna, A., Getz, G., Ligon, K.L., Palescandolo, E., Van Hummelen, P., Ducar, M.D. and Raza, A., 2013. Genomic sequencing of meningiomas identifies oncogenic SMO and AKT1 mutations. *Nature genetics*, 45(3), pp.285-289.
- Bretag, A.H., 1987. Muscle chloride channels. *Physiological reviews*, 67(2), pp.618-724.
- Briscoe, J. and Théron, P.P., 2013. The mechanisms of Hedgehog signalling and its roles in development and disease. *Nature reviews Molecular cell biology*, 14(7), p.416.
- Brzozowski, J.S. and Skelding, K.A., 2019. The multi-functional calcium/calmodulin stimulated protein kinase (CaMK) family: emerging targets for anti-cancer therapeutic intervention. *Pharmaceuticals*, 12(1), p.8.
- Budhu, A.S. and Noy, N., 2002. Direct channeling of retinoic acid between cellular retinoic acid-binding protein II and retinoic acid receptor sensitizes mammary carcinoma cells to retinoic acid-induced growth arrest. *Molecular and cellular biology*, 22(8), pp.2632-2641.
- Buerki, R.A., Horbinski, C.M., Kruser, T., Horowitz, P.M., James, C.D. and Lukas, R.V., 2018. An overview of meningiomas. *Future Oncology*, 14(21), pp.2161-2177.
- Burandt, E., Lübbersmeyer, F., Gorbokon, N., Büscheck, F., Luebke, A.M., Menz, A., Kluth, M., Hube-Magg, C., Hinsch, A., Höflmayer, D. and Weidemann, S., 2021. E-Cadherin expression in human tumors: a tissue microarray study on 10,851 tumors. *Biomarker research*, 9(1), pp.1-17.

- Burghardt, I., Ventura, E., Weiss, T., Schroeder, J.J., Seystahl, K., Zielasek, C., Gramatzki, D. and Weller, M., 2021. Endoglin and TGF- $\beta$  signaling in glioblastoma. *Cell and tissue research*, 384(3), pp.613-624.
- Burnett, R.C., David, J.C., Harden, A.M., Le Beau, M.M., Rowley, J.D. and Diaz, M.O., 1991. The LCK Gene Is Involved in the t (1; 7) (p34; q34) in the T-Cell Acute Lymphoblastic Leukemia Derived Cell Line, HSB-2. *Genes, Chromosomes and Cancer*, 3(6), pp.461-467.
- Burris, H.3., Moore, M.J., Andersen, J., Green, M.R., Rothenberg, M.L., Modiano, M.R., Christine Cripps, M., Portenoy, R.K., Storniolo, A.M. and Tarassoff, P., 1997. Improvements in survival and clinical benefit with gemcitabine as first-line therapy for patients with advanced pancreas cancer: a randomized trial. *Journal of clinical oncology*, 15(6), pp.2403-2413.
- Cagney, D.N., Sul, J., Huang, R.Y., Ligon, K.L., Wen, P.Y. and Alexander, B.M., 2018. The FDA NIH Biomarkers, EndpointS, and other Tools (BEST) resource in neuro-oncology. *Neuro-oncology*, 20(9), pp.1162-1172.
- Calmon, M.F., Rodrigues, R.V., Kaneto, C.M., Moura, R.P., Silva, S.D., Mota, L.D.C., Pinheiro, D.G., Torres, C., De Carvalho, A.F., Cury, P.M. and Nunes, F.D., 2009. Epigenetic silencing of CRABP2 and MX1 in head and neck tumors. *Neoplasia*, 11(12), pp.1329-IN9.
- Caltabiano, R., Barbagallo, G.M., Castaing, M., Cassenti, A., Senetta, R., Cassoni, P., Albanese, V. and Lanzafame, S., 2013. Prognostic value of EGFR expression in de novo and progressed atypical and anaplastic meningiomas: an immunohistochemical and fluorescence in situ hybridization pilot study. *J Neurosurg Sci*, 57(2), pp.139-51.
- Campos, B., Warta, R., Chaisaingmongkol, J., Geiselhart, L., Popanda, O., Hartmann, C., Von Deimling, A., Unterberg, A., Plass, C., Schmezer, P. and Herold-Mende, C., 2012. Epigenetically mediated downregulation of the differentiation-promoting chaperon protein CRABP2 in astrocytic gliomas. *International journal of cancer*, 131(8), pp.1963-1968.
- Carafa, V., Rotili, D., Forgione, M., Cuomo, F., Serrettiello, E., Hailu, G.S., Jarho, E., Lahtela-Kakkonen, M., Mai, A. and Altucci, L., 2016. Sirtuin functions and modulation: from chemistry to the clinic. *Clinical epigenetics*, 8(1), pp.1-21.
- Carpten, J.D., Faber, A.L., Horn, C., Donoho, G.P., Briggs, S.L., Robbins, C.M., Hostetter, G., Boguslawski, S., Moses, T.Y., Savage, S. and Uhlik, M., 2007. A transforming mutation in the pleckstrin homology domain of AKT1 in cancer. *Nature*, 448(7152), p.439.
- Castonguay, R., Werner, E.D., Matthews, R.G., Presman, E., Mulivor, A.W., Solban, N., Sako, D., Pearsall, R.S., Underwood, K.W., Seehra, J. and Kumar, R., 2011. Soluble endoglin specifically binds bone morphogenetic proteins 9 and 10 via its orphan domain, inhibits blood vessel formation, and suppresses tumor growth. *Journal of Biological Chemistry*, 286(34), pp.30034-30046.
- Cazaubon, S., Bornancin, F. and Parker, P.J., 1994. Threonine-497 is a critical site for permissive activation of protein kinase  $\alpha$ . *Biochemical Journal*, 301(2), pp.443-448.
- Celay, J., Lozano, T., Concepcion, A.R., Beltrán, E., Rudilla, F., García-Barchino, M.J., Robles, E.F., Rabal, O., de Miguel, I., Panizo, C. and Casares, N., 2018. Targeting the anion exchanger 2 with specific peptides as a new therapeutic approach in B lymphoid neoplasms. *Haematologica*, 103(6), p.1065.
- Chamberlain, M.C. and Barnholtz-Sloan, J.S., 2011. Medical treatment of recurrent meningiomas. *Expert review of neurotherapeutics*, 11(10), pp.1425-1432.

- Chamberlain, M.C. and Johnston, S.K., 2011. Hydroxyurea for recurrent surgery and radiation refractory meningioma: a retrospective case series. *Journal of neuro-oncology*, 104(3), pp.765-771.
- Chambon, P., 1996. A decade of molecular biology of retinoic acid receptors. *The FASEB journal*, 10(9), pp.940-954.
- Chambrion, C. and Le Naour, F., 2010. The tetraspanins CD9 and CD81 regulate CD9P1-induced effects on cell migration. *PloS one*, 5(6), p.e11219.
- Chapman, P.B., Hauschild, A., Robert, C., Haanen, J.B., Ascierto, P., Larkin, J., Dummer, R., Garbe, C., Testori, A., Maio, M. and Hogg, D., 2011. Improved survival with vemurafenib in melanoma with BRAF V600E mutation. *New England Journal of Medicine*, 364(26), pp.2507-2516.
- Charras, G. and Sahai, E., 2014. Physical influences of the extracellular environment on cell migration. *Nature reviews Molecular cell biology*, 15(12), p.813.
- Cheetham, G.M., Knegt, R.M., Coll, J.T., Renwick, S.B., Swenson, L., Weber, P., Lippke, J.A. and Austen, D.A., 2002. Crystal structure of aurora-2, an oncogenic serine/threonine kinase. *Journal of Biological Chemistry*, 277(45), pp.42419-42422.
- Cheifetz, S., Bellón, T., Calés, C., Vera, S., Bernabeu, C., Massague, J. and Letarte, M., 1992. Endoglin is a component of the transforming growth factor-beta receptor system in human endothelial cells. *Journal of Biological Chemistry*, 267(27), pp.19027-19030.
- Chen, F., Xiang, C.X., Zhou, Y., Ao, X.S., Zhou, D.Q., Peng, P., Zhang, H.Q., Liu, H.D. and Huang, X., 2015. Gene expression profile for predicting survival of patients with meningioma. *International journal of oncology*, 46(2), pp.791-797.
- Chen, S., Crabill, G.A., Pritchard, T.S., McMiller, T.L., Wei, P., Pardoll, D.M., Pan, F. and Topalian, S.L., 2019. Mechanisms regulating PD-L1 expression on tumor and immune cells. *Journal for immunotherapy of cancer*, 7(1), pp.1-12.
- Chen, Y., Huang, L., Dong, Y., Tao, C., Zhang, R., Shao, H. and Shen, H., 2020. Effect of AKT1 (p. E17K) hotspot mutation on malignant tumorigenesis and prognosis. *Frontiers in Cell and Developmental Biology*, 8, p.573599.
- Chen, Y.C., Aguan, K., Yang, C.W., Wang, Y.T., Pal, N.R. and Chung, I.F., 2011. Discovery of protein phosphorylation motifs through exploratory data analysis. *PloS one*, 6(5), p.e20025.
- Chen, Y.C., Aguan, K., Yang, C.W., Wang, Y.T., Pal, N.R. and Chung, I.F., 2011. Discovery of protein phosphorylation motifs through exploratory data analysis. *PloS one*, 6(5), p.e20025.
- Cheung, M. and Testa, J.R., 2017. BAP1, a tumor suppressor gene driving malignant mesothelioma. *Translational lung cancer research*, 6(3), p.270.
- Chi, M., Evans, H., Gilchrist, J., Mayhew, J., Hoffman, A., Pearsall, E.A., Jankowski, H., Brzozowski, J.S. and Skelding, K.A., 2016. Phosphorylation of calcium/calmodulin-stimulated protein kinase II at T286 enhances invasion and migration of human breast cancer cells. *Scientific reports*, 6(1), pp.1-12.
- Chiambaretta, F., De Graeve, F., Turet, G., Marceau, G., Gain, P., Dastugue, B., Rigal, D. and Sapin, V., 2004. Cell and tissue specific expression of human Kruppel-like transcription factors in human ocular surface. *Mol Vis*, 10, pp.901-909.

- Chiba, M., Iizuka, M. and Masamune, O., 1988. Ubiquitous expression of HLA-DR antigens on human small intestinal epithelium. *Gastroenterologia Japonica*, 23(2), pp.109-116.
- Cho, S.H., Toouli, C.D., Fujii, G.H., Crain, C. and Parry, D., 2005. Chk1 is essential for tumor cell viability following activation of the replication checkpoint. *Cell cycle*, 4(1), pp.131-139.
- Christiansen, M.N., Chik, J., Lee, L., Anugraham, M., Abrahams, J.L. and Packer, N.H., 2014. Cell surface protein glycosylation in cancer. *Proteomics*, 14(4-5), pp.525-546.
- Chua, M.M., Ortega, C.E., Sheikh, A., Lee, M., Abdul-Rassoul, H., Hartshorn, K.L. and Dominguez, I., 2017. CK2 in cancer: cellular and biochemical mechanisms and potential therapeutic target. *Pharmaceuticals*, 10(1), p.18.
- Chueh, F.Y. and Yu, C.L., 2012. Engagement of T-cell antigen receptor and CD4/CD8 co-receptors induces prolonged STAT activation through autocrine/paracrine stimulation in human primary T cells. *Biochemical and biophysical research communications*, 426(2), pp.242-246.
- Cirak, Y., Furuncuoglu, Y., Yapicier, O., Aksu, A. and Cubukcu, E., 2015. Aurora A overexpression in breast cancer patients induces taxane resistance and results in worse prognosis. *J BUON*, 20(6), pp.1414-9.
- Clark, V.E., Erson-Omay, E.Z., Serin, A., Yin, J., Cotney, J., Özduman, K., Avşar, T., Li, J., Murray, P.B., Henegariu, O. and Yilmaz, S., 2013. Genomic analysis of non-NF2 meningiomas reveals mutations in TRAF7, KLF4, AKT1, and SMO. *Science*, 339(6123), pp.1077-1080.
- Clark, V.E., Harmanci, A.S., Bai, H., Youngblood, M.W., Lee, T.I., Baranoski, J.F., Ercan-Sencicek, A.G., Abraham, B.J., Weintraub, A.S., Hnisz, D. and Simon, M., 2016. Recurrent somatic mutations in POLR2A define a distinct subset of meningiomas. *Nature genetics*, 48(10), p.1253.
- Claus, E.B., Black, P.M., Bondy, M.L., Calvocoressi, L., Schildkraut, J.M., Wiemels, J.L. and Wrensch, M., 2007. Exogenous hormone use and meningioma risk: what do we tell our patients. *Cancer: Interdisciplinary International Journal of the American Cancer Society*, 110(3), pp.471-476.
- Claus, E.B., Calvocoressi, L., Bondy, M.L., Wrensch, M., Wiemels, J.L. and Schildkraut, J.M., 2013. Exogenous hormone use, reproductive factors, and risk of intracranial meningioma in females. *Journal of neurosurgery*, 118(3), pp.649-656.
- Claus, E.B., Cornish, A.J., Broderick, P., Schildkraut, J.M., Dobbins, S.E., Holroyd, A., Calvocoressi, L., Lu, L., Hansen, H.M., Smirnov, I. and Walsh, K.M., 2018. Genome-wide association analysis identifies a meningioma risk locus at 11p15.5. *Neuro-oncology*, 20(11), pp.1485-1493.
- Codreanu, S.G., Hoeksema, M.D., Slebos, R.J., Zimmerman, L.J., Rahman, S.J., Li, M., Chen, S.C., Chen, H., Eisenberg, R., Liebler, D.C. and Massion, P.P., 2017. Identification of proteomic features to distinguish benign pulmonary nodules from lung adenocarcinoma. *Journal of proteome research*, 16(9), pp.3266-3276.
- Cohen, G., Makranz, C., Spira, M., Kodama, T., Reichert, F. and Rotshenker, S., 2006. Non-PKC DAG/Phorbol-Ester receptor (s) inhibit complement receptor-3 and nPKC inhibit scavenger receptor-AI/II-mediated myelin phagocytosis but cPKC, PI3k, and PLC $\gamma$  activate myelin phagocytosis by both. *Glia*, 53(5), pp.538-550.

- Cohen, H., Ben-Hamo, R., Gidoni, M., Yitzhaki, I., Kozol, R., Zilberberg, A. and Efroni, S., 2014. Shift in GATA3 functions, and GATA3 mutations, control progression and clinical presentation in breast cancer. *Breast Cancer Research*, 16(6), pp.1-16.
- Colbran, R.J., Schworer, C.M., Hashimoto, Y., Fong, Y.L., Rich, D.P., Smith, M.K. and Soderling, T.R., 1989. Calcium/calmodulin-dependent protein kinase II. *Biochemical Journal*, 258(2), p.313.
- Coultrap, S.J., Buard, I., Kulbe, J.R., Dell'Acqua, M.L. and Bayer, K.U., 2010. CaMKII autonomy is substrate-dependent and further stimulated by Ca<sup>2+</sup>/calmodulin. *Journal of Biological Chemistry*, 285(23), pp.17930-17937.
- Courtney, A.H., Lo, W.L. and Weiss, A., 2018. TCR signaling: mechanisms of initiation and propagation. *Trends in biochemical sciences*, 43(2), pp.108-123.
- Crosio, C., Fimia, G.M., Loury, R., Kimura, M., Okano, Y., Zhou, H., Sen, S., Allis, C.D. and Sassone-Corsi, P., 2002. Mitotic phosphorylation of histone H3: spatio-temporal regulation by mammalian Aurora kinases. *Molecular and cellular biology*, 22(3), pp.874-885.
- Cui, G.Q., Jiao, A.H., Xiu, C.M., Wang, Y.B., Sun, P., Zhang, L.M. and Li, X.G., 2014. Proteomic analysis of meningiomas. *Acta Neurologica Belgica*, 114(3), pp.187-194.
- Curto, M., Cole, B.K., Lallemand, D., Liu, C.H. and McClatchey, A.I., 2007. Contact-dependent inhibition of EGFR signaling by Nf2/Merlin. *J Cell Biol*, 177(5), pp.893-903.
- Dalan, A.B., Gulluoglu, S., Tuysuz, E.C., Kuskucu, A., Yaltirik, C.K., Ozturk, O., Ture, U. and Bayrak, O.F., 2017. Simultaneous analysis of miRNA-mRNA in human meningiomas by integrating transcriptome: A relationship between PTX3 and miR-29c. *BMC cancer*, 17(1), pp.1-9.
- David, L., Mallet, C., Mazerbourg, S., Feige, J.J. and Bailly, S., 2007. Identification of BMP9 and BMP10 as functional activators of the orphan activin receptor-like kinase 1 (ALK1) in endothelial cells. *Blood*, 109(5), pp.1953-1961.
- Davidson, B., Nymoen, D.A., Elgaaen, B.V., Staff, A.C., Tropé, C.G., Kærn, J., Reich, R. and Falkenthal, T.E.H., 2014. BUB1 mRNA is significantly co-expressed with AURKA and AURKB mRNA in advanced-stage ovarian serous carcinoma. *Virchows Archiv*, 464(6), pp.701-707.
- De Matos, L.L., Trufelli, D.C., De Matos, M.G.L. and da Silva Pinhal, M.A., 2010. Immunohistochemistry as an important tool in biomarkers detection and clinical practice. *Biomarker insights*, 5, pp.BMI-S2185.
- DeBerardinis, R.J. and Chandel, N.S., 2020. We need to talk about the Warburg effect. *Nature metabolism*, 2(2), pp.127-129.
- DeBerardinis, R.J. and Cheng, T., 2010. Q's next: the diverse functions of glutamine in metabolism, cell biology and cancer. *Oncogene*, 29(3), pp.313-324.
- DeBerardinis, R.J., Lum, J.J., Hatzivassiliou, G. and Thompson, C.B., 2008. The biology of cancer: metabolic reprogramming fuels cell growth and proliferation. *Cell metabolism*, 7(1), pp.11-20.
- Delva, L., Bastie, J.N., Rochette-Egly, C., Kraïba, R., Balitrand, N., Despouy, G., Chambon, P. and Chomienne, C., 1999. Physical and functional interactions between cellular retinoic acid

binding protein II and the retinoic acid-dependent nuclear complex. *Molecular and cellular biology*, 19(10), pp.7158-7167.

Deracinois, B., Flahaut, C., Duban-Deweer, S. and Karamanos, Y., 2013. Comparative and quantitative global proteomics approaches: an overview. *Proteomes*, 1(3), pp.180-218.

Desvergne, B., Michalik, L. and Wahli, W., 2006. Transcriptional regulation of metabolism. *Physiological reviews*, 86(2), pp.465-514.

Di Chen, X.Z., Sui, Z., Niu, H., Chen, L., Hu, C., Xuan, Q., Hou, X., Zhang, R., Zhou, L., Li, Y. and Yuan, H., 2020. A multi-omics investigation of the molecular characteristics and classification of six metabolic syndrome relevant diseases. *Theranostics*, 10(5), p.2029.

Di Maira, G., Salvi, M., Arrigoni, G., Marin, O., Sarno, S., Brustolon, F., Pinna, L.A. and Ruzzene, M., 2005. Protein kinase CK2 phosphorylates and upregulates Akt/PKB. *Cell Death & Differentiation*, 12(6), pp.668-677.

Di Paolo, V., Russo, I., Boldrini, R., Ravà, L., Pezzullo, M., Benedetti, M.C., Galardi, A., Colletti, M., Rota, R., Orlando, D. and Crocoli, A., 2018. Evaluation of Endoglin (CD105) expression in pediatric rhabdomyosarcoma. *BMC cancer*, 18(1), pp.1-11.

Dieplinger, B., Schiefermeier, N., Juchum-Pasquazzo, M., Gstir, R., Huber, L.A., Klimaschewski, L. and Vietor, I., 2007. The transcriptional corepressor TPA-inducible sequence 7 regulates adult axon growth through cellular retinoic acid binding protein II expression. *European Journal of Neuroscience*, 26(12), pp.3358-3367.

Di-Poi, N., Michalik, L., Tan, N.S., Desvergne, B. and Wahli, W., 2003. The anti-apoptotic role of PPAR $\beta$  contributes to efficient skin wound healing. *The Journal of steroid biochemistry and molecular biology*, 85(2-5), pp.257-265.

Di-Poi, N., Tan, N.S., Michalik, L., Wahli, W. and Desvergne, B., 2002. Antiapoptotic role of PPAR $\beta$  in keratinocytes via transcriptional control of the Akt1 signaling pathway. *Molecular cell*, 10(4), pp.721-733.

Diviani, D. and Scott, J.D., 2001. AKAP signaling complexes at the cytoskeleton. *Journal of cell science*, 114(8), pp.1431-1437.

Dobbins, S.E., Broderick, P., Melin, B., Feychting, M., Johansen, C., Andersson, U., Brännström, T., Schramm, J., Olver, B., Lloyd, A. and Ma, Y.P., 2011. Common variation at 10p12.31 near MLLT10 influences meningioma risk. *Nature genetics*, 43(9), pp.825-827.

Domingues, P.H., Sousa, P., Otero, A., Gonçalves, J.M., Ruiz, L., de Oliveira, C., Lopes, M.C., Orfao, A. and Tabertero, M.D., 2014. Proposal for a new risk stratification classification for meningioma based on patient age, WHO tumor grade, size, localization, and karyotype. *Neuro-oncology*, 16(5), pp.735-747.

Dominguez, I., Mizuno, J., Wu, H., Imbrie, G.A., Symes, K. and Seldin, D.C., 2005. A role for CK2 $\alpha/\beta$  in *Xenopus* early embryonic development. *Molecular and cellular biochemistry*, 274(1), pp.125-131.

Dominguez, I., Sonenshein, G.E. and Seldin, D.C., 2009. Protein Kinase CK2 in Health and Disease. *Cellular and Molecular Life Sciences*, 66(11), pp.1850-1857.



Donato, L.J. and Noy, N., 2005. Suppression of mammary carcinoma growth by retinoic acid: proapoptotic genes are targets for retinoic acid receptor and cellular retinoic acid-binding protein II signaling. *Cancer research*, 65(18), pp.8193-8199.

Donato, L.J., Suh, J.H. and Noy, N., 2007. Suppression of mammary carcinoma cell growth by retinoic acid: the cell cycle control gene Btg2 is a direct target for retinoic acid receptor signaling. *Cancer research*, 67(2), pp.609-615.

Dong, D., Ruuska, S.E., Levinthal, D.J. and Noy, N., 1999. Distinct roles for cellular retinoic acid-binding proteins I and II in regulating signaling by retinoic acid. *Journal of Biological Chemistry*, 274(34), pp.23695-23698.

Dong, W., Wu, X., Ma, S., Wang, Y., Nalin, A.P., Zhu, Z., Zhang, J., Benson, D.M., He, K., Caligiuri, M.A. and Yu, J., 2019. The mechanism of Anti-PD-L1 antibody efficacy against PD-L1-Negative tumors identifies NK cells expressing PD-L1 as a cytolytic effector. *Cancer discovery*, 9(10), pp.1422-1437.

Dos Santos Dias, A.I.B., Fachin, C.G., Avó, L.R.S., Frazão, C.V.G., Caran, E.M.M., Schettini, S.T., Alves, M.T.S., Ribeiro, R.C. and Abib, S.D.C.V., 2015. Correlation between selected angiogenic markers and prognosis in pediatric adrenocortical tumors: Angiogenic markers and prognosis in pediatric ACTs. *Journal of Pediatric Surgery*, 50(8), pp.1323-1328.

Downward, J., Parker, P. and Waterfield, M.D., 1984. Autophosphorylation sites on the epidermal growth factor receptor. *Nature*, 311(5985), pp.483-485.

Dozynkiewicz, M.A., Jamieson, N.B., MacPherson, I., Grindlay, J., van den Berghe, P.V., von Thun, A., Morton, J.P., Gourley, C., Timpson, P., Nixon, C. and McKay, C.J., 2012. Rab25 and CLIC3 collaborate to promote integrin recycling from late endosomes/lysosomes and drive cancer progression. *Developmental cell*, 22(1), pp.131-145.

Drakos, S.S., Anifantaki, F., Zarros, A. and Liapi, C., 2010. The role of folate metabolism-related gene polymorphisms in the development of meningiomas. *Cancer Genomics & Proteomics*, 7(2), pp.105-109.

Du, R., Liu, B., Zhou, L., Wang, D., He, X., Xu, X., Zhang, L., Niu, C. and Liu, S., 2018. Downregulation of annexin A3 inhibits tumor metastasis and decreases drug resistance in breast cancer. *Cell death & disease*, 9(2), pp.1-11.

Du, Z., Abedalthagafi, M., Aizer, A.A., McHenry, A.R., Sun, H.H., Bray, M.A., Viramontes, O., Machaidze, R., Brastianos, P.K., Reardon, D.A. and Dunn, I.F., 2015. Increased expression of the immune modulatory molecule PD-L1 (CD274) in anaplastic meningioma. *Oncotarget*, 6(7), p.4704.

Dunn, I.F., Du, Z., Touat, M., Sisti, M.B., Wen, P.Y., Umeton, R., Dubuc, A.M., Ducar, M., Canoll, P.D., Severson, E. and Elvin, J.A., 2018. Mismatch repair deficiency in high-grade meningioma: a rare but recurrent event associated with dramatic immune activation and clinical response to PD-1 blockade. *JCO precision oncology*, 2.

Dunn, J., Ferluga, S., Sharma, V., Futschik, M., Hilton, D.A., Adams, C.L., Lasonder, E. and Hanemann, C.O., 2019. Proteomic analysis discovers the differential expression of novel proteins and phosphoproteins in meningioma including NEK9, HK2 and SET and deregulation of RNA metabolism. *EBioMedicine*, 40, pp.77-91.

- Dunn, J., Lenis, V.P., Hilton, D.A., Warta, R., Herold-Mende, C., Hanemann, C.O. and Futschik, M.E., 2020. Integration and comparison of transcriptomic and proteomic data for meningioma. *Cancers*, 12(11), p.3270.
- Eckel-Passow, J.E., Lachance, D.H., Molinaro, A.M., Walsh, K.M., Decker, P.A., Sicotte, H., Pekmezci, M., Rice, T., Kosel, M.L., Smirnov, I.V. and Sarkar, G., 2015. Glioma groups based on 1p/19q, IDH, and TERT promoter mutations in tumors. *New England Journal of Medicine*, 372(26), pp.2499-2508.
- Elbitar, S., Renard, M., Arnaud, P., Hanna, N., Jacob, M.P., Guo, D.C., Tsutsui, K., Gross, M.S., Kessler, K., Tosolini, L. and Dattilo, V., 2021. Pathogenic variants in THSD4, encoding the ADAMTS-like 6 protein, predispose to inherited thoracic aortic aneurysm. *Genetics in Medicine*, 23(1), pp.111-122.
- Eller, M.S., Muz, P. and Gilchrist, B.A., 1995. Regulation of CRABP II mRNA expression in human keratinocytes. *Experimental dermatology*, 4(2), pp.97-103.
- Elsberger, B., Fullerton, R., Zino, S., Jordan, F., Mitchell, T.J., Brunton, V.G., Mallon, E.A., Shiels, P.G. and Edwards, J., 2010. Breast cancer patients' clinical outcome measures are associated with Src kinase family member expression. *British journal of cancer*, 103(6), pp.899-909.
- Engholm-Keller, K., Waardenberg, A.J., Müller, J.A., Wark, J.R., Fernando, R.N., Arthur, J.W., Robinson, P.J., Dietrich, D., Schoch, S. and Graham, M.E., 2019. The temporal profile of activity-dependent presynaptic phospho-signalling reveals long-lasting patterns of poststimulus regulation. *PLoS biology*, 17(3), p.e3000170.
- Epstein, R.J. and Lin, F.P., 2017. Cancer and the omics revolution. *Australian Family Physician*, 46(4), pp.189-193.
- Esaulova, E., Artyomov, M. and Dunn, G.P., 2017. Genomic landscape of high-grade meningiomas.
- Esteban, F., Ruiz-Cabello, F., Concha, A., Pérez-Ayala, A., Sanchez-Rozas, J.A. and Garrido, F., 1990. HLA-DR expression is associated with excellent prognosis in squamous cell carcinoma of the larynx. *Clinical & experimental metastasis*, 8(4), pp.319-328.
- Estoppey, D., Schutzius, G., Kolter, C., Salathe, A., Wunderlin, T., Meyer, A., Nigsch, F., Bouwmeester, T., Hoepfner, D. and Kirkland, S., 2021. Genome-wide CRISPR-Cas9 screens identify mechanisms of BET bromodomain inhibitor sensitivity. *Iscience*, 24(11), p.103323.
- Evans, D.G.R., Salvador, H., Chang, V.Y., Erez, A., Voss, S.D., Schneider, K.W., Scott, H.S., Plon, S.E. and Tabori, U., 2017. Cancer and central nervous system tumor surveillance in pediatric neurofibromatosis 1. *Clinical Cancer Research*, 23(12), pp.e46-e53.
- Everson, R.G., Hashimoto, Y., Freeman, J.L., Hodges, T.R., Huse, J., Zhou, S., Xiu, J., Spetzler, D., Sanai, N., Kim, L. and Kesari, S., 2018. Multiplatform profiling of meningioma provides molecular insight and prioritization of drug targets for rational clinical trial design. *Journal of neuro-oncology*, 139(2), pp.469-478.
- Falck, J., Mailand, N., Syljuåsen, R.G., Bartek, J. and Lukas, J., 2001. The ATM-Chk2-Cdc25A checkpoint pathway guards against radioresistant DNA synthesis. *Nature*, 410(6830), pp.842-847.

- Fan, X., Liang, J., Wu, Z., Shan, X., Qiao, H. and Jiang, T., 2017. Expression of HLA-DR genes in gliomas: correlation with clinicopathological features and prognosis. *Chinese Neurosurgical Journal*, 3(03), pp.154-162.
- Fathi, A.R. and Roelcke, U., 2013. Meningioma. *Current neurology and neuroscience reports*, 13(4), p.337.
- Fawcett, D., Pasceri, P., Fraser, R., Colbert, M., Rossant, J. and Giguère, V., 1995. Postaxial polydactyly in forelimbs of CRABP-II mutant mice. *Development*, 121(3), pp.671-679.
- FDA-NIH Biomarker Working Group, BEST (Biomarkers, EndpointS, and other Tools) Resource. Maryland: Food and Drug Administration-National Institutes of Health Biomarker Working Group 2016.
- Feist, P. and Hummon, A.B., 2015. Proteomic challenges: sample preparation techniques for microgram-quantity protein analysis from biological samples. *International journal of molecular sciences*, 16(2), pp.3537-3563.
- Feske, S., Skolnik, E.Y. and Prakriya, M., 2012. Ion channels and transporters in lymphocyte function and immunity. *Nature Reviews Immunology*, 12(7), pp.532-547.
- Finley, L.W., Haas, W., Desquiret-Dumas, V., Wallace, D.C., Procaccio, V., Gygi, S.P. and Haigis, M.C., 2011. Succinate dehydrogenase is a direct target of sirtuin 3 deacetylase activity. *PloS one*, 6(8), p.e23295.
- Fischer-Huchzermeyer, S., Dombrowski, A., Hagel, C., Mautner, V.F., Schittenhelm, J. and Harder, A., 2017. The cellular retinoic acid binding protein 2 promotes survival of malignant peripheral nerve sheath tumor cells. *The American journal of pathology*, 187(7), pp.1623-1632.
- Flint-Richter, P., Mandelzweig, L., Oberman, B. and Sadetzki, S., 2011. Possible interaction between ionizing radiation, smoking, and gender in the causation of meningioma. *Neuro-oncology*, 13(3), pp.345-352.
- Fong, Y.L., Taylor, W.L., Means, A.R. and Soderling, T.R., 1989. Studies of the regulatory mechanism of Ca<sup>2+</sup>/calmodulin-dependent protein kinase II: mutation of threonine 286 to alanine and aspartate. *Journal of Biological Chemistry*, 264(28), pp.16759-16763.
- Fouladi, M., Perentesis, J.P., Phillips, C.L., Leary, S., Reid, J.M., McGovern, R.M., Ingle, A.M., Ahern, C.H., Ames, M.M., Houghton, P. and Doyle, L.A., 2014. A phase I trial of MK-2206 in children with refractory malignancies: a Children's Oncology Group study. *Pediatric blood & cancer*, 61(7), pp.1246-1251.
- Fujiwara, K., Ohuchida, K., Ohtsuka, T., Mizumoto, K., Shindo, K., Ikenaga, N., Cui, L., Takahata, S., Aishima, S. and Tanaka, M., 2013. Migratory activity of CD105+ pancreatic cancer cells is strongly enhanced by pancreatic stellate cells. *Pancreas*, 42(8), pp.1283-1290.
- Gao, F., Shi, L., Russin, J., Zeng, L., Chang, X., He, S., Chen, T.C., Giannotta, S.L., Weisenberger, D.J., Zada, G. and Mack, W.J., 2013. DNA methylation in the malignant transformation of meningiomas. *PloS one*, 8(1), p.e54114.
- Gao, P.T., Cheng, J.W., Gong, Z.J., Hu, B., Sun, Y.F., Cao, Y., Qiu, S.J., Zhou, J., Fan, J. and Yang, X.R., 2017. Low SLC29A1 expression is associated with poor prognosis in patients with hepatocellular carcinoma. *American journal of cancer research*, 7(12), p.2465.
- Gawenis, L.R., Ledoussal, C., Judd, L.M., Prasad, V., Alper, S.L., Stuart-Tilley, A., Woo, A.L., Grisham, C., Sanford, L.P., Doetschman, T. and Miller, M.L., 2004. Mice with a targeted

disruption of the AE2 Cl<sup>-</sup>/HCO<sub>3</sub><sup>-</sup> exchanger are achlorhydric. *Journal of Biological Chemistry*, 279(29), pp.30531-30539.

Geiger, T., Madden, S.F., Gallagher, W.M., Cox, J. and Mann, M., 2012. Proteomic portrait of human breast cancer progression identifies novel prognostic markers. *Cancer research*, 72(9), pp.2428-2439.

Gerber, D.E., Grossman, S.A., Zeltzman, M., Parisi, M.A. and Kleinberg, L., 2007. The impact of thrombocytopenia from temozolomide and radiation in newly diagnosed adults with high-grade gliomas. *Neuro-oncology*, 9(1), pp.47-52.

Gerke, V. and Moss, S.E., 2002. Annexins: from structure to function. *Physiological reviews*, 82(2), pp.331-371.

Ghaleb, A.M. and Yang, V.W., 2017. Krüppel-like factor 4 (KLF4): what we currently know. *Gene*, 611, pp.27-37.

Ghavidel, A. and Schultz, M.C., 2001. TATA binding protein-associated CK2 transduces DNA damage signals to the RNA polymerase III transcriptional machinery. *Cell*, 106(5), pp.575-584.

Ghosh, R., Gilda, J.E. and Gomes, A.V., 2014. The necessity of and strategies for improving confidence in the accuracy of western blots. *Expert review of proteomics*, 11(5), pp.549-560.

Giles, A.J., Hao, S., Padget, M., Song, H., Zhang, W., Lynes, J., Sanchez, V., Liu, Y., Jung, J., Cao, X. and Fujii, R., 2019. Efficient ADCC killing of meningioma by avelumab and a high-affinity natural killer cell line, haNK. *JCI insight*, 4(20).

Gnad, F., Gunawardena, J. and Mann, M., 2010. PHOSIDA 2011: the posttranslational modification database. *Nucleic acids research*, 39(suppl\_1), pp.D253-D260.

Goldbrunner, R., Stavrinou, P., Jenkinson, M.D., Sahm, F., Mawrin, C., Weber, D.C., Preusser, M., Minniti, G., Lund-Johansen, M., Lefranc, F. and Houdart, E., 2021. EANO guideline on the diagnosis and management of meningiomas. *Neuro-oncology*, 23(11), pp.1821-1834.

Gonzalez de Castro, D., Clarke, P.A., Al-Lazikani, B. and Workman, P., 2013. Personalized cancer medicine: molecular diagnostics, predictive biomarkers, and drug resistance. *Clinical Pharmacology & Therapeutics*, 93(3), pp.252-259.

González Muñoz, T., Amaral, A.T., Puerto-Camacho, P., Peinado, H. and de Álava, E., 2021. Endoglin in the Spotlight to Treat Cancer. *International Journal of Molecular Sciences*, 22(6), p.3186.

Goodwin, J.W., Crowley, J., Eyre, H.J., Stafford, B., Jaeckle, K.A. and Townsend, J.J., 1993. A phase II evaluation of tamoxifen in unresectable or refractory meningiomas: a Southwest Oncology Group study. *Journal of neuro-oncology*, 15(1), pp.75-77.

Gorgoulis, V.G., Vassiliou, L.V.F., Karakaidos, P., Zacharatos, P., Kotsinas, A., Liloglou, T., Venere, M., DiTullio, R.A., Kastriakis, N.G., Levy, B. and Kletsas, D., 2005. Activation of the DNA damage checkpoint and genomic instability in human precancerous lesions. *Nature*, 434(7035), pp.907-913.

Gottlob, K., Majewski, N., Kennedy, S., Kandel, E., Robey, R.B. and Hay, N., 2001. Inhibition of early apoptotic events by Akt/PKB is dependent on the first committed step of glycolysis and mitochondrial hexokinase. *Genes & development*, 15(11), pp.1406-1418.

- Götz, C. and Montenarh, M., 2017. Protein kinase CK2 in development and differentiation. *Biomedical reports*, 6(2), pp.127-133.
- Gougos, A. and Letarte, M., 1990. Primary structure of endoglin, an RGD-containing glycoprotein of human endothelial cells. *Journal of Biological Chemistry*, 265(15), pp.8361-8364.
- Goulart, B.H., Martins, R.G. and Lynch, T.J., 2001. Twenty-two years of phase III trials for patients with advanced non-small-cell lung cancer: sobering results. *Journal of Clinical Oncology: Official Journal of the American Society of Clinical Oncology*, 19(20), pp.4089-4089.
- Goutagny, S., Yang, H.W., Zucman-Rossi, J., Chan, J., Dreyfuss, J.M., Park, P.J., Black, P.M., Giovannini, M., Carroll, R.S. and Kalamirides, M., 2010. Genomic profiling reveals alternative genetic pathways of meningioma malignant progression dependent on the underlying NF2 status. *Clinical cancer research*, 16(16), pp.4155-4164.
- Graves, P.R. and Haystead, T.A., 2002. Molecular biologist's guide to proteomics. *Microbiology and molecular biology reviews*, 66(1), pp.39-63.
- Grunberg, S.M., Weiss, M.H., Russell, C.A., Spitz, I.M., Ahmadi, J., Sadun, A. and Sitruk-Ware, R., 2006. Long-term administration of mifepristone (RU486): clinical tolerance during extended treatment of meningioma. *Cancer investigation*, 24(8), pp.727-733.
- Grunberg, S.M., Weiss, M.H., Spitz, I.M., Ahmadi, J., Sadun, A., Russell, C.A., Lucci, L. and Stevenson, L.L., 1991. Treatment of unresectable meningiomas with the antiprogestosterone agent mifepristone. *Journal of neurosurgery*, 74(6), pp.861-866.
- Guang, M.H.Z., McCann, A., Bianchi, G., Zhang, L., Dowling, P., Bazou, D., O’Gorman, P. and Anderson, K.C., 2018. Overcoming multiple myeloma drug resistance in the era of cancer ‘omics’. *Leukemia & lymphoma*, 59(3), pp.542-561.
- Guerra, B. and Issinger, O.G., 1999. Protein kinase CK2 and its role in cellular proliferation, development and pathology. *ELECTROPHORESIS: An International Journal*, 20(2), pp.391-408.
- Guerrero-Esteo, M., Sánchez-Elsner, T., Letamendia, A. and Bernabéu, C., 2002. Extracellular and cytoplasmic domains of endoglin interact with the transforming growth factor- $\beta$  receptors I and II. *Journal of Biological Chemistry*, 277(32), pp.29197-29209.
- Guilford, P., 1999. E-cadherin downregulation in cancer: fuel on the fire. *Molecular medicine today*, 5(4), pp.172-177.
- Guilmain, W., Colin, S., Legrand, E., Vannier, J.P., Steverlynck, C., Bongaerts, M., Vasse, M. and Al-Mahmood, S., 2011. CD9P-1 expression correlates with the metastatic status of lung cancer, and a truncated form of CD9P-1, GS-168AT2, inhibits in vivo tumour growth. *British journal of cancer*, 104(3), pp.496-504.
- Gupta, A., Williams, B.R., Hanash, S.M. and Rawwas, J., 2006. Cellular Retinoic Acid–Binding Protein II Is a Direct Transcriptional Target of MycN in Neuroblastoma. *Cancer research*, 66(16), pp.8100-8108.
- Gupta, S., Bi, W.L. and Dunn, I.F., 2018. Medical management of meningioma in the era of precision medicine. *Neurosurgical Focus*, 44(4), p.E3.

- Gygi, S.P., Rochon, Y., Franza, B.R. and Aebersold, R., 1999. Correlation between protein and mRNA abundance in yeast. *Molecular and cellular biology*, 19(3), pp.1720-1730.
- Gysin, S. and Imber, R., 1996. Replacement of Ser657 of Protein Kinase C- $\alpha$  by Alanine Leads to Premature Down Regulation After Phorbol-Ester-Induced Translocation to the Membrane. *European journal of biochemistry*, 240(3), pp.747-750.
- Habela, C.W., Olsen, M.L. and Sontheimer, H., 2008. CLC3 is a critical regulator of the cell cycle in normal and malignant glial cells. *Journal of Neuroscience*, 28(37), pp.9205-9217.
- Han, S.S., Kim, W.J., Hong, Y., Hong, S.H., Lee, S.J., Ryu, D.R., Lee, W., Cho, Y.H., Lee, S., Ryu, Y.J. and Won, J.Y., 2014. RNA sequencing identifies novel markers of non-small cell lung cancer. *Lung Cancer*, 84(3), pp.229-235.
- Hao, S., Huang, G., Feng, J., Li, D., Wang, K., Wang, L., Wu, Z., Wan, H., Zhang, L. and Zhang, J., 2019. Non-NF2 mutations have a key effect on inhibitory immune checkpoints and tumor pathogenesis in skull base meningiomas. *Journal of Neuro-Oncology*, 144(1), pp.11-20.
- Hara, H., 2012. Endoglin (CD105) and claudin-5 expression in cutaneous angiosarcoma. *The American Journal of Dermatopathology*, 34(7), pp.779-782.
- Harding, M.A. and Theodorescu, D., 2010. RhoGDI signaling provides targets for cancer therapy. *European journal of cancer*, 46(7), pp.1252-1259.
- Harper, J.W. and Elledge, S.J., 2007. The DNA damage response: ten years after. *Molecular cell*, 28(5), pp.739-745.
- Havenga, M.J.E., Bosman, G.J.C.G.M., Appelhans, H. and De Grip, W.J., 1994. Expression of the anion exchanger (AE) gene family in human brain. Identification of a new AE protein: AE0. *Molecular brain research*, 25(1-2), pp.97-104.
- He, C., Holme, J. and Anthony, J., 2014. SNP genotyping: the KASP assay. In *Crop Breeding* (pp. 75-86). Humana Press, New York, NY.
- He, S., Pham, M.H., Pease, M., Zada, G., Giannotta, S.L., Wang, K. and Mack, W.J., 2013. A review of epigenetic and gene expression alterations associated with intracranial meningiomas. *Neurosurgical focus*, 35(6), p.E5.
- Hell, J.W., 2014. CaMKII: claiming center stage in postsynaptic function and organization. *Neuron*, 81(2), pp.249-265.
- Heo, Y.J., Hwa, C., Lee, G.H., Park, J.M. and An, J.Y., 2021. Integrative Multi-Omics Approaches in Cancer Research: From Biological Networks to Clinical Subtypes. *Molecules and cells*, 44(7), p.433.
- Hernandez-Fernaund, J.R., Ruengeler, E., Casazza, A., Neilson, L.J., Pulleine, E., Santi, A., Ismail, S., Lilla, S., Dhayade, S., MacPherson, I.R. and McNeish, I., 2017. Secreted CLIC3 drives cancer progression through its glutathione-dependent oxidoreductase activity. *Nature communications*, 8(1), pp.1-17.
- Hilton, D.A., Shivane, A., Kirk, L., Bassiri, K., Enki, D.G. and Hanemann, C.O., 2016. Activation of multiple growth factor signalling pathways is frequent in meningiomas. *Neuropathology*, 36(3), pp.250-261.

- Hirao, A., Kong, Y.Y., Matsuoka, S., Wakeham, A., Ruland, J., Yoshida, H., Liu, D., Elledge, S.J. and Mak, T.W., 2000. DNA damage-induced activation of p53 by the checkpoint kinase Chk2. *Science*, 287(5459), pp.1824-1827.
- Hoffmann, E.K. and Dunham, P.B., 1995. Membrane mechanisms and intracellular signalling in cell volume regulation. *International review of cytology*, 161, pp.173-262.
- Hofmann, A., Raguénès-Nicol, C., Favier-Perron, B., Mesonero, J., Huber, R., Russo-Marie, F. and Lewit-Bentley, A., 2000. The Annexin A3– Membrane Interaction Is Modulated by an N-Terminal Tryptophan. *Biochemistry*, 39(26), pp.7712-7721.
- Holappa, K., Suokas, M., Soinen, P. and Kellokumpu, S., 2001. Identification of the full-length AE2 (AE2a) isoform as the Golgi-associated anion exchanger in fibroblasts. *Journal of Histochemistry & Cytochemistry*, 49(2), pp.259-269.
- Honda, H., Takamura, M., Yamagiwa, S., Genda, T., Horigome, R., Kimura, N., Setsu, T., Tominaga, K., Kamimura, H., Matsuda, Y. and Wakai, T., 2017. Overexpression of a disintegrin and metalloproteinase 21 is associated with motility, metastasis, and poor prognosis in hepatocellular carcinoma. *Scientific reports*, 7(1), pp.1-10.
- Hong, J., Hu, K., Yuan, Y., Sang, Y., Bu, Q., Chen, G., Yang, L., Li, B., Huang, P., Chen, D. and Liang, Y., 2012. CHK1 targets spleen tyrosine kinase (L) for proteolysis in hepatocellular carcinoma. *The Journal of clinical investigation*, 122(6), pp.2165-2175.
- Honma, K., Nakanishi, R., Nakanoko, T., Ando, K., Saeki, H., Oki, E., Iimori, M., Kitao, H., Kakeji, Y. and Maehara, Y., 2014. Contribution of Aurora-A and-B expression to DNA aneuploidy in gastric cancers. *Surgery today*, 44(3), pp.454-461.
- Horgan, R.P. and Kenny, L.C., 2011. ‘Omic’ technologies: genomics, transcriptomics, proteomics and metabolomics. *The Obstetrician & Gynaecologist*, 13(3), pp.189-195.
- Hosking, F.J., Feldman, D., Bruchim, R., Olver, B., Lloyd, A., Vijaykrishnan, J., Flint-Richter, P., Broderick, P., Houlston, R.S. and Sadetzki, S., 2011. Search for inherited susceptibility to radiation-associated meningioma by genomewide SNP linkage disequilibrium mapping. *British journal of cancer*, 104(6), pp.1049-1054.
- Hsu, A.H., Lum, M.A., Shim, K.S., Frederick, P.J., Morrison, C.D., Chen, B., Lele, S.M., Sheinin, Y.M., Daikoku, T., Dey, S.K. and Leone, G., 2018. Crosstalk between PKC $\alpha$  and PI3K/AKT signaling is tumor suppressive in the endometrium. *Cell reports*, 24(3), pp.655-669.
- Hsu, L.C., Chang, W.C., Shibuya, A. and Yoshida, A., 1992. Human stomach aldehyde dehydrogenase cDNA and genomic cloning, primary structure, and expression in *Escherichia coli*. *Journal of Biological Chemistry*, 267(5), pp.3030-3037.
- Hu, J., Guan, W., Liu, P., Dai, J., Tang, K., Xiao, H., Qian, Y., Sharrow, A.C., Ye, Z., Wu, L. and Xu, H., 2017. Endoglin is essential for the maintenance of self-renewal and chemoresistance in renal cancer stem cells. *Stem cell reports*, 9(2), pp.464-477.
- Huang, D.W., Sherman, B.T. and Lempicki, R.A., 2009. Systematic and integrative analysis of large gene lists using DAVID bioinformatics resources. *Nature protocols*, 4(1), pp.44-57.
- Huang, G., Lai, Y., Pan, X., Zhou, L., Quan, J., Zhao, L., Li, Z., Lin, C., Wang, J., Li, H. and Yuan, H., 2020. Tumor suppressor miR-33b-5p regulates cellular function and acts a prognostic biomarker in RCC. *American Journal of Translational Research*, 12(7), p.3346.

- Hubmacher, D. and Apte, S.S., 2015. ADAMTS proteins as modulators of microfibril formation and function. *Matrix Biology*, 47, pp.34-43.
- Hudmon, A. and Schulman, H., 2002. Structure–function of the multifunctional Ca<sup>2+</sup>/calmodulin-dependent protein kinase II. *Biochemical Journal*, 364(3), pp.593-611.
- Huiping, C., Sigurgeirsdottir, J.R., Jonasson, J.G., Eiriksdottir, G., Johannsdottir, J.T., Egilsson, V. and Ingvarsson, S., 1999. Chromosome alterations and E-cadherin gene mutations in human lobular breast cancer. *British journal of cancer*, 81(7), pp.1103-1110.
- Hunter, T., 2000. Signaling—2000 and beyond. *Cell*, 100(1), pp.113-127.
- Hunter, T., 2009. Tyrosine phosphorylation: thirty years and counting. *Current opinion in cell biology*, 21(2), pp.140-146.
- Huttlin, E.L., Jedrychowski, M.P., Elias, J.E., Goswami, T., Rad, R., Beausoleil, S.A., Villén, J., Haas, W., Sowa, M.E. and Gygi, S.P., 2010. A tissue-specific atlas of mouse protein phosphorylation and expression. *Cell*, 143(7), pp.1174-1189.
- Inoue, T., Hiratsuka, M., Osaki, M., Yamada, H., Kishimoto, I., Yamaguchi, S., Nakano, S., Katoh, M., Ito, H. and Oshimura, M., 2007. SIRT2, a tubulin deacetylase, acts to block the entry to chromosome condensation in response to mitotic stress. *Oncogene*, 26(7), pp.945-957.
- Iruela-Arispe, M.L., Liska, D.J., Sage, E.H. and Bornstein, P., 1993. Differential expression of thrombospondin 1, 2, and 3 during murine development. *Developmental Dynamics*, 197(1), pp.40-56.
- Isenberg, J.S., Ridnour, L.A., Perruccio, E.M., Espey, M.G., Wink, D.A. and Roberts, D.D., 2005. Thrombospondin-1 inhibits endothelial cell responses to nitric oxide in a cGMP-dependent manner. *Proceedings of the National Academy of Sciences*, 102(37), pp.13141-13146.
- Ito, Y., Miyauchi, A., Yoshida, H., Uruno, T., Nakano, K., Takamura, Y., Miya, A., Kobayashi, K., Yokozawa, T., Matsuzuka, F. and Taniguchi, N., 2003. Expression of  $\alpha$ 1, 6-fucosyltransferase (FUT8) in papillary carcinoma of the thyroid: its linkage to biological aggressiveness and anaplastic transformation. *Cancer letters*, 200(2), pp.167-172.
- Izquierdo-Garcia, J.L., Cai, L.M., Chaumeil, M.M., Eriksson, P., Robinson, A.E., Pieper, R.O., Phillips, J.J. and Ronen, S.M., 2014. Glioma cells with the IDH1 mutation modulate metabolic fractional flux through pyruvate carboxylase. *PloS one*, 9(9), p.e108289.
- Jenkinson, M.D., Santarius, T., Zadeh, G. and Aldape, K.D., 2016. Atypical meningioma—is it time to standardize surgical sampling techniques. *Neuro-oncology*, 19(3), pp.453-454.
- Jeong, S.G. and Cho, G.W., 2017. The tubulin deacetylase sirtuin-2 regulates neuronal differentiation through the ERK/CREB signaling pathway. *Biochemical and biophysical research communications*, 482(1), pp.182-187.
- Jia, H., Liu, Y., Xia, R., Tong, C., Yue, T., Jiang, J. and Jia, J., 2010. Casein kinase 2 promotes Hedgehog signaling by regulating both smoothed and Cubitus interruptus. *Journal Of Biological Chemistry*, 285(48), pp.37218-37226.
- Jiang, C., Ma, Z., Zhang, G., Yang, X., Du, Q. and Wang, W., 2019. CSNK2A1 promotes gastric cancer invasion through the PI3K-Akt-mTOR signaling pathway. *Cancer Management and Research*, 11, p.10135.



- Jiang, J.N., Hong, Q.Y., Gao, H.J., Lai, B.L., Lan, J.F. and Yang, Q., 2019. Lnc00908 promotes the development of ovarian cancer by regulating microRNA-495-5p. *Eur Rev Med Pharmacol Sci*, 23(4), pp.1388-1396.
- Jiang, X., Wang, J., Deng, X., Xiong, F., Ge, J., Xiang, B., Wu, X., Ma, J., Zhou, M., Li, X. and Li, Y., 2019. Role of the tumor microenvironment in PD-L1/PD-1-mediated tumor immune escape. *Molecular cancer*, 18(1), pp.1-17.
- Jing, E., Gesta, S. and Kahn, C.R., 2007. SIRT2 regulates adipocyte differentiation through FoxO1 acetylation/deacetylation. *Cell metabolism*, 6(2), pp.105-114.
- John, P., Waldt, N., Liebich, J., Kessler, C., Schnabel, S., Angenstein, F., Sandalcioglu, I.E., Scherlach, C., Sahm, F., Kirches, E. and Mawrin, C., 2022. AKT1E17K-mutated meningioma cell lines respond to treatment with the AKT inhibitor AZD5363. *Neuropathology and Applied Neurobiology*, 48(2), p.e12780.
- Johnson, J.L., Erickson, J.W. and Cerione, R.A., 2009. New insights into how the Rho guanine nucleotide dissociation inhibitor regulates the interaction of Cdc42 with membranes. *Journal of biological chemistry*, 284(35), pp.23860-23871.
- Johnson, M.D., Sade, B., Milano, M.T., Lee, J.H. and Toms, S.A., 2008. New prospects for management and treatment of inoperable and recurrent skull base meningiomas. *Journal of Neuro-oncology*, 86(1), pp.109-122.
- Jung, E.J., Moon, H.G., Park, S.T., Cho, B.I., Lee, S.M., Jeong, C.Y., Ju, Y.T., Jeong, S.H., Lee, Y.J., Choi, S.K. and Ha, W.S., 2010. Decreased annexin A3 expression correlates with tumor progression in papillary thyroid cancer. *PROTEOMICS–Clinical Applications*, 4(5), pp.528-537.
- Kaempchen, K., Mielke, K., Utermark, T., Langmesser, S. and Hanemann, C.O., 2003. Upregulation of the Rac1/JNK signaling pathway in primary human schwannoma cells. *Human molecular genetics*, 12(11), pp.1211-1221.
- Kalamarides, M., Stemmer-Rachamimov, A.O., Niwa-Kawakita, M., Chareyre, F., Taranchon, E., Han, Z.Y., Martinelli, C., Lusic, E.A., Hegedus, B., Gutmann, D.H. and Giovannini, M., 2011. Identification of a progenitor cell of origin capable of generating diverse meningioma histological subtypes. *Oncogene*, 30(20), pp.2333-2344.
- Kaley, T., Barani, I., Chamberlain, M., McDermott, M., Panageas, K., Raizer, J., Rogers, L., Schiff, D., Vogelbaum, M., Weber, D. and Wen, P., 2014. Historical benchmarks for medical therapy trials in surgery-and radiation-refractory meningioma: a RANO review. *Neuro-oncology*, 16(6), pp.829-840.
- Kang, H.G., Jenabi, J.M., Zhang, J., Keshelava, N., Shimada, H., May, W.A., Ng, T., Reynolds, C.P., Triche, T.J. and Sorensen, P.H., 2007. E-cadherin cell-cell adhesion in ewing tumor cells mediates suppression of anoikis through activation of the ErbB4 tyrosine kinase. *Cancer research*, 67(7), pp.3094-3105.
- Kang, S., Bader, A.G. and Vogt, P.K., 2005. Phosphatidylinositol 3-kinase mutations identified in human cancer are oncogenic. *Proceedings of the National Academy of Sciences*, 102(3), pp.802-807.
- Kantak, S.S. and Kramer, R.H., 1998. E-cadherin regulates anchorage-independent growth and survival in oral squamous cell carcinoma cells. *Journal of Biological Chemistry*, 273(27), pp.16953-16961.

- Karakas, B., Bachman, K.E. and Park, B.H., 2006. Mutation of the PIK3CA oncogene in human cancers. *British journal of cancer*, 94(4), p.455.
- Karhemo, P.R., Ravela, S., Laakso, M., Ritamo, I., Tatti, O., Mäkinen, S., Goodison, S., Stenman, U.H., Hölttä, E., Hautaniemi, S. and Valmu, L., 2012. An optimized isolation of biotinylated cell surface proteins reveals novel players in cancer metastasis. *Journal of proteomics*, 77, pp.87-100.
- Karimi, S., Mansouri, S., Nassiri, F., Bunda, S., Singh, O., Brastianos, P.K., Dunn, I.F. and Zadeh, G., 2021. Clinical significance of checkpoint regulator “Programmed death ligand-1 (PD-L1)” expression in meningioma: review of the current status. *Journal of Neuro-oncology*, 151(3), pp.443-449.
- Karlsson, R., Pedersen, E.D., Wang, Z. and Brakebusch, C., 2009. Rho GTPase function in tumorigenesis. *Biochimica et Biophysica Acta (BBA)-Reviews on Cancer*, 1796(2), pp.91-98.
- Karumanchi, S.A., Jiang, L., Knebelmann, B., Stuart-tilley, A.K., Alper, S.L. and Sukhatme, V.P., 2001. VHL tumor suppressor regulates Cl<sup>-</sup>/HCO<sub>3</sub><sup>-</sup> exchange and Na<sup>+</sup>/H<sup>+</sup> exchange activities in renal carcinoma cells. *Physiological Genomics*, 5(3), pp.119-128.
- Kask, K., Ruisu, K., Tikker, L., Karis, K., Saare, M., Meier, R., Karis, A., Tõnissoo, T. and Pooga, M., 2015. Deletion of RIC8A in neural precursor cells leads to altered neurogenesis and neonatal lethality of mouse. *Developmental Neurobiology*, 75(9), pp.984-1002.
- Katar, S., Baran, O., Evran, S., Cevik, S., Akkaya, E., Baran, G., Antar, V., Hanimoglu, H. and Kaynar, M.Y., 2017. Expression of miRNA-21, miRNA-107, miRNA-137 and miRNA-29b in meningioma. *Clinical neurology and neurosurgery*, 156, pp.66-70.
- Kato, Y., Ozawa, S., Miyamoto, C., Maehata, Y., Suzuki, A., Maeda, T. and Baba, Y., 2013. Acidic extracellular microenvironment and cancer. *Cancer cell international*, 13(1), pp.1-8.
- Katz, L.M., Hielscher, T., Liechty, B., Silverman, J., Zagzag, D., Sen, R., Wu, P., Golfinos, J.G., Reuss, D., Neidert, M.C. and Wirsching, H.G., 2018. Loss of histone H3K27me3 identifies a subset of meningiomas with increased risk of recurrence. *Acta neuropathologica*, 135(6), pp.955-963.
- Kauer, J., Schwartz, K., Tandler, C., Hinterleitner, C., Roerden, M., Jung, G., Salih, H.R., Heitmann, J.S. and Märklin, M., 2019. CD105 (Endoglin) as negative prognostic factor in AML. *Scientific reports*, 9(1), pp.1-11.
- Kavanagh, M.E., O’Sullivan, K.E., O’Hanlon, C., O’Sullivan, J.N., Lysaght, J. and Reynolds, J.V., 2014. The esophagitis to adenocarcinoma sequence; the role of inflammation. *Cancer letters*, 345(2), pp.182-189.
- Kemler, R., 1993. From cadherins to catenins: cytoplasmic protein interactions and regulation of cell adhesion. *Trends in genetics*, 9(9), pp.317-321.
- Khan, M.I., Czarnecka, A.M., Lewicki, S., Helbrecht, I., Brodaczewska, K., Koch, I., Zdanowski, R., Król, M. and Szczylik, C., 2016. Comparative gene expression profiling of primary and metastatic renal cell carcinoma stem cell-like cancer cells. *PLoS One*, 11(11), p.e0165718.
- Kia-Ki, H. and Martinage, A., 1992. Post-translational chemical modification (s) of proteins. *International journal of biochemistry*, 24(1), pp.19-28.

- Kiesel, V.A., Sheeley, M.P., Coleman, M.F., Cotul, E.K., Donkin, S.S., Hursting, S.D., Wendt, M.K. and Teegarden, D., 2021. Pyruvate carboxylase and cancer progression. *Cancer & metabolism*, 9(1), pp.1-13.
- Kim, D.J., Kim, W.J., Lim, M., Hong, Y., Lee, S.J., Hong, S.H., Heo, J., Lee, H.Y. and Han, S.S., 2018. Plasma CRABP2 as a novel biomarker in patients with non-small cell lung cancer. *Journal of Korean Medical Science*, 33(26).
- Kim, J., Kim, K.H. and Kim, Y.Z., 2017. The clinical outcome of hydroxyurea chemotherapy after incomplete resection of atypical meningiomas. *Brain tumor research and treatment*, 5(2), pp.77-86.
- Kim, J.Y., Jung, E.J., Park, H.J., Lee, J.H., Song, E.J., Kwag, S.J., Park, J.H., Park, T., Jeong, S.H., Jeong, C.Y. and Ju, Y.T., 2018. Tumor-suppressing effect of silencing of Annexin A3 expression in breast cancer. *Clinical Breast Cancer*, 18(4), pp.e713-e719.
- Kim, R.K., Yoon, C.H., Hyun, K.H., Lee, H., An, S., Park, M.J., Kim, M.J. and Lee, S.J., 2010. Role of lymphocyte-specific protein tyrosine kinase (LCK) in the expansion of glioma-initiating cells by fractionated radiation. *Biochemical and biophysical research communications*, 402(4), pp.631-636.
- Kim, R.K., Yoon, C.H., Hyun, K.H., Lee, H., An, S., Park, M.J., Kim, M.J. and Lee, S.J., 2010. Role of lymphocyte-specific protein tyrosine kinase (LCK) in the expansion of glioma-initiating cells by fractionated radiation. *Biochemical and biophysical research communications*, 402(4), pp.631-636.
- Kim, S.K., Kang, S., Kim, B.S., Kim, K.S. and Chung, J.H., 2008. Association between THSD4 Gene Polymorphisms and Hepatocellular Carcinoma in Korean Population.
- King, F.W., Skeen, J., Hay, N. and Shtivelman, E., 2004. Inhibition of Chk1 by activated PKB/Akt. *Cell Cycle*, 3(5), pp.632-635.
- Klaeboe, L., Lonn, S., Scheie, D., Auvinen, A., Christensen, H.C., Feychting, M., Johansen, C., Salminen, T. and Tynes, T., 2005. Incidence of intracranial meningiomas in Denmark, Finland, Norway and Sweden, 1968–1997. *International journal of cancer*, 117(6), pp.996-1001.
- Knowles, L.M., Zewe, J., Malik, G., Parwani, A.V., Gingrich, J.R. and Pilch, J., 2013. CLT1 targets bladder cancer through integrin  $\alpha 5\beta 1$  and CLIC3. *Molecular Cancer Research*, 11(2), pp.194-203.
- Koivunen, J., Aaltonen, V. and Peltonen, J., 2006. Protein kinase C (PKC) family in cancer progression. *Cancer letters*, 235(1), pp.1-10.
- Kokaji, E., Shimomura, A., Minamisaka, T., Nakajima, T., Miwa, S., Hatta, H., Nishida, T., Kiya, C. and Imura, J., 2018. Endoglin (CD105) and SMAD4 regulate spheroid formation and the suppression of the invasive ability of human pancreatic cancer cells. *International Journal of Oncology*, 52(3), pp.892-900.
- Kolch, W., Heidecker, G., Kochs, G., Hummel, R., Vahidi, H., Mischak, H., Finkenzeller, G., Marmé, D. and Rapp, U.R., 1993. Protein kinase C $\alpha$  activates RAF-1 by direct phosphorylation. *Nature*, 364(6434), pp.249-252.

- Koleva, R.I., Conley, B.A., Romero, D., Riley, K.S., Marto, J.A., Lux, A. and Vary, C.P., 2006. Endoglin structure and function: determinants of endoglin phosphorylation by transforming growth factor- $\beta$  receptors. *Journal of Biological Chemistry*, 281(35), pp.25110-25123.
- Kopito, R.R., 1990. Molecular biology of the anion exchanger gene family. *International review of cytology*, 123, pp.177-199.
- Kopito, R.R., Lee, B.S., Simmons, D.M., Lindsey, A.E., Morgans, C.W. and Schneider, K., 1989. Regulation of intracellular pH by a neuronal homolog of the erythrocyte anion exchanger. *Cell*, 59(5), pp.927-937.
- Kowalski, P.E. and Mager, D.L., 1998. A human endogenous retrovirus suppresses translation of an associated fusion transcript, PLA2L. *Journal of virology*, 72(7), pp.6164-6168.
- Kreutz, M., Fritsche, J., Andreesen, R. and Krause, S.W., 1998. Regulation of Cellular Retinoic Acid Binding Protein (CRABP II) during Human Monocyte Differentiation in Vitro. *Biochemical and biophysical research communications*, 248(3), pp.830-834.
- Kristensen, B.W., Priesterbach-Ackley, L.P., Petersen, J.K. and Wesseling, P., 2019. Molecular pathology of tumors of the central nervous system. *Annals of oncology*, 30(8), pp.1265-1278.
- Krzyszczuk, P., Acevedo, A., Davidoff, E.J., Timmins, L.M., Marrero-Berrios, I., Patel, M., White, C., Lowe, C., Sherba, J.J., Hartmanshenn, C. and O'Neill, K.M., 2018. The growing role of precision and personalized medicine for cancer treatment. *Technology*, 6(03n04), pp.79-100.
- Kuefer, R., Hofer, M.D., Gschwend, J.E., Pienta, K.J., Sanda, M.G., Chinnaiyan, A.M., Rubin, M.A. and Day, M.L., 2003. The role of an 80 kDa fragment of E-cadherin in the metastatic progression of prostate cancer. *Clinical Cancer Research*, 9(17), pp.6447-6452.
- Larue, L. and Bellacosa, A., 2005. Epithelial–mesenchymal transition in development and cancer: role of phosphatidylinositol 3' kinase/AKT pathways. *Oncogene*, 24(50), pp.7443-7454.
- Lastres, P., Letamendia, A., Zhang, H., Rius, C., Almendro, N., Raab, U., López, L.A., Langa, C., Fabra, A., Letarte, M. and Bernabéu, C., 1996. Endoglin modulates cellular responses to TGF-beta 1. *The Journal of cell biology*, 133(5), pp.1109-1121.
- Lastres, P., Martin-Perez, J., Langa, C. and Bernabéu, C., 1994. Phosphorylation of the human-transforming-growth-factor- $\beta$ -binding protein endoglin. *Biochemical Journal*, 301(3), pp.765-768.
- Le Cabec, V. and Maridonneau-Parini, I., 1994. Annexin 3 is associated with cytoplasmic granules in neutrophils and monocytes and translocates to the plasma membrane in activated cells. *Biochemical Journal*, 303(2), pp.481-487.
- Lee, J.H., Choy, M.L., Ngo, L., Venta-Perez, G. and Marks, P.A., 2011. Role of checkpoint kinase 1 (Chk1) in the mechanisms of resistance to histone deacetylase inhibitors. *Proceedings of the National Academy of Sciences*, 108(49), pp.19629-19634.
- Lee, S.H., Lee, E.H., Lee, S.H., Lee, Y.M., Kim, H.D. and Kim, Y.Z., 2015. Epigenetic role of histone 3 lysine methyltransferase and demethylase in regulating apoptosis predicting the recurrence of atypical meningioma. *Journal of Korean Medical Science*, 30(8), pp.1157-1166.

- Lee, Y., Liu, J., Patel, S., Cloughesy, T., Lai, A., Farooqi, H., Seligson, D., Dong, J., Liau, L., Becker, D. and Mischel, P., 2010. Genomic landscape of meningiomas. *Brain pathology*, 20(4), pp.751-762.
- Leibetseder, A., Preusser, M. and Berghoff, A.S., 2022. New Approaches with Precision Medicine in Adult Brain Tumors. *Cancers*, 14(3), p.712.
- Lek, M., Karczewski, K.J., Minikel, E.V., Samocha, K.E., Banks, E., Fennell, T., O'Donnell-Luria, A.H., Ware, J.S., Hill, A.J., Cummings, B.B. and Tukiainen, T., 2016. Analysis of protein-coding genetic variation in 60,706 humans. *Nature*, 536(7616), pp.285-291.
- Lelias, J.M., Adra, C.N., Wulf, G.M., Guillemot, J.C., Khagad, M., Caput, D. and Lim, B., 1993. cDNA cloning of a human mRNA preferentially expressed in hematopoietic cells and with homology to a GDP-dissociation inhibitor for the rho GTP-binding proteins. *Proceedings of the National Academy of Sciences*, 90(4), pp.1479-1483.
- Lerner, C., Ketter, R., Linsler, S., Henn, W., Oertel, J. and Urbschat, S., 2014. Establishment of a molecular cytogenetic analysis for native tumor tissue of meningiomas-suitable for clinical application. *Molecular cytogenetics*, 7(1), pp.1-8.
- Lewy-Trenda, I., Omulecka, A., Janczukowicz, J. and Papierz, W., 2004. CD44 expression in human meningiomas: an immunohistochemical analysis. *Pol J Pathol*, 55(1), pp.33-37.
- Li, D., Mallory, T. and Satomura, S., 2001. AFP-L3: a new generation of tumor marker for hepatocellular carcinoma. *Clinica chimica acta*, 313(1-2), pp.15-19.
- Li, J. and Stern, D.F., 2005. Regulation of CHK2 by DNA-dependent protein kinase. *Journal of Biological Chemistry*, 280(12), pp.12041-12050.
- Li, J., Zhou, T., Liu, L., Ju, Y.C., Chen, Y.T., Tan, Z.R. and Wang, J., 2018. The regulatory role of Annexin 3 in a nude mouse bearing a subcutaneous xenograft of MDA-MB-231 human breast carcinoma. *Pathology-Research and Practice*, 214(10), pp.1719-1725.
- Li, W., Zhang, B., Tang, J., Cao, Q., Wu, Y., Wu, C., Guo, J., Ling, E.A. and Liang, F., 2007. Sirtuin 2, a mammalian homolog of yeast silent information regulator-2 longevity regulator, is an oligodendroglial protein that decelerates cell differentiation through deacetylating  $\alpha$ -tubulin. *Journal of Neuroscience*, 27(10), pp.2606-2616.
- Lin, Q., Fuji, R.N., Yang, W. and Cerione, R.A., 2003. RhoGDI is required for Cdc42-mediated cellular transformation. *Current Biology*, 13(17), pp.1469-1479.
- Liu, J., Huang, Z., Chen, H.N., Qin, S., Chen, Y., Jiang, J., Zhang, Z., Luo, M., Ye, Q., Xie, N. and Zhou, Z.G., 2021. ZNF37A promotes tumor metastasis through transcriptional control of THSD4/TGF- $\beta$  axis in colorectal cancer. *Oncogene*, 40(19), pp.3394-3407.
- Liu, J., Xia, C. and Wang, G., 2020. Multi-omics analysis in initiation and progression of meningiomas: from pathogenesis to diagnosis. *Frontiers in Oncology*, p.1491.
- Liu, Q., Guntuku, S., Cui, X.S., Matsuoka, S., Cortez, D., Tamai, K., Luo, G., Carattini-Rivera, S., DeMayo, F., Bradley, A. and Donehower, L.A., 2000. Chk1 is an essential kinase that is regulated by Atr and required for the G2/M DNA damage checkpoint. *Genes & development*, 14(12), pp.1448-1459.

- Liu, R.Z., Li, S., Garcia, E., Glubrecht, D.D., Yin Poon, H., Easaw, J.C. and Godbout, R., 2016. Association between cytoplasmic CRABP2, altered retinoic acid signaling, and poor prognosis in glioblastoma. *Glia*, 64(6), pp.963-976.
- Liu, X., Wang, J., Chen, M., Liu, S., Yu, X. and Wen, F., 2019. Combining data from TCGA and GEO databases and reverse transcription quantitative PCR validation to identify gene prognostic markers in lung cancer. *OncoTargets and therapy*, 12, p.709.
- Liu, X.B. and Murray, K.D., 2012. Neuronal excitability and calcium/calmodulin-dependent protein kinase type II: location, location, location. *Epilepsia*, 53, pp.45-52.
- Liu, Y., Wang, Y., Zhang, Y., Miao, Y., Zhao, Y., Zhang, P.X., Jiang, G.Y., Zhang, J.Y., Han, Y., Lin, X.Y. and Yang, L.H., 2009. Abnormal expression of p120-catenin, E-cadherin, and small GTPases is significantly associated with malignant phenotype of human lung cancer. *Lung cancer*, 63(3), pp.375-382.
- Liu, Y., Zuo, T., Zhu, X., Ahuja, N. and Fu, T., 2017. Differential expression of hENT1 and hENT2 in colon cancer cell lines. *Genet. Mol. Res*, 16, p.gmr16019549.
- Liu, Y.F., Xiao, Z.Q., Li, M.X., Li, M.Y., Zhang, P.F., Li, C., Li, F., Chen, Y.H., Yi, H., Yao, H.X. and Chen, Z.C., 2009. Quantitative proteome analysis reveals annexin A3 as a novel biomarker in lung adenocarcinoma. *The Journal of Pathology: A Journal of the Pathological Society of Great Britain and Ireland*, 217(1), pp.54-64.
- Liu, Z., Han, G., Cao, Y., Wang, Y. and Gong, H., 2014. Calcium/calmodulin-dependent protein kinase II enhances metastasis of human gastric cancer by upregulating nuclear factor- $\kappa$ B and Akt-mediated matrix metalloproteinase-9 production. *Molecular medicine reports*, 10(5), pp.2459-2464.
- Liu, Z.Y., Wang, J.Y., Liu, H.H., Ma, X.M., Wang, C.L., Zhang, X.P., Tao, Y.Q., Lu, Y.C., Liao, J.C. and Hu, G.H., 2013. Retinoblastoma protein-interacting zinc-finger gene 1 (RIZ1) dysregulation in human malignant meningiomas. *Oncogene*, 32(10), pp.1216-1222.
- Lloyd, C., 1980. Hot foot. *Nature*, 288(5786), pp.13-14.
- Loizou, J.I., El-Khamisy, S.F., Zlatanou, A., Moore, D.J., Chan, D.W., Qin, J., Sarno, S., Meggio, F., Pinna, L.A. and Caldecott, K.W., 2004. The protein kinase CK2 facilitates repair of chromosomal DNA single-strand breaks. *Cell*, 117(1), pp.17-28.
- Lopez, E., Lopez, I., Ferreira, A. and Sequi, J., 2013. Clinical and technical phosphoproteomic research (Retraction of vol 9, pg 27, 2011). *Proteome science*, 11.
- López-Contreras, A.J., Gutierrez-Martinez, P., Specks, J., Rodrigo-Perez, S. and Fernandez-Capetillo, O., 2012. An extra allele of Chk1 limits oncogene-induced replicative stress and promotes transformation. *Journal of Experimental Medicine*, 209(3), pp.455-461.
- Louis, D.N., Perry, A., Reifenberger, G., Von Deimling, A., Figarella-Branger, D., Cavenee, W.K., Ohgaki, H., Wiestler, O.D., Kleihues, P. and Ellison, D.W., 2016. The 2016 World Health Organization classification of tumors of the central nervous system: a summary. *Acta neuropathologica*, 131(6), pp.803-820.
- Louis, D.N., Perry, A., Wesseling, P., Brat, D.J., Cree, I.A., Figarella-Branger, D., Hawkins, C., Ng, H.K., Pfister, S.M., Reifenberger, G. and Soffiatti, R., 2021. The 2021 WHO classification of tumors of the central nervous system: a summary. *Neuro-oncology*, 23(8), pp.1231-1251.

- Lozano, E., Frasa, M.A., Smolarczyk, K., Knaus, U.G. and Braga, V.M., 2008. PAK is required for the disruption of E-cadherin adhesion by the small GTPase Rac. *Journal of cell science*, 121(7), pp.933-938.
- Lu, Q., Longo, F.M., Zhou, H., Massa, S.M. and Chen, Y.H., 2009. Signaling through Rho GTPase pathway as viable drug target. *Current medicinal chemistry*, 16(11), pp.1355-1365.
- Lui, V.C.H., Lung, S.S.S., Pu, J.K.S., Hung, K.N. and Leung, G.K.K., 2010. Invasion of human glioma cells is regulated by multiple chloride channels including ClC-3. *Anticancer Research*, 30(11), pp.4515-4524.
- Lundgren, K., Holm, K., Nordenskjöld, B., Borg, Å. and Landberg, G., 2008. Gene products of chromosome 11q and their association with CCND1 gene amplification and tamoxifen resistance in premenopausal breast cancer. *Breast cancer research*, 10(5), pp.1-14.
- Lundgren, K., Holm, K., Nordenskjöld, B., Borg, Å. and Landberg, G., 2008. Gene products of chromosome 11q and their association with CCND1 gene amplification and tamoxifen resistance in premenopausal breast cancer. *Breast cancer research*, 10(5), pp.1-14.
- Ma, J., Hou, X., Li, M., Ren, H., Fang, S., Wang, X. and He, C., 2015. Genome-wide methylation profiling reveals new biomarkers for prognosis prediction of glioblastoma. *Journal of cancer research and therapeutics*, 11(6), p.212.
- Ma, M.Z., Zhang, Y., Weng, M.Z., Wang, S.H., Hu, Y., Hou, Z.Y., Qin, Y.Y., Gong, W., Zhang, Y.J., Kong, X. and Wang, J.D., 2016. Long noncoding RNA GCASPC, a target of miR-17-3p, negatively regulates Pyruvate Carboxylase-dependent cell proliferation in gallbladder cancer. *Cancer research*, 76(18), pp.5361-5371.
- Maallem, S., Wierinckx, A., Lachuer, J., Kwon, M.H. and Tappaz, M.L., 2008. Gene expression profiling in brain following acute systemic hypertonicity: novel genes possibly involved in osmoadaptation. *Journal of neurochemistry*, 105(4), pp.1198-1211.
- Maas, S.L., Stichel, D., Hielscher, T., Sievers, P., Berghoff, A.S., Schrimpf, D., Sill, M., Euskirchen, P., Blume, C., Patel, A. and Dogan, H., 2021. Integrated Molecular-Morphologic Meningioma Classification: A Multicenter Retrospective Analysis, Retrospectively and Prospectively Validated. *Journal of Clinical Oncology*.
- Machado, J.C., Soares, P., Carneiro, F., Rocha, A., Beck, S., Blin, N., Berx, G. and Sobrinho-Simoes, M., 1999. E-cadherin gene mutations provide a genetic basis for the phenotypic divergence of mixed gastric carcinomas. *Laboratory investigation*, 79(4), pp.459-466.
- Madhav, A., Andres, A., Duong, F., Mishra, R., Haldar, S., Liu, Z., Angara, B., Gottlieb, R., Zumsteg, Z.S. and Bhowmick, N.A., 2018. Antagonizing CD105 enhances radiation sensitivity in prostate cancer. *Oncogene*, 37(32), pp.4385-4397.
- Madoz-Gurpide, J., Cañamero, M., Sanchez, L., Solano, J., Alfonso, P. and Casal, J.I., 2007. A proteomics analysis of cell signaling alterations in colorectal cancer. *Molecular & Cellular Proteomics*, 6(12), pp.2150-2164.
- Maecker, H.T., Todd, S.C. and Levy, S., 1997. The tetraspanin superfamily: molecular facilitators. *The FASEB Journal*, 11(6), pp.428-442.
- Magill, S.T., Vasudevan, H.N., Seo, K., Villanueva-Meyer, J.E., Choudhury, A., John Liu, S., Pekmezci, M., Findakly, S., Hilz, S., Lastella, S. and Demaree, B., 2020. Multiplatform genomic profiling and magnetic resonance imaging identify mechanisms underlying intratumor heterogeneity in meningioma. *Nature communications*, 11(1), p.4803.

- Mahmoudi, T., Boj, S.F., Hatzis, P., Li, V.S., Taouatas, N., Vries, R.G., Teunissen, H., Begthel, H., Korving, J., Mohammed, S. and Heck, A.J., 2010. The leukemia-associated Mllt10/Af10-Dot11 are Tcf4/ $\beta$ -catenin coactivators essential for intestinal homeostasis. *PLoS biology*, 8(11), p.e1000539.
- Maitra, S., Kulikauskas, R.M., Gavilan, H. and Fehon, R.G., 2006. The tumor suppressors Merlin and Expanded function cooperatively to modulate receptor endocytosis and signaling. *Current Biology*, 16(7), pp.702-709.
- Majolini, M.B., Boncristiano, M. and Baldari, C., 1999. Dysregulation of the protein tyrosine kinase LCK in lymphoproliferative disorders and in other neoplasias. *Leukemia & lymphoma*, 35(3-4), pp.245-254.
- Mallikarjuna, K., Sundaram, C.S., Sharma, Y., Deepa, P.R., Khetan, V., Gopal, L., Biswas, J., Sharma, T. and Krishnakumar, S., 2010. Comparative proteomic analysis of differentially expressed proteins in primary retinoblastoma tumors. *PROTEOMICS—Clinical Applications*, 4(4), pp.449-463.
- Man, T., Noélia, C., Lei, Z., Luk, S.T., Kau, P.W., Stella, C., Ngan, E.S., Chung-Mau, L., Kwan, M., Jin, D. and Lee, T.K., 2018. Efficacy of annexin A3 blockade in sensitizing hepatocellular carcinoma to sorafenib and regorafenib. *J Hepatol*, 69(4), pp.826-839.
- Mandil, R., Ashkenazi, E., Blass, M., Kronfeld, I., Kazimirsky, G., Rosenthal, G., Umansky, F., Lorenzo, P.S., Blumberg, P.M. and Brodie, C., 2001. Protein kinase C $\alpha$  and protein kinase C $\delta$  play opposite roles in the proliferation and apoptosis of glioma cells. *Cancer research*, 61(11), pp.4612-4619.
- Manning, G., Whyte, D.B., Martinez, R., Hunter, T. and Sudarsanam, S., 2002. The protein kinase complement of the human genome. *Science*, 298(5600), pp.1912-1934.
- Manor, D., Schmidt, E.N., Budhu, A., Flesken-Nikitin, A., Zgola, M., Page, R., Nikitin, A.Y. and Noy, N., 2003. Mammary carcinoma suppression by cellular retinoic acid binding protein-II. *Cancer research*, 63(15), pp.4426-4433.
- Margolis, B.L., Lax, I., Kris, R., Dombalagian, M., Honegger, A.M., Howk, R., Givol, D., Ullrich, A. and Schlessinger, J., 1989. All autophosphorylation sites of epidermal growth factor (EGF) receptor and HER2/neu are located in their carboxyl-terminal tails: identification of a novel site in EGF receptor. *Journal of Biological Chemistry*, 264(18), pp.10667-10671.
- Marosi, C., Hassler, M., Roessler, K., Reni, M., Sant, M., Mazza, E. and Vecht, C., 2008. Meningioma. *Critical reviews in oncology/hematology*, 67(2), pp.153-171.
- Martiny-Baron, G., Kazanietz, M.G., Mischak, H., Blumberg, P.M., Kochs, G., Hug, H., Marme, D. and Schächtele, C.H., 1993. Selective inhibition of protein kinase C isozymes by the indolocarbazole Gö 6976. *Journal of Biological Chemistry*, 268(13), pp.9194-9197.
- Marumoto, T., Zhang, D. and Saya, H., 2005. Aurora-A—a guardian of poles. *Nature Reviews Cancer*, 5(1), pp.42-50.
- Matsuoka, S., Huang, M. and Elledge, S.J., 1998. Linkage of ATM to cell cycle regulation by the Chk2 protein kinase. *Science*, 282(5395), pp.1893-1897.
- Matsuoka, S., Rotman, G., Ogawa, A., Shiloh, Y., Tamai, K. and Elledge, S.J., 2000. Ataxia telangiectasia-mutated phosphorylates Chk2 in vivo and in vitro. *Proceedings of the National Academy of Sciences*, 97(19), pp.10389-10394.



- Mawrin, C. and Perry, A., 2010. Pathological classification and molecular genetics of meningiomas. *Journal of neuro-oncology*, 99(3), pp.379-391.
- Mawrin, C., Chung, C. and Preusser, M., 2015. Biology and clinical management challenges in meningioma. In *American Society of Clinical Oncology educational book. American Society of Clinical Oncology. Annual Meeting* (pp. e106-15).
- McConnell, B.B. and Yang, V.W., 2010. Mammalian Krüppel-like factors in health and diseases. *Physiological reviews*, 90(4), pp.1337-1381.
- McGuirk, S., Audet-Delage, Y. and St-Pierre, J., 2020. Metabolic fitness and plasticity in cancer progression. *Trends in Cancer*, 6(1), pp.49-61.
- Meggio, F. and Pinna, L.A., 2003. One-thousand-and-one substrates of protein kinase CK2. *The FASEB Journal*, 17(3), pp.349-368.
- Meimoun, P., Ambard-Bretteville, F., Colas-des Francs-Small, C., Valot, B. and Vidal, J., 2007. Analysis of plant phosphoproteins. *Analytical biochemistry*, 371(2), pp.238-246.
- Mendonsa, A.M., Na, T.Y. and Gumbiner, B.M., 2018. E-cadherin in contact inhibition and cancer. *Oncogene*, 37(35), pp.4769-4780.
- Mertins, P., Yang, F., Liu, T., Mani, D.R., Petyuk, V.A., Gillette, M.A., Clauser, K.R., Qiao, J.W., Gritsenko, M.A., Moore, R.J. and Levine, D.A., 2014. Ischemia in tumors induces early and sustained phosphorylation changes in stress kinase pathways but does not affect global protein levels. *Molecular & cellular proteomics*, 13(7), pp.1690-1704.
- Merzoug-Larabi, M., Spasojevic, C., Eymard, M., Hugonin, C., Auclair, C. and Karam, M., 2017. Protein kinase C inhibitor Gö6976 but not Gö6983 induces the reversion of E-to N-cadherin switch and metastatic phenotype in melanoma: identification of the role of protein kinase D1. *BMC cancer*, 17(1), pp.1-22.
- Meyer, T., Hanson, P.I., Stryer, L. and Schulman, H., 1992. Calmodulin trapping by calcium-calmodulin-dependent protein kinase. *Science*, 256(5060), pp.1199-1202.
- Michalik, L. and Wahli, W., 2007. Guiding ligands to nuclear receptors. *Cell*, 129(4), pp.649-651.
- Michie, A.M. and Nakagawa, R., 2005. The link between PKC $\alpha$  regulation and cellular transformation. *Immunology letters*, 96(2), pp.155-162.
- Mihaila, D., Jankowski, M., Gutiérrez, J.A., Rosenblum, M.L., Newsham, I.F., Böglér, O. and Rempel, S.A., 2003. Meningiomas: loss of heterozygosity on chromosome 10 and marker-specific correlations with grade, recurrence, and survival. *Clinical cancer research*, 9(12), pp.4443-4451.
- Mirian, C., Duun-Henriksen, A.K., Juratli, T., Sahm, F., Spiegl-Kreinecker, S., Peyre, M., Biczok, A., Tonn, J.C., Goutagny, S., Bertero, L. and Maier, A.D., 2020. Poor prognosis associated with TERT gene alterations in meningioma is independent of the WHO classification: an individual patient data meta-analysis. *Journal of Neurology, Neurosurgery & Psychiatry*, 91(4), pp.378-387.
- Money, T.T., King, R.G., Wong, M.H., Stevenson, J.L., Kalionis, B., Erwich, J.J.H.M., Huisman, M.A., Timmer, A., Hiden, U., Desoye, G. and Gude, N.M., 2007. Expression and

cellular localisation of chloride intracellular channel 3 in human placenta and fetal membranes. *Placenta*, 28(5-6), pp.429-436.

Moore, L.D., Le, T. and Fan, G., 2013. DNA methylation and its basic function. *Neuropsychopharmacology*, 38(1), pp.23-38.

Morgan, M.R., Humphries, M.J. and Bass, M.D., 2007. Synergistic control of cell adhesion by integrins and syndecans. *Nature reviews Molecular cell biology*, 8(12), pp.957-969.

Moss, S.E. and Morgan, R.O., 2004. The annexins. *Genome biology*, 5(4), pp.1-8.

Mostafa, R.R. and Khairy, R.A., 2017. CD44 expression in meningioma and its correlation with proliferation indices. *Journal of Clinical and Diagnostic Research: JCDR*, 11(8), p.EC12.

Muinelo-Romay, L., Vazquez-Martin, C., Villar-Portela, S., Cuevas, E., Gil-Martin, E. and Fernandez-Briera, A., 2008. Expression and enzyme activity of alpha (1, 6) fucosyltransferase in human colorectal cancer (vol 123, pg 641, 2008). *International journal of cancer*, 123(10), pp.2472-2472.

Mussunoor, S. and Murray, G.I., 2008. The role of annexins in tumour development and progression. *The Journal of Pathology: A Journal of the Pathological Society of Great Britain and Ireland*, 216(2), pp.131-140.

Nagaishi, M., Nobusawa, S., Tanaka, Y., Ikota, H., Yokoo, H. and Nakazato, Y., 2012. Slug, twist, and E-cadherin as immunohistochemical biomarkers in meningeal tumors.

Najm, P., Zhao, P., Steklov, M., Sewduth, R.N., Baietti, M.F., Pandolfi, S., Criem, N., Lechat, B., Maia, T.M., Van Haver, D. and Corthout, N., 2021. Loss-of-Function Mutations in TRAF7 and KLF4 Cooperatively Activate RAS-Like GTPase Signaling and Promote Meningioma Development. *Cancer Research*, 81(16), pp.4218-4229.

Nakane, Y., Natsume, A., Wakabayashi, T., Oi, S., Ito, M., Inao, S., Saito, K. and Yoshida, J., 2007. Malignant transformation-related genes in meningiomas: allelic loss on 1p36 and methylation status of p73 and RASSF1A. *Journal of neurosurgery*, 107(2), pp.398-404.

Narumi, R., Murakami, T., Kuga, T., Adachi, J., Shiromizu, T., Muraoka, S., Kume, H., Kodera, Y., Matsumoto, M., Nakayama, K. and Miyamoto, Y., 2012. A strategy for large-scale phosphoproteomics and SRM-based validation of human breast cancer tissue samples. *Journal of proteome research*, 11(11), pp.5311-5322.

Nassiri, F., Cusimano, M.D., Scheithauer, B.W., Rotondo, F., Fazio, A., Yousef, G.M., Syro, L.V., Kovacs, K. and Lloyd, R.V., 2011. Endoglin (CD105): a review of its role in angiogenesis and tumor diagnosis, progression and therapy. *Anticancer research*, 31(6), pp.2283-2290.

Nassiri, F., Liu, J., Patil, V., Mamatjan, Y., Wang, J.Z., Hugh-White, R., Macklin, A.M., Khan, S., Singh, O., Karimi, S. and Corona, R.I., 2021. A clinically applicable integrative molecular classification of meningiomas. *Nature*, 597(7874), pp.119-125.

Nassiri, F., Wang, J.Z., Singh, O., Karimi, S., Dalcourt, T., Ijad, N., Pirouzman, N., Ng, H.K., Saladino, A., Pollo, B. and Dimeco, F., 2021. Loss of H3K27me3 in meningiomas. *Neuro-oncology*, 23(8), pp.1282-1291.

Negrone, C., Hilton, D.A., Ercolano, E., Adams, C.L., Kurian, K.M., Baiz, D. and Hanemann, C.O., 2020. GATA-4, a potential novel therapeutic target for high-grade meningioma, regulates

miR-497, a potential novel circulating biomarker for high-grade meningioma. *EBioMedicine*, 59, p.102941.

Newman, A., 1998. RNA splicing. *Current Biology*, 8(25), pp.R903-R905.

Newton, A.C., 2001. Protein kinase C: structural and spatial regulation by phosphorylation, cofactors, and macromolecular interactions. *Chemical reviews*, 101(8), pp.2353-2364.

Newton, A.C., 2018. Protein kinase C: perfectly balanced. *Critical reviews in biochemistry and molecular biology*, 53(2), pp.208-230.

Niessen, C.M., Leckband, D. and Yap, A.S., 2011. Tissue organization by cadherin adhesion molecules: dynamic molecular and cellular mechanisms of morphogenetic regulation. *Physiological reviews*, 91(2), pp.691-731.

Nigg, E.A., 2001. Mitotic kinases as regulators of cell division and its checkpoints. *Nature reviews Molecular cell biology*, 2(1), pp.21-32.

Nigim, F., Wakimoto, H., Kasper, E.M., Ackermans, L. and Temel, Y., 2018. Emerging medical treatments for meningioma in the molecular era. *Biomedicines*, 6(3), p.86.

Nikiteas, N.I., Tzanakis, N., Theodoropoulos, G., Atsaves, V., Christoni, Z., Karakitsos, P., Lazaris, A.C., Papachristodoulou, A., Klonaris, C. and Gazouli, M., 2007. Vascular endothelial growth factor and endoglin (CD-105) in gastric cancer. *Gastric Cancer*, 10(1), pp.12-17.

Noda, K., Miyoshi, E., Gu, J., Gao, C.X., Nakahara, S., Kitada, T., Honke, K., Suzuki, K., Yoshihara, H., Yoshikawa, K. and Kawano, K., 2003. Relationship between elevated FX expression and increased production of GDP-L-fucose, a common donor substrate for fucosylation in human hepatocellular carcinoma and hepatoma cell lines. *Cancer research*, 63(19), pp.6282-6289.

Nordh, S., Ansari, D. and Andersson, R., 2014. hENT1 expression is predictive of gemcitabine outcome in pancreatic cancer: a systematic review. *World journal of gastroenterology: WJG*, 20(26), p.8482.

North, B.J., Marshall, B.L., Borra, M.T., Denu, J.M. and Verdin, E., 2003. The human Sir2 ortholog, SIRT2, is an NAD<sup>+</sup>-dependent tubulin deacetylase. *Molecular cell*, 11(2), pp.437-444.

Noy, N., 2010. Between death and survival: retinoic acid in regulation of apoptosis. *Annual review of nutrition*, 30(1), pp.201-217.

Nunes, F.P., Merker, V.L., Jennings, D., Caruso, P.A., di Tomaso, E., Muzikansky, A., Barker II, F.G., Stemmer-Rachamimov, A. and Plotkin, S.R., 2013. Bevacizumab treatment for meningiomas in NF2: a retrospective analysis of 15 patients. *PLoS One*, 8(3), p.e59941.

O'Neill, W.C., 1999. Physiological significance of volume-regulatory transporters. *American Journal of Physiology-Cell Physiology*, 276(5), pp.C995-C1011.

Ohgaki, H. and Kleihues, P., 2005. Epidemiology and etiology of gliomas. *Acta neuropathologica*, 109, pp.93-108.

Okamoto, H., Li, J., Vortmeyer, A.O., Jaffe, H., Lee, Y.S., Gläscher, S., Sohn, T.S., Zeng, W., Ikejiri, B., Proescholdt, M.A. and Mayer, C., 2006. Comparative proteomic profiles of meningioma subtypes. *Cancer research*, 66(20), pp.10199-10204.

- Okuducu, A.F., Janzen, V., Ko, Y., Hahne, J.C., Lu, H., Ma, Z.L., Albers, P., Sahin, A., Wellmann, A., Scheinert, P. and Wernert, N., 2005. Cellular retinoic acid-binding protein 2 is down-regulated in prostate cancer. *International journal of oncology*, 27(5), pp.1273-1282.
- Olar, A., Goodman, L.D., Wani, K.M., Boehling, N.S., Sharma, D.S., Mody, R.R., Gumin, J., Claus, E.B., Lang, F.F., Cloughesy, T.F. and Lai, A., 2018. A gene expression signature predicts recurrence-free survival in meningioma. *Oncotarget*, 9(22), p.16087.
- Olayioye, M.A., Neve, R.M., Lane, H.A. and Hynes, N.E., 2000. The ErbB signaling network: receptor heterodimerization in development and cancer. *The EMBO journal*, 19(13), pp.3159-3167.
- Oliveira, C., Faoro, H., Alves, L.R. and Goldenberg, S., 2017. RNA-binding proteins and their role in the regulation of gene expression in *Trypanosoma cruzi* and *Saccharomyces cerevisiae*. *Genetics and molecular biology*, 40, pp.22-30.
- Olsen, M.L., Schade, S., Lyons, S.A., Amaral, M.D. and Sontheimer, H., 2003. Expression of voltage-gated chloride channels in human glioma cells. *Journal of Neuroscience*, 23(13), pp.5572-5582.
- Onda, T., Uzawa, K., Nakashima, D., Saito, K., Iwadate, Y., Seki, N., Shibahara, T. and Tanzawa, H., 2007. Lin-7C/VELI3/MALS-3: an essential component in metastasis of human squamous cell carcinoma. *Cancer research*, 67(20), pp.9643-9648.
- Oplawski, M., Dziobek, K., Adwent, I., Dąbrus, D., Grabarek, B., Zmarzły, N., Plewka, A. and Boroń, D., 2018. Expression profile of endoglin in different grades of endometrial cancer. *Current pharmaceutical biotechnology*, 19(12), pp.990-995.
- Orlicky, D.J., 1996. Negative regulatory activity of a prostaglandin F2 $\alpha$  receptor associated protein (FPRP). *Prostaglandins, leukotrienes and essential fatty acids*, 54(4), pp.247-259.
- Orlicky, D.J., Lieber, J.G., Morin, C.L. and Evans, R.M., 1998. Synthesis and accumulation of a receptor regulatory protein associated with lipid droplet accumulation in 3T3-L1 cells. *Journal of lipid research*, 39(6), pp.1152-1161.
- O'shea, K.S. and Dixit, V.M., 1988. Unique distribution of the extracellular matrix component thrombospondin in the developing mouse embryo. *The Journal of cell biology*, 107(6), pp.2737-2748.
- Ostrom, Q.T., Cioffi, G., Waite, K., Kruchko, C. and Barnholtz-Sloan, J.S., 2021. CBTRUS statistical report: primary brain and other central nervous system tumors diagnosed in the United States in 2014–2018. *Neuro-oncology*, 23(Supplement\_3), pp.iii1-iii105.
- Ostrom, Q.T., Gittleman, H., Fulop, J., Liu, M., Blanda, R., Kromer, C., Wolinsky, Y., Kruchko, C. and Barnholtz-Sloan, J.S., 2015. CBTRUS statistical report: primary brain and central nervous system tumors diagnosed in the United States in 2008-2012. *Neuro-oncology*, 17(4), pp.iv1-iv62.
- Ostrom, Q.T., Gittleman, H., Liao, P., Rouse, C., Chen, Y., Dowling, J., Wolinsky, Y., Kruchko, C. and Barnholtz-Sloan, J., 2014. CBTRUS statistical report: primary brain and central nervous system tumors diagnosed in the United States in 2007–2011. *Neuro-oncology*, 16(4), pp.iv1-iv63.

- Ostrom, Q.T., Gittleman, H., Xu, J., Kromer, C., Wolinsky, Y., Kruchko, C. and Barnholtz-Sloan, J.S., 2016. CBTRUS statistical report: primary brain and other central nervous system tumors diagnosed in the United States in 2009–2013. *Neuro-oncology*, 18(suppl\_5), pp.v1-v75.
- Owen, O.E., Kalhan, S.C. and Hanson, R.W., 2002. The key role of anaplerosis and cataplerosis for citric acid cycle function. *Journal of Biological Chemistry*, 277(34), pp.30409-30412.
- Oxford, G. and Theodorescu, D., 2003. Ras superfamily monomeric G proteins in carcinoma cell motility. *Cancer letters*, 189(2), pp.117-128.
- Oxmann, D., Held-Feindt, J., Stark, A.M., Hattermann, K., Yoneda, T. and Mentlein, R., 2008. Endoglin expression in metastatic breast cancer cells enhances their invasive phenotype. *Oncogene*, 27(25), pp.3567-3575.
- Paez, J.G., Janne, P.A., Lee, J.C., Tracy, S., Greulich, H., Gabriel, S., Herman, P., Kaye, F.J., Lindeman, N., Boggon, T.J. and Naoki, K., 2004. EGFR mutations in lung cancer: correlation with clinical response to gefitinib therapy. *Science*, 304(5676), pp.1497-1500.
- Palacios, E.H. and Weiss, A., 2004. Function of the Src-family kinases, Lck and Fyn, in T-cell development and activation. *Oncogene*, 23(48), pp.7990-8000.
- Pan, Q.Z., Pan, K., Wang, Q.J., Weng, D.S., Zhao, J.J., Zheng, H.X., Zhang, X.F., Jiang, S.S., Lv, L., Tang, Y. and Li, Y.Q., 2015. Annexin A3 as a potential target for immunotherapy of liver cancer stem-like cells. *Stem cells*, 33(2), pp.354-366.
- Pan, Q.Z., Pan, K., Weng, D.S., Zhao, J.J., Zhang, X.F., Wang, D.D., Lv, L., Jiang, S.S., Zheng, H.X. and Xia, J.C., 2015. Annexin A3 promotes tumorigenesis and resistance to chemotherapy in hepatocellular carcinoma. *Molecular carcinogenesis*, 54(8), pp.598-607.
- Pandey, A. and Mann, M., 2000. Proteomics to study genes and genomes. *Nature*, 405(6788), pp.837-846.
- Parada, C.A., Osburn, J., Kaur, S., Yakkoui, Y., Shi, M., Pan, C., Busald, T., Karasozen, Y., Gonzalez-Cuyar, L.F., Rostomily, R. and Zhang, J., 2018. Kinome and phosphoproteome of high-grade meningiomas reveal AKAP12 as a central regulator of aggressiveness and its possible role in progression. *Scientific reports*, 8(1), pp.1-14.
- Parada, C.A., Osburn, J.W., Busald, T., Karasozen, Y., Kaur, S., Shi, M., Barber, J., Adidharma, W., Cimino, P.J., Pan, C. and Gonzalez-Cuyar, L.F., 2020. Phosphoproteomic and kinomic signature of clinically aggressive grade I (1.5) meningiomas reveals RB1 signaling as a novel mediator and biomarker. *Clinical Cancer Research*, 26(1), pp.193-205.
- Pardali, E., Van Der Schaft, D.W.J., Wiercinska, E., Gorter, A., Hogendoorn, P.C.W., Griffioen, A.W. and Ten Dijke, P., 2011. Critical role of endoglin in tumor cell plasticity of Ewing sarcoma and melanoma. *Oncogene*, 30(3), pp.334-345.
- Parekh, D.B., Ziegler, W. and Parker, P.J., 2000. Multiple pathways control protein kinase C phosphorylation. *The EMBO journal*, 19(4), pp.496-503.
- Park, J., 2012. Human Equilibrative Nucleoside Transporter Subtype 1: Structure-Function Analysis Using Cysteine Mutagenesis and Thiol Modifying Techniques.

- Parker, C.E. and Borchers, C.H., 2014. Mass spectrometry based biomarker discovery, verification, and validation—quality assurance and control of protein biomarker assays. *Molecular oncology*, 8(4), pp.840-858.
- Pasteur, L., 1861. *Expériences et vues nouvelles sur la nature des fermentations*.
- Pavlova, N.N. and Thompson, C.B., 2016. The emerging hallmarks of cancer metabolism. *Cell metabolism*, 23(1), pp.27-47.
- Pawson, T. and Scott, J.D., 2005. Protein phosphorylation in signaling—50 years and counting. *Trends in biochemical sciences*, 30(6), pp.286-290.
- Pećina-Šlaus, N., 2003. Tumor suppressor gene E-cadherin and its role in normal and malignant cells. *Cancer cell international*, 3(1), pp.1-7.
- Pećina-Šlaus, N., Nikuševa Martić, T., Deak, A.J., Zeljko, M., Hrašćan, R., Tomas, D. and Musani, V., 2010. Genetic and protein changes of E-cadherin in meningiomas. *Journal of cancer research and clinical oncology*, 136(5), pp.695-702.
- Peraldo-Neia, C., Migliardi, G., Mello-Grand, M., Montemurro, F., Segir, R., Pignochino, Y., Cavalloni, G., Torchio, B., Mosso, L., Chiorino, G. and Aglietta, M., 2011. Epidermal Growth Factor Receptor (EGFR) mutation analysis, gene expression profiling and EGFR protein expression in primary prostate cancer. *BMC cancer*, 11(1), pp.1-12.
- Perego, C., Vanoni, C., Massari, S., Raimondi, A., Pola, S., Cattaneo, M.G., Francolini, M., Vicentini, L.M. and Pietrini, G., 2002. Invasive behaviour of glioblastoma cell lines is associated with altered organisation of the cadherin-catenin adhesion system. *Journal of Cell Science*, 115(16), pp.3331-3340.
- Pérez-Gómez, E., Del Castillo, G., Santibáñez, J.F., Lêpez-Novoa, J.M., Bernabéu, C. and Quintanilla, M., 2010. The role of the TGF- $\beta$  coreceptor endoglin in cancer. *TheScientificWorldJOURNAL*, 10, pp.2367-2384.
- Perez-Gomez, E., Eleno, N., Lopez-Novoa, J.M., Ramón Ramirez, J., Velasco, B., Letarte, M., Bernabeu, C. and Quintanilla, M., 2005. Characterization of murine S-endoglin isoform and its effects on tumor development. *Oncogene*, 24(27), pp.4450-4461.
- Peri, S., Navarro, J.D., Kristiansen, T.Z., Amanchy, R., Surendranath, V., Muthusamy, B., Gandhi, T.K., Chandrika, K.N., Deshpande, N., Suresh, S. and Rashmi, B.P., 2004. Nucleic Acids Res, 32 Database issue. *D497-501*.
- Perry, A., Giannini, C., Raghavan, R., Scheithauer, B.W., Banerjee, R., Margraf, L., Bowers, D.C., Lytle, R.A., Newsham, I.F. and Gutmann, D.H., 2001. Aggressive phenotypic and genotypic features in pediatric and NF2-associated meningiomas: a clinicopathologic study of 53 cases. *Journal of Neuropathology & Experimental Neurology*, 60(10), pp.994-1003.
- Perry, A., Scheithauer, B.W., Stafford, S.L., Lohse, C.M. and Wollan, P.C., 1999. “Malignancy” in meningiomas: a clinicopathologic study of 116 patients, with grading implications. *Cancer: Interdisciplinary International Journal of the American Cancer Society*, 85(9), pp.2046-2056.
- Petrilli, A.M. and Fernández-Valle, C., 2016. Role of Merlin/NF2 inactivation in tumor biology. *Oncogene*, 35(5), p.537.
- Phannasil, P., Israr-ul, H.A., El Azzouny, M., Longacre, M.J., Rattanapornsompong, K., Burant, C.F., MacDonald, M.J. and Jitrapakdee, S., 2017. Mass spectrometry analysis shows

the biosynthetic pathways supported by pyruvate carboxylase in highly invasive breast cancer cells. *Biochimica et Biophysica Acta (BBA)-Molecular Basis of Disease*, 1863(2), pp.537-551.

Phannasil, P., Thuwajit, C., Warnnissorn, M., Wallace, J.C., MacDonald, M.J. and Jitrapakdee, S., 2015. Pyruvate carboxylase is up-regulated in breast cancer and essential to support growth and invasion of MDA-MB-231 cells. *PloS one*, 10(6), p.e0129848.

Pichumani, K., Ijare, O.B. and Baskin, D.S., 2019. Metabolic fate of glucose in atypical meningioma studied by <sup>13</sup>C NMR isotopomer analysis. In *Metabolic fate of glucose in atypical meningioma studied by <sup>13</sup>C NMR isotopomer* (p. 2507). International Society for magnetic resonance in medicine.

Pinna, L.A. and Ruzzene, M., 1996. How do protein kinases recognize their substrates. *Biochimica et Biophysica Acta (BBA)-Molecular Cell Research*, 1314(3), pp.191-225.

Polakis, P., 2000. Wnt signaling and cancer. *Genes & development*, 14(15), pp.1837-1851.

Pommier, Y., Sordet, O., Rao, A., Zhang, H. and Kohn, K.W., 2005. Targeting chk2 kinase: molecular interaction maps and therapeutic rationale. *Current pharmaceutical design*, 11(22), p.2855.

Postiglione, L., Di Domenico, G., Caraglia, M., Marra, M., Giuberti, G., Del Vecchio, L., Montagnani, S., Macri, M., Bruno, E.M., Abbruzzese, A. and Rossi, G., 2005. Differential expression and cytoplasm/membrane distribution of endoglin (CD105) in human tumour cell lines: Implications in the modulation of cell proliferation. *International journal of oncology*, 26(5), pp.1193-1201.

Powell, J.A., Rieger, F., Blondet, B., Dreyfus, P. and Pinçon-Raymond, M., 1984. Distribution and quantification of ACh receptors and innervation in diaphragm muscle of normal and mdg mouse embryos. *Developmental biology*, 101(1), pp.168-180.

Powers, J.T., Hong, S., Mayhew, C.N., Rogers, P.M., Knudsen, E.S. and Johnson, D.G., 2004. E2F1 Uses the ATM Signaling Pathway to Induce p53 and Chk2 Phosphorylation and Apoptosis. American Cancer Society (ES Knudsen) and NIH (grants CA98601, ES11047, ES07784, CA16672, and T32ESO7247). *Molecular Cancer Research*, 2(4), pp.203-214.

Preusser, M., Brastianos, P.K. and Mawrin, C., 2018. Advances in meningioma genetics: novel therapeutic opportunities. *Nature Reviews Neurology*, 14(2), pp.106-115.

Preusser, M., Silvani, A., Le Rhun, E., Soffietti, R., Lombardi, G., Sepulveda, J.M., Brandal, P., Brazil, L., Bonneville-Levard, A., Lorgis, V. and Vauleon, E., 2022. Trabectedin for recurrent WHO grade 2 or 3 meningioma: a randomized phase II study of the EORTC Brain Tumor Group (EORTC-1320-BTG). *Neuro-oncology*, 24(5), pp.755-767.

Preusser, M., Spiegl-Kreinecker, S., Lötsch, D., Wöhrer, A., Schmook, M., Dieckmann, K., Saringer, W., Marosi, C. and Berger, W., 2012. Trabectedin has promising antineoplastic activity in high-grade meningioma. *Cancer*, 118(20), pp.5038-5049.

Pridham, K.J., Varghese, R.T. and Sheng, Z., 2017. The role of class IA phosphatidylinositol-4, 5-bisphosphate 3-kinase catalytic subunits in glioblastoma. *Frontiers in oncology*, 7, p.312.

- Provenzano, L., Ryan, Y., Hilton, D.A., Lyons-Rimmer, J., Dave, F., Maze, E.A., Adams, C.L., Rigby-Jones, R., Ammoun, S. and Hanemann, C.O., 2017. Cellular prion protein (PrPC) in the development of Merlin-deficient tumours. *Oncogene*, 36(44), pp.6132-6142.
- Puc, J., Keniry, M., Li, H.S., Pandita, T.K., Choudhury, A.D., Memeo, L., Mansukhani, M., Murty, V.V., Gaciong, Z., Meek, S.E. and Piwnica-Worms, H., 2005. Lack of PTEN sequesters CHK1 and initiates genetic instability. *Cancer cell*, 7(2), pp.193-204.
- Pujuguet, P., Del Maestro, L., Gautreau, A., Louvard, D. and Arpin, M., 2003. Ezrin regulates E-cadherin-dependent adherens junction assembly through Rac1 activation. *Molecular biology of the cell*, 14(5), pp.2181-2191.
- Qian, Z., Okuhara, D., Abe, M.K. and Rosner, M.R., 1999. Molecular cloning and characterization of a mitogen-activated protein kinase-associated intracellular chloride channel. *Journal of Biological Chemistry*, 274(3), pp.1621-1627.
- Qin, C., He, B., Dai, W., Lin, Z., Zhang, H., Wang, X., Wang, J., Zhang, X., Wang, G., Yin, L. and Zhang, Q., 2014. The impact of a chlorotoxin-modified liposome system on receptor MMP-2 and the receptor-associated protein CIC-3. *Biomaterials*, 35(22), pp.5908-5920.
- Qiu, S., Lin, S., Hu, D., Feng, Y., Tan, Y. and Peng, Y., 2013. Interactions of miR-323/miR-326/miR-329 and miR-130a/miR-155/miR-210 as prognostic indicators for clinical outcome of glioblastoma patients. *Journal of translational medicine*, 11(1), pp.1-11.
- Rabjerg, M., 2016. *Identification and validation of novel prognostic markers in renal cell carcinoma* (Doctoral dissertation, Syddansk Universitet).
- Rachinger, W., Stoecklein, V.M., Terpolilli, N.A., Haug, A.R., Ertl, L., Pöschl, J., Schüller, U., Schichor, C., Thon, N. and Tonn, J.C., 2015. Increased <sup>68</sup>Ga-DOTATATE uptake in PET imaging discriminates meningioma and tumor-free tissue. *Journal of Nuclear Medicine*, 56(3), pp.347-353.
- Ramani, P., Sowa-Avugrah, E. and May, M.T., 2015. High proliferation index, as determined by immunohistochemical expression of Aurora kinase B and geminin, indicates poor prognosis in neuroblastomas. *Virchows Archiv*, 467(3), pp.319-327.
- Ramroach, S., Joshi, A. and John, M., 2020. Optimisation of cancer classification by machine learning generates an enriched list of candidate drug targets and biomarkers. *Molecular omics*, 16(2), pp.113-125.
- Rappsilber, J., Ishihama, Y. and Mann, M., 2003. Stop and go extraction tips for matrix-assisted laser desorption/ionization, nanoelectrospray, and LC/MS sample pretreatment in proteomics. *Analytical chemistry*, 75(3), pp.663-670.
- Reshkin, S.J., Cardone, R.A. and Harguindey, S., 2012. Na-H Exchanger, pH Regulation and Cancer. *Recent Patents on Anti-Cancer Drug Discovery*, 8, pp.000-000.
- Reuss, D.E., Piro, R.M., Jones, D.T., Simon, M., Ketter, R., Kool, M., Becker, A., Sahm, F., Pusch, S., Meyer, J. and Hagenlocher, C., 2013. Secretory meningiomas are defined by combined KLF4 K409Q and TRAF7 mutations. *Acta neuropathologica*, 125(3), pp.351-358.
- Riemenschneider, M.J., Perry, A. and Reifenberger, G., 2006. Histological classification and molecular genetics of meningiomas. *The Lancet Neurology*, 5(12), pp.1045-1054.
- Robey, R.B. and Hay, N., 2009, February. Is Akt the “Warburg kinase”?—Akt-energy metabolism interactions and oncogenesis. In *Seminars in cancer biology* (Vol. 19, No. 1, pp. 25-31). Academic Press.



- Robinson, D., He, F., Pretlow, T. and Kung, H.J., 1996. A tyrosine kinase profile of prostate carcinoma. *Proceedings of the National Academy of Sciences*, 93(12), pp.5958-5962.
- Rodrigues, G.A., Falasca, M., Zhang, Z., Ong, S.H. and Schlessinger, J., 2000. A novel positive feedback loop mediated by the docking protein Gab1 and phosphatidylinositol 3-kinase in epidermal growth factor receptor signaling. *Molecular and cellular biology*, 20(4), pp.1448-1459.
- Rodriguez-Enriquez, S., Maria, H.A. and Saaverdra, E., 2007. Energy metabolism in tumor cells. *FEBS Journal*, 274(6), pp.1393-1418.
- Rogers, L., Barani, I., Chamberlain, M., Kaley, T.J., McDermott, M., Raizer, J., Schiff, D., Weber, D.C., Wen, P.Y. and Vogelbaum, M.A., 2015. Meningiomas: knowledge base, treatment outcomes, and uncertainties. A RANO review. *Journal of neurosurgery*, 122(1), pp.4-23.
- Rojas, M., Yao, S. and Lin, Y.Z., 1996. Controlling epidermal growth factor (EGF)-stimulated Ras activation in intact cells by a cell-permeable peptide mimicking phosphorylated EGF receptor. *Journal of Biological Chemistry*, 271(44), pp.27456-27461.
- Rosen, L.S., Gordon, M.S., Robert, F. and Matei, D.E., 2014. Endoglin for targeted cancer treatment. *Current oncology reports*, 16(2), pp.1-9.
- Rouleau, G.A., Merel, P., Lutchman, M., Sanson, M., Zucman, J., Marineau, C., Hoang-Xuan, K., Demczuk, S., Desmaze, C., Plougastel, B. and Pulst, S.M., 1993. Alteration in a new gene encoding a putative membrane-organizing protein causes neuro-fibromatosis type 2. *Nature*, 363(6429), p.515.
- Ruan, L., Wang, G.L., Chen, Y., Yi, H., Tang, C.E., Zhang, P.F., Li, M.Y., Li, C., Peng, F., Li, J.L. and Chen, Z.C., 2010. Identification of tyrosine phosphoproteins in signaling pathway triggered TGF- $\alpha$  by using functional proteomics technology. *Medical Oncology*, 27(4), pp.1407-1414.
- Rutten, I., Cabay, J.E., Withofs, N., Lemaire, C., Aerts, J., Baart, V. and Hustinx, R., 2007. PET/CT of skull base meningiomas using 2-18F-fluoro-L-tyrosine: initial report. *Journal of Nuclear Medicine*, 48(5), pp.720-725.
- Ruttledge, M.H., Sarrazin, J., Rangaratnam, S., Phelan, C.M., Twist, E., Merel, P., Delattre, O., Thomas, G., Nordenskjöld, M., Collins, V.P. and Dumanski, J.P., 1994. Evidence for the complete inactivation of the NF2 gene in the majority of sporadic meningiomas. *Nature genetics*, 6(2), pp.180-184.
- Sadetzki, S., Flint-Richter, P., Ben-Tal, T. and Nass, D., 2002. Radiation-induced meningioma: a descriptive study of 253 cases. *Journal of neurosurgery*, 97(5), pp.1078-1082.
- Saha, B., Arase, A., Imam, S.S., Tsao-Wei, D., Naritoku, W.Y., Groshen, S., Jones, L.W. and Imam, S.A., 2008. Overexpression of E-cadherin and  $\beta$ -Catenin proteins in metastatic prostate cancer cells in bone. *The Prostate*, 68(1), pp.78-84.
- Sahm, F., Schrimpf, D., Olar, A., Koelsche, C., Reuss, D., Bissel, J., Kratz, A., Capper, D., Schefzyk, S., Hielscher, T. and Wang, Q., 2015. TERT promoter mutations and risk of recurrence in meningioma. *Journal of the National Cancer Institute*, 108(5), p.djv377.
- Sahm, F., Schrimpf, D., Stichel, D., Jones, D.T., Hielscher, T., Schefzyk, S., Okonechnikov, K., Koelsche, C., Reuss, D.E., Capper, D. and Sturm, D., 2017. DNA methylation-based

classification and grading system for meningioma: a multicentre, retrospective analysis. *The Lancet Oncology*, 18(5), pp.682-694.

Sakaguchi, K., Okabayashi, Y., Kido, Y., Kimura, S., Matsumura, Y., Inushima, K. and Kasuga, M., 1998. Shc phosphotyrosine-binding domain dominantly interacts with epidermal growth factor receptors and mediates Ras activation in intact cells. *Molecular endocrinology*, 12(4), pp.536-543.

Sala-Valdés, M., Ursa, Á., Charrin, S., Rubinstein, E., Hemler, M.E., Sánchez-Madrid, F. and Yáñez-Mó, M., 2006. EWI-2 and EWI-F link the tetraspanin web to the actin cytoskeleton through their direct association with ezrin-radixin-moesin proteins. *Journal of Biological Chemistry*, 281(28), pp.19665-19675.

Santini, D., Vincenzi, B., Fratto, M.E., Perrone, G., Lai, R., Catalano, V., Cass, C., Ruffini, P.A., Spoto, C., Muretto, P. and Rizzo, S., 2010. Prognostic role of human equilibrative transporter 1 (hENT1) in patients with resected gastric cancer. *Journal of cellular physiology*, 223(2), pp.384-388.

Sato, T. and Sekido, Y., 2018. Nf2/merlin inactivation and potential therapeutic targets in mesothelioma. *International journal of molecular sciences*, 19(4), p.988.

Saydam, O., Senol, O., Schaaïj-Visser, T.B., Pham, T.V., Piersma, S.R., Stemmer-Rachamimov, A.O., Wurdinger, T., Peerdeman, S.M. and Jimenez, C.R., 2010. Comparative protein profiling reveals minichromosome maintenance (MCM) proteins as novel potential tumor markers for meningiomas. *Journal of proteome research*, 9(1), pp.485-494.

Scatena, R., 2012. Mitochondria and cancer: a growing role in apoptosis, cancer cell metabolism and dedifferentiation. *Advances in Mitochondrial Medicine*, pp.287-308.

Schmidt, M., Mock, A., Jungk, C., Sahm, F., Ull, A.T., Warta, R., Lamszus, K., Gousias, K., Ketter, R., Roesch, S. and Rapp, C., 2016. Transcriptomic analysis of aggressive meningiomas identifies PTTG1 and LEPR as prognostic biomarkers independent of WHO grade. *Oncotarget*, 7(12), p.14551.

Schneider, B., Pülhorn, H., Röhrig, B. and Rainov, N.G., 2005. Predisposing conditions and risk factors for development of symptomatic meningioma in adults. *Cancer detection and prevention*, 29(5), pp.440-447.

Schneider, M., Neoptolemos, J.P. and Büchler, M.W., 2020. Commentary: Neoadjuvant treatment of resectable pancreatic cancer: lack of level III evidence. *Surgery*, 168(6), pp.1015-1016.

Schönwasser, D.C., Marais, R.M., Marshall, C.J. and Parker, P.J., 1998. Activation of the mitogen-activated protein kinase/extracellular signal-regulated kinase pathway by conventional, novel, and atypical protein kinase C isotypes. *Molecular and cellular biology*, 18(2), pp.790-798.

Schroeder, F., Petrescu, A.D., Huang, H., Atshaves, B.P., McIntosh, A.L., Martin, G.G., Hostetler, H.A., Vespa, A., Landrock, D., Landrock, K.K. and Payne, H.R., 2008. Role of fatty acid binding proteins and long chain fatty acids in modulating nuclear receptors and gene transcription. *Lipids*, 43(1), pp.1-17.

Schuetz, A., Nana, D., Rose, C., Zocher, G., Milanovic, M., Koenigsmann, J., Blasig, R., Heinemann, U. and Carstanjen, D., 2011. The structure of the Klf4 DNA-binding domain links

- to self-renewal and macrophage differentiation. *Cellular and Molecular Life Sciences*, 68(18), pp.3121-3131.
- Schug, T.T., Berry, D.C., Shaw, N.S., Travis, S.N. and Noy, N., 2007. Opposing effects of retinoic acid on cell growth result from alternate activation of two different nuclear receptors. *Cell*, 129(4), pp.723-733.
- Schug, T.T., Berry, D.C., Toshkov, I.A., Cheng, L., Nikitin, A.Y. and Noy, N., 2008. Overcoming retinoic acid-resistance of mammary carcinomas by diverting retinoic acid from PPAR $\beta/\delta$  to RAR. *Proceedings of the National Academy of Sciences*, 105(21), pp.7546-7551.
- Schunke, D., Span, P., Ronneburg, H., Dittmer, A., Vetter, M., Holzhausen, H.J., Kantelhardt, E., Krenkel, S., Müller, V., Sweep, F.C. and Thomssen, C., 2007. Cyclooxygenase-2 is a target gene of Rho GDP dissociation inhibitor  $\beta$  in breast cancer cells. *Cancer research*, 67(22), pp.10694-10702.
- Schwartzbaum, J.A., Fisher, J.L., Aldape, K.D. and Wrensch, M., 2006. Epidemiology and molecular pathology of glioma. *Nature clinical practice Neurology*, 2(9), pp.494-503.
- Seldin, D.C., Landesman-Bollag, E., Farago, M., Currier, N., Lou, D. and Dominguez, I., 2005. CK2 as a positive regulator of Wnt signalling and tumourigenesis. *Molecular and cellular biochemistry*, 274(1), pp.63-67.
- Sellers, K., Fox, M.P., Bousamra, M., Slone, S.P., Higashi, R.M., Miller, D.M., Wang, Y., Yan, J., Yuneva, M.O., Deshpande, R. and Lane, A.N., 2015. Pyruvate carboxylase is critical for non-small-cell lung cancer proliferation. *The Journal of clinical investigation*, 125(2), pp.687-698.
- Senyavina, N.V., Gerasimenko, T.N., Fomicheva, K.A., Tonevitskaya, S.A. and Kaprin, A.D., 2016. Localization and expression of nucleoside transporters ENT1 and ENT2 in polar cells of intestinal epithelium. *Bulletin of experimental biology and medicine*, 160(6), pp.771-774.
- Seol, H.J., Yoo, H.Y., Jin, J., Joo, K.M., Kim, H.S., Yoon, S.J., Choi, S.H., Kim, Y., Pyo, H.R., Lim, D.H. and Kim, W., 2011. The expression of DNA damage checkpoint proteins and prognostic implication in metastatic brain tumors. *Oncology Research Featuring Preclinical and Clinical Cancer Therapeutics*, 19(8-9), pp.381-390.
- Serrano, L., Martínez-Redondo, P., Marazuela-Duque, A., Vazquez, B.N., Dooley, S.J., Voigt, P., Beck, D.B., Kane-Goldsmith, N., Tong, Q., Rabanal, R.M. and Fondevila, D., 2013. The tumor suppressor SirT2 regulates cell cycle progression and genome stability by modulating the mitotic deposition of H4K20 methylation. *Genes & development*, 27(6), pp.639-653.
- Sette, G., Salvati, V., Mottolese, M., Visca, P., Gallo, E., Fecchi, K., Piloizzi, E., Duranti, E., Policicchio, E., Tartaglia, M. and Milella, M., 2015. Tyr1068-phosphorylated epidermal growth factor receptor (EGFR) predicts cancer stem cell targeting by erlotinib in preclinical models of wild-type EGFR lung cancer. *Cell death & disease*, 6(8), pp.e1850-e1850.
- Seyfried, T.N. and Shelton, L.M., 2010. Cancer as a metabolic disease. *Nutrition & metabolism*, 7(1), pp.1-22.
- Seyhan, A.A., Varadarajan, U., Choe, S., Liu, W. and Ryan, T.E., 2012. A genome-wide RNAi screen identifies novel targets of neratinib resistance leading to identification of potential drug resistant genetic markers. *Molecular bioSystems*, 8(5), pp.1553-1570.

- Seystahl, K., Tritschler, I., Szabo, E., Tabatabai, G. and Weller, M., 2015. Differential regulation of TGF- $\beta$ -induced, ALK-5-mediated VEGF release by SMAD2/3 versus SMAD1/5/8 signaling in glioblastoma. *Neuro-oncology*, 17(2), pp.254-265.
- Shackelford, D.B., Abt, E., Gerken, L., Vasquez, D.S., Seki, A., Leblanc, M., Wei, L., Fishbein, M.C., Czernin, J., Mischel, P.S. and Shaw, R.J., 2013. LKB1 inactivation dictates therapeutic response of non-small cell lung cancer to the metabolism drug phenformin. *Cancer cell*, 23(2), pp.143-158.
- Shah, N.R., Tancioni, I., Ward, K.K., Lawson, C., Chen, X.L., Jean, C., Sulzmaier, F.J., Uryu, S., Miller, N.L., Connolly, D.C. and Schlaepfer, D.D., 2014. Analyses of merlin/NF2 connection to FAK inhibitor responsiveness in serous ovarian cancer. *Gynecologic oncology*, 134(1), pp.104-111.
- Shankar, G.M. and Santagata, S., 2017. BAP1 mutations in high-grade meningioma: implications for patient care. *Neuro-oncology*, 19(11), pp.1447-1456.
- Shao, H., Chung, J., Balaj, L., Charest, A., Bigner, D.D., Carter, B.S., Hochberg, F.H., Breakefield, X.O., Weissleder, R. and Lee, H., 2012. Protein typing of circulating microvesicles allows real-time monitoring of glioblastoma therapy. *Nature medicine*, 18(12), pp.1835-1840.
- Sharma, S., Ray, S., Moiyadi, A., Sridhar, E. and Srivastava, S., 2014. Quantitative proteomic analysis of meningiomas for the identification of surrogate protein markers. *Scientific reports*, 4(1), pp.1-11.
- Sharma, S., Ray, S., Mukherjee, S., Moiyadi, A., Sridhar, E. and Srivastava, S., 2015. Multipronged quantitative proteomic analyses indicate modulation of various signal transduction pathways in human meningiomas. *Proteomics*, 15(2-3), pp.394-407.
- Shaw, R.J., Paez, J.G., Curto, M., Yaktine, A., Pruitt, W.M., Saotome, I., O'Bryan, J.P., Gupta, V., Ratner, N., Der, C.J. and Jacks, T., 2001. The Nf2 tumor suppressor, merlin, functions in Rac-dependent signaling. *Developmental cell*, 1(1), pp.63-72.
- Shen, M.R., Wilkins, R.J., Chou, C.Y. and Ellory, J.C., 2002. Anion exchanger isoform 2 operates in parallel with Na<sup>+</sup>/H<sup>+</sup> exchanger isoform 1 during regulatory volume decrease of human cervical cancer cells. *FEBS letters*, 512(1-3), pp.52-58.
- Sher, I., Hanemann, C.O., Karplus, P.A. and Bretscher, A., 2012. The tumor suppressor merlin controls growth in its open state and is converted by phosphorylation to a less-active more-closed state. *Developmental cell*, 22(4), p.703.
- Shevchenko, A., Tomas, H., Havli, J., Olsen, J.V. and Mann, M., 2006. In-gel digestion for mass spectrometric characterization of proteins and proteomes. *Nature protocols*, 1(6), p.2856.
- Shi, R., Wang, P.Y., Li, X.Y., Chen, J.X., Li, Y., Zhang, X.Z., Zhang, C.G., Jiang, T., Li, W.B., Ding, W. and Cheng, S.J., 2015. Exosomal levels of miRNA-21 from cerebrospinal fluids associated with poor prognosis and tumor recurrence of glioma patients. *Oncotarget*, 6(29), p.26971.
- Shimada, M., Niida, H., Zineldeen, D.H., Tagami, H., Tanaka, M., Saito, H. and Nakanishi, M., 2008. Chk1 is a histone H3 threonine 11 kinase that regulates DNA damage-induced transcriptional repression. *Cell*, 132(2), pp.221-232.

- Shinde, A., Wilmanski, T., Chen, H., Teegarden, D. and Wendt, M.K., 2018. Pyruvate carboxylase supports the pulmonary tropism of metastatic breast cancer. *Breast Cancer Research*, 20(1), pp.1-12.
- Shiozaki, A., Hikami, S., Ichikawa, D., Kosuga, T., Shimizu, H., Kudou, M., Yamazato, Y., Kobayashi, T., Shoda, K., Arita, T. and Konishi, H., 2018. Anion exchanger 2 suppresses cellular movement and has prognostic significance in esophageal squamous cell carcinoma. *Oncotarget*, 9(40), p.25993.
- Shoelson, S.E., 1997. SH2 and PTB domain interactions in tyrosine kinase signal transduction. *Current opinion in chemical biology*, 1(2), pp.227-234.
- Siegel, P.M. and Massagué, J., 2003. Cytostatic and apoptotic actions of TGF- $\beta$  in homeostasis and cancer. *Nature Reviews Cancer*, 3(11), pp.807-820.
- Sievers, P., Hielscher, T., Schrimpf, D., Stichel, D., Reuss, D.E., Berghoff, A.S., Neidert, M.C., Wirsching, H.G., Mawrin, C., Ketter, R. and Paulus, W., 2020. CDKN2A/B homozygous deletion is associated with early recurrence in meningiomas. *Acta neuropathologica*, 140(3), pp.409-413.
- Silinsky, E.M. and Searl, T.J., 2003. Phorbol esters and neurotransmitter release: more than just protein kinase C. *British journal of pharmacology*, 138(7), pp.1191-1201.
- Silva, G.B.R.F.D., Silva, T.G.A., Duarte, R.A., Neto, N.L., Carrara, H.H.A., Donadi, E.A., Gonçalves, M.A.G., Soares, E.G. and Soares, C.P., 2013. Expression of the classical and nonclassical HLA molecules in breast cancer. *International journal of breast cancer*, 2013.
- Silva, J.M., Wippel, H.H., Santos, M.D., Verissimo, D.C., Santos, R.M., Nogueira, F., Passos, G.A., Sprengel, S.L., Borba, L.A., Carvalho, P.C. and Fischer, J.D.S.D.G., 2020. Proteomics pinpoints alterations in grade I meningiomas of male versus female patients. *Scientific reports*, 10(1), pp.1-11.
- Simpson, D., 1957. The recurrence of intracranial meningiomas after surgical treatment. *Journal of neurology, neurosurgery, and psychiatry*, 20(1), p.22.
- Singh, P.K., Kashyap, A. and Silakari, O., 2018. Exploration of the therapeutic aspects of Lck: A kinase target in inflammatory mediated pathological conditions. *Biomedicine & Pharmacotherapy*, 108, pp.1565-1571.
- Skelding, K.A. and Rostas, J.A., 2009. Regulation of CaMKII in vivo: the importance of targeting and the intracellular microenvironment. *Neurochemical research*, 34(10), pp.1792-1804.
- Slattery, M.L., Mullany, L.E., Sakoda, L., Samowitz, W.S., Wolff, R.K., Stevens, J.R. and Herrick, J.S., 2018. The NF- $\kappa$ B signalling pathway in colorectal cancer: associations between dysregulated gene and miRNA expression. *Journal of cancer research and clinical oncology*, 144(2), pp.269-283.
- Smyth, M.S. and Martin, J.H.J., 2000. X-ray crystallography. *Molecular Pathology*, 53(1), p.8.
- Sofela, A. A., Hilton, D. A., Ammoun, S., Baiz, D., Adams, C. L., Ercolano, E., Jenkinson, M. D., Kurian, K. M., Teo, M., Whitfield, P. C., Sahn, F., & Hanemann, C. O. (2021). Fibulin-2: A Novel Biomarker for Differentiating Grade II from Grade I Meningiomas. *International journal of molecular sciences*, 22(2), 560.

- Soh, J.W. and Weinstein, I.B., 2003. Roles of specific isoforms of protein kinase C in the transcriptional control of cyclin D1 and related genes. *Journal of Biological Chemistry*, 278(36), pp.34709-34716.
- Solari, F.A., Dell'Aica, M., Sickmann, A. and Zahedi, R.P., 2015. Why phosphoproteomics is still a challenge. *Molecular BioSystems*, 11(6), pp.1487-1493.
- Song, L.J., Liu, R.J., Zeng, Z., Alper, S.L., Cui, H.J., Lu, Y., Zheng, L., Yan, Z.W. and Fu, G.H., 2012. Gastrin inhibits a novel, pathological colon cancer signaling pathway involving EGR1, AE2, and P-ERK. *Journal of molecular medicine*, 90(6), pp.707-718.
- Sontheimer, H., 2008. An unexpected role for ion channels in brain tumor metastasis. *Experimental biology and medicine*, 233(7), pp.779-791.
- Sopkova, J., Raguene-Nicol, C., Vincent, M., Chevalier, A., Lewit-Bentley, A., Russo-Marie, F. and Gallay, J., 2002. Ca<sup>2+</sup> and membrane binding to annexin 3 modulate the structure and dynamics of its N terminus and domain III. *Protein science*, 11(7), pp.1613-1625.
- Soprano, D.R., Qin, P. and Soprano, K.J., 2004. Retinoic acid receptors and cancers. *Annual review of nutrition*, 24, p.201.
- Sørensen, C.S., Hansen, L.T., Dziegielewski, J., Syljuåsen, R.G., Lundin, C., Bartek, J. and Helleday, T., 2005. The cell-cycle checkpoint kinase Chk1 is required for mammalian homologous recombination repair. *Nature cell biology*, 7(2), pp.195-201.
- Soyuer, S., Chang, E.L., Selek, U., Shi, W., Maor, M.H. and DeMonte, F., 2004. Radiotherapy after surgery for benign cerebral meningioma. *Radiotherapy and oncology*, 71(1), pp.85-90.
- Spratlin, J.L. and Mackey, J.R., 2010. Human equilibrative nucleoside transporter 1 (hENT1) in pancreatic adenocarcinoma: towards individualized treatment decisions. *Cancers*, 2(4), pp.2044-2054.
- Sriuranpong, V., Mutirangura, A., Gillespie, J.W., Patel, V., Amornphimoltham, P., Molinolo, A.A., Kerekhanjanarong, V., Supanakorn, S., Supiyaphun, P., Rangaeng, S. and Voravud, N., 2004. Global gene expression profile of nasopharyngeal carcinoma by laser capture microdissection and complementary DNA microarrays. *Clinical Cancer Research*, 10(15), pp.4944-4958.
- St-Denis, N.A. and Litchfield, D.W., 2009. Protein kinase CK2 in health and disease. *Cellular and Molecular Life Sciences*, 66(11), pp.1817-1829.
- Steinmeyer, K., Ortlund, C. and Jentsch, T.J., 1991. Primary structure and functional expression of a developmentally regulated skeletal muscle chloride channel. *Nature*, 354(6351), pp.301-304.
- Stenina, O.I., Topol, E.J. and Plow, E.F., 2007. Thrombospondins, their polymorphisms, and cardiovascular disease. *Arteriosclerosis, thrombosis, and vascular biology*, 27(9), pp.1886-1894.
- Stevens, C., Smith, L. and La Thangue, N.B., 2003. Chk2 activates E2F-1 in response to DNA damage. *Nature cell biology*, 5(5), pp.401-409.
- Strange, K.E.V.I.N., 1991. Volume regulatory Cl<sup>-</sup> loss after Na<sup>+</sup> pump inhibition in CCT principal cells. *American Journal of Physiology-Renal Physiology*, 260(2), pp.F225-F234.

- Strickaert, A., Corbet, C., Spinette, S.A., Craciun, L., Dom, G., Andry, G., Larsimont, D., Wattiez, R., Dumont, J.E., Feron, O. and Maenhaut, C., 2019. Reprogramming of energy metabolism: increased expression and roles of pyruvate carboxylase in papillary thyroid cancer. *Thyroid*, 29(6), pp.845-857.
- Strickland, M.R., Gill, C.M., Nayyar, N., D'Andrea, M.R., Thiede, C., Juratli, T.A., Schackert, G., Borger, D.R., Santagata, S., Frosch, M.P. and Cahill, D.P., 2017. Targeted sequencing of SMO and AKT1 in anterior skull base meningiomas. *Journal of neurosurgery*, 127(2), pp.438-444.
- Su, P., Wen, S., Zhang, Y., Li, Y., Xu, Y., Zhu, Y., Lv, H., Zhang, F., Wang, M. and Tian, Z., 2016. Identification of the key genes and pathways in esophageal carcinoma. *Gastroenterology research and practice*, 2016.
- Sulman, E.P., White, P.S. and Brodeur, G.M., 2004. Genomic annotation of the meningioma tumor suppressor locus on chromosome 1p34. *Oncogene*, 23(4), pp.1014-1020.
- Sun, S.Q., Gu, X., Gao, X.S., Li, Y., Yu, H., Xiong, W., Yu, H., Wang, W., Li, Y., Teng, Y. and Zhou, D., 2016. Overexpression of AKR1C3 significantly enhances human prostate cancer cells resistance to radiation. *Oncotarget*, 7(30), p.48050.
- Sun, S.Q., Hawasli, A.H., Huang, J., Chicoine, M.R. and Kim, A.H., 2015. An evidence-based treatment algorithm for the management of WHO Grade II and III meningiomas. *Neurosurgical focus*, 38(3), p.E3.
- Suppiah, S., Nassiri, F., Bi, W.L., Dunn, I.F., Hanemann, C.O., Horbinski, C.M., Hashizume, R., James, C.D., Mawrin, C., Noushmehr, H. and Perry, A., 2019. Molecular and translational advances in meningiomas. *Neuro-oncology*, 21(Supplement\_1), pp.i4-i17.
- Sutandy, F.R., Qian, J., Chen, C.S. and Zhu, H., 2013. Overview of protein microarrays. *Current protocols in protein science*, 72(1), pp.27-1.
- Swairjo, M.A. and Seaton, B.A., 1994. Annexin structure and membrane interactions: a molecular perspective. *Annual review of biophysics and biomolecular structure*, 23(1), pp.193-213.
- Takahashi, K. and Yamanaka, S., 2006. Induction of pluripotent stem cells from mouse embryonic and adult fibroblast cultures by defined factors. *Cell*, 126(4), pp.663-676.
- Takai, H., Tominaga, K., Motoyama, N., Minamishima, Y.A., Nagahama, H., Tsukiyama, T., Ikeda, K., Nakayama, K., Nakanishi, M. and Nakayama, K.I., 2000. Aberrant cell cycle checkpoint function and early embryonic death in *Chk1*<sup>-/-</sup> mice. *Genes & development*, 14(12), pp.1439-1447.
- Tan, M., Li, P., Sun, M., Yin, G. and Yu, D., 2006. Upregulation and activation of PKC $\alpha$  by ErbB2 through Src promotes breast cancer cell invasion that can be blocked by combined treatment with PKC $\alpha$  and Src inhibitors. *Oncogene*, 25(23), pp.3286-3295.
- Tan, Y., Wu, F., Lin, W., Wei, Y., Lin, Y., Chao, N. and Zhou, Q., 2021. Upregulation of PTGFRN in Hepatocellular Carcinoma Predicts Poor Prognosis: A Study Based on the TCGA Database.
- Tang, W., Zhu, Y., Gao, J., Fu, J., Liu, C., Liu, Y., Song, C., Zhu, S., Leng, Y., Wang, G. and Chen, W., 2014. MicroRNA-29a promotes colorectal cancer metastasis by regulating matrix metalloproteinase 2 and E-cadherin via KLF4. *British journal of cancer*, 110(2), pp.450-458.

- Tavolari, S., Deserti, M., Vasuri, F., Curti, S., Palloni, A., Pinna, A.D., Cescon, M., Frega, G., De Lorenzo, S., Barbera, M.A. and Garajova, I., 2019. Membrane human equilibrative nucleoside transporter 1 is associated with a high proliferation rate and worse survival in resected intrahepatic cholangiocarcinoma patients not receiving adjuvant treatments. *European Journal of Cancer*, 106, pp.160-170.
- Taylor, K.M. and LaBonne, C., 2007. Modulating the activity of neural crest regulatory factors. *Current opinion in genetics & development*, 17(4), pp.326-331.
- Theodorescu, D., Sapinoso, L.M., Conaway, M.R., Oxford, G., Hampton, G.M. and Frierson Jr, H.F., 2004. Reduced expression of metastasis suppressor RhoGDI2 is associated with decreased survival for patients with bladder cancer. *Clinical Cancer Research*, 10(11), pp.3800-3806.
- Theret, N., Bouezzeddine, F., Azar, F., Diab-Assaf, M. and Legagneux, V., 2021. ADAM and ADAMTS Proteins, New Players in the Regulation of Hepatocellular Carcinoma Microenvironment. *Cancers*, 13(7), p.1563.
- Thiery, J.P., Acloque, H., Huang, R.Y. and Nieto, M.A., 2009. Epithelial-mesenchymal transitions in development and disease. *Cell*, 139(5), pp.871-890.
- Tian, H., Mythreye, K., Golzio, C., Katsanis, N. and Blobel, G.C., 2012. Endoglin mediates fibronectin/ $\alpha 5\beta 1$  integrin and TGF- $\beta$  pathway crosstalk in endothelial cells. *The EMBO journal*, 31(19), pp.3885-3900.
- Tiwari, N., Meyer-Schaller, N., Arnold, P., Antoniadis, H., Pachkov, M., van Nimwegen, E. and Christofori, G., 2013. Klf4 is a transcriptional regulator of genes critical for EMT, including Jnk1 (Mapk8). *PloS one*, 8(2), p.e57329.
- Tong, M., Che, N., Zhou, L., Luk, S.T., Kau, P.W., Chai, S., Ngan, E.S., Lo, C.M., Man, K., Ding, J. and Lee, T.K., 2018. Efficacy of annexin A3 blockade in sensitizing hepatocellular carcinoma to sorafenib and regorafenib. *Journal of Hepatology*, 69(4), pp.826-839.
- Tong, M., Fung, T.M., Luk, S.T., Ng, K.Y., Lee, T.K., Lin, C.H., Yam, J.W., Chan, K.W., Ng, F., Zheng, B.J. and Yuan, Y.F., 2015. ANXA3/JNK signaling promotes self-renewal and tumor growth, and its blockade provides a therapeutic target for hepatocellular carcinoma. *Stem cell reports*, 5(1), pp.45-59.
- Torres-Martin, M., Lassaletta, L., Isla, A., De Campos, J.M., Pinto, G.R., Burbano, R.R., Castresana, J.S., Melendez, B. and Rey, J.A., 2014. Global expression profile in low grade meningiomas and schwannomas shows upregulation of PDGFD, CDH1 and SLIT2 compared to their healthy tissue. *Oncology reports*, 32(6), pp.2327-2334.
- Toyama, A., Suzuki, A., Shimada, T., Aoki, C., Aoki, Y., Umino, Y., Nakamura, Y., Aoki, D. and Sato, T.A., 2012. Proteomic characterization of ovarian cancers identifying annexin-A 4, phosphoserine aminotransferase, cellular retinoic acid-binding protein 2, and serpin B 5 as histology-specific biomarkers. *Cancer science*, 103(4), pp.747-755.
- Trofatter, J.A., MacCollin, M.M., Rutter, J.L., Murrell, J.R., Duyao, M.P., Parry, D.M., Eldridge, R., Kley, N., Menon, A.G., Pulaski, K. and Haase, V.H., 1993. A novel moesin-, ezrin-, radixin-like gene is a candidate for the neurofibromatosis 2 tumor suppressor. *Cell*, 72(5), pp.791-800.



- Tsai, C.H., Chen, Y.T., Chang, Y.H., Hsueh, C., Liu, C.Y., Chang, Y.S., Chen, C.L. and Yu, J.S., 2018. Systematic verification of bladder cancer-associated tissue protein biomarker candidates in clinical urine specimens. *Oncotarget*, 9(56), p.30731.
- Tsuchiya, Y., Nakabayashi, O. and Nakano, H., 2015. FLIP the Switch: Regulation of Apoptosis and Necroptosis by cFLIP. *International journal of molecular sciences*, 16(12), pp.30321-30341.
- Tsutsui, K., Manabe, R.I., Yamada, T., Nakano, I., Oguri, Y., Keene, D.R., Sengle, G., Sakai, L.Y. and Sekiguchi, K., 2010. ADAMTSL-6 Is a Novel Extracellular Matrix Protein That Binds to Fibrillin-1 and Promotes Fibrillin-1 Fibril Formation 2. *Journal of Biological Chemistry*, 285(7), pp.4870-4882.
- Tufan, K., Dogulu, F., Kurt, G., Emmez, H., Ceviker, N. and Baykaner, M.K., 2005. Intracranial meningiomas of childhood and adolescence. *Pediatric neurosurgery*, 41(1), pp.1-7.
- Turbin, R.E., Thompson, C.R., Kennerdell, J.S., Cockerham, K.P. and Kupersmith, M.J., 2002. A long-term visual outcome comparison in patients with optic nerve sheath meningioma managed with observation, surgery, radiotherapy, or surgery and radiotherapy. *Ophthalmology*, 109(5), pp.890-899.
- Tyers, M. and Mann, M., 2003. From genomics to proteomics. *Nature*, 422(6928), pp.193-197.
- Uchida, T., Park, S.B., Inuzuka, T., Zhang, M., Allen, J.N., Chayama, K. and Liang, T.J., 2021. Genetically edited hepatic cells expressing the NTCP-S267F variant are resistant to hepatitis B virus infection. *Molecular Therapy-Methods & Clinical Development*, 23, pp.597-605.
- Uzawa, K., Kasamatsu, A., Shimizu, T., Saito, Y., Baba, T., Sakuma, K., Fushimi, K., Sakamoto, Y., Ogawara, K., Shiiba, M. and Tanzawa, H., 2014. Suppression of metastasis by mirtazapine via restoration of the Lin-7C/ $\beta$ -catenin pathway in human cancer cells. *Scientific reports*, 4(1), pp.1-8.
- Vadivelu, S., Sharer, L. and Schulder, M., 2010. Regression of multiple intracranial meningiomas after cessation of long-term progesterone agonist therapy: Case report. *Journal of neurosurgery*, 112(5), pp.920-924.
- Vaezeslami, S., Mathes, E., Vasileiou, C., Borhan, B. and Geiger, J.H., 2006. The structure of apo-wild-type cellular retinoic acid binding protein II at 1.4 Å and its relationship to ligand binding and nuclear translocation. *Journal of molecular biology*, 363(3), pp.687-701.
- Vahedi, S., Chueh, F.Y., Chandran, B. and Yu, C.L., 2015. Lymphocyte-specific protein tyrosine kinase (Lck) interacts with CR6-interacting factor 1 (CRIF1) in mitochondria to repress oxidative phosphorylation. *BMC cancer*, 15(1), pp.1-14.
- Van Gool, A., Corrales, F., Čolović, M., Krstić, D., Oliver-Martos, B., Martínez-Cáceres, E., Jakasa, I., Gajski, G., Brun, V., Kyriacou, K. and Burzynska-Pedziwiatr, I., 2020. Analytical techniques for multiplex analysis of protein biomarkers. *Expert review of proteomics*, 17(4), pp.257-273.
- Van Laethem, F., Tikhonova, A.N., Pobezinsky, L.A., Tai, X., Kimura, M.Y., Le Saout, C., Guintier, T.I., Adams, A., Sharrow, S.O., Bernhardt, G. and Feigenbaum, L., 2013. Lck availability during thymic selection determines the recognition specificity of the T cell repertoire. *Cell*, 154(6), pp.1326-1341.

- Van Laethem, F., Tikhonova, A.N., Pobezinsky, L.A., Tai, X., Kimura, M.Y., Le Saout, C., Guintier, T.I., Adams, A., Sharrow, S.O., Bernhardt, G. and Feigenbaum, L., 2013. Lck availability during thymic selection determines the recognition specificity of the T cell repertoire. *Cell*, 154(6), pp.1326-1341.
- Van Roy, F. and Berx, G., 2008. The cell-cell adhesion molecule E-cadherin. *Cellular and molecular life sciences*, 65(23), pp.3756-3788.
- Vega, F.M. and Ridley, A.J., 2008. Rho GTPases in cancer cell biology. *FEBS letters*, 582(14), pp.2093-2101.
- Veillette, A., Foss, F.M., Sausville, E.A., Bolen, J.B. and Rosen, N., 1987. Expression of the lck tyrosine kinase gene in human colon carcinoma and other non-lymphoid human tumor cell lines. *Oncogene research*, 1(4), pp.357-374.
- Velasco, S., Alvarez-Muñoz, P., Pericacho, M., Dijke, P.T., Bernabéu, C., López-Novoa, J.M. and Rodríguez-Barbero, A., 2008. L- and S-endoglin differentially modulate TGFβ1 signaling mediated by ALK1 and ALK5 in L6E9 myoblasts. *Journal of Cell Science*, 121(6), pp.913-919.
- Verlinden, L., Bempt, I.V., Eelen, G., Drijkoningen, M., Verlinden, I., Marchal, K., De Wolf-Peeters, C., Christiaens, M.R., Michiels, L., Bouillon, R. and Verstuyf, A., 2007. The E2F-regulated gene Chk1 is highly expressed in triple-negative estrogen receptor-/progesterone receptor-/HER-2- breast carcinomas. *Cancer research*, 67(14), pp.6574-6581.
- Vesuna, F., van Diest, P., Chen, J.H. and Raman, V., 2008. Twist is a transcriptional repressor of E-cadherin gene expression in breast cancer. *Biochemical and biophysical research communications*, 367(2), pp.235-241.
- Viaene, A.N., Zhang, B., Martinez-Lage, M., Xiang, C., Tosi, U., Thawani, J.P., Gungor, B., Zhu, Y., Roccograndi, L., Zhang, L. and Bailey, R.L., 2019. Transcriptome signatures associated with meningioma progression. *Acta neuropathologica communications*, 7(1), pp.1-13.
- Villén, J., Beausoleil, S.A., Gerber, S.A. and Gygi, S.P., 2007. Large-scale phosphorylation analysis of mouse liver. *Proceedings of the National Academy of Sciences*, 104(5), pp.1488-1493.
- Vinagre, J., Almeida, A., Pópulo, H., Batista, R., Lyra, J., Pinto, V., Coelho, R., Celestino, R., Prazeres, H., Lima, L. and Melo, M., 2013. Frequency of TERT promoter mutations in human cancers. *Nature communications*, 4, p.2185.
- Vivanco, I. and Sawyers, C.L., 2002. The phosphatidylinositol 3-kinase–AKT pathway in human cancer. *Nature Reviews Cancer*, 2(7), p.489.
- Vogelstein, B., Papadopoulos, N., Velculescu, V.E., Zhou, S., Diaz Jr, L.A. and Kinzler, K.W., 2013. Cancer genome landscapes. *Science*, 339(6127), pp.1546-1558.
- Von Spreckelsen, N., Waldt, N., Poetschke, R., Kessler, C., Dohmen, H., Jiao, H.K., Nemeth, A., Schob, S., Scherlach, C., Sandalcioglu, I.E. and Deckert, M., 2020. KLF4K409Q-mutated meningiomas show enhanced hypoxia signaling and respond to mTORC1 inhibitor treatment. *Acta neuropathologica communications*, 8(1), pp.1-11.
- Vos, L.J., Yusuf, D., Lui, A., Abdelaziz, Z., Ghosh, S., Spratlin, J.L. and Mackey, J.R., 2019. Predictive and prognostic properties of human equilibrative nucleoside transporter 1 expression

- in gemcitabine-treated pancreatobiliary cancer: a meta-analysis. *JCO Precision Oncology*, 3, pp.1-22.
- Vreeland, A.C., Levi, L., Zhang, W., Berry, D.C. and Noy, N., 2014. Cellular retinoic acid-binding protein 2 inhibits tumor growth by two distinct mechanisms. *Journal of Biological Chemistry*, 289(49), pp.34065-34073.
- Vreeland, A.C., Yu, S., Levi, L., de Barros Rossetto, D. and Noy, N., 2014. Transcript stabilization by the RNA-binding protein HuR is regulated by cellular retinoic acid-binding protein 2. *Molecular and cellular biology*, 34(12), pp.2135-2146.
- Vucic, E.A., Thu, K.L., Robison, K., Rybaczyk, L.A., Chari, R., Alvarez, C.E. and Lam, W.L., 2012. Translating cancer 'omics' to improved outcomes. *Genome research*, 22(2), pp.188-195.
- Wadt, K., Choi, J., Chung, J.Y., Kiilgaard, J., Heegaard, S., Drzewiecki, K.T., Trent, J.M., Hewitt, S.M., Hayward, N.K., Gerdes, A.M. and Brown, K.M., 2012. A cryptic BAP1 splice mutation in a family with uveal and cutaneous melanoma, and paraganglioma. *Pigment cell & melanoma research*, 25(6), pp.815-818.
- Waite, K.A. and Eng, C., 2003. From developmental disorder to heritable cancer: it's all in the BMP/TGF- $\beta$  family. *Nature Reviews Genetics*, 4(10), pp.763-773.
- Walcott, B.P., Nahed, B.V., Brastianos, P.K. and Loeffler, J.S., 2013. Radiation treatment for WHO grade II and III meningiomas. *Frontiers in oncology*, 3, p.227.
- Walworth, N., Davey, S. and Beach, D., 1993. Fission yeast chk1 protein kinase links the rad checkpoint pathway to cdc2. *Nature*, 363(6427), pp.368-371.
- Walworth, Nancy, Scott Davey, and David Beach. "Fission yeast chk1 protein kinase links the rad checkpoint pathway to cdc2." *Nature* 363, no. 6427 (1993): 368-371.
- Wan, H., Zhu, J., Chen, F., Xiao, F., Huang, H., Han, X., Zhong, L., Zhong, H., Xu, L., Ni, B. and Zhong, J., 2014. SLC29A1 single nucleotide polymorphisms as independent prognostic predictors for survival of patients with acute myeloid leukemia: an in vitro study. *Journal of Experimental & Clinical Cancer Research*, 33(1), pp.1-10.
- Wan, X., Guo, D., Zhu, Q. and Qu, R., 2020. microRNA-382 suppresses the progression of pancreatic cancer through the PI3K/Akt signaling pathway by inhibition of Anxa3. *American Journal of Physiology-Gastrointestinal and Liver Physiology*, 319(3), pp.G309-G322.
- Wang, D., Wang, H., Guo, Y., Ning, W., Katkuri, S., Wahli, W., Desvergne, B., Dey, S.K. and DuBois, R.N., 2006. Crosstalk between peroxisome proliferator-activated receptor  $\delta$  and VEGF stimulates cancer progression. *Proceedings of the National Academy of Sciences*, 103(50), pp.19069-19074.
- Wang, J., Guo, Y., Chu, H., Guan, Y., Bi, J. and Wang, B., 2013. Multiple functions of the RNA-binding protein HuR in cancer progression, treatment responses and prognosis. *International journal of molecular sciences*, 14(5), pp.10015-10041.
- Wang, K. and Li, J., 2016. Overexpression of ANXA3 is an independent prognostic indicator in gastric cancer and its depletion suppresses cell proliferation and tumor growth. *Oncotarget*, 7(52), p.86972.

- Wang, L., Li, X., Ren, Y., Geng, H., Zhang, Q., Cao, L., Meng, Z., Wu, X., Xu, M. and Xu, K., 2019. Cancer-associated fibroblasts contribute to cisplatin resistance by modulating ANXA 3 in lung cancer cells. *Cancer Science*, 110(5), pp.1609-1620.
- Wang, S., Liechty, B., Patel, S., Weber, J.S., Hollmann, T.J., Snuderl, M. and Karajannis, M.A., 2018. Programmed death ligand 1 expression and tumor infiltrating lymphocytes in neurofibromatosis type 1 and 2 associated tumors. *Journal of Neuro-oncology*, 138(1), pp.183-190.
- Wang, S., Yang, Q., Fung, K.M. and Lin, H.K., 2008. AKR1C2 and AKR1C3 mediated prostaglandin D2 metabolism augments the PI3K/Akt proliferative signaling pathway in human prostate cancer cells. *Molecular and cellular endocrinology*, 289(1-2), pp.60-66.
- Wang, T., Fei, H.J., Yang, Y., Jiang, X.S., Yan, M., Zeng, Z., Wu, J., Song, L.J., Tian, H. and Fu, G.H., 2016. Expression of AE1/p16 promoted degradation of AE2 in gastric cancer cells. *BMC cancer*, 16(1), pp.1-11.
- Wang, X., Ma, Z., Xiao, Z., Liu, H., Dou, Z., Feng, X. and Shi, H., 2012. Chk1 knockdown confers radiosensitization in prostate cancer stem cells. *Oncology reports*, 28(6), pp.2247-2254.
- Wang, Z., Ling, S., Rettig, E., Sobel, R., Tan, M., Fertig, E.J., Considine, M., El-Naggar, A.K., Brait, M., Fakhry, C. and Ha, P.K., 2015. Epigenetic screening of salivary gland mucoepidermoid carcinoma identifies hypomethylation of CLIC3 as a common alteration. *Oral oncology*, 51(12), pp.1120-1125.
- Wang, Z., Liu, H., Liu, B., Ma, W., Xue, X., Chen, J. and Zhou, Q., 2010. Gene expression levels of CSNK1A1 and AAC-11, but not NME1, in tumor tissues as prognostic factors in NSCLC patients. *Medical Science Monitor*, 16(8), pp.CR357-CR364.
- Warburg, O., Wind, F. and Negelein, E., 1927. The metabolism of tumors in the body. *The Journal of general physiology*, 8(6), p.519.
- Wardlaw, S.A., Bucco, R.A., Zheng, W.L. and Ong, D.E., 1997. Variable expression of cellular retinol-and cellular retinoic acid-binding proteins in the rat uterus and ovary during the estrous cycle. *Biology of reproduction*, 56(1), pp.125-132.
- Watts, J., Box, G., Galvin, A., Brotchie, P., Trost, N. and Sutherland, T., 2014. Magnetic resonance imaging of meningiomas: a pictorial review. *Insights into imaging*, 5(1), pp.113-122.
- Ways, D.K., Kukoly, C.A., deVente, J., Hooker, J.L., Bryant, W.O., Posekany, K.J., Fletcher, D.J., Cook, P.P. and Parker, P.J., 1995. MCF-7 breast cancer cells transfected with protein kinase C-alpha exhibit altered expression of other protein kinase C isoforms and display a more aggressive neoplastic phenotype. *The Journal of clinical investigation*, 95(4), pp.1906-1915.
- Webb, B.A., Chimenti, M., Jacobson, M.P. and Barber, D.L., 2011. Dysregulated pH: a perfect storm for cancer progression. *Nature Reviews Cancer*, 11(9), pp.671-677.
- Wei, X., Zhang, K., Qin, H., Zhu, J., Qin, Q., Yu, Y. and Wang, H., 2018. GMDS knockdown impairs cell proliferation and survival in human lung adenocarcinoma. *BMC cancer*, 18(1), p.600.
- Weinberg, S.E. and Chandel, N.S., 2015. Targeting mitochondria metabolism for cancer therapy. *Nature chemical biology*, 11(1), pp.9-15.

- Weiss, A., 1993. T cell antigen receptor signal transduction: a tale of tails and cytoplasmic protein-tyrosine kinases. *Cell*, 73(2), pp.209-212.
- Weller, M., Roth, P., Sahm, F., Burghardt, I., Schuknecht, B., Rushing, E.J., Regli, L., Lindemann, J.P. and von Deimling, A., 2017. Durable control of metastatic AKT1-mutant WHO grade 1 meningeal meningioma by the AKT inhibitor, AZD5363. *Journal Of The National Cancer Institute*, 109(3), p.djw320.
- Weller, M., Stupp, R., Reifenberger, G., Brandes, A.A., Van Den Bent, M.J., Wick, W. and Hegi, M.E., 2010. MGMT promoter methylation in malignant gliomas: ready for personalized medicine? *Nature Reviews Neurology*, 6(1), pp.39-51.
- Welsh, M.J., 1990. Abnormal regulation of ion channels in cystic fibrosis epithelia. *The FASEB Journal*, 4(10), pp.2718-2725.
- Whittle, I.R., Smith, C., Navoo, P. and Collie, D., 2004. Meningiomas. *The Lancet*, 363(9420), pp.1535-1543.
- Wibom, C., Mören, L., Aarhus, M., Knappskog, P.M., Lund-Johansen, M., Antti, H. and Bergenheim, A.T., 2009. Proteomic profiles differ between bone invasive and noninvasive benign meningiomas of fibrous and meningeal subtype. *Journal of neuro-oncology*, 94(3), pp.321-331.
- Wickremesekera, A., Hovens, C.M. and Kaye, A.H., 2010. Expression of ErbB-1 and ErbB-2 in meningioma. *Journal of Clinical Neuroscience*, 17(9), pp.1155-1158.
- Wiemels, J., Wrensch, M. and Claus, E.B., 2010. Epidemiology and etiology of meningioma. *Journal of neuro-oncology*, 99(3), pp.307-314.
- Wiese, S., Reidegeld, K.A., Meyer, H.E. and Warscheid, B., 2007. Protein labeling by iTRAQ: a new tool for quantitative mass spectrometry in proteome research. *Proteomics*, 7(3), pp.340-350.
- Wilkins, M.R., Gasteiger, E., Sanchez, J.C., Appel, R.D. and Hochstrasser, D.F., 1996. Protein identification with sequence tags. *Current Biology*, 6(12), pp.1543-1544.
- Willems, E., Dedobbeleer, M., Digregorio, M., Lombard, A., Lumapat, P.N. and Rogister, B., 2018. The functional diversity of Aurora kinases: a comprehensive review. *Cell division*, 13(1), pp.1-17.
- Wirbel, J., Cutillas, P. and Saez-Rodriguez, J., 2018. Phosphoproteomics-based profiling of kinase activities in cancer cells. In *Cancer Systems Biology* (pp. 103-132). Humana Press, New York, NY.
- Wiredja, D.D., Koyutürk, M. and Chance, M.R., 2017. The KSEA App: a web-based tool for kinase activity inference from quantitative phosphoproteomics. *Bioinformatics*, 33(21), pp.3489-3491.
- Wojtkowiak, J.W., Verduzco, D., Schramm, K.J. and Gillies, R.J., 2011. Drug resistance and cellular adaptation to tumor acidic pH microenvironment. *Molecular pharmaceuticals*, 8(6), pp.2032-2038.
- Worrell, R.T., Butt, A.G., Cliff, W.H. and Frizzell, R.A., 1989. A volume-sensitive chloride conductance in human colonic cell line T84. *American Journal of Physiology-Cell Physiology*, 256(6), pp.C1111-C1119.

- Wu, J., Li, X., Luo, F., Yan, J. and Yang, K., 2020. Screening key miRNAs and genes in prostate cancer by microarray analysis. *Translational Cancer Research*, 9(2), p.856.
- Wu, J.I., Lin, Y.P., Tseng, C.W., Chen, H.J. and Wang, L.H., 2019. Crabp2 promotes metastasis of lung cancer cells via HuR and integrin  $\beta$ 1/FAK/ERK signaling. *Scientific reports*, 9(1), pp.1-14.
- Wu, N., Liu, S., Guo, C., Hou, Z. and Sun, M.Z., 2013. The role of annexin A3 playing in cancers. *Clinical and Translational Oncology*, 15(2), pp.106-110.
- Wu, T., Hsieh, Y., Wu, C., Tsai, J., Hsieh, Y., Huang, C. and Liu, J., 2006. Overexpression of anion exchanger 2 in human hepatocellular carcinoma. *Chinese Journal of Physiology*, 49(4), p.192.
- Wu, X., Xing, X., Dowlut, D., Zeng, Y., Liu, J. and Liu, X., 2019. Integrating phosphoproteomics into kinase-targeted cancer therapies in precision medicine. *Journal of proteomics*, 191, pp.68-79.
- Xiao, W., Hong, H., Awadallah, A., Yu, S., Zhou, L. and Xin, W., 2014. CRABP-II is a highly sensitive and specific diagnostic molecular marker for pancreatic ductal adenocarcinoma in distinguishing from benign pancreatic conditions. *Human pathology*, 45(6), pp.1177-1183.
- Xie, Z.C., Tang, R.X., Gao, X., Xie, Q.N., Lin, J.Y., Chen, G. and Li, Z.Y., 2018. A meta-analysis and bioinformatics exploration of the diagnostic value and molecular mechanism of miR-193a-5p in lung cancer. *Oncology Letters*, 16(4), pp.4114-4128.
- Xiong, J., 2006. *Essential bioinformatics*. Cambridge University Press.
- Xu, L.G., Li, L.Y. and Shu, H.B., 2004. TRAF7 potentiates MEKK3-induced AP1 and CHOP activation and induces apoptosis. *Journal of Biological Chemistry*, 279(17), pp.17278-17282.
- Xu, N., Hegarat, N., Black, E.J., Scott, M.T., Hochegger, H. and Gillespie, D.A., 2010. Akt/PKB suppresses DNA damage processing and checkpoint activation in late G2. *Journal of Cell Biology*, 190(3), pp.297-305.
- Xu, R., Yin, J., Zhang, Y. and Zhang, S., 2019. Annexin A3 depletion overcomes resistance to oxaliplatin in colorectal cancer via the MAPK signaling pathway. *Journal of Cellular Biochemistry*, 120(9), pp.14585-14593.
- Xu, Z., Zhu, C., Chen, C., Zong, Y., Feng, H., Liu, D., Feng, W., Zhao, J. and Lu, A., 2018. CCL19 suppresses angiogenesis through promoting miR-206 and inhibiting Met/ERK/Elk-1/HIF-1 $\alpha$ /VEGF-A pathway in colorectal cancer. *Cell death & disease*, 9(10), pp.1-16.
- Yamamoto, M., Dräger, U.C., Ong, D.E. and McCaffery, P., 1998. Retinoid-binding proteins in the cerebellum and choroid plexus and their relationship to regionalized retinoic acid synthesis and degradation. *European journal of biochemistry*, 257(2), pp.344-350.
- Yamamoto, M., Sanomachi, T., Suzuki, S., Uchida, H., Yonezawa, H., Higa, N., Takajo, T., Yamada, Y., Sugai, A., Togashi, K. and Seino, S., 2021. Roles for hENT1 and dCK in gemcitabine sensitivity and malignancy of meningioma. *Neuro-oncology*, 23(6), pp.945-954.
- Yamanaka, R., Hayano, A. and Kanayama, T., 2017. Radiation-induced meningiomas: an exhaustive review of the literature. *World neurosurgery*, 97, pp.635-644.
- Yamaoka, T., Frey, M.R., Dise, R.S., Bernard, J.K. and Polk, D.B., 2011. Specific epidermal growth factor receptor autophosphorylation sites promote mouse colon epithelial cell

chemotaxis and restitution. *American Journal of Physiology-Gastrointestinal and Liver Physiology*, 301(2), pp.G368-G376.

Yamashita, D., Sano, Y., Adachi, Y., Okamoto, Y., Osada, H., Takahashi, T., Yamaguchi, T., Osumi, T. and Hirose, F., 2007. hDREF regulates cell proliferation and expression of ribosomal protein genes. *Molecular and cellular biology*, 27(6), pp.2003-2013.

Yan, Y., Zhiwei, L.I., Kong, X., Jia, Z., Zuo, X., Gagea, M., Huang, S., Wei, D. and Xie, K., 2016. KLF4-mediated suppression of CD44 signaling negatively impacts pancreatic cancer stemness and metastasis. *Cancer research*, 76(8), pp.2419-2431.

Yáñez-Mó, M., Barreiro, O., Gordon-Alonso, M., Sala-Valdés, M. and Sánchez-Madrid, F., 2009. Tetraspanin-enriched microdomains: a functional unit in cell plasma membranes. *Trends in cell biology*, 19(9), pp.434-446.

Yang, H.W., Kim, T.M., Song, S.S., Shrinath, N., Park, R., Kalamarides, M., Park, P.J., Black, P.M., Carroll, R.S. and Johnson, M.D., 2012. Alternative splicing of CHEK2 and codeletion with NF2 promote chromosomal instability in meningioma. *Neoplasia*, 14(1), pp.20-28.

Yang, L., Lu, P., Yang, X., Li, K. and Qu, S., 2021. Annexin A3, a Calcium-dependent Phospholipid-Binding Protein: Implication in Cancer. *Frontiers in Molecular Biosciences*, 8.

Yang, Q., Roehrl, M.H. and Wang, J.Y., 2018. Proteomic profiling of antibody-inducing immunogens in tumor tissue identifies PSMA1, LAP3, ANXA3, and maspin as colon cancer markers. *Oncotarget*, 9(3), p.3996.

Yang, Q., Wang, R., Xiao, W., Sun, F., Yuan, H. and Pan, Q., 2016. Cellular retinoic acid binding protein 2 is strikingly downregulated in human esophageal squamous cell carcinoma and functions as a tumor suppressor. *PLoS One*, 11(2), p.e0148381.

Yang, Y., Wu, P.P., Wu, J., Shen, W.W., Wu, Y.L., Fu, A.F., Zheng, L., Jin, X.L. and Fu, G.H., 2008. Expression of anion exchanger 2 in human gastric cancer. *Experimental Oncology*.

Yao, H., Yang, Z. and Li, Y., 2010. Expression of checkpoint kinase 1 and polo-like kinase 1 and its clinicopathological significance in benign and malignant lesions of the stomach. *Zhong nan da xue xue bao. Yi xue ban= Journal of Central South University. Medical sciences*, 35(10), pp.1080-1084.

Yao, Y., Kubota, T., Takeuchi, H. and Sato, K., 2005. Prognostic significance of microvessel density determined by an anti-CD105/endoglin monoclonal antibody in astrocytic tumors: Comparison with an anti-CD31 monoclonal antibody. *Neuropathology*, 25(3), pp.201-206.

Yasuda, K., Kosugi, A., Hayashi, F., Saitoh, S.I., Nagafuku, M., Mori, Y., Ogata, M. and Hamaoka, T., 2000. Serine 6 of Lck tyrosine kinase: a critical site for Lck myristoylation, membrane localization, and function in T lymphocytes. *The Journal of Immunology*, 165(6), pp.3226-3231.

Yates III, J.R., 1998. Database searching using mass spectrometry data. *Electrophoresis*, 19(6), pp.893-900.

Yesilöz, Ü., Kirches, E., Hartmann, C., Scholz, J., Kropf, S., Sahm, F., Nakamura, M. and Mawrin, C., 2017. Frequent AKT1 E17K mutations in skull base meningiomas are associated with mTOR and ERK1/2 activation and reduced time to tumor recurrence. *Neuro-oncology*, 19(8), pp.1088-1096.

- Yori, J.L., Johnson, E., Zhou, G., Jain, M.K. and Keri, R.A., 2010. Krüppel-like factor 4 inhibits epithelial-to-mesenchymal transition through regulation of E-cadherin gene expression. *Journal of Biological Chemistry*, 285(22), pp.16854-16863.
- Young, J.D., Yao, S.Y., Baldwin, J.M., Cass, C.E. and Baldwin, S.A., 2013. The human concentrative and equilibrative nucleoside transporter families, SLC28 and SLC29. *Molecular aspects of medicine*, 34(2-3), pp.529-547.
- Yuzawa, S., Nishihara, H. and Tanaka, S., 2016. Genetic landscape of meningioma. *Brain tumor pathology*, 33(4), pp.237-247.
- Zhang, G., Annan, R.S., Carr, S.A. and Neubert, T.A., 2010. Overview of peptide and protein analysis by mass spectrometry. *Current protocols in protein science*, 62(1), pp.16-1.
- Zhang, G., Kazanietz, M.G., Blumberg, P.M. and Hurley, J.H., 1995. Crystal structure of the Cys2 activator-binding domain of protein kinase C $\delta$  in complex with phorbol ester. *Cell*, 81(6), pp.917-924.
- Zhang, H., Yu, Z., Sun, F. and Jin, J., 2021. Overexpression of CRABP2 inhibits dexamethasone-induced apoptosis in human osteoblast cells. *Journal of Orthopaedic Surgery and Research*, 16(1), pp.1-8.
- Zhang, J., Yang, P.L. and Gray, N.S., 2009. Targeting cancer with small molecule kinase inhibitors. *Nature reviews cancer*, 9(1), pp.28-39.
- Zhang, J., Yuan, B., Zhang, H. and Li, H., 2019. Human epithelial ovarian cancer cells expressing CD105, CD44 and CD106 surface markers exhibit increased invasive capacity and drug resistance. *Oncology letters*, 17(6), pp.5351-5360.
- Zhang, L.J., Lu, R., Song, Y.N., Zhu, J.Y., Xia, W., Zhang, M., Shao, Z.Y., Huang, Y., Zhou, Y., Zhang, H. and Guo, L., 2017. Knockdown of anion exchanger 2 suppressed the growth of ovarian cancer cells via mTOR/p70S6K1 signaling. *Scientific reports*, 7(1), pp.1-11.
- Zhang, T., Ma, Y., Fang, J., Liu, C. and Chen, L., 2019. A deregulated PI3K-AKT signaling pathway in patients with colorectal cancer. *Journal of Gastrointestinal Cancer*, 50(1), pp.35-41.
- Zhang, W., Xiong, Z., Wei, T., Li, Q., Tan, Y., Ling, L. and Feng, X., 2018. Nuclear factor 90 promotes angiogenesis by regulating HIF-1 $\alpha$ /VEGF-A expression through the PI3K/Akt signaling pathway in human cervical cancer. *Cell death & disease*, 9(3), pp.1-13.
- Zhang, X., Jia, H., Lu, Y., Dong, C., Hou, J., Wang, Z., Wang, F., Zhong, H., Wang, L. and Wang, K., 2014. Exome sequencing on malignant meningiomas identified mutations in neurofibromatosis type 2 (NF2) and meningioma 1 (MN1) genes. *Discovery medicine*, 18(101), p.301.
- Zhang, X., Yang, W., Chen, K., Zheng, T., Guo, Z., Peng, Y. and Yang, Z., 2021. The potential prognostic values of the ADAMTS-like protein family: an integrative pan-cancer analysis. *Annals of Translational Medicine*, 9(20).
- Zhang, Y. and Hunter, T., 2014. Roles of Chk1 in cell biology and cancer therapy. *International journal of cancer*, 134(5), pp.1013-1023.
- Zhang, Y., Wang, H., Wang, J., Bao, L., Wang, L., Huo, J. and Wang, X., 2015. Global analysis of chromosome 1 genes among patients with lung adenocarcinoma, squamous carcinoma, large-cell carcinoma, small-cell carcinoma, or non-cancer. *Cancer and Metastasis Reviews*, 34(2), pp.249-264.



- Zhang, Y., Xu, J. and Zhu, X., 2018. A 63 signature genes prediction system is effective for glioblastoma prognosis. *International journal of molecular medicine*, 41(4), pp.2070-2078.
- Zhao, J., Ma, W. and Zhao, H., 2014. Loss of heterozygosity 1p/19q and survival in glioma: a meta-analysis. *Neuro-oncology*, 16(1), pp.103-112.
- Zheng, W.L., Bucco, R.A., Schmitt, M.C., Wardlaw, S.A. and Ong, D.E., 1996. Localization of cellular retinoic acid-binding protein (CRABP) II and CRABP in developing rat testis. *Endocrinology*, 137(11), pp.5028-5035.
- Zheng, Y., Qin, H., Frank, S.J., Deng, L., Litchfield, D.W., Tefferi, A., Pardanani, A., Lin, F.T., Li, J., Sha, B. and Benveniste, E.N., 2011. A CK2-dependent mechanism for activation of the JAK-STAT signaling pathway. *Blood, The Journal of the American Society of Hematology*, 118(1), pp.156-166.
- Zhou, K., Wang, G., Wang, Y., Jin, H., Yang, S. and Liu, C., 2010. The potential involvement of E-cadherin and  $\beta$ -catenins in meningioma. *PloS one*, 5(6), p.e11231.
- Zhou, L. and Hanemann, C.O., 2012. Merlin, a multi-suppressor from cell membrane to the nucleus. *FEBS letters*, 586(10), pp.1403-1408.
- Zhou, T., Liu, S., Yang, L., Ju, Y. and Li, C., 2018. The expression of ANXA3 and its relationship with the occurrence and development of breast cancer. *J buon*, 23(3), pp.713-719.
- Zhou, W., Ross, M.M., Tessitore, A., Ornstein, D., VanMeter, A., Liotta, L.A. and Petricoin III, E.F., 2009. An initial characterization of the serum phosphoproteome. *Journal of proteome research*, 8(12), pp.5523-5531.
- Zhou, W., Ross, M.M., Tessitore, A., Ornstein, D., VanMeter, A., Liotta, L.A. and Petricoin III, E.F., 2009. An initial characterization of the serum phosphoproteome. *Journal of proteome research*, 8(12), pp.5523-5531.
- Ziebarth, A.J., Nowsheen, S., Steg, A.D., Shah, M.M., Katre, A.A., Dobbin, Z.C., Han, H.D., Lopez-Berestein, G., Sood, A.K., Conner, M. and Yang, E.S., 2013. Endoglin (CD105) contributes to platinum resistance and is a target for tumor-specific therapy in epithelial ovarian cancer. *Clinical Cancer Research*, 19(1), pp.170-182.
- Zoppoli, G., Solier, S., Reinhold, W.C., Liu, H., Connelly, J.W., Monks, A., Shoemaker, R.H., Abaan, O.D., Davis, S.R., Meltzer, P.S. and Doroshow, J.H., 2012. CHEK2 genomic and proteomic analyses reveal genetic inactivation or endogenous activation across the 60 cell lines of the US National Cancer Institute. *Oncogene*, 31(4), pp.403-418.
- Zotti, T., Uva, A., Ferravante, A., Vessichelli, M., Scudiero, I., Ceccarelli, M. and Vito, P., 2011. TRAF7 protein promotes Lys-29-linked polyubiquitination of I $\kappa$ B kinase (IKK $\gamma$ )/NF- $\kappa$ B essential modulator (NEMO) and p65/RelA protein and represses NF- $\kappa$ B activation. *Journal of Biological Chemistry*, 286(26), pp.22924-22933.
- Zotti, T., Vito, P. and Stilo, R., 2012. The seventh ring: exploring TRAF7 functions. *Journal of cellular physiology*, 227(3), pp.1280-1284.

Vismodegib and FAK Inhibitor GSK2256098 in treating patients with progressive meningiomas

Available at:

<https://ClinicalTrials.gov/show/NCT02523014> (2015)

Accessed, June 15, 2018

Vistusertib (AZD2014) For Recurrent Grade II-III Meningiomas

Available at:

<https://ClinicalTrials.gov/show/NCT03071874> (2015)

Accessed, June 15, 2018

## Appendix

Uniprot ID	Protein name	Log2 FC <i>AKT1<sup>E17K</sup>/TRAF7</i> vs. NMT	<i>P-value</i> <i>AKT1<sup>E17K</sup>/TRAF7</i> vs. NMT	Log2 FC <i>AKT1<sup>E17K</sup>/TRAF7</i> vs. <i>NF2<sup>-/-</sup></i>	<i>P-value</i> <i>AKT1<sup>E17K</sup>/TRAF7</i> vs. <i>NF2<sup>-/-</sup></i>	Log2 FC <i>AKT1<sup>E17K</sup>/TRAF7</i> vs. <i>KLF4<sup>K409Q</sup>/TRAF7</i>	<i>P-value</i> <i>AKT1AKT1<sup>E17K</sup>/TRAF7</i> vs. <i>KLF4<sup>K409Q</sup>/TRAF7</i>
A0A024R5C5	Pyruvate carboxylase	8.998	0.007346	4.969	0.006696	4.795	0.003284
O95833	Chloride intracellular channel protein 3	8.302	0.000489	5.460	0.003681	5.947	0.000105
A0A024RC61	Aminopeptidase	8.060	1.66E-05	4.202	0.000899	3.062	0.001302
Q96FL8	Multidrug and toxin extrusion protein 1	7.764	0.004934	4.410	0.002489	3.530	0.01284
P29373	Cellular retinoic acid-binding protein 2	7.286	3.99E-05	4.803	0.007235	7.042	0.000192
Q53FA7	Quinone oxidoreductase PIG3	7.088	2.65E-05	2.212	0.004485	6.720	1.42E-06
O60547	GDP-mannose 4,6 dehydratase	6.109	4.15E-05	3.222	0.016223	2.901	0.008747
Q92542	Nicastrin	6.013	0.001413	3.139	0.013796	4.408	0.002519
Q6FGU2	DTYMK protein (Fragment)	5.960	1.81E-05	3.027	0.022986	2.937	0.000451
Q9BUH6	Protein PAXX	5.922	0.00116	3.220	0.020508	4.244	0.000599
A0A024R9E4	Mal, T-cell differentiation protein 2, isoform	5.858	2.1E-05	5.645	0.000868	3.333	0.028326
Q53ZR1	Bumetanide-sensitive Na-K-Cl cotransporter	5.833	0.003951	4.328	0.0018	3.805	0.002589
P17568	NADH dehydrogenase [ubiquinone] 1 beta subcomplex subunit 7	5.748	0.010775	4.229	0.004276	4.172	0.000819

A8K644	Splicing factor, arginine/serine-rich 4, isoform	5.747	0.004112	3.414	0.020559	4.031	0.000883
A0A024R6G6	NADH dehydrogenase (Ubiquinone) 1 beta subcomplex, 1, 7kDa	5.703	0.016721	4.953	1.9E-05	3.771	0.000278
A0A0C4DFM1	Transmembrane 9 superfamily member	5.664	1.68E-06	2.971	0.025847	5.109	3.8E-08
Q53F37	SAR1a gene homolog 2 variant (Fragment)	5.473	0.007176	4.511	0.000472	2.559	0.014871
A0A024R2Q7	C-type lectin domain family 3, member B, isoform	5.447	0.006926	6.697	0.000267	4.562	0.005208
Q8N4V1	Membrane magnesium transporter 1	5.344	6.28E-06	3.596	0.009005	2.911	0.014074
I3UJJ7	Angiotensin-converting enzyme	5.324	0.033408	4.079	0.004055	4.410	0.000226
A0A024R482	GDP-mannose pyrophosphorylase A	5.303	0.000111	3.233	0.009396	3.573	3.92E-05
O75396	Vesicle-trafficking protein SEC22b	5.275	0.003691	1.573	0.035466	1.656	0.043726
O60613	Selenoprotein F	5.196	7.31E-05	3.595	0.016396	5.445	4.55E-06
A0A140VJE4	Testicular tissue protein Li 18	5.177	0.000178	3.188	0.005478	2.942	0.005422
A0A024R4I7	Leucine zipper and CTNNBIP1 domain containing, isoform	5.175	0.000213	2.480	0.034108	4.708	7.01E-07
Q53FN7	BZW1 protein variant (Fragment)	5.161	0.009929	3.497	0.016168	3.978	0.000972
H0YGR4	Oligoribonuclease, mitochondrial (Fragment)	5.051	0.000313	4.828	0.000377	5.734	1.9E-08
Q9HAT2	Sialate O-acetyltransferase	5.048	0.00165	3.096	0.0088	2.797	0.007372

P10109	Adrenodoxin, mitochondrial	5.017	0.000109	3.511	0.002304	4.019	4.59E-05
U3KQU4	Uncharacterized protein	4.887	0.000423	3.008	0.012908	2.897	0.000119
D3DVF0	F11 receptor, isoform	4.874	0.000229	5.083	1.9E-05	3.344	0.028501
J3QLB2	Zinc transporter ZIP11 (Fragment)	4.831	0.002671	4.721	1.35E-05	3.694	0.001954
B3KW5	Galectin	4.828	0.002486	3.223	0.00873	3.700	0.000187
A0A024R6M6	BCL2-associated athanogene 5	4.824	0.005239	3.232	0.005997	2.401	0.006626
D3DP75	RAB3 GTPase activating protein subunit 1 (Catalytic), isoform	4.754	0.039638	5.941	0.001812	5.193	0.001105
H0Y382	Calcium-activated potassium channel subunit alpha-1	4.745	0.001183	3.817	0.005355	3.460	0.00083
P36405	ADP-ribosylation factor-like protein 3	4.726	0.000508	3.192	0.045466	3.441	0.004946
Q9HC07	Transmembrane protein 165	4.680	0.00204	4.027	0.00168	2.250	0.013832
A0A024R156	Guanine nucleotide-binding protein subunit gamma	4.640	0.018766	4.570	0.000134	3.634	0.000155
P32321	Deoxycytidylate deaminase	4.618	0.005087	2.844	0.023401	4.946	2.18E-06
Q53H18	Beta-galactosidase (Fragment)	4.579	0.000199	4.119	0.000949	4.293	5.24E-08
D3DUJ0	AFG3 ATPase family gene 3-like 2 (Yeast), isoform	4.556	0.012717	2.588	0.006171	3.680	0.00055
Q16643	Drebrin	4.435	0.016951	3.038	0.049177	3.562	0.00995
Q96CN7	Isochorismatase domain-containing protein 1	4.405	0.029054	3.697	0.003504	4.323	0.001751
A0A024R179	Nuclear cap binding protein subunit 1, 80kDa, isoform	4.394	1.69E-06	2.113	0.029015	2.262	0.00491

Q9UII2	ATPase inhibitor, mitochondrial	4.344	0.042906	3.561	0.008886	3.067	0.024349
A0A024R7W9	COP9 constitutive photomorphogenic homolog subunit 5	4.330	0.000927	3.558	0.021253	3.383	0.006502
A0A024R0K8	HCG1995540, isoform	4.320	1.81E-05	3.494	2.38E-05	3.316	0.000323
A0A286LWX1	AOX1	4.261	0.007431	2.540	0.013701	5.804	2.99E-05
A0A024RD41	RAB23, member RAS oncogene family, isoform	4.242	0.00255	3.675	0.030544	4.081	0.001552
B1AJY7	26S proteasome non-ATPase regulatory subunit 10	4.224	0.004478	2.858	0.045459	3.539	0.010586
A0A024R366	Fragile histidine triad gene, isoform	4.196	0.00329	2.906	0.012969	2.424	0.028134
A8K3J4	Carbonic anhydrase XIV	4.182	0.002578	3.678	1.19E-05	2.680	0.005168
Q9GZT4	Serine racemase	4.180	0.031512	2.727	0.016869	2.872	0.005301
Q9NX47	E3 ubiquitin-protein ligase MARCH5	4.163	1.36E-06	3.824	0.000836	3.332	0.000499
O75884	Putative hydrolase RBBP9	4.123	0.018527	5.899	0.000502	6.195	6.73E-06
A0A024R277	Serine palmitoyltransferase, long chain base subunit 1	4.088	0.001525	3.128	0.004113	2.459	0.033034
A0A0C4DGH0	CD276 antigen	4.073	0.016427	2.681	0.024101	2.790	0.035023
Q96JZ5	Transmembrane 9 superfamily member	4.071	0.029846	3.043	0.014012	2.054	0.034188
A0A0A0MTI6	Elongation of very long chain fatty acids protein	4.052	0.002365	2.457	0.006603	2.802	0.000148
A0A024R4E7	Peroxisomal biogenesis factor 11B	4.035	0.014445	4.231	0.002548	5.119	9.52E-07
Q96FV2	Secernin-2	4.015	0.003262	3.094	0.020929	3.259	0.005157

B4DS5 7	cDNA FLJ53176, highly similar to Nuclear autoantigenic sperm	3.986	0.00053 7	4.394	1.14E-07	2.453	0.024865
B7Z9F 3	cDNA, FLJ78817, highly similar to Metaxin-2	3.916	0.00111 7	5.292	4.78E-05	4.807	7.13E-05
M4VP5 2	Apolipoprotein B editing enzyme catalytic polypeptide- like 3C	3.898	0.02457 5	2.534	0.00646 6	2.174	0.018059
B4DL6 6	cDNA FLJ56297, highly similar to Rattus norvegicus ubiquitin	3.862	0.02546 6	2.110	0.02438 4	2.158	0.00356
A0A0S 2Z3H2	Cleft lip and palate associated transmembrane protein 1	3.834	0.00312 9	3.989	0.00048 9	3.251	1.94E-05
O9516 9	NADH dehydrogenase [ubiquinone] 1 beta subcomplex subunit 8,	3.812	0.00051 5	4.441	0.00064 3	3.407	0.002704
M0QZ Q8	Trafficking protein particle complex subunit 5	3.758	1.62E-05	3.278	8.38E-06	2.919	6.09E-05
B5MC E7	Basic leucine zipper and W2 domain- containing protein 2	3.735	0.01804 6	2.322	0.03116 8	2.746	0.00151
B2RA W8	cDNA, FLJ95164, highly similar to Homo sapiens SEC14- like 2 (	3.729	0.04485 4	3.156	0.01319 8	3.721	5.61E-06
Q2M38 9	WASH complex subunit 4	3.725	0.00161 4	2.928	0.00036 3	2.682	1.43E-05
K7EID 2	Chitobiosyldip hosphodolichol beta-	3.721	0.00297 5	3.463	0.00285 9	4.019	1.07E-06

	mannosyltransferase (Fragment)						
O95379	Tumor necrosis factor alpha-induced protein 8	3.708	0.006427	2.663	0.018581	2.857	0.000356
Q659C9	Uncharacterized protein DKFZp434L1715	3.681	0.047045	3.372	0.002169	2.700	0.005033
Q8NE86	Calcium uniporter protein, mitochondrial	3.614	0.000808	3.688	5.57E-05	2.533	0.000541
P48163	NADP-dependent malic enzyme	3.610	0.018801	3.539	0.006844	4.604	3.44E-05
A0A087WUR6	Calcium/calmodulin-dependent protein kinase type 1D	3.600	0.000758	2.668	0.006498	2.104	0.007507
Q9HB R0	Putative sodium-coupled neutral amino acid transporter 10	3.588	0.002031	3.714	0.006331	1.844	0.001618
A0A024R8C8	TBC1 domain family, member 13, isoform	3.587	0.001979	2.226	0.040386	2.101	0.000423
E9PP55	E3 ubiquitin-protein ligase RNF170 (Fragment)	3.579	0.000458	2.157	0.01373	2.240	0.000195
Q96GX9	Methylthioribulose-1-phosphate dehydratase	3.572	0.001813	3.719	0.000355	3.132	0.025493
E9PJE4	COMM domain-containing protein 5 (Fragment)	3.568	0.019483	2.512	0.027369	2.360	0.001229
Q9NT62	Ubiquitin-like-conjugating enzyme ATG3	3.558	0.000217	3.262	0.005969	2.845	0.001141
Q6NT72	UNC84B protein (Fragment)	3.542	0.012102	2.493	0.033749	2.260	0.001556
A0A024R184	Asparagine-linked glycosylation 2 homolog	3.526	0.009796	3.061	3.55E-05	2.138	0.001633



Q96DG6	Carboxymethyl enebutenolidase homolog	3.526	0.003004	5.343	0.008785	4.582	9.36E-05
A0A0S2Z3K9	V-crk sarcoma virus CT10 oncogene-like protein isoform 2	3.511	9.31E-05	3.290	0.01224	2.844	0.000321
B1AUU8	Epidermal growth factor receptor substrate 15	3.497	0.000367	2.448	0.03692	2.981	6.71E-05
A4D0Z3	ADP-ribosylation factor 5	3.478	0.03387	2.876	0.003926	2.641	0.049112
V9HWE1	Epididymis luminal protein 113	3.468	0.001479	1.898	0.046622	1.562	0.00199
Q92896	Golgi apparatus protein 1	3.453	0.000397	2.487	0.000408	1.769	0.013504
B7Z5Q8	cDNA FLJ52519, weakly similar to LIM domain only protein 7	3.449	0.006906	2.956	0.036475	3.510	1.37E-05
Q9UPE4	Mitochondrial import inner membrane translocase subunit TIM44	3.446	0.004604	3.533	0.000269	2.806	4.44E-05
P14854	Cytochrome c oxidase subunit 6B1	3.432	0.001896	2.989	0.004415	3.023	0.004544
E7EMC7	Sequestosome-1	3.418	0.031022	2.214	0.018613	2.673	0.003448
I3L1T3	Derlin (Fragment)	3.345	0.000392	2.138	0.001105	2.487	0.000132
S4R329	ER membrane protein complex subunit 4	3.328	0.005546	3.171	0.015111	2.081	0.040855
C9IYF5	Exostosin-like 2 (Fragment)	3.323	0.011994	3.734	1.1E-05	2.307	0.003042
Q549N5	Signal recognition particle receptor beta subunit	3.320	0.001993	4.060	0.035236	4.577	0.011054
A0A087WY55	Chromosome 6 open reading frame 55, isoform	3.312	0.024012	2.766	0.023574	3.219	0.000931

J3QK W2	28S ribosomal protein S7, mitochondrial	3.288	0.000479	3.012	9.87E-05	2.040	0.004604
B7ZLD 8	Integrin beta	3.270	0.032341	2.260	0.031023	2.418	0.024842
Q1578 5	Mitochondrial import receptor subunit TOM34	3.265	0.046288	4.405	0.0011	3.783	1.88E-05
Q6FG H9	DNCL1 protein	3.210	0.002867	3.438	0.048065	4.887	0.003109
Q53GR 7	Solute carrier family 25, member 13 (Citrin) variant	3.166	0.00298	3.916	0.001262	2.467	0.044691
P56134	ATP synthase subunit f, mitochondrial	3.075	0.035324	2.141	0.032774	2.062	0.006269
Q6IBU 4	SDF2 protein	3.065	0.047169	2.648	0.039376	3.530	1.97E-05
O7588 6	Signal transducing adapter molecule 2	3.034	0.02115	2.658	0.016103	2.190	0.001088
Q0197 0	1-phosphatidylinositol 4,5-bisphosphate phosphodiesterase beta	3.034	0.027553	2.023	0.034986	1.945	0.009031
B7Z3M 6	Phosphomannomutase	3.026	0.00092	3.535	0.013756	4.172	6.95E-06
A0A14 0VK39	Protein phosphatase methylesterase 1	2.966	0.022641	2.886	0.013414	2.002	0.002636
B4E1G 2	Serine hydroxymethyltransferase	2.936	0.00589	3.205	0.009296	2.479	0.007477
Q9UM S0	NFU1 iron-sulfur cluster scaffold homolog, mitochondrial	2.909	0.005328	2.129	0.000208	2.142	7.35E-05
E9PSI1	Transmembrane 9 superfamily member	2.893	0.008006	4.768	0.000298	3.699	0.000108
Q5QP Q0	Acyl-protein thioesterase 2	2.866	0.004337	2.362	0.04526	1.949	0.013816
O9521 9	Sorting nexin-4	2.838	0.049551	2.516	0.01233	2.280	0.002137
A8K2I 7	cDNA FLJ76072, highly similar	2.819	0.000696	1.979	0.007607	1.298	0.013448

	to Homo sapiens GIPC PDZ domain						
O75962	Triple functional domain protein	2.805	0.021584	3.609	0.001166	4.041	4.02E-06
Q9H2D6	TRIO and F-actin-binding protein	2.795	0.045016	3.238	0.000707	2.085	0.011408
E9PJ81	UBX domain-containing protein 1 (Fragment)	2.782	0.024246	3.101	9.28E-05	1.860	0.013713
P07311	Acylphosphatase-1	2.741	0.006545	4.189	0.004437	3.065	0.015098
P51153	Ras-related protein Rab-13	2.686	0.001855	2.300	0.049145	2.703	0.008704
Q86TY2	Full-length cDNA clone CS0DI035YL21 of Placenta of Homo sapiens	2.663	0.011152	2.846	0.00391	3.272	5.08E-05
Q5T6L4	Argininosuccinate synthase 1 isoform 1	2.635	0.0038	3.839	0.004477	1.321	0.046331
Q9BRQ6	MICOS complex subunit MIC25	2.5852	0.012558	3.661	0.025617	3.672	0.000383
A0A024R151	Solute carrier family 44, member 1, isoform CRA	2.580	0.013553	5.605	0.001072	4.284	0.000893
Q9H8S9	MOB kinase activator 1A	2.569	0.001009	2.382	0.049859	4.584	0.002728
B0LPE5	V-akt murine thymoma viral oncogene homolog 1	2.541	0.017573	2.748	0.006457	2.152	0.006408
Q9UBQ0	Vacuolar protein sorting-associated protein 29	2.507	0.011061	2.346	0.034723	3.780	0.009396
A6NP52	PRA1 family protein	2.485	0.04496	5.606	0.000441	3.578	0.004262
A0A024R8B2	Frequenin homolog (Drosophila), isoform	2.482	0.023974	3.929	0.001449	3.364	2.66E-06
B2RDK6	cDNA, FLJ96656, highly similar to Homo sapiens SPFH domain	2.392	0.021117	2.496	0.013203	3.328	0.00143

Q1333 2	Receptor-type tyrosine-protein phosphatase S	2.319	0.02677 5	1.535	0.00720 2	1.261	0.019329
P53007	Tricarboxylate transport protein, mitochondrial	2.300	0.03644	5.583	0.00126	2.628	0.015755
E9PM7 5	NAD-dependent protein deacetylase sirtuin-3, mitochondrial	2.287	0.01990 4	1.725	0.01141 7	1.371	0.040727
A0A02 4R745	NADH dehydrogenase (Ubiquinone) 1 alpha subcomplex, 5, 13kDa	2.272	0.00050 9	3.355	0.04484	4.407	0.004063
Q96HN 2	Adenosylhomocysteinase 3	2.271	0.00188 1	1.616	0.02523 5	1.990	0.035979
F6RU0 0	Golgi SNAP receptor complex member 1	2.254	0.00050 7	2.522	0.01473 1	2.991	1.35E-06
Q5SRT 3	Chloride intracellular channel protein	2.214	0.01741 1	3.362	0.04755 4	1.495	0.014717
Q53FR 9	COMM domain containing 9 variant (Fragment)	2.179	0.01729	2.770	0.01732 1	2.194	5.03E-06
Q4KM Q2	Anoctamin-6	2.170	0.02519 3	2.377	0.02049 5	2.382	0.001617
I4AY8 7	Macrophage migration inhibitory factor (Fragment)	2.004	0.01298 4	3.516	0.03924 9	5.368	0.000664
Q9Y68 0	Peptidyl-prolyl cis-trans isomerase FKBP7	2.004	0.03304 3	3.096	0.04096 8	3.633	0.003713
Q53HN 4	DNAation factor, 45kDa, alpha polypeptide isoform 1 variant	1.952	0.00989 9	2.801	0.01194 5	3.251	1.93E-07
A0A02 4RDT3	Calcium binding protein 39-like, isoform	1.885	0.02801 8	2.326	0.02485 9	5.976	1.15E-05

J3KP58	CAP-Gly domain-containing linker protein 1	1.879	0.015958	3.684	0.022718	1.036	0.005889
IISRC5	UBE2L3/KRAS fusion protein	1.841	0.02984	1.617	0.001467	4.108	0.016834
Q9NUF9	Nucleoside diphosphate kinase (Fragment)	1.752	0.006099	3.698	0.021157	2.899	0.032792
Q08AM6	Protein VAC14 homolog	1.727	0.025974	1.842	0.025876	1.857	0.004587
A0A087X054	Hypoxia up-regulated protein 1	1.702	0.005079	1.503	0.002919	2.734	9.76E-05
A0A024R8T9	Synaptogyrin	1.652	0.04522	4.042	0.003216	3.928	0.002714
Q9P0P8	Uncharacterized protein C6orf203	1.623	0.026778	3.412	9.3E-06	2.585	1.01E-06
A0A0A0MSB8	Exocyst complex component 7	1.537	0.02348	2.739	0.009028	3.408	2.27E-06
A0A140VJP2	Methionine adenosyltransferase 2 subunit beta	1.510	0.0264	1.633	0.010963	1.498	0.034544
A4D0W0	LSM8 homolog, U6 small nuclear RNA associated ( <i>S. cerevisiae</i> )	1.502	0.011986	3.377	0.020679	4.415	6.94E-06
B7Z756	cDNA FLJ56256, highly similar to Choline/ethanol amine kinase	1.461	0.024023	1.269	0.003442	1.434	0.000713
X6RC K5	Dynalectin subunit 3 (Fragment)	1.306	0.001685	3.830	0.011726	4.031	0.010174
P28288	ATP-binding cassette sub-family D member 3	1.276	0.038148	2.663	0.028198	2.019	0.009023
C9JFR7	Cytochrome c (Fragment)	1.250	0.045389	5.401	0.005036	5.125	0.001513
Q8N766	ER membrane protein complex subunit 1	1.098	0.003202	2.085	0.023915	2.153	0.025929

**Table: 1 Complete lists of significantly upregulated proteins common to *AKT1<sup>E17K</sup>/TRAF7* mutational subtype**

Uniprot ID	Protein Name	Log2 FC <i>NF2<sup>-/-</sup></i> vs. <i>AKT1<sup>E17K</sup>/TRAF7</i>	P-value <i>NF2<sup>-/-</sup></i> vs. <i>AKT1<sup>E17K</sup>/TRAF7</i>	Log2 FC <i>NF2<sup>-/-</sup></i> vs. <i>KLF4<sup>K409Q</sup>/TRAF7</i>	P-value <i>NF2<sup>-/-</sup></i> vs. <i>KLF4<sup>K409Q</sup>/TRAF7</i>	Log 2 FC <i>NF2<sup>-/-</sup></i> vs. NMT	P-value <i>NF2<sup>-/-</sup></i> vs. NMT
E9PN66	Tumor protein p53-inducible protein 11 (Fragment)	-2.77858	0.026205	-2.74788	0.00407	-6.40615	0.002673
Q53EW7	Branched-chain-amino-acid aminotransferase (Fragment)	-4.86843	1.49E-05	-4.37141	0.000442	-7.63052	0.000211
O43405	Cochlin	-1.01525	0.024436	-1.11593	0.045237	-5.03383	3.75E-05
Q53HG3	Peroxisomal D3,D2-enoyl-CoA isomerase isoform 1 variant (Fragment)	-2.97296	0.002052	-2.13039	0.04309	-4.62381	0.00769
O75891	Cytosolic 10-formyltetrahydrofolate dehydrogenase	-3.8657	0.002568	-3.07241	0.010052	-8.5665	0.001306
O95202	Mitochondrial proton/calcium exchanger protein	-3.83879	0.000768	-2.31771	0.019141	-4.29932	0.029969
O95670	V-type proton ATPase subunit G 2	-1.27107	0.007679	-2.02653	0.006442	-2.4858	0.004557
O95822	Malonyl-CoA decarboxylase, mitochondrial	-1.18941	0.040742	-1.67386	0.015041	-3.81802	0.001289
A0A024R6W0	Aspartate aminotransferase	-3.09171	0.020452	-2.82353	0.031122	-5.91946	0.02467
P02741	C-reactive protein	-1.2158	0.038834	-1.51266	0.022464	-11.3629	1.89E-07

Uniprot ID	Protein Name	Log2 FC <i>NF2<sup>-/-</sup></i> vs. <i>AKT1<sup>E17K</sup>/TRAF7</i>	P-value <i>NF2<sup>-/-</sup></i> vs. <i>AKT1<sup>E17K</sup>/TRAF7</i>	Log2 FC <i>NF2<sup>-/-</sup></i> vs. <i>KLF4<sup>K409Q</sup>/TRAF7</i>	P-value <i>NF2<sup>-/-</sup></i> vs. <i>KLF4<sup>K409Q</sup>/TRAF7</i>	Log 2 FC <i>NF2<sup>-/-</sup></i> vs. NMT	P-value <i>NF2<sup>-/-</sup></i> vs. NMT
P02760	Protein AMBP	-2.89882	0.046662	-3.0338	0.034087	-5.11976	0.048562
P05090	Apolipoprotein D	-3.21346	0.010089	-2.58716	0.024219	-8.30714	0.001549
F5GY80	Complement component C8 beta chain	-2.81246	0.005627	-2.68512	0.022743	-5.69153	0.0015
F5GZS6	4F2 cell-surface antigen heavy chain	-1.77439	0.024767	-2.69529	0.004745	-8.69954	1.69E-05
F5H345	Porphobilinogen deaminase	-3.17992	0.000151	-2.78994	0.001644	-4.74911	5.46E-05
H0YD13	CD44 antigen	-3.94396	0.01357	-8.34147	4.32E-08	-5.02649	0.038104
P16298	Serine/threonine-protein phosphatase 2B catalytic subunit beta isoform	-2.99138	0.002498	-2.22906	0.016561	-3.40288	0.049801
B2R950	cDNA, FLJ94213, highly similar to Homo sapiens pregnancy-zone protein	-1.64806	0.036282	-1.75594	0.013653	-5.56173	0.002528
P23141	Liver carboxylesterase 1	-1.96694	0.019132	-1.46494	0.04257	-12.4123	1.37E-07
A0A140VJX1	Testicular tissue protein Li 198	-2.02901	0.008173	-2.97365	0.005822	-4.04372	0.003463
E9PF59	Dipeptidyl aminopeptidase-like protein 6	-1.57624	0.022309	-1.90894	0.002514	-3.70716	0.010872
B4DKB2	Endothelin-converting enzyme 1	-3.65165	0.001505	-2.68215	0.009936	-3.43487	0.02796

Uniprot ID	Protein Name	Log2 FC <i>NF2<sup>-/-</sup></i> vs. <i>AKT1<sup>E17K</sup>/TRAF7</i>	P-value <i>NF2<sup>-/-</sup></i> vs. <i>AKT1<sup>E17K</sup>/TRAF7</i>	Log2 FC <i>NF2<sup>-/-</sup></i> vs. <i>KLF4<sup>K409Q</sup>/TRAF7</i>	P-value <i>NF2<sup>-/-</sup></i> vs. <i>KLF4<sup>K409Q</sup>/TRAF7</i>	Log 2 FC <i>NF2<sup>-/-</sup></i> vs. NMT	P-value <i>NF2<sup>-/-</sup></i> vs. NMT
D2JYH4	Actin, alpha 2, smooth muscle, aorta	-4.38259	0.013182	-4.84418	0.003068	-11.0237	0.002125
Q6LES8	TFAM protein (Fragment)	-2.63151	0.021108	-3.48615	0.006126	-4.93761	0.026796
Q05707	Collagen alpha-1(XIV) chain	-5.20999	0.003448	-6.12994	0.000397	-11.963	0.000903
Q0ZGT2	Nexilin	-1.54327	0.019586	-1.74128	0.005486	-6.76022	0.000627
A0A0A0MRK6	Metaxin 1, isoform	-4.49963	2.62E-05	-1.8445	0.016973	-2.91344	0.000665
Q13683	Integrin alpha-7	-3.32436	0.000673	-2.73608	0.001694	-6.68213	1.39E-05
Q15120	[Pyruvate dehydrogenase (acetyl-transferring)] kinase isozyme 3, mitochondria	-1.84379	0.011192	-1.03262	0.037185	-3.07289	0.005978
A0A140VJL0	3-hydroxyisobutyryl-CoA hydrolase, mitochondrial	-4.13723	0.000814	-3.59664	0.00214	-5.21741	0.016909
Q6PCE3	Glucose 1,6-bisphosphate synthase	-1.53608	0.011512	-2.00035	0.001078	-5.03605	0.002604
A8K6Q3	cDNA FLJ75880, highly similar to Homo sapiens synaptic vesicle glycoprotein	-1.23173	0.014859	-1.03432	0.02715	-6.28487	0.000266
V9HW32	Epididymis secretory protein Li 298	-2.11555	0.0138	-2.2423	0.02678	-2.91437	0.042878



Uniprot ID	Protein Name	Log2 FC <i>NF2<sup>-/-</sup></i> vs. <i>AKT1<sup>E17K</sup>/TRAF7</i>	P-value <i>NF2<sup>-/-</sup></i> vs. <i>AKT1<sup>E17K</sup>/TRAF7</i>	Log2 FC <i>NF2<sup>-/-</sup></i> vs. <i>KLF4<sup>K409Q</sup>/TRAF7</i>	P-value <i>NF2<sup>-/-</sup></i> vs. <i>KLF4<sup>K409Q</sup>/TRAF7</i>	Log 2 FC <i>NF2<sup>-/-</sup></i> vs. NMT	P-value <i>NF2<sup>-/-</sup></i> vs. NMT
Q8TB36	Ganglioside-induced differentiation-associated protein 1	-2.65768	0.001123	-1.40781	0.027759	-3.3896	0.042494
A0A1U9X7U3	HSD17B8	-3.16829	0.005351	-2.67275	0.039595	-4.48884	0.025352
C9JYY6	Neuronal cell adhesion molecule	-1.03374	0.045467	-1.23126	0.043114	-5.56134	0.000477
Q969E2	Secretory carrier-associated membrane protein 4	-3.61839	8.68E-06	-2.44489	0.002585	-1.85811	0.01995
A0A024R687	Pleckstrin homology domain containing, family C (With FERM domain) member	-2.40596	0.000462	-1.57483	0.002705	-5.23773	0.000283
Q96GW7	Brevican core protein	-1.53876	0.012891	-2.09144	0.001721	-5.99594	0.000986
B7ZA99	cDNA, FLJ79113, highly similar to Zinc finger SWIM domain-containing protein	-1.3387	0.039162	-1.27861	0.020994	-3.66573	0.019642
X5DNA9	HCG2002594, isoform	-1.59311	0.040497	-1.57716	0.005939	-7.16485	0.000253
A0A087WTL4	Bcl-2-like protein 13	-4.13027	0.001212	-5.57889	8.79E-06	-3.64247	0.048206
Q9GZM7	Tubulointerstitial nephritis antigen-like	-1.44468	0.044566	-2.6585	0.000708	-6.15407	0.000149

Uniprot ID	Protein Name	Log2 FC <i>NF2<sup>-/-</sup></i> vs. <i>AKT1<sup>E17K</sup>/TRAF7</i>	P-value <i>NF2<sup>-/-</sup></i> vs. <i>AKT1<sup>E17K</sup>/TRAF7</i>	Log2 FC <i>NF2<sup>-/-</sup></i> vs. <i>KLF4<sup>K409Q</sup>/TRAF7</i>	P-value <i>NF2<sup>-/-</sup></i> vs. <i>KLF4<sup>K409Q</sup>/TRAF7</i>	Log 2 FC <i>NF2<sup>-/-</sup></i> vs. NMT	P-value <i>NF2<sup>-/-</sup></i> vs. NMT
Q9NSD5	Sodium- and chloride-dependent GABA transporter 2	-1.7259	0.046538	-1.44243	0.042807	-9.09166	6.17E-06
A8K9L8	cDNA FLJ76964, highly similar to Homo sapiens tropomodulin 2 (neuronal)	-3.64013	0.004891	-2.29267	0.001372	-5.48188	0.000184
Q9P2U7	Vesicular glutamate transporter 1	-2.06889	0.00487	-1.54069	0.023013	-5.21816	0.003607
Q9Y698	Voltage-dependent calcium channel gamma-2 subunit	-1.35774	0.005683	-1.09724	0.016537	-2.18093	0.010083
A0A024R5W6	Tropomyosin 1 (Alpha), isoform	-1.81545	0.049184	-1.48906	0.047562	-9.95476	6.95E-06
A0A087WWA5	Tenascin-X	-2.60883	0.008032	-3.04697	0.002824	-5.38577	0.001233
A2VBC8	ATPase, Ca <sup>++</sup> transporting, plasma membrane 2 (Fragment)	-1.022	0.044506	-1.51334	0.009663	-2.18944	0.007712
A8K5T0	cDNA FLJ75416, highly similar to Homo sapiens complement factor H (CFH)	-1.50509	0.035776	-1.26814	0.02332	-4.76136	0.012547
H7BXR3	Sorbin and SH3 domain-containing protein 2 (Fragment)	-1.52907	0.018195	-2.0398	0.004016	-5.89666	0.000567

Uniprot ID	Protein Name	Log2 FC <i>NF2<sup>-/-</sup></i> vs. <i>AKT1<sup>E17K</sup>/TRAF7</i>	P-value <i>NF2<sup>-/-</sup></i> vs. <i>AKT1<sup>E17K</sup>/TRAF7</i>	Log2 FC <i>NF2<sup>-/-</sup></i> vs. <i>KLF4<sup>K409Q</sup>/TRAF7</i>	P-value <i>NF2<sup>-/-</sup></i> vs. <i>KLF4<sup>K409Q</sup>/TRAF7</i>	Log 2 FC <i>NF2<sup>-/-</sup></i> vs. NMT	P-value <i>NF2<sup>-/-</sup></i> vs. NMT
Q9H4D2	Tubby-like protein (Fragment)	-1.36654	0.048097	-1.65867	0.010826	-3.63737	0.005368
X5DNI1	Collapsin response mediator protein 1 isoform A (Fragment)	-2.55889	0.029399	-1.83589	0.022085	-6.22995	0.011189

**Table: 2 Complete lists of significantly deregulated proteins common to *NF2<sup>-/-</sup>* mutational subtype.**

Uniprot ID	Protein name	Log2 FC <i>KLF4<sup>K409Q</sup>/TRAF7</i> vs. <i>AKT1<sup>E17K</sup>/TRAF7</i>	P-value <i>KLF4<sup>K409Q</sup>/TRAF7</i> vs. <i>AKT1<sup>E17K</sup>/TRAF7</i>	Log2 FC <i>KLF4<sup>K409Q</sup>/TRAF7</i> vs. <i>NF2<sup>-/-</sup></i>	P-value <i>KLF4<sup>K409Q</sup>/TRAF7</i> vs. <i>NF2<sup>-/-</sup></i>	Log2 FC <i>KLF4<sup>K409Q</sup>/TRAF7</i> NMT	P-value <i>KLF4<sup>K409Q</sup>/TRAF7</i> NMT
P04920	Anion exchange protein 2	4.311079	0.004411	6.715718	1.1E-05	6.890585	0.018494
D3XNU5	E-cadherin 1	3.073486	0.010845	3.939768	0.006387	5.714101	0.003263
H0YD13	CD44 antigen	4.311307	0.000305	8.425873	7.01E-08	3.314977	0.00021
Q5T9B9	Endoglin (Osler-Rendu-Weber syndrome 1)	2.079189	0.000397	2.201567	0.002244	2.841178	0.001218
B2R8K9	Aminopeptidase	4.137402	0.000781	5.232938	6.12E-06	6.093094	0.000304
E9PQW1	Caspase recruitment domain-containing protein 16 (Fragment)	1.431636	0.009845	1.684484	0.000861	1.793876	0.047454
A0A0S2Z548	Sulfatase modifying factor 2 isoform 3	1.603546	0.01292	2.497712	0.035562	1.88763	0.012925
Q8NF91	Nesprin-1	2.71291	0.028219	2.575034	0.033208	3.246015	0.034617
J3KPX7	Prohibitin-2	1.260482	0.001069	2.560642	0.003899	1.673822	0.005009
A0A024R9M9	Calcium binding protein P22, isoform	1.648322	0.002596	4.795829	0.000647	7.348162	3.3E-05

H0YL Y3	Ceramide synthase 4 (Fragment)	1.008019	0.028518	1.171341	0.01558	1.862582	0.043516
Q9UJZ 1	Stomatin-like protein 2, mitochondrial	1.302364	0.005855	3.975603	0.000343	1.74825	0.048533
A0A02 4R5X2	HCG2001986, isoform	2.212798	3.06E-05	3.207731	0.000164	1.475752	0.029288
F2Z2J 1	Ribosomal protein S6 kinase	4.014948	4.07E-05	4.636334	1.74E-07	3.455334	0.021941

**Table: 3** Complete lists of significantly upregulated proteins unique to *KLF4<sup>K409Q</sup>* mutational subtype.

Uniprot ID	Protein name	Log2 FC <i>KLF4<sup>K409Q</sup></i> <i>Q/TRAF7</i> vs. <i>AKT1<sup>E17K</sup></i> <i>/TRAF7</i>	P-value <i>KLF4<sup>K409Q</sup></i> <i>Q/TRAF7</i> vs. <i>AKT1<sup>E17K</sup></i> <i>/TRAF7</i>	Log2 FC <i>KLF4<sup>K409Q</sup></i> <i>Q/TRAF7</i> vs. <i>NF2<sup>-/-</sup></i>	P-value <i>KLF4<sup>K409Q</sup></i> <i>Q/TRAF7</i> vs. <i>NF2<sup>-/-</sup></i>	Log2 FC <i>KLF4<sup>K409Q</sup></i> <i>Q/TRAF7</i> NMT	P-value <i>KLF4<sup>K409Q</sup></i> <i>Q/TRAF7</i> NMT
Q6ZN4 0	Tropomyosin 1 (Alpha), isoform	-6.3347	0.000219	-6.2827	0.000103	-10.9713	0.000865
Q53FI7	Four and a half LIM domains 1 variant (Fragment)	-6.873	1.02E-05	-7.22534	7.91E-05	-10.1997	3.54E-05
A0A02 4RBB5	Cysteine and glycine-rich protein 2, isoform	-2.4665	0.005647	-3.19157	0.00132	-9.88956	1.95E-08
P13591	Neural cell adhesion molecule 1	-5.1497	0.000117	-3.92071	0.011197	-9.11525	6.84E-05
V9HW C9	Superoxide dismutase [Cu-Zn]	-3.8219	0.001119	-4.688	0.00195	-9.07859	0.000337
P01861	Immunoglobulin heavy constant gamma 4	-3.1529	0.009836	-3.21098	0.024828	-8.75455	2.31E-06
A0A0S 2Z3X8	Rab GDP dissociation inhibitor (Fragment)	-3.5417	0.000973	-5.52259	7.92E-07	-8.27719	0.000141
Q6FHH 6	LANCL1 protein (Fragment)	-6.1055	1.93E-06	-3.03975	0.030007	-8.15241	2.13E-06
A0A08 7WV90	Dystrophin	-4.4579	0.000287	-3.7166	0.036626	-8.03634	0.000106

A0A140VK69	Aspartate aminotransferase	-3.8878	0.000838	-3.28214	0.015176	-7.27627	0.001927
A0A024QZ64	Fructose-bisphosphate aldolase	-1.3354	0.044573	-2.13922	0.003261	-6.67647	8.01E-05
Q53G58	Coronin (Fragment)	-3.8882	0.000121	-3.32796	0.011258	-6.60118	0.000323
Q14019	Coactosin-like protein	-5.2721	0.001893	-6.07065	7.72E-05	-6.25731	0.006682
A8K413	NADH dehydrogenase [ubiquinone] 1 alpha subcomplex subunit 10, mitochondria	-4.5168	9.14E-05	-1.91361	0.013112	-6.0363	8.76E-07
A0A024R1S8	LIM and SH3 protein 1, isoform	-5.2553	2.71E-05	-3.91215	0.000506	-5.99344	0.000712
Q5JR08	Rho-related GTP-binding protein RhoC (Fragment)	-5.3601	0.000155	-4.2073	0.005369	-5.85327	2E-05
A0A140VJJ2	S-formylglutathione hydrolase	-4.4359	0.000364	-4.96492	5.85E-06	-5.83688	0.005973
C9J0K6	Sorcin	-4.2049	0.002573	-3.1225	0.032662	-5.76733	0.023831
A0A024R9H2	Heat-responsive protein 12, isoform	-5.5754	3.3E-08	-2.57622	0.03831	-5.751	3.48E-06
E7DVW5	Fatty acid binding protein 5 (Psoriasis-associated)	-3.193	0.040248	-7.51627	2.73E-05	-5.74374	0.043352
A0A0A0MRJ6	Protein-L-isoaspartate O-methyltransferase	-5.4054	0.000362	-4.07712	0.005578	-5.68737	0.030451
A0A024RB09	RAB5B, member RAS oncogene family, isoform	-4.4481	7.97E-05	-3.16759	0.017888	-5.67608	0.000142

A0A024RDM2	Crystallin, lambda 1, isoform	-5.438	0.000667	-3.28636	0.016425	-5.63252	0.039888
B2R659	cDNA, FLJ92803, highly similar to Homo sapiens hydroxysteroid (17-beta)	-5.0539	0.000191	-4.02064	9.46E-05	-5.54992	0.01266
B4DDF4	Calponin	-2.3281	0.012179	-2.87316	0.049023	-5.37876	0.002183
Q8N335	Glycerol-3-phosphate dehydrogenase 1-like protein	-4.1888	0.002358	-3.81561	0.001707	-5.34085	0.00201
Q86SZ7	Full-length cDNA clone CS0DJ015Y J12 of T cells (Jurkat cell line)	-6.4662	1.61E-08	-6.86721	1.22E-10	-5.09271	0.000794
A0A140VKA9	Testis secretory sperm-binding protein Li 236P	-3.4077	0.00339	-2.75695	0.049047	-5.04328	0.023823
A0A140T8Z0	Protein diaphanous homolog 1	-4.2305	2.33E-05	-2.46392	0.009665	-4.6743	9.43E-05
A0A140VK19	Testicular secretory protein Li 19	-2.3511	0.010606	-3.81462	0.000622	-4.27559	0.015461
R4GNH3	26S proteasome regulatory subunit 6A	-4.478	6.91E-05	-3.5696	0.01208	-4.19206	0.000143
J3KN29	26S proteasome non-ATPase regulatory subunit 9	-4.3186	4.87E-06	-2.80999	0.020754	-4.12452	0.001033
A0A024RDT3	Calcium binding protein 39-like, isoform	-5.966	9.93E-06	-3.63969	0.002033	-4.08048	0.036973
P40123	Adenylyl cyclase-associated protein 2	-3.2534	0.000224	-3.61868	5.61E-05	-4.05947	0.005295

P50135	Histamine N-methyltransferase	-6.6068	9.17E-08	-6.06671	1.69E-05	-4.02076	0.002598
Q96CV8	Thimet oligopeptidase 1	-2.5146	0.00143	-2.85041	3.11E-06	-3.82362	0.000107
O75116	Rho-associated protein kinase 2	-2.2683	0.003703	-3.07244	0.000245	-3.79972	0.000941
O95182	NADH dehydrogenase [ubiquinone] 1 alpha subcomplex subunit 7	-5.7459	3.2E-05	-3.74109	0.002421	-3.76284	0.001101
A0A024R496	Calcium binding protein 39, isoform	-4.9694	2.78E-05	-2.55005	0.034822	-3.74406	0.037735
A8K8F9	Phosphoinositide phospholipase C	-2.3463	0.02733	-3.46458	0.000248	-3.74393	0.023554
Q9UBV8	Peflin	-4.7139	6.94E-05	-4.21483	9.86E-05	-3.62835	0.013653
Q53HJ0	COP9 constitutive photomorphogenic homolog subunit 2 variant (Fragment)	-3.0067	0.005331	-2.93723	0.007678	-3.62264	0.023663
A8K6K2	cDNA FLJ75877, highly similar to Homo sapiens 5-nucleotidase	-3.9682	0.000342	-5.05614	2.66E-06	-3.51137	0.040274
Q5TZV6	Cytochrome P450, family 1, subfamily B, polypeptide 1	-4.7008	3.54E-05	-2.66495	0.023389	-3.50252	0.024877
P46952	3-hydroxyanth	-2.9006	0.010346	-3.82784	0.000255	-3.46999	0.000927

	ranilate 3,4-dioxygenase						
A8K646	cDNA FLJ75699, highly similar to Homo sapiens osteoclast stimulating	-4.4789	0.000479	-3.80034	0.014879	-3.4435	0.013379
P07814	Bifunctional glutamate/proline--tRNA ligase	-3.4074	0.000844	-2.93274	0.000654	-3.43663	0.013344
B5BU72	Phosphatidylinositol-binding clathrin assembly protein isoform 2	-3.9119	2.21E-05	-3.49124	0.01126	-3.4218	0.014414
A0A024R8R4	Nuclear protein localization 4 homolog (S. cerevisiae), isoform	-3.1889	9.63E-06	-2.2263	0.04077	-3.40023	0.002877
Q75T13	GPI inositol-deacylase	-6.3767	7.16E-07	-3.16981	0.020085	-3.28167	0.048874
O75663	TIP41-like protein	-1.4556	0.049293	-2.15324	0.046333	-3.25704	0.000195
A0A0S2A4E4	Amylo-1, 6-glucosidase, 4-alpha-glucanotransferase (Glycogen debranch	-2.8091	0.000762	-3.72759	8.08E-06	-3.24729	0.005925
P26368	Splicing factor U2AF 65 kDa subunit	-1.6016	0.037575	-3.42898	0.01793	-3.18724	0.026721
D6RCD0	Estradiol 17-beta-dehydrogenase 11	-2.4897	0.001532	-2.08876	0.025081	-3.01459	0.025808
A0A024RDY0	RAN binding protein 5, isoform	-2.2189	0.004883	-1.80488	0.005228	-2.92566	0.004781
A8K8U1	cDNA FLJ77762, highly	-2.6662	0.001088	-1.98152	0.00812	-2.90259	0.032335



	similar to Homo sapiens cullin-associated and						
Q96FJ2	Dynein light chain 2, cytoplasmic	-3.6587	0.000264	-3.4431	0.02668	-2.88964	0.034236
B1AKK2	Dimethylarginine dimethylaminohydrolase 1, isoform	-2.2888	0.000105	-1.3999	0.007855	-2.71002	0.01452
O00291	Huntingtin-interacting protein 1	-1.7763	0.006471	-1.93902	0.013344	-2.43088	0.02455
Q5U077	L-lactate dehydrogenase	-1.129	0.006161	-2.26836	9.66E-05	-2.38026	0.001853
O14531	Dihydropyrimidinase-related protein 4	-2.0661	0.009501	-2.72579	0.008807	-2.2362	0.029101
Q9NQE9	Histidine triad nucleotide-binding protein 3	-1.7958	0.006493	-2.30769	0.047776	-2.08748	0.026189
V9HWI5	Cofilin 1 (Non-muscle), isoform	-1.6832	0.000666	-1.58534	0.015567	-1.82176	0.038808
B2R7T8	cDNA, FLJ93598, highly similar to Homo sapiens capping protein	-1.0943	0.003123	-1.21767	0.000447	-1.00528	0.049147

**Table: 4** Complete lists of significantly downregulated proteins unique to *KLF4*<sup>K409Q</sup> mutational subtype.

Uniprot ID	Protein name	Log2 FC <i>AKT1</i> <sup>E17K/T</sup> / <i>RAF7</i> vs. NMT	P-value <i>AKT1</i> <sup>E17K/T</sup> / <i>RAF7</i> vs. NMT	Log2 FC <i>KLF4</i> <sup>K409Q</sup> / <i>TRAF7</i> vs. NMT	P-value <i>KLF4</i> <sup>K409Q</sup> / <i>TRAF7</i> vs. NMT	Log2 FC <i>NF2</i> <sup>-/-</sup> vs. NMT	P value <i>NF2</i> <sup>-/-</sup> vs. NMT
Q6ZMP0	Thrombospondin type-1 domain-containing protein 4	9.0513	0.000134	8.681101	0.001383	9.76963	2.07E-05
Q9P2B2	Prostaglandin F2 receptor negative regulator	7.872114	3.21E-05	7.022715	0.000844	4.313749	0.026003
B0UXD8	HUMAN HLA-DRA	5.720575	0.000101	7.636087	0.000784	7.309523	0.005213
Q07812	Apoptosis regulator BAX	5.101104	4.7E-05	4.852595	0.000659	4.31843	0.002286
A0A024R5K8	Serpin peptidase inhibitor, clade H (Heat shock protein 47), member 1, (Collagen binding protein 1), isoform	4.924363	0.000344	4.138257	0.000356	5.728439	0.000271
A0A1S5UZ19	Protein transport protein Sec31A	5.361034	0.014039	3.46793	0.018982	4.226442	0.02477
A0A140VJN8	Perilipin	3.96963	0.010434	3.893778	5.22E-05	4.179601	0.000456
A0A024R2F9	Transmembrane protein 43 isoform 1	3.599154	0.001119	3.70057	0.002477	3.010133	0.033565
B4DP27	cDNA FLJ52153, highly similar to Transmembrane emp24 domain-containing protein 2	2.941337	0.035053	3.736768	0.003384	2.238144	0.015004

P09525	Annexin A4	1.855169	0.0036	1.871707	0.018686	1.658012	0.04326
Q53FX5	Lin-7 homolog C variant	6.618656	0.000119	4.809913	0.040019	4.555417	0.078835

**Table: 5** Complete lists of significantly upregulated proteins unique to benign meningioma compared to NMT.

Uniprot ID	Protein name	Log2 FC <i>AKT1<sup>E17K</sup>/TRAF7</i> vs. NMT	P-value <i>AKT1<sup>E17K</sup>/TRAF7</i> vs. NMT	Log2 FC <i>KLF4<sup>K409Q</sup>/TRAF7</i> vs. NMT	P-value <i>KLF4<sup>K409Q</sup>/TRAF7</i> vs. NMT	Log2 FC <i>NF2<sup>-/-</sup></i> vs. NMT	P value <i>NF2<sup>-/-</sup></i> vs. NMT
A0A024QZJ4	Myosin, heavy polypeptide 11, smooth muscle, isoform	-13.2699	7.79E-05	-13.3154	1.88E-07	-8.67893	0.002138
Q16853	Membrane primary amine oxidase	-12.9434	9.61E-06	-11.6156	2.62E-05	-13.5585	4.57E-08
D6RGG3	Collagen alpha-1(XII) chain OS	-11.4378	1.28E-06	-9.4238	0.008816	-11.7305	0.000163
K7EMP8	Glial fibrillary acidic protein OS	-11.0712	0.002148	-10.7083	8.64E-05	-11.2581	4.74E-07
V9HWA5	Calponin OS	-10.9918	2.91E-05	-11.6264	1.93E-06	-12.6444	2.33E-05
P23141	Liver carboxylesterase 1 OS	-10.633	0.000288	-10.9765	9.43E-06	-12.4123	1.37E-07
A0A0U4BW16	Non-muscle myosin heavy chain 9 OS	-10.6194	2.09E-06	-9.22858	7.34E-06	-10.7338	1.05E-06
O94875	Sorbin and SH3 domain-containing protein 2 OS	-10.5649	4.02E-06	-9.36423	4.22E-05	-10.7652	4.27E-07
F5GZ08	Amyloid-like protein 1 OS	-10.0662	3.44E-05	-8.95279	2.52E-05	-10.1929	3.7E-07
P02741	C-reactive protein OS	-10.0172	2.21E-05	-9.87212	1.92E-05	-11.3629	1.89E-07

F8VVB6	Protein kinase C-binding protein NELL2 OS	-9.98857	3.01E-05	-9.76128	1.22E-06	-10.7496	3.21E-06
L8E853	von Willebrand factor OS	-9.96659	2.15E-06	-8.01642	0.000345	-9.80875	1.63E-09
B2RMS9	Inter-alpha (Globulin) inhibitor H4 (Plasma Kallikrein-sen	-9.91793	0.016102	-6.91785	0.037078	-10.1699	0.000878
A0A024RDI5	Alcohol dehydrogenase IB (Class I), beta polypeptide, isof	-9.88503	8.45E-08	-8.97135	4.66E-06	-9.75221	0.002587
A0A024R8G3	Prostaglandin D2 synthase 21kDa (Brain), isoform CRA	-9.5854	0.004748	-10.5776	4.39E-05	-11.7201	2.26E-09
H9KV75	Alpha-actinin-1 OS	-9.52518	1.47E-05	-8.32222	4.67E-07	-9.06468	1.69E-06
P30837	Aldehyde dehydrogenase X, mitochondrial OS	-8.99154	3.57E-05	-8.89764	1.1E-07	-9.60351	1.1E-06
C0JYY2	Apolipoprotein B (Including Ag(X) antigen) OS	-8.8662	0.027018	-6.52248	0.037337	-10.5223	0.001213
A0A142CHG9	GO2-q chimeric G-protein OS	-8.82468	0.002468	-8.73814	0.002163	-10.1676	0.000197
V9HW83	Aldehyde dehydrogenase 1 family, member A1, isoform CRA	-8.76388	6.73E-08	-8.57437	3.91E-05	-8.38787	0.000179
Q4L233	Brain-specific protein p25 alpha, isoform CRA	-8.70686	0.008438	-6.10337	0.022129	-8.11511	0.000324
B4E3Q1	cDNA FLJ61580, highly similar to	-8.65661	7.83E-08	-7.48398	0.000104	-7.89558	0.003209

	Calsyntenin-1 OS						
A0A024 RAB6	Heparan sulfate proteoglycan 2 (Perlecan), isoform CRA	-8.65651	0.000682	-6.92158	0.013418	-5.94605	0.01862
B4E3S9	cDNA FLJ53443, highly similar to Leiomodrin-1 OS	-8.5786	3.45E-05	-8.41149	1.81E-05	-9.67203	2.14E-06
O15540	Fatty acid-binding protein, brain OS	-8.5279	5.11E-05	-7.84009	6.09E-05	-9.30854	9.14E-07
D3DSM4	Collagen, type XVIII, alpha 1, isoform CRA	-8.48685	0.000397	-6.90757	0.003826	-9.90757	0.000282
P04003	C4b-binding protein alpha chain OS	-8.40557	0.017808	-8.58186	0.00075	-11.2083	0.00025
V9HWF6	Alpha-1-acid glycoprotein OS	-8.23883	0.017115	-6.43046	0.025753	-8.51746	0.034869
P14543	Nidogen-1 OS	-8.23787	0.00066	-6.72097	0.000553	-6.5002	0.001961
P11277	Spectrin beta chain, erythrocytic OS	-8.06936	0.010874	-6.5919	0.034405	-8.99113	0.000693
Q5VU97	VWFA and cache domain-containing protein 1 OS	-8.05962	0.007062	-7.20349	0.005817	-8.90179	0.000272
A0A024 R5W6	Tropomyosin 1 (Alpha), isoform CRA	-8.04557	0.001586	-8.62648	6.25E-05	-9.95476	6.95E-06
I7L574	Lutheran blood group OS	-7.90471	0.011138	-6.97194	0.022969	-7.55761	0.014928
A0A087 WW43	Inter-alpha-trypsin inhibitor heavy chain H3 OS	-7.8023	1.38E-06	-7.24416	2.29E-06	-8.44982	4.96E-05
Q8N4S1	Proliferation-inducing protein 33 OS	-7.69783	0.000385	-7.7725	4.73E-06	-8.09639	5.16E-05

A1L306	TNR protein OS	-7.69479	0.029969	-7.78668	0.01144	-8.47953	0.017029
O15230	Laminin subunit alpha-5 OS	-7.67689	2.95E-05	-5.22142	0.003225	-7.77454	0.003751
A0A024R104	Contactin 1, isoform CRA	-7.64453	0.004109	-5.99136	0.002401	-8.74174	0.000578
B9EG60	Synaptopodin 2 OS	-7.64409	0.000209	-7.32494	7.88E-06	-7.17364	0.001123
A0A0G2JPR0	Complement C4-A OS	-7.60725	4.61E-05	-5.37512	0.033654	-7.73396	0.000909
B4DI69	cDNA FLJ59893, highly similar to Dickkopf-related protein	-7.53643	3.6E-05	-6.91397	0.000166	-7.22708	1.66E-05
A0A024RBB5	Cysteine and glycine-rich protein 2, isoform CRA	-7.42303	0.00468	-9.88956	1.95E-08	-6.76043	0.007293
Q86YB0	Glycoprotein M6A OS	-7.29816	0.001376	-5.82319	0.001204	-7.50747	5.07E-06
Q8TCF0	LBP protein OS	-7.28891	9.71E-05	-7.45331	3.01E-05	-8.13596	6.52E-05
Q9NSD5	Sodium- and chloride-dependent GABA transporter 2 OS	-7.26367	0.000887	-7.93595	2.38E-05	-9.09166	6.17E-06
A0A140VJW3	Sushi domain containing 2, isoform CRA	-7.23563	0.000415	-7.94138	0.000502	-8.45714	0.000109
Q8N169	Amino acid transporter OS	-7.14957	0.000312	-6.76977	0.005002	-6.79549	0.000375
B3KX75	cDNA FLJ44930 fis, clone BRAMY3015549, highly similar to N	-7.13708	0.000674	-7.28955	0.000159	-7.7349	3.3E-05
P14415	Sodium/potassium-transporting ATPase	-7.13101	5.58E-05	-6.04999	1.33E-05	-7.15097	6.57E-05

	subunit beta-2 OS						
A0A024 R778	Pleiotrophin (Heparin binding growth factor 8, neurite gro	-7.09757	7.3E-06	-7.14086	2.82E-05	-7.16835	0.000107
A0A024 RC55	Milk fat globule-EGF factor 8 protein, isoform CRA	-6.92852	0.002963	-7.78781	0.001346	-6.85927	0.012191
F5GZS6	4F2 cell-surface antigen heavy chain OS	-6.92514	9.04E-05	-6.00425	0.004074	-8.69954	1.69E-05
Q53YE7	Amine oxidase OS	-6.9122	0.001259	-5.83279	0.000651	-6.5301	0.003873
Q8WX93	Palladin OS	-6.86377	0.002864	-7.59721	0.000451	-5.8498	0.030306
C9JFZ1	Synaptojanin-1 OS	-6.83342	0.019536	-7.10027	0.003998	-7.13658	0.003938
P16452	Erythrocyte membrane protein band 4.2 OS	-6.82337	0.005754	-5.66283	0.015438	-6.77483	0.001192
A0A024 R231	Guanine deaminase, isoform CRA	-6.79291	0.01014	-5.16331	0.009302	-6.52189	0.004621
Q9UN36	Protein NDRG2 OS	-6.78749	8.3E-05	-8.33261	4.02E-08	-8.62556	0.001628
Q05707	Collagen alpha-1(XIV) chain OS	-6.75305	0.003436	-5.8331	0.018457	-11.963	0.000903
Q6FHV6	ENO2 protein OS	-6.69365	0.00769	-6.51955	0.026704	-8.48062	0.008674
A0A286 YF37	F-box only protein 2 (Fragment) OS	-6.68522	1.98E-06	-6.16608	1.17E-06	-6.78627	4.36E-05
G5E9D8	Inter-alpha (Globulin) inhibitor H5, isoform CRA	-6.65093	0.000156	-7.44572	0.007436	-7.3477	0.028752
D2JYH4	Actin, alpha 2, smooth muscle, aorta OS	-6.64112	0.004996	-6.26	0.01466	-11.0237	0.002125

A0A0A0MQY0	PDZ and LIM domain protein 3 OS	-6.63922	5.03E-05	-6.19169	1.99E-06	-7.08536	4.43E-06
P23471	Receptor-type tyrosine-protein phosphatase zeta OS	-6.56453	0.019745	-5.96265	0.014349	-7.8188	0.004187
Q8TDR6	Cytoplasmic protein Ndr1 OS	-6.5155	7.83E-05	-5.67204	4.51E-05	-6.65353	2.63E-06
A1L4H1	Soluble scavenger receptor cysteine-rich domain-containing	-6.49656	4.87E-06	-6.29407	0.000239	-6.43966	0.006947
P12532	Creatine kinase U-type, mitochondrial OS	-6.47609	0.024447	-6.28024	0.002271	-8.09325	0.000834
C9J7L4	Solute carrier family 13 member 3 (Fragment) OS	-6.45573	0.000141	-6.45511	2.23E-07	-5.86462	0.018068
Q9UKV8	Protein argonaute-2 OS	-6.43231	1.78E-06	-6.61162	1.18E-05	-6.71892	0.000144
A0A024R5Z9	Pyruvate kinase OS	-6.42911	1.62E-05	-7.01755	3.95E-05	-7.64842	0.001444
Q15746	Myosin light chain kinase, smooth muscle OS	-6.42851	0.000329	-4.72523	0.016429	-7.44077	0.005273
S6BGD6	IgG L chain OS	-6.40186	3.51E-06	-6.0307	0.000278	-5.72871	0.02856
A0A024RA98	Peptidyl arginine deiminase, type II, isoform CRA	-6.39789	7.94E-05	-7.1652	2.66E-05	-7.14854	0.018109
A0A024R7R3	Beta-synuclein (Fragment) OS	-6.35891	0.000281	-5.48892	0.000373	-6.32466	0.002248
Q4VB86	EPB41 protein OS	-6.35315	0.010848	-6.28064	0.001683	-6.7638	0.004558



A8K9L3	Proteolipid protein 1 (Pelizaeus-Merzbacher disease, spast	-6.33465	0.020845	-6.24349	0.011604	-6.2696	0.005694
A0A024R9Y0	Microtubule-associated protein OS	-6.30381	0.00599	-6.71331	0.0037	-7.77394	0.000721
A0A0M4FEM1	Alpha-1,4 glucan phosphorylase OS	-6.29454	0.001573	-4.75036	0.018368	-7.12552	0.001283
A0A024R0S6	EH-domain containing 2, isoform CRA	-6.25644	0.006273	-4.99079	0.010015	-6.16486	0.002902
P01031	Complement C5 OS	-6.24605	0.017156	-6.78578	0.021339	-8.73465	0.001445
O94856	Neurofascin OS	-6.23407	0.019933	-4.70811	0.027629	-6.9395	0.006051
P02750	Leucine-rich alpha-2-glycoprotein OS	-6.20896	0.001309	-5.11909	0.021061	-5.71382	0.017573
Q9HCB6	Spondin-1 OS	-6.20289	0.00242	-5.91991	7.76E-05	-6.20166	0.000967
Q9HB00	Desmocollin 1, isoform CRA	-6.19828	4.43E-06	-6.51878	8.26E-05	-5.06548	0.028328
Q53HU9	Complement component 1, r subcomponent variant (Fragment)	-6.17174	0.004921	-7.17411	3.05E-06	-6.49212	0.004972
P22792	Carboxypeptidase N subunit 2 OS	-6.17115	0.000155	-5.47453	0.000126	-5.77771	6.83E-06
W0UV93	Ribonuclease A C1 OS	-6.13275	1.36E-05	-6.43917	1.42E-06	-6.86512	2.96E-06
Q13938	Calcyphosin OS	-6.12905	0.000198	-5.73957	7.83E-05	-6.25582	1.7E-05
V9HW25	Epididymis secretory protein Li 273 OS	-6.10716	0.004005	-6.58371	0.002731	-6.04373	0.018695
A0A0K0K1J1	Cystatin OS	-6.06706	0.00315	-9.22071	0.002007	-7.75885	0.024804

P09871	Complement C1s subcomponent OS	-6.00005	0.008483	-5.32945	0.004574	-6.39975	0.009844
P05230	Fibroblast growth factor 1 OS	-5.87864	2.03E-05	-5.28247	0.000234	-6.74982	0.00019
A0A140VKB1	Testis secretory sperm-binding protein Li 238E OS	-5.86317	0.013331	-5.51622	2.76E-06	-5.22963	0.005186
A2NB45	Cold agglutinin FS-1 L-chain (Fragment) OS	-5.81859	9.2E-05	-5.34191	3.87E-06	-5.47313	0.033461
Q53QT6	Uncharacterized protein FRZB (Fragment) OS	-5.78248	2.48E-07	-5.96189	0.000412	-6.08405	0.002907
Q86UY8	5-nucleotidase domain-containing protein 3 OS	-5.77592	0.000103	-6.00921	5.71E-07	-5.17121	1.77E-05
O00468	Agrin OS	-5.76266	0.000354	-6.27613	0.014961	-5.39023	0.005237
Q5KU26	Collectin-12 OS	-5.76003	0.000535	-4.43742	0.024992	-5.3047	0.00347
A0A024R7M3	Chondroitin sulfate proteoglycan 3 (Neurocan), isoform CRA	-5.70079	0.017537	-5.87855	0.017965	-6.35957	0.004429
P15259	Phosphoglycerate mutase 2 OS	-5.65944	0.000111	-4.44242	0.004805	-6.49961	8.3E-05
Q08495	Dematin OS	-5.61847	7.93E-06	-4.51778	0.00127	-5.49494	0.000509
A0A0X9UWL5	GCT-A5 light chain variable region (Fragment) OS	-5.61232	0.000174	-5.56529	7.22E-05	-5.40277	0.009367
A0A218KGR2	Amyloid beta A4 protein isoform a OS	-5.60576	0.007092	-7.16414	0.001185	-8.39693	0.000589

Q0ZGT2	Nexilin OS	-5.59169	0.007119	-4.8791	0.00345	-6.76022	0.000627
X5DNA9	HCG2002594, isoform CRA	-5.57174	0.014548	-6.29153	0.000652	-7.16485	0.000253
P35625	Metalloproteinase inhibitor 3 OS	-5.57081	0.020415	-5.89893	4.78E-06	-7.047	0.000133
X5D8S1	4-aminobutyrate aminotransferase isoform A (Fragment) OS	-5.53344	0.002951	-5.89701	0.000331	-7.01832	0.004411
Q15124	Phosphoglucosyltransferase-like protein 5 OS	-5.46731	0.000645	-7.81494	0.00163	-7.70206	0.003694
Q9BQI0	Allograft inflammatory factor 1-like OS	-5.37995	0.000136	-4.89662	3.04E-05	-5.98271	6.12E-06
A8K6Q3	cDNA FLJ75880, highly similar to Homo sapiens synaptic ves	-5.3689	0.006401	-5.46161	0.001938	-6.28487	0.000266
A0A024QZ64	Fructose-bisphosphate aldolase OS	-5.3411	0.000187	-6.67647	8.01E-05	-4.53725	0.001933
P0DOX8	Immunoglobulin lambda-1 light chain OS	-5.33182	0.000355	-5.86548	0.018043	-5.68702	0.001835
J3QL64	Myelin basic protein OS	-5.32527	0.020365	-4.32685	0.020641	-5.28505	0.008851
P62760	Visinin-like protein 1 OS	-5.30622	0.025786	-5.11848	0.010128	-6.10371	0.001302
P63096	Guanine nucleotide-binding protein G(i) subunit alpha-1 OS	-5.28818	0.008543	-6.11573	2.01E-05	-6.25441	0.000428
C8YAE4	Cytochrome c oxidase subunit 1 OS	-5.27921	0.001546	-3.71383	0.037792	-4.92221	0.004882
S6BAM6	IgG H chain OS	-5.27082	0.002281	-6.09652	0.000124	-6.41198	0.005553

E9PBC5	Plasma kallikrein OS	-5.26591	0.020386	-6.30303	2.76E-05	-6.86871	2.39E-06
Q53H91	Phospholipid transfer protein isoform a variant (Fragment)	-5.24938	0.000904	-3.69882	0.047456	-4.46769	0.005417
A0A0B4J2A4	3-ketoacyl-CoA thiolase, mitochondrial OS	-5.16728	0.001755	-4.36823	0.010331	-6.50576	0.009167
P05090	Apolipoprotein D OS	-5.09368	0.000959	-5.99655	0.005883	-8.30714	0.001549
B0AZM0	cDNA, FLJ79460, highly similar to Voltage-gated potassium	-5.07695	0.00019	-4.71252	0.000146	-4.17888	0.005725
O43837	Isocitrate dehydrogenase [NAD] subunit beta, mitochondrial	-5.03324	0.004009	-6.52633	0.000712	-6.22492	0.004686
A0A1B0GWJ0	Adenylosuccinate lyase OS	-5.01517	0.025238	-6.77963	2.94E-06	-6.76898	0.003093
Q5U0D2	Transgelin OS	-4.97628	0.001322	-5.43507	1.91E-06	-5.49589	0.002497
Q8IVN3	Musculoskeletal embryonic nuclear protein 1 OS	-4.97282	0.000192	-4.38065	0.00015	-5.3731	0.000291
B7Z544	cDNA FLJ51742, highly similar to Inter-alpha-trypsin inhib	-4.96049	0.002437	-3.69391	0.004526	-5.40157	0.005595
H7BXR3	Sorbin and SH3 domain-containing protein 2 (Fragment) OS	-4.93786	0.005344	-3.76471	0.023031	-5.89666	0.000567
B2R4C5	Lysozyme OS	-4.93291	0.00427	-6.7637	0.001428	-6.54247	0.015547

X5D7N2	Proline dehydrogenase (Fragment) OS	-4.91111	0.000205	-5.12297	1.62E-06	-5.44347	0.000327
Q13825	Methylglutac onyl-CoA hydratase, mitochondrial OS	-4.90649	6.44E-06	-6.58658	0.002872	-6.53205	0.000427
O43405	Cochlin OS	-4.89673	0.000112	-4.02893	0.003751	-5.03383	3.75E-05
Q16716	Pyruvate kinase OS	-4.88345	1.36E-05	-4.38429	1.44E-05	-5.30132	0.001883
Q9UL83	Myosin-reactive immunoglobulin light chain variable region	-4.81922	0.00107	-4.18664	3.78E-05	-4.79941	0.003298
A0A109P SY4	MS-A1 light chain variable region (Fragment) OS	-4.80022	2.53E-05	-4.29219	4.22E-05	-5.16455	0.011697
K7EJH8	Alpha-actinin-4 (Fragment) OS	-4.7956	0.000335	-5.1947	0.000583	-5.05061	0.0002
Q9GZM7	Tubulointerstitial nephritis antigen-like OS	-4.79487	1.46E-05	-3.28372	0.019517	-6.15407	0.000149
B4DGP4	cDNA FLJ53288, moderately similar to LIM domain-binding pr	-4.7812	0.00015	-4.57924	0.000621	-5.3798	0.000256
A0A024 RAD8	Aldehyde dehydrogenase 4 family, member A1, isoform CRA	-4.76421	0.004224	-7.04805	0.000584	-8.4191	3.76E-05
P48735	Isocitrate dehydrogenase [NADP], mitochondrial OS	-4.75652	0.003171	-7.82484	0.000725	-5.45136	0.022272
Q7Z3B1	Neuronal growth regulator 1 OS	-4.71526	0.004363	-6.9057	7.37E-07	-7.2743	0.000122

O75891	Cytosolic 10-formyltetrahydrofolate dehydrogenase OS	-4.70081	0.002046	-5.5449	0.009665	-8.5665	0.001306
Q4VAR4	INPP5A protein OS	-4.68618	1.88E-05	-4.2434	0.000566	-4.77979	0.002455
Q6MZQ6	Uncharacterized protein DKFZp686G11190 OS	-4.68053	0.003003	-5.0299	2.78E-06	-6.08487	0.000528
B9EJA8	Mannose receptor, C type 1-like 1 OS	-4.65909	0.025875	-5.17036	0.024701	-6.80189	0.01488
P53814	Smoothelin OS	-4.65176	0.008242	-4.14005	0.005885	-4.79766	0.00243
Q5TDH0	Protein DDI1 homolog 2 OS	-4.64722	3.61E-06	-4.73632	0.000164	-4.72774	0.002276
P02787	Serotransferrin OS	-4.64233	9.06E-05	-3.43018	0.032789	-4.88972	0.001162
Q6ZN40	Tropomyosin 1 (Alpha), isoform CRA	-4.63653	0.006377	-10.9713	0.000865	-4.68858	0.038989
F5H5G1	Limbic system-associated membrane protein OS	-4.60602	0.010398	-4.98518	0.003509	-6.10317	0.002343
A0A0S2Z4C6	Serine/threonine-protein phosphatase (Fragment) OS	-4.59461	0.012197	-6.84139	0.00595	-7.25827	0.001456
O95631	Netrin-1 OS	-4.55872	0.000348	-4.84617	0.000205	-5.86306	0.001342
B4DPK0	cDNA FLJ55736, highly similar to Homo sapiens solute carrier	-4.55685	0.000318	-4.39381	0.015315	-4.7247	0.000477
Q05682	Caldesmon OS	-4.54197	0.021749	-4.33429	0.029409	-2.99321	0.02953
Q9P1X0	Cystine/glutamate transporter	-4.53571	0.001133	-4.20572	0.000201	-5.30925	2.26E-05

	(Fragment) OS						
Q96GW7	Brevican core protein OS	-4.53324	0.032739	-4.15019	0.042193	- 5.995 94	0.000 986
A0A024 R782	Phosphoglyce rate mutase OS	-4.48157	0.004403	-5.82888	0.027924	- 6.202 91	0.028 905
A0A024 R6V8	NDRG family member 4, isoform CRA	-4.47589	0.002456	-4.86813	0.000137	- 5.192 13	0.002 059
B7Z997	cDNA FLJ54581, highly similar to Homo sapiens sorbin and S	-4.46671	0.022638	-4.82643	0.002756	- 5.242 78	0.005 678
X5D8T4	Aldehyde dehydrogenas e 5 family member A1 isoform B (Fragm	-4.45319	0.044028	-5.42662	0.029613	- 6.987 01	0.000 508
E5KLM2	Mitochondria l dynamin- like 120 kDa protein OS	-4.44671	0.023702	-5.31784	0.007379	- 4.943 24	0.039 736
A0A087 WYF1	Laminin subunit alpha-2 OS	-4.41652	0.014761	-5.48304	0.001661	- 4.863 06	0.049 331
Q92743	Serine protease HTRA1 OS	-4.40033	0.008988	-3.86678	0.013554	- 5.110 72	0.015 757
Q9UI15	Transgelin-3 OS	-4.3901	0.049702	-3.95482	0.028855	- 5.498 99	0.003 24
Q6ZV30	Acetyl- coenzyme A synthetase OS	-4.37947	0.000513	-3.72414	0.009765	- 3.990 29	0.011 008
Q6PCE3	Glucose 1,6- biphosphate synthase OS	-4.37898	0.019787	-3.43724	0.024901	- 5.036 05	0.002 604
A0A125 QYY9	IBM-B2 heavy chain variable region (Fragment) OS	-4.36692	0.017739	-5.40808	0.000108	- 4.535 14	0.037 95
V9HWI6	Epididymis secretory protein Li 51 OS	-4.36638	0.000726	-3.9767	0.000195	- 4.768 66	0.014 326

A0A0S2Z4H2	Protein S100 (Fragment) OS	-4.34064	0.004142	-3.94399	0.006651	-4.76543	0.002415
B4DY28	cDNA FLJ61189, highly similar to Cysteine and glycine-rich	-4.32878	6.43E-05	-10.9507	0.000388	-8.03146	0.044663
Q14289	Protein-tyrosine kinase 2-beta OS	-4.29829	0.01078	-3.90452	0.000499	-4.42095	0.014331
A0A140VK65	Testicular secretory protein Li 65 OS	-4.29191	0.011879	-7.20554	0.002737	-5.38097	0.021181
C9JYY6	Neuronal cell adhesion molecule OS	-4.25697	0.01625	-4.40364	0.013275	-5.56134	0.000477
A0A024RDA6	Insulin-like growth factor binding protein 7, isoform CRA	-4.24857	0.000604	-3.78931	0.001956	-4.31098	0.012743
A0A1W2PPH1	Malic enzyme OS	-4.24713	0.007745	-6.09898	0.000249	-4.69048	0.043622
P60880	Synaptosomal-associated protein 25 OS	-4.22893	0.029058	-4.44841	0.001086	-5.03872	0.005661
V9HWF8	Epididymis secretory protein Li 41 OS	-4.22309	0.003424	-3.62838	0.000423	-3.99988	0.005319
Q9UH03	Neuronal-specific septin-3 OS	-4.21413	0.040461	-4.95606	0.008095	-5.13839	0.004791
B4DI16	cDNA FLJ58063, highly similar to 6-phosphofructo-2-kinase/	-4.11986	0.002714	-3.72106	0.01063	-4.73098	0.000316
E7EUY3	Propionyl-CoA carboxylase beta chain, mitochondrial OS	-4.08217	0.0153	-4.97459	0.000763	-5.64107	0.013457
H3BNU1	TBC1 domain family	-4.07664	0.02729	-6.58	0.000197	-5.9033	0.003621



	member 24 OS						
A0A096LPE2	SAA2-SAA4 readthrough OS	-4.03732	0.005358	-3.75669	0.000245	-4.15396	0.0049
Q1HP67	Lipoprotein, Lp(A) OS	-4.03509	0.025655	-4.38919	0.026598	-5.04328	0.010879
Q53XB4	Full-length cDNA clone CS0DF032Y M23 of Fetal brain of Homo	-4.03215	0.000527	-3.23411	0.002748	-3.69556	0.006662
P11177	Pyruvate dehydrogenase E1 component subunit beta, mitochondrion	-4.01674	0.001642	-4.50676	0.033017	-5.17272	0.013889
B2R950	cDNA, FLJ94213, highly similar to Homo sapiens pregnancy-z	-3.93624	0.020049	-3.65749	0.008046	-5.56173	0.002528
H3BM30	Enoyl-[acyl-carrier-protein] reductase, mitochondrial (Fragment)	-3.93525	0.000379	-3.08023	0.001901	-4.42865	0.005265
D3DSC5	Neural cell adhesion molecule 2, isoform CRA1	-3.90304	0.007015	-4.6908	0.00036	-4.78454	0.020142
P0DOX5	Immunoglobulin gamma-1 heavy chain OS	-3.89021	0.00101	-3.42042	0.020986	-5.00529	0.004472
A0A1W2PQV2	Glycine cleavage system H protein, mitochondrial (Fragment)	-3.85347	0.01766	-3.32848	0.001232	-3.87988	0.012189
K7ENT6	Tropomyosin alpha-4 chain (Fragment) OS	-3.83605	0.011487	-4.37399	0.030094	-5.72393	0.000105
P78324	Tyrosine-protein phosphatase non-receptor	-3.82943	0.04724	-5.39801	0.001429	-5.92061	0.000437

	type substrate 1						
A0A024 R694	Actinin, alpha 1, isoform CRA	-3.76953	0.015952	-3.74089	0.016212	- 2.590 21	0.003 254
Q59FG2	Low density lipoprotein- related protein 1 variant (Fragmen	-3.75294	0.045947	-3.10024	0.005098	- 4.366 48	0.013 39
O00408	cGMP- dependent 3,5-cyclic phosphodiesterase OS	-3.71053	0.001905	-3.29293	0.004637	- 2.959 99	0.043 46
B4DRD3	Plasminogen activator OS	-3.70635	0.002218	-3.64129	0.005006	- 4.537 74	0.000 106
Q6FHG5	Gamma- synuclein OS	-3.70511	0.006848	-2.32921	0.040743	- 4.214 46	0.001 482
Q6GMX6	IGH@ protein OS	-3.67498	0.049044	-7.00825	0.000108	- 6.575 99	0.000 558
Q16798	NADP- dependent malic enzyme, mitochondrial OS	-3.6389	0.008538	-3.22228	0.010571	- 4.326 46	0.037 918
S6BGF5	IgG H chain OS	-3.61727	0.007318	-3.38168	0.015634	- 3.856 79	0.002 584
A0A1R3 UCE8	Kallikrein I OS	-3.59286	0.002468	-2.781	0.002126	- 3.985 63	0.000 691
P60520	Gamma- aminobutyric acid receptor- associated protein-like 2	-3.58896	0.02431	-4.58979	0.009393	- 4.450 08	0.014 346
Q6N089	Uncharacteriz ed protein OS	-3.57796	0.0471	-3.69045	0.009647	- 4.436 44	0.000 761
P21333	Filamin-A OS	-3.49005	0.001535	-3.17456	0.00336	- 3.204 6	0.000 148
B4DEQ0	cDNA FLJ59482, highly similar to Electron transfer flavopr	-3.48895	0.008431	-4.75431	0.006487	- 6.028 1	0.001 673

X5DNH4	Contactin associated protein-like 2 isoform B (Fragment) O	-3.47868	0.019875	-3.59931	0.030196	-4.51574	0.022799
Q12929	Epidermal growth factor receptor kinase substrate 8 OS	-3.47113	0.002901	-3.07895	0.00469	-4.16398	0.002091
A0A024R0Y5	ATP-dependent 6-phosphofructokinase OS	-3.46513	0.004628	-5.04446	0.002018	-4.18768	0.029995
P35609	Alpha-actinin-2 OS	-3.4643	0.035137	-3.83984	0.022473	-4.2352	0.009113
A7E2D8	Calcium-transporting ATPase OS	-3.3121	0.026558	-3.03216	0.019028	-3.16369	0.029261
B4DPI4	cDNA FLJ53456, highly similar to Homo sapiens solute carri	-3.30236	0.020668	-3.118	0.011634	-4.54896	0.002333
A0A024R702	Brain specific protein, isoform CRA	-3.30101	0.029343	-5.47514	0.031175	-7.09002	0.023959
E9PCG9	D-beta-hydroxybutyrate dehydrogenase, mitochondrial OS	-3.2735	0.042934	-6.19706	1.86E-06	-5.92483	0.000382
A0A024R040	Succinyl-CoA:3-ketoacid-coenzyme A transferase OS	-3.27183	0.020713	-5.82499	0.041841	-5.05037	0.001099
Q6B0I4	Opioid binding protein/cell adhesion molecule-like OS	-3.22757	0.002911	-3.02378	0.011701	-3.84424	0.002021
B4DWZ7	cDNA FLJ56802, highly similar to LanC-like protein 2 OS	-3.22443	0.010172	-4.44755	0.006976	-5.55553	0.034869

B4DVS4	cDNA FLJ57619, highly similar to Delta 3,5-delta 2,4-dieno	-3.18746	0.004108	-2.77232	0.007285	-3.11833	0.024392
P60660	Myosin light polypeptide 6 OS	-3.13078	0.018458	-2.97906	0.039264	-2.72345	0.001567
D3DUU0	CD163 antigen, isoform CRA	-3.12943	0.036333	-2.79911	0.005504	-4.34673	0.002991
P35442	Thrombospondin-2 OS	-3.08763	0.021475	-3.49575	0.000252	-3.34832	0.019114
O43866	CD5 antigen-like OS	-3.05464	0.040128	-3.23205	0.012273	-3.924	0.014335
Q8N2G2	cDNA PSEC0187 fis, clone HEMBA1000034, highly similar to R	-3.03933	0.002284	-6.0742	0.001785	-6.72776	0.000816
B2RB70	Neurocalcin delta, isoform CRA	-3.03645	0.019756	-4.9576	0.000171	-4.08905	0.004192
Q6UWP8	Suprabasin OS	-3.01754	0.001967	-3.02256	0.000706	-3.2216	0.015673
A0A024R216	Hepatoma-derived growth factor, related protein 3, isoform	-2.93498	0.017102	-3.40591	0.000475	-3.53012	0.029991
B1AP58	Carboxypeptidase N catalytic chain (Fragment) OS	-2.92307	0.001068	-2.80032	0.006423	-3.26925	0.005283
Q9H4D2	Tubby-like protein (Fragment) OS	-2.91382	0.001277	-2.09078	0.04672	-3.63737	0.005368
P49247	Ribose-5-phosphate isomerase OS	-2.8753	0.021773	-4.30679	0.008662	-5.10458	0.006827
Q9H479	Fructosamine-3-kinase OS	-2.84302	0.007085	-4.89956	0.046735	-4.84566	0.023135
A0A024R687	Pleckstrin homology domain	-2.83177	0.001017	-3.6629	7.75E-06	-5.23773	0.000283

	containing, family C (With FERM						
E9PPJ5	Midkine (Fragment) OS	-2.76012	0.018622	-3.12367	0.008852	- 3.658 18	0.002 332
H0Y630	Serine/threoni ne-protein kinase 24 (Fragment) OS	-2.74061	0.005859	-2.28314	0.019165	- 2.709 14	0.037 494
O15240	Neurosecretor y protein VGF OS	-2.71148	0.031563	-3.15504	0.002132	- 3.520 97	0.018 074
Q14BN4	Sarcolemmal membrane- associated protein OS	-2.65389	0.005727	-2.67764	0.023439	- 2.929 73	0.046 213
A0A024 RE27	Fumarylaceto acetate hydrolase domain containing 2A, isoform	-2.60992	0.043465	-4.25964	0.002851	- 4.502 19	0.026 52
A0A024 R3N3	Amyloid beta (A4)-like protein 2, isoform CRA	-2.60391	0.00159	-2.39016	0.049936	- 3.472 79	0.000 113
X5DQN2	Aldehyde dehydrogenas e 5 family member A1 isoform B (Fragm	-2.56689	0.025946	-2.40217	0.039674	- 3.988 54	0.006 304
H7C144	Alpha- actinin-4 (Fragment) OS	-2.56113	0.001475	-3.11121	0.000968	- 3.689 07	0.001 718
B7Z2D6	Cystathionine beta-synthase OS	-2.50972	0.000497	-3.12293	0.014528	- 3.540 75	0.020 497
B1AKY9	Sodium/potas sium- transporting ATPase subunit alpha OS	-2.41113	0.00015	-2.85373	0.040026	- 2.496 82	0.005 492
Q13976	cGMP- dependent protein kinase 1 OS	-2.40437	0.016247	-4.91267	0.001259	- 4.799 43	0.008 276
Q53HW4	Claudin (Fragment) OS	-2.40328	0.015072	-2.59556	0.002579	- 2.183 28	0.023 922

F8WE86	Transcobalamin-2 OS	-2.39859	0.009098	-2.71888	0.008395	-2.95845	0.013518
F5H065	Nuclear receptor-interacting protein 2 (Fragment) OS	-2.39484	0.018734	-2.12356	0.026185	-2.47675	0.00125
A0A1W6IYJ0	N90-VRC38.03 heavy chain variable region (Fragment) OS	-2.36325	0.032393	-2.56858	0.024517	-3.20554	0.006671
Q8IZZ5	Coagulation factor XII-Mie OS	-2.34293	0.04741	-3.08147	0.00039	-3.38886	0.028248
B7Z7C0	Serine/threonine-protein phosphatase 2A 56 kDa regulatory	-2.32134	0.003429	-2.64414	0.01206	-3.05899	0.021084
E7EQB2	Lactotransferrin (Fragment) OS	-2.2684	0.015027	-2.55593	0.001624	-3.4769	0.003149
Q3LGB0	Osteopontin (Fragment) OS	-2.25563	0.009076	-2.8403	0.001335	-3.52793	0.007658
K7EIJ0	WW domain-binding protein 2 (Fragment) OS	-1.73378	0.000487	-2.79251	0.000498	-4.04148	0.013727
J3KS22	L-xylulose reductase (Fragment) OS	-1.72026	0.035759	-5.804	0.00569	-4.10517	0.048649
A0A024QZN4	Vinculin, isoform CRA	-1.44446	0.042353	-2.36749	0.007016	-1.92755	0.01041

**Table: 6** Complete lists of significantly downregulated proteins unique to benign meningioma compared to NMT.

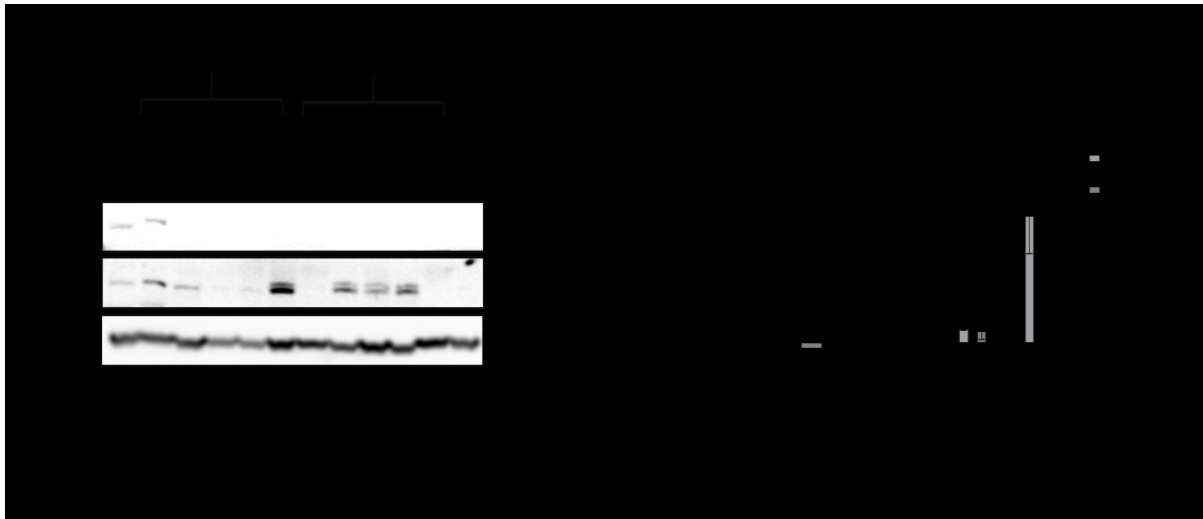


**Figure 1: Validation of predicted kinase CHEK2 as significantly upregulated in  $AKT1^{E17K}/TRAF7$  compared to  $NF2^{-/-}$  mutational subtype and NMT.** A) Western blot of upregulated kinase p-CHEK2-Thr68 and Total CHEK2 in meningioma and normal meningeal tissue lysates. GAPDH as a loading control. NMT ( $n=2$ );  $NF2^{-/-}$  ( $n=5$ ) and  $AKT1^{E17K}/TRAF7$  ( $n=5$ ). A1) Histogram showing quantification of kinase p-CHEK2-Thr68 normalized at Total CHEK2 and GAPDH. A2) First, histogram showing quantification of p-CHEK2-Thr68 normalized only at GAPDH and second histogram showing quantification of Total CHEK2-Thr68 normalized only at GAPDH respectively. Data represented as  $\pm$ SEM and statistical significance One-way ANOVA is shown by: ns= not significant;  $p>0.05$ ; \*  $p\leq 0.05$ ; \*\*  $p\leq 0.01$ ; \*\*\*  $p\leq 0.001$ ; \*\*\*\*  $p\leq 0.0001$ .

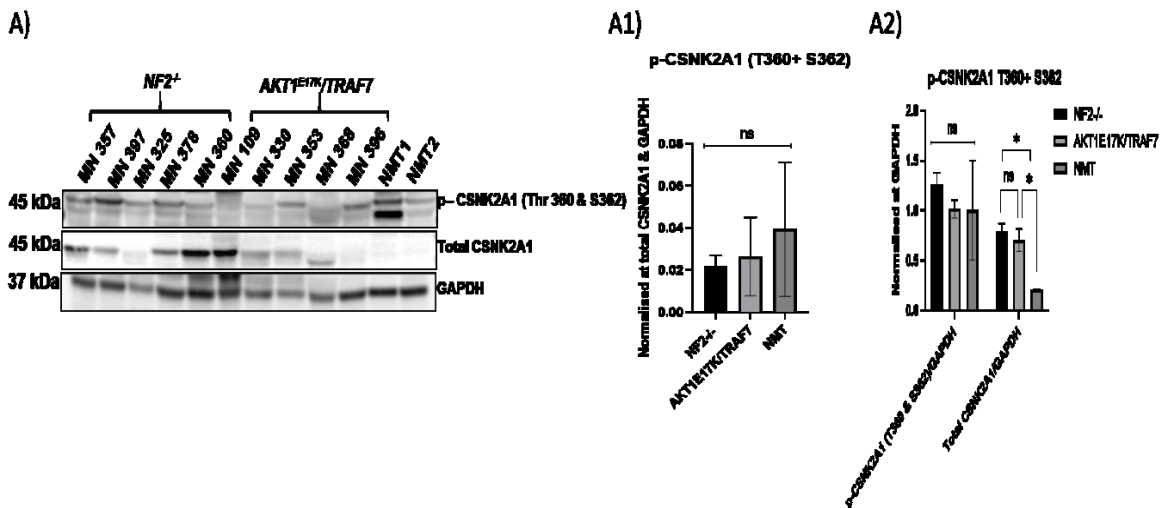


**Figure 2: Validation of predicted kinase CSNK2A1 as significantly upregulated in  $NF2^{-/-}$  compared to  $AKT1^{E17K}/TRAF7$  mutational subtype and NMT.** A) Western blot of upregulated kinase p-CSNK2A1-Thr360+Ser-362 and Total CSNK2A1 in meningioma and normal meningeal tissue lysates. GAPDH as a loading control. NMT ( $n=2$ );  $NF2^{-/-}$  ( $n=5$ ) and  $AKT1^{E17K}/TRAF7$  ( $n=5$ ). A1) Histogram showing quantification of kinase p-CSNK2A1-Thr360+Ser-362 normalized at Total CSNK2A1 and GAPDH. A2) First, histogram showing quantification of p-CSNK2A1-Thr360+Ser-362 normalized only at GAPDH and second histogram showing quantification of Total CSNK2A1 normalized only at GAPDH respectively. Data represented as  $\pm$ SEM and statistical significance One-way ANOVA is shown by: ns= not significant;  $p>0.05$ ; \*  $p\leq 0.05$ ; \*\*  $p\leq 0.01$ ; \*\*\*  $p\leq 0.001$ ; \*\*\*\*  $p\leq 0.0001$ .

